Geochemical Heterogeneity in the Hawaiian Plume: Constraints from Hawaiian Volcanoes and Emperor Seamounts

By

Shichun Huang

B.S. Geochemistry
University of Science and Technology of China, 1998

Submitted to the Department of Earth, Atmospheric and Planetary Sciences in Partial Fulfillment of the Requirement for the Degree of

DOCTOR OF PHILOSOPHY
in
GEOCHEMISTRY
at the
MASSACHUSETTS INSTITUTE OF TECHNOLOGY

SEPTEMBER 2005

Signature of Author:_____
Department of Earth, Atmospheric and Planetary Sciences
August 10, 2005

Certified by:_____
Frederick A. Frey
Professor of Geochemistry
Thesis Supervisor

Accepted by:_____
Maria Zuber
E.A. Griswold Professor of Geophysics and Planetary Science
Department Head

Abstract:

The 6000-km long, age-progressive linear Hawaii-Emperor Chain is one of the best defined hotspot tracks. This hotspot track plays an important role in the plume hypothesis. In this research, geochemical data on the Hawaiian-Emperor lavas are used to evaluate the plume hypothesis. There are important geochemical similarities among lavas from the Hawaii-Emperor Chain, such as high Ba/Th (>100), high $^{3}He/^{4}He$ (>10 R/R_A) and enrichment in incompatible elements. These distinctive geochemical characteristics are not present in mid-ocean ridge basalt (MORB). Consequently, it is inferred that a common mantle source has been contributing to the Hawaiian-Emperor volcanism for over 80 My, which provides the strongest geochemical argument supporting the plume hypothesis.

The distinctive geochemical characteristics of Makapuu-stage Koolau lavas, such as high SiO_2 content, $^{87}Sr/^{86}Sr$, $^{208}Pb^{*}/^{206}Pb^{*}$, $\delta^{18}O$, $^{187}Os/^{188}Os$, La/Nb, Sr/Nb and low CaO content, $^{143}Nd/^{144}Nd$, $^{206}Pb/^{204}Pb$, Th/La, require that recycled ancient oceanic crust including sediments is present in the Hawaiian plume. Some of these distinctive geochemical characteristics are also present in other Hawaiian shields. For example, Kahoolawe lavas also range to low $^{206}Pb/^{204}Pb$. However, Kahoolawe lavas are not characterized by relatively high SiO_2 content, Sr/Nb and La/Nb and low CaO content that are characteristic of Makapuu-stage Koolau lavas, and they are offset from other Hawaiian shield lavas to high $^{87}Sr/^{86}Sr$ at a given $^{143}Nd/^{144}Nd$. Since Hawaiian shield lavas have similar Sr/Nd (variation less than a factor of three), I speculate that the $^{87}Sr/^{86}Sr$ offset is a result of varying roles of recycled plagioclase-rich gabbro in Hawaiian shield lavas.

Modern Hawaiian volcanoes form two offset trends, i.e., the Loa and Kea trends. Lavas from Loa and Kea trends have important geochemical differences. Specifically, Loa trend lavas have relatively higher $^{208}Pb/^{204}Pb$ at a given $^{206}Pb/^{204}Pb$ than Kea trend lavas, that is, Loa trend lavas have higher $^{208}Pb^*/^{206}Pb^*$ than Kea trend lavas. Loa and Kea trend lavas form different trends in plots of $^{208}Pb^*/^{206}Pb^*$ vs Sr-Nd-Hf-He isotopic ratios, and the Loihi component (high $^3He/^4He$) is a common source component for Loa and Kea trend lavas. The Loa-Kea geochemical differences are inferred to reflect source differences; consequently, different models of plume structure have been proposed. However, I propose an alternative model in which Loa and Kea trend volcanoes sample a common geochemically heterogeneous source. The observed Loa-Kea geochemical differences is inferred as a result of temperature difference between Loa and Kea trend volcanoes which reflects their distances from the center of the hot plume core.

Thesis Supervisor: Frederick A. Frey
Title: Professor of Geochemistry

ACKNOWLEDGEMENT

I am indebted to my thesis committee, Fred Frey, Tim Grove, Sam Bowring, Mark Kurz, Dan Shim and Sujoy Mukhopadhyay, as well as Rob van der Hilst who cannot participate in my thesis defense, for their constructive criticism and many fruitful discussions over the years. Particularly, I would like to thank Fred Frey. As an academic advisor and a mentor, he teaches me almost everything from igneous geochemistry, ABC of scientific research to English. I have benefited from discussions with Mike Garcia, Francis Albarède, Thor Thordarson, Marcel Regelous, Janna Blichert-Toft, Randy Keller, Rob Duncan, Vincent Salters, Ron Fodor, and Glenn Bauer.

I would like to thank the science teams of Hawaiian Scientific Drilling Project, Koolau Scientific Drilling Project and Ocean Drilling Program Leg 197. My thesis could not have been completed without their cooperation. Most of the analytical work of my thesis was done at MIT and Univ. of Mass. at Amherst. I thank Mark Schmitz for teaching me clean lab ABC and ICP-MS analysis. I would like to thank Sam Bowring and Ed Boyle who let me use the clean lab and ICP-MS facilities at MIT for years, and their lab managers, Frank Dudas, Barry Grant and Rick Kayser for the help in the clean lab, ICP-MS and TIMS analysis. I thank Michael Rhodes for access the XRF facility at Univ. of Mass. at Amherst, and Michael Vollinger for his help in XRF analysis. I thank Neal Chatterjee for assisting electron microprobe analysis at MIT. I thank Carol Zayotti for administrative support.

I benefited from the discussion in the informal trace element seminars given by Fred every year. I learned a lot from discussions with my fellow graduate students and postdocs: Kirsten Nicolaysen, Mark Schmitz, Steve Parman, Alberto Saal, Haui-Jen

Yang, Jim van Orman, Lindy Elkins-Tanton, Steve Singletary, Guangping Xu, Jeff Standish, Rhea Workman, and Matt Jackson. They make MIT a stimulating and fun place to work.

I also thank the MIT Dragon team and the crEAPS team. These soccer and volleyball games keep me healthy at MIT.

Last, but the most important, I am grateful to my family for their continuous support and confidence in me.

TABLE OF CONTENTS

Introduction

The Hawaiian Ridge-Emperor Seamount Chain (Fig. 1) is one of the best defined hotspot tracks (Wilson, 1963). It ranges from the active volcanoes at the south-eastern end of the Hawaiian ridge to > 80 My old volcanoes at the northern end of the Emperor Seamount chain. Although there is evidence for southward migration of the Hawaiian hotspot (e.g., DePaolo et al., 2001; Tarduno et al., 2003), this linear hotspot track is attributed to the passage of the Pacific plate over a relatively fixed mantle source of magma (hotspot), perhaps a mantle plume (e.g., Morgan, 1971). Most Hawaiian volcanoes systematically evolve through four growth stages: pre-shield, shield, post-shield and rejuvenated-stage, which are consistent with a volcano forming as it approaches, over-rides and leaves the hotspot (e.g., Chen and Frey, 1985; Clague and Dalrymple, 1987). The shield stage is the main growth stage of a Hawaiian volcano, and ~95% mass of a volcano is built within this stage. An understanding of how a mantle plume "works" requires documentation and understanding of geochemical variation in plume-derived lavas on both short-term (intra-shield) and long-term (inter-shield) time scales. In this study, I present geochemical data on basalt recovered from four volcanoes of varying ages: Mauna Kea volcano (<1 Ma), Kahoolawe volcano (1-2 Ma), Koolau volcano (2-3 Ma) and Detroit Seamount (76-81Ma) (Fig. 1). Each of these studies comprises a thesis chapter. The fifth chapter is a synthesis chapter summarizing tests of the plume hypothesis using Hawaiian-Emperor volcanism as an example. Chapters 1, 2 and 4 are published. Below are the references:

Chapter 1: Huang, S. and Frey, F. A., Trace element abundances of Mauna Kea basalt from Phase 2 of the Hawaiian Scientific Drilling Project: Petrogenetic implications of correlations with major element content and isotopic ratios, Geochem. Geophys., Geosys, 4(6), 8711, doi, 1029/2002 GC000322, 2003.

Chapter 2: Huang, S. and Frey, F. A., Recycled Oceanic Crust in the Hawaiian Plume: Evidence from Temporal Geochemical Variations Within the Koolau Shield. Contrib. Mineral. Petrol. 149(5): 556-575, DOI:10.1007/s00410-005-0664-9, 2005.

Chapter 4: Huang, S., Regelous, M., Thordarson, T. and Frey, F. A., Petrogenesis of Lavas from Detroit Seamount: Geochemical Differences Between Emperor Chain and Hawaiian Volcanoes. Geochem. Geophys. Geosystem. 6(1), Q01L06, doi:10.1029/2004GC000756, 2005.

In detail, Chapter 2 differs slightly from the published version. Chapter 3 was re-submitted to Geochem. Geophys. Geosyst. after revision on August 4, 2005.

Reference

Chen, C.-Y. and Frey, F.A., Trace element and isotope geochemistry of lavas from Haleakala Volcano, East Maui: Implications for the origin of Hawaiian basalts, J. Geophys. Res., 90, B10, 8743-8768, 1985.

Clague, D. A., and Dalrymple, B. G., The Hawaiian-Emperor volcanic chain; Part I, Geologic evolution, in Decker, R. W. (editor), Wright, T. L. (editor), Stauffer, P. H. (editor), Volcanism in Hawaii, U. S. Geological Survey Professional Paper, P 1350, 5-73, 1987.

DePaolo, D. J., Bryce, J. G., Dodson, A., Shuster, D. L., Kennedy, B. M., Isotopic evolution of Mauna Loa and the chemical structure of the Hawaiian plume, Geochem. Geophys. Geosyst. 2 paper number 2000GC000139, 2001.

Morgan, W. J., Convection plumes in the lower mantle, Nature (London), 230 (5288), 42-43, 1971.

Tarduno, J. A., Duncan, R. A., Scholl, D. W., Cottrell, R. D., Steinberger, B., Thordarson, T., Kerr, B. C., Neal, C. R., Frey, F. A., Torii, M., Carvallo, C., The Emperor Seamounts; southward motion of the Hawaiian Hotspot plume in Earth's mantle, Science, 301 (5636), 1064-1069, 2003.

Wilson, T. J., A possible origin of the Hawaiian Islands, Canadian Journal of Physics, 41 (6), 863-870, 1963.

Figure Caption

Fig. 1 Map shows volcanoes along the Emperor Seamount Chain (eruption ages within parenthesis). Inset shows the Hawaiian Islands (green), locations of Loa and Kea trend shields (blue and black, respectively) and rejuvenated stage volcanism (red) and North Arch volcanic field. Volcanoes and seamount studied in this research are labeled with larger letters.

Fig 1

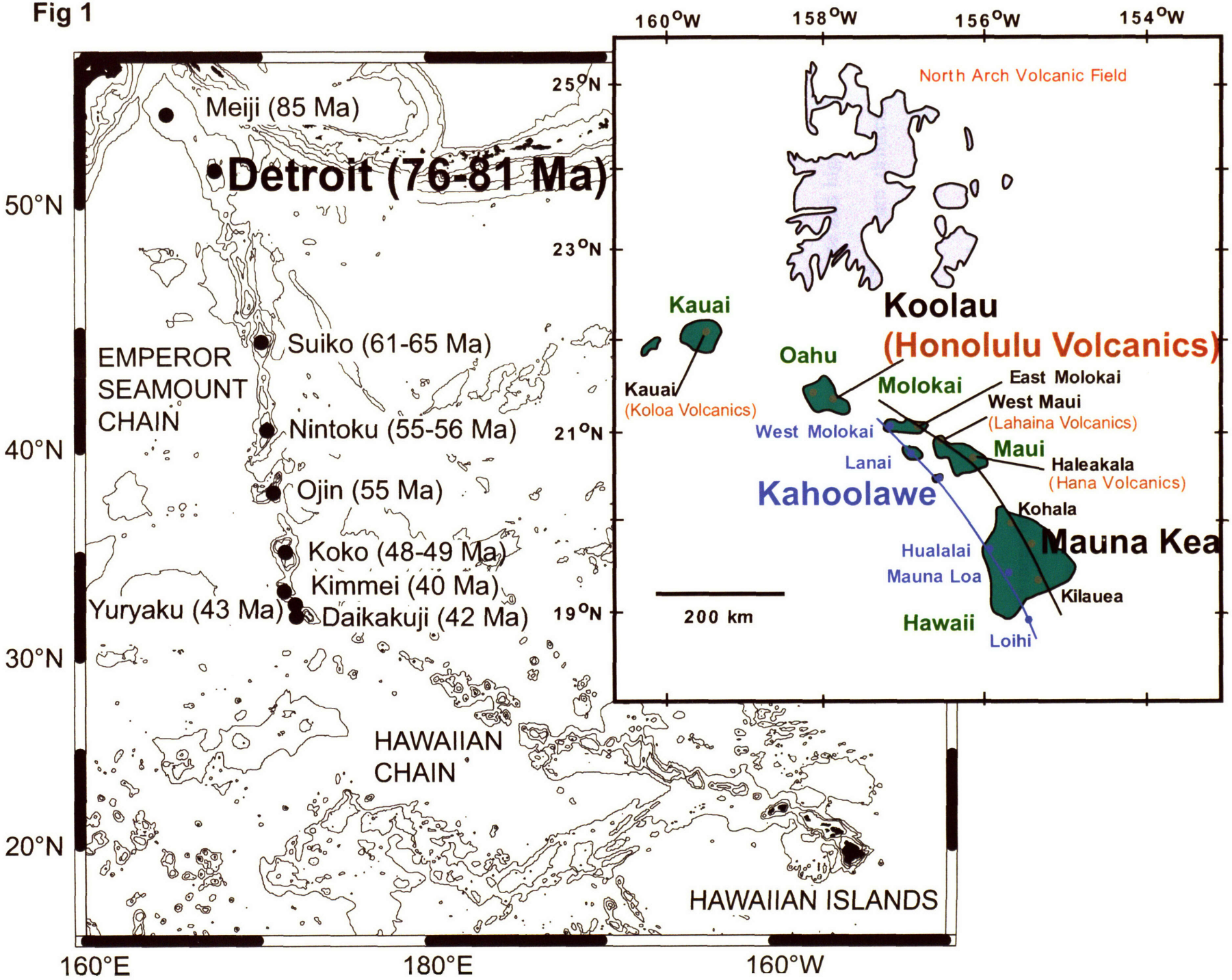
160°W
158°W
156°W
154°W
25°N
23°N
21°N
19°N
North Arch Volcanic Field
Koolau
(Honolulu Volcanics)
Kauai
Kauai
(Koloa Volcanics)
Oahu
Molokai
East Molokai
West Maui
(Lahaina Volcanics)
West Molokai
Maui
Lanai
Haleakala
(Hana Volcanics)
Kahoolawe
Kohala
Mauna Kea
Hualalai
Mauna Loa
Kilauea
200 km
Hawaii
Loihi
Meiji (85 Ma)
Detroit (76-81 Ma)
Suiko (61-65 Ma)
EMPEROR
SEAMOUNT
CHAIN
Nintoku (55-56 Ma)
Ojin (55 Ma)
Koko (48-49 Ma)
Kimmei (40 Ma)
Yuryaku (43 Ma)
Daikakuji (42 Ma)
HAWAIIAN
CHAIN
HAWAIIAN ISLANDS
50°N
40°N
30°N
20°N
160°E
180°E
160°W

CHAPTER 1: TRACE ELEMENT ABUNDANCES OF MAUNA KEA BASALT FROM PHASE 2 OF THE HAWAII SCIENTIFIC DRILLING PROJECT: PETROGENETIC IMPLICATIONS OF CORRELATIONS WITH MAJOR ELEMENT CONTENT AND ISOTOPIC RATIOS

ABSTRACT

The temporal geochemical variations defined by lavas erupted throughout the growth of a single volcano provide important information for understanding how the Hawaiian plume works. The Hawaii Scientific Drilling Project (HSDP) sampled the shield of Mauna Kea volcano to a depth of 3100 meters below sea level during Phase 2 of the HSDP. Incompatible element abundance ratios, such as La/Yb, Sm/Yb, Nb/Zr, and Ti/Zr, in conjunction with SiO_2 abundance and radiogenic isotopic ratios, especially He and Pb, in the reference sample suites of the Mauna Kea portion of cores from Phases 1 and 2 of the HSDP define three distinct geochemical groups. The upper 550m of Mauna Kea lavas in the Phase 2 core include the Postshield Group with eruption ages of ~200ka to <370ka. These lavas have relatively low SiO_2 content, $^{3}He/^{4}He$ and $^{206}Pb/^{204}Pb$, and they define a trend to relatively high La/Yb, Sm/Yb, and Nb/Zr. The eruption of these lavas coincides with migration of the Mauna Kea shield off the hotspot. As a result, extent of melting decreased, melt segregation occurred at greater depth, within the garnet stability field, and a geochemically distinct component associated with the periphery of the plume was sampled. Deeper in the Phase 2 core two other geochemical groups of lava are intercalated. One group has relatively low SiO_2 abundance and high Nb/Zr Ti/Zr, $^{3}He/^{4}He$ and high $^{208}Pb/^{204}Pb$ at a given $^{206}Pb/^{204}Pb$. These are distinctive geochemical characteristics of lavas erupted at Loihi seamount. Variations in incompatible element abundance ratios (e.g., Sm/Yb vs. Nb/Zr and La/Yb vs. Ti/Zr) define mixing trends between these low SiO_2 lavas (Loihi-type) and lavas belonging to a high SiO_2 group that are the dominant lava type in the shield part of the core (Kea-type). These two groups are presumed to reflect components intrinsic to the plume.

Correlations of incompatible element abundance ratios, such as La/Nb, with radiogenic isotope ratios show that Hawaiian shields contain different proportions of geochemically distinctive components. The Koolau shield contains a recycled sedimentary component that is not present in the Mauna Kea shield. The anomalously high Ba/Th in Hawaiian lavas is inferred to be a source characteristic. Ba/Th is correlated with some radiogenic isotope ratios in Kilauea and Mauna Loa lavas, but there is no correlation in Mauna Kea lavas which range in Ba/Th by a factor of 2.6.

1. INTRODUCTION

In order to understand processes occurring within the earth's mantle, it is necessary to determine the role of mantle plumes in creating ocean island volcanoes. The strongest evidence for long-lived mantle plumes arises from volcanic chains that define age progressive hotspot tracks; the Hawaiian Ridge and Emperor Seamount Chain are well documented examples. An important approach for determining how a plume "works" is to study the life history of a single volcano as it approaches, passes over and moves away from the hotspot. This is a principal objective of the Hawaiian Scientific Drilling Project (HSDP) which is focussed on sampling a large portion of the growth of Mauna Kea Volcano (Stolper et al., 1996).

Core from the pilot hole of HSDP (designated Phase 1 in following text) drilled near Hilo, Hawaii recovered 280 m of lavas derived from Mauna Loa Volcano overlying 776 m of subaerially erupted Mauna Kea lavas ranging in age from <200ka to ~400 ka (Sharp et al., 1996). Based on the success of this Phase 1 hole, Phase 2 of HSDP drilled and cored (95% recovery) Mauna Loa and Mauna Kea shield lavas to a depth of 3098 meters below sea level (mbsl) at a site ~2 km south of the Phase I hole (De Paolo et al., 1999). From top to bottom this core includes 246 m of subaerially erupted Mauna Loa lavas, 833 m (~120 flow units) of subaerially erupted Mauna Kea lavas which at the depth of 1079 mbsl abruptly change to 905 m of submarine lavas, dominantly basaltic hyaloclastite debris flows but with a significant proportion of massive basalt with relatively low vesicularity. The lowermost 1114 m of Phase 2 core is ~60% pillow lavas intercalated with volcaniclastic sediment. Also thirteen intrusive units occur in the deepest parts of the core forming ~7% of the core from 2500 to 3100 mbsl. Both cores

are dominantly tholeiitic basalt, but alkalic basalt occurs in the uppermost parts of the Mauna Kea section in both the Phase 1 (nine flow units, Yang et al., 1996) and Phase 2 cores (two flow units, Rhodes and Vollinger, 2004). Eruption ages for Mauna Kea lavas in the Phase 2 core range from <230 ka to 630 ka (all ages mentioned in this text are measured, interpolated or extrapolated data from Sharp and Renne, 2005).

Our research effort is part of a team effort to determine and interpret temporal geochemical variations of lavas forming the shield of Mauna Kea Volcano. I have determined abundances of trace elements in the reference suite of samples (DePaolo et al., 1999) from the Mauna Kea portion of the Phase 2 core (100 samples) by instrumental neutron activation (INAA) and inductively coupled plasma mass spectrometry (ICP-MS) **(Table 1)**. I analyzed aliquots of the reference suite powders prepared by Rhodes and Vollinger (2004). Details of the analytical procedures, estimates of accuracy and precision are discussed in **Appendix 1**. Many trace elements were analyzed by ICP-MS, INAA and XRF (Rhodes and Vollinger, 2004), and the comparisons of the three data sets are in **Appendix 1**. Figures in this paper show ICP-MS data unless noted otherwise in the figure captions. Our objective is to use these data along with major and trace element abundances determined by X-ray fluorescence (XRF) (Rhodes and Vollinger, 2004) and radiogenic isotopic ratios (Blichert-Toft et al., 2003; Bryce et al., 2005; Kurz et al., 2004) to understand how the geochemical characteristics of these lavas were affected by post-magmatic alteration, crystal fractionation within the crust, and mantle processes, such as extent of melting. To constrain the source components contributing to Hawaiian shield building lavas, I also evaluate correlations between abundance ratios of incompatible

elements and radiogenic isotopic ratios in lavas from Mauna Kea and other Hawaiian shields.

2. RESULTS: Incompatible Trace Elements

Abundances of incompatible elements that are not very sensitive to post-magmatic alteration, such as Nb, are inversely correlated with MgO content. This correlation is not linear because at a given MgO content the alkalic basalts are offset to higher Nb content (Fig. 1). Within the HSDP Phase 2 reference suite of samples, the abundance range of incompatible elements varies from ~3 for moderately incompatible elements such as heavy rare earth elements (REE) to ~5 to 8 for highly incompatible elements, such as Ba, Th, U, Nb and light REE (Fig. 2a). Generally this is also the order of increasing variability in abundance as indicated by the percent standard deviation (Fig. 2b). For most incompatible elements the highest abundances are in the two alkalic lavas, SR 121 and SR 131 **(Table 1, Fig. 3)**. Note that the complete sample identification numbers are given in **Table 1**, but for brevity in the text I identify each reference sample only by SR number for Phase 2 and R number for Phase 1.

Based on compositional similarity, alkalic basalt SR 131 from the Phase 2 core is from the same flow as sample R 177 from the Phase 1 core **(Table 2)**. Both R 177 and SR 131 have unusually low SiO_2 contents and high alkalinity; they define the extremes in their respective cores (see fig. 1a of Yang et al., 1996 and fig. 3 of Rhodes and Vollinger, 2004), In addition these samples are from units with similar eruption ages of ~240ka (Table 2).

The systematic increase in abundance range from moderately to highly incompatible elements is consistent with control of incompatible element abundances

(except Rb) by igneous processes involving mafic minerals such as olivine, pyroxenes, and perhaps garnet. Based on analyses of multiple samples from individual flow units in the Phase 2 core (unpublished data of Huang, Vollinger, Frey and Rhodes), the extremely large range in Rb abundance (~40, Fig. 2a inset) reflects the effects of post-magmatic processes whereas Nb and Th are highly incompatible elements whose abundances were not affected by post-magmatic alteration. Abundance of Ba, Th and light REE are highly correlated, and in x-y plots the trends have near zero intercepts indicating that these elements were similarly incompatible (Fig 3a). The correlations are not as good for U, and especially Rb (Fig. 3a); I infer that these poorer correlations reflect the effects of post-magmatic alteration (e.g., Kennedy et al., 1991; Cohen et al., 1996; Yang et al., 1996 and unpublished data of Huang, Vollinger, Frey and Rhodes). Although Sr, Sm and Hf abundances versus Th abundance are also highly correlated, the trends clearly define convex upwards trends; such convexity is even more apparent for Y and heavy rare earth element abundance (Fig. 3b). Non-linearity in abundance variation plots involving elements of differing incompatibility is characteristic of melts derived by different extents of melting of a common source. This result arises from the mass balance equations

$$C_\ell^x / C_o^x = 1/[F + D_x(1-F)] \text{ and } (C^x / C^y)_\ell / (C^x / C^y)_o = [F + D_y(1-F)]/[F + D_x(1-F)]$$

(where x and y are generic incompatible elements; C_l^x and C_o^x are melt and source concentrations, respectively; F = melt fraction; D_x and D_y are bulk solid/melt partition coefficients). When Ds of incompatible elements are much less than the extent of melting (F), the abundance ratio $(C_x/C_y)_l$ is constant (i.e., trends with constant slope intersecting the origin in Fig. 3a); therefore $(C_x/C_y)_l$ is independent of F and is equal to the source ratio. In contrast when Ds of incompatible elements are comparable to F, the abundance ratio $(C_x/C_y)_l$ varies with extent of melting; i.e., the slope changes in a x-y variation plot (e.g., Fig. 3 of Hanson, 1989). The convexity in Fig. 3b trends indicates

that the bulk solid/melt partition coefficient for Th was smaller than that for Sr, Sm, Hf, Y and Lu.

3. DISCUSSION: HSDP CORES

3.1 Effects of Post-Magmatic Alteration on Lava Compositions

For subaerially erupted Hawaiian tholeiitic basalt, the abundance ratios K/Rb and K_2O/P_2O_5 are sensitive indicators of post-magmatic alteration because K and especially Rb are preferentially leached from the basalts leading to unusually low K_2O/P_2O_5 (<1) and high K/Rb (>1000) and Ba/Rb (>20) (e.g., Feigenson et al., 1983; Frey et al., 1991, 1994; Yang et al., 1996). For the HSDP samples the effects of such alteration are obvious in a plot of Ba/Rb versus K_2O/P_2O_5 where Ba/Rb, a ratio that is quite constant, 11.6± 0.2, in unaltered oceanic basalts (Hofmann and White, 1983), reaches values of >100 (Fig. 4a). What is surprising about the HSDP trend in Fig. 4a is that the subaerial and submarine lavas define sub-parallel trends with the submarine lavas slightly offset to lower Ba/Rb at a given K_2O/P_2O_5. Submarine seawater alteration of MORB typically leads to increases in abundances of K and Rb (Staudigel et al., 1995), but submarine HSDP samples show no evidence for addition of K and Rb. Alkali loss is especially characteristic of the second pillow zone (2234 to 2470 mbsl, see Fig. 4b) which is composed of low density, vesicular pillow lava (Moore, 2001). I infer that this pillow zone is a region of fresh water migration. Additional geochemical effects of postmagmatic alteration are discussed by Chan and Frey (2003) for lithium.

3.2 Role of Crystal Fractionation

Plagioclase: Only about 20% of the HSDP cores contains phenocrysts of plagioclase or clinopyroxene, and only a few of these lavas have >1% plagioclase or

clinopyroxene phenocrysts (Garcia, 1996; De Paolo et al., 1999). The role of plagioclase fractionation can be evaluated using Al_2O_3 abundance, $(Sr/Nd)_{PM}$ and relative abundance of Eu (subscript PM indicates normalized to primitive mantle). Samples from Phase 1 and 2 cores define an inverse correlation between Al_2O_3 and MgO (Fig. 5a). The increased scatter at the low MgO end of the trend reflects the tendency of alkalic basalt to have higher Al_2O_3; e.g., samples SR 121, SR 131 and R177; tholeiitic sample SR 129 is also offset to high Al_2O_3 and CaO (Fig. 5a,b). Since the Al_2O_3 content of plagioclase exceeds that of coexisting equilibrium melts, segregation of mineral assemblages including significant plagioclase result in decreasing Al_2O_3 abundance with increasing differentiation. Consequently, the inverse Al_2O_3 versus MgO trend shows that plagioclase fractionation was not an important process. Because Sr and Eu are relatively compatible in plagioclase the variation of $(Sr/Nd)_{PM}$ and (Eu/Eu*) with MgO content in an individual shield can also be used to evaluate the role of plagioclase fractionation. In general, HSDP Phase 2 samples have $(Sr/Nd)_{PM}$ close to unity, ranging from 0.8 to 1.2, and $(Sr/Nd)_{PM}$ does not vary systematically with MgO content (Fig. 5c). Sample SR 129 has an anomalously high $(Sr/Nd)_{PM}$ >1.4 (Fig. 5c). Also it is the sample with the largest enrichment in Eu (Eu/Eu* = 1.06, Fig. 5d). Sample SR129 is from Unit 47 which contains up to 13% plagioclase phenocrysts (De Paolo et al., 1999), and it is the only obvious plagioclase cumulate in the Phase 2 core.

Sample SR125 has several anomalous geochemical characteristics. It has the lowest $(Sr/Nd)_{PM}$ (Fig. 5c) and an unusually low Na_2O content (1.27%) which is confirmed by similar values determined by XRF and INAA (Rhodes and Vollinger, 2004 and Table 1, this paper). This sample has a relatively high Loss on Ignition (3.43%), low

K_2O/P_2O_5 (0.55) and high Ba/Rb (92) (Fig. 4). It appears to have lost a plagioclase component during alteration; its CaO abundance, however, is not unusually low (Fig. 5b), and Eu/Eu* is 0.98. In addition, it has an anomalously high Sc content (Fig. 5e).

Clinopyroxene: Clinopyroxene is also a rare phenocryst in HSDP lavas (Garcia, 1996; De Paolo et. al., 1999). The role of clinopyroxene fractionation can be evaluated using CaO and Sc abundances. The CaO versus MgO trend is inverse and like the Al_2O_3 versus MgO trend, there is more scatter at low MgO; in this case the scatter is caused by the relatively low CaO content of alkalic basalt (Fig. 5b), perhaps indicating a role for clinopyroxene fractionation in generating alkalic basalt. Consistent with this inference some of the alkalic lavas, such as SR 131 and R177, have relatively low Sc and Cr contents (Fig. 5e and Table 1). The only Phase 2 tholeiitic basalt which may have experienced clinopyroxene fractionation is SR 850 which has high abundances of incompatible elements (Fig. 3a) and a low MgO content (6.44%); for this MgO content, it has relatively low Sc abundance (Fig. 5e). However, no clinopyroxene phenocrysts were observed in this sample (De Paolo et. al., 1999).

Olivine: Olivine is the dominant phenocryst/xenocryst in most of the HSDP tholeiitic basalts and petrographic observation shows that in contrast to plagioclase and clinopyroxene fractionation, olivine accumulation and fractionation was an important process (e.g., Baker et al., 1996; Garcia, 1996; Rhodes and Vollinger, 2004). A reflection of the role of olivine is the wide variation in MgO content (6% to 29%) and the positive correlation between MgO and Ni abundance (Fig. 5f). In order to adjust for the effects of olivine fractionation and accumulation for each of the Phase 2 lavas, I added or subtracted olivine in 1% increments with $K_D^{Fe/Mg} = 0.3$ until the calculated composition

was in equilibrium with Fo_{90} olivine, typical of the most Mg-rich olivine phenocrysts in the core, or Fo_{85} which is closer to the average olivine composition (Baker et al., 1996; Garcia, 1996). This adjustment greatly reduces the MgO variation (~10 to 13% for Fo_{85} and ~16.6 to 19.6% for Fo_{90}), and decreases the abundance range of incompatible elements (Fig 2a). In summary, olivine addition and fractionation was a dominant process controlling the compositions of HSDP lavas (see also Rhodes and Vollinger, 2004). Although this process can explain much of the variation in abundance of incompatible elements (Figs. 2, 3), it cannot explain the convexity of trends in Fig. 3b.

3.3 Geochemical Groups in HSDP Cores

Postshield Group: As with Al_2O_3 and CaO versus MgO abundance (Fig. 5a, b), the abundance of SiO_2 and TiO_2 are scattered at low MgO content because the eleven samples of alkalic basalt (nine in Phase 1 core and two in Phase 2 core) in the upper part of the cores have relatively low SiO_2 and high TiO_2 content (Fig. 6a, b) and relatively high total iron contents (Rhodes, 1996; Rhodes and Vollinger, 2004). The upper 152 m of the Mauna Kea section in the Phase 2 core (samples SR121 through SR175) includes intercalated alkalic and tholeiitic basalt which define a trend to relatively low SiO_2 content (Fig. 7c,f). In the range of 6 to 10% MgO, at a given MgO content these low SiO_2 lavas within the upper 152 m have the highest abundance of Nb and other incompatible elements (Fig. 3a), Al_2O_3 (Fig. 5a) and TiO_2 (Fig. 6b). Although there is considerable scatter in downhole trends for incompatible element abundance ratios, such as Nb/Zr and La/Yb, these ratios are relatively high in the alkalic samples SR 121 and SR 131 near the top of the Mauna Kea section (Fig. 7a, b). Moreover, within the uppermost

Mauna Kea lavas, there is a trend to relatively high Nb/Zr and La/Yb with decreasing depth and age (Fig. 7a, b, d, e).

The age range of samples SR121 to SR175, ~200ka to 330 ka (Fig. 7f), overlaps with the oldest of the Hamakua Volcanics, ~70ka to 250 ka, which form the basaltic postshield stage that is exposed on the lower subaerial flanks of Mauna Kea volcano (Frey et al., 1990, 1991; Wolfe et al., 1997). The Hamakua Volcanics also include intercalated tholeiitic and alkalic basalt. Yang et al. (fig. 9, 1996) showed that the trend to high La/Yb at the top of the Phase 1 core is continuous with that defined by the Hamakua Volcanics. Therefore, I refer to the intercalated alkalic and tholeiitic basalt in the upper parts of the Phase 1 and 2 cores as the Postshield Group. The gradual increase of La/Yb and Nb/Zr with decreasing age shows that the transition from shield to postshield stage was gradual and prolonged over a span of ~130 ka (Fig. 7d,e). Also, during the shield to postshield transition there were systematic changes in radiogenic isotopic ratios. For example, beginning at ~830 m $^{3}He/^{4}He$ decreases upward in the core (Fig. 8a). The Postshield Group also has relatively low $^{206}Pb/^{204}Pb$, $^{208}Pb/^{204}Pb$ and ε_{Hf}, but relatively high ε_{Nd} (Fig. 8b,c,d,e). Based on their relatively low $^{3}He/^{4}He$ (Fig. 8a) and $^{208}Pb/^{204}Pb$ at a given $^{206}Pb/^{204}Pb$ (Fig. 8f), I include samples of SR232, SR276, SR328 and SR340 in this Postshield Group, thereby increasing the initiation of postshield volcanism to ~370 ka (Fig. 7f).

Low SiO_2 Shield Group: Lavas with relatively low SiO_2 content (Fig. 6a,c) are not restricted to the Postshield Group. In the Phase 2 core some of the deeper and older (>834 mbsl and >380 ka) lavas have relatively low SiO_2 content (Fig. 7c,f). I identify these as the Low SiO_2 Shield Group (individual samples are labeled in Fig. 7c). This

group is characterized by relatively high $^{3}He/^{4}He$ and high $^{208}Pb/^{204}Pb$ at a given $^{206}Pb/^{204}Pb$, Fig. 8a,f). Based on these isotopic parameters, the youngest lava in the Low SiO_2 Shield Group is subaerial sample SR354, and samples SR750, SR756 and SR762 also belong to this group (Fig. 8a,f), despite their adjusted SiO_2 contents of >48.8% (Fig. 7c); that is I conclude that the arbitrary SiO_2 discriminant does not perfectly identify this group. In part this difficulty arises from SiO_2 mobility during postmagmatic alteration (Vollinger and Rhodes, 2002). In addition, as emphasized in later discussion, there is within group variation in geochemical characteristics, e.g., La/Yb and Zr/Nb; that is some samples are transitional between the groups. Nevertheless $^{3}He/^{4}He$ and delta $^{208}Pb/^{204}Pb$ clearly distinguish the Low SiO_2 Shield Group (Fig. 8).

High SiO_2 Shield Group: Most of the lavas have adjusted SiO_2 contents >48.8% (Fig. 7c,f), and they define the main inverse trends in MgO variation plots (Figs. 5, 6). These samples form the High SiO_2 Shield Group.

3.4 Comparison of Geochemical Groups Defined by this paper with those Defined by Rhodes and Vollinger (2004)

Rhodes and Vollinger (2004) used adjusted SiO_2 content and Zr/Nb as principle criteria for defining lava types in the Phase 2 core whereas I use adjusted SiO_2 content, incompatible element abundance ratios, $^{3}He/^{4}He$ and Pb isotopic ratios to define geochemical groups. Consequently, the lava types defined by Rhodes and Vollinger (2004) are generally similar to our groups, but there are some important differences.

Postshield: Rhodes and Vollinger include only samples SR121 (246.2 mbsl) through SR152 (337 mbsl) in this type. I extend this grouping to include samples SR167,

SR175, SR232, SR276, SR328 and SR340 (794 mbsl) that also have relatively low SiO_2 (Fig. 7f).

Type 1 of Rhodes and Vollinger (2004): These are the dominant type of tholeiitic basalt in the core (61% of the Mauna Kea lavas analyzed by Rhodes and Vollinger, 2004). They are present from 337 to 3098 mbsl and are equivalent to the High SiO_2 Shield Group in Fig. 7c, f.

Type 2 of Rhodes and Vollinger (2004): This type includes low SiO_2 lavas restricted to the upper part of the Mauna Kea section (above 1739 mbsl); these lavas are most abundant between 337 and 850 mbsl. This type includes tholeiitic lavas that resemble tholeiitic basalt occurring within the postshield group. Rhodes and Vollinger (2004) include low SiO_2 subaerial lavas SR276, SR328, SR340 and SR354, as well as the low SiO_2 submarine lavas SR531, SR545, SR560 and SR675 in this type (Fig. 7c). Because of their relatively high $^{3}He/^{4}He$ and delta $^{208}Pb/^{204}Pb$ (Fig. 8a,f) I include samples SR354, SR531, SR545, SR560 and SR675 in our Low SiO_2 Shield Group. These samples, however lack the high Nb/Zr that distinguishes older lavas in this group (Fig. 7a,d). I agree that samples SR276, SR328 and SR340 are similar to the Postshield group and I include them in this group (Figs. 7, 8).

Type 3 of Rhodes and Vollinger (2004): These are low SiO_2 lavas confined to the submarine portion of the core. They are equivalent to our Low SiO_2 Shield Group. They are a distinctive group because low SiO_2 is coupled with relatively high Nb/Zr, $^{3}He/^{4}He$ and delta $^{208}Pb/^{204}Pb$ (Figs. 7a,d, 8a,f). As noted by Rhodes and Vollinger (2004) these are also characteristics of Loihi lavas. An important difference in our grouping is that sample SR354 is a Type 2 sample in the Rhodes and Vollinger

classification because it has "normal" Nb/Zr, low SiO_2 and is in the subaerial part of the core. However, it has relatively low SiO_2, high $^3He/^4He$ and delta $^{208}Pb/^{204}Pb$; these are characteristics of of our Low SiO_2 Shield Group (Figs. 7c,f, 8a,f). This sample is important because it occurs high in the core within the subaerial section (834 mbsl with an inferred age of 380 ka). It is the uppermost sample of our Low SiO_2 Shield Group.

Type 4 of Rhodes and Vollinger (2004): This type includes only 4 samples (two are from unit 92) and is defined by relatively high Nb/Zr but they do not have relatively low SiO_2 contents. I analyzed three of these samples (SR222, SR860 and SR956) and also find that they have relatively high Nb/Zr (Fig. 7a). However, unlike Group 3 lavas, they do not have relatively high $^3He/^4He$ and delta $^{208}Pb/^{204}Pb$ (Fig. 8a,f); therefore, I do not recognize them as a distinct group.

3.5 Petrogenesis of Geochemical Groups

Postshield Group: The abundance ratios La/Sm, La/Yb, Sm/Yb and Nb/Zr are positively correlated with incompatible element content in the Postshield Group (e.g., Th in Fig. 9), and the highest La/Yb and Nb/Zr ratios are in samples from the upper part of the core (Fig. 7a,b,d,e). Although radiogenic isotope ratios vary systematically with depth in this group (Fig. 8), a plausible inference is that changes in proportions of source components were accompanied by variations in extent of melting with the alkalic lavas representing the lowest degree of melting (Yang et al., 1996). To test this hypothesis I did forward modeling for partial melting of spinel- and garnet-peridotite (see Fig. 10 and Appendix 2). The relatively large variations of La/Yb, Nb/Zr and Sm/Yb within the Postshield Group (Fig. 10a,b,c) are consistent with variable extents of batch melting of garnet peridotite with La/Yb, Nb/Zr and Sm/Yb ratios slightly greater than estimates for

primitive mantle (Table A-4 of Appendix 2). It is surprising that the range in La/Yb and Nb/Zr in the Postshield Group is similar to that for historical, ~200 yr, Kilauea lavas (Fig. 10e). These variations in Kilauea shield lavas have been explained by a factor of two change in extent of melting of garnet peridotite (Pietruszka and Garcia, 1999).

Segregation of the primary magmas for the Postshield Group within the stability field of garnet is consistent with the inverse modeling of rare earth element abundances by Feigenson et al. (2003) who inferred that alkalic lavas in the upper part of the core formed by low degrees of melting of a garnet-bearing source. In addition, I suggest that the Ti/Zr ratio is useful for identifying a role for residual garnet because $D_{cpx/melt}^{Ti/Zr} > 1$ whereas $D_{gt/melt}^{Ti/Zr} < 1$, especially for Ca-rich garnet (Table A-4). The Postshield Group trend of varying La/Yb at nearly constant Ti/Zr is clearly most consistent with partial melting of garnet peridotite (Fig. 10d). Melt segregation of the postshield lavas at relatively high pressure is also consistent with their relatively low SiO_2 content (Fig. 7f) and high FeO content (fig 6 of Rhodes and Vollinger, 2004). Hence the petrogenetic inferences for the Postshield Group are consistent with the "overall trend of increasing pressure of melt segregation and decreasing extent of melting with decreasing eruption age" inferred by Yang et al., (1996) for the HSDP 1 core.

In addition to variable extents of melting, Mauna Kea postshield lavas experienced more extensive crustal processing than shield lavas; for example, samples showing the effects of plagioclase or clinopyroxene fractionation are dominantly confined to subaerially erupted lavas (Fig. 5). Moreover, samples with relatively low (~7%) MgO content are also abundant in the upper part of the Phase 2 core (Fig. 5 of Rhodes and Vollinger, 2004). The relatively low MgO content and a role for fractionation of

plagioclase and clinopyroxene in the upper part of the core are consistent with longer residence times in crustal magma reservoirs as the magma supply from the mantle decreased during the transition from shield-stage to postshield-stage volcanism (e.g., Frey et al., 1990, 1991; De Paolo and Stolper, 1996).

Shield Groups: The trends in Fig. 10 for the High SiO_2 Shield Group are not as clearly defined as those for the Postshield Group, but they may also reflect variations in extent of melting. However, variations in radiogenic isotopic ratios within the core and even within the defined lava groups (Fig. 11) shows that the petrogenesis of each group is more complex than variable extents of melting of a geochemically homogeneous source. As an example, the inverse Sm/Yb-Nb/Zr trend (Fig. 10b) and relatively constant La/Yb but variable Ti/Zr of the Low SiO_2 Shield Group (Fig. 10d) are inconsistent with variable extents of melting of a common peridotite source. Rhodes and Vollinger (2004) noted that each of their major lava types ranges widely in MgO content. They argued that the near linear trends in MgO variation plots (e.g., Fig. 5a,b, 6a,b) reflect magma mixing in addition to olivine accumulation and fractionation. Although this complexity does not mask the compositional groups that I identify, the recognition of magma mixing as a significant process is important in explaining geochemical variations within these groups because the mixing endmembers may be derived from geochemically distinct sources.

An important observation is that the high Ti/Zr and Nb/Zr portion of the trends defined by the Low SiO_2 Shield Group is defined by the low SiO_2 lavas erupted in two distinct intervals (Fig. 10e), the 5 samples from SR732 to SR762 (depth range of 1974 to 2124 mbsl and inferred age range of 503ka to 520ka) and the 7 samples from SR791 to SR842 (depth range of 2280 to 2504 mbsl and inferred age range of 537ka to 561ka).

Also, a lower pillow basalt SR871 and intrusive sample SR940 are included in this subgroup. In addition to high Ti/Zr and Nb/Zr and relatively low SiO_2 contents these samples have relatively high $^3He/^4He$ (Fig. 8a), and they define the low $^{206}Pb/^{204}Pb$ end of the Kea high 8 Pb array of Eisele et al. (2003, see their Fig. 2). A plot of $^3He/^4He$ versus delta $^{208}Pb/^{204}Pb$ (see Fig. 7 of Kurz et al., 2004) shows that for He and Pb isotopes these lavas trend toward the field of lavas from Loihi Seamount (also see Fig.11a). Based on SiO_2 content, Nb/Zr and $^3He/^4He$, Rhodes (2000) and Kurz and Curtice (2000) were the first to note the similarity of these Mauna Kea lavas to lavas from Loihi Seamount. In addition to high Nb/Zr (Fig. 10f), high Ti/Zr is typical of some Loihi lavas (Fig. 10g). Therefore, I conclude that samples of the Low SiO_2 Shield Group with the lowest $^{206}Pb/^{204}Pb$ and highest Nb/Zr and Ti/Zr contain the largest proportion of a Loihi-type component (Figs.10f,g, 11a).

3.6 Abundance Ratios Involving Elements of Similar Incompatibility

Each of the abundance ratios Nb/La, Nb/Ta, Nb/Th, Nb/U, Zr/Hf and Ce/Pb involve elements with similar geochemical characteristics. These ratios are not highly variable in oceanic basalt; typically they vary by less than a factor of two. However, numerous recent studies have shown that significant variations in these ratios are found in mid-ocean ridge and oceanic island basalt. These variations are inferred to reflect magmatic processes, specifically differences in partition coefficients, e.g., $D_{Hf} > 2D_{Zr}$ for clinopyroxene/melt (Blundy et al., 1998). However, these ratios in the Phase 2 core are typical for ocean island basalt and there are few significant differences between the Postshield and Shield groups (Fig. 12).

Nb/Th: The mean Nb/Th for the Phase 2 reference suite is 15.4±1.4 (in this section the ± value indicates two standard deviations) very similar to that for the Phase 1 core (15.0±3.6 and 16.2±2.4, Albarede, 1996; Hofmann and Jochum, 1996, respectively), for postshield lavas on the subaerial slopes of Mauna Kea (14.3, Kennedy et al., 1991) and to the average (15.2±1.7) reported for Hawaiian shield basalt by Hofmann (1986). It is notable that the Nb/Th ratio is greater than the primitive mantle estimate (8.6, Sun and McDonough, 1989) but to date there is no indication that Nb/Th is a useful discriminant for the different components contributing to Hawaiian volcanism.

Nb/U: The mean Nb/U for the two groups of shield lavas is 45±10, well within the global average of 47±10 for oceanic basalt (Hofmann, 1986), and similar to that for the Phase 1 core (48±12 and 53±14, Albarede, 1996; Hofmann and Jochum, 1996, respectively). The Postshield lavas range to higher Nb/U, but given the similarity of Nb/Th in all groups, the higher Nb/U in upper lavas probably reflects U loss during post-magmatic alteration as proposed by Kennedy et al. (1991) for postshield lavas erupted on the high rainfall east flank of Mauna Kea. In the Phase 2 core, sample SR129 has the highest Nb/U (74), and its altered nature is indicated in Fig 4a.

Nb/Ta: The average Nb/Ta of the shield lavas is 13±2, similar to that reported for the Phase 1 core (12±6, Albarede, 1996) and close to that for average MORB and OIB (16.7±1.8 and 17.1±2, respectively; Kamber and Collerson, 2000). The highest Nb/Ta (up to 15.7 in SR125) occurs in the youngest postshield lavas. The slightly lower Nb/Ta of Phase 2 samples compared to OIB and MORB probably reflects Ta contamination arising from use of a WC shatterbox (see Rhodes, 1996 for description of sample preparation for Phase 1 and 2 reference suite). Surprisingly Phase 1 Mauna Kea samples

analyzed by Albarede (1996) range to much lower Nb/Ta of 2 to 3, hence the large standard deviation. Apparently, the samples of Albarede (1996) were contaminated by Ta.

Nb/La: There is a general trend, with considerable scatter, for Nb/La to decrease upwards in the HSDP core (Fig.12). The mean value of 1.19±0.10 of the Phase 2 data overlaps with the Phase 1 mean (1.18±0.24 and 1.19±0.08, Albarede, 1996 and Yang et al. 1996, respectively). All of these values exceed that of the primitive mantle estimate of 1.04 (Sun and McDonough, 1989). Like Nb/Zr, the Nb/La ratio of Hawaiian shield lavas is correlated with radiogenic isotopic ratios (see subsequent Discussion in Section 4).

Zr/Hf: The Zr/Hf ratio does not vary systematically with depth in the core and the mean value, 39±3. is within the range for primitive OIB ~37 to 44 (David et al., 2000) and similar to that for the Phase 1 core (42±2, Yang et al. 1996).

Ce/Pb: Similarly, Ce/Pb does not vary with depth in the core and the mean 29±8 (excluding two samples with anomalously high Pb content, see Fig 3) is similar to that typical of oceanic basalt (25±5, Hofmann et al., 1986). The range to low Ce/Pb (<20 in a few HSDP samples may reflect Pb contamination, but the lowest Ce/Pb occur over the depth interval from ~300 to 1300m. Possibly this is a zone of Pb mobility, but it does not overlap with the uppermost lavas with high Nb/U. The Ce/Pb ratios in the Phase 2 core are lower than the 40±4 reported by Kennedy et al. (1991) for postshield Mauna Kea lavas but similar to the Phase 1 average (33±8 and 40±11, Albarede, 1996 and Yang et al. 1996, respectively).

3.7 Implications of Temporal Geochemical Trends in HSDP Cores

In summary, the temporal geochemical trends defined by Mauna Kea lavas in the HSDP cores leads to the following conclusions.

(a) HSDP lavas show that at Mauna Kea volcano there was a gradual and prolonged transition from shield- to postshield-stage volcanism commencing at ~370ka (sample SR 340), and entering a phase of intercalated tholeiitic and alkalic basalt at ~230ka (SR 131, Table 2). Studies of subaerially exposed Mauna Kea lavas show that postshield basaltic volcanism (Hamakua Volcanics) continued until 70-65ka and was followed by a hawaiitic substage (Laupahoehoe Volcanics) erupted from 65-4ka (Frey et al., 1990, 1991; Wolfe et al., 1997). Although the HSDP postshield lavas are not highly evolved (MgO > 6.3%), they, in general, are more evolved than the underlying shield lavas, thereby providing evidence for increased crystal fractionation resulting from a decreasing magma supply to the crust, an inference that is consistent with the long time interval represented by these lavas (Fig. 7f).

Within the intercalated tholeiitic and alkalic basalt of the postshield-stage, the alkalic basalt does not have distinctive isotopic characteristics (Fig. 8); hence I infer that low SiO_2 content and incompatible element enrichment of alkalic basalt was, at least in part, controlled by process. Specifically, I conclude that the uppermost HSDP lavas in the Mauna Kea section, the Postshield Group including intercalated alkalic and tholeiitic basalt, segregated at a lower extent of melting and higher pressure, within the stability field of garnet, than the underlying Mauna Kea lavas. Similar inferences were made from studies of the Phase 1 core (Yang et al., 1996) and onland sections of Mauna Kea basalt (Frey et al., 1991). In addition the source of the Postshield Group had lower $^3He/^4He$ and

less radiogenic Pb isotope ratios than older shield lavas. Similar results were obtained for the HSDP Phase 1 core (Kurz et al., 1996; Lassiter et al., 1996) and for other Hawaiian shields, such as Haleakala (Kurz et al., 1987; Chen et al., 1991). Hence as a Hawaiian volcano migrates away from the hotspot, shield-stage volcanism wanes, extent of melting decreases, depth of melt segregation increases, magma supply to the crust decreases, crystal fractionation within the crust is enhanced, and there is an increased role for a depleted component with typically lower $^{3}He/^{4}He$ and $^{87}Sr/^{86}Sr$, higher $^{143}Nd/^{144}Nd$ and $^{176}Hf/^{177}Hf$ and less radiogenic Pb. In detail the trend to lower ε_{Hf} for the Postshield Group (Fig. 8c) is anomalous.

Lassiter et al. (1996, see their Fig. 9) interpreted results for the Phase I core as reflecting a thermally and geochemically zoned plume. As the volcano moves over the relatively cool and depleted plume margin, melting extent decreases, melt segregation occurs at relatively higher pressure and partial melts have isotopic characteristics reflecting a role for a depleted source; i.e., relatively low $^{3}He/^{4}He$ and non-radiogenic Pb. The geochemical data for the Postshield Group of the Phase 2 core are consistent with this interpretation.

(b) A new conclusion inferred from the lower part of the HSDP 2 core, deeper than 800 m, is that the Low SiO_2 Shield Group sampled a source whose partial melting led to relatively low SiO_2 content, relatively uniform La/Yb, relatively high Nb/Zr and Ti/Zr, high $^{3}He/^{4}He$ and high $^{208}Pb/^{204}Pb$ at a given $^{206}Pb/^{204}Pb$ (i.e., high delta $^{208}Pb/^{204}Pb$). This group cannot be distinguished on the basis of Sr, Nd or Hf isotopes or specific incompatible element abundance ratios, such as La/Yb and Nb/Zr. However, distinctive trends are defined by this group in ratio-ratio plots, such as Sm/Yb vs. Nb/Zr and La/Yb

vs. Ti/Zr (Fig.10e,g); moreover, these ratios are correlated with delta $^{208}Pb/^{204}Pb$ (Fig. 11). This Low SiO_2 Shield Group occurs throughout the core from ~800 to 3000 mbsl) forming clusters of samples (e.g., the 3 subgroups formed by SR531-SR545-SR560, and SR732-SR741-SR750-SR756-SR762, and SR791-SR796-SR800-SR814-SR826-SR836-SR842) which are intercalated with high SiO_2 lavas (Figs. 7 and 8). In addition to relatively low SiO_2 content the two older subgroups (SR732 to SR762 and SR791 to SR842) are characterized by relatively high Nb/Zr and Ti/Zr (Fig. 10d,e) and high $^{3}He/^{4}He$ and delta $^{208}Pb/^{204}Pb$ (Fig. 8a,f). These are characteristics of lavas from Loihi seamount. This is a surprising result because it requires that volcanoes on both the Loa (Loihi) and Kea (Mauna Kea) trends (e.g., De Paolo et al., 2001) sampled similar source materials early in their evolution. If this Loihi component is associated with the core of the Hawaiian plume, the conclusion of Lassiter et al. (1996, see their Fig. 10) that Mauna Kea volcano sampled only the relatively cool peripheral part of the plume thereby bypassing the central part of the hotspot (plume source) is incorrect. However, if sample SR354, a relatively young (380ka) subaerially erupted sample, also sampled the Loihi component, as I infer by including it in the Low SiO_2 Shield Group (Fig. 8), this component contributed to the growth of Mauna Kea for 200ka.

(c) Despite the complexities arising from the role of geochemically distinct source components, the well-defined positive correlations between abundances of incompatible elements (Fig. 3) show that these source components were not markedly different in abundance ratios involving highly incompatible elements (Fig. 12).

4. DISCUSSION: COMPARISONS OF HAWAIIAN SHIELDS

4.1 Intershield Differences in Abundance Ratios Involving Nb and Correlations With Radiogenic Isotope Ratios

Like Mauna Kea samples in the HSDP core, lavas from different Hawaiian shields define positive trends between La/Yb and Nb/Zr, but the Koolau shield is offset to lower Nb/Zr (Fig. 13a); this offset is much larger than Nb/Zr differences between groups within the Mauna Kea part of the HSDP cores. I infer that correlations between La/Yb and Nb/Zr reflect differences in extent of melting whereas intershield differences in these ratios reflect source heterogeneity. For example the La/Yb-Nb/Zr variation in HSDP postshield lavas is inferred to reflect varying extents of melting (Fig. 10a), and relatively low extent of melting is also the likely explanation for the alkalic lavas from Loihi seamount that range to high La/Yb and Nb/Zr (Fig. 13a). In contrast, the relatively low Nb/Zr and high La/Nb (a ratio that is less sensitive than Nb/Zr to variations in extent of melting) of Koolau shield lavas is inferred to reflect source differences (Fig. 13). Although the Low SiO_2 Shield Group at Mauna Kea is not distinct in La/Nb (Fig. 12), I infer that their high Nb/Zr also reflects source control (Fig. 10a,b).

It is well established for Hawaiian shield lavas that incompatible element abundance ratios involving Nb correlate with radiogenic isotopic ratios (Frey and Rhodes, 1993; Roden et al., 1994; Yang et al., 1994; Rhodes and Hart, 1995, Chen et al., 1996). Such correlations provide the opportunity to identify compositional characteristics of the different source components contributing to Hawaiian lavas. Two ratios which provide good correlations with isotopic ratios are Nb/Zr and La/Nb (Fig. 14a, b). Clearly, lavas from Koolau and to a lesser extent Mauna Loa are deficient in Nb, and their lavas trend to

relatively low $^{206}Pb/^{204}Pb$, $^{143}Nd/^{144}Nd$ and high $^{87}Sr/^{86}Sr$. Based on extrapolation of the intershield trends, the distinctive Koolau component has $^{206}Pb/^{204}Pb$ ~17.8 and $^{87}Sr/^{86}Sr$ ~0.7045 (Fig. 14b). This constraint on $^{206}Pb/^{204}Pb$ is identical to that arising from the ε_{Hf} versus $^{206}Pb/^{204}Pb$ trend defined by Hawaiian shield lavas (see Fig. 3 of Blichert-Toft et al., 1999). In contrast, the Kea component defined by lavas from Mauna Kea and Kilauea has $^{87}Sr/^{86}Sr$ ~0.7036, $^{143}Nd/^{144}Nd$ ~0.5130 and $^{206}Pb/^{204}Pb$ ~18.6 (but see Eisle et al. (2003) for a discussion of Pb isotopic complexity in HSDP 2 lavas)

It is also well known that abundance ratios involving Nb are strongly fractionated by the processes involved in arc magmatism. As a consequence, arc lavas and continental rocks have distinctly high La/Nb ratios (e.g., Hofmann, 1986). Therefore, a plausible inference is that the relative deficiency of Nb in some Hawaiian shield lavas, such as Koolau lavas, reflects recycled source components derived from an arc tectonic setting. In addition to a Nb depletion, the Koolau component has high Pb/Hf, relatively high $^{18}O/^{16}O$, $^{87}Sr/^{86}Sr$, $^{187}Os/^{188}Os$, high $^{176}Hf/^{177}Hf$ for a given $^{143}Nd/^{144}Nd$ and relatively low $^{143}Nd/^{144}Nd$, $^{206}Pb/^{204}Pb$, $^{207}Pb/^{204}Pb$ and $^{208}Pb/^{204}Pb$ (Roden et al., 1994; Eiler et al., 1996; Lassiter and Hauri, 1998; Blichert-Toft et al., 1999; Jackson et al., 1999). All of these geochemical characteristics are consistent with the conclusion that the distinctive Koolau component was derived from ancient recycled oceanic crust including pelagic sediment with a continental signature, i.e., relative depletion in Nb and enrichment in Pb (Lassiter and Hauri, 1998; Blichert-Toft et al., 1999; Jackson et al., 1999). Although subduction zone processing must modify subducted oceanic crust, it is evident that in some cases important geochemical characteristics of at least some parts of subducted plates are recycled into the mantle and returned to the surface via plume-

related volcanism. Moreover, the distinctive major element characteristics of Koolau shield lavas, notably high SiO_2/FeO and low CaO/Al_2O_3 (Frey et al., 1994), can be explained by partial melting of a peridotite source that was refertilized by melts derived from recycled oceanic crust occurring as eclogite within peridotite (Hauri, 1996; Green et al., 2001).

4.2 Abundance Ratios Involving Ba

Abundance ratios involving Th, Ba, Nb and La are potentially useful in identifying components in the source of Hawaiian lava. These elements are highly incompatible in anhydrous phases; consequently, ratios such as Ba/Th, Ba/Nb and Ba/La in melts derived by >1% melting are equal to the source ratios. However residues from partial melting will have ratios that differ significantly from those of the source. Also these ratios in melts are not very sensitive to fractional crystallization of anhydrous minerals, but cumulate phases, such as plagioclase, may have quite different ratios than the coexisting melts.

High Ba/Th (>100) relative to that of primitive mantle is characteristic of most Hawaiian shield lavas (Fig. 15; Hofmann and Jochum, 1996), melt inclusions within olivine phenocrysts in Mauna Loa lavas (Sobolev et al., 2000) and even postshield- and rejuvenated-stage lavas (Yang et al., 2003). As shown by Hofmann and Jochum (1996), Ba/Th ratios in Hawaiian lavas are higher than those of MORB and most other ocean island basalt (Iceland is an exception, Chauvel and Hemond, 2000). Hofmann and Jochum (1996) concluded that relatively high Ba/Th is characteristic of the present-day Hawaiian source and not a result of melting or post-melting processes; they proposed that the high Ba/Th signature results from an eclogite component in the source that formed as plagioclase-rich cumulate gabbro. Such a component is apparently ubiquitous in the

source of Hawaiian lavas; an inference that contrasts with the localized presence of the component creating relative Nb deficiencies.

If Ra/Th ratio is a proxy for Ba/Th, further insight into Ba/Th fractionation during the melting process creating Hawaiian tholeiitic basalt is provided by measurements of ($^{226}Ra/^{230}Th$) disequilibria; e.g., Pietruszka et al. (2001) found that the activity ratio ($^{226}Ra/^{230}Th$) is typically ~1.1 in historic tholeiitic basalt from Kilauea Volcano. This 10% disequilibrium can arise from the melting process (a consequence of different partition coefficients for Ra and Th), and from radiogenic ingrowth of ^{226}Ra during the melting process. Figure 7 of Pietruszka et al. (2001) shows that at very low extents of melting (<<1%), ~10% disequilibrium results from the difference in partition coefficients. However, at the 5 to 10% extent of melting generally proposed for Kilauea lavas (e.g., Pietruszka and Garcia, 1999) most of the ($^{226}Ra/^{230}Th$) disequilibria results form radiogenic ingrowth. I conclude that Ra/Th and Ba/Th were not controlled by the melting process; therefore anomalously high Ba/Th is a characteristic of the source for Hawaiian lavas.

Within the Phase 2 core, Ba/La, Ba/Nb and Ba/Th are quite variable but strongly correlated; these ratios vary by a factor of ~2.6 with one standard deviation of ~15% (Figure 16). In contrast to these ratios involving Ba, other ratios involving only highly incompatible elements, such as La/Nb, are much less variable, especially within a shield (Figs. 15c and 16). Even the variability of several ratios involving elements with significant differences in their incompatibility (e.g., La/Sm, Sm/Yb and Nb/Zr) is less than that of Ba/(La, Nb, Th) ratios; in fact, the ranges for Ba/La, Ba/Nb and Ba/Th are

similar to that found for Nb/Y and La/Yb, ratios involving elements of very different incompatability (Fig. 16).

If high Ba/Th is a source characteristic, I expect this ratio to correlate with radiogenic isotope ratios. Historic Kilauea lavas define an inverse trend for Ba/Th vs. $^{206}Pb/^{204}Pb$ and Mauna Loa lavas (<30 ka) show correlations of Ba/Th with Sr, Nd and Pb isotopic ratios (Fig. 14c). However, in older and more altered lavas, e.g., from the HSDP cores and Koolau shield, Ba/Th ratios are considerably more variable than in lavas from Kilauea and Mauna Loa (Fig. 15). Analyses of 101 Phase 1 Mauna Kea samples (not the reference suite) by Albarede (1996) showed that for the lower parts of the Phase 1 core (689 to 1041m) ratios of Rb/Th, Cs/Th and to a lesser extent Ba/Th decrease upwards in the core. A Principal Component Analysis of the data showed that a component, accounting for 5.1% of the variance, has maximum loading on Rb and Cs, moderate loading on Ba and marginal loading on U (Albarede, 1996). Given the well-documented post-magmatic mobility of Rb, Cs, and U, a plausible inference is that relatively low Ba/Th reflects Ba loss and that the variable Ba/Th in the upper part of the Phase 1 core reflects lateral fluid (H_2O) advection (see Fig. 3 of Albarede, 1996). In the Phase 2 core Ba/Th ranges from 70 to 185, but there is no correlation with depth or compositional group (see inset in Fig. 14c). To determine the effects of post-magmatic processes on Ba abundance in the Phase 2 core, Huang, Vollinger, Frey and Rhodes are determining compositional variations within four flow units. Based on data for 6 to 7 samples from these units, I find that Ba is not correlated with K. This result is consistent with the lack of correlation between K_2O/P_2O_5 and Ba/Th in the reference suite of samples. Nevertheless, variable Ba abundance at nearly constant Th content within individual units

leads me to conclude that some of the Ba/Th variability in the Phase 2 core arises from post-magmatic alteration. Because there is evidence for both loss and addition of Ba, I infer that the extremes of Ba/Th (<100 and >150) may reflect alteration.

In summary the data arrays in Fig. 14c could be explained by mixing of components with distinct combinations of Ba/Th and isotopic ratios. Particularly important are the diverse Ba/Th vs. $^{87}Sr/^{86}Sr$ and $^{143}Nd/^{144}Nd$ trends defined by Koolau and Mauna Loa lavas. If these trends reflect magmatic characteristics, they convey important information about source components. However, Koolau lavas (~2 to 3 Ma) are variably altered (Frey et al., 1994), and it is necessary to determine if their systematic Ba/Th-isotope ratio trends in Fig. 14c are a fortuitous combination of source heterogeneity (isotopic ratios) and alteration (Ba/Th).

5. SUMMARY

Based on study of Mauna Kea lavas in reference sample suites from the two HSDP cores I identify 3 major types of geochemically distinct magmas.

(1) Lavas within the upper 150m (<200ka to ~330ka) of the Mauna Kea section are low SiO_2 basalt with intercalated alkalic and tholeiitic basalt in the upper 50m; these lavas form the Postshield Group. Their relatively low SiO_2 is coupled with high incompatible element content, and high La/Yb and Sm/Yb; hence, relative to underlying lavas they were derived by lower extents of melting and segregated at higher pressure within the stability field of garnet. Relative to underlying lavas they also contain more of a component with relatively low $^3He/^4He$, high ε_{Nd} and non-radiogenic Pb. These changes in

process and source are interpreted to have occurred as the Mauna Kea shield passed over the periphery of the thermally and geochemically zoned plume.

(2) Deeper in the Phase 2 core, >800 mbsl, two other groups, presumably intrinsic to the plume, are intercalated. These shield lavas are distinguished by different SiO_2 contents at a given MgO content. Most of the HSDP Mauna Kea lavas belong to the relatively high SiO_2 group (~49-51% SiO_2 after adjusting lava composition to be in equilibrium with Fo_{85} olivine). This group defines the Kea component.

Like the Postshield Group, the other group is distinguished by a relatively low SiO_2 content (<48.8% after adjusting lava compositions to be in equilibrium with Fo_{85} olivine). Unlike the Postshield Group, this shield group has relatively high Nb/Zr, Ti/Zr and $^3He/^4He$ and high $^{208}Pb/^{204}Pb$ at a given $^{206}Pb/^{204}Pb$. These are the characteristics of tholeiitic lavas erupted at Loihi seamount. This geochemically distinctive component contributes to early shield volcanism at both Kea and Loa trend volcanoes. Based on abundance ratios such as La/Yb, Sm/Yb and Nb/Zr this group did not segregate within the garnet stability field.

Although in detail the HSDP cores contain distinctive geochemical groups of lavas, within the context of all Hawaiian shields Mauna Kea shield lavas are not highly heterogeneous in isotopic ratios of Sr, Nd and Hf or in La/Nb and Nb/Zr. Ratios involving Nb reflect the Koolau component (recycled oceanic crust including pelagic sediment), and there is no evidence for this component in Mauna Kea lavas. Like other Hawaiian lavas, Mauna Kea lavas have high Ba/Th

(>100), but this ratio is highly variable, possibly a result of alteration, and it is not correlated with radiogenic isotope ratios.

Appendix I: Analytical Procedures

1. Instrumental Neutron Activation Analysis (INAA)

Determination of Na, Cr, Sc, La, Ce, Nd, Sm, Eu, Tb, Yb, Lu, Hf and Th abundances by INAA followed the procedures of Ila and Frey (1984, 2000). The accuracy and precision of this procedure for analyses of Hawaiian basalt are documented in Table 1d of Frey et al. (1990) and for HSDP 1 samples in Table 1 of Yang et al. (1996). Also analyses of USGS standards are reported in Ila and Frey (2000); BHVO-2 data are in Table A-3.

2. Inductively Coupled Plasma Mass Spectrometry (ICP-MS)

2.1 Sample Dissolution

Samples were dissolved using a HF-HNO_3 multi-stage digestion procedure in Teflon Savillex beakers. Rock powder, 50 to 100 mg, was weighed into a pre-cleaned Teflon Savillex beaker; then 2 ml concentrated HF and 0.5 ml 14M HNO_3 were added. The mixture of acids and rock powder in uncapped beakers was dried at 350°F to form a moist sample cake. Then 3.5 ml concentrated HF and 0.5 ml of 7M HNO_3 were added to this sample cake. The capped beaker was heated at 250°F for 3 to 5 days. Then the sample was dried at 350°F to form a thick liquid gel, and 5 ml of 7M HNO_3 were added. Again the sample was dried at 350°F to form a moist cake, and 5 ml of 7M HNO_3 were added. Then the capped beaker was heated at 250°F overnight. Approximately 10% of the samples were not totally dissolved at this stage. These samples were transferred to a Teflon bomb and the same procedure outlined above was followed. The bomb treatment was repeated until the sample was totally dissolved. The samples were then diluted by a factor of 2000 to 8000 using 1M HNO_3 and spiked with a solution, containing three

isotopes, ^{77}Se, ^{115}In and ^{209}Bi, with known concentrations prior to aspiration into a Fissons (VG) Plasmaquad 2+S ICP-MS.

2.2 Analytical Procedure

Our procedure typically involves sequential analysis of 37 sample solutions over a ~6 hour time span. One to three isotopes are selected for each element based on high natural abundances and no or minimal isobaric and oxide interferences (Table A-1a). Data are collected and reported as count rates (counts per second or 'CPS') for these isotopes. I use a standard calibration curve to convert these ion count rates into elemental abundances. Several USGS standard samples, BHVO-1, BCR-1 and AGV-1, are used to obtain the standard calibration curve (Table A-2). The sensitivity of the instrument at a given mass is not stable with time. In addition, this temporal fluctuation in signal strength varies with isotope mass. These mass- and time-dependent variations are described as "sensitivity drift" (Fig A-1).

In order to correct for sensitivity drift, both internal and external drift monitors are used. Three spiked isotopes, ^{77}Se, ^{115}In and ^{209}Bi, are used as internal drift monitors (IDM). They record the sensitivity drift for these three isotopes in every analyzed solution. Beginning with the first solution in the analytical procedure, every sixth solution is an identical solution, such as BHVO-1, known as the external drift monitor (EDM). I use these EDMs to record the sensitivity drift in all the analyzed isotopes. Table A-1b shows the typical sequence of analysis: external drift monitor, standard sample solution, 4 unknown solutions, etc.

Figure A-1 shows the sensitivity drift in the three spiked isotopes, ^{77}Se, ^{115}In and ^{209}Bi, in all solutions during one analytical procedure (~6 hours). The first drift

correction, the internal drift correction, is based on these 3 spiked isotopes. Since the concentrations of the three spiked isotopes are known in every solution, CPS for these three isotopes are firstly normalized by their isotope concentrations; then are normalized to CPS of the first EDM. Hence, for each of the three isotopes I have a correction factor for every solution. I call this the internal drift correction factor (IDF). I assign an IDF to each analyzed isotope mass using a linear interpolation (extrapolation for ^{232}Th, ^{238}U and ^{45}Sc).

In most situations, the internal drift correction does not adequately correct the sensitivity drift for all analyzed isotopes; therefore, I also correct for sensitivity drift using the external drift monitors. Figure A-2 shows the sensitivity drift, after internal drift correction, in all the analyzed isotopes in EDMs during one procedure (~6 hours). Clearly, the range in internal drift corrected CPS from 0.92 to 1.08 (Fig A-2) shows that internal drift correction has not adequately corrected the sensitivity drift. Therefore, I also apply an external drift correction. I normalize the CPS in all EDMs to that in the first one; hence, I have a correction factor for each of the analyzed isotopes in every external drift monitor. I call this the external drift correction factor (EDF). Because an external drift monitor is analyzed as every sixth solution in the analytical sequence (Table A-1b), I must interpolate to determine the EDF for each intervening solutions, i.e. the 4 unknown and one standard solutions. This interpolation is done using a cubic spline fit. After application of the EDF, the reproducibility of all analyzed elements is better than ±6%, and better than ±3% for most of these elements. The only "cost" is that seven EDMs are analyzed (Table A-1b), which increases machine time by 20%.

3. Estimation of Precision and Accuracy

Most of the uncertainty in ICP-MS data are caused by sensitivity drift during the analysis. Therefore, the sensitivity drift correction factors are very important in controlling the precision and accuracy of the data determined by ICP-MS. In order to evaluate our sensitivity drift correction procedure, I repeatedly analyzed a BHVO-1 solution using our typical analytical procedure, i.e., in this procedure all the unknown and standard sample solutions and EDMs are a BHVO-1 solution. In this experiment, after sensitivity drift corrections (IDF and EDF), all the solutions should have the same signal strength, i.e., the same CPS. For comparison, I normalized the CPS of all the solutions to that of the first solution. Figure A-3 shows the normalized CPS values for each of the 25 analyzed elements. Overall, the normalized CPS values are within ±6% for all the solutions, most are within ±3%. The uncertainties, one standard deviation in percent, of these 25 elements are ~1-2%

In order to evaluate accuracy, I analyzed, BHVO-2, a newly prepared USGS standard sample. The average values and standard deviations of 11 replicate analyses obtained over ~5 months are reported in Table A-3. For comparison, Table A-3 also shows the trace element abundances in BHVO-2 reported by Ila and Frey (2000), Lin et al. (2000), Raczek et al. (2001) and the USGS recommended values. Except for Tb and Yb, the trace element abundances in BHVO-2 analyzed by ICP-MS at MIT are within ±5% of the INAA values reported by Ila and Frey (2000). Values of Tb and Yb in BHVO-2 analyzed by MIT ICP-MS are about 8% higher than reported by Ila and Frey (2000). Our reported values for BHVO-2 are also within ±5% of the values reported by Raczek et al. (2001), and for most of the elements the differences between the two reported values are

within analytical uncertainties (Table A-3). Taking the uncertainty into account, except for Gd and Y, our results are also in agreement with that reported by Lin et al. (2000). Compared with the USGS recommended values, the difference between our reported values for BHVO-2 and the recommended values are within the reported standard deviations (Table A-3).

4. Comparison with Other Techniques (XRF and INAA) and another ICP-MS Facility

Trace element abundances for HSDP Phase 2 reference samples have also been determined by X-ray fluorescence (Rhodes and Vollinger, 2004), INAA at MIT (this paper) and ICP-MS at Rutgers (Feigenson et al. (2003). These multiple data sets for the same samples provide the opportunity for comparison of results obtained by different techniques or the same technique (ICP-MS) in different facilities.

4.1 ICP-MS (MIT) compared to XRF (Univ. Massachusetts)

In Figure A-4, I compare results obtained by ICP-MS (MIT) and XRF (Univ. Massachusetts). The linear correlation coefficients between the two data sets for Ba, Sr, Zr, Nb, Rb and Y are greater than 0.96 (Figure 4). These results show that the precision of both techniques is comparable, ~3-6%, and the slopes are near unity for each element (except Y), thereby indicating that both analytical techniques yield similar abundances. However, for Y abundance there is a systematic difference between the two techniques with the Y abundance determined by ICP-MS approximately 12% higher than that determined by XRF.

4.2 ICP-MS (MIT compared to Rutgers)

In Figure A-5 I compare ICP-MS results for REE abundances obtained at MIT and Rutgers. For La, Ce, Pr, Nd, Sm and Eu the correlation coefficients are 0.98 to 0.99 and systematic differences are <4%. Correlation coefficients for Gd, Tb, Dy, Ho, Er, Tm, Yb and Lu are lower 0.93 to 0.96 and systematic differences are ≤5%, except for Tm, Yb and Lu whose abundances determined at MIT are 6 to 7% higher than those determined at Rutgers.

4.3 ICP-MS (MIT) compared to INAA (MIT)

In Figure A-5, I also compare results obtained by ICP-MS and INAA for REE, Hf and Th. Except for Tb and Th the linear correlation coefficients between the results from ICP-MS and INAA are greater than 0.96. The poorer correlation for Tb and Th reflects the poorer precision of INAA data for these elements (see precision estimates in Table 1 of Yang et al., 1996). Also there is a systematic discrepancy between the two techniques for Tb, Yb and Lu. The INAA results are ~8% lower than the ICP-MS data; this same discrepancy was found for analyses of BHVO-2 (Table A-3).

Appendix II

In order to evaluate the relationships between HSDP 2 lavas, I calculated La/Yb-Nb/Zr, Sm/Yb-Nb/Zr, Sm/Yb-La/Yb and La/Yb-Ti/Zr trends for variable extents of batch melting of garnet- and spinel- peridotite (Fig 10). Source abundances and mineral proportions and melting reactions are in Table A-4. The partition coefficients are assumed to be zero for olivine/melt and spinel/melt. For clinopyroxene and garnet the partition coefficients vary with mineral composition and the values used are in Table A-4. For garnet peridotite I used data for high pressure clinopyroxene and garnet (TM 694-6) from Salters and Longhi (1999). For spinel peridotite I used data for a lower pressure clinopyroxene (TM 1094-9) from Salters and Longhi (1999). For orthopyroxene, I estimated partition coefficients from measured $D^{opx/cpx}$ ratios (Eggins et al., 1998). For more detailed information, see the footnote of Table A-4.

REFERENCES

Abouchami, W., Galer, S. J. G., and Hofmann, A. W., High precision lead isotope systematics of lavas from the Hawaiian Scientific Drilling Project. *Chem. Geol.* 169, 187-209, 2000.

Albarede, F., High-resolution geochemical stratigraphy of Mauna Kea flows from the Hawaii Scientific Drilling Project core. *J. Geophys. Res.* 101, 11,841-11,853, 1996.

Baker, M. B., Alves, S., and Stolper, E. M. , Petrography and petrology of the Hawaii Scientific Drilling Project lavas: Inferences from olivine phenocryst abundances and compositions. *J. Geophys. Res.* 101, 11,715-11,727, 1996.

Blichert-Toft, J., Frey, F.A., and Albarède, F., Hf isotope evidence for pelagic sediments in the source of Hawaiian basalts, *Science*, 285, 879-882, 1999.

Blichert-Toft, J., D. Weis, C. Maerschalk, A. Agranier, and F. Albarède, Hawaiian hot spot dynamics as inferred from the Hf and Pb isotope evolution of Mauna Kea volcano, Geochem. Geophys. Geosyst., 4(2), 8704, doi:10.1029/2002GC000340, 2003.

Blundy, J. D., Robinson, J. A. C., and Wood, B. J., Heavy REE are compatible in clinopyroxene on the spinel lherzolite solidus. *Earth Planet. Sci. Lett.* 160, 493-504, 1998.

Bryce, J. G., DePaolo, J. D. and Lassiter, J., Sr, Nd and Os isotopes in the 2.8 km HSDP-2 section of Mauna Kea volcano, submitted to Geochem. Geophys. Geosyst.

Chan, L.-H., and Frey, F. A., Lithium isotope geochemistry of the Hawaiian plume: Results from the Hawaii Scientific Drilling Project and Koolau volcano. Geochem., Geophys., Geosyst. 4(3), 8707, doi:10.1029/2002GC000365, 2003.

Chauvel, C., and Hemond, C., Melting of a complete section of recycled oceanic crust: Trace element and Pb isotopic evidence from Iceland, *Geochem. Geophys. Geosys.*, 1[Paper number 1999 GC000002] 2000.

Chen, C.-Y., Frey, F. A., Garcia, M. O., Dalrymple B., and Hart S. R., The tholeiite to alkalic basalt transition at Haleakala Volcano, Maui, Hawaii: Petrogenetic interpretations based on major and trace element and isotope geochemistry. *Contrib. Mineral. Petrol.* 106, 183-200, 1991.

Chen, C.-Y., Frey, F. A., Garcia, M. O., Dalrymple, G. B., and Hart, S. R., The tholeiitic to alkalic basalt transition at Haleakala volcano, Maui, Hawaii. *Contrib. Mineral. Petrol.* 106, 183–200, 1990.

Chen, C.-Y., Frey, F. A., Rhodes, J. M., and Easton, R. M., Temporal geochemical evolution of Kilauea Volcano: Comparison of Hilina and Puna Basalt. in Earth Processes: Reading the isotopic code, *Geophysical Monograph Series*, vol. 95, edited by A. Basu and S. R. Hart, 161-181, AGU, Washington, D.C., 1996.

Cohen, A. S., O'Nions, R. K., and Kurz, M. D., Chemical and isotopic variations in Mauna Loa tholeiites. *Earth Planet. Sci. Lett.* 143, 111-124, 1996.

David, K., Schiano, P., and Allegre, C. J., Assessment of the Zr/Hf fractionation in oceanic basalts and continental materials during petrogenetic processes. *Earth Planet. Sci. Lett.* 178, 285-301, 2000.

DePaolo, D. J., Bryce, J. G., Dodson, A., Shuster, D. L., and Kennedy, B. M., Isotopic evolution of Mauna Loa and the chemical structure of the Hawaiian plume. *Geochem., Geophys. Geosystems,* 2(Paper number 2000 GC000139), 2001.

DePaolo, D. J., and Stolper, E. M., Models of Hawaiian volcano growth and plume structure; implications of results from the Hawaii Scientific Drilling Project, *J. Geophys. Res.* 101, 11,643-11,654, 1996.

DePaolo, D. J., Stolper, E. M., Thomas, D. M., and Garcia, M. O., Hawaii Scientific Drilling Project: Core logs and summarizing data [CD-ROM], 1999.

Eggins, S.M. Rudnick, R.L. and McDonough, W.F., The composition of peridotites and their minerals: a laser ablation ICP-MS study. *Earth Planet. Sci. Letts.,* 154, 53-71, 1998.

Eiler, J. M., Valley, J. W., and Stolper, E. M., Oxygen isotope ratios in olivine from the Hawaii Scientific Drilling Project. *J. Geophys. Res.,* 101, 11,807-11,813, 1996.

Eisele, J., Abouchami, W., Galer, S. J. G. and Hofmann, A. W., The 320 kyr Pb isotope evolution of Mauna Kea lavas recorded in the HSDP-2 drill core, Geochem. Geophys. Geosyst., 4(5), 8710, doi:10.1029/2002GC000339, 2003.

Feigenson, M. D., L. L. Bolge, M. J. Carr, and C. T. Herzberg, REE inverse modeling of HSDP2 basalts: Evidence for multiple sources in the Hawaiian plume, Geochem. Geophys. Geosyst., 4(2), 8706, doi:10.1029/2001GC000271, 2003.

Feigenson, M. D., Hofmann, A. W., and Spera, F. J., Case studies on the origin of basalt. II. The transition from tholeiitic to alkalic volcanism on Kohala volcano, Hawaii. *Contrib. Mineral. Petrol.* 84, 390-405, 1983.

Frey, F. A., and Clague, D. A., Geochemistry of diverse basalt types from Loihi Seamount, Hawaii; petrogenetic implications. *Earth Planet Sci Letts.* 66, 337-355, 1983.

Frey, F. A., and Rhodes, J. M., Inter-shield geochemical differences among Hawaiian volcanoes: implications for source compositions, melting processes and magma ascent paths. *Phil. Trans. Roy. Soc. Lond. A.,* 342, 121-136, 1993.

Frey, F. A., Garcia, M. O., and Roden, M. F., Geochemical characteristics of Koolau Volcano: Implications of intershield geochemical differences among Hawaiian volcanoes. *Geochim. Cosmochim. Acta* 58, 1441-1462, 1994.

Frey, F. A., Garcia, M. O., Wise, W. S., Kennedy, A., Gurriet, P., Albarede, F., The evolution of Mauna Kea volcano, Hawaii: Petrogenesis of tholeiitic and alkalic basalts, *J. Geophys. Res.*, 96, 14,347-14,375, 1991.

Frey, F. A., Wise, W. S., Garcia, West, H., Kwon, S. T., and Kennedy, A., Evolution of Mauna Kea volcano, Hawaii: Petrologic and geochemical constraints on postshield volcanism, *J. Geophys. Res., 95*, 1271-1300, 1990.

Garcia, M. O., Foss, D. J. P., West, H. B. and Mahoney, J. J., Geochemical and isotopic evolution of Loihi Volcano, Hawaii, *Journal of Petrology*, 36, 1647-1644, 1995.

Garcia, M. O., Jorgenson, B. A., Mahoney, J. J., Ito E., and Irving, A. J., An evaluation of temporal geochemical evolution of Loihii summit lavas: Results from Alvin submersible dives. *J. Geophys. Res.* 98, 535-550, 1993.

Garcia, M. O., Rhodes, J. M., Trusdell, F. A., and Pietruszka, A., Petrology of lavas from Puu Oo eruption of Kilauea Volcano, III. The Pond Stage (1986-1992). *Bull. Volcanology* 58, 359-379, 1996.

Garcia, M. O., Rubin, K. H., Norman, M. D., Rhodes, J. M., Graham, D. W., Muenow, D W., Spencer, K., Petrology and geochronology of basalt breccia from the 1996 earthquake swarm of Loihi Seamount, Hawaii; magmatic history of its 1996 eruption. *Bulletin of Volcanology.*, 59, 577-592, 1998.

Green, D. H., Falloon, T., Eggins, S. M., and Yaxley, G. M., Primary magmas and mantle temperaturesAnonymous, Experimental mineralogy, petrology and geochemistry. *Eur. J. Mineral.*, 13, 437-451, 2001.

Hanson, G. N., An approach to trace element modeling using a simple igneous system as an example in geochemistry and mineralogy of rare earth elements, vol. 21, Reviews in Mineralogy, pp. 79-97, *Mineralogical Society of America*, Washington, D.c., 1989.

Hart, S. R., A large-scale isotope anomaly in the Southern Hemisphere mantle. *Nature* 309, 753-757, 1984.

Hart, S. R. and Dunn, T., Experimental clinopyroxene/melt partitioning for 24 trace elements. *Contrib. Mineral. Petrol.*, 113, 108, 1993.

Hauri, E. H., Major-element variability in the Hawaiian mantle plume. *Nature* 382, 415-419, 1996.

Hawaii Scientific Drilling Project, Core-Logs, edited by E. Stopler, and M. Baker., 471 pp. Calif. Inst. of Tech. Pasadena, 1994.

Hofmann, A. W., Nb in Hawaiian magmas; constraints on source composition and evolution. *Chem. Geol.* 57, 17-30, 1986.

Hofmann, A. W., Chemical differentiation of the earth: the relationship between mantle, continental crust, and oceanic crust. *Earth Planet. Sci. Lett.* 90, 297-314, 1988.

Hofmann, A. W. and Jochum, K. P., Source characteristics derived from very incompatible trace elements in Mauna Loa and Mauna Kea basalts (Hawaiian Scientific Drilling Project). *J. Geophys. Res.* 101, 11,831-11,839, 1996.

Hofmann, A. W. and White, W. M., Ba, Rb and Cs in the Earth's mantle. *Z. Naturforssch* 38a, 258-266, 1983.

Ila, P. and Frey, F.A., Utilization of neutron activation analysis in the study of geologic materials, in Use and development of Low and Medium Flux Research Reactors. eds. harling, O.K., Clark, L. and von der Hardt, P., Atomkerenergie Kerntechnik, suppl. to vol. 44, 710-716, 1984.

Ila, P. and Frey, F.a., Trace element analysis of USGS standards AGV2, BCR2, GHVO2, DTS2 and GSP2 by INAA. J. Radioanal. *Nuclear Chem.*, 244, 599-602, 2000.

Jackson, M. C., Wilmoth, R. A., and Frey, F. A., Geology and petrology of basaltic lavas and dikes of the Koolau Volcano in the Trans-Koolau exploratory tunnels, Oahu, Hawaii. *Bull. Volcan.* 60, 381-401, 1999.

Johnson, K.T.M., Experimental determination of partition coefficients for rare earth and high-field-strength elements between clinopyroxene, garnet, and basaltic melt at high pressures. *Contrib. Mineral. Petrol.*, 133, 60-68, 1998.

Kamber, B. S., and Collerson, K. D., Zr/Nb systematics of ocean island basalts reassessed - the case for binary mixing. *J. Petrol.* 41, 1007-1021, 2000.

Kennedy, A. K., Kwon, S. T., Frey, F. A., West, H. B., The isotopic composition of postshield lavas from Mauna Kea Volcano, Hawaii. *Earth Planet Sci Letts.* 103, 339-353, 1991.

Kurz, M. D., Curtice, J., Lott III, D. E. and Solow, A., Rapid helium isotopic variability in Mauna Kea shield lavas from the Hawaiian Scientific Drilling Project, Geochem. Geophys. Geosyst., 5, Q04G14, doi:10.1029/2002GC000439, 2004.

Kurz, M. D., and Curtice, J. M., Helium Isotopic Evolution of Mauna Kea Volcano: New Results From the 3 Km Drill Core. *EOS. Trans. AGU, 81(48), Fall Meet. Suppl., Abstract V11D-09,* 2000.

Kurz, M. D., Garcia, M. O., Frey, F. A., and O'Brien, P. A., Temporal helium isotopic variations within Hawaiian volcanoes: basalts from Mauna Loa and Haleakala. *Geochim. Cosmochim. Acta* 51, 2905-2914, 1987.

Kurz, M. D., Kenna, T. C., Kammer, D. P., Rhodes, J. M., and Garcia, M. O., Isotopic evolution of Mauna Loa volcano: a view from the submarine southwest rift Mauna Loa: A Decade Volcano. in Mauna Loa Revealed, *Geophysical Monograph Series*, vol. 92, edited by J.M. Rhodes and J.P. Lockwood, . 289-306, AGU, Washington, D.C., 1995.

Kurz, M. D., Kenna, T. C., Lassiter, J. C., and DePaolo, D. J., Helium isotopic evolution of Mauna Kea volcano: First results from the 1-km drill core. *J. Geophys. Res.* 101, 11,781-11,791, 1996.

Lassiter, J. C., DePaolo, D. J., and Tatsumoto, M., Isotopic evolution of Mauna Kea volcano: Results from the initial phase of the Hawaiian Scientific Drilling Project. *J. Geophys. Res.* 101, 11,769-11,780, 1996.

Lassiter, J. C. and Hauri, E. H., Osmium-iosotope variations in Hawaiian lavas: Evidence for recycled oceanic lithosphere in the Hawaiian plume. *Earth Planet Sci Letts.* 164, 483-496, 1998.

Lin, S., He, M., Hu, H., Yuan, H. and Gas, S., Precise determination of trace elements in geological samples by ICP-MS using compromise conditions and fine matrix-matching strategy. *Analytical Sciences,* 16, 1291-1296, 2000.

Moore, J. G., Density of basalt core from Hilo drill hole, Hawaii. *J. Volcanol. Geotherm. Res.,* 112, 221-230, 2001.

Norman, M. D., and Garcia, M. O., Primitive magmas and source characteristics of the Hawaiian Plume; petrology and geochemistry of shield picrites. *Earth Planet Sci Letts.* 168, 27-44, 1999.

Pietruszka, A. J. and Garcia, M. O., A rapid fluctuation in the mantle source and melting history of Kilauea Volcano inferred from the geochemistry of its historical summit lavas (1790-1982). *J. Petrol.* 40, 1321-1342, 1999.

Pietruszka, A. J., Rubin, K. H., and Garcia, M. O., ^{226}Ra-^{230}Th-^{238}U disequilibria of historical Kilauea lavas (1790-1982) and the dynamics of mantle melting within the Hawaiian Plume. *Earth Planet. Sci. Lett.* 186, 15-31, 2001.

Raczek, I., Stoll, B., Hofmann, A.W., and Jochum, K.P., High precision trace element data for USGS reference materials BCR-1, BCR-2, BHVO-1, BHVO-2, AGU-1, AGU-2,

DTS-1, DTS-2, GSP-1, and GSP-2 by ID-TIMS and MIC-SSMS. Geostandards Newsletter, 25, 77-86, 2001.

Rhodes, J. M., The 1852 and 1868 Mauna Loa picrite eruptions: clues to parental magma compositions and the magmatic plumbing system, in Mauna Loa Revealed, *Geophysical Monograph Series*, vol. 92, edited by J.M. Rhodes and J.P. Lockwood, . 241-262, AGU, Washington, D.C., 1995.

Rhodes, J. M., Geochemical stratigraphy of lava flows sampled by the Hawaii Scientific Drilling Project. *J. Geophys. Res.* 101, 11,729-11,746, 1996.

Rhodes, J. M., Geochemistry of Mauna Loa and Mauna Kea Lavas Sampled by the Hawaii Scientific Drilling Project. *EOS. Trans. AGU, 81(48), Fall Meet. Suppl., Abstract V11D-02,* 2000.

Rhodes, J. M. and Hart, S. R., Episodic trace element and isotopic variation in historical Mauna Loa lavas. in Mauna Loa Revealed, *Geophysical Monograph Series*, vol. 92, edited by J.M. Rhodes and J.P. Lockwood, 263-288, AGU, Washington, D.C., 1995.

Rhodes, J. M. and Vollinger, M., Geochemical stratigraphy of basaltic lavas from HSDP 2. *Geochem., Geophys. Geosystem,* submitted..

Roden, M. F., Trull, T., Hart, S. R., and Frey, F. A., New He, Sr, Nd and Pb isotopic constraints on the constitution of the Hawaiian plume: Results from Koolau Volcano, Oahu, Hawaii. *Geochim. Cosmochim. Acta* 58, 1431-1440, 1994.

Salters, V.J.M., The generation of mid-ocean ridge basalts from the Hf and Nd isotope perspective. *Earth Planet. Sci. Letts.,* 141, 109-123, 1996.

Salters, V.J.M. and Longhi, J., Trace element partitioning during the initial stages of melting beneath mid-ocean ridges. *Earth Planet. Sci. Letts.,* 166, 15-30, 1999.

Sharp, W. D. and Renne, P. R., $^{40}Ar/^{39}Ar$ dating of core recovered by the Hawaii Scientific Drilling Project (Phase 2) Hilo, Hawaii, Geochem. Geophys. Geosyst. 6, Q04G17, doi:10.1029/2004GC000846, 2005.

Sharp, W., Turrin B., Renne P., and Lanphere M., The $^{40}Ar/^{39}Ar$ and K/Ar dating of lavas from the Hilo 1-km core hold, Hawaiian Scientific Drilling Project. *J. Geophys. Res.* 101, 11,604-11,616, 1996.

Skulski, T., Minarik, W. and Watson, E.B., High pressure experimental trace-element partitioning between clinopyroxene and basaltic melts. *Chem. Geol.,* 117, 127-147, 1994.

Sobolev, A.V., Hofmann, A.W., and Nikogosian, I. K., Recycled oceanic crust observed in ghost plagioclase within the source of Mauna Loa lavas. *Nature* 404, 986-990, 2000.

Staudigel, H., Davies, G.R., Hart, S.R., Marchant, K.M. and Smith, B.M., Large scale isotopic Sr, Nd and O isotopic anatomy of altered oceanic crust: DSDP/ODP sites 417/418, *Earth Planet. Sci. Lett.,* 130, 169-185, 1995.

Stolper, E M., DePaolo, D. J., and Thomas, D. M., Introduction to special section; Hawaii Scientific Drilling Project. . *J. Geophys. Res.* 101, 11,593-11,598, 1996.

Sun, S.-S. and McDonough, W. F., Chemical and isotopic systematics of oceanic basalts: implications for mantle composition and processes. In *Magmatism in the Ocean Basins*, Vol. 42 (ed. A. D. Saunders and M. J. Norry), 313-345, 1989.

Thomas, D., Implications of downhole temperature and fluid chemistry from the HSDP well for subsurface hydrology under Hilo. *Geochem., Geophys. Geosystems,* submitted.

van Westrenen, W., Blundy, J., and Wood, B., Crystal-chemical controls on trace element partitioning between garnet and anhydrous silicate melt. *Am. Mineral.*, 84, 838-847, 1999.

Wolfe, E. W., Wise, W. S., and Dalrymple, G. B., The geology and petrology of Mauna Kea Volcano, Hawaii; a study of postshield volcanism. *U S Geol Surv Prof Pap, 1557, 1-129*, 1997.

Yang, H.-J., Frey, F. A., Garcia, M. O., and Clague, D. A., Submarine lavas from Mauna Kea volcano, Hawaii: Implications for Hawaiian shield-stage processes. *J. Geophys. Res.* 99, 15,577-15,594, 1994.

Yang, H.-J., Frey, F. A., Rhodes, J. M., and Garcia, M. O., Evolution of Mauna Kea volcano: Inferences from lava compositions recovered in the Hawaii Scientific Drilling Project. *J. Geophys. Res.* 101, 11,747-11,767, 1996.

Yang, H.-J., Frey, F. A. and Clague, D. A., Constraints on the source components of lavas forming the Hawaiian North Arch and Honolulu Volcanoes, J. Petrol., 44, 603-627, 2003.

Figure Captions

Figure 1. Nb abundance (ppm) versus MgO content (wt.%) showing that Nb abundance is inversely correlated with MgO content in tholeiitic basalt from the Phase 1 and 2 cores of the HSDP. The wide range in MgO and inverse trend reflects olivine accumulation and magma mixing (Rhodes and Vollinger, 2004). The eleven samples of alkalic basalt, (nine from Phase 1 hole, two, SR121 and SR131, from Phase 2 hole) however, are offset to higher Nb abundance at a given MgO content. In this and following figures, data are for the reference suites of HSDP samples (Hawaii Scientific Drilling Project, 1994; De Paolo et al., 1999). Data for MgO are from Rhodes (1996) for the Phase 1 hole and Rhodes and Vollinger (2004) for the Phase 2 hole. Data for Nb are from Rhodes (1996) for the Phase 1 hole and this paper for the Phase 2 core.

Figure 2. The abundance range (i.e., for each element the highest abundance in HSDP 2 samples is divided by the lowest abundance) and one standard deviation (in percent of the mean abundance) for reference suite samples from the Phase 2 HSDP core. Elements are arranged in order of incompatibility for peridotite/melt partitioning with the most incompatible elements on the left.

Both the abundance range and percent standard deviation increase with increasing incompatibility (for unknown reasons Pb is an exception). As discussed later in the text much of the abundance variation arises from accumulation of olivine. Abundance variation for each incompatible element decreases significantly (assuming $D_x^{ol/melt} = 0$) after lava compositions are adjusted to be in equilibrium with a common olivine composition (Fo_{85} or Fo_{90}). In general, this adjustment decreases the the range and

percent standard deviation by a factor of two. Insets show that Rb abundance is much more variable than abundances of other elements.

Figure 3. (a) Abundances of the highly incompatible elements Rb, U, Ba, Pb, La and Nb versus Th abundance (all in ppm) in basalt from the Phase 2 core. Th is the most incompatible element, i.e., the largest abundance range in Figure 2a, that was not mobile during post-magmatic alteration. The abundance trends for Rb and U are scattered because of their mobility during post-magmatic alterations. Ba and Pb are positively correlated with Th content but especially for Pb there is significant scatter. The correlation coefficient for Pb excludes the two labeled samples with anomalously high Pb content. These samples may have been contaminated with Pb (see Eisele et al., 2003, for isotopic evidence for Pb contamination of subaerially erupted samples). Abundance of La and Nb are highly correlated with near zero intercepts, as indicated by equations for the best-fit line. Data symbols indicate the various types of basalt samples recovered in the HSDP Phase 2 core. There is no correlation of composition with lava type (i.e., subaerial eruptive, pillow basalt, etc.), but the 7 samples with >l.1 ppm Th include the two samples of alkalic basalt and 5 of the 10 tholeiitic basalt lavas from the upper 132 m of the Mauna Kea section (circled in the La panel). In addition, SR 850, a low MgO (6.44%) tholeiitic basalt from deep in the core has high abundances of incompatible elements.

(b) Abundances of the moderately incompatible elements, Sr, Sm, Hf, Y and Lu versus Th abundance (all in ppm). At less than ~1 ppm Th these trends are linear, but at higher

Th abundance the trends become convex upwards indicating that if these samples are genetically related, the elements Sr, Sm, Zr, Hf, Y and Lu were more compatible than Th.

Figure 4. **(a)** Ba/Rb versus K_2O/P_2O_5 for basalt from the HSDP Phase 1 and 2 cores. K_2O and Rb abundances are decreased during subaerial alteration in the Hawaiian enrivonment (e.g., Yang et al., 1996). Hence, the trend to low K_2O/P_2O_5 and high Ba/Rb reflects increasing amounts of post-magmatic alteration. Unaltered Hawaiian basalt has K_2O/P_2O_5 >1.5 and Ba/Rb close to that of average oceanic basalt (11.6±0.2, Hofmann and White, 1983). It is surprising that submarine lavas from the HSDP Phase 2 core also define an inverse trend, which is offset to lower Ba/Rb. Data for HSDP Phase 1 from Rhodes (1996) and HSDP Phase 2 from Rhodes and Vollinger (2004) and this paper. Shown for comparison are data for subaerial lavas from Koolau volcano (Frey et al., 1994; Jackson et al., 1999; Haskins and Garcia, unpublished) which define the same trend as the subaerially erupted HSDP samples, and data for Mauna Loa (Rhodes 1996) and for Loihi (Garcia et al. 1993, 1995, 1998; Norman and Garcia, 1999).

(b) K_2O/P_2O_5 versus Ba/Rb for the various types of the HSDP Phase 2 submarine lavas. Lavas from above and below 2200 m are distinguished because below 2200 m the lavas are relatively undegassed, indicating eruption in a submarine environment (Moore, 2001). An important result is that the trend to low K_2O/P_2O_5 and high Ba/Rb is in part defined by pillow lavas from >2200 m especially those from the vesicular pillow zone 2 that extends from 2234 to 2470 mbsl (Moore, 2001).

Figure 5. **(a,b)** Al_2O_3 and CaO versus MgO content (all in wt.%). Major oxide abundances are from Rhodes and Vollinger (2004). The inverse trends dominantly reflect the effects of olivine fractionation and accumulation and perhaps magma mixing (Rhodes and Vollinger, 2004). In detail, however, the alkalic basalts at ~6 to 8% MgO scatter to high Al_2O_3 and low CaO; also a subgroup of the tholeiitic basalt from both holes which have relatively low SiO_2 (see Figure 6a) are slightly offset to higher Al_2O_3 at a given MgO content in the range of 6 to 14% MgO.

(c,d) $(Sr/Nd)_{PM}$ and Eu/Eu^* versus MgO content. Subscript PM indicates normalized to a primitive mantle ratio of 15.6 (Sun and McDonough, 1989). Eu* is an estimate of Eu abundance based on extrapolation between Sm and Gd in a chondrite-normalized plot for REE and Eu is the measured abundance. These ratios are indicators of plagioclase accumulation. For $(Sr/Nd)_{PM}$ all samples are within 0.8 to 1.2 except for higher ratios for SR129 and R164 and lower values for R174 and SR125. The mean ratio in the Phase 1 core is >1 and larger than that in the Phase 2 core. Different analytical techniques were used (XRF and INAA for Phase 1, ICP-MS for Phase 2); hence the systematic differences probably reflect inter-laboratory bias. All Phase 2 samples have Eu/Eu* in the range 0.95 to 1.05, except for SR129 which has a ratio of 1.06.

(e,f). Sc and Ni abundances (in ppm) versus MgO content (wt.%). The Sc trend is generally inverse, reflecting the incompatibility of Sc in olivine. The most obvious deviations are: the high Sc of SR125, a sample with many anomalous geochemical characteristics (see text); and the low Sc content (also Cr which is not plotted) of alkalic basalt R177 and SR131 which are from the same flow (Table 2). Sample SR 850 is the tholeiitic basalt with a low MgO content and high abundances of incompatible elements

(Fig. 3a); it is offset from the general trend to low CaO (panel b) and Sc, thereby indicating a role for clinopyroxene fractionation. Sc abundance determined by INAA (Table 1).

The positive correlation between Ni and MgO abundance reflects olivine accumulation, but at <7% MgO, Ni contents become less variable, presumably because of combined plagioclase, clinopyroxene and olivine fractionation (Ni abundance data from Rhodes and Vollinger, 2004).

Figure 6 (a,b). SiO_2 and TiO_2 versus MgO content (all in wt.%). The alkalic lavas including the three labeled tholeiitic lavas from the upper part of the Mauna Kea section, are offset to relatively low SiO_2 and high TiO_2 contents. Also there is a subgroup of tholeiitic lavas with relatively low SiO_2 at a given MgO content. These two subsets of tholeiitic lavas are labeled as low and high SiO_2 lavas. Inset shows that the main trend of data for SiO_2-MgO intersects the trajectory of olivine compositions at ~Fo_{85}.
(c) SiO_2 versus MgO content (wt.%) showing the abundance range after adjusting each sample to be in equilibrium with Fo_{85}. This adjustment reduces the range of MgO abundance, but a significant range in SiO_2 content persists.

Figure 7. (a,b,c) Nb/Zr, La/Yb, and SiO_2 contents (adjusted to be in equilibrium with olivine of Fo_{85}) versus depth in the HSDP Phase 2 core in meters below sea level (mbsl). Significant results are the high Nb/Zr and La/Yb in 12 of the uppermost 13 lavas. These lavas also have relatively low SiO_2 contents; in each plot the most extreme values are for alkali basalt samples SR121 and SR131, but 10 of the uppermost 11 tholeiitic lavas also

have relatively low SiO_2 content. These samples are defined as the Postshield Group. Samples SR232, SR276, SR328 and SR340 are also included in this group (see text). Underlying samples with relatively low SiO_2, labeled samples SR354 through SR940 in panel c, are defined as the Low SiO_2 Tholeiitic Shield Group. The 48.8% SiO_2 dividing line is arbitrary, and samples SR750, 756 and 762 with >48.8% SiO_2 are included in this group (see text). In panel "a" the 3 labelled high Nb/Zr samples are Type 4 of Rhodes and Vollinger (2004). In panel "b" two samples with anomalously high La/Yb are labeled; their relatively high ratios are confirmed by the data of Feigenson et al. (2003).

(d,e,f) La/Yb, Nb/Zr and SiO_2 contents (adjusted to be in equilibrium with olivine of Fo_{85}) versus age in the HSDP Phase 2 core. Inferred ages are from Sharp et al. (2002). These panels show the prolonged transition from the shield groups to the postshield group. The age span from SR121 to SR340 is ~180 Ka.

Figure 8. (a to f) Depth profiles for isotopic ratios: $^{3}He/^{4}He$; ε_{Nd}; ε_{Hf}; $^{206}Pb/^{204}Pb$, $^{208}Pb/^{204}Pb$ and delta $^{208}Pb/^{204}Pb$ (delta $^{208}Pb/^{204}Pb = [(^{208}Pb/^{204}Pb)-(^{208}Pb/^{204}Pb)_{NHRL}]$ x 100 where NHRL is northern hemisphere reference line (see Hart, 1984). ε_{Nd} and ε_{Hf} are related to $^{143}Nd/^{144}Nd$ and $^{176}Hf/^{177}Hf$, respectively (see Bryce and De Paolo., 2002; Blichert-Toft et al., 2003). The Postshield Group and intercalated subaerial High SiO_2 Tholeiitic lavas have relatively low $^{3}He/^{4}He$, high ε_{Nd}, low ε_{Hf} and low $^{206}Pb/^{204}Pb$, $^{208}Pb/^{204}Pb$ and delta $^{208}Pb/^{204}Pb$. In contrast, the labeled lavas forming the Low SiO_2 Shield Group are distinguished by relatively high $^{3}He/^{4}He$ (SR871 is anomalously low) and relatively high delta $^{208}Pb/^{204}Pb$. Data sources are Kurz et al. (2004) for He; Bryce et al. (2005) for Sr and Nd, Blichert-Toft et al. (2003) for Hf and Pb.

Figure 9. La/Sm, La/Yb and Nb/Zr versus Th content (adjusted so that each sample has a Mg/Fe ratio in equilibrium with olivine of Fo_{85}) for two groups of Phase 2 Mauna Kea lavas.

Figure 10 (a,b,c,d). La/Yb and Sm/Yb versus Nb/Zr, and La/Yb versus Sm/Yb and Ti/Zr in HSDP Phase 2 samples. Symbols as defined in Fig. 8. In panels a,b,c there are positive correlations with the highest La/Yb and Sm/Yb ratios in the uppermost samples in the Mauna Kea part of the core (also see Fig. 7b,e). The difference between the two groups of shield lavas is significant in the La/Yb and Sm/Yb vs. Nb/Zr panels where the Low-SiO_2 Group shows relatively little variation in La/Yb and Sm/Yb (sample SR 791 is an exception) and an inverse trend for Sm/Yb vs. Nb/Zr. This group also ranges to the highest Ti/Zr found in the Mauna Kea portion of the core. The relatively high La/Yb for SR 791 is confirmed by the data of Feigenson et al. (2003). SR791 at a depth of ~2280m is from Unit 288 which is a thick sequence of pillows (De Paolo et al., 1999). ICP-MS data are used in panels a, b and c; in panel d, La and Yb are ICP-MS data, Ti and Zr are XRF data from Rhodes and Vollinger, 2004.

In each panel calculated melting trajectories are shown for batch partial melting (1% increments with total extents of melting indicated at both ends of the trajectories) of spinel peridotite, and garnet peridotite. Details of the models, such as source abundances, mineral modes, melting reactions, and mineral/melt partition coefficients, are in **appendix II**.

Figure 10 (e,f,g). Panels are equivalent to panels "a" and "d", but their objective is to compare Phase 2 Mauna Kea lavas with shield lavas from Kilauea, Mauna Loa and Loihi. Panel "e" shows that Phase 2 Mauna Kea Shield lavas are intermediate between historic Kilauea lavas (Pietruszka and Garcia, 1999) and historic Mauna Loa lavas (Rhodes and Hart, 1995). Most notable is that the range of La/Yb and Nb/Zr during the last 200 years of Kilauea volcanism (dashed field) exceeds that of the >300,000 years of Mauna Kea volcanism recorded in the Phase 2 core.

Panels "f" and "g" show data for Loihi seamount. At high ratios, the trend labeled "Loihi lavas" reflects the higher ratios of alkalic lavas created by the lower degrees of melting (Frey and Clague, 1983; Garcia et al., 1993). Most important is the Loihi Glasses field (outlined in blue and from Garcia et al., 1998) which shows that recent tholeiitic glasses from Loihi seamount have relatively high Nb/Zr and Ti/Zr overlapping with the Low SiO_2 Shield Group of Mauna Kea. The field labeled Loihi Picrites (outlined in red and from Norman and Garcia, 1999) also has high Nb/Zr but in contrast to the glasses, these picrites do not have La/Yb and Ti/Zr similar to the Low SiO_2 Group of Mauna Kea lavas.

Figure 11. Delta $^{208}Pb/^{204}Pb$ (see Figure caption 8 for definition) versus the incompatible element abundance ratios, Nb/Zr, Nb/Y and Sm/Yb. Within each group of Mauna Kea lavas these abundance ratios correlate with delta $^{208}Pb/^{204}Pb$. Sample SR791 is an anomalous member of the Low SiO_2 Shield Group. It is also distinguished by having the lowest Ba/Th ratio (Fig. 15). The Low SiO_2 Shield Group ranges to high delta $^{208}Pb/^{204}Pb$ and it overlaps with the field for lavas from Loihi seamount (panel "a"). In

these panels the array of Mauna Kea data requires at least 3 mixing components. Trace element data for Mauna Kea lavas are from this paper, and delta $^{208}Pb/^{204}Pb$ is calculated from Pb isotopic data in Blichert-Toft et al. (2003). Field for Loihi lavas is from Garcia et al. (1993, 1998) and Norman and Garcia (1999).

Figure 12. Abundance ratios of Nb/Th, Nb/U, Nb/Ta, Nb/La, Zr/Hf, and Ce/Pb versus depth in the Phase 2 core. All of these ratios involve highly incompatible elements or elements with similar geochemical characteristics (charge and ionic radius). Symbols as defined in Figure 8. There is no distinction between the two Shield Groups. There is a slight tendency for Postshield lavas to have relatively low Nb/La, and high Nb/U, Ce/Pb and Nb/Ta. The greater dispersion of Ce/Pb may reflect Pb contamination whereas that of Nb/U may reflect U mobility during alteration.

Figure 13 (a). La/Yb versus Nb/Zr for several Hawaiian shields. Although within shields these ratios are correlated, the Koolau shield lavas are offset to low Nb/Zr. Loihi alkalic lavas extend to the highest La/Yb and Nb/Zr, presumably reflecting a relatively low extent of melting (Frey and Clague, 1983; Garcia et al., 1993).

(b). La/Nb versus Sr/Nb for several Hawaiian shields. Compared to La/Yb and Nb/Zr these ratios are less sensitive to variations in extent of melting. The shields define a positive trend with Mauna Loa and especially Koolau showing a relative Nb depletion, i.e, high La/Nb and Sr/Nb. The fields for Mauna Kea, Kilauea and Loihi overlap.

Data sources: HSDP 1 (Yang et al., 1996; Rhodes, 1996); HSDP 2 (this paper); Koolau (Frey et al., 1994; Jackson et al., 1999; unpublished data of Huang and Frey), Mauna Loa

(Rhodes, 1995; Rhodes and Hart, 1995; Kurz et al., 1995; Cohen et al., 1996); Loihi (Frey and Clague, 1983; Garcia et al., 1993, 1998; Norman and Garcia, 1998); Kilauea (historic from Pietruszka and Garcia, 1999; Hilina from Chen et al. 1996).

Figure 14 (a,b,c). Correlations of Nb/Zr, La/Nb and Ba/Th with isotopic ratios of Sr, Nd and Pb in the HSDP core and other Hawaiian shields. Inset in "c" shows that the distinctive geochemical groups for HSDP Mauna Kea lavas overlap in Ba/Th. Data Sources: HSDP 2 (this paper; Bryce et al., 2005; Blichert-Toft et al. 2003); HSDP 1 (Rhodes, 1996; Lassiter et al., 1996); Koolau (Roden et al., 1994 and unpublished data of Huang and Frey); Mauna Loa (Rhodes and Hart, 1995; Kurz et al., 1995; Cohen et al., 1996); Loihi (Garcia et al., 1993, 1995, 1998; Norman and Garcia, 1998); Kilauea (Chen et al., 1996; Pietruszka and Garcia, 1999).

Figure 15. Abundance ratios involving highly incompatible elements: Ba/Nb, Ba/La and La/Nb versus Ba/Th for HSDP lavas and basalt from other Hawaiian shields. In the Ba/Nb-Ba/Th panel HSDP lavas and Hawaiian shields in general define a positive trend that extends toward depleted mantle (DM) estimates (Hofmann, 1988) but not toward primitive mantle (PM) estimates (Sun and McDonough, 1989). A positive trend is also defined by Ba/La-Ba/Th, but basalt from the Koolau shield is offset to lower Ba/La at a given Ba/Th. In contrast to the more than a factor of two variation in Ba/Nb, Ba/La and Ba/Th, the La/Nb ratio is relatively constant, although Koolau lavas have high La/Nb at a given Ba/Th. Data sources are as given in Fig. 13 caption.

Figure 16. Variability [(one standard deviation/mean) x 100] in abundance ratios of incompatible elements in HSDP 2 lavas.

Appendix Figure Captions

Fig. A-1. Sensitivity drift in internal drift monitors. Counts per second (CPS) normalized by the isotope concentrations in the solutions, and then normalized to CPS of the first external drift monitor (EDM), for the 3 internal drift monitors (^{77}Se, ^{115}In, ^{203}Bi) in a sequence of solutions, 1 to 37, analyzed over 6 hours. Generally, the statistical uncertainty in CPS is less than 3% (2σ). The non-uniform behavior of the 3 isotopes indicates that sensitivity drift is a function of time and mass. Because the sensitivity drift is a complicated function of mass, use of only 3 isotopes does not adequately correct for drift as a function of mass (See Fig A-2). Solution 18 in the sequence is a blank solution (i.e., it contains only the internal drift monitors and acid.). It has very high CPS because of the absence of a dissolved rock matrix which depresses the signal strength.

Fig. A-2. Sensitivity drift in external drift monitors. CPS (normalized by their isotope concentrations in the solutions), after applying the internal drift correction factor (IDF), normalized by CPS of the first external drift monitor, in 7 external drift monitors for all the analyzed isotopes. The 7 external drift monitors were run in the order of DM-a, DM-b, DM-c, DM-d, DM-e, DM-f, DM-g. Notice that after applying the IDF, the normalized CPS do not define a horizontal line at unity. However the shapes of IDF corrected CPS in EDMs, relatively low at lower mass and high at higher mass, are similar for each EDM.

Clearly, the internal drift correction has not sufficiently corrected for sensitivity drift as a function of mass.

Fig. A-3. Normalized CPS in 37 solutions of BHVO-1 for 25 elements. Both internal drift correction factor (IDF) and external drift Correction Factor (EDF) were applied following the procedure described in the text. Solutions labeled as EDM are external drift monitors which were normalized to the CPS of the first EDM in order to determine the EDF; therefore for each element in every EDM, the normalized CPS are unity. For solutions run between two EDM (Table A-1b), the EDF was determined for each analyzed isotope using a cubic spline fit to the EDF for each EDM. Ideally, since all analyzed solutions are from the same solution of BHVO-1, the normalized CPS in all the solutions should be unity. The discrepancy from unity provides estimates of the uncertainty resulting from both the analytical technique and sensitivity drift correction procedures.

Fig. A-4. Comparisons between MIT ICP-MS and XRF. Comparisons between trace element abundances in HSDP-2 lavas obtained by ICP-MS at MIT (this paper) and XRF at UMASS (Rhodes and Vollinger, 2004). Regression equations are forced to intersect the origin. R^2 is linear correlation coefficient.

Fig. A-5. Comparison between ICP-MS and INAA. Comparisons between trace element abundances in HSDP 2 lavas obtained by ICP-MS at MIT (this paper), ICP MS at

Rutgers (Feigenson et al., 2003) and INAA at MIT (this paper). Regression equations are forced to intersect the origin. R^2 is linear correlation coefficient.

Table 1. Trace Element Abundances in Mauna Kea Lavas Recovered from HSDP Phase 2 Drill Hole

	SR0121 -4.40	SR0124 -3.90	SR0125 -6.25	SR0127 -4.75	SR0129 -5.20	SR0131 -6.92	SR0133 -8.20	SR0137 -5.98	SR0141 -7.90	SR0148 -8.50	SR0157 -6.25	SR0167 -5.90	SR0175 -5.25	SR0184 -2.80	SR0193 -0.00	SR0205 -1.30	SR0212 -8.20
Depth (mbsl)	246.2	252.9	256.5	261.7	267.5	274.4	281.3	293.0	305.8	326.7	353	378.4	398.1	421.2	443.6	467.8	490.9
Rock Type	subaerial	subaerial	subaerial	subaerial	subaerial	subaerial	subaerial	subaerial	subaerial	subaerial	subaerial	subaerial	subaerial	subaerial	subaerial	subaerial	subaerial
UNIT	U0042	U0043	U0045	U0046	U0047	U0048	U0049	U0053	U0056	U0060	U0065	U0070	U0073	U0076	U0080	U0083	U0088
ICP-MS																	
Rb	13.0	1.68	1.96	9.72	1.36	14.0	5.03	3.40	3.48	0.531	3.16	1.38	0.356	4.40	6.51	4.88	3.78
Sr	470	414	318	462	496	604	364	389	416	211	213	375	151	228	297	268	238
Y	39.5	35.6	29.8	31.3	29.2	38.9	26.2	30.8	34.1	18.1	18.5	32.8	14.2	21.0	26.0	22.3	20.7
Zr	248	234	195	198	162	293	168	188	210	102	101	193	75.3	122	152	131	116
Nb	28.4	23.0	20.1	19.4	14.9	29.4	15.9	16.1	19.8	8.71	8.05	16.5	6.13	9.28	13.0	11.9	9.60
Ba	317	204	181	173	155	248	134	137	166	62.9	68.7	137	52.5	78.0	107	91.9	80.6
La	24.8	19.9	18.7	16.8	13.1	24.4	14.0	13.9	16.9	7.59	7.20	14.8	5.26	8.14	11.1	9.82	8.26
Ce	52.9	46.8	42.5	41.0	31.7	59.0	33.8	34.2	40.9	18.6	18.1	37.4	12.8	20.6	27.4	24.8	20.2
Pr	7.98	7.05	6.18	5.98	4.84	8.67	5.00	5.22	6.18	2.91	2.81	5.67	2.07	3.18	4.13	3.74	3.19
Nd	34.9	31.7	28.1	27.0	22.7	38.7	22.9	24.2	28.4	13.7	13.5	26.2	9.69	15.7	20.1	17.6	15.2
Sm	8.58	7.92	7.25	6.87	6.02	9.69	5.79	6.40	7.28	3.70	3.72	7.13	2.72	4.34	5.32	4.68	4.16
Eu	2.89	2.64	2.33	2.25	2.13	3.15	1.90	2.21	2.48	1.24	1.24	2.31	0.935	1.44	1.83	1.58	1.44
Gd	8.60	8.09	7.15	6.94	6.22	9.66	5.80	6.54	7.52	3.85	3.82	7.27	3.00	4.35	5.40	4.91	4.35
Tb	1.33	1.27	1.12	1.09	1.00	1.48	0.919	1.05	1.19	0.621	0.615	1.14	0.471	0.717	0.914	0.770	0.710
Dy	6.97	6.66	5.88	5.92	5.48	7.66	4.91	5.80	6.46	3.43	3.42	6.31	2.67	3.97	4.94	4.25	3.93
Ho	1.37	1.28	1.07	1.12	1.04	1.42	0.911	1.12	1.25	0.64	0.685	1.20	0.518	0.769	0.957	0.798	0.773
Er	3.27	3.20	2.57	2.75	2.58	3.35	2.23	2.68	3.03	1.60	1.70	2.90	1.30	1.83	2.29	2.00	1.90
Tm	0.445	0.424	0.364	0.440	0.351	0.458	0.312	0.379	0.415	0.222	0.224	0.393	0.177	0.265	0.334	0.279	0.257
Yb	2.63	2.43	2.06	2.22	2.01	2.64	1.80	2.18	2.45	1.30	1.38	2.33	1.01	1.53	1.86	1.62	1.55
Lu	0.355	0.333	0.292	0.300	0.280	0.358	0.245	0.303	0.334	0.175	0.190	0.323	0.145	0.212	0.260	0.222	0.219
Hf	6.19	5.94	4.92	4.94	4.22	7.06	4.14	4.59	5.35	2.57	2.69	5.07	1.95	3.07	3.78	3.37	3.01
Ta[1]	1.86	1.57	1.28	1.31	1.01	2.01	1.11	1.14	1.37	0.664	0.673	1.16	0.576	0.735	0.980	0.916	0.800
Pb	1.51	1.38	1.28	1.22	0.989	1.61	0.962	1.00	1.17	0.91	0.593	1.18	0.484	0.649	0.787	0.820	0.665
Th	1.71	1.49	1.44	1.36	0.945	1.97	1.06	0.994	1.24	0.526	0.542	1.14	0.382	0.607	0.858	0.801	0.597
U	0.471	0.440	0.382	0.409	0.202	0.610	0.286	0.285	0.300	0.152	0.192	0.260	0.0976	0.188	0.270	0.252	0.201
INAA																	
Na_2O	2.05	1.83	1.29	2.35	2.21	2.81	1.81	2.03	2.35	1.07	1.25	2.11	0.88	1.35	1.88	1.4	1.51
Cr	140	328	609	182	271	129	839	454	214	1830	1268	349	1660	1209	592	1038	1204
Sc	29.3	29.2	35.9	29.8	29.8	25.8	25.9	30.5	30.1	22.5	22.1	27.8	17	21.9	28.7	22.1	25.7
La	22.8	18.6	18.7	16.4	12.9	23.6	13.9	13.8	16.4	7.39	6.92	13.7	4.85	7.41	11	8.96	8.08
Ce	51.7	45.8	44.3	42	33.4	59.9	35	36.2	43.1	18.6	18.4	35.3	12.3	19.4	28	23.5	20.8
Nd	32.9	30.7	30.3	27.8	23	39.1	23.1	23.2	28.2	13.8	11.8	24.2	8.8	13.5	19.3	15.9	16.1
Sm	7.92	7.65	7.24	6.7	6.02	9.3	5.66	6.34	7.13	3.46	3.44	6.42	2.53	3.81	5.16	4.21	4.08
Eu	2.71	2.56	2.31	2.24	2.09	3.1	1.91	2.17	2.41	1.2	1.25	2.18	0.88	1.3	1.76	1.46	1.46
Tb	1.16	1.1	1.19	1.08	0.94	1.4	0.85	1.08	1.09	0.56	0.59	1.09	0.43	0.62	0.76	0.58	0.68
Yb	2.32	2.31	1.92	2.03	1.95	2.41	1.53	2.13	2.33	1.14	1.17	1.98	0.89	1.3	1.71	1.4	1.48
Lu	0.36	0.33	0.275	0.29	0.27	0.33	0.23	0.28	0.33	0.17	0.18	0.29	0.12	0.19	0.25	0.19	0.2
Hf	5.69	5.28	4.73	4.69	4.08	6.61	4.02	4.38	4.93	2.39	2.27	4.8	1.71	2.67	3.76	2.86	2.96
Th	1.4	1.2	1.17	0.98	0.78	1.68	0.94	0.79	1.06	0.28	0.42	0.82	0.36	0.51	0.8	0.8	0.84

Trace Element abundances were determined by ICP-MS and INAA separately, and are reported in ppm, except for Na_2O which is reported in %.

n.d. : not determined.

For discussion of accuracy and precision see Appendix 1.

(1)Samples were powdered in WC shatterbox (Rhodes and Vollinger, 2002); therefore, the Ta contents may be anomalously high. However, this effect appears to be minor (see text and Fig 12c).

Table 1 (continue)

	SR0222 -2.00	SR0232 -8.50	SR0240 -3.30	SR0256 -0.95	SR0267 -6.85	SR0276 -7.85	SR0284 -1.75	SR0294 -7.65	SR0300 -6.50	SR0311 -4.40	SR0328 -3.10	SR0340 -1.00	SR0346 -5.60	SR0354 -7.75	SR0372 -2.80	SR0379 -3.00	SR0392 -4.30
Depth (mbsl)	516.2	542.1	563.5	589.0	615.8	636.0	658.3	678.6	695.9	724.1	759.8	793.6	812.7	833.9	871.2	888.4	921.8
Rock Type	subaerial	subaerial	subaerial	subaerial	subaerial	subaerial	subaerial	subaerial	subaerial	subaerial	subaerial	subaerial	subaerial	subaerial	subaerial	subaerial	subaerial
UNIT	U0092	U0094	U0098	U0103	U0107	U0110	U0114	U0116	U0119	U0124	U0127	U0132	U0136	U0138	U0142	U0144	U0148
ICP-MS																	
Rb	5.75	1.25	4.89	6.86	3.62	0.817	2.37	8.02	5.28	5.02	3.61	3.52	3.19	3.19	5.87	5.60	3.75
Sr	289	280	287	343	204	215	182	340	285	270	181	177	240	195	303	289	179
Y	21.8	25.2	24.2	31.5	18.4	21.1	17.3	29.0	26.4	23.3	16.1	16.5	22.6	17.4	29.2	27.5	17.7
Zr	125	143	144	180	101	123	92.1	166	152	131	88.1	94.4	118	95.0	152	144	95.2
Nb	12.6	11.7	12.1	14.7	8.71	10.3	8.01	16.0	12.9	10.8	7.57	8.42	9.98	8.15	12.9	11.8	7.65
Ba	95.8	71.6	91.2	109	60.2	84.0	68.4	124	76.4	87.0	57.6	68.3	103	68.0	100	82.9	59.8
La	10.3	10.1	10.4	12.5	7.17	8.82	6.77	12.9	10.9	9.78	6.43	6.86	8.37	6.76	10.7	9.80	6.76
Ce	25.4	25.6	25.8	32.1	18.0	22.2	16.8	32.0	28.0	24.0	15.7	16.9	21.5	17.1	27.5	25.7	16.9
Pr	3.79	3.96	4.05	5.02	2.84	3.42	2.63	4.94	4.29	3.65	2.49	2.65	3.39	2.62	4.30	4.01	2.69
Nd	17.2	18.6	18.4	23.2	13.5	15.8	12.4	22.1	20.2	18.1	12.1	12.4	16.4	11.7	19.9	18.3	12.6
Sm	4.63	5.03	4.91	6.48	3.60	4.36	3.34	5.83	5.39	4.74	3.27	3.32	4.42	3.40	5.31	5.15	3.41
Eu	1.55	1.68	1.65	2.15	1.25	1.47	1.12	1.92	1.80	1.62	1.08	1.14	1.53	1.16	1.90	1.71	1.17
Gd	4.62	5.25	5.09	6.68	3.84	4.52	3.53	6.04	5.67	4.96	3.34	3.47	4.70	3.61	5.91	5.41	3.67
Tb	0.755	0.821	0.804	1.091	0.636	0.744	0.558	0.961	0.910	0.807	0.548	0.567	0.759	0.574	0.951	0.871	0.597
Dy	4.12	4.63	4.38	6.04	3.51	4.00	3.15	5.25	4.96	4.41	3.01	3.15	4.09	3.19	5.37	4.96	3.36
Ho	0.785	0.892	0.836	1.15	0.656	0.792	0.620	0.972	0.966	0.848	0.580	0.610	0.808	0.617	1.05	0.927	0.656
Er	1.91	2.20	2.06	2.84	1.65	1.98	1.52	2.48	2.44	2.06	1.43	1.52	2.06	1.50	2.72	2.38	1.56
Tm	0.264	0.293	0.287	0.384	0.227	0.274	0.212	0.348	0.332	0.304	0.201	0.206	0.278	0.220	0.370	0.327	0.221
Yb	1.58	1.73	1.71	2.32	1.35	1.62	1.22	2.00	1.95	1.68	1.17	1.23	1.63	1.29	2.14	1.99	1.37
Lu	0.210	0.248	0.243	0.321	0.190	0.226	0.178	0.280	0.274	0.238	0.170	0.168	0.229	0.183	0.304	0.279	0.180
Hf	3.15	3.49	3.53	4.72	2.69	3.16	2.27	3.92	3.96	3.34	2.42	2.50	3.03	2.27	3.87	3.47	2.58
Ta	0.970	0.849	0.911	1.17	0.692	0.739	0.630	1.05	0.948	0.849	0.723	0.681	0.733	0.648	0.981	0.856	0.671
Pb	0.747	0.756	0.721	0.982	0.714	1.05	0.910	1.00	1.12	0.942	0.637	1.01	1.53	1.03	1.04	0.939	0.625
Th	0.779	0.778	0.788	1.01	0.570	0.676	0.534	1.02	0.906	0.743	0.499	0.564	0.634	0.527	0.815	0.769	0.527
U	0.269	0.212	0.248	0.333	0.192	0.194	0.178	0.319	0.312	0.229	0.183	0.179	0.211	0.160	0.282	0.260	0.163
INAA																	
Na_2O	1.63	n.d.	1.7	2.07	n.d.	1.38	n.d.	2.11	1.8	1.69	1.13	1.12	n.d.	1.33	2.06	n.d.	1.27
Cr	961	n.d.	858	249	n.d.	1148	n.d.	504	750	790	1482	1450	n.d.	1262	399	n.d.	1140
Sc	26.9	n.d.	25.2	28.8	n.d.	21.4	n.d.	30.7	26	27.3	20.2	18.7	n.d.	20.6	30.7	n.d.	21.5
La	10.1	n.d.	10.2	12	n.d.	8.56	n.d.	13.1	10.5	9.31	6.26	6.52	n.d.	6.64	10.5	n.d.	6.5
Ce	26	n.d.	26.6	32.4	n.d.	22	n.d.	33.8	28	24.8	15.6	18	n.d.	17.5	27.8	n.d.	17
Nd	16.9	n.d.	18.7	22.9	n.d.	15.7	n.d.	21.2	19.1	18.7	11.7	12.3	n.d.	12.1	20	n.d.	12.1
Sm	4.35	n.d.	4.84	5.93	n.d.	4.07	n.d.	5.65	5.01	4.53	3.08	3.08	n.d.	3.23	5.26	n.d.	3.37
Eu	1.46	n.d.	1.66	2.1	n.d.	1.46	n.d.	1.97	1.77	1.67	1.05	1.14	n.d.	1.15	1.85	n.d.	1.17
Tb	0.6	n.d.	0.76	0.79	n.d.	0.55	n.d.	0.88	0.83	0.68	0.43	0.39	n.d.	0.47	0.83	n.d.	0.63
Yb	1.45	n.d.	1.73	2.11	n.d.	1.46	n.d.	2.02	1.78	1.6	1.08	1.07	n.d.	1.22	1.98	n.d.	1.19
Lu	0.2	n.d.	0.23	0.29	n.d.	0.2	n.d.	0.27	0.24	0.22	0.15	0.15	n.d.	0.18	0.28	n.d.	0.17
Hf	3.23	n.d.	3.57	3.97	n.d.	2.93	n.d.	3.97	3.85	3.18	2.32	2.27	n.d.	2.29	3.54	n.d.	2.38
Th	0.6	n.d.	0.68	0.84	n.d.	0.68	n.d.	0.77	1.01	0.94	0.4	0.8	n.d.	0.53	0.62	n.d.	0.44

Table 1 (continue)

	SR0401 -2.85	SR0413 -3.10	SR0423 -3.65	SR0431 -8.50	SR0441 -9.10	SR0450 -3.55	SR0455 -7.40	SR0472 -1.00	SR0490 -1.50	SR0502 -4.85	SR0518 -0.80	SR0531 -4.40	SR0545 -8.35	SR0548 -8.00	SR0560 -7.50	SR0574 -1.90	SR0582 -10.00
Depth (mbsl)	948.9	984.2	1012.4	1037.7	1061.2	1083.7	1098.2	1123.2	1229.6	1265.2	1311.9	1352.6	1395.0	1404.1	1435.4	1474.7	1497.7
Rock Type	subaerial	subaerial	subaerial	subaerial	subaerial	massive	massive	massive	Hyalo-clastite	massive	massive	Hyalo-clastite	Hyalo-clastite	massive	Hyalo-clastite	Hyalo-clastite	massive
UNIT	U0151	U0155	U0157	U0160	U0166	U0171	U0179	U0185	U0190	U0191	U0195	U0198	U0198	U0199	U0202	U0202	U0207
ICP-MS																	
Rb	3.09	4.89	6.98	7.14	6.41	1.19	0.763	4.41	3.07	0.977	2.31	3.38	2.03	3.22	2.89	4.43	3.89
Sr	148	302	344	325	300	194	168	279	214	157	186	263	261	202	241	217	208
Y	14.3	27.2	29.3	30.4	28.5	16.1	15.2	27.0	22.0	15.2	18.5	22.3	22.5	19.4	21.1	21.1	20.4
Zr	75.8	141	163	169	154	87.1	77.6	139	115	79.8	97.3	121	121	104	114	116	108
Nb	6.03	10.8	14.1	15.7	13.0	7.26	6.47	10.3	9.15	6.54	7.60	10.8	10.8	8.08	10.0	10.0	9.04
Ba	50.4	80.9	114	114	98.3	61.4	52.6	74.8	64.1	66.4	55.8	81.0	68.3	66.9	57.7	53.0	71.1
La	5.27	9.16	11.7	13.1	11.2	6.12	5.24	8.96	7.72	5.89	6.54	8.70	8.77	7.30	8.33	7.66	7.87
Ce	13.3	23.3	29.7	32.2	28.1	15.6	13.2	22.7	19.1	14.9	16.9	22.4	22.0	17.7	21.0	20.4	19.7
Pr	2.10	3.64	4.61	4.91	4.35	2.44	2.09	3.62	3.04	2.31	2.57	3.48	3.36	2.84	3.21	3.12	3.12
Nd	9.91	17.3	21.1	23.4	20.3	11.7	9.76	17.4	15.3	10.5	12.5	15.8	15.9	13.5	15.0	14.9	14.6
Sm	2.72	5.14	5.74	6.15	5.56	3.19	2.76	4.86	4.00	2.99	3.54	4.37	4.37	3.70	4.05	4.03	4.03
Eu	0.921	1.73	1.98	2.06	1.84	1.07	0.924	1.70	1.38	1.02	1.20	1.51	1.47	1.25	1.39	1.38	1.37
Gd	2.89	5.47	6.17	6.58	5.70	3.34	2.82	5.34	4.40	3.14	3.78	4.54	4.69	4.04	4.35	4.24	4.28
Tb	0.472	0.870	0.968	1.018	0.919	0.550	0.462	0.890	0.717	0.510	0.611	0.747	0.738	0.650	0.712	0.700	0.704
Dy	2.66	5.01	5.58	5.68	5.31	3.10	2.65	4.88	3.96	2.87	3.43	4.36	4.15	3.60	3.93	3.88	3.94
Ho	0.507	0.961	1.07	1.09	1.00	0.574	0.500	0.958	0.769	0.534	0.665	0.790	0.806	0.701	0.760	0.751	0.738
Er	1.28	2.41	2.63	2.77	2.66	1.41	1.27	2.35	1.89	1.34	1.63	2.05	2.07	1.77	1.94	1.92	1.89
Tm	0.181	0.354	0.368	0.380	0.342	0.198	0.162	0.346	0.274	0.193	0.238	0.281	0.285	0.240	0.273	0.271	0.267
Yb	1.04	2.01	2.16	2.23	2.16	1.18	1.01	1.98	1.57	1.12	1.38	1.65	1.71	1.51	1.58	1.56	1.56
Lu	0.144	0.292	0.287	0.318	0.303	0.166	0.148	0.278	0.222	0.157	0.187	0.240	0.230	0.211	0.217	0.218	0.207
Hf	1.86	3.53	4.13	4.50	3.71	2.24	1.77	3.47	2.97	2.01	2.44	3.12	3.30	2.72	2.83	3.01	2.98
Ta	0.510	0.788	1.07	1.09	0.963	0.521	0.453	0.781	0.671	0.547	0.621	0.809	0.782	0.611	0.834	0.808	0.722
Pb	0.788	0.898	1.07	0.972	0.978	0.727	0.588	0.708	0.660	0.513	0.737	1.47	0.920	1.00	0.952	0.611	0.683
Th	0.375	0.684	0.934	1.05	0.839	0.490	0.383	0.654	0.560	0.436	0.519	0.700	0.710	0.564	0.631	0.645	0.671
U	0.119	0.216	0.322	0.316	0.278	0.199	0.133	0.241	0.236	0.148	0.206	0.242	0.248	0.186	0.201	0.227	0.221
INAA																	
Na_2O	n.d.	2.02	n.d.	2.11	n.d.	0.96	0.86	n.d.	n.d.	0.89	1.25	1.61	1.6	1.41	1.55	1.43	1.37
Cr	n.d.	283	n.d.	524	n.d.	1516	1603	n.d.	n.d.	1579	1191	859	910	1138	976	984	930
Sc	n.d.	31.3	n.d.	29	n.d.	19.7	19.4	n.d.	n.d.	21.3	21.1	23.3	22.4	22.9	21.9	22.4	22.4
La	n.d.	8.79	n.d.	12.3	n.d.	5.86	4.79	n.d.	n.d.	5.58	6.55	8.62	8.42	7.22	8.16	7.79	7.55
Ce	n.d.	24	n.d.	32	n.d.	15.3	13	n.d.	n.d.	14.5	17.7	22.6	21.7	19.8	20.7	19.9	20.6
Nd	n.d.	16.7	n.d.	22.3	n.d.	11.3	9.1	n.d.	n.d.	10.7	12.2	16	14.2	14.7	14	14.5	13.6
Sm	n.d.	4.82	n.d.	5.77	n.d.	2.91	2.49	n.d.	n.d.	2.84	3.34	4.16	4.01	3.75	3.86	3.83	3.87
Eu	n.d.	1.73	n.d.	1.91	n.d.	1.01	0.91	n.d.	n.d.	0.98	1.17	1.49	1.41	1.29	1.37	1.36	1.41
Tb	n.d.	0.86	n.d.	0.95	n.d.	0.46	0.39	n.d.	n.d.	0.46	0.61	0.77	0.67	0.6	0.66	0.67	0.65
Yb	n.d.	1.94	n.d.	2.03	n.d.	1.01	0.86	n.d.	n.d.	1.14	1.23	1.54	1.43	1.35	1.42	1.37	1.41
Lu	n.d.	0.26	n.d.	0.28	n.d.	0.16	0.12	n.d.	n.d.	0.16	0.17	0.22	0.21	0.2	0.2	0.2	0.2
Hf	n.d.	3.38	n.d.	4.23	n.d.	2.1	1.58	n.d.	n.d.	2.13	2.47	3	2.69	2.73	2.67	2.64	2.63
Th	n.d.	0.6	n.d.	0.69	n.d.	0.4	0.52	n.d.	n.d.	0.35	0.51	0.75	0.56	0.58	0.41	0.39	0.4

Table 1 (continue)

	SR0594 -8.70	SR0603 -8.90	SR0604 -2.50	SR0622 -7.10	SR0630 -6.20	SR0641 -1.00	SR0655 -4.00	SR0664 -5.10	SR0675 -6.90	SR0683 -5.75	SR0694 -9.00	SR0705 -0.15	SR0709 -13.35	SR0714 -11.55	SR0720 -18.25	SR0723 -13.70	SR0732 -1.10
Depth (mbsl)	1521.4	1548.2	1549.3	1581.2	1605.0	1636.4	1678.7	1705.5	1739.3	1763.2	1794.8	1823.2	1852.0	1883.6	1921.6	1933.8	1973.8
Rock Type	massive	Hyalo-clastite	massive	Hyalo-clastite	massive	massive	Hyalo-clastite	Hyalo-clastite	Hyalo-clastite	massive	massive	Hyalo-clastite	Hyalo-clastite	intrusive	intrusive	Hyalo-clastite	Hyalo-clastite
UNIT	U0213	U0216	U0217	U0218	U0224	U0226	U0238	U0238	U0243	U0245	U0253	U0260	U0261	U0263	U0268	U0270	U0274
ICP-MS																	
Rb	3.36	3.58	4.70	4.41	2.29	n.d.	4.45	0.715	3.98	2.47	5.08	2.41	1.79	4.65	3.13	5.16	5.35
Sr	223	254	254	261	204	n.d.	256	249	273	205	281	262	163	281	169	273	315
Y	20.8	23.7	24.4	25.0	19.5	n.d.	23.8	23.4	24.4	19.2	25.3	23.8	16.4	26.0	16.9	28.0	27.7
Zr	113	120	124	137	105	n.d.	124	144	132	103	136	125	85.5	137	90.2	145	139
Nb	9.67	10.1	10.5	11.1	8.17	n.d.	11.2	13.6	11.3	7.88	12.3	9.98	7.24	12.5	6.91	11.7	14.1
Ba	70.6	76.2	77.4	72.2	60.2	n.d.	86.2	64.9	69.1	76.3	90.1	57.4	39.6	88.4	55.8	79.6	86.8
La	7.97	8.24	8.71	9.01	6.81	n.d.	9.65	10.6	9.47	7.02	10.4	8.84	6.05	10.8	6.12	9.89	11.2
Ce	20.6	20.9	21.5	22.9	17.6	n.d.	24.2	26.6	23.8	17.5	25.7	22.0	15.2	25.9	15.5	25.1	27.1
Pr	3.18	3.36	3.40	3.65	2.81	n.d.	3.72	4.11	3.63	2.81	3.79	3.36	2.40	3.91	2.40	3.98	4.10
Nd	14.9	16.1	15.9	17.4	13.7	n.d.	17.3	18.8	17.5	13.1	18.6	16.5	11.5	18.9	12.0	18.9	19.0
Sm	4.05	4.39	4.41	4.75	3.67	n.d.	4.62	4.98	4.56	3.73	4.88	4.44	3.04	5.17	3.21	5.22	5.02
Eu	1.35	1.53	1.53	1.65	1.25	n.d.	1.61	1.65	1.59	1.29	1.64	1.54	1.02	1.72	1.07	1.76	1.71
Gd	4.27	4.77	4.77	5.25	3.93	n.d.	5.17	5.10	4.94	4.08	5.19	4.80	3.33	5.27	3.39	5.61	5.36
Tb	0.692	0.764	0.786	0.850	0.658	n.d.	0.813	0.802	0.808	0.653	0.839	0.786	0.537	0.872	0.563	0.927	0.877
Dy	3.90	4.30	4.42	4.63	3.61	n.d.	4.54	4.61	4.47	3.58	4.56	4.38	2.90	4.85	3.13	5.14	4.91
Ho	0.754	0.844	0.874	0.898	0.705	n.d.	0.851	0.829	0.840	0.697	0.884	0.846	0.579	0.951	0.613	1.02	0.954
Er	1.88	2.15	2.13	2.23	1.74	n.d.	2.15	2.05	2.20	1.73	2.17	2.13	1.48	2.35	1.53	2.54	2.43
Tm	0.301	0.295	0.300	0.317	0.246	n.d.	0.295	0.288	0.302	0.259	0.320	0.311	0.198	0.334	0.209	0.363	0.340
Yb	1.54	1.69	1.75	1.83	1.43	n.d.	1.78	1.70	1.77	1.44	1.80	1.79	1.18	1.90	1.28	2.09	2.05
Lu	0.211	0.252	0.244	0.261	0.203	n.d.	0.249	0.228	0.253	0.197	0.248	0.252	0.166	0.269	0.183	0.287	0.293
Hf	2.91	3.02	3.07	3.36	2.55	n.d.	3.34	3.53	3.22	2.65	3.46	3.23	2.18	3.70	2.37	3.58	3.42
Ta	0.716	0.747	0.743	0.879	0.679	n.d.	0.846	0.906	0.834	0.624	0.921	0.710	0.606	0.968	0.567	0.985	1.08
Pb	n.d.	0.672	0.677	0.716	0.633	n.d.	0.855	0.765	0.794	0.801	0.883	0.729	0.493	0.838	0.557	0.765	0.900
Th	0.637	0.611	0.659	0.704	0.527	n.d.	0.741	0.876	0.707	0.557	0.814	0.700	0.468	0.859	0.495	0.785	0.836
U	0.223	0.238	0.230	0.277	0.181	n.d.	0.285	0.415	0.240	0.185	0.252	0.214	0.179	0.287	0.171	0.261	0.275
INAA																	
Na_2O	1.4	1.62	n.d.	1.52	n.d.	1.6	n.d.	1.35	n.d.	1.32	1.84	1.7	n.d.	1.93	1.22	n.d.	2.17
Cr	955	689	n.d.	771	n.d.	997	n.d.	934	n.d.	1044	718	705	n.d.	488	1166	n.d.	516
Sc	22.5	29.2	n.d.	26.7	n.d.	24.8	n.d.	24.2	n.d.	22.1	27.8	27	n.d.	29	19.8	n.d.	29.5
La	7.78	8.27	n.d.	9	n.d.	7.78	n.d.	10.2	n.d.	6.61	9.9	8.28	n.d.	10.2	6.06	n.d.	10.9
Ce	20.2	20.7	n.d.	23.6	n.d.	20.2	n.d.	27	n.d.	17.3	25.4	22.3	n.d.	25.1	16.1	n.d.	29.5
Nd	14.7	14.8	n.d.	16.2	n.d.	15.7	n.d.	18.4	n.d.	12.7	18.5	15.3	n.d.	18.9	11.1	n.d.	17.5
Sm	3.88	4.17	n.d.	4.58	n.d.	4.08	n.d.	4.76	n.d.	3.46	4.62	4.3	n.d.	4.58	3.16	n.d.	4.86
Eu	1.35	1.5	n.d.	1.6	n.d.	1.51	n.d.	1.6	n.d.	1.2	1.64	1.5	n.d.	1.64	1.09	n.d.	1.72
Tb	0.64	0.77	n.d.	0.91	n.d.	0.72	n.d.	0.72	n.d.	0.52	0.79	0.66	n.d.	0.79	0.49	n.d.	0.79
Yb	1.38	1.56	n.d.	1.64	n.d.	1.59	n.d.	1.39	n.d.	1.2	1.62	1.67	n.d.	1.73	1.13	n.d.	1.85
Lu	0.21	0.22	n.d.	0.25	n.d.	0.24	n.d.	0.2	n.d.	0.18	0.24	0.23	n.d.	0.24	0.17	n.d.	0.28
Hf	2.55	2.82	n.d.	3.1	n.d.	2.8	n.d.	3.23	n.d.	2.47	3.28	2.92	n.d.	3.26	2.28	n.d.	3.31
Th	0.58	0.6	n.d.	0.45	n.d.	0.19	n.d.	0.59	n.d.	0.54	0.57	0.67	n.d.	0.63	0.52	n.d.	0.64

Table 1 (continue)

	SR0741 -7.90	SR0750 -12.45	SR0756 -13.25	SR0762 -4.60	SR0768 -11.20	SR0776 -17.70	SR0778 -3.20	SR0791 -9.50	SR0796 -6.70	SR0800 -13.20	SR0814 -14.40	SR0826 -20.60	SR0836 -5.80	SR0842 -2.35	SR0846 -2.80	SR0850 -5.95	SR0855 -0.10
Depth (mbsl)	2009.8	2062.7	2098.6	2123.7	2157.4	2209.5	2218.2	2280.2	2300.2	2321.6	2357.0	2414.1	2467.3	2503.5	2525.4	2550.9	2581.8
Rock Type	pillow	pillow	pillow	pillow	Hyalo-clastite	Hyalo-clastite	Hyalo-clastite	pillow	pillow	pillow	pillow	pillow	pillow	massive	Hyalo-clastite	Hyalo-clastite	Hyalo-clastite
UNIT	U0278	U0283	U0284	U0284	U0285	U0286	U0287	U0288	U0290	U0291	U0292	U0293	U0295	U0298	U0303	U0305	U0305
ICP-MS																	
Rb	2.82	3.04	3.83	3.86	6.41	6.20	4.66	0.960	3.11	2.70	1.24	3.07	1.50	6.17	5.20	9.68	6.44
Sr	254	243	225	221	302	319	277	289	295	241	262	256	243	249	286	359	278
Y	22.7	20.8	19.6	19.3	30.5	31.0	25.9	23.8	23.7	22.9	23.2	23.3	22.3	23.1	30.5	39.1	30.9
Zr	114	105	101	98.3	166	168	134	150	127	115	123	122	112	118	164	227	165
Nb	11.6	10.3	9.55	9.54	13.5	13.6	11.1	15.1	11.9	11.3	12.0	12.0	10.7	11.4	13.5	21.3	14.0
Ba	70.3	54.7	61.9	64.3	102	98.6	80.4	64.1	102	89.8	63.5	103	73.7	104	95.2	146	97.4
La	9.27	8.13	7.64	7.95	11.7	11.5	9.48	11.7	10.1	8.83	9.58	9.38	8.65	9.35	11.3	17.0	11.8
Ce	22.8	21.3	19.3	19.3	29.7	28.2	24.5	29.4	24.3	22.0	23.6	23.8	21.6	22.8	28.7	42.3	29.5
Pr	3.40	3.18	2.95	2.99	4.61	4.39	3.80	4.35	3.65	3.42	3.65	3.63	3.32	3.55	4.44	6.41	4.60
Nd	15.9	14.3	13.7	14.0	21.6	21.5	18.0	20.0	17.4	15.6	17.2	16.7	15.6	16.6	20.9	29.1	21.9
Sm	4.17	3.86	3.67	3.64	5.83	5.74	4.85	5.25	4.52	4.18	4.59	4.44	4.29	4.38	5.76	7.69	5.88
Eu	1.43	1.35	1.23	1.24	1.98	1.91	1.63	1.75	1.54	1.45	1.55	1.50	1.45	1.49	1.94	2.51	1.94
Gd	4.44	4.20	3.94	3.88	6.08	6.09	5.11	5.36	4.92	4.54	4.87	4.69	4.47	4.69	6.01	7.80	6.14
Tb	0.720	0.683	0.646	0.634	1.02	0.944	0.866	0.846	0.832	0.757	0.802	0.767	0.743	0.768	1.02	1.262	1.031
Dy	4.09	3.79	3.64	3.54	5.60	5.44	4.67	4.52	4.40	4.17	4.31	4.39	4.17	4.33	5.54	7.19	5.62
Ho	0.803	0.740	0.704	0.713	1.09	1.04	0.938	0.860	0.887	0.808	0.870	0.843	0.805	0.835	1.07	1.36	1.10
Er	2.08	1.84	1.75	1.77	2.80	2.69	2.32	2.09	2.15	2.04	2.20	2.09	2.03	2.15	2.62	3.51	2.79
Tm	0.276	0.267	0.251	0.251	0.393	0.361	0.326	0.287	0.311	0.283	0.309	0.334	0.284	0.300	0.388	0.456	0.390
Yb	1.71	1.60	1.46	1.51	2.25	2.16	1.95	1.73	1.84	1.69	1.77	1.73	1.64	1.76	2.18	2.83	2.26
Lu	0.242	0.224	0.218	0.207	0.318	0.309	0.273	0.235	0.248	0.236	0.253	0.244	0.230	0.239	0.314	0.380	0.322
Hf	2.96	2.80	2.49	2.53	4.25	3.80	3.50	3.65	3.21	2.93	3.24	3.14	2.95	3.19	4.10	5.34	4.21
Ta	0.973	0.852	0.767	0.782	1.06	1.08	0.937	1.031	0.836	0.755	0.842	0.804	0.756	0.842	1.00	1.53	1.14
Pb	0.857	0.893	0.664	0.693	1.09	0.848	0.701	0.952	0.816	0.779	0.810	0.856	0.760	0.872	0.909	1.24	0.896
Th	0.708	0.623	0.591	0.617	0.908	0.859	0.747	0.909	0.767	0.704	0.793	0.727	0.648	0.741	0.873	1.36	0.982
U	0.216	0.204	0.184	0.180	0.315	0.360	0.246	0.305	0.267	0.229	0.304	0.276	0.206	0.222	0.294	0.590	0.391
INAA																	
Na_2O	1.71	1.61	1.48	1.53	2.09	2.11	1.8	1.58	1.57	1.52	1.41	1.57	n.d.	1.65	1.98	2.45	2.08
Cr	812	787	865	874	187	346	723	527	541	617	552	564	n.d.	595	523	195	407
Sc	24.2	23.5	22.7	23.2	29.2	30.5	29.1	24.8	25.8	25	25.5	25.7	n.d.	25.2	27.6	27.8	27.9
La	8.75	8.01	7.51	7.63	11.4	11.1	9.11	11.5	9.41	8.84	9.18	9.05	n.d.	8.68	10.7	16	11.6
Ce	22.5	21.1	18.9	19.7	29.1	29.4	24.4	29.9	24.2	22.8	24.2	23.7	n.d.	23.2	28.2	41.9	30.3
Nd	12.8	13.2	12.9	13.6	19.7	19.7	16.5	20.4	16.9	15.1	16.7	16.1	n.d.	15.3	20	28.4	21.5
Sm	3.89	3.69	3.48	3.5	5.7	5.56	4.69	5.17	4.41	4.15	4.32	4.26	n.d.	4.16	5.33	7.18	5.57
Eu	1.36	1.3	1.23	1.21	1.98	1.89	1.67	1.72	1.53	1.43	1.52	1.45	n.d.	1.46	1.87	2.4	1.89
Tb	0.63	0.61	0.58	0.59	0.87	0.92	0.73	0.78	0.79	0.73	0.68	0.96	n.d.	0.69	0.89	1.17	0.97
Yb	1.53	1.36	1.34	1.46	2.16	2.01	1.66	1.63	1.65	1.54	1.64	1.68	n.d.	1.67	2.04	2.58	2.2
Lu	0.23	0.2	0.21	0.2	0.29	0.28	0.26	0.23	0.24	0.23	0.23	0.24	n.d.	0.23	0.28	0.36	0.29
Hf	2.7	2.5	2.31	2.41	3.91	3.98	3.28	3.6	3.03	2.8	2.93	3.04	n.d.	2.93	3.78	5.38	4.02
Th	0.64	0.73	0.54	0.52	0.73	0.6	0.67	0.75	0.61	0.68	0.61	0.55	n.d.	0.37	0.52	1.1	0.71

Table 1 (continue)

	SR0860 -8.10	SR0871 -13.00	SR0891 -15.10	SR0896 -2.40	SR0899 -2.45	SR0907 -1.65	SR0913 -2.40	SR0916 -1.15	SR0930 -15.85	SR0939 -18.10	SR0940 -18.35	SR0954 -8.00	SR0956 -18.35	SR0964 -4.30	SR0967 -2.75
Depth (mbsl)	2615.0	2654.1	2730.2	2759.3	2770.9	2789.9	2825.8	2837.6	2919.5	2961.0	2967.8	3009.2	3019.0	3058.0	3068.9
Rock Type	pillow	pillow	pillow	Hyalo-clastite	pillow	pillow	intrusive	pillow	pillow	pillow	intrusive	pillow	intrusive	pillow	pillow
UNIT	U0310e	U0312	U0316	U0319	U0320	U0321	U0327	U0330	U0333	U0335a	U0336c	U0339	U0341b	U0340e	U0343a
ICP-MS															
Rb	5.61	3.32	1.84	4.71	3.67	4.98	4.09	3.44	2.36	3.75	3.95	3.95	6.80	2.00	4.32
Sr	348	246	171	278	248	284	240	233	185	240	264	214	360	125	225
Y	27.6	20.9	18.1	25.9	23.0	26.6	24.0	21.5	18.3	24.9	23.1	20.8	28.7	11.8	22.3
Zr	155	108	90.2	132	117	135	117	115	96.7	138	118	116	155	65.4	120
Nb	15.2	10.6	7.29	10.7	9.29	11.1	9.57	9.89	8.12	11.6	11.6	9.86	15.4	5.42	9.58
Ba	114	74.0	68.8	70.6	76.4	87.7	69.8	61.2	71.3	90.0	84.5	79.4	126	43.4	77.1
La	12.2	8.63	6.19	9.15	7.97	9.36	7.89	7.63	6.89	9.11	8.99	8.08	12.5	4.13	8.41
Ce	30.5	21.8	15.7	23.6	20.7	23.4	20.2	20.0	17.0	22.7	22.8	20.5	30.8	11.1	21.1
Pr	4.52	3.32	2.52	3.65	3.10	3.72	3.19	3.01	2.71	3.62	3.48	3.23	4.71	1.65	3.25
Nd	20.8	14.4	12.2	17.7	15.2	17.9	15.5	14.4	12.8	16.5	16.2	14.9	21.2	7.68	15.4
Sm	5.68	3.89	3.28	5.01	4.15	4.78	4.38	4.00	3.41	4.50	4.23	4.14	5.64	2.22	4.41
Eu	1.93	1.38	1.13	1.68	1.45	1.71	1.50	1.37	1.16	1.53	1.48	1.38	1.89	0.745	1.44
Gd	5.84	4.28	3.61	5.21	4.57	5.31	4.66	4.42	3.61	5.02	4.60	4.42	5.89	2.42	4.72
Tb	0.937	0.688	0.591	0.864	0.756	0.862	0.788	0.696	0.595	0.783	0.752	0.710	0.937	0.386	0.748
Dy	5.27	3.98	3.26	4.76	4.19	4.93	4.36	3.94	3.40	4.36	4.23	3.91	5.17	2.18	4.21
Ho	1.02	0.777	0.630	0.947	0.795	0.957	0.858	0.784	0.67	0.838	0.818	0.751	1.02	0.416	0.818
Er	2.52	1.96	1.62	2.37	2.00	2.45	2.18	1.98	1.64	2.15	2.03	1.88	2.57	1.09	2.05
Tm	0.366	0.276	0.232	0.330	0.284	0.332	0.310	0.275	0.231	0.307	0.292	0.269	0.351	0.148	0.293
Yb	2.02	1.63	1.34	1.92	1.69	1.97	1.80	1.64	1.36	1.75	1.70	1.58	2.10	0.884	1.68
Lu	0.283	0.220	0.188	0.273	0.231	0.286	0.264	0.227	0.203	0.252	0.232	0.219	0.288	0.127	0.242
Hf	3.88	2.84	2.39	3.49	2.91	3.53	3.17	3.00	2.51	3.25	3.04	2.95	3.92	1.69	3.15
Ta	1.12	0.861	0.582	0.820	0.658	0.819	0.820	0.661	0.570	0.762	0.774	0.674	1.07	0.385	0.668
Pb	1.06	0.729	0.532	0.749	0.671	0.812	0.665	0.656	0.521	0.691	0.760	0.656	1.08	0.372	0.695
Th	0.990	0.681	0.479	0.699	0.595	0.724	0.644	0.615	0.529	0.741	0.685	0.644	0.963	0.334	0.684
U	0.322	0.215	0.189	0.290	0.230	0.254	0.212	0.227	0.212	0.249	0.205	0.212	0.319	0.144	0.319
INAA															
Na_2O	2.22	1.58	1.11	n.d.	1.65	n.d.	n.d.	n.d.	n.d.	1.6	1.57	n.d.	n.d.	n.d.	n.d.
Cr	314	834	1224	n.d.	824	n.d.	n.d.	n.d.	n.d.	620	1016	n.d.	n.d.	n.d.	n.d.
Sc	29.1	23.5	19.6	n.d.	27.8	n.d.	n.d.	n.d.	n.d.	25.7	24	n.d.	n.d.	n.d.	n.d.
La	11.8	8.21	5.81	n.d.	7.71	n.d.	n.d.	n.d.	n.d.	8.63	9.04	n.d.	n.d.	n.d.	n.d.
Ce	30.9	21.1	16	n.d.	20.8	n.d.	n.d.	n.d.	n.d.	22.6	23.2	n.d.	n.d.	n.d.	n.d.
Nd	20.7	12.9	11.1	n.d.	14.2	n.d.	n.d.	n.d.	n.d.	14.6	16.6	n.d.	n.d.	n.d.	n.d.
Sm	5.31	3.63	3.06	n.d.	3.99	n.d.	n.d.	n.d.	n.d.	4.11	4.48	n.d.	n.d.	n.d.	n.d.
Eu	1.84	1.28	1.07	n.d.	1.42	n.d.	n.d.	n.d.	n.d.	1.4	1.49	n.d.	n.d.	n.d.	n.d.
Tb	0.87	0.67	0.51	n.d.	0.64	n.d.	n.d.	n.d.	n.d.	0.64	0.73	n.d.	n.d.	n.d.	n.d.
Yb	1.98	1.39	1.21	n.d.	1.53	n.d.	n.d.	n.d.	n.d.	1.52	1.68	n.d.	n.d.	n.d.	n.d.
Lu	0.27	0.2	0.18	n.d.	0.22	n.d.	n.d.	n.d.	n.d.	0.23	0.2	n.d.	n.d.	n.d.	n.d.
Hf	3.7	2.51	2.12	n.d.	2.86	n.d.	n.d.	n.d.	n.d.	2.75	3.19	n.d.	n.d.	n.d.	n.d.
Th	0.72	0.5	0.37	n.d.	0.51	n.d.	n.d.	n.d.	n.d.	0.44	0.4	n.d.	n.d.	n.d.	n.d.

Table 2. Comparison of Alkalic Basalt From HSDP Phase 1 and 2 Cores

	Phase 1		Phase 2
Reference Sample	R177-2.60		SR131-6.92
Flow Unit	58		48
	analysis 1	analysis 2	
Depth (m)	331.7		274.7
Age[1] (Ka)	240±14		234±32
Isotopic Ratios[2]			
$^{87}Sr/^{86}Sr$	0.70356		0.703559
$^{176}Hf/^{197}Hf$	0.283129		0.283124
$^{206}Pb/^{204}Pb$	18.437		18.436
$^{207}Pb/^{204}Pb$	15.482		15.479
$^{208}Pb/^{204}Pb$	38.024		37.997
X-ray Fluorescence[3] (U. Mass.)			
SiO_2	43.68	43.60	43.75
TiO_2	3.96	3.95	3.99
Al_2O_3	14.39	14.38	14.40
Fe_2O_3	15.33	15.26	15.33
MnO	0.19	0.19	0.19
MgO	8.21	8.05	8.27
CaO	9.77	9.77	9.83
Na_2O	3.24	2.99	2.72 (2.81)
K_2O	0.84	0.84	0.84
P_2O_5	0.47	0.48	0.49
Rb	15.0		13.8
Sr	628		613
Ba	253		242
V	267		271
Cr	116		134
Ni	151		137
Zn	129		136
Y	34.8		34.1
R	287		283
Nb	28.0		27.3
Instrumental Neutron Activation[3] (MIT)			
Sc	25.5		25.8
Cr	127		129
La	23.7		23.6
Ce	59.3		59.6
Nd	36.5		39.1
Sm	9.00		9.30
Eu	3.13		3.10
Tb	1.31		1.40
Yb	2.40		2.41
Lu	0.33		0.33
Hf	6.58		6.61
Th	1.51		1.68

1) Argon isochron ages are for samples R177-6.0 and SR132-1.5 which are from the same units as the respective reference samples (Sharp et al., 1996; 2005).

2) Isotopic data from Lassiter and Hauri (1998), Blichert-Toft and Albarede (1999), Abouchami et al. (2000), Blichert-Toft et al. (2003), Bryce et al. (2005).

3) Oxides in wt.%, trace elements in ppm. Phase 1 abundances data from Rhodes (1996) and Yang et al. (1996). The second column of major element data for R177-2.60 indicates result from a second (April, 2003) analysis; the agreement with the first analysis is excellent except for Na_2O which was the only significant difference between R177-2.60 and SR131-6.92. The new Na_2O value for R177-2.60 is in better agreement with the SR131-6.42 value. Phase 2 abundance data from Rhodes and Vollinger (2002) and this paper. Na_2O value in parentheses was determined by INAA.

Table A1-a. Isotopes Analyzed by ICP-MS at MIT

Sc 45
Cr 53
Ni 61
Ni 62
Se 77
Rb 85
Sr 86
Y 89
Zr 91
Nb 93
In 115
Cs 133
Ba 135
Ba 137
La 139
Ce 140
Pr 141
Nd 143
Nd 145
Sm 147
Sm 149
Eu 151
Sm 152
Eu 153
Tb 159
Gd 160
Dy 163
Ho 165
Er 167
Tm 169
Yb 174
Lu 175
Hf 178
Hf 179
Ta 181
Pb 206
Pb 208
Bi 209
Th 232
U 238

Table A1-b. MIT ICP-MS Typical Procedure

Position	SOLUTION
1	EDM
2	STD
3	UNKNOWN
4	UNKNOWN
5	UNKNOWN
6	UNKNOWN
7	EDM
8	STD
9	UNKNOWN
10	UNKNOWN
11	UNKNOWN
12	UNKNOWN
13	EDM
14	STD
15	UNKNOWN
16	UNKNOWN
17	UNKNOWN
18	BLANK
19	EDM
20	STD
21	UNKNOWN
22	UNKNOWN
23	UNKNOWN
24	UNKNOWN
25	EDM
26	STD
27	UNKNOWN
28	UNKNOWN
29	UNKNOWN
30	UNKNOWN
31	EDM
32	STD
33	UNKNOWN
34	UNKNOWN
35	UNKNOWN
36	UNKNOWN
37	EDM

EDM	external drift monitor solution
STD	standard sample solution
BLANK	blank solution
UNKNOWN	unknown solution

Table A-2. Trace element abundances (ppm) in 3 USGS standard samples used in ICP-MS at MIT

	AGV-1	BCR-1	BHVO-1
Rb	68	48	9.50
Sr	655	326	390
Y	21	39	27.6
Zr	227	190	179
Nb	14.5	12.5	19.0
Ba	1223	687	133
La	38	24.9	15.5
Ce	67	53.7	39.0
Pr	8.45	6.88	5.70
Nd	31.6	28.8	25.2
Sm	5.9	6.6	6.20
Eu	1.64	1.95	2.06
Gd	5	6.69	6.03
Tb	0.664	1.068	0.96
Dy	3.6	6.35	5.20
Ho	0.69	1.315	0.990
Er	1.856	3.7	2.40
Tm	0.34	0.56	0.330
Yb	1.644	3.35	2.02
Lu	0.248	0.505	0.278
Hf	5	4.97	4.38
Ta	0.9	0.81	1.23
Pb	36	13.5	2.10
Th	6.5	6.19	1.16
U	1.92	1.7	0.420

Table A-3. Trace element abundances in BHVO-2 analyzed by MIT ICP-MS and other techniques

	MIT ICPMS		MIT INAA		Lin et al. ICP-MS		Raczek et al. *		USGS recommend	
	mean of 11	uncertainty(%)	mean of 6	uncertainty(%)	mean of 6	uncertainty(%)	mean of 3	uncertainty(%)	mean	uncertainty(%)
Rb	9.48	1			9.04	5.8	9.08	0.7	9.8	10
Sr	399	2			399	3.1	396	0.2	389	6
Y	28.3	2			25.6	5			26	8
Zr	178	1			170	4.7			172	6
Nb	19.0	1			18.2	4.7			18	11
Ba	135	2			134	4.5	131		130	10
La	15.2	2	14.8	2	15.1	2.7	15.2	0.4	15	7
Ce	38.4	1	38.8	1	37.6	4.6	37.5	0.3	38	5
Pr	5.57	1			5.13	1.2	5.29	0.9		
Nd	24.9	1	24.6	3	25.1	1	24.5		25.0	7
Sm	6.16	1	6.0	1	6.31	5.1	6.07	0.1	6.2	6
Eu	2.03	1	2.01	1	1.94	3.5	2.07	0.7		
Gd	6.13	2			5.76	6.1	6.24	0.4	6.3	3
Tb	0.963	2	0.88	5	0.9	3.3	0.936	1.7	0.9	
Dy	5.30	2			5.3	2	5.31	0.3		
Ho	1.01	2			1.05	2.7	0.972		1.04	4
Er	2.50	1			2.68	8.9	2.54	0.2		
Tm	0.350	3			0.35	7.1	0.341	2.3		
Yb	2.05	1	1.89	3	2.2	6	2.00	0.3	2	10
Lu	0.286	3	0.275	4	0.3	5.7	0.274		0.28	4
Hf	4.42	2	4.2	2	4.52	6.2			4.1	7
Ta	1.22	2	1.04	5	1.35	3.7			1.4	
Pb	1.53	2								
Th	1.30	3	1.06	2	1.2	12			1.2	25
U	0.446	2			0.45	10				

uncertainty = (1 s/mean)x100%

* All element abundances were determined by ID-TIMS, except for Pr, Tb, Ho and Tm which were determined by MIC-SSMS.

Table A-4. Input Parameters for Melting Model

	Mineral Proportions						Source Composition				
	Olivine	OPX	CPX	Sp	Grt		Nb/Zr	La/Sm	La/Yb	Sm/Yb	Ti/Zr
Source Mode[1]											
Grt Peridotite	0.53	0.04	0.33	0	0.1		0.076	1.9	1.8	0.9	80
Sp Peridotite	0.53	0.2	0.25	0.02	0	normalized to PM	1.20	1.20	1.22	1.02	0.72
Melting Reaction[1]											
Grt Peridotite	0.05	-0.49	1.31	0	0.13						
Sp Peridotite	0.375	-0.5	1.125	0	0						

	Partition Coefficients						
	OPX [2]			CPX			
	Grt Peridotite	Sp Peridotite	Olivine	Grt Peridotite [3]	Sp Peridotite[4]	Spinel	Garnet[3]
La	0.00001	0.00008	0	0.008[5]	0.045[5]	0	0.023[5]
Sm	0.00083	0.0038	0	0.07	0.319	0	0.318
Yb	0.02	0.0569	0	0.174	0.503	0	5.17
Nb	0.00022	0.0013	0	0.008	0.045	0	0.023
Zr	0.0013	0.0066	0	0.027	0.138	0	0.411
Ti	0.017	0.087	0	0.081[6]	0.414[6]	0	0.2/0.03[7]

(1) from Table 2 of Salters (1996)
(2) calculated using $K_d^{OPX/CPX}$ values of sample 2905 from Eggins et al., 1998
(3) from Salters and Longhi, 1999, sample TM 694-6 (2.8GPa and 1537°C)
(4) from Salters and Longhi, 1999, sample TM 1094-9 (1.5GPa and 1502°C)
(5)$Kd_{La}^{CPX/melt} = Kd_{Nb}^{CPX/melt}$ and $Kd_{La}^{Grt/melt} = Kd_{Nb}^{Grt/melt}$ are assumed.
(6)Since $(Ti/Zr)_{CPX}/(Ti/Zr)_{melt}$ is ~3 (Hart and Dunn, 1993; Skulski et al., 1994; Johnson, 1998), $Kd_{Ti}^{CPX/melt}=3Kd_{Zr}^{CPX/melt}$.
(7)Since $Kd_{Ti}^{Grt/CPX}$ ranges from 0.4 to 2 (Harte and Kirkley, 1997), two values are used for $Kd_{Ti}^{Grt/melt}$. In model "garnet peridotite a", $Kd_{Ti}^{Grt/melt} = 0.2$;
in model "garnet peridotite b", $Kd_{Ti}^{Grt/melt} = 0.03$. These yield $(Ti/Zr)_{grt}/(Ti/Zr)_{melt} = 0.07$ and 0.49; the latter value is similar to the ratio (0.3 to 0.7) found by van Westrenen et al. (1999).

Figure 1

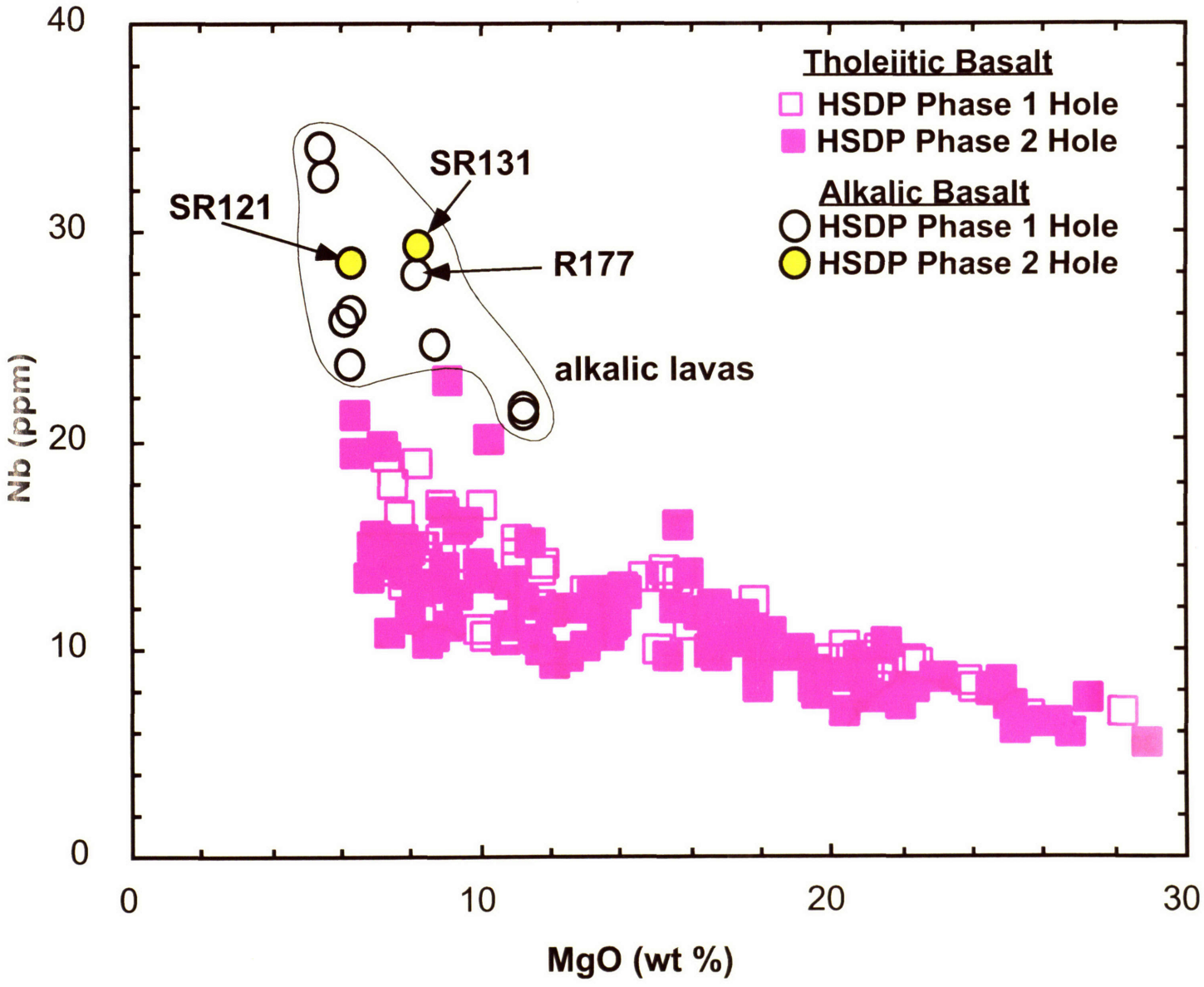
Tholeiitic Basalt
HSDP Phase 1 Hole
HSDP Phase 2 Hole
Alkalic Basalt
HSDP Phase 1 Hole
HSDP Phase 2 Hole
SR131
SR121
R177
alkalic lavas
Nb (ppm)
MgO (wt %)
0
10
20
30
40

Figure 2

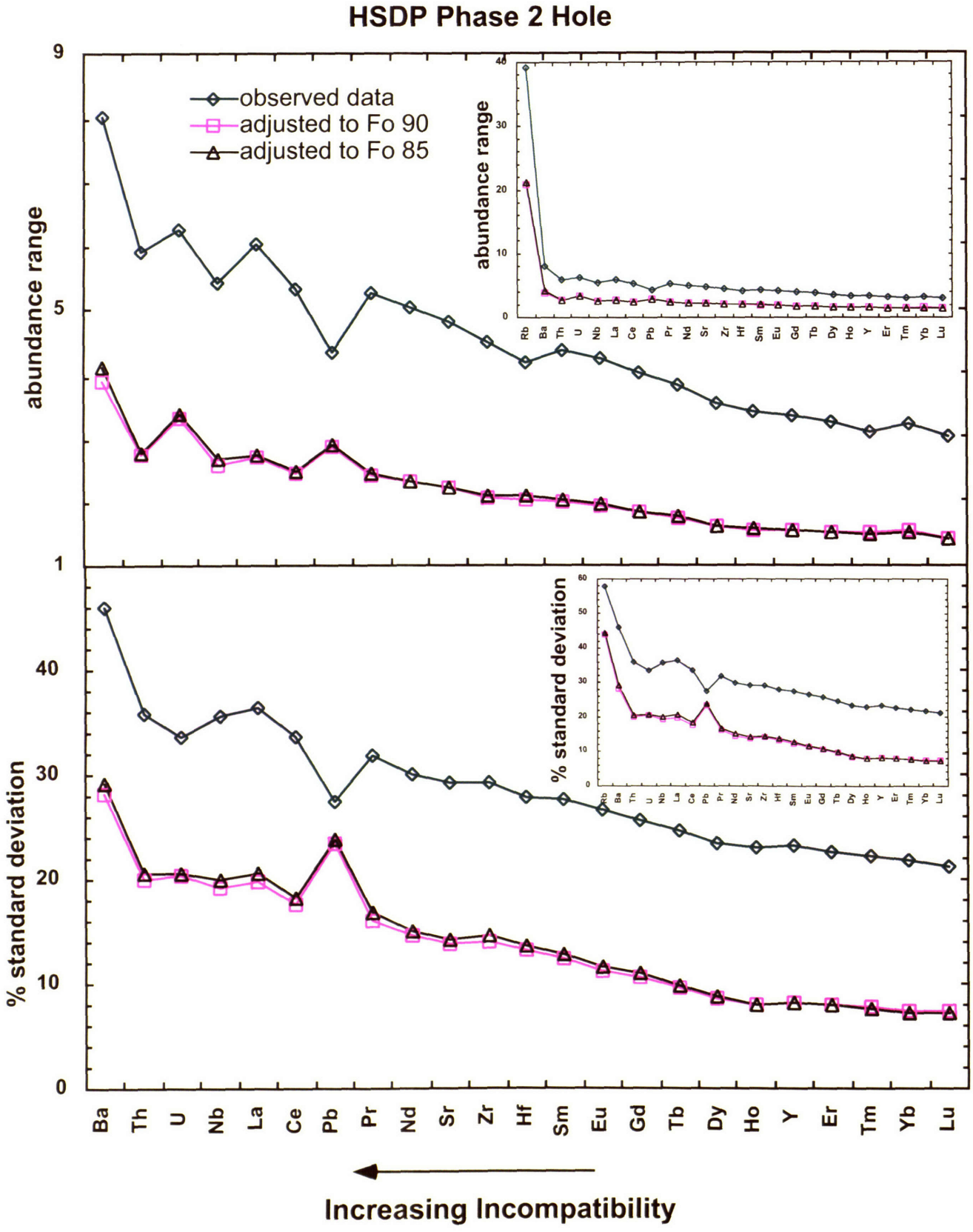
HSDP Phase 2 Hole
observed data
adjusted to Fo 90
adjusted to Fo 85
abundance range
% standard deviation
Ba Th U Nb La Ce Pb Pr Nd Sr Zr Hf Sm Eu Gd Tb Dy Ho Y Er Tm Yb Lu
Increasing Incompatibility

Figure 3a

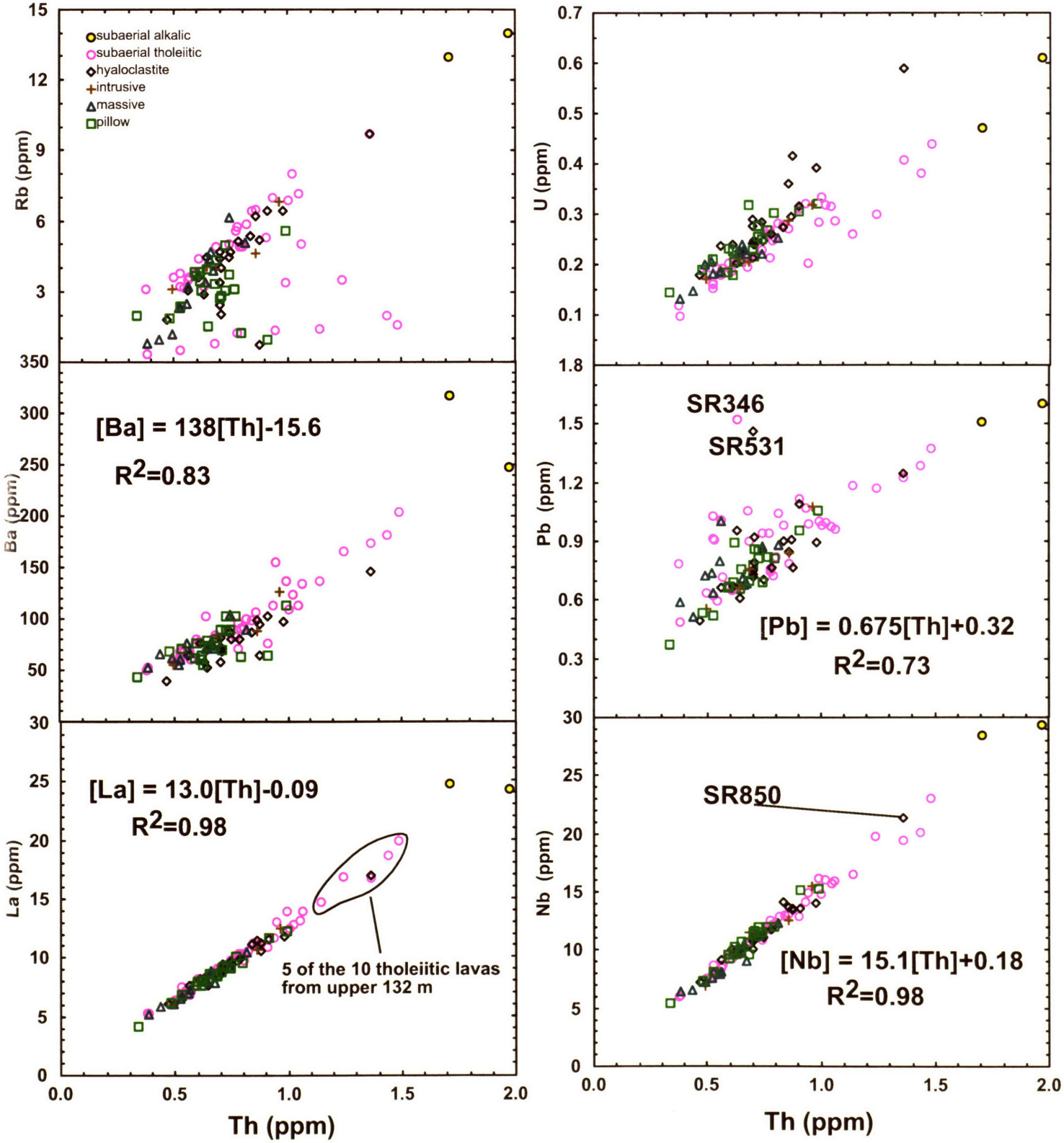
subaerial alkalic
subaerial tholeiitic
hyaloclastite
intrusive
massive
pillow
Rb (ppm)
U (ppm)
Ba (ppm)
[Ba] = 138[Th]-15.6
R2=0.83
SR346
SR531
Pb (ppm)
[Pb] = 0.675[Th]+0.32
R2=0.73
La (ppm)
[La] = 13.0[Th]-0.09
R2=0.98
5 of the 10 tholeiitic lavas from upper 132 m
SR850
Nb (ppm)
[Nb] = 15.1[Th]+0.18
R2=0.98
Th (ppm)
Th (ppm)

Figure 3b

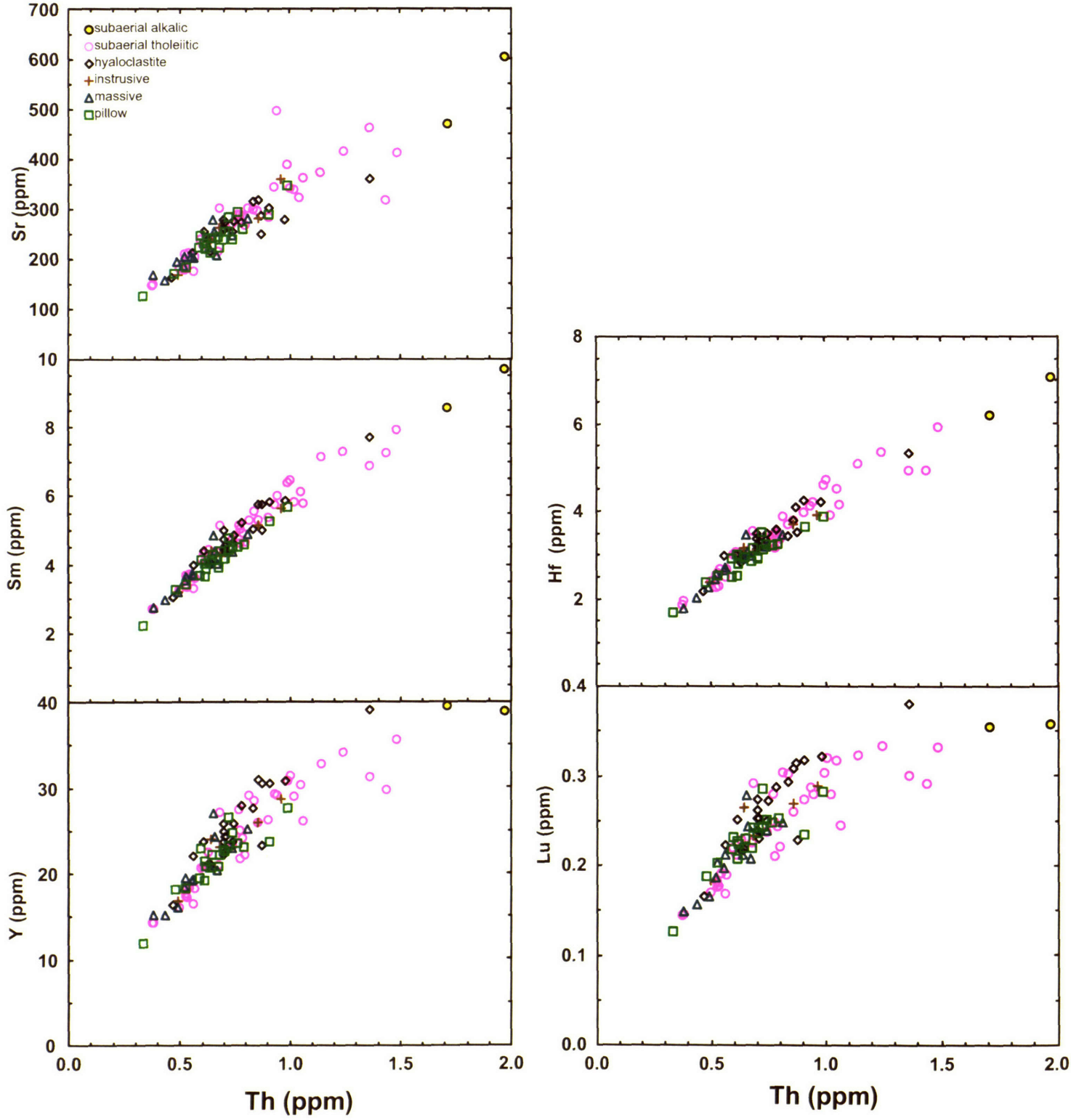
subaerial alkalic
subaerial tholeiitic
hyaloclastite
instrusive
massive
pillow
Sr (ppm)
Sm (ppm)
Y (ppm)
Hf (ppm)
Lu (ppm)
Th (ppm)
Th (ppm)

Figure 4

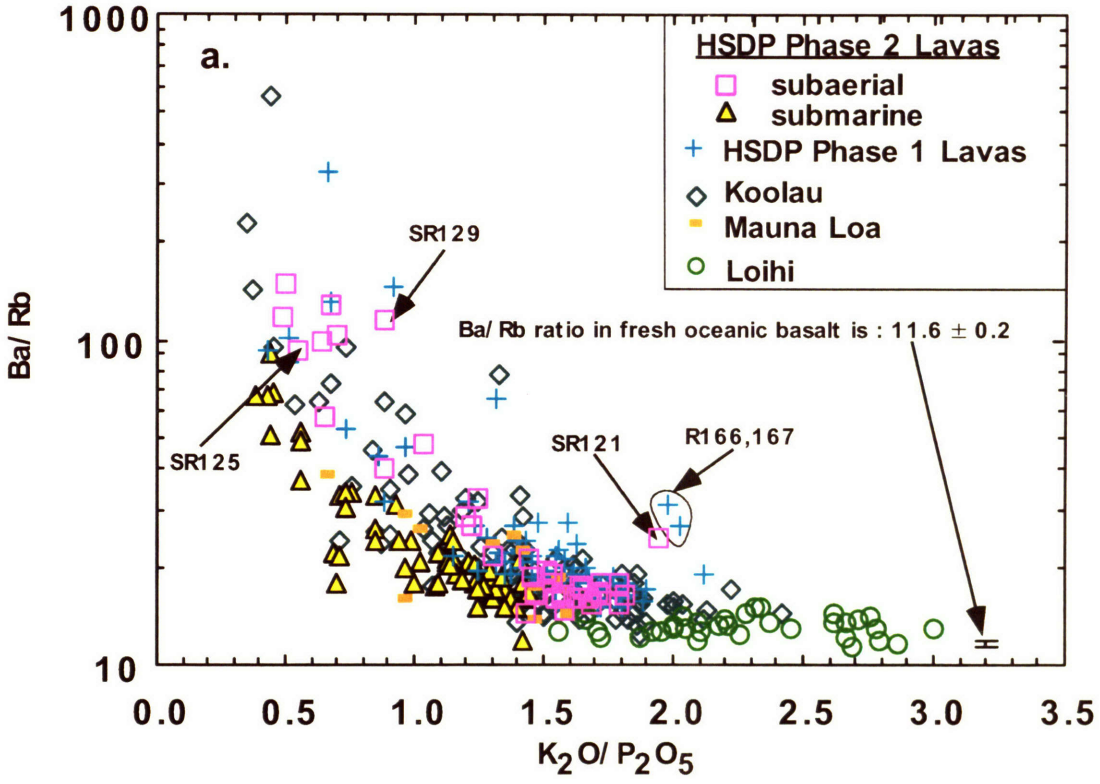
a.
HSDP Phase 2 Lavas
subaerial
submarine
HSDP Phase 1 Lavas
Koolau
Mauna Loa
Loihi
Ba/ Rb ratio in fresh oceanic basalt is : 11.6 ± 0.2
SR129
SR125
SR121
R166,167
Ba/ Rb
1000
100
10
0.0
0.5
1.0
1.5
2.0
2.5
3.0
3.5
K2O/ P2O5

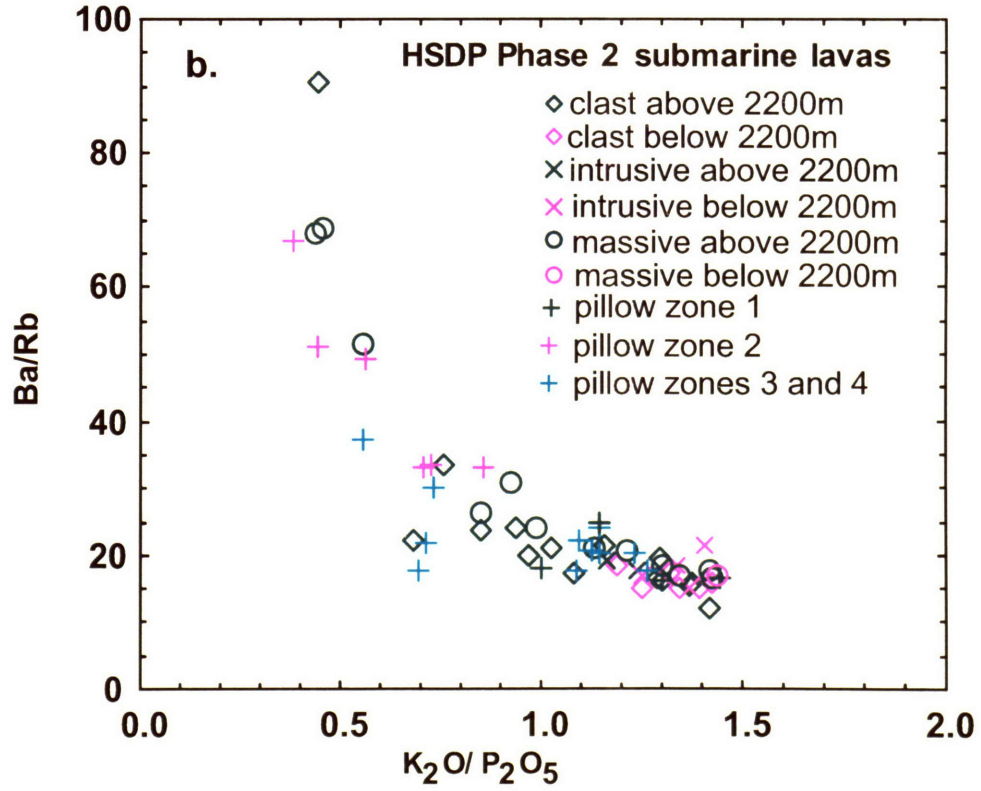
b.
HSDP Phase 2 submarine lavas
clast above 2200m
clast below 2200m
intrusive above 2200m
intrusive below 2200m
massive above 2200m
massive below 2200m
pillow zone 1
pillow zone 2
pillow zones 3 and 4
Ba/Rb
100
80
60
40
20
0
0.0
0.5
1.0
1.5
2.0
K2O/ P2O5

Figure 5

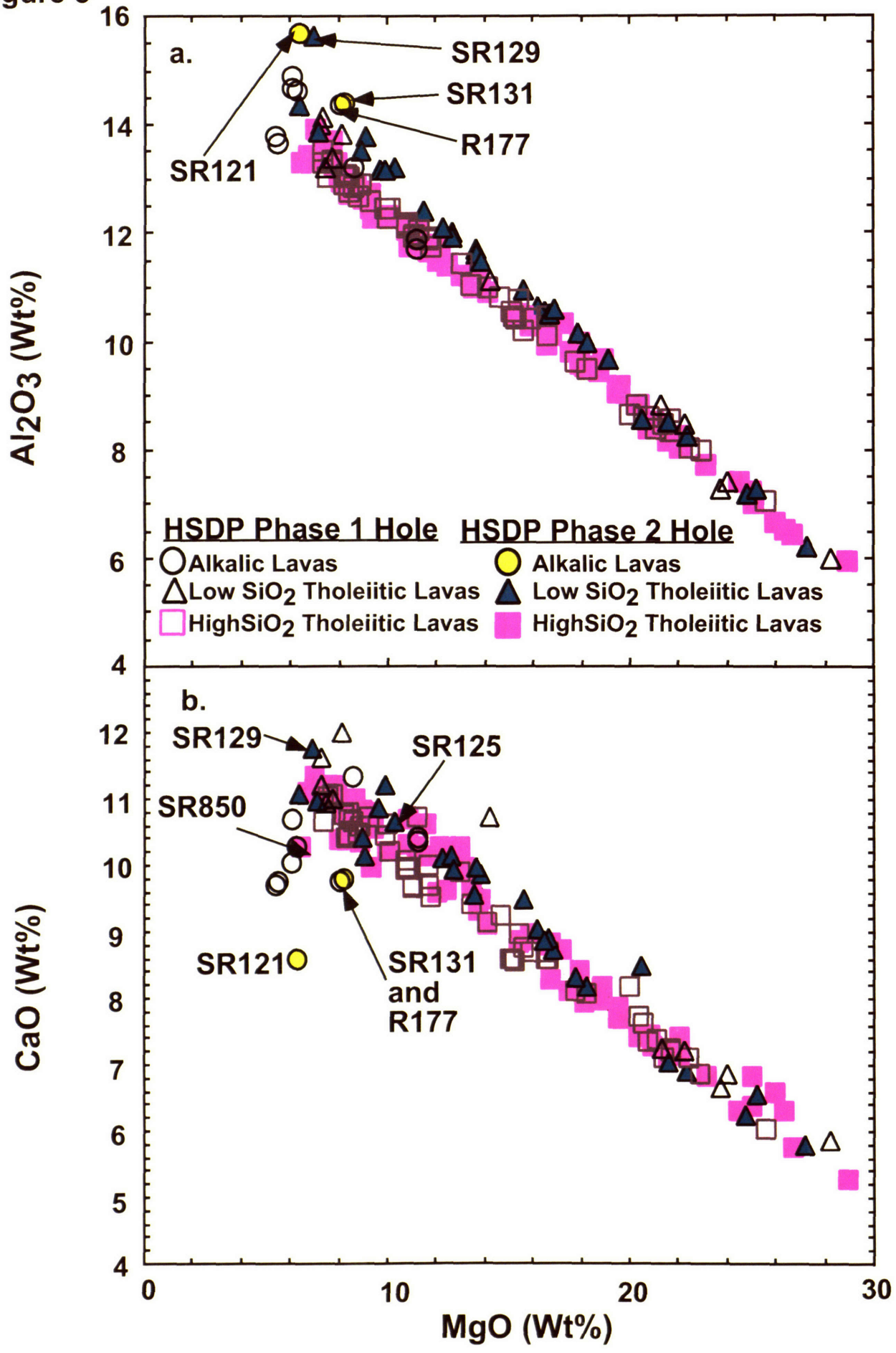
a.
SR129
SR131
R177
SR121
HSDP Phase 1 Hole
Alkalic Lavas
Low SiO2 Tholeiitic Lavas
HighSiO2 Tholeiitic Lavas
HSDP Phase 2 Hole
Alkalic Lavas
Low SiO2 Tholeiitic Lavas
HighSiO2 Tholeiitic Lavas
Al2O3 (Wt%)
b.
SR129
SR125
SR850
SR121
SR131
and
R177
CaO (Wt%)
MgO (Wt%)

Figure 5

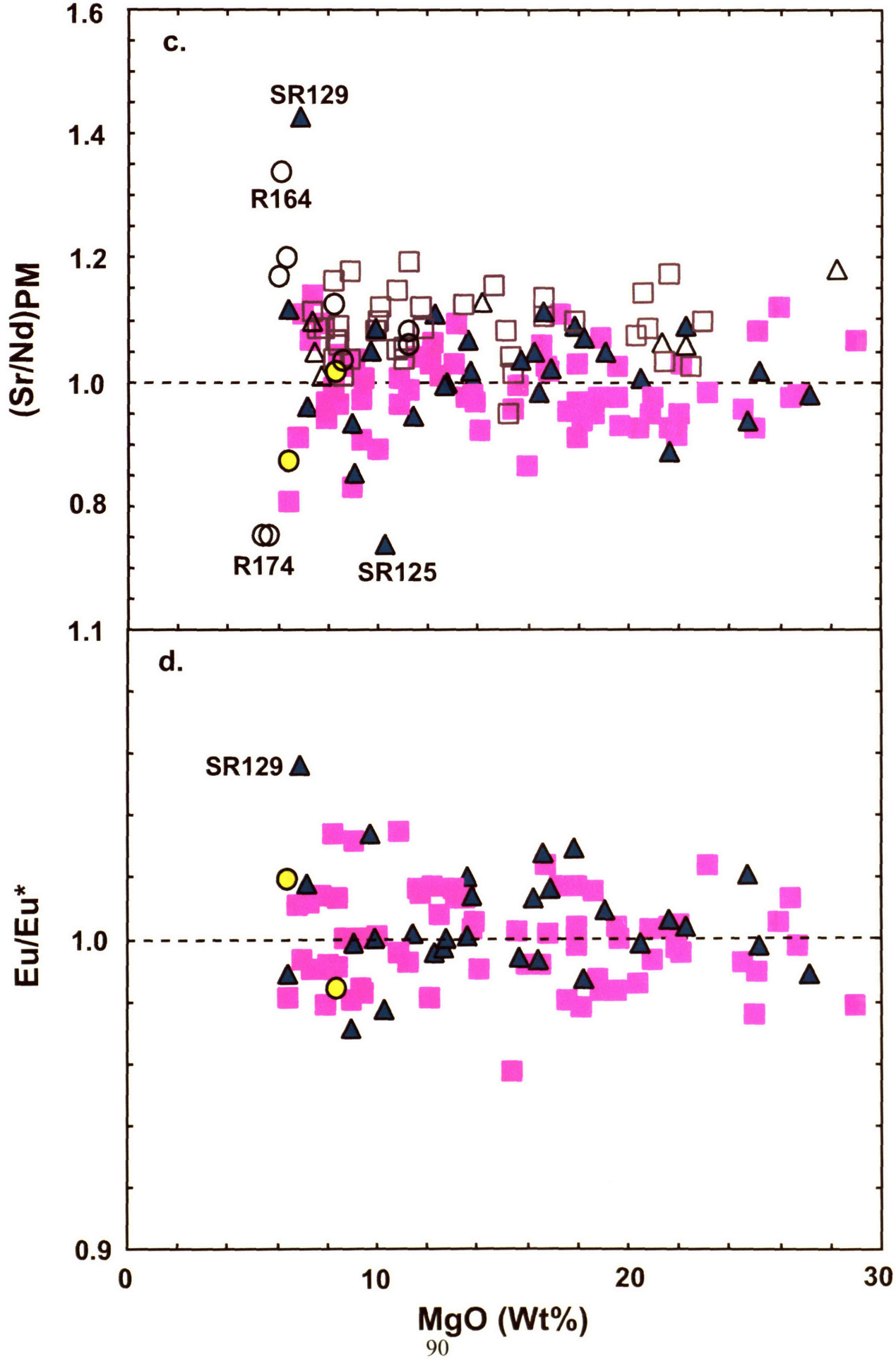
c.
SR129
R164
R174
SR125
(Sr/Nd)PM
1.6
1.4
1.2
1.0
0.8
1.1
d.
SR129
Eu/Eu*
1.0
0.9
0
10
20
30
MgO (Wt%)

Figure 5

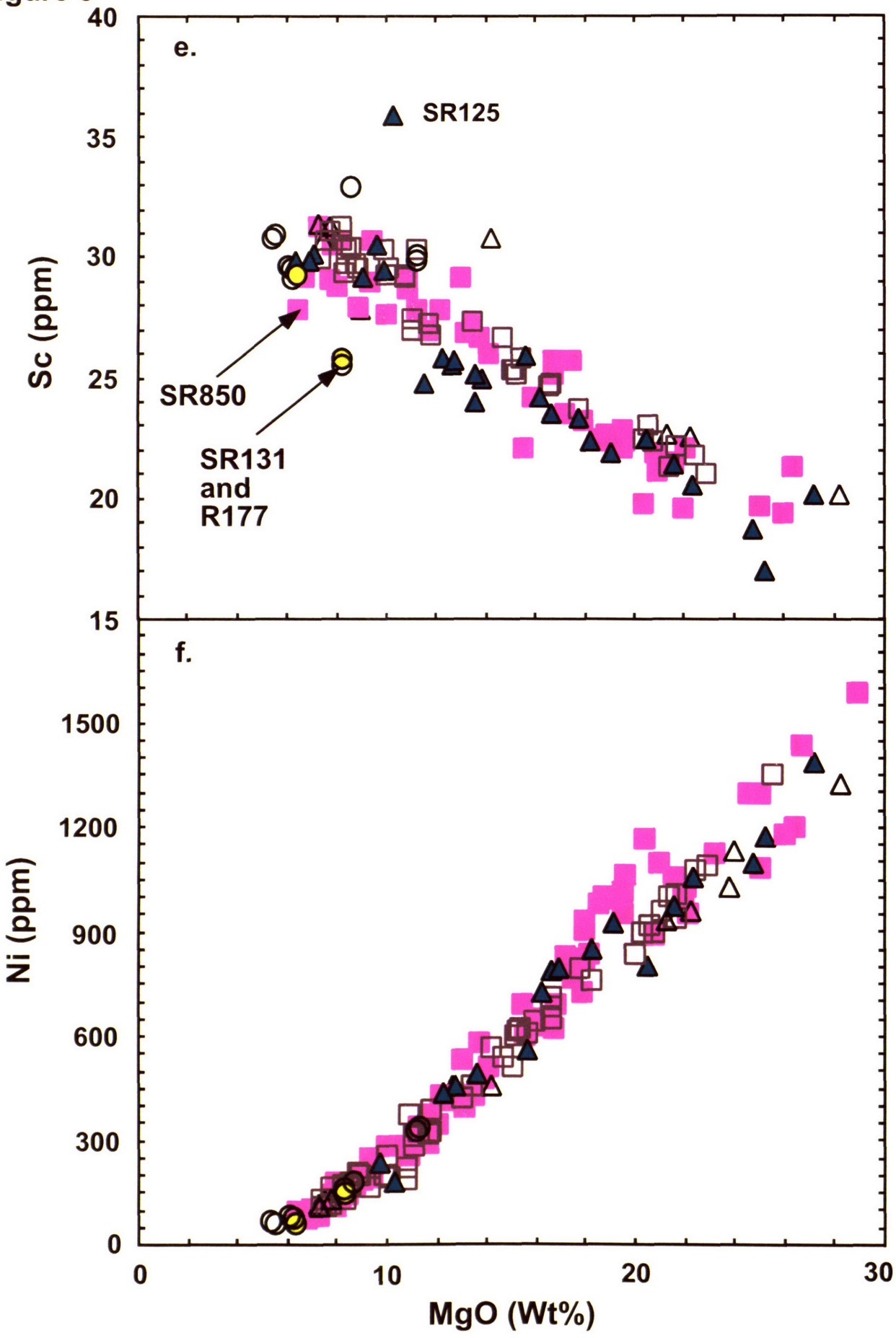
e.
SR125
SR850
SR131
and
R177
Sc (ppm)
40
35
30
25
20
15
f.
Ni (ppm)
1500
1200
900
600
300
0
0
10
20
30
MgO (Wt%)

Figure 6

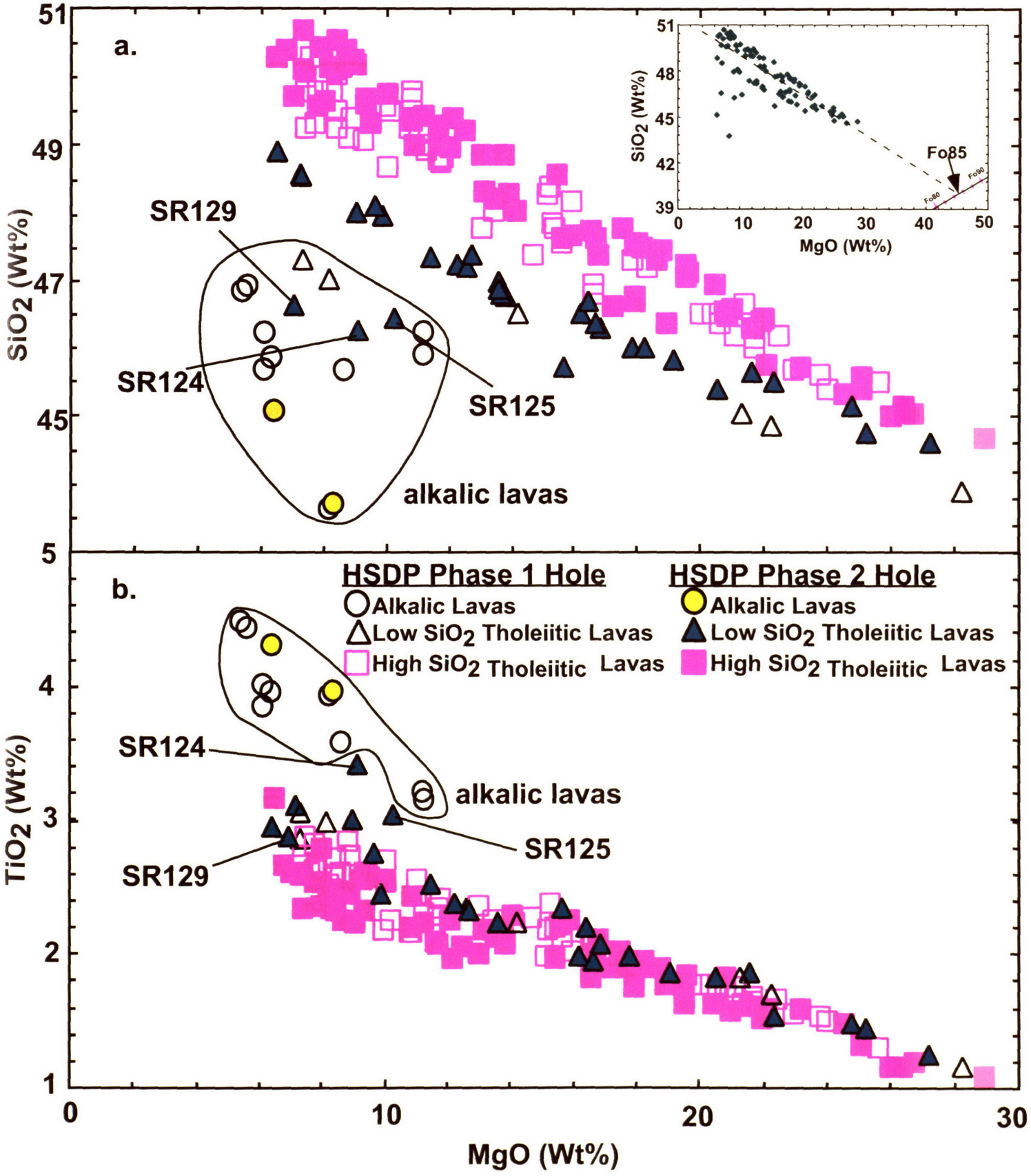
a.
SR129
SR124
SR125
alkalic lavas
SiO2 (Wt%)
51
49
47
45
5
SiO2 (Wt%)
MgO (Wt%)
Fo85
Fo80
Fo90
39
42
48
0
10
20
30
40
50
b.
HSDP Phase 1 Hole
Alkalic Lavas
Low SiO2 Tholeiitic Lavas
High SiO2 Tholeiitic Lavas
HSDP Phase 2 Hole
Alkalic Lavas
Low SiO2 Tholeiitic Lavas
High SiO2 Tholeiitic Lavas
SR124
alkalic lavas
SR125
SR129
TiO2 (Wt%)
4
3
2
1
0
10
20
30
MgO (Wt%)

Figure 6c.

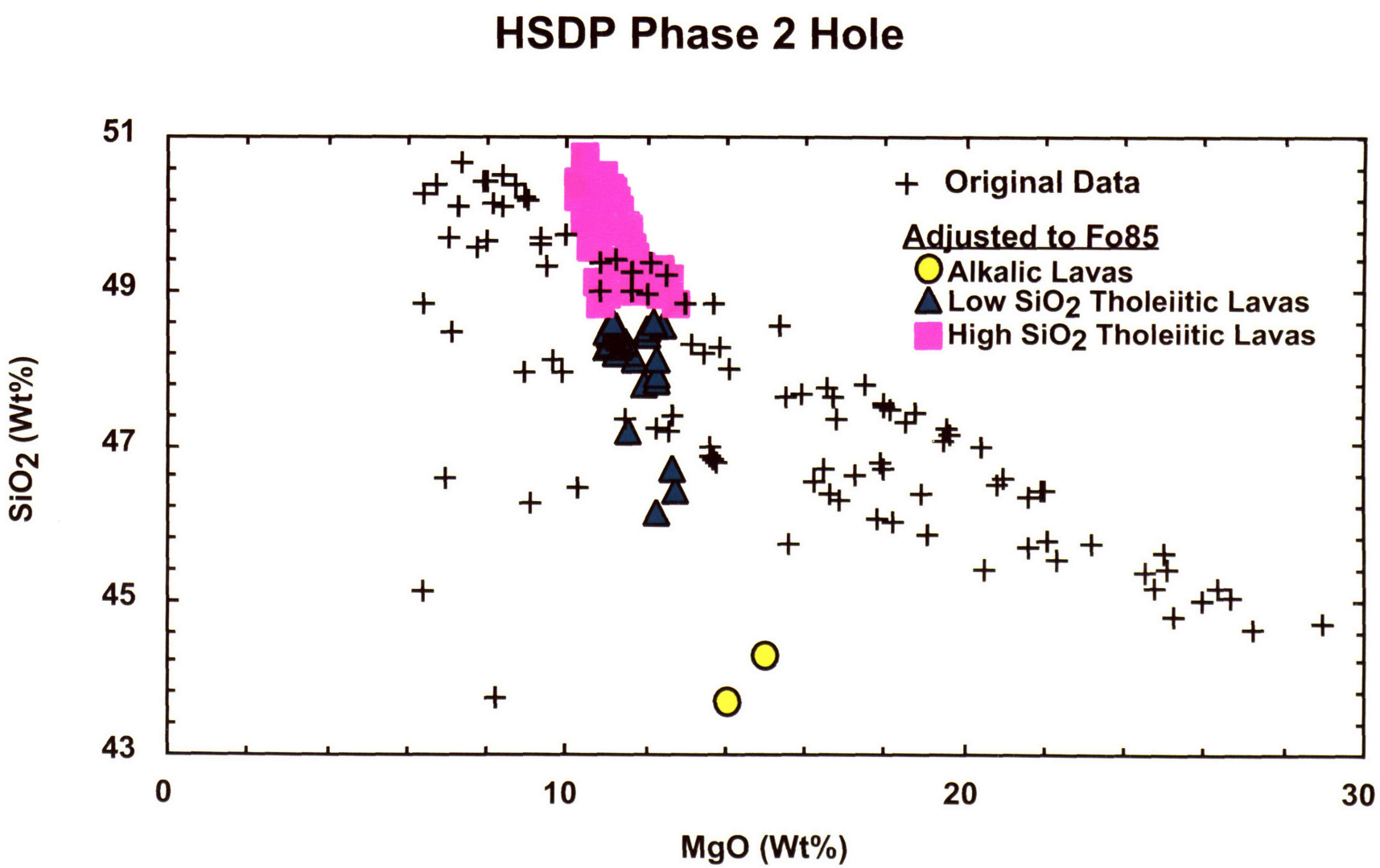
HSDP Phase 2 Hole
Original Data
Adjusted to Fo85
Alkalic Lavas
Low SiO2 Tholeiitic Lavas
High SiO2 Tholeiitic Lavas
SiO2 (Wt%)
MgO (Wt%)
51
49
47
45
43
0
10
20
30

Figure 7

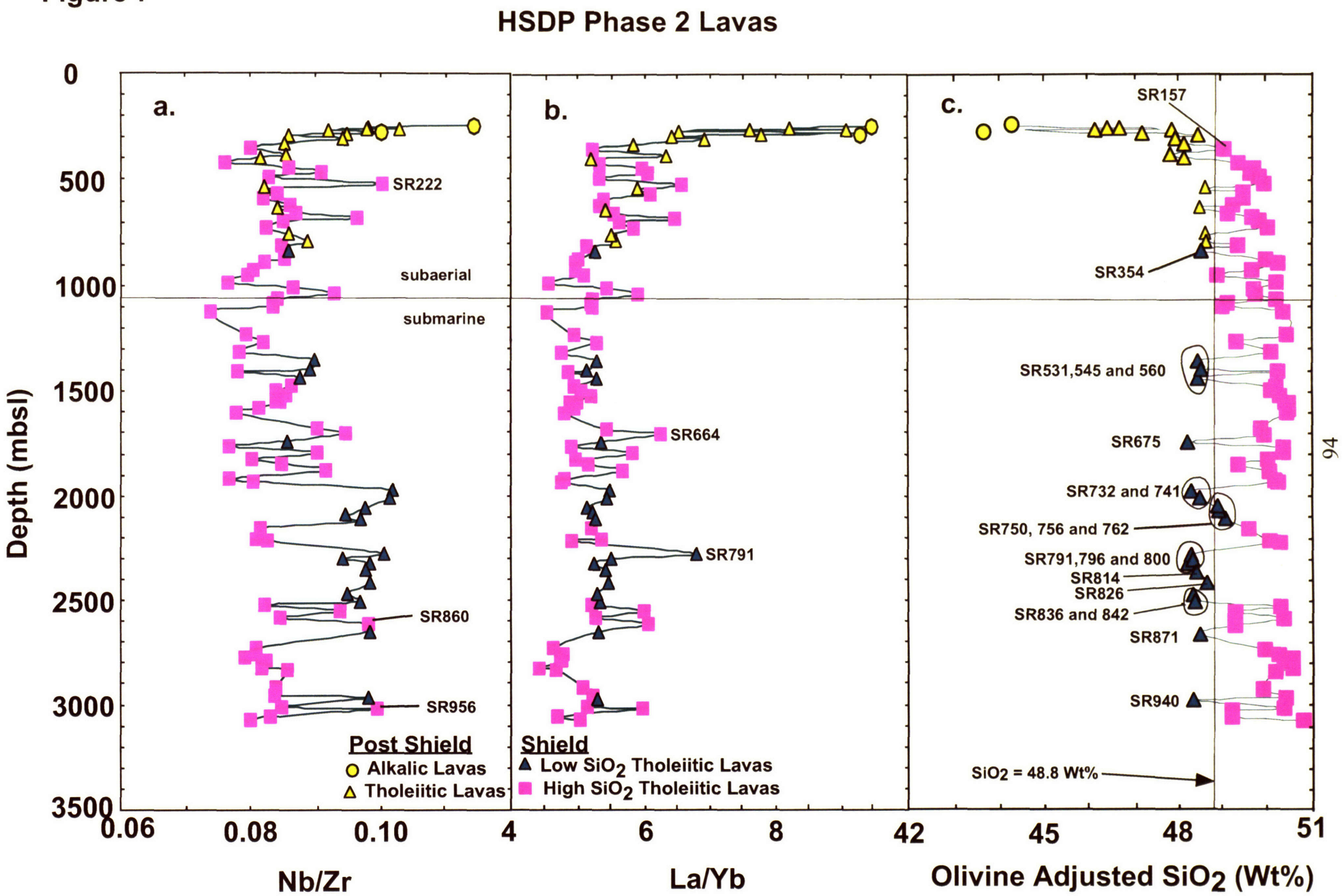
HSDP Phase 2 Lavas
a.
b.
c.
Depth (mbsl)
0
500
1000
1500
2000
2500
3000
3500
subaerial
submarine
SR222
SR860
SR956
SR664
SR791
SR157
SR354
SR531,545 and 560
SR675
SR732 and 741
SR750, 756 and 762
SR791,796 and 800
SR814
SR826
SR836 and 842
SR871
SR940
SiO2 = 48.8 Wt%
Post Shield
Alkalic Lavas
Tholeiitic Lavas
Shield
Low SiO2 Tholeiitic Lavas
High SiO2 Tholeiitic Lavas
0.06
0.08
0.10
Nb/Zr
4
6
8
La/Yb
42
45
48
51
Olivine Adjusted SiO2 (Wt%)

Figure 7

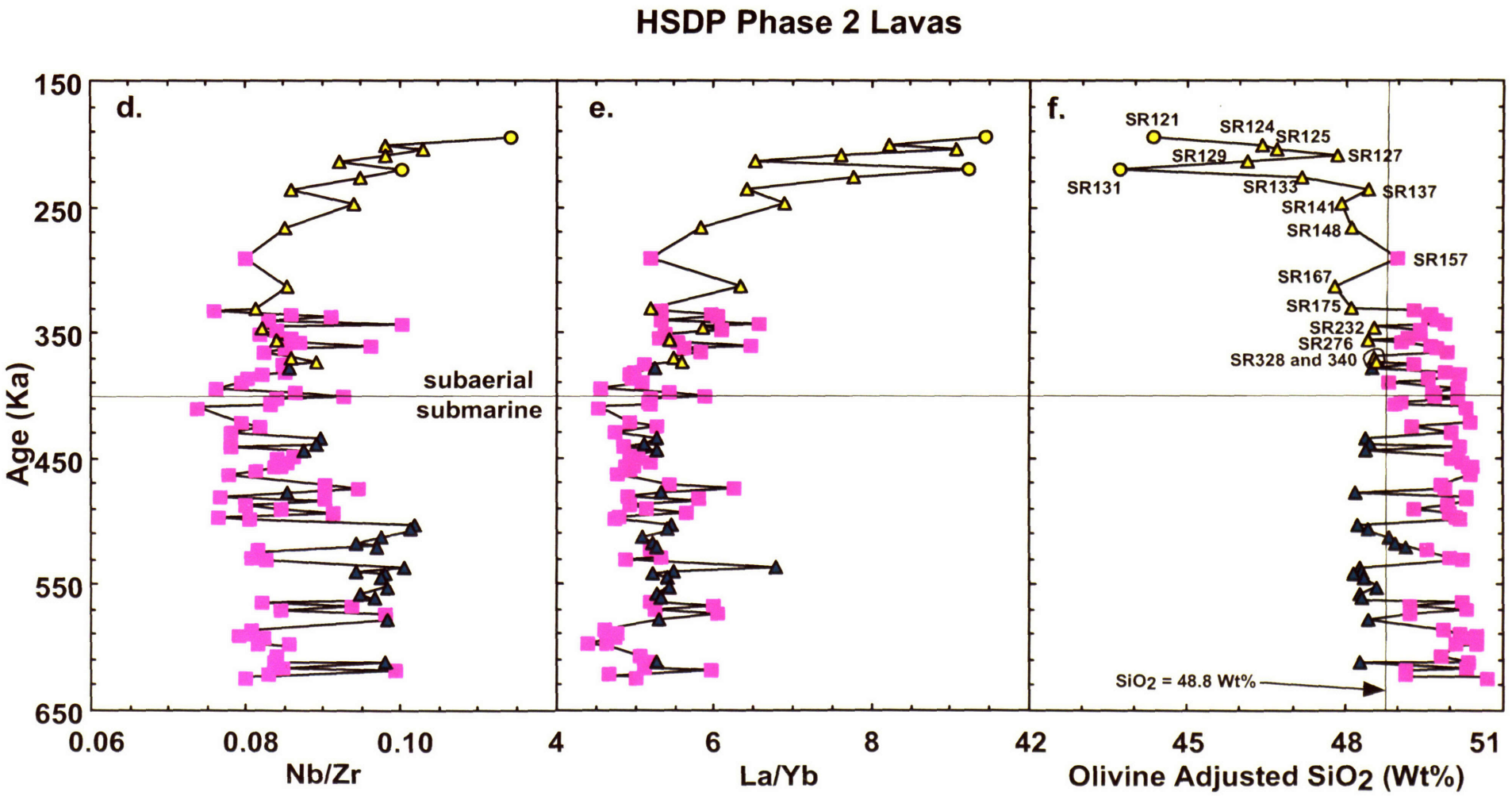
HSDP Phase 2 Lavas
d.
e.
f.
Age (Ka)
150
250
350
450
550
650
subaerial
submarine
0.06
0.08
0.10
Nb/Zr
4
6
8
La/Yb
42
45
48
51
Olivine Adjusted SiO2 (Wt%)
SR121
SR124
SR125
SR129
SR127
SR131
SR133
SR137
SR141
SR148
SR157
SR167
SR175
SR232
SR276
SR328 and 340
SiO2 = 48.8 Wt%

Figure 8.

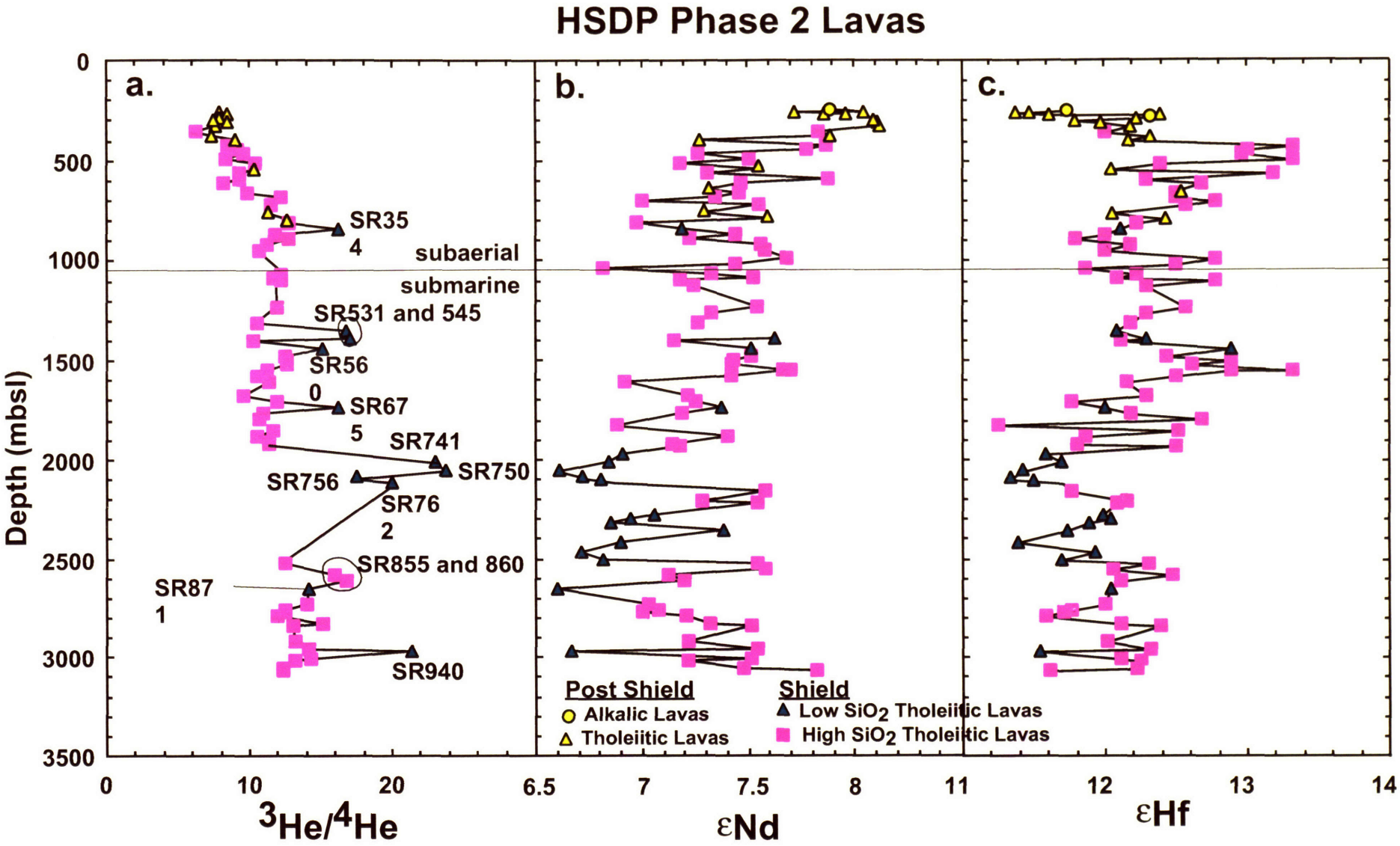
HSDP Phase 2 Lavas
a.
b.
c.
Depth (mbsl)
0
500
1000
1500
2000
2500
3000
3500
subaerial
submarine
SR35
4
SR531 and 545
SR56
0
SR67
5
SR741
SR750
SR756
SR76
2
SR855 and 860
SR87
1
SR940
Post Shield
Alkalic Lavas
Tholeiitic Lavas
Shield
Low SiO2 Tholeiitic Lavas
High SiO2 Tholeiitic Lavas
0
10
20
3He/4He
6.5
7
7.5
8
11
εNd
12
13
14
εHf

Figure 8

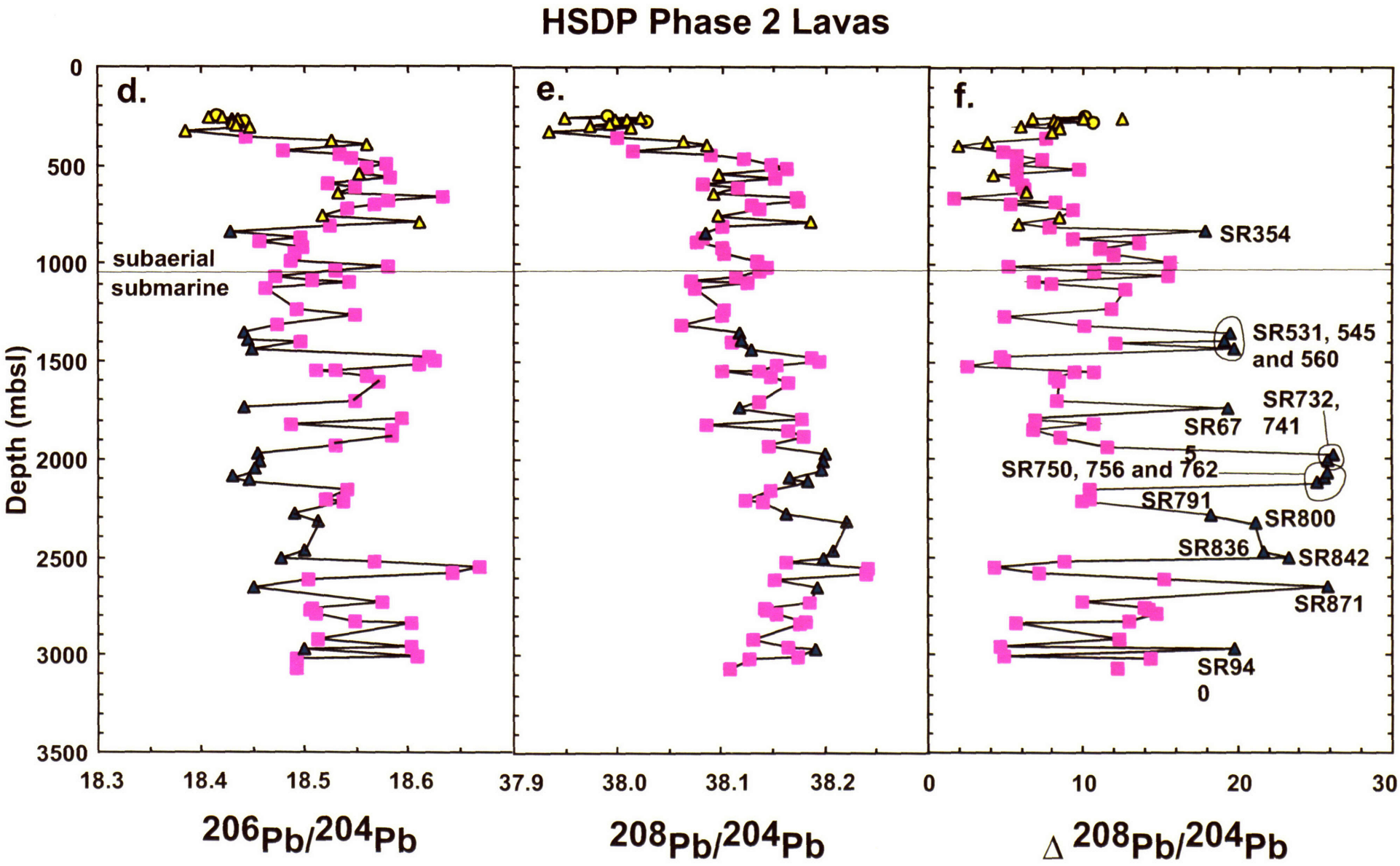
HSDP Phase 2 Lavas
d.
e.
f.
subaerial
submarine
SR354
SR531, 545 and 560
SR732, 741
SR67 5
SR750, 756 and 762
SR791
SR800
SR836
SR842
SR871
SR94 0
Depth (mbsl)
0
500
1000
1500
2000
2500
3000
3500
18.3
18.4
18.5
18.6
37.9
38.0
38.1
38.2
0
10
20
30
206Pb/204Pb
208Pb/204Pb
Δ 208Pb/204Pb

Figure 9

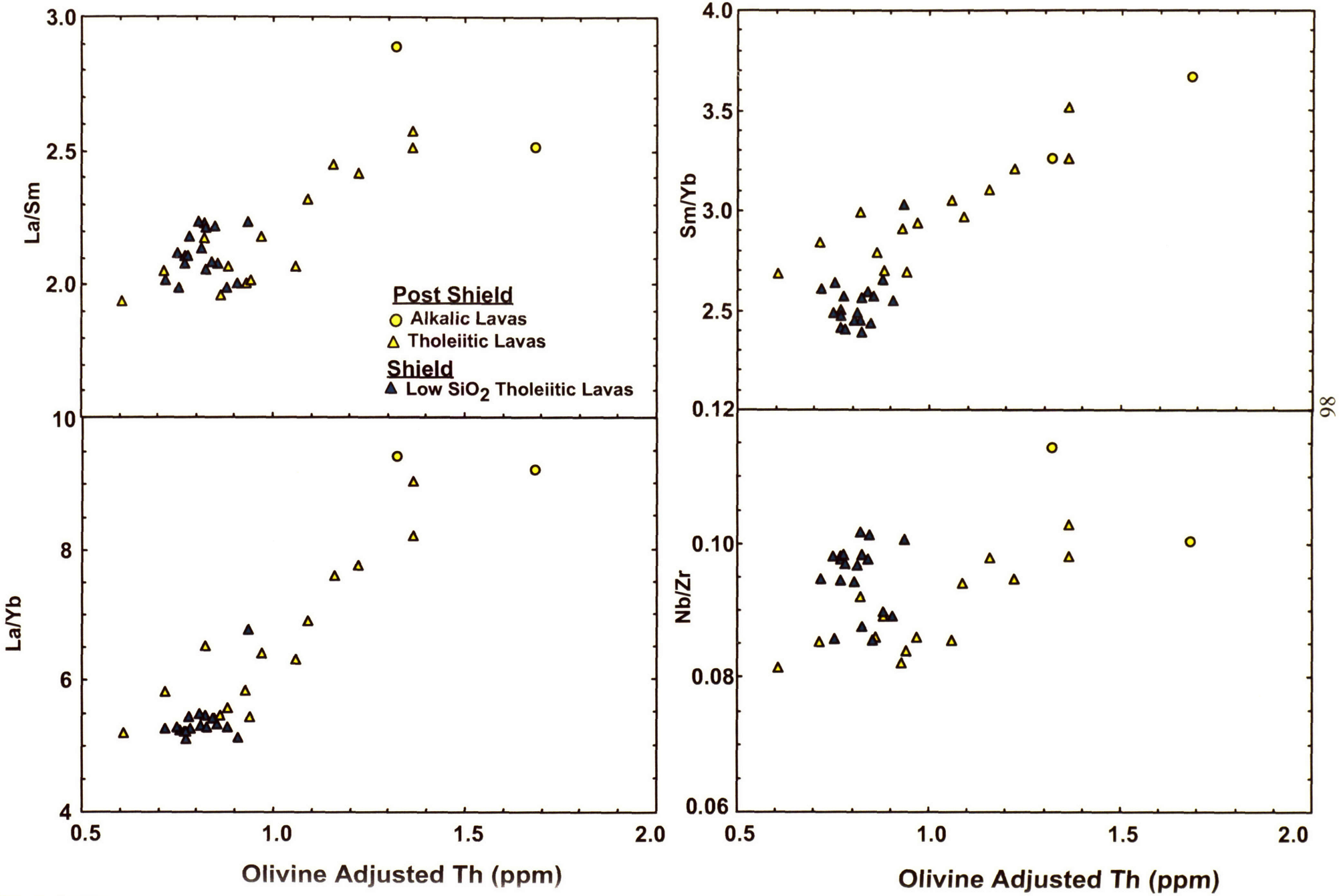
La/Sm
La/Yb
Sm/Yb
Nb/Zr
Post Shield
Alkalic Lavas
Tholeiitic Lavas
Shield
Low SiO2 Tholeiitic Lavas
Olivine Adjusted Th (ppm)
Olivine Adjusted Th (ppm)

Figure 10

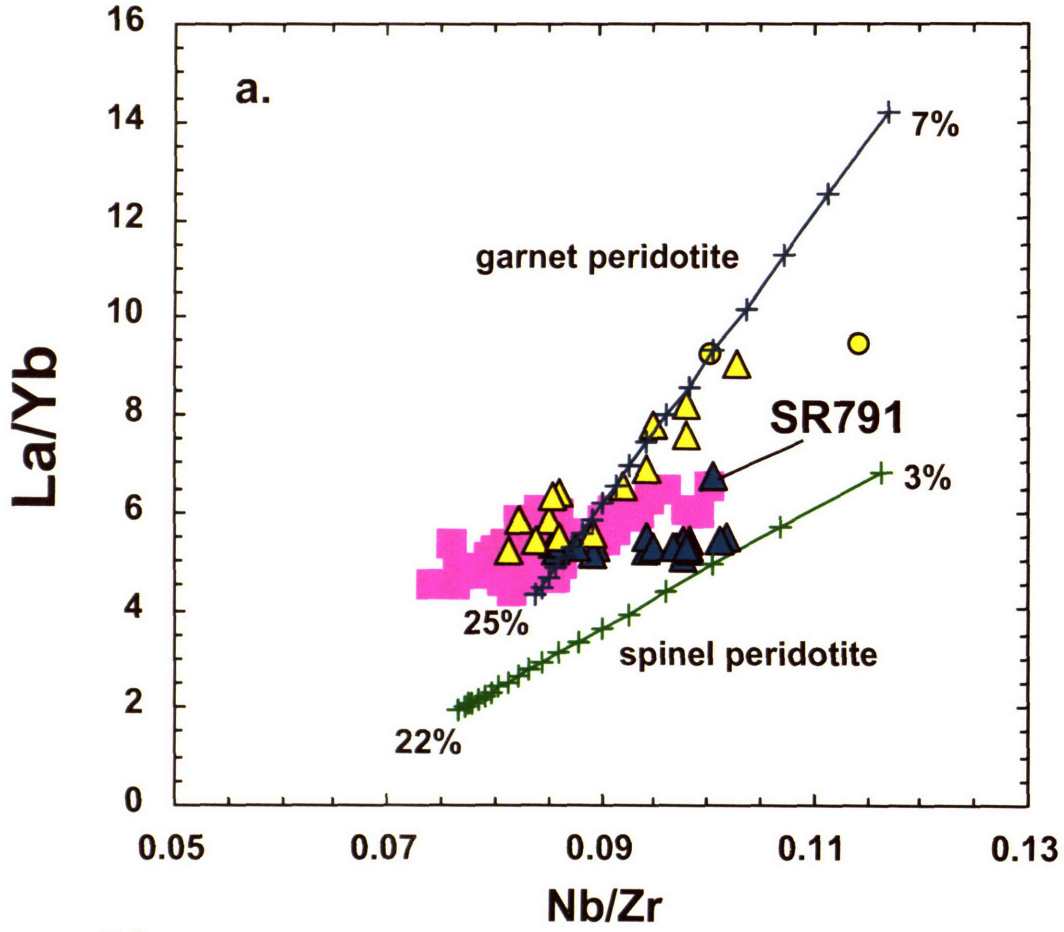
a.
La/Yb
Nb/Zr
garnet peridotite
spinel peridotite
SR791
7%
3%
25%
22%
0
2
4
6
8
10
12
14
16
0.05
0.07
0.09
0.11
0.13

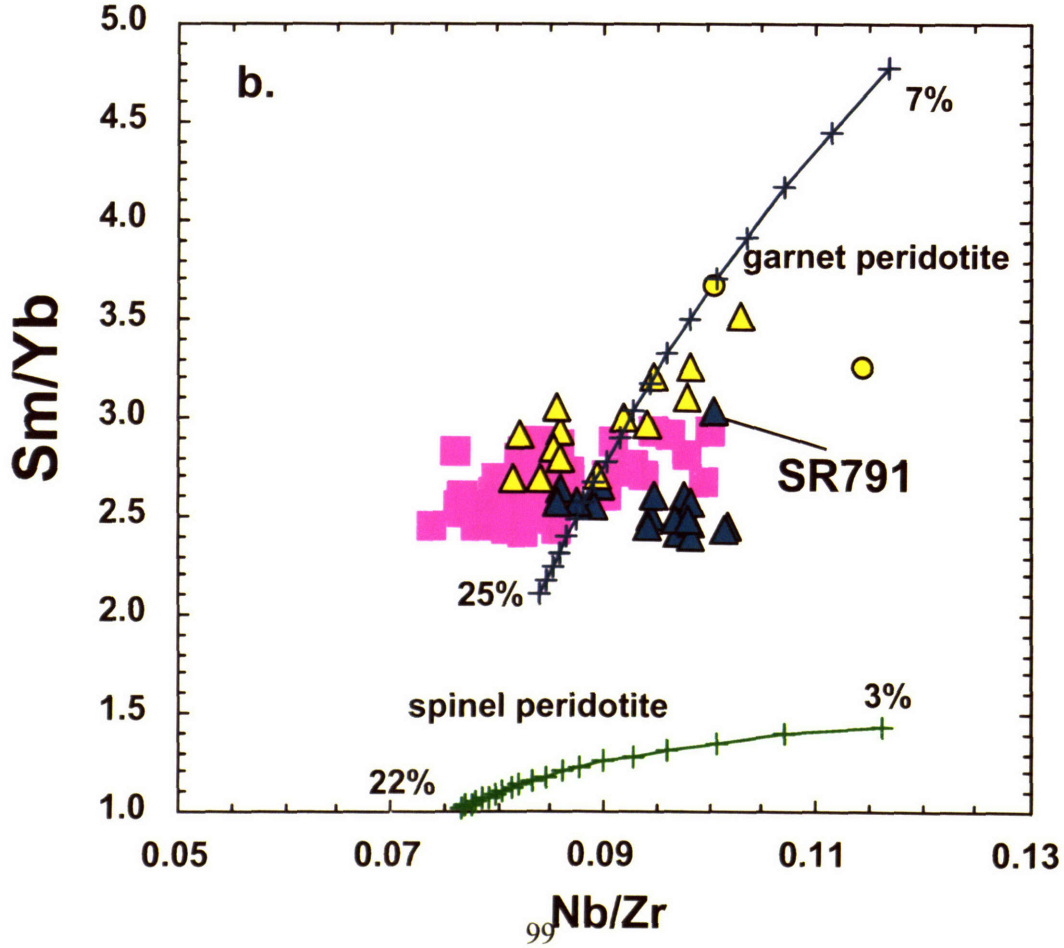
b.
Sm/Yb
Nb/Zr
garnet peridotite
spinel peridotite
SR791
7%
3%
25%
22%
1.0
1.5
2.0
2.5
3.0
3.5
4.0
4.5
5.0
0.05
0.07
0.09
0.11
0.13

Figure 10

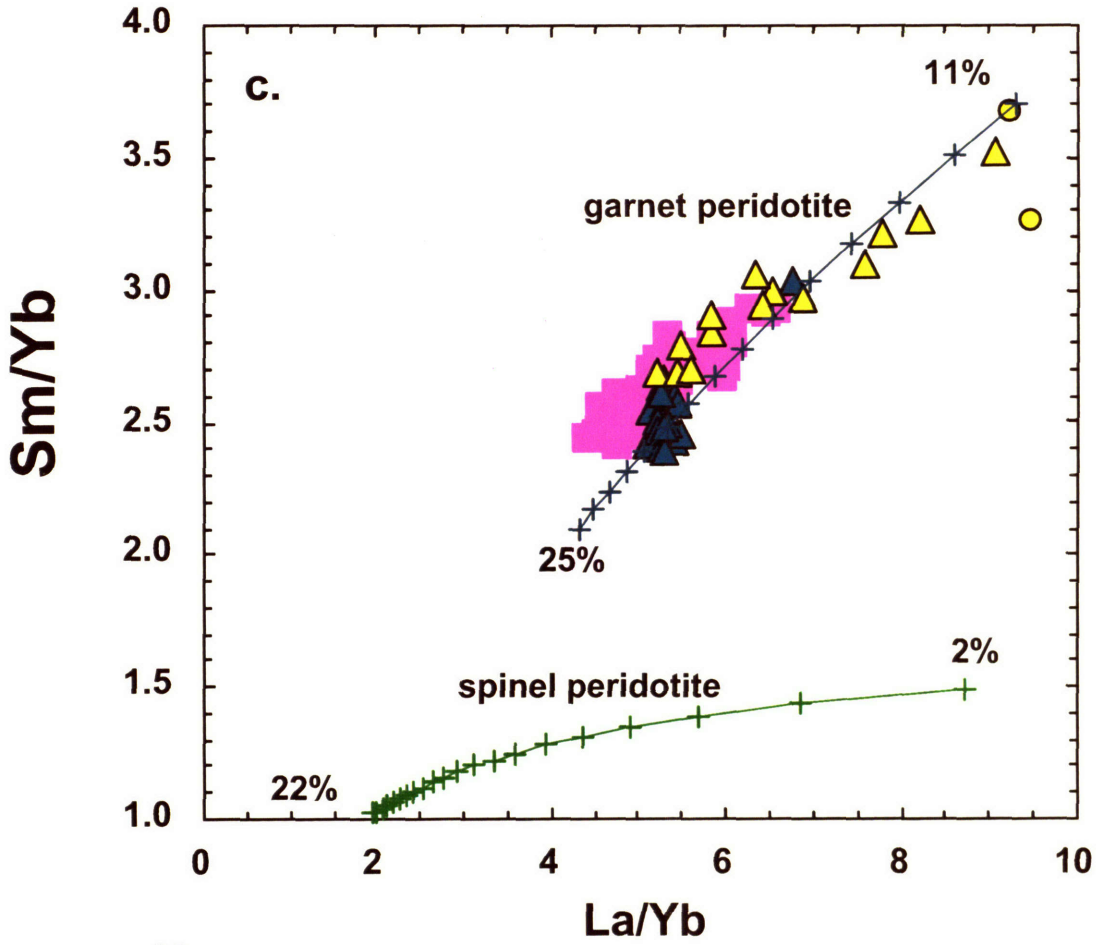
c.
11%
garnet peridotite
25%
2%
spinel peridotite
22%
Sm/Yb
La/Yb
4.0
3.5
3.0
2.5
2.0
1.5
1.0
0
2
4
6
8
10

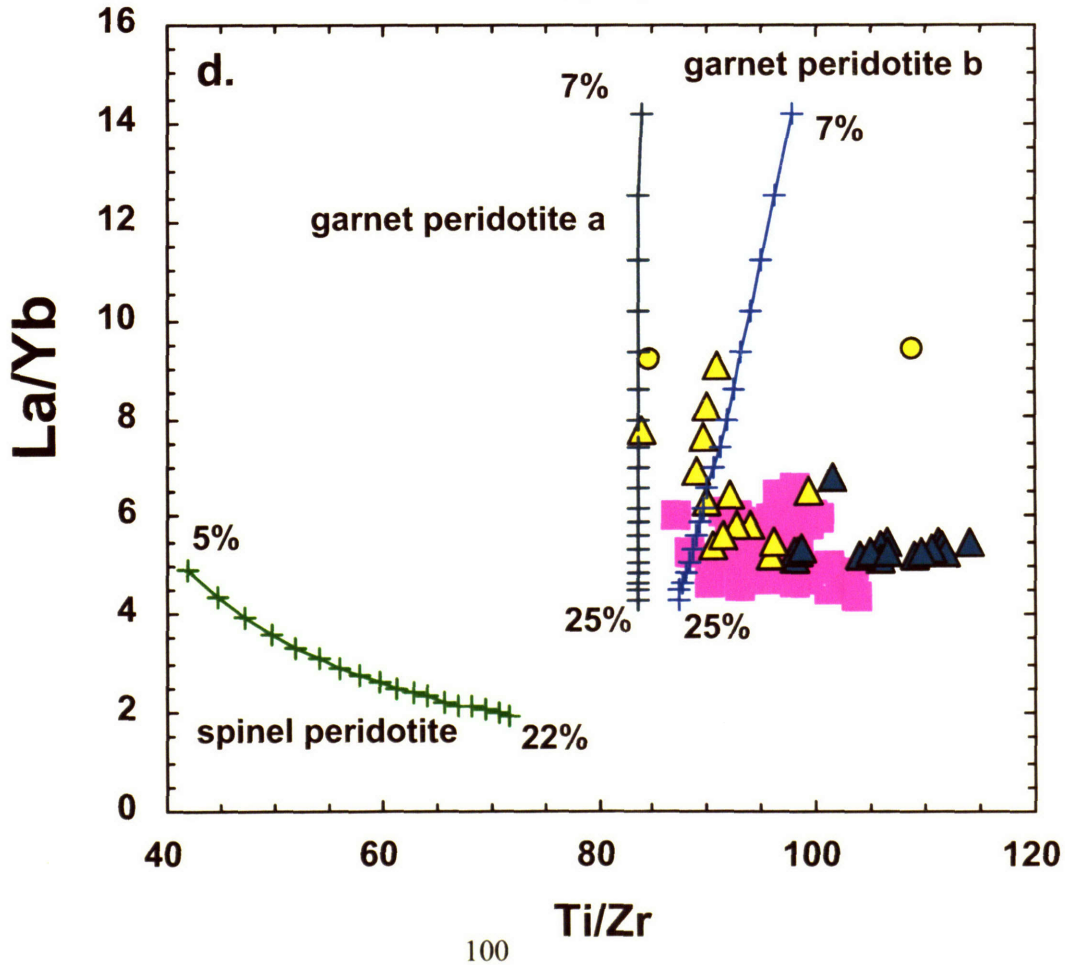
d.
7%
garnet peridotite b
7%
garnet peridotite a
5%
25%
25%
spinel peridotite
22%
La/Yb
Ti/Zr
16
14
12
10
8
6
4
2
0
40
60
80
100
120

Figure 10

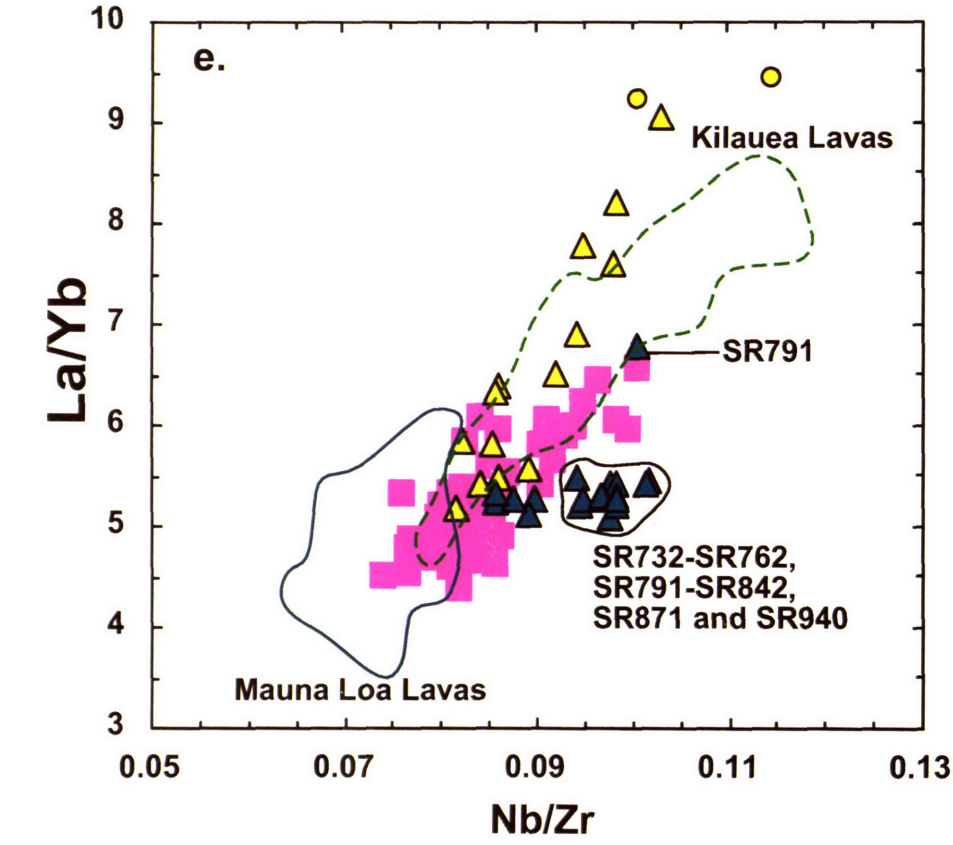
e.
Kilauea Lavas
SR791
SR732-SR762,
SR791-SR842,
SR871 and SR940
Mauna Loa Lavas
La/Yb
Nb/Zr
10
9
8
7
6
5
4
3
0.05
0.07
0.09
0.11
0.13

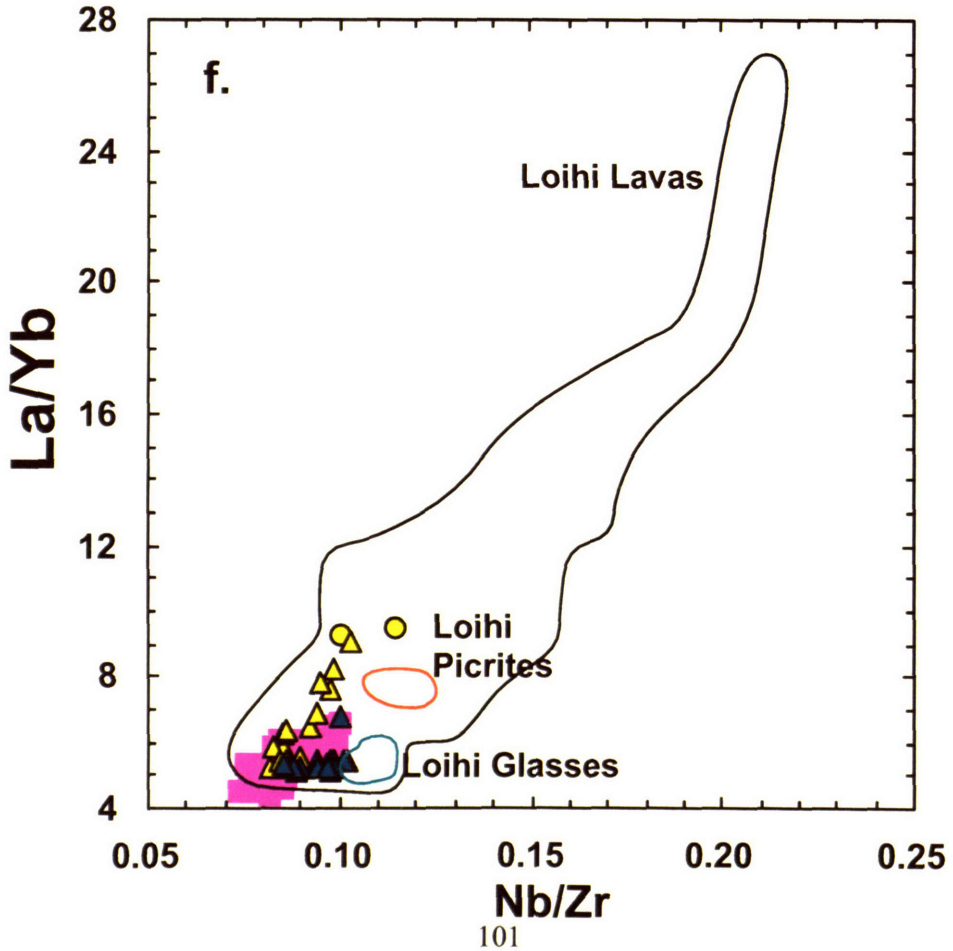
f.
Loihi Lavas
Loihi
Picrites
Loihi Glasses
La/Yb
Nb/Zr
28
24
20
16
12
8
4
0.05
0.10
0.15
0.20
0.25

Figure 10

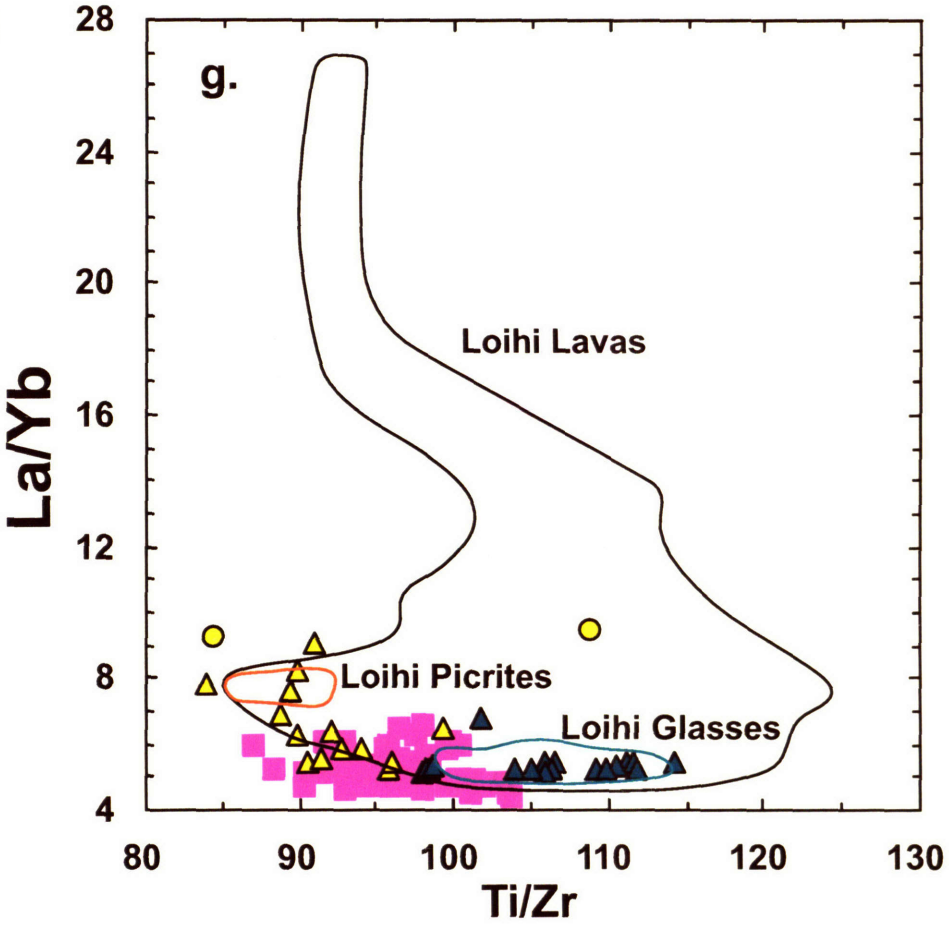
g.
28
24
20
16
12
8
4
La/Yb
80
90
100
110
120
130
Ti/Zr
Loihi Lavas
Loihi Picrites
Loihi Glasses

Figure 11

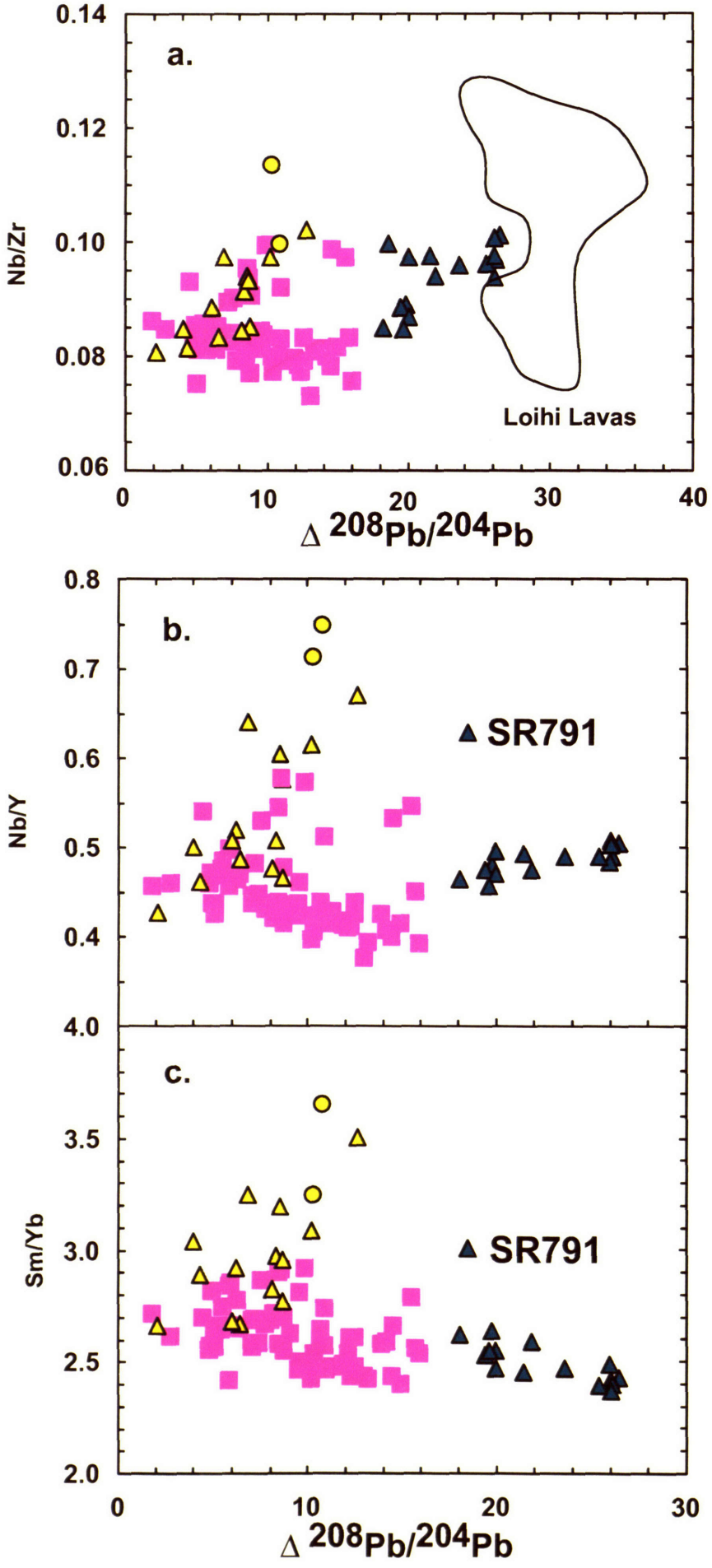
a.
Nb/Zr
0.14
0.12
0.10
0.08
0.06
Loihi Lavas
0
10
20
30
40
Δ 208Pb/204Pb
b.
Nb/Y
0.8
0.7
0.6
0.5
0.4
SR791
c.
Sm/Yb
4.0
3.5
3.0
2.5
2.0
SR791
0
10
20
30
Δ 208Pb/204Pb

Figure 12

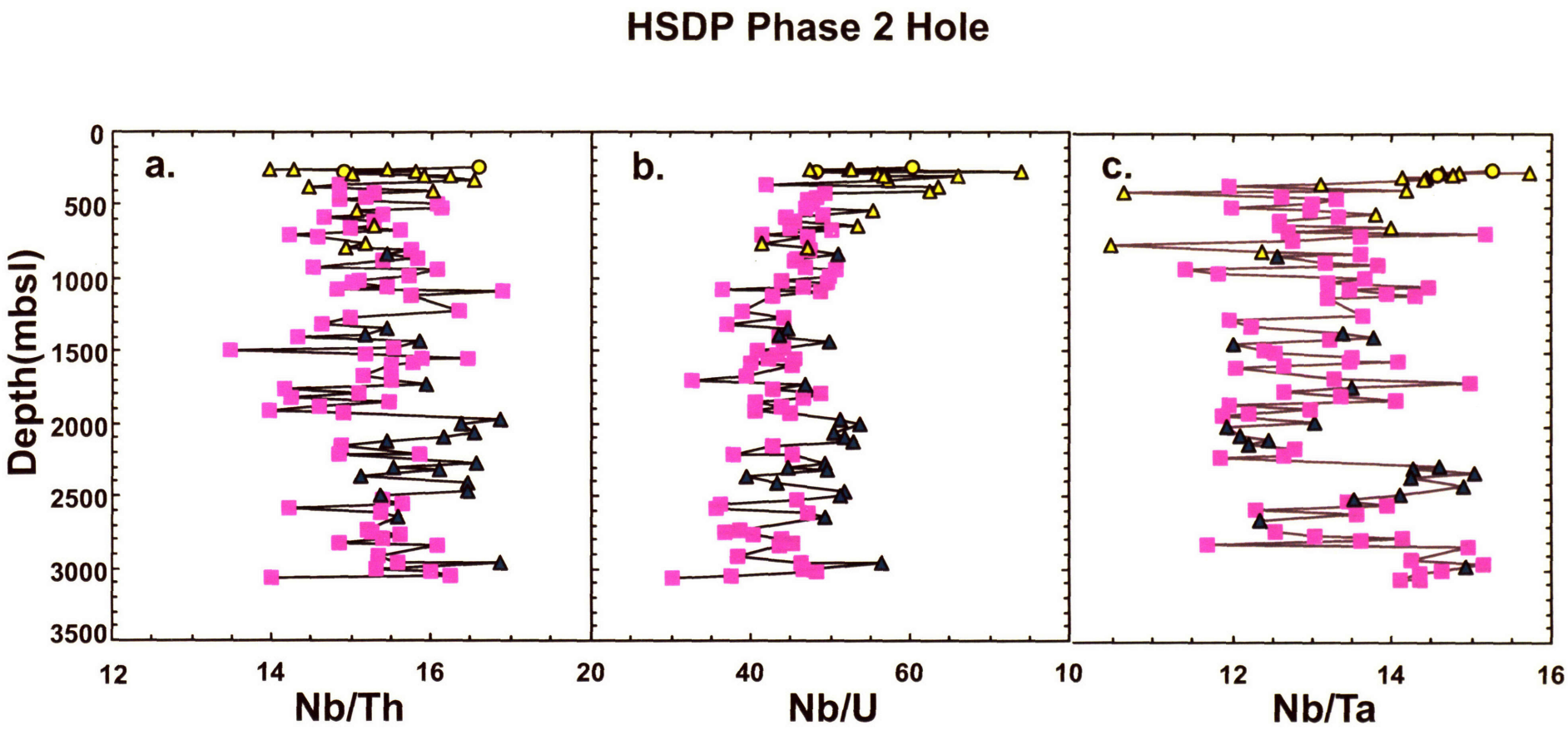
HSDP Phase 2 Hole
a.
b.
c.
Depth(mbsl)
0
500
1000
1500
2000
2500
3000
3500
12
14
16
20
Nb/Th
40
60
10
Nb/U
12
14
16
Nb/Ta

Figure 12

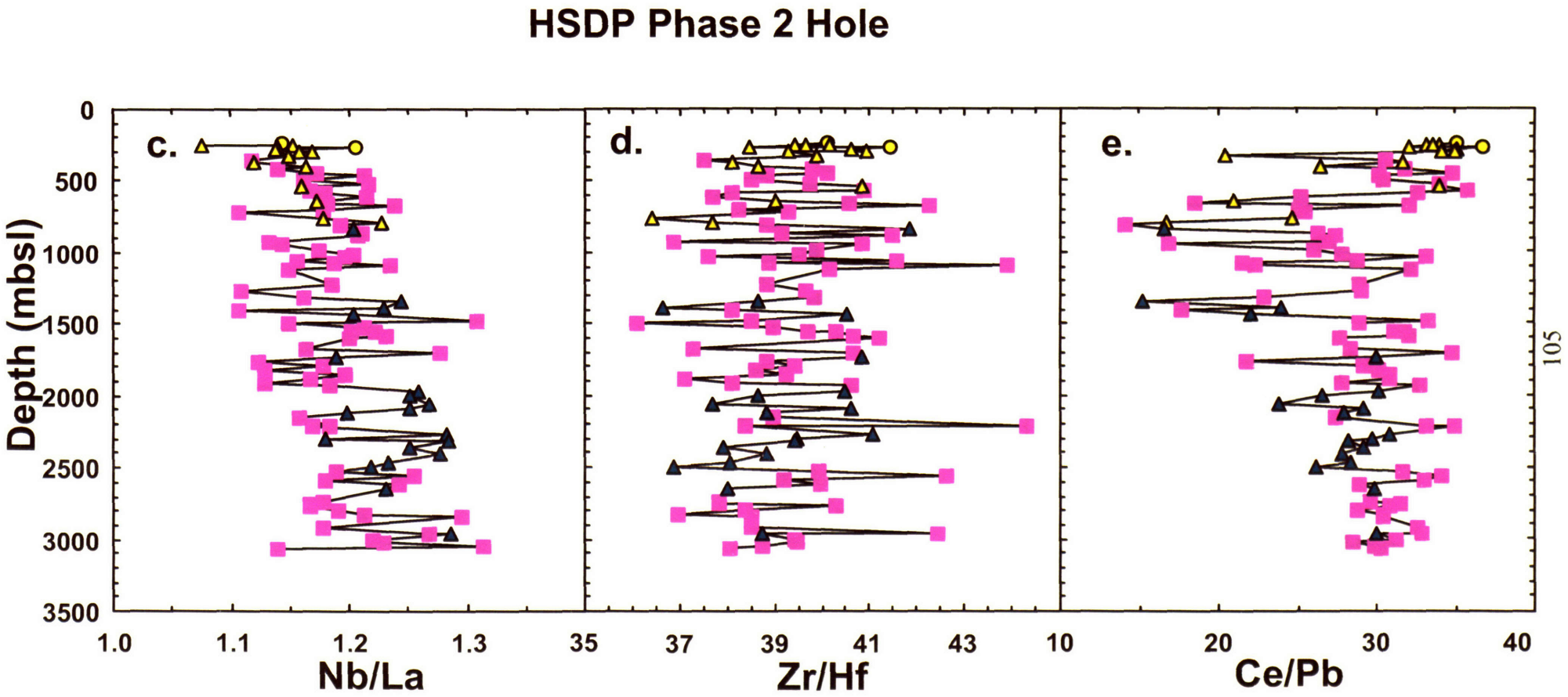
HSDP Phase 2 Hole
c.
d.
e.
Depth (mbsl)
0
500
1000
1500
2000
2500
3000
3500
1.0
1.1
1.2
1.3
Nb/La
35
37
39
41
43
Zr/Hf
10
20
30
40
Ce/Pb

Figure 13

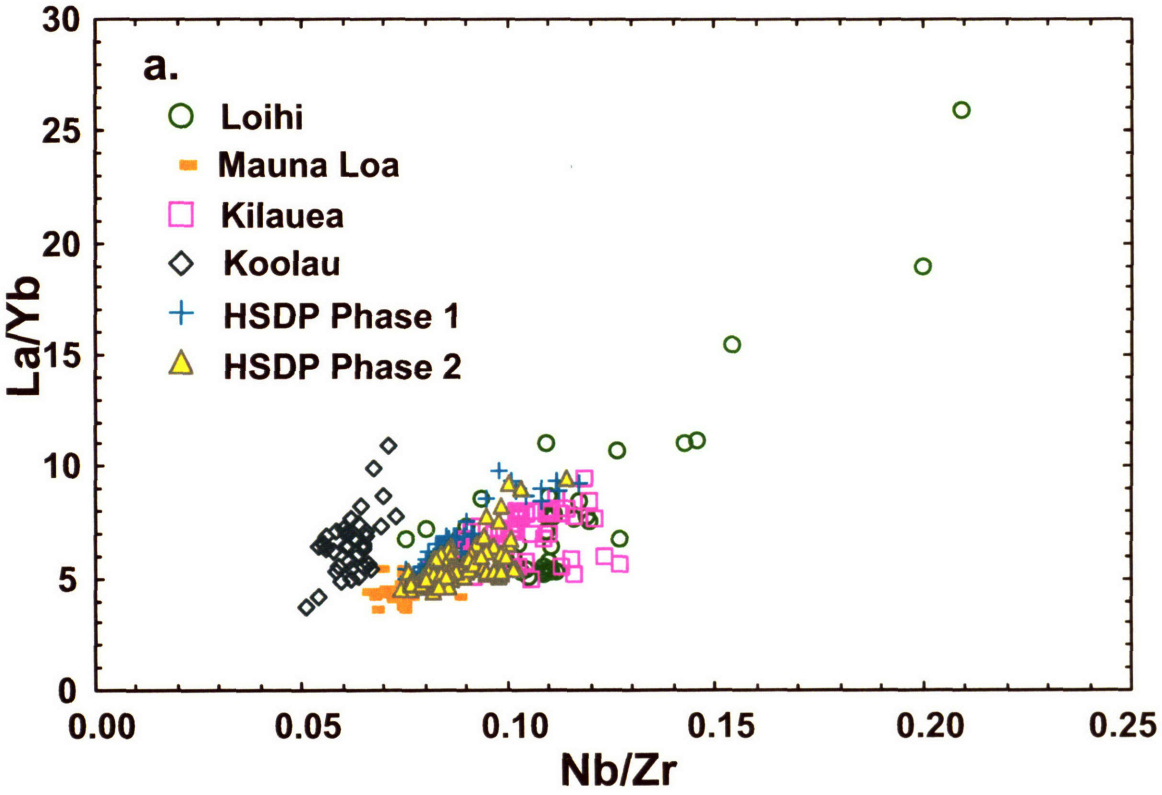
a.
Loihi
Mauna Loa
Kilauea
Koolau
HSDP Phase 1
HSDP Phase 2
La/Yb
Nb/Zr
0
5
10
15
20
25
30
0.00
0.05
0.10
0.15
0.20
0.25

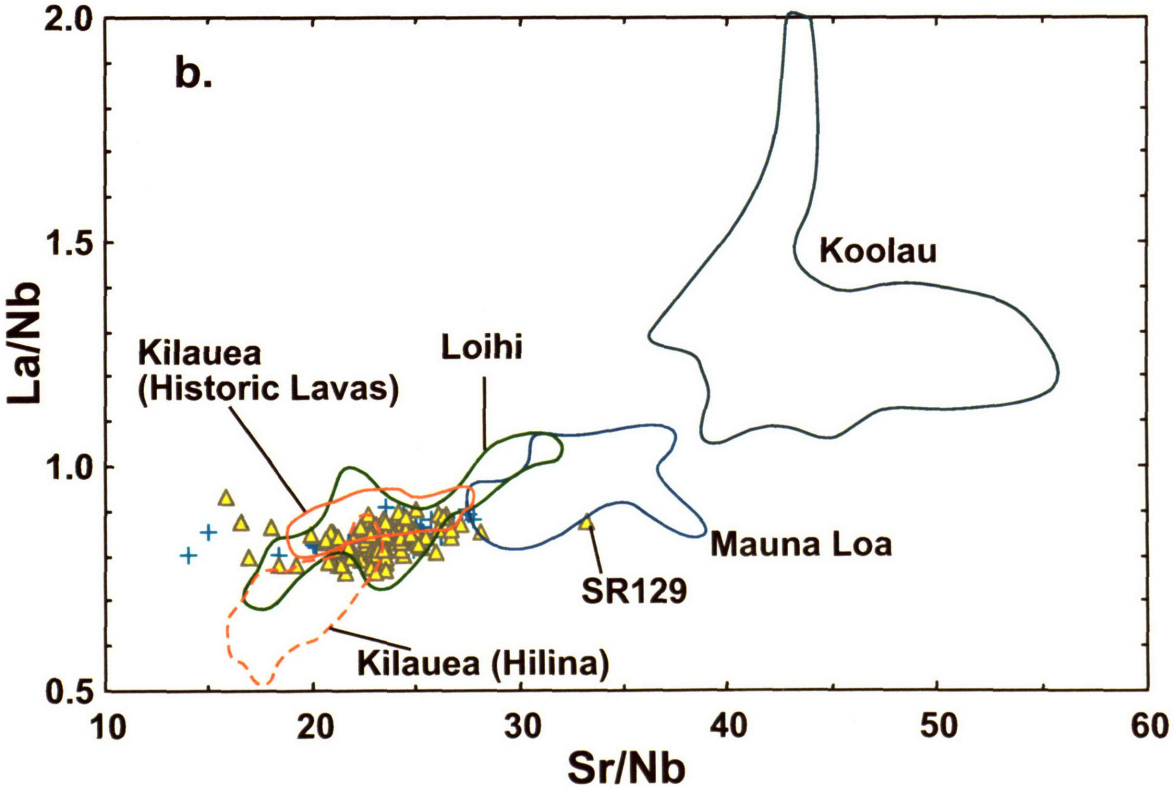
b.
Koolau
Kilauea
(Historic Lavas)
Loihi
Mauna Loa
SR129
Kilauea (Hilina)
La/Nb
Sr/Nb
0.5
1.0
1.5
2.0
10
20
30
40
50
60

Figure 14a

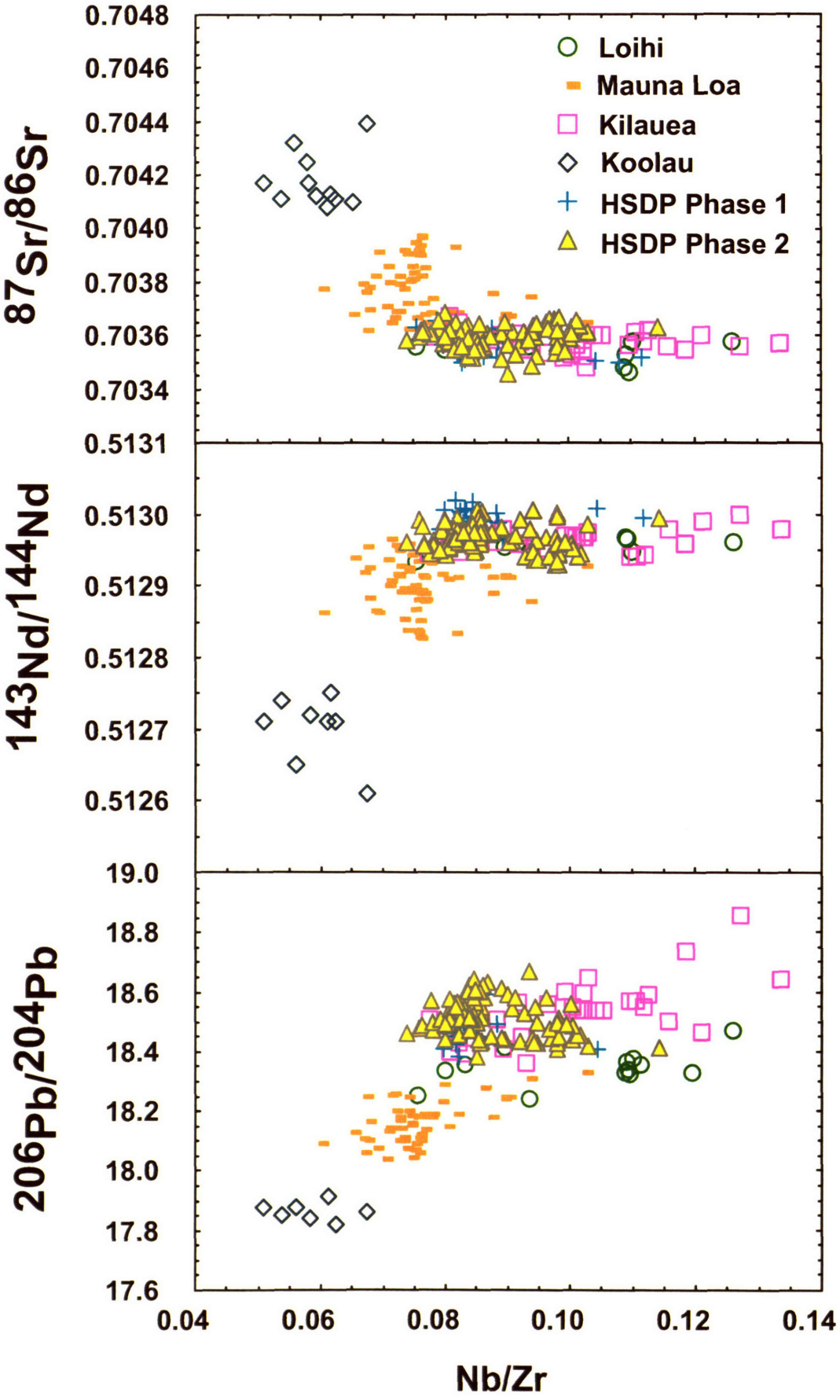
Loihi
Mauna Loa
Kilauea
Koolau
HSDP Phase 1
HSDP Phase 2
87Sr/86Sr
143Nd/144Nd
206Pb/204Pb
Nb/Zr
0.7048
0.7046
0.7044
0.7042
0.7040
0.7038
0.7036
0.7034
0.5131
0.5130
0.5129
0.5128
0.5127
0.5126
19.0
18.8
18.6
18.4
18.2
18.0
17.8
17.6
0.04
0.06
0.08
0.10
0.12
0.14

Figure 14b

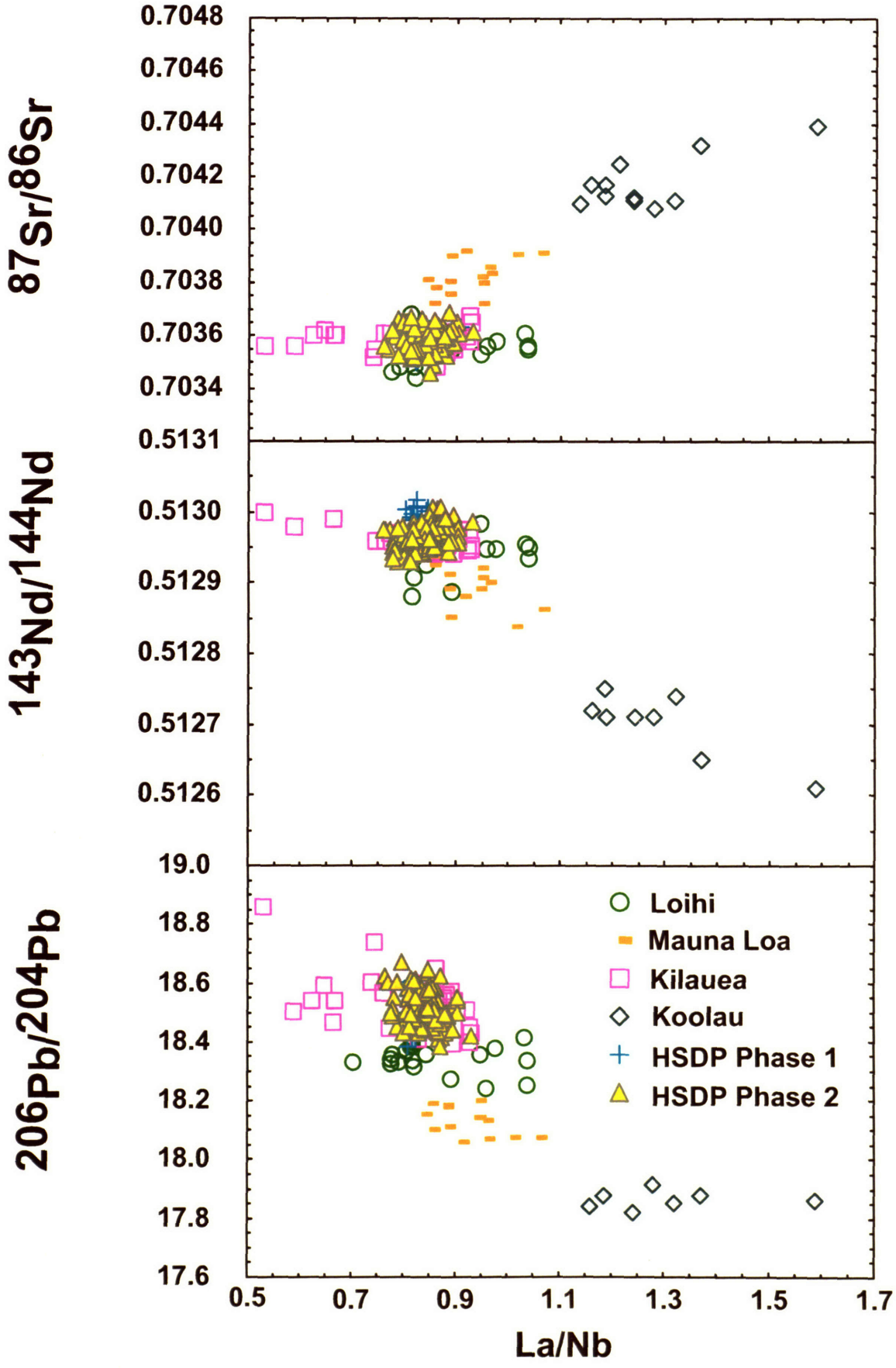
0.7048
0.7046
0.7044
0.7042
0.7040
0.7038
0.7036
0.7034
87Sr/86Sr
0.5131
0.5130
0.5129
0.5128
0.5127
0.5126
143Nd/144Nd
19.0
18.8
18.6
18.4
18.2
18.0
17.8
17.6
206Pb/204Pb
Loihi
Mauna Loa
Kilauea
Koolau
HSDP Phase 1
HSDP Phase 2
0.5
0.7
0.9
1.1
1.3
1.5
1.7
La/Nb

Figure 14c

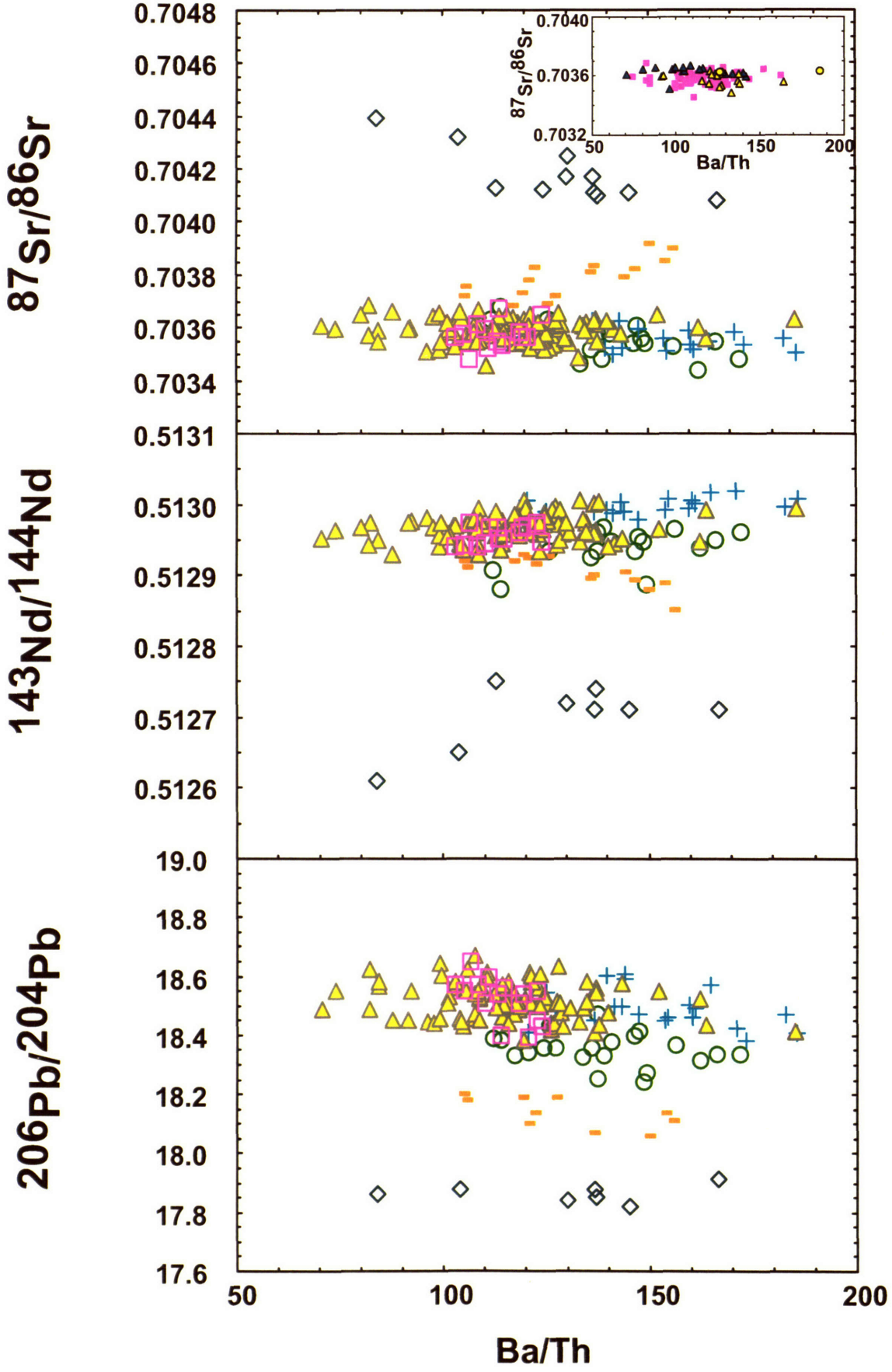
0.7048
0.7046
0.7044
0.7042
0.7040
0.7038
0.7036
0.7034
87Sr/86Sr
0.7040
0.7036
0.7032
87Sr/86Sr
50
100
150
200
Ba/Th
0.5131
0.5130
0.5129
0.5128
0.5127
0.5126
143Nd/144Nd
19.0
18.8
18.6
18.4
18.2
18.0
17.8
17.6
206Pb/204Pb
50
100
150
200
Ba/Th

Figure 15

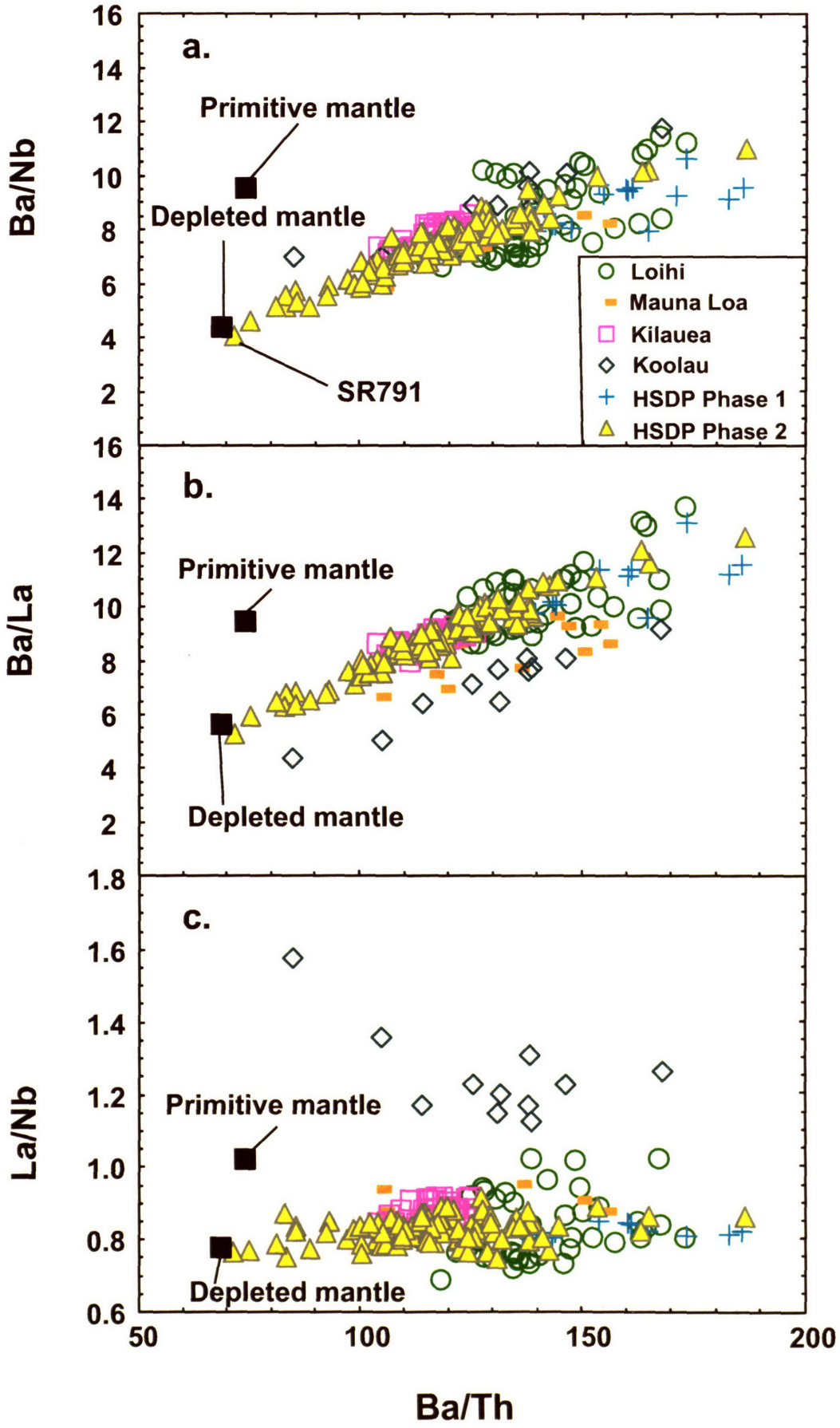
a.
Primitive mantle
Depleted mantle
SR791
Loihi
Mauna Loa
Kilauea
Koolau
HSDP Phase 1
HSDP Phase 2
Ba/Nb
b.
Primitive mantle
Depleted mantle
Ba/La
c.
Primitive mantle
Depleted mantle
La/Nb
Ba/Th

Figure 16

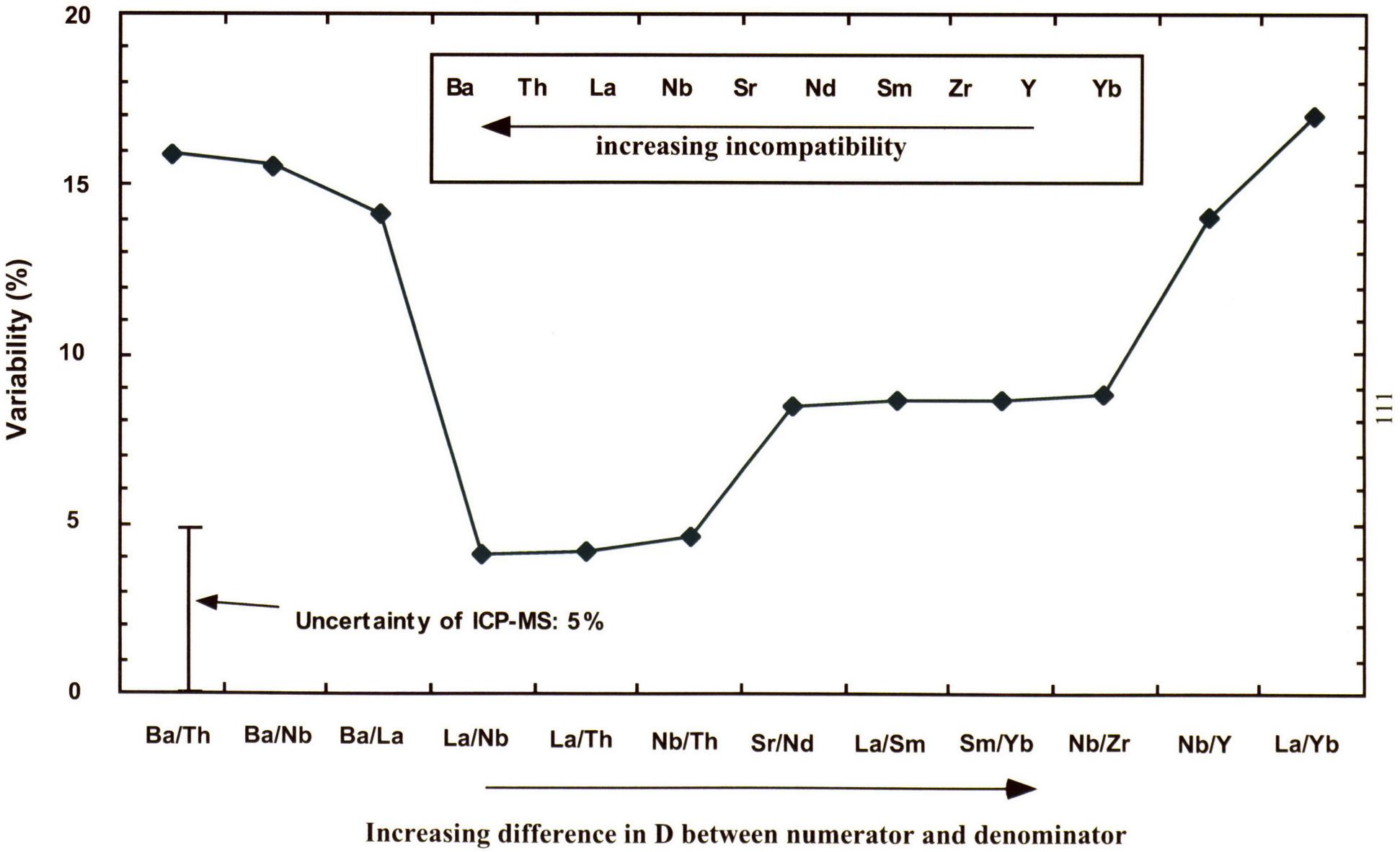
20
15
10
5
0
Variability (%)
Ba Th La Nb Sr Nd Sm Zr Y Yb
increasing incompatibility
Uncertainty of ICP-MS: 5%
Ba/Th
Ba/Nb
Ba/La
La/Nb
La/Th
Nb/Th
Sr/Nd
La/Sm
Sm/Yb
Nb/Zr
Nb/Y
La/Yb
Increasing difference in D between numerator and denominator

Figure A-1

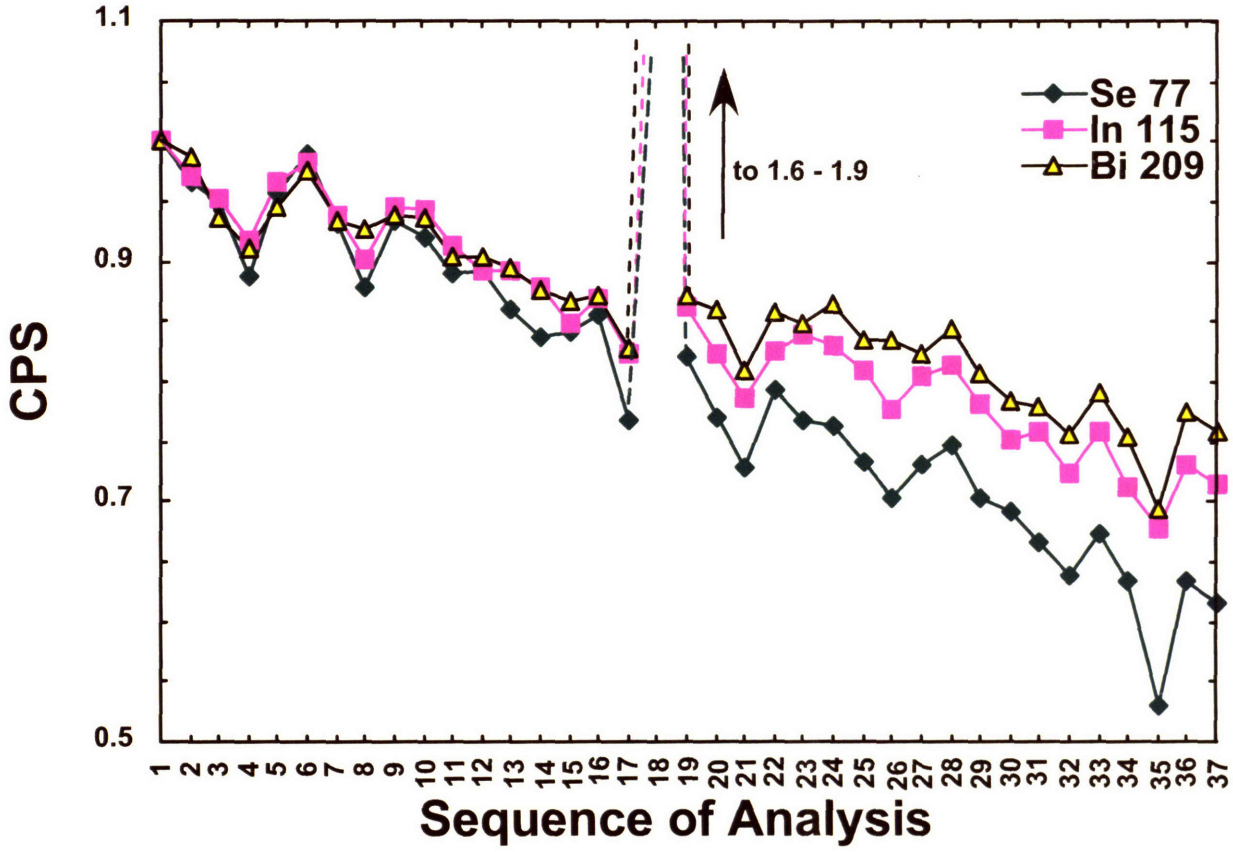
1.1
0.9
0.7
0.5
CPS
to 1.6 - 1.9
Se 77
In 115
Bi 209
1 2 3 4 5 6 7 8 9 10 11 12 13 14 15 16 17 18 19 20 21 22 23 24 25 26 27 28 29 30 31 32 33 34 35 36 37
Sequence of Analysis

Figure A-2

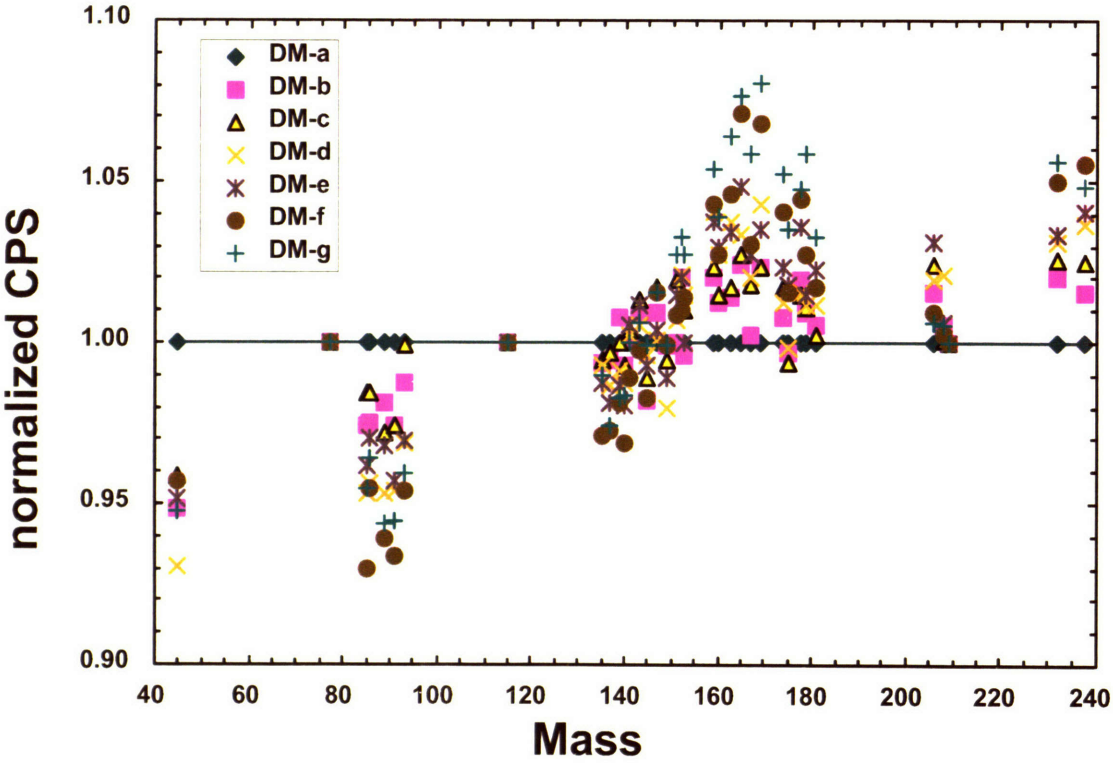
1.10
1.05
1.00
0.95
0.90
normalized CPS
DM-a
DM-b
DM-c
DM-d
DM-e
DM-f
DM-g
40
60
80
100
120
140
160
180
200
220
240
Mass

Figure A-3

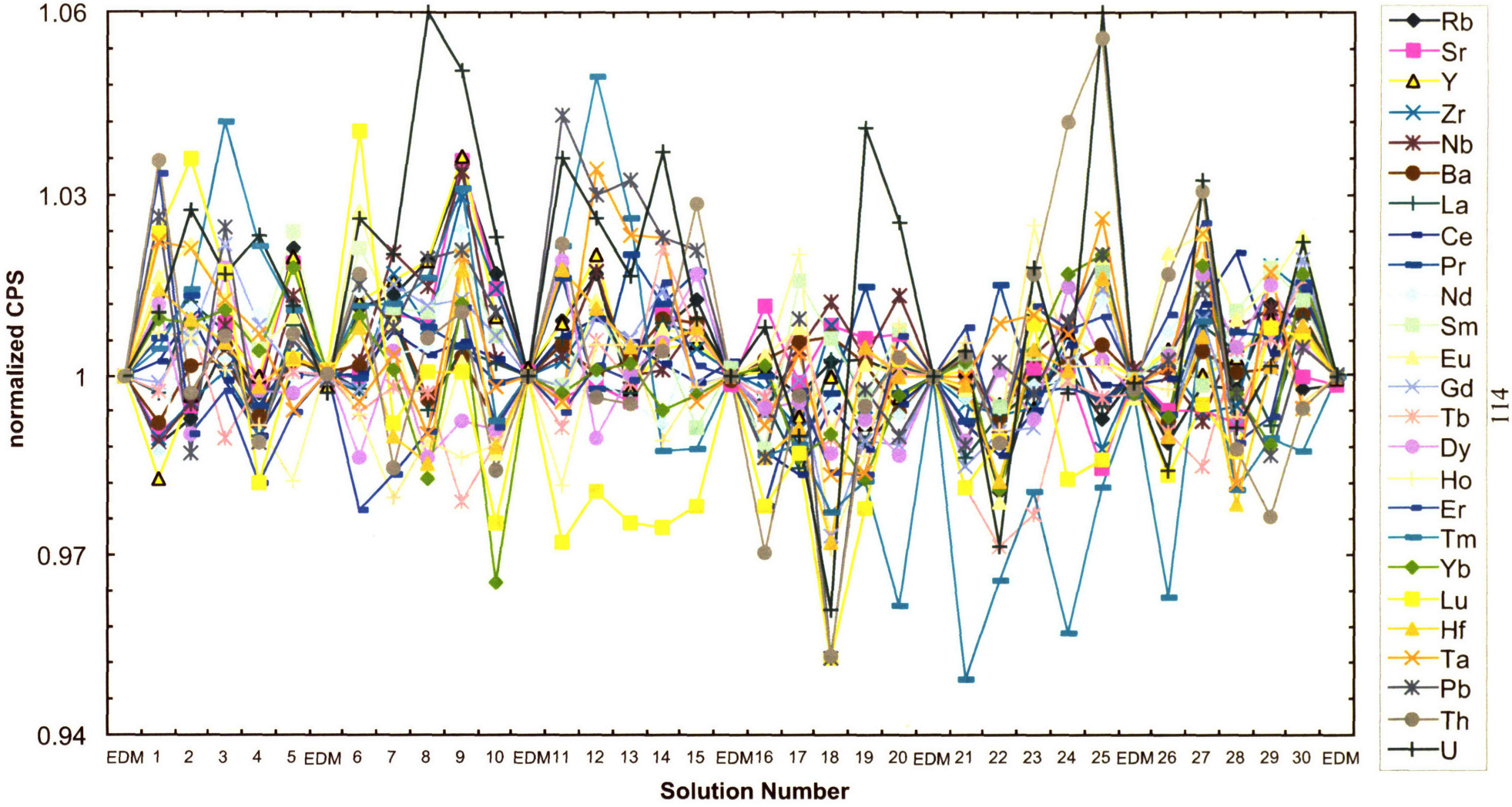
1.06
1.03
1
0.97
0.94
normalized CPS
EDM 1 2 3 4 5 EDM 6 7 8 9 10 EDM11 12 13 14 15 EDM16 17 18 19 20 EDM 21 22 23 24 25 EDM 26 27 28 29 30 EDM
Solution Number
Rb
Sr
Y
Zr
Nb
Ba
La
Ce
Pr
Nd
Sm
Eu
Gd
Tb
Dy
Ho
Er
Tm
Yb
Lu
Hf
Ta
Pb
Th
U

Figure A-4

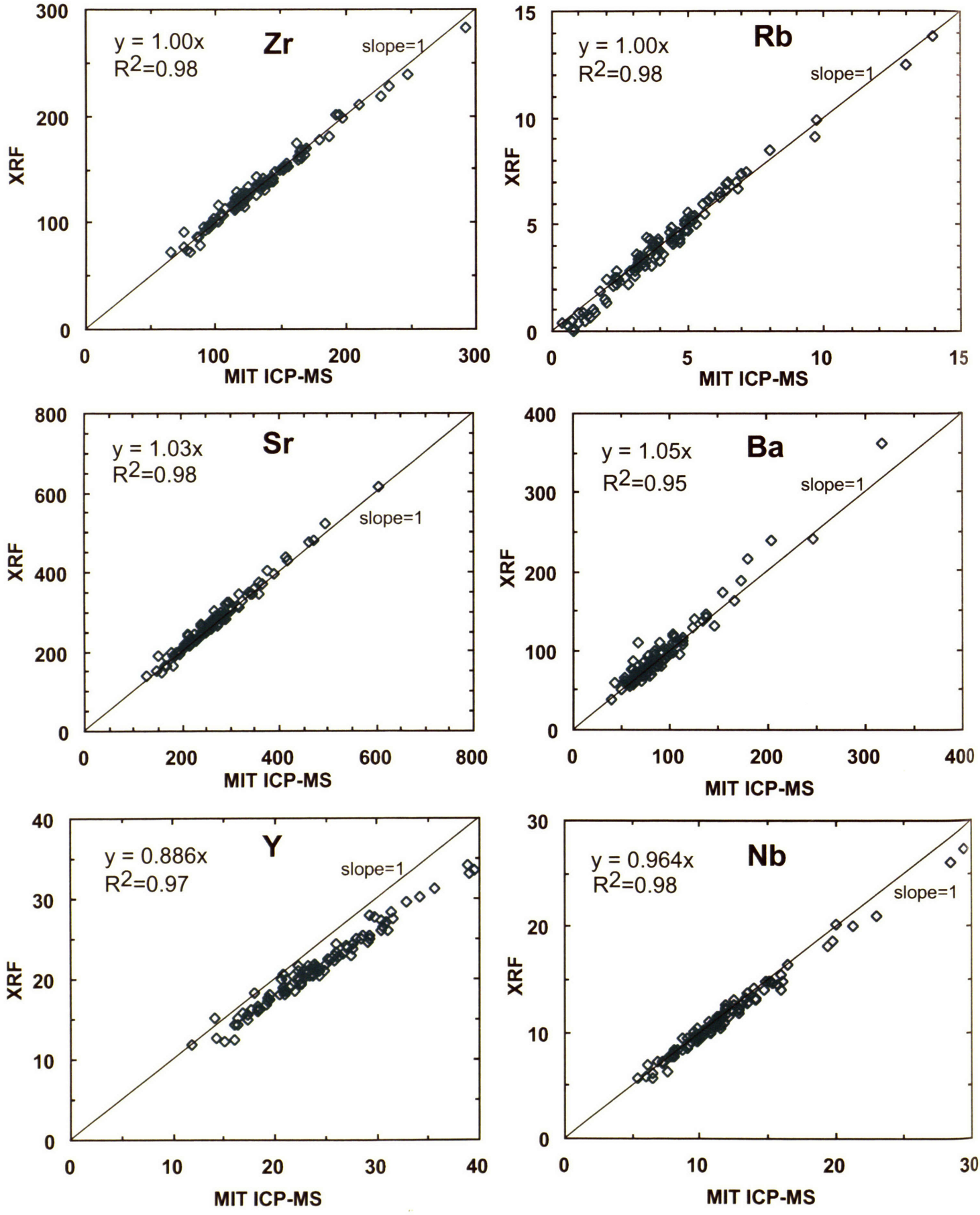
Zr
y = 1.00x
R2=0.98
slope=1
Rb
y = 1.00x
R2=0.98
slope=1
Sr
y = 1.03x
R2=0.98
slope=1
Ba
y = 1.05x
R2=0.95
slope=1
Y
y = 0.886x
R2=0.97
slope=1
Nb
y = 0.964x
R2=0.98
slope=1
XRF
MIT ICP-MS

Figure A-5a.

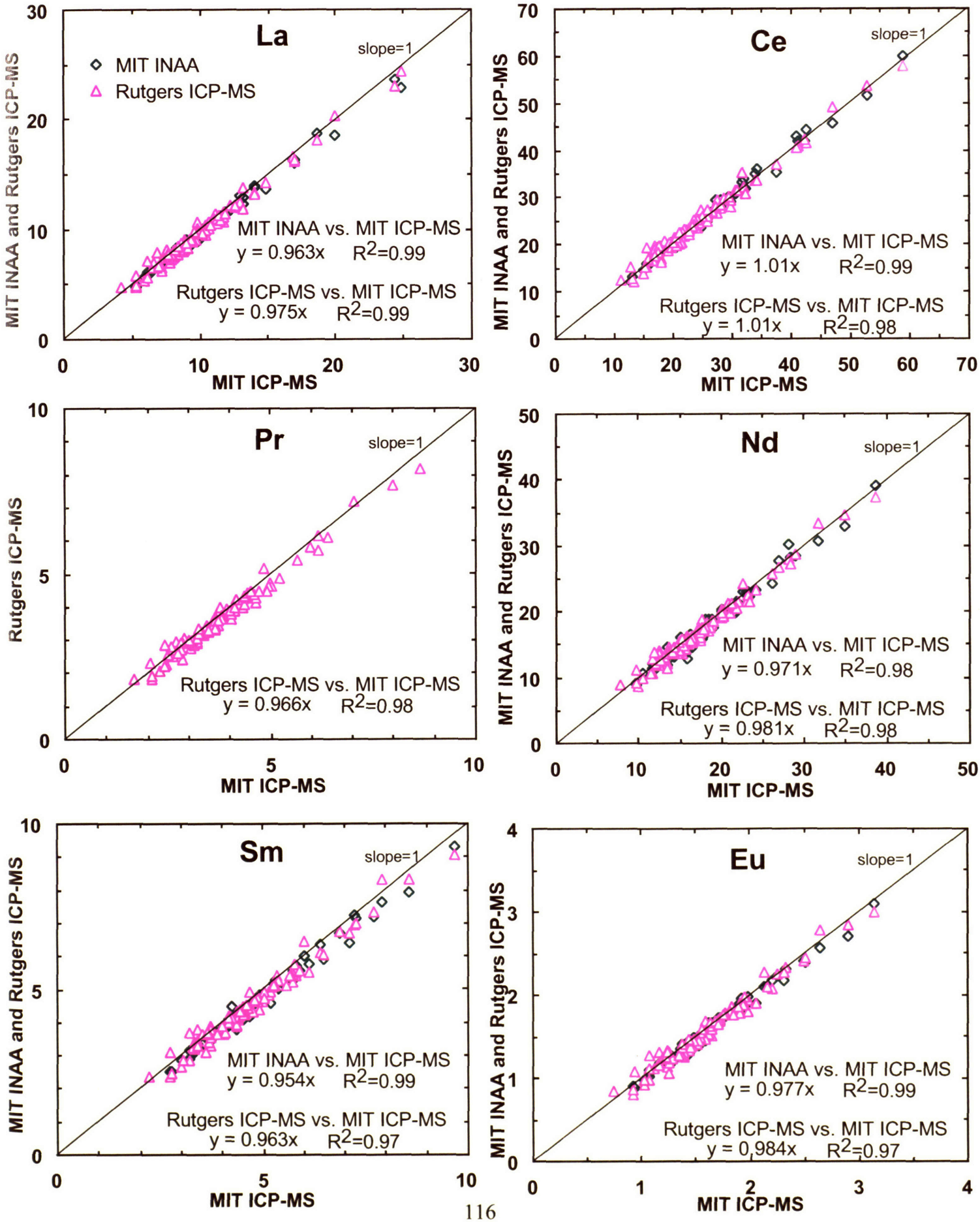
La
slope=1
MIT INAA
Rutgers ICP-MS
MIT INAA vs. MIT ICP-MS
y = 0.963x R2=0.99
Rutgers ICP-MS vs. MIT ICP-MS
y = 0.975x R2=0.99
MIT INAA and Rutgers ICP-MS
MIT ICP-MS
Ce
slope=1
MIT INAA vs. MIT ICP-MS
y = 1.01x R2=0.99
Rutgers ICP-MS vs. MIT ICP-MS
y = 1.01x R2=0.98
MIT INAA and Rutgers ICP-MS
MIT ICP-MS
Pr
slope=1
Rutgers ICP-MS vs. MIT ICP-MS
y = 0.966x R2=0.98
Rutgers ICP-MS
MIT ICP-MS
Nd
slope=1
MIT INAA vs. MIT ICP-MS
y = 0.971x R2=0.98
Rutgers ICP-MS vs. MIT ICP-MS
y = 0.981x R2=0.98
MIT INAA and Rutgers ICP-MS
MIT ICP-MS
Sm
slope=1
MIT INAA vs. MIT ICP-MS
y = 0.954x R2=0.99
Rutgers ICP-MS vs. MIT ICP-MS
y = 0.963x R2=0.97
MIT INAA and Rutgers ICP-MS
MIT ICP-MS
Eu
slope=1
MIT INAA vs. MIT ICP-MS
y = 0.977x R2=0.99
Rutgers ICP-MS vs. MIT ICP-MS
y = 0,984x R2=0.97
MIT INAA and Rutgers ICP-MS
MIT ICP-MS

Figure A-5b.

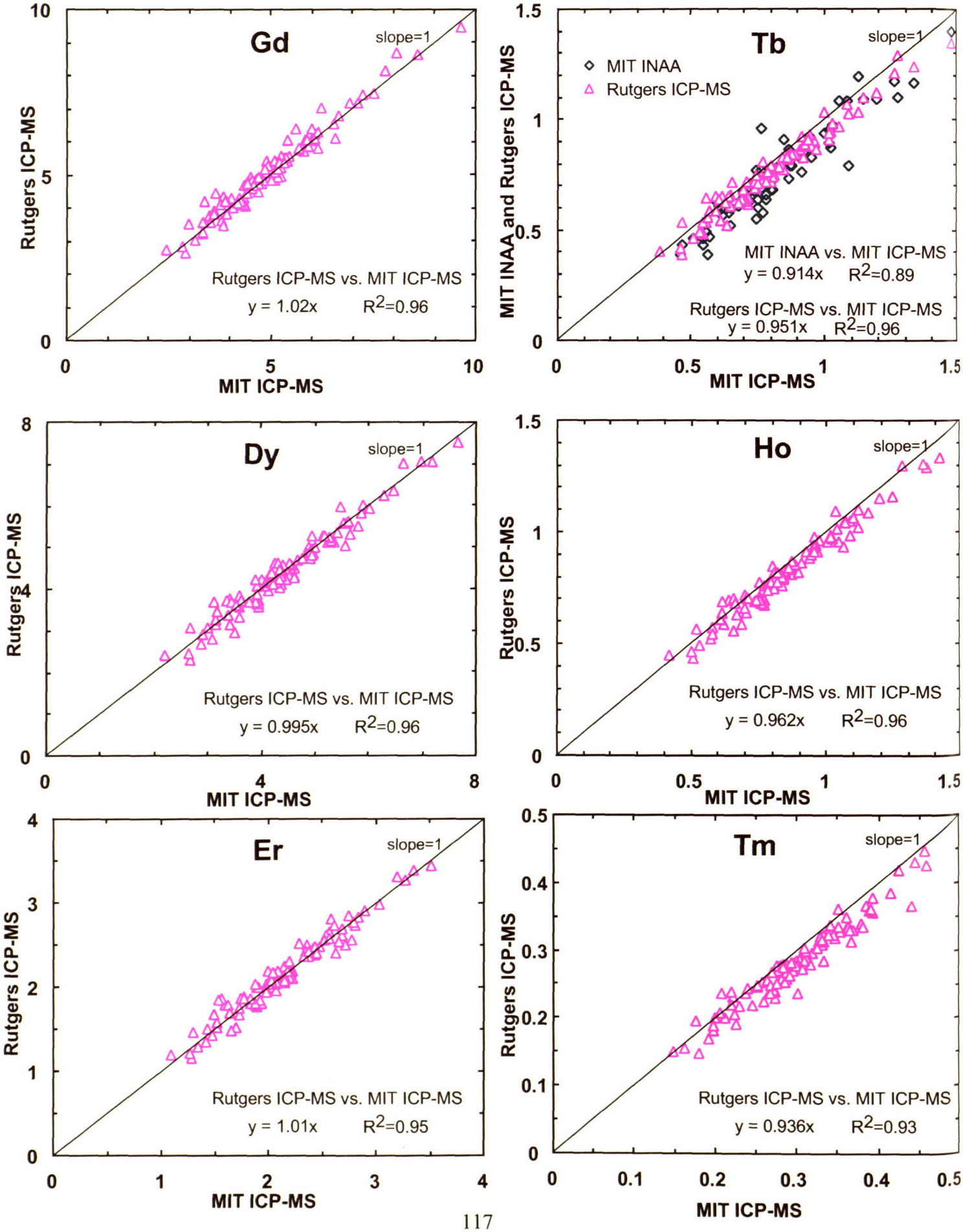
Gd
slope=1
Rutgers ICP-MS vs. MIT ICP-MS
y = 1.02x R2=0.96
Rutgers ICP-MS
MIT ICP-MS
Tb
slope=1
MIT INAA
Rutgers ICP-MS
MIT INAA vs. MIT ICP-MS
y = 0.914x R2=0.89
Rutgers ICP-MS vs. MIT ICP-MS
y = 0.951x R2=0.96
MIT INAA and Rutgers ICP-MS
MIT ICP-MS
Dy
slope=1
Rutgers ICP-MS vs. MIT ICP-MS
y = 0.995x R2=0.96
Rutgers ICP-MS
MIT ICP-MS
Ho
slope=1
Rutgers ICP-MS vs. MIT ICP-MS
y = 0.962x R2=0.96
Rutgers ICP-MS
MIT ICP-MS
Er
slope=1
Rutgers ICP-MS vs. MIT ICP-MS
y = 1.01x R2=0.95
Rutgers ICP-MS
MIT ICP-MS
Tm
slope=1
Rutgers ICP-MS vs. MIT ICP-MS
y = 0.936x R2=0.93
Rutgers ICP-MS
MIT ICP-MS

Figure A-5c.

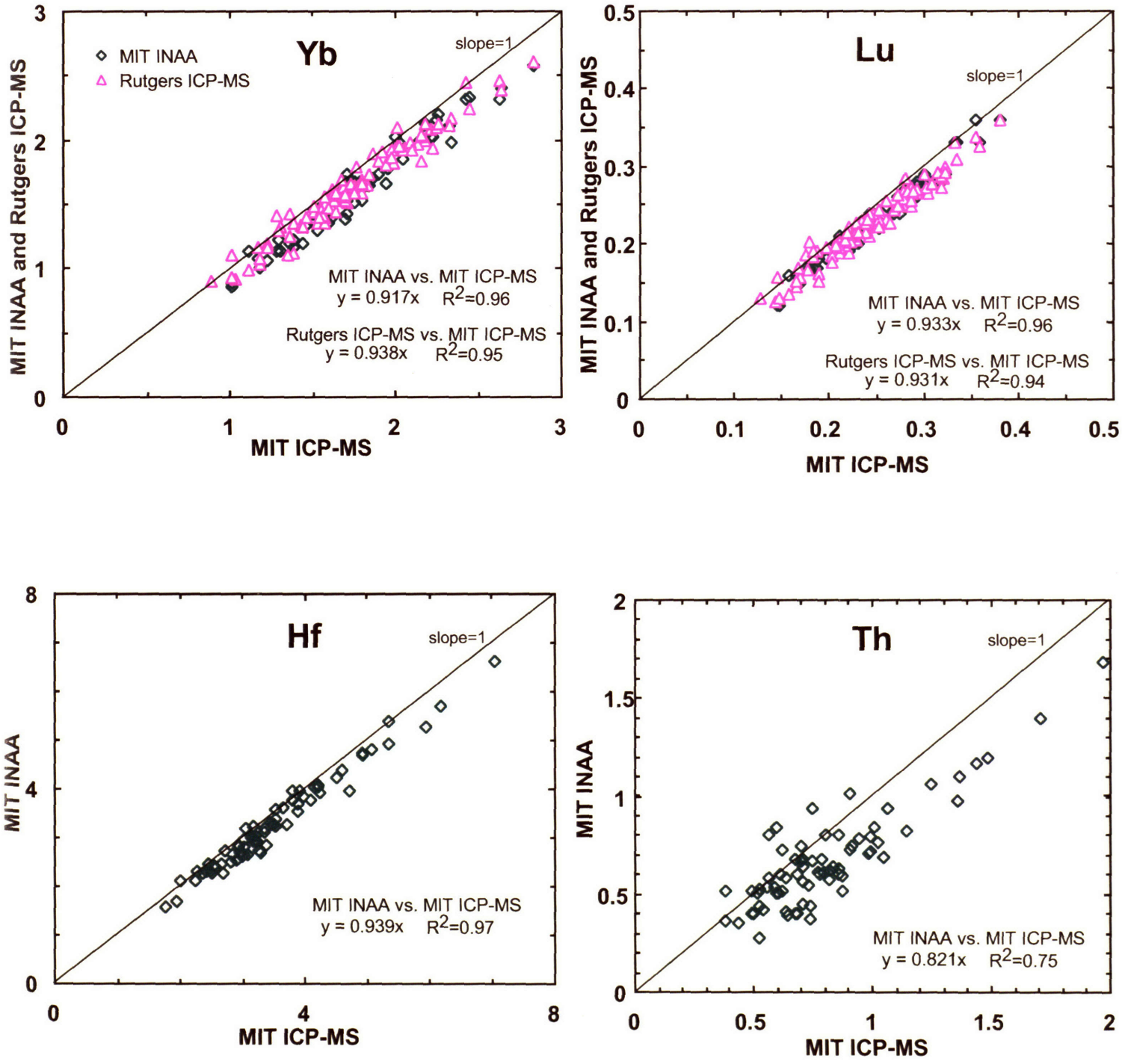
Yb
MIT INAA
Rutgers ICP-MS
slope=1
MIT INAA vs. MIT ICP-MS
y = 0.917x R2=0.96
Rutgers ICP-MS vs. MIT ICP-MS
y = 0.938x R2=0.95
MIT INAA and Rutgers ICP-MS
MIT ICP-MS
Lu
slope=1
MIT INAA vs. MIT ICP-MS
y = 0.933x R2=0.96
Rutgers ICP-MS vs. MIT ICP-MS
y = 0.931x R2=0.94
MIT INAA and Rutgers ICP-MS
MIT ICP-MS
Hf
slope=1
MIT INAA vs. MIT ICP-MS
y = 0.939x R2=0.97
MIT INAA
MIT ICP-MS
Th
slope=1
MIT INAA vs. MIT ICP-MS
y = 0.821x R2=0.75
MIT INAA
MIT ICP-MS

CHAPTER 2: RECYCLED OCEANIC CRUST IN THE HAWAIIAN PLUME: EVIDENCE FROM TEMPORAL GEOCHEMICAL VARIATIONS WITHIN THE KOOLAU SHIELD.

Abstract:

The subaerial surface of Koolau volcano is composed of lavas that define the distinctive endmember composition for Hawaiian shield lavas, known as the Koolau component, now designated as the Makapuu-stage. The geochemical characteristics of lavas recovered by the Koolau Scientific Drilling Project (KSDP) show that this distinctive composition forms a <300 m veneer. Below this veneer, from ~300 to 470 m below sea level, Koolau shield lavas transition to a composition similar to Mauna Loa lavas, now designated as the Kalihi-stage. This transition was gradual, occurring over >80 ka; therefore it was not caused by an abrupt event, such as a landslide.

Among all Koolau shield lavas, there are correlations between radiogenic isotopic ratios of Sr, Nd and Pb and compositional characteristics, such as SiO_2 content (adjusted to be in equilibrium with Fo_{90} olivine), Sr/Nb, La/Nb and Th/La. These long-term compositional and isotopic trends show that as the shield aged there was an increasing role for an ancient recycled marine sediment component (<3% of the source) accompanied by up to 20% SiO_2-rich dacitic melt. This melt was generated by partial melting of garnet pyroxenite, probably kilometers in size, that formed from recycled basaltic oceanic crust. In detail, time series analyses of depth profiles of Al_2O_3/CaO, Sr/Nb, La/Nb and Th/La in the KSDP drill core show correlations among these ratios indicating that recycled oceanic crust contributed episodically, ~29 ka period, to the magma source during the prolonged transition from Kalihi- to Makapuu-stage lava compositions. The long-term geochemical trends show that recycled oceanic crust was

increasingly important as the Koolau shield moved away from the plume and encountered lower temperature.

1.Introduction:

Although shield-stage lavas of Hawaiian volcanoes are derived from the Hawaiian hotspot, commonly inferred to be a mantle plume, many Hawaiian shields are distinct from one another in major and trace element abundances, as well as isotopic ratios (e.g., Frey and Rhodes, 1993; Frey et al., 1994; Hauri, 1996; Lassiter and Hauri, 1998). Some of these geochemical differences may be related to melting processes, but there is no doubt that the mantle source for Hawaiian shield lavas is geochemically heterogeneous. Compositions of lavas collected from subaerial exposures of the Koolau shield on Oahu (Fig. 1 in Introduction Chapter) define an extreme endmember. They are characterized by relatively high SiO_2 content, SiO_2/total iron, Al_2O_3/CaO, La/Nb, Sr/Nb, $^{87}Sr/^{86}Sr$, $^{187}Os/^{188}Os$, $\delta^{18}O$ and low total iron and CaO contents, $^{143}Nd/^{144}Nd$, $^{176}Hf/^{177}Hf$ and $^{206}Pb/^{204}Pb$ (e.g., Frey et al., 1994; Roden et al., 1994; Lassiter and Hauri, 1998; Blichert-Toft et al., 1999). These geochemical characteristics have provided support for recycled oceanic crust, including sediments, in the source of Koolau lavas.

It is also well established that there are important temporal geochemical changes within individual Hawaiian shields. At some shields there are large variations, e.g., Mauna Loa (Rhodes and Hart, 1995; Kurz et al., 1995), whereas at others, such as Mauna Kea, the temporal changes are relatively subtle (e.g., Special Section of Hawaii Scientific Drilling Project in J. Geophys. Res., 1996 Vol. 101, pp11,593-pp11,864; Theme of Hawaii Scientific Drilling Project in Geochem. Geophys. Geosyst. 2003). Hence, an important question is – **Does the entire Koolau shield have the end-member geochemical characteristics manifested by the subaerially exposed lavas?** Studies of lavas recovered from a highway (H3) tunnel (Jackson et al., 1999) and from the

submarine landslide blocks (Shinozaki et al., 2002; Tanaka et al., 2002) indicate that the geochemical characteristics of older Koolau lavas may not be similar to the surface Koolau lavas. Specifically, Tanaka et al. (2002) argue for a temporal transition from Mauna Kea-like to Mauna Loa-like to Koolau-like with decreasing age. However, determining the origin and relative age of lavas from landslide blocks is difficult. A more direct approach to determining temporal geochemical variations in Koolau shield lavas is drilling and coring. This goal was achieved by the Koolau Scientific Drilling Project (KSDP) which deepened and cored a ~351 m water well to a depth of ~679 m (Haskins and Garcia, 2004). The upper 351 m were rotary drilled and only rock chips are available, whereas nearly continuous core was recovered from the lower 328 m using a diamond drill bit. This core samples 103 subaerially erupted lava flows and one sedimentary unit. Ar-Ar plateau ages of three drill hole lavas are 2.8 to 2.9 Ma (Haskins and Garcia, 2005). Based on petrography and compositions of whole-rocks and glasses, Haskins and Garcia (2004) conclude that the distinctive geochemical features of uppermost Koolau lavas (hereafter referenced as Makapuu-stage lavas) "**form a veneer only 175-250 m thick at the drill site".** This veneer overlies lavas with Mauna Loa-like major element compositions which Haskins and Garcia (2004) define as the Kalihi-stage of the Koolau shield.

As part of a team effort studying the KSDP core, I report 26 trace element abundances in 91 KSDP core samples (Table 1a) analyzed by inductively coupled plasma mass spectrometry (ICP-MS); see Appendix A2 of Huang and Frey (2003) for procedures and discussion of accuracy and precision. I use these data, in conjunction with major element compositions and Nd-Hf-Pb isotopic ratios (Haskins and Garcia, 2004;

Fekiacova et al., in prep.; Salters et al., in prep.), to understand the temporal evolution of Koolau shield lavas.

Makapuu-stage lavas have been studied by Frey et al. (1994), who used X-ray fluorescence (XRF) and instrumental neutron activation (INAA) to obtain trace element data. In order to minimize bias caused by using different analytical methods, I re-analyzed by ICP-MS 15 Makapuu-stage lavas which have been analyzed for Sr-Nd-Pb isotopic ratios (Roden et al., 1994) and major and trace elements (Frey et al., 1994) (Table 1b).

2. Results: Incompatible Elements

Abundances of incompatible elements that are immobile during alteration, such as Nb and La, are positively correlated with Th abundance for both Makapuu-stage lavas and Kalihi-stage lavas (Fig. 1a, 1b). Sr and Rb abundances are generally correlated with Th abundance; however, these trends are more scattered (Fig. 1c, 1d). Some of this scatter, e.g., to relatively low Rb abundance, is caused by altered samples. There are significant differences between Makapuu-stage and Kalihi-stage lavas; at a given Th abundance Makapuu-stage lavas have higher La and Sr abundances than Kalihi-stage lavas (Fig. 1a, 1c).

Fig. 2 shows the primitive mantle normalized trace element abundances of Makapuu-stage and Kalihi-stage lavas. Both lava suites have been adjusted to be in equilibrium with mantle olivine composition (Fo_{90}) to minimize the effect of crystal fractionation. The most obvious difference between the two lava suites is the relative Sr enrichment in the Makapuu-stage lavas. Since only relatively unaltered lavas are plotted, the enrichment of Sr in Makapuu-stage lavas is not a result of post-magmatic alteration.

In contrast to the large variations in highly incompatible elements, abundances of heavy rare earth elements are nearly constant in both Makapuu-stage and Kalihi-stage lavas (Fig. 2).

3. Discussion:

3.1 The Transition from Makapuu-Stage to Kalihi-Stage Lavas: Constraints from the KSDP Core

Haskins and Garcia (Fig. 10, 2004) used Al_2O_3/CaO to define a change from the Makapuu-stage ($Al_2O_3/CaO > 1.45$) to Kalihi-stage ($Al_2O_3/CaO < 1.45$) within the uppermost 250 m of the KSDP hole. There is, however, considerable structure in the downhole variation of Al_2O_3/CaO within the KSDP drill core (Fig. 3a). Within the upper part of the KSDP core, at a depth level inferred to be Kalihi-stage lavas, there are two groups of lavas which have Al_2O_3/CaO near the boundary between Makapuu- and Kalihi-stage lavas. Units 4, 5, 6 and 9, 10, 12 have $Al_2O_3/CaO = 1.42$ to 1.44 (Fig. 3a). Deeper in the core, Unit 70 has $Al_2O_3/CaO = 1.43$, Unit 85 has a ratio of 1.45 and Unit 88 has a ratio of 1.54. Units 85 and 88 are altered lavas; e.g., among Kalihi-Stage lavas, Unit 88 has the highest Loss on Ignition (L.O.I. = 3.65%), and Unit 85 has a L.O.I. of 2.89% (Table 4 of Haskins and Garcia, 2004).

The presence of orthopyroxene is a diagnostic petrographic characteristic of Makapuu-stage lavas (Frey et al., 1994), but orthopyroxene also occurs in KSDP cored lavas classified as Kalihi-stage lavas, that is, orthopyroxene is present in 6 of the uppermost 11 lava flows, including Units 9, 10 and 12 with high Al_2O_3/CaO, is absent in the underlying 44 lava flows, and is sporadically present in 7 of the lowermost 35 lava flows (Table 2 of Haskins and Garcia, 2004).

Surface Koolau lavas, i.e., Makapuu-stage lavas, are distinguished from other Hawaiian shield lavas by their relatively high La/Nb and Sr/Nb (Fig. 11 of Frey et al., 1994; Fig. 13b of Huang and Frey, 2003). A distinct difference between Makapuu-stage and Kalihi-stage lavas in La/Nb and Sr/Nb is apparent in Fig. 4a where the lower ratios of the Kalihi-stage lavas overlap with the Mauna Loa field. These differences are not a function of MgO content (Fig. 4b). In detail, however, Units 4, 5 and 6 of the KSDP core overlap with Makapuu-stage lavas in Sr/Nb and Units 4, 6, 14, 73 and 81 overlap in La/Nb (Fig. 3).

An objective is to use trace element geochemistry to understand the transition from Kalihi-stage to Makapuu-stage compositions. In particular to address the question – was the transition abrupt or gradual? As shown in Fig. 3, within the uppermost 32 m of the KSDP core, classed as Kalihi-stage by Haskins and Garcia (2004), there are six flows (Units 4, 5, 6, 9, 10 and 12) with geochemical characteristics that are transitional between Makapuu-stage and Kalihi-stage groups. Also, La/Nb and Sr/Nb generally increase upwards from an elevation of ~470 m below sea level, but there are high frequency variations superimposed on these general trends. Within the KSDP core there is no indication that there was an abrupt change from only Kalihi-stage composition to the distinctive Makapuu-stage composition. Rather the Makapuu-stage geochemical signature gradually appears towards the top of the core and is most evident in two groups, Units 4, 5, 6, and Units 9, 10, 12.

Haskins and Garcia (2004) argue that the transition from Kalihi- to Makapuu-stage compositions occurred over a 60-m-thick sequence of lavas; consequently, this transition lasted over 2,600–4,600 years assuming a lava accumulation rate of 13-23 mm

per year (DePaolo and Stolper, 1996). These accumulation rates may be too high for late shield growth (c.f., 8.6 to 0.4 mm per year for Mauna Kea, Sharp and Renne, in press). Moreover, I infer that the transition from typical Kalihi-stage composition to Makapuu-stage composition began at the elevation of ~470 mbsl in the KSDP drill hole, and continued to the top of the cored section at ~300 mbsl (Fig. 3). This transition corresponds to at least ~60 lava flows (Table 1a). If the time interval between flows at a given location is ~1400 years (estimated from the Mauna Kea portion of the Phase 2 of the Hawaii Scientific Drilling Project core which consists of ~300 shield and late-shield lava flow units erupted over ~410 ka, Sharp and Renne, in press), the transition in composition from Kalihi-stage lavas to Makapuu-stage lavas lasted for ~84 ka which corresponds to a growth rate of ~2 mm per year, and is much longer than the estimate, 2.6-4.6 ka, of Haskins and Garcia (2004). Consequently, I conclude that the transition was not caused by a catastrophic event, such as the Nuuanu landslide (Haskins and Garcia, 2004).

3.2 Role of Recycled Marine Sediment in the Source of Koolau Lavas

What is the source of the distinctive Makapuu-stage geochemical signature? Depth profiles of $^{208}Pb^*/^{206}Pb^*$ (defined in Fig. 5 caption), $^{143}Nd/^{144}Nd$ and $^{176}Hf/^{177}Hf$ (Fekiacova et al., in prep.; Salters et al., in prep.) are similar to those of La/Nb and Sr/Nb. Consequently, Makapuu-stage and Kalihi-stage lavas form trends in La/Nb versus $^{208}Pb^*/^{206}Pb^*$, $^{143}Nd/^{144}Nd$ and $^{176}Hf/^{177}Hf$ plots (Fig. 5a-c). Koolau lavas (Makapuu-stage and Kalihi-stage) also form trends in Th/La versus $^{208}Pb^*/^{206}Pb^*$, $^{143}Nd/^{144}Nd$ and $^{176}Hf/^{177}Hf$ plots (Fig. 5d-f). Clearly, these lavas were derived from a source containing two geochemically distinct components. One component is like Mauna Loa lavas (Fig.

5a, 5c), but the other component defines an extreme endmember for Hawaiian shield lavas. The characteristics of Makapuu-stage lavas, high La/Nb, high $^{176}Hf/^{177}Hf$ at a given $^{143}Nd/^{144}Nd$ and relatively high $^{187}Os/^{188}Os$ and $\delta^{18}O$, have been proposed as recycled sediment signatures (Lassiter and Hauri, 1998; Jackson et al., 1999; Blichert-Toft et al., 1999; Huang and Frey, 2003). Since marine sediments typically have higher $^{232}Th/^{238}U$ and lower $^{238}U/^{204}Pb$ than primitive mantle values (e.g., Figs. 11 and 12 of Ben Othman et al., 1989), ancient recycled sediments are characterized by relatively low $^{206}Pb/^{204}Pb$ and high $^{208}Pb/^{204}Pb$ at a given $^{206}Pb/^{204}Pb$, i.e., high $^{208}Pb^*/^{206}Pb^*$. Therefore, several of the extreme geochemical characteristics of Makapuu-stage lavas are consistent with ancient recycled marine sediment in their source. The correlations in Figs. 4 and 5 require that this component also has high La/Nb (>1.6), Sr/Nb (>55) and low Th/La (<0.05). I ask – Are these characteristics of marine sediment? Sr/Nb and Th/La are highly variable in marine sediments (Fig. 6; Fig. 2 of Plank, 2005); however, most carbonate- and phosphate-rich ($CaO>20\%$, $Al_2O_3/P_2O_5<10$) sediments are characterized high Sr/Nb (>55) and low Th/La (<0.05) (Fig. 6). In addition, the hydrothermal clay section recovered from east of the Tonga trench, which is also phosphate-rich, has these geochemical characteristics (Fig. 6; Table 1 of Plank and Langmuir, 1998). These two types of sediments are possible sedimentary components in Makapuu-stage lavas.

Can phosphate-bearing carbonate and hydrothermal clay also explain the Makapuu-stage characteristic of high $^{176}Hf/^{177}Hf$ at a given $^{143}Nd/^{144}Nd$ (Fig. 7)? Rare earth elements are abundant in phosphate; consequently, phosphate-rich sediment is characterized by high Lu/Hf (e.g., Table 1 of Plank and Langmuir, 1998). Time-integrated high Lu/Hf leads to high $^{176}Hf/^{177}Hf$ at a given $^{143}Nd/^{144}Nd$. For example, the

carbonate section from the Guatemala trench has Lu/Hf = 1.4 and Sm/Nd = 0.25 (Table 2a). A mixture of 3% 2Ga sediment with such Lu/Hf and Sm/Nd ratios and 97% primitive mantle has ε_{Nd} = -2.7 and ε_{Hf} = 4.4, which are appropriate as an end-member component for Makapuu-stage lavas (Table 2a; Fig. 7). The hydrothermal clay section from east of the Tonga trench has Lu/Hf = 0.47 and Sm/Nd = 0.20 (Table 2b). A mixture of 0.25% 2Ga sediment with such Lu/Hf and Sm/Nd ratios and 99.75% primitive mantle has ε_{Nd} = -4.2 and ε_{Hf} = 1.8, which are also appropriate as an end-member component for Makapuu-stage lavas (Table 2b; Fig. 7). The lower amount of hydrothermal sediment required arises from their high trace element abundances (Table 2b).

Small amounts of phosphate-bearing carbonate (3%) or hydrothermal clay (0.25%) can also explain the high La/Nb and low Th/La that are characteristic of Makapuu-stage lavas (see source compositions in Table 3). The required high Sr/Nb (>55) is also consistent with 3% phosphate-bearing carbonate but is inconsistent with only 0.25% hydrothermal clay, similar to that recovered from east of the Tonga trench (see source compositions in Table 3). However, given the variable Sr content of hydrothermal sediments (e.g., Thompson et al., 1988; Honnorez et al., 1999), I do not preclude hydrothermal sediment as a possible component in the source of Makapuu-stage lavas.

Carbonate-rich sediments with high Sr/Nb and low Th/La are a regional feature of the equatorial eastern Pacific Ocean; e.g., they occur in the Guatemala trench and basin, as well as the Peru and Columbia trenches (Plank and Langmuir, 1998; Patino et al., 2000; Plank et al., 2002). However, these carbonate-rich sediments are associated with biological activity, such as nannofossil and foram deposits that did not exist at 2 Ga. Nevertheless, the high rare earth element content of Proterozoic marine carbonate

sediments, such as phosphorites and carbonates associated with banded iron formations, indicate that these sediments are likely to have low Th/La accompanied by high Sr/Nb (e.g., Tu et al., 1985).

The sedimentary component in Koolau lavas is also characterized by high $^{87}Sr/^{86}Sr$ (~0.7045, Fig. 14 of Huang and Frey, 2003). Hydrothermal sediments are characterized by high Rb/Sr. For example, the hydrothermal clay section from east of the Tonga trench has Rb/Sr = 0.09 (Table 1 of Plank and Langmuir, 1998), and the primitive mantle value is 0.03 (Hofmann, 1988). Consequently, aged recycled hydrothermal sediments are characterized by high $^{87}Sr/^{86}Sr$. In contrast, phosphate-bearing carbonate-rich sediments are characterized by low Rb/Sr. For example, the carbonate section from the Guatemala trench has Rb/Sr = 0.005 (Table 1 of Plank and Langmuir, 1998). Can ancient recycled phosphate-bearing carbonate-rich sediments have high $^{87}Sr/^{86}Sr$? At 2Ga, seawater $^{87}Sr/^{86}Sr$ was > 0.704 (Fig. 3 of Ray et al., 2002). Consequently, ancient recycled phosphate-bearing carbonate-rich sediments, which inherit $^{87}Sr/^{86}Sr$ from seawater, can explain the high $^{87}Sr/^{86}Sr$ in Makapuu-stage lavas.

Additional evidence supporting marine sediments as a source component for Makapuu-stage lavas arises from correlations between Ce/Pb and La/Nb, Th/La and Ba/Th in Koolau glasses that extrapolate toward a component with low Ce/Pb and Th/La and high Ba/Th and La/Nb (Fig. 8). Compared with MORB and OIB, marine sediments are generally characterized by low Ce/Pb (e.g., Hofmann, 1997). Specifically, the carbonate section at Guatemala and the hydrothermal clay section from Tonga have Ce/Pb =0.6-0.8 (Table 1 of Plank and Langmuir, 1998; Table 2 of Patino et al., 2000). In addition, these sediments have high Ba/Th (>1000), low Th/La (0.02-0.03) and high

La/Nb (18-56). In contrast to the glass data, whole rock data (even after applying an alteration filter) do not form obvious trends in Fig. 8, implying that Ce/Pb and Ba/Th were affected by post-magmatic alteration even in these relatively less altered whole rocks. Nevertheless the linear trends formed by glass data in Fig. 8 imply a source component with low Th/La, Ce/Pb and high La/Nb and Ba/Th, which is consistent with phosphate-bearing carbonate-rich or hydrothermal sediments as a source component for Koolau lavas.

3.3 The Transition from Makapuu-Stage to Kalihi-Stage Lavas: Constraints from Nuuanu Landslide Deposits.

With decreasing age, there was a greater proportion of a recycled sedimentary component in the source of Koolau lavas, but the proportion of this component in the source did not change abruptly or systematically with time in the Kalihi-stage (Fig. 3) or Makapuu-stage (Frey et al., 1994; Roden et al., 1994). This inference of a gradual transition from Kalihi-stage geochemical characteristics contrasts with that of Shinozaki et al. (2002), Takahashi and Nakajima (2002) and Tanaka et al. (2002) who described the transition from Mauna Loa-like composition (Kalihi-stage) to Makapuu-stage composition as "very sharp and abrupt" occurring over an interval of ~10 m in subaerial outcrops on the Nuuanu Pali. I note, however, that their data form linear trends overlapping with the trends defined by KSDP and Makapuu-stage lavas in La/Nb vs Sr/Nb, $^{143}Nd/^{144}Nd$ and $^{208}Pb^*/^{206}Pb^*$ plots (Fig. 9). In detail, the relatively old Nuuanu landslide samples overlap with the Kalihi-stage field; the submarine Oahu North and subaerial Makapuu samples overlap with the Makapuu-stage field; and the subaerial lavas from Nuuanu Pali straddle the boundaries between Kalihi-stage and Makapuu-stage lavas

(Fig. 9). Consequently, I argue for a gradual, rather than abrupt, transition between Kalihi-stage and Makapuu-stage volcanism (Figs. 3 and 9).

3.4 Relative Role of Garnet Pyroxenite/Eclogite and Peridotite as Sources for Koolau Lavas: Trace Element Constraints

After Koolau whole rock compositions are adjusted to be in equilibrium with a common mantle olivine composition (Fo_{90}), the abundance of heavy rare earth elements are much less variable than those of highly incompatible elements (Fig. 2). This result reflects garnet as a residual mineral during partial melting (Hofmann et al., 1984). Compared with other Hawaiian shield lavas, Makapuu-stage lavas at a given MgO content have lower Sc, Y and Yb abundances, a result interpreted to reflect a larger proportion of residual garnet during generation of Makapuu-stage lavas (Budahn and Schmitt, 1985; Frey et al., 1994; Jackson et al., 1999). This observation is confirmed by our ICP-MS data of Makapuu-stage lavas (Fig. 10). Kalihi-stage lavas have higher Sc, Y and Yb abundances than Makapuu-stage lavas, and overlap with (Sc) or are on the lower part of (Y and Yb) the fields defined by Mauna Kea and Mauna Loa lavas (Fig. 10a-d). Among these elements, Sc is the best discriminant between Makapuu-stage and Kalihi-stage lavas. This may reflect the greater compatibility of Sc, relative to Y and Yb, in both garnet and clinopyroxene (e.g., Pertermann et al., 2004).

The variable presence of a sedimentary component in Koolau lavas indicates that garnet pyroxenite, formed from recycled basaltic oceanic crust, may also be a source component. In subsequent discussion, I use garnet pyroxenite as a general rock name that includes eclogite. Hauri (1996) concluded that Makapuu-stage lavas contain a dacitic component derived from partial melting of quartz-bearing garnet pyroxenite formed from

recycled oceanic crust. More recently, Takahashi and Nakajima (2002) inferred that Makapuu-stage lavas were derived from eclogite formed from recycled Fe-rich Archean basalt, whereas Garcia (2002) argued that picritic submarine lavas from the slope of Koolau Volcano were primarily derived from partial melting of peridotite. Hence the source of Koolau lavas may have been peridotite with embedded garnet pyroxenite heterogeneities. How does melting of such a mixed source proceed? Since the solidi of most garnet pyroxenites are lower than those of peridotite (e.g., Hirschmann and Stolper, 1996), one modeling approach is to fertilize the unmelted peridotite with partial melt of garnet pyroxenite to form a homogeneous modified garnet peridotite source. This process is consistent with the experiments by Yaxley and Green (1998) and was used by Sobolev et al. (2000) to model the origin of melt inclusions in olivine in Mauna Loa lavas.

Koolau data consistent with variable partial melting of a garnet peridotite source are the correlated variations in ratios that are controlled by residual garnet, such as La/Yb, Sc/Y and Tb/Yb, in Kalihi-stage and Makapuu-stage lavas (Fig. 11). The La/Yb-Sc/Y, La/Yb-Zr/Yb and La/Yb-Tb/Yb trends can be explained by partial melting of a garnet peridotite, with uniform La/Yb, Sc/Y, Zr/Yb and Tb/Yb (Fig. 11). These ratios may have been similar in the sources of Kalihi-stage and Makapuu-stage lavas because adding a small amount (<3%) of sediment into the proposed source for Kalihi-stage lavas has little effect on these ratios. For example, adding 3% phosphate-bearing carbonate-rich sediment into the proposed source for Kalihi-stage lavas markedly increases La/Nb from 0.95 to 1.5, Sr/Nb from 35 to 98 and decreases Th/La from 0.07 to 0.05, but only changes La/Yb by <50%, and Sc/Y, Zr/Yb and Tb/Yb by <15% (Table 3). In contrast, La/Yb, Sc/Y, Zr/Yb and Tb/Yb in Makapuu-stage and Kalihi-stage lavas vary by a factor of >2,

~1.7, >2 and ~1.2, respectively (Fig. 11). I infer that Makapuu-stage lavas were derived by lower extents of melting than Kalihi-stage lavas. Consequently, they equilibrated with a larger amount of residual garnet.

Although I am confident that abundance ratios sensitive to control by residual garnet were controlled by the melting process, the simple model of variable extents of partial melting of garnet peridotite is not suitable. Eggins (1992) and Wagner and Grove (1998) showed that the estimated primary magma compositions for Hawaiian shield lavas, and especially Makapuu-stage lavas (Hauri, 1996), are not in equilibrium with garnet peridotite. More complex models are required.

One possibility is mixing of melts derived from garnet peridotite and garnet pyroxenite. However, La/Yb is not correlated with Sr-Nd-Pb isotopic ratios; therefore, the trends formed by Koolau lavas in Fig. 11 are not magma mixing trends. Rather I infer that Koolau lavas reflect both variable extents of partial melting and magma mixing processes. That is, the transition from Kalihi-stage to Makapuu-stage was accompanied by decreasing melting extent and an increasing proportion of a garnet pyroxenite melt component. In this scenario a complexity is that melts of garnet pyroxenite are very reactive with peridotite and require transport in isolated channels (e.g., Yaxley and Green, 1998; Takahashi and Nakajima, 2002; Kogiso et al., 2004). That is, the SiO_2-rich melts derived by partial melting of garnet pyroxenite react with peridotite and convert olivine to orthopyroxene (e.g., Yaxley and Green, 1998; Takahashi and Nakajima, 2002). It is possible that the orthopyroxene band formed between SiO_2-rich and peridotite precludes further reaction. Consequently, there is a possibility that SiO_2-rich melts ascend to a magma chamber or even to the Earth's surface. The presence of adakite, which is

proposed as partial melt of subducting oceanic crust (e.g., Yogodzinski et al., 1995), provides evidence for this possibility. A requirement of this hypothesis is that the garnet pyroxenite body should be large in size, probably several kilometers, in order to generate sufficient SiO_2-rich melt to form isolated channels insulated from reaction by orthopyroxene bands (Takahashi and Nakajima, 2002). Since melt derived from garnet pyroxenite has been proposed to be a significant (Hauri, 1996) or even dominant component (Takahashi and Nakajima, 2002) for the Makapuu-stage of Koolau, I ask: is it possible to use trace element abundances to distinguish between garnet pyroxenite and garnet peridotite as sources for Makapuu-stage lavas?

Based on experiments in the CMAS (CaO, MgO, Al_2O_3 and SiO_2) system, van Westrenen et al. (Fig. 5d, 2001) proposed that Zr/Yb can be used to distinguish between melts derived from garnet pyroxenite and garnet peridotite. This discriminant arises because $D_{Zr}^{garnet/melt}>1$ for the Ca-rich garnet in garnet pyroxenite, and consequently D_{Zr} is similar to D_{Yb}, but $D_{Zr}^{garnet/melt} < D_{Yb}^{garnet/melt}$ for the Mg-rich garnet in garnet peridotite. However, recent experimental results for more complex compositional systems, notably including Ti, show that Zr is not compatible in Ca-rich garnet (Pertermann et al., 2004). Rather than Zr/Yb, Pertermann et al. (2004) propose Zr/Hf as a discriminant for distinguishing residual eclogite (high clinopyroxene/garnet ratio) from residual garnet peridotite (low clinopyroxene/garnet ratio). The suitability of Zr/Hf as a discriminant arises because: (1) $(K_D)_{Zr/Hf}$ for clinopyroxene/melt is ~0.5 whereas it is ~1 for garnet/melt; and (2) the very different clinopyroxene/garnet ratios for eclogite and garnet peridotite used by Pertermann et al. (2004). However clinopyroxene/garnet ratios in peridotite are very dependent upon pressure and temperature (e.g., Walter, 1998), and

may overlap with the ratios in eclogite; therefore, I suggest that Zr/Hf is not a reliable discriminant (Fig. 12). Moreover, Fig. 10 of Pertermann et al. (2004) is misleading because as Koolau lavas they include data from both tholeiitic Koolau shield stage lavas and highly alkalic rejuvenated stage lavas erupted onto the Koolau shield (i.e., the Honolulu Volcanics). If only Koolau shield lavas are plotted, it is intriguing that Kalihi-stage and Makapuu-stage lavas may define different trends (Fig. 12). If this difference is substantiated with more high quality data, it requires a higher clinopyroxene/garnet ratio in the residue of Makapuu-stage lavas.

3.5 Relative Role of Garnet Pyroxenite/Eclogite and Peridotite as Sources for Koolau Lavas: Major Element Constraints

An early hypothesis for explaining the distinctive major element composition of Makapuu-stage lavas, i.e., relatively high SiO_2 and low total iron and CaO contents, was melt segregation at relatively low pressure (Frey et al., 1994; Putirka, 1999). However, Hauri (1996) noted problems with this interpretation. Namely the high SiO_2 content of Makapuu-stage lavas requires melt segregation at depths of 30-45 km, less than the thickness of Hawaiian lithosphere (Li et al., 2004). Also at low pressure, the experimental total iron contents are lower than observed (Fig. 2 of Hauri, 1996). He proposed an alternative hypothesis that the distinctive Makapuu-stage composition reflects SiO_2-rich partial melts derived from a garnet pyroxenite component in the plume.

Based on melt-peridotite reactions first discussed in Kelemen (1986), a third alternative for generating relatively high SiO_2 content was proposed by Stolper et al. (2004) for the High-SiO_2 Group Mauna Kea lavas recovered in Phase 2 of the Hawaii Scientific Drilling Project (HSDP). Specifically, melt generated from peridotite

(relatively low SiO_2 content) reacts with an overlying residual peridotite by assimilating orthopyroxene, clinopyroxene and crystallizing olivine thereby increasing the SiO_2 content in the melt. This reaction is similar to the models proposed by Eggins (1992) and Wagner and Grove (1998) to explain the high MgO Kilauea glasses. No attempt has yet been made to explain incompatible element abundance and isotopic ratios of HSDP lavas by this process. In addition, since Ni is much more compatible in olivine than other phases, this process will simultaneously increase SiO_2 content and decrease Ni content. Using mineral and melt compositions given in Table 3 of Stolper et al. (2004) and Equation 39 of Beattie et al. (1991), I obtain $D_{Ni}^{olivine/melt}=6.59$ and $D_{Ni}^{orthopyroxene/melt}=1.92$. Since $D_{Ni}^{clinopyroxene/orthopyroxene}<0.5$ (e.g, Table 2 of Seitz et al., 1999), I take $D_{Ni}^{clinopyroxene/melt}=0.96$ as a maximum estimate. Consequently, the reaction (Fit A) given in Table 3 of Stolper et al. (2004) predicts that Ni content in High-SiO_2 Mauna Kea Group lavas should be ~70% of that in Low-SiO_2 Mauna Kea Group lavas. However, this is not observed in HSDP2 whole rocks (Fig. 5f of Huang and Frey, 2003).

With respect to Koolau lavas, the reaction proposed by Stolper et al. (2004) does not significantly affect CaO and Al_2O_3 contents (see their Fig. 18). Therefore, this process does not explain the low CaO and high Al_2O_3/CaO of Makapuu-stage lavas (Fig. 11 of Frey et al., 1994; Fig. 10 of Haskins and Garcia, 2004). In addition, Garcia (2002) noted the unusually high Ni contents of olivine in Koolau lavas and in detail Makapuu-stage lavas have higher Ni contents than Kalihi-stage lavas (Fig. 10e). Consequently, the melt-peridotite reaction fails to explain important compositional features (low CaO and high Ni) of Makapuu-stage lavas. Therefore, this model is not suitable for explaining the SiO_2 difference between Makapuu-stage and Kalihi-stage lavas.

To further evaluate the role of melt derived from garnet pyroxenite in controlling major element compositions of Koolau lavas, the Makapuu-stage and Kalihi-stage lavas, with $K_2O/P_2O_5>1.2$ and MgO>6.5%, were adjusted to be in equilibrium with Fo_{90} olivine, which is the highest Fo olivine found in Makapuu-stage lavas (Norman and Garcia, 1999; Garcia, 2002), by adding or subtracting equilibrium olivine in 0.1% steps assuming $(Fe/Mg)_{olivine}/(Fe/Mg)_{melt}=0.30$. After this adjustment, there is still considerable variation in major element composition of Makapuu-stage and Kalihi-stage lavas (Figs. 13 and 14). Surprisingly, SiO_2 content does not distinguish Makapuu-stage and Kalihi-stage lavas. Some Kalihi-stage lavas, Units 6 and 9, also have high SiO_2 content (Fig. 13). These two units, along with samples from Units 4, 5, 10 and 12 which are not plotted in Fig. 13, also have the distinctive high Sr/Nb, a characteristic of Makapuu-stage lavas (Fig. 3c). The best major element discriminant between Makapuu-stage and Kalihi-stage lavas is CaO content (Fig. 14b; Fig. 5 of Haskins and Garcia; 2004). I argue in **Section 3.2** that Makapuu-stage lavas sampled more of a recycled phosphate-bearing carbonate-rich or hydrothermal sedimentary component. Since only small amounts (<3%) of a sedimentary component is required to explain the distinctive trace element geochemical signatures of Makapuu-stage lavas (Fig. 7; Table 3), the sedimentary component has negligible effect on the major element content, such as CaO, of Koolau lavas.

Olivine adjusted SiO_2 content in Koolau lavas is correlated with Nd-Hf-Pb isotopic ratios (Fig. 13). Therefore, the large variations in olivine adjusted major element contents are not artifacts of olivine adjustment. In the olivine adjusted SiO_2-$^{143}Nd/^{144}Nd$ plot (Fig. 13b), the averages for different Hawaiian shields (from Table 1 of Hauri, 1996) largely overlap with Koolau lavas (Makapuu-stage and Kalihi-stage lavas), implying that

a single shield (Koolau) may sample all the source components contributing to Hawaiian shields. Reiners (2002) also noted correlations between composition and isotopic ratios in individual sequences of basaltic eruptives, and he argued for mixing of melts derived from pyroxenite and peridotite. In detail, Makapuu-stage and Kalihi-stage lavas form subparallel trends in Fig. 13. A possible interpretation for these trends is that both Makapuu-stage and Kalihi-stage lavas contain varying proportions of a SiO_2-rich component derived from garnet pyroxenite but that the Makapuu-stage lavas contain more of an isotopically distinctive sedimentary component.

The calculated dacitic magma of Hauri (1996) has an unusual composition in having quite high MgO (6%) for its high SiO_2 content (64%). No experimentally derived melt of eclogite/garnet pyroxenite has these characteristics; in fact, Pertermann and Hirschmann (2003a) concluded that "no eclogitic partial melt has been identified that is capable of explaining all of compositional features of the exotic Koolau component". I ask – Is the 6% MgO-64% SiO_2 a robust estimate? A concern about the Hauri compilation of shield lava composition is SiO_2 mobility during alteration. A significant fraction (26%) of lavas in Hauri's data compilation have $K_2O/P_2O_5 < 1$, and Frey et al. (1994) showed that SiO_2 contents are commonly lower in such altered lavas. However, using our alteration discriminant ($2.2>K_2O/P_2O_5>1.2$) leads to similar averages for Makapuu-stage lavas (Table 4).

The mismatch between the 6% MgO-64% SiO_2 composition with partial melts of eclogite/garnet pyroxenite is apparent in Fig. 14a. This discrepancy can be avoided by choosing a more SiO_2-rich (~66%) component with ~2% MgO. Although such a dacitic component is consistent with experimentally determined melts of eclogite/garnet

pyroxenite, Pertermann and Hirschmann (2003a) suggest that there are two problems with this interpretation:

(a) Low degrees of melting of garnet pyroxenite are required to create a SiO_2-rich melt; hence a relatively low temperature is inferred. In contrast, high MgO-low SiO_2 picritic magma requires partial melting of peridotite at higher temperature. Generally, garnet pyroxenite melts to a very high extent (60%) at the peridotite solidus temperature (e.g., Fig. 4 of Pertermann and Hirschmann, 2003b). Consequently, Pertermann and Hirschmann (2003a) suggest that "dacitic partial melts could form from eclogite in the deeper portions or the cold periphery of the plume, with peridotite partial melting predominantly in the hot core"; therefore, they conclude that dacitic and picritic melts are unlikely to be in close proximity. I argue, however, that mixing of such melts is consistent with a physical model for the Hawaiian plume. For example, the radius of the Hawaiian plume is ~50-70 km and the potential temperature in the center of the plume may be ~300-400 degrees higher than ambient mantle (Ribe and Christensen, 1999; Zhang and Watt, 2002). Consequently, there is large horizontal temperature gradient within the Hawaiian plume (Figs. 4a and 5a of Ribe and Christensen, 1999). Since a Hawaiian volcano captures magma generated over a circular area (magma capture area) with radius ranging from 20 to 35 km (DePaolo and Stolper, 1996; Ribe and Christensen, 1999), the magma capture area can include melts derived over a large temperature range. Using Fig. 4 of Pertermann and Hirschmann (2003b), a temperature difference less than 200 degrees is required to generate low extent (10-20%) partial melts of garnet pyroxenite and high extent (~20%) partial melts

of peridotite. Since Makapuu-stage lavas formed as Koolau shield volcanism waned, i.e., when the shield was moving off the plume, the magma capture area included lower temperature dacitic melts.

(b) Referring to Norman and Garcia (1999), Pertermann and Hirschmann (2003a) argue that the trace element features created by residual garnet, e.g., high Sr/Y and Sm/Yb, are absent in Koolau lavas. However, in Figs. 2, 10 and 11 I provide evidence for garnet as an important residual phase for Makapuu-stage lavas. Moreover, Fig. 6c of Haskins and Garcia (2004) also shows that a relatively high Sr/Y in Makapuu-stage lavas is consistent with a dacitic component.

Finally Hawaiian shield lavas define a clear inverse MgO-SiO_2 trend with Makapuu-stage lavas as one extreme (Fig. 14a), but the MgO-CaO plot is scattered (Fig. 14b). Nevertheless, Makapuu-stage lavas are offset to low CaO at a given MgO, and this result is consistent with a low CaO, dacitic component in these lavas (Fig. 14b). Additional evidence in favor of a dacitic component is the positive SiO_2 versus Na_2O+K_2O trend for Koolau lavas (Fig. 14c). This trend can be explained by mixing low SiO_2-low (Na_2O+K_2O) picritic melt and high SiO_2-high (Na_2O+K_2O) dacitic melt. If the picrite endmember has 48% SiO_2 and 16% MgO, and the dacite endmember has 66% SiO_2 and 2% MgO (Fig. 14a), the maximum amount of dacite endmember in Koolau lavas is ~20%.

3.6 Relative Role of Garnet Pyroxenite/Eclogite and Peridotite as Sources for Koolau Lavas: Ni Constraints

Olivine and whole rocks from Koolau Volcano have unusually high Ni content (Fig. 4 of Garcia, 2002; Fig. 10e). Sobolev et al. (in press) noted that Ni/MgO and SiO_2

(both corrected for olivine fractionation) are positively correlated in Hawaiian shield lavas, with Makapuu-stage lavas defining the high SiO_2 and Ni/MgO endmember. In **section 3.5** I used the relatively high Ni content to argue against a melt-mantle reaction model for explaining high SiO_2. Based on major element contents, I inferred that the high SiO_2 component in Koolau lavas is a dacitic melt; however dacitic partial melts of eclogites formed from recycled oceanic crust are expected to have low Ni content. In contrast, Sobolev et al. (in press) suggest that high Ni/MgO may be associated with SiO_2-rich melt. They argue that partial melt of garnet pyroxenite reacts with peridotite, replaces olivine with pyroxene, and generates olivine-free, secondary garnet pyroxenite (e.g., Yaxley and Green, 1998; Takahashi and Nakajima, 2002). Partial melts of this secondary olivine-free, garnet pyroxenite have high Ni and SiO_2 content; therefore their model accounts for the previously unexplained relatively high Ni and SiO_2 in Makapuu-stage lavas. I note, however, that several aspects of their model need testing. Specifically, can partial melting of olivine-free, secondary garnet pyroxenite generate melts with ~15% MgO and >49% SiO_2 (Table 1 of Sobolev et al., in press)? The high MgO content of this melt is required to keep the bulk-solid/melt partition coefficient for Ni ~1 (Table S2 of Sobolev et al., in press) rather than >10 for partial melting of MORB-like eclogite (see Table 9 of Pertermann et al., 2004). Finally, a characteristic of Makapuu-stage lavas is relatively low CaO content (Fig. 5 of Haskins and Garcia, 2004 and Fig. 14b, this paper), but low CaO is inconsistent with the relatively high CaO of the calculated melt derived from secondary garnet pyroxenite (Table 1 of Sobolev et al., in press). Consequently, the model proposed by Sobolev et al. (in press) needs testing and refining before it can be accepted as a suitable model for Makapuu-stage lavas. I agree,

however, that mixing of partial melt derived from peridotite and dacitic melt derived from garnet pyroxenite formed from MORB cannot account for anomalously high Ni abundance.

3.7 Summary of Evidence for Ancient Recycled Oceanic Crust in the Hawaiian Plume:

In **Sections 3.2**, **3.4** and **3.5**, I used major and trace element abundances and isotopic data to evaluate garnet pyroxenite as a source component for Koolau lavas. These data show that as Koolau Volcano migrated away from the plume and reached the end of shield building, garnet became increasingly important as a residual phase, the extent of melting decreased and up to 20% of a dacitic melt (relatively high SiO_2 and low MgO and CaO) contributed to the late shield (Makapuu-stage) lavas. The distinctive trace element, relatively high Sr/Nb and low Th/La, and isotopic, relatively low $^{143}Nd/^{144}Nd$, $^{176}Hf/^{177}Hf$, and high $^{208}Pb^*/^{206}Pb^*$, characteristics of Makapuu-stage lavas can be explained by <3% of a sedimentary component, either ancient recycled phosphate-bearing carbonate or perhaps sediment with an abundant hydrothermal component, in the source. The evidence for a small amount of ancient recycled sediment in the source of late shield Koolau lavas coupled with up to 20% of a dacitic melt derived from garnet pyroxenite are consistent with recycled oceanic crust in the Hawaiian plume. The mixing of high temperature MgO-rich melts required by olivine with Fo_{88-90} (Garcia, 2002) with low temperature dacitic melts is plausible in the Hawaiian plume setting, especially at the end of shield-building, when melts are captured from a region that includes the high temperature plume core and the cooler plume periphery (See Fig. 1 of DePaolo and Stolper, 1996).

3.8 Temporal Geochemical Variations Within the KSDP core

The relative age of lava flows recovered from the KSDP core is constrained; hence, it is possible to use the time-dependent geochemical variations to constrain temporal changes in process and the spatial distribution of geochemical heterogeneity. In order to avoid complications caused by alteration, I consider only unaltered lavas ($1.2<K_2O/P_2O_5<2.2$ and L.O.I.<0.8) in a time series analysis; in particular, I do not consider the bottom of the core where altered lavas are dominant (Fig. 3). I follow the assumption of Blichert-Toft et al. (2003) that the resurfacing time was constant, i.e., the time differences between lava flows were equal. Using the Mauna Kea portion of the Phase 2 of the Hawaii Scientific Drilling Project (HSDP2) core as an analogy for late shield growth of Koolau, I estimate ~1400 years for resurfacing time (~410 ka for ~300 lava flow units in the Mauna Kea section, Sharp and Renne, in press). Note that this estimate of resurfacing time exceeds that of 350 years inferred by Blichert-Toft et al. (2003) who erroneously assumed ~1000 Mauna Kea flow units in the HSDP2 core.

Following the method described in Press et al. (pp. 575-579, 1992) for time series analysis of an unevenly sampled system, I calculate the Lomb normalized periodograms for Al_2O_3/CaO, Th/La, Sr/Nb, La/Nb, La/Yb and Tb/Yb (Fig. 15). There are two peaks in these periodograms for Al_2O_3/CaO, Th/La, Sr/Nb and La/Nb: one is at very low frequency (unlabeled) and the other is at around ~21 times resurfacing time (Fig. 15a-d). These peaks, except the Th/La peak at very low frequency, are significant at the 95% confidence level. The low frequency peak reflects the long-term secular trend shown in Fig. 3. After removal of this secular trend, only the peak at ~21 times resurfacing time exists in the Lomb normalized periodogram (e.g., Al_2O_3/CaO in Fig. 15e). In contrast,

there is only one peak at ~30 times resurfacing time (significant at 95% confidence level) in the Lomb normalized periodograms for La/Yb and Tb/Yb.

Time series analyses show that the variations of Al_2O_3/CaO, Th/La, Sr/Nb and La/Nb are highly correlated and share a period of ~21 times resurfacing time, which corresponds to ~29 ka using 1400 years for resurfacing time. The correlations among these ratios are consistent with our inference that high Al_2O_3/CaO arises from partial melting of garnet pyroxenite and the high Sr/Nb, La/Nb with low Th/La arise from an ancient sediment component in this garnet pyroxenite. These variations reflect horizontal (e.g., DePaolo et al., 2001) or vertical (e.g., see Figs. 12 and 13 of Blichert-Toft et al., 2003) geochemical heterogeneity in the Hawaiian plume. Blichert-Toft et al. (2003) note that plume upwelling velocity is greater than plate velocity; therefore magma extraction may homogenize horizontal heterogeneity thereby implying that temporal geochemical variations in lavas reflect vertical heterogeneity within the plume. This implication is valid for piston or pipe flow where there is an abrupt velocity gradient between the plume core and rim, but it is less likely if there is a broad velocity gradient (e.g., Hauri et al., 1994).

If the observed variations of Al_2O_3/CaO, La/Nb, Sr/Nb and Th/La in the KSDP core reflect vertical spacing of a garnet pyroxenite component within the Hawaiian plume, the spacing is 2.9-29 km given 10 cm/year and 1 m/year as the lower and upper limits of the plume upwelling velocity (e.g., Ribe and Christensen, 1999). This range encompasses the estimate of Takahashi and Nakajima (2002), based on the volume of Makapuu-stage lavas, that entrained eclogite blocks in the Hawaiian plume "may reach up to 10 km in size or larger". The approach of Eisele et al. (2003) for the HSDP drill

core at Mauna Kea calculates the spacing of Pb isotopic heterogeneities by integrating over a non-linear ascent path beneath the HSDP drill site (see their Fig. 13); they infer 21 to 86 km as the minimum length scale of the Pb heterogeneity. However, this approach requires information about the distance between the shield and plume center as a function of time. Such information is not available for Koolau.

The lack of a significant peak (at 95% confidence level) at ~21 times resurfacing time in the Lomb normalized periodograms for La/Yb and Tb/Yb implies that these ratios were not affected by the recycled oceanic crust component. That is, La/Yb and Tb/Yb are controlled by the partial melting process. The variations of La/Yb and Tb/Yb, at a period of ~30 times resurfacing time which corresponds to ~42 ka, imply that there was substantial variation in melting extent during the shield building stage (Figs. 3d and 11). Variable extents of melting during shield construction have also been inferred for Kilauea (Pietruszka and Garcia, 1999), Mauna Loa (Rhodes and Hart, 1995) and Mauna Kea (Stolper et al., 2004).

4. Summary

Geochemical and petrographic studies of surface lavas erupted on the Koolau shield and drill core from the Koolau Scientific Drilling Project show that the shield lavas changed markedly near the end of shield-building (Frey et al., 1994; Roden et al., 1994; Jackson et al., 1999; Haskins and Garcia, 2004; this paper). Specifically, as shield building ended, tholeiitic shield basalt changed gradually from a Mauna Loa-like composition to the well known geochemical endmember that characterizes subaerially exposed Koolau lavas (i.e., the Kalihi- and Makapuu-stages, respectively of Haskins and Garcia, 2004). This transition, occurring over ~84 ka, was not abrupt; therefore it was not

caused by a rapid catastrophic event, such as the Nuuanu landslide. The transition from Kalihi-stage to Makapuu-stage lavas reflects changes in source material that occurred as Koolau volcano migrated away from the plume.

The distinctive geochemical characteristics of Makapuu-stage basalt is manifested in major and trace element abundances as well as isotopic ratios. Relatively low abundances of MgO, CaO, Sc and Yb coupled with high SiO_2 content are consistent with up to 20% of a dacitic melt derived from garnet pyroxenite. Distinctive trace element ratios, such as high Sr/Nb and low Th/La, which correlate with isotopic ratios of Nd, Hf and Pb, provide evidence for <3% of ancient recycled (phosphate-bearing carbonate-rich or hydrothermal) sediment in the source. The combination of km-size garnet pyroxenite and a sedimentary geochemical signature strongly suggests recycled oceanic crust in the Hawaiian plume as Koolau Volcano entered the late-stage of shield construction. Mixing of low temperature dacitic melt formed from garnet pyroxenite and high temperature melt derived from peridotite is possible at this stage of volcano growth, because the magma capture area includes high temperature melts from the plume center and low temperature melts from the cooler periphery of the plume.

References:

Beattie, P., Ford, C., Russell, D., Partition coefficients for olivine-melt and orthopyroxene-melt system, Contrib. Mineral. Petrol., 109 (2), 212-224, 1991.

Ben Othman, D., White, W. M., Patchett, J., The geochemistry of marine sediments, island arc magma genesis, and crust-mantle recycling, Earth Planet Sci Letts., 94 (1-2), 1-21, 1989.

Blichert-Toft, J., Frey, F. A., and Albarede, F., Hf isotope evidence for pelagic sediments in the source of Hawaiian basalts, Science, 285 (5429), 879-882, 1999.

Blichert-Toft, J., Weis, D., Maerschalk, C., Agranier, A., and Albarède, F., Hawaiian hot spot dynamics as inferred from the Hf and Pb isotope evolution of Mauna Kea volcano, Geochem. Geophys. Geosyst., 4(2), 8704, doi:10.1029/2002GC000340, 2003.

Blundy, J. D., Robinson, J. A. C., and Wood, B. J., Heavy REE are compatible in clinopyroxene on the spinel lherzolite solidus. Earth Planet. Sci. Lett., 160, 493-504, 1998.

Budahn, J. R., Schmitt, R. A., Petrogenetic modeling of Hawaiian tholeiitic basalts; a geochemical approach, Geochim. Cosmochim. Acta., 49 (1), 67-87, 1985.

Chen, C.-Y., Frey, F. A., Rhodes, J. M., and Easton, R. M., Temporal geochemical evolution of Kilauea Volcano: Comparison of Hilina and Puna Basalt. in Earth Processes: Reading the isotopic code, Geophysical Monograph Series, vol. 95, edited by A. Basu and S. R. Hart, 161-181, AGU, Washington, D.C., 1996.

Cohen, A. S., O'Nions, R. K., and Kurz, M. D., Chemical and isotopic variations in Mauna Loa tholeiites, Earth Planet. Sci. Lett., 143, 111-124, 1996.

DePaolo, D. J. and Stolper, E. M., Models of Hawaiian volcano growth and plume structure; implications of results from the Hawaii Scientific Drilling Project, J. Geophys. Res., 101 (5), 11,643-11,654, 1996.

DePaolo, D., J. Bryce, A. Dodson, D. Shuster, and B. Kennedy, Isotopic evolution of Mauna Loa and the chemical structure of the Hawaiian plume, Geochem. Geophys. Geosyst., 2, doi:10.1029/2000GC000139, 2001.

Eggins, S. M., Petrogenesis of Hawaiian tholeiites; 1, Phase equilibria constraints, Contrib. Mineral. Petrol., 110 (2-3), 387-397, 1992.

Eisele, J., Abouchami, W., Galer, S. J. G. and Hofmann, A. W., The 320 kyr Pb isotope evolution of Mauna Kea lavas recorded in the HSDP-2 drill core, Geochem. Geophys. Geosyst., 4(5), 8710, doi:10.1029/2002GC000339, 2003.

Fodor, R. V., Frey, F. A., Bauer, G. R., Clague, D. A., Ages, rare-earth element enrichment, and petrogenesis of tholeiitic and alkalic basalts from Kahoolawe Island, Hawaii, Contrib. Mineral. Petrol., 110, 442-462, 1992.

Frey, F. A., and Clague, D. A., Geochemistry of diverse basalt types from Loihi Seamount, Hawaii; petrogenetic implications. Earth Planet Sci. Letts. 66, 337-355, 1983.

Frey, F.A. and Rhodes, J.M., Inter-shield geochemical differences among Hawaiian volcanoes: implications for source compositions, melting processes and magma ascent paths. Phil. Trans. Roy. Soc. Lond. A., 342, 121-136, 1993.

Frey, F. A., Garcia, M. O., and Roden, M. F., Geochemical characteristics of Koolau Volcano: Implications of intershield geochemical differences among Hawaiian volcanoes. Geochim. Cosmochim. Acta., 58, 1441-1462, 1994.

Galer, S. J. G., and O'Nions, R. K., Residence time of thorium, uranium and lead in the mantle with implications for mantle convection, Nature, 316 (6031), 778-782, 1985.

Garcia, M. O., Jorgenson, B. A., Mahoney, J. J., Ito E., and Irving, A. J., An evaluation of temporal geochemical evolution of Loihii summit lavas: Results from Alvin submersible dives. J. Geophys. Res. 98, 535-550, 1993.

Garcia, M. O., Foss, D. J. P., West, H. B. and Mahoney, J. J., Geochemical and isotopic evolution of Loihi Volcano, Hawaii, J. Petrol., 36, 1647-1644, 1995b.

Garcia, M. O., Hulsebosch, T. P., Rhodes, J. M., Olivine-rich submarine basalts from the southwest rift zone of Mauna Loa Volcano; implications for magmatic processes and geochemical evolution, in Mauna Loa Revealed, Geophysical Monograph Series, vol. 92, (eds, J.M. Rhodes and J.P. Lockwood) 219-239, AGU, Washington, D.C., 1995a.

Garcia, M. O., Rubin, K. H., Norman, M. D., Rhodes, J. M., Graham, D. W., Muenow, D W., Spencer, K., Petrology and geochronology of basalt breccia from the 1996 earthquake swarm of Loihi Seamount, Hawaii; magmatic history of its 1996 eruption, Bull. Volcan., 59, 577-592, 1998.

Garcia, M. O., Pietruszka, A. J., Rhodes, J. M., Swanson, K., Magmatic processes during the prolonged Pu'u O'o eruption of Kilauea volcano, Hawaii, J. Petrol, 41(7), 967-990, 2000.

Garcia, M. O., Giant landslides in the northeast of O'ahu; when, why and how? in Hawaiian volcanoes; deep underwater perspectives, Geophysical Monograph Series, vol. 128, (eds, Takahashi, E., Lipman, P. W., Garcia, M. O., Naka, J., Aramaki, S), 221-222, 2002.

Hart, S. R. and Dunn, T., Experimental cpx/melt partitioning of 24 trace elements, Contrib. Mineral. Petrol., 113 (1), 1-8, 1993.

Haskins, E. R., and Garcia M. O., Scientific drilling reveals geochemical heterogeneity within the Ko'olau shield, Hawai'i, Contrib. Mineral. Petrol., 147, 162-188, 2004.

Hauri, E. H., Wagner, T. P., Grove, T. L., Experimental and natural partitioning of Th, U, Pb and other trace elements between garnet, clinopyroxene and basaltic melts, Chem. Geol., 117 (1-4), 149-166, 1994.

Hauri, E. H., Major-element variability in the Hawaiian mantle plume, Nature 382, 415-419, 1996.

Hirschmann, M. M., Stolper, E. M., A possible role for garnet pyroxenite in the origin of the "garnet signature" in MORB, Contrib. Mineral. Petrol., 124 (2), 185-208, 1996.

Hofmann, A. W., Feigenson, M. D., Raczek, I., Case studies on the origin of basalt; III, Petrogenesis of the Mauna Ulu eruption, Kilauea, 1969-1971, Contrib. Mineral. Petrol., 88 (1-2), 24-35, 1984.

Hofmann, A. W., Chemical differentiation of the earth: the relationship between mantle, continental crust, and oceanic crust, Earth Planet. Sci. Lett. 90, 297-314, 1988.

Hofmann, A. W., Mantle geochemistry; the message from oceanic volcanism, Nature, 385 (6613), 219-229, 1997.

Honnorez, J., Mevel, C., Honnerez-Guerstein, B. M. and Tomschi, H. P., Mineralogy and chemistry of sulfide deposits drilled from hydrothermal mound of the snake pit active field, MAR, in Detrick, R., Honnorez. J., Bryan, W. B., Juteau, T., et al., Proceedings of the Ocean Drilling Program, Scientific Results, Vol. 106/109: 145-162, Washington, D.C.: U.S. Government Printing Office. 1990.

Huang, S. and Frey, F.A., Trace element abundances of Mauna Kea basalt from Phase 2 of the Hawaiian Scientific Drilling Project: Petrogenetic implications of correlations with major element content and isotopic ratios, Geochem. Geophys., Geosys, 4(6), 8711, doi, 1029/2002 GC000322, 2003.

Jackson, M. C., Wilmoth, R. A., and Frey, F. A., Geology and petrology of basaltic lavas and dikes of the Koolau Volcano in the Trans-Koolau exploratory tunnels, Oahu, Hawaii. Bull. Volcan. 60, 381-401, 1999.

Kelemen, P. B., Assimilation of ultramafic rock in subduction-related magmatic arcs, J. Geol., 94 (6), 829-843, 1986.

Kogiso, T., Hirschmann, M. M., Reiners, P. W., Length scales of mantle heterogeneities and their relationship to ocean island basalt geochemistry, Geochim. Cosmochim. Acta., 68(2), 345-360, doi, 10.1016/S0016-7037(03)00419-8, 2004.

Kurz, M. D., Kenna, T. C., Kammer, D. P., Rhodes, J. M., and Garcia, M. O., Isotopic evolution of Mauna Loa volcano: a view from the submarine southwest rift Mauna Loa: A Decade Volcano, in Mauna Loa Revealed, Geophysical Monograph Series, vol. 92, (eds, J.M. Rhodes and J.P. Lockwood) 289-306, AGU, Washington, D.C., 1995.

Lassiter, J. C. and Hauri, E. H., Osmium-iosotope variations in Hawaiian lavas: Evidence for recycled oceanic lithosphere in the Hawaiian plume. Earth Planet Sci Letts., 164, 483-496, 1998.

Leeman, W. P., Gerlach, D. C., Garcia, M. O., West, H. B., Geochemical variations in lavas from Kahoolawe volcano, Hawaii: evidence for open system evolution of plume-derived magmas, Contrib. Mineral. Petrol., 116, 62-77, 1994.

Li, X., Kind, R., Yuan, X., Wölbern I. and & HANKA, W., Rejuvenation of the lithosphere by the Hawaiian plume, Nature 427, 827-829 doi:10.1038/nature02349, 2004.

Norman, M. D., and Garcia, M. O., Primitive magmas and source characteristics of the Hawaiian Plume; petrology and geochemistry of shield picrites, Earth Planet Sci. Letts., 168, 27-44, 1999.

Norman, M. D., Garcia, M. O. and Bennett, V. C., Rhenium and chalcophile elements in basaltic glasses from Ko'olau and Moloka'i volcanoes: Magmatic outgassing and composition of the Hawaiian plume, Geochim. Cosmochim. Acta., 68(18), 3761-3777, doi: 10.1016/j.gca.2004.02.025, 2004.

Patino, L, C., Carr, M. J. and Feigenson, M. D., Local and regional variations in Central American arc lavas controlled by variations in subducted sediment input, Contrib. Mineral. Petrol., 138(3), 265-283, 2000.

Pertermann, M. and Hirschmann M. M., Anhydrous partial melting experiments on MORB-like eclogite: Phase reactions, phase compositions and mineral-melt partitioning of major elements at 2-3 GPa, J. Petrol., 44(12), 2173-2201, 2003a.

Pertermann, M. and Hirschmann, M. M., Partial melting experiments on a MORB-like pyroxenite between 2 and 3 GPa; constraints on the presence of pyroxenite in basalt source regions from solidus location and melting rate, J. Geophys. Res., 108(B2), 2125, doi: 10.1029/2000JB000118, 2003b.

Pertermann, M., Hirschmann, M. M., Hametner, K., Gunther, D., Schmidt, M. W., Experimental determination of trace element partitioning between garnet and silica-rich liquid during anhydrous partial melting of MORB-like eclogite, Geochem. Geophys, Geosyst, 5, Q05A01, doi:10.1029/2003GC000638, 2004.

Pietruszka, A. J. and Garcia, M. O., A rapid fluctuation in the mantle source and melting history of Kilauea Volcano inferred from the geochemistry of its historical summit lavas (1790-1982), J. Petrol., 40 (8), 1321-1342, 1999.

Plank, T., and Langmuir, C. H., The chemical composition of subducting sediment and its consequences for the crust and mantle, Chem. Geol., 145 (3-4), 325-394, 1998.

Plank, T., Constraints from Thorium/Lanthanum on Sediment Recycling at Subduction Zones and the Evolution of the Continents, J. Petrol., doi: 10.1093/petrology/egi005, 2005.

Plank, T., Balzer, V. and Carr, M., Nicaraguan volcanoes record paleoceanographic changes accompanying closure of the Panama gateway, Geology, 30(12), 1087-1090, 2002.

Press, W. H., S. A. Teukolsky, W. T. Vetterling, and B. P. Flannery, Numerical Recipes in C, 2nd ed., 994 pp., Cambridge Univ. Press, New York, 1992.

Putirka, K., Melting depths and mantle heterogeneity beneath Hawaii and the East Pacific Rise; constraints from Na/Ti and rare earth element ratios, J. Geophys. Res., 104(2), 2817-2829, 1999.

Quane, S. L., Garcia, M. O., Guillou, H., Hulsebosch, T. P., Magmatic history of the East Rift Zone of Kilauea Volcano, Hawaii based on drill core from SOH 1, J. Volcanol. Geotherm. Res., 102 (3-4), 319-338, 2000.

Ray, J. S., Martin, M. W., Veizer, J. and Bowring, S. A., U-Pb zircon dating and Sr isotope systematics of the Vindhyan Supergroup, India, Geology, 30(2), 131-134, 2002.

Reiners, P. W., Temporal-compositional trends in intraplate basalt eruptions: Implications for mantle heterogeneity and melting processes, Geochem. Geophys. Geosyst., 3(2), 10.1029/2001GC000250, 2002.

Rhodes, J. M. and Hart, S. R., Episodic trace element and isotopic variation in historical Mauna Loa lavas, in Mauna Loa Revealed, Geophysical Monograph Series, vol. 92, (eds, J.M. Rhodes and J.P. Lockwood) 263-288, AGU, Washington, D.C., 1995.

Rhodes, J. M., Geochemical stratigraphy of lava flows sampled by the Hawaii Scientific Drilling Project, J. Geophys. Res. 101, 11,729-11,746, 1996.

Rhodes, J. M., and M. J. Vollinger, Composition of basaltic lavas sampled by phase-2 of the Hawaii Scientific Drilling Project: Geochemical stratigraphy and magma types, Geochem. Geophys. Geosyst., 5, Q03G13, doi:10.1029/2002GC000434, 2004.

Ribe, N. M. and Christensen, U. R., The dynamical origin of Hawaiian volcanism, Earth Planet. Sci. Lett., 171(4), 517-531, 1999.

Roden, M. F., Trull, T., Hart, S. R., and Frey, F. A., New He, Sr, Nd and Pb isotopic constraints on the constitution of the Hawaiian plume: Results from Koolau Volcano, Oahu, Hawaii. Geochim. Cosmochim. Acta., 58, 1431-1440, 1994.

Salters, V. J. M., The generation of mid-ocean ridge basalts from the Hf and Nd isotope perspective. Earth Planet. Sci. Letts., 141, 109-123, 1996.

Salters, V. J. M. and Longhi, J., Trace element partitioning during the initial stages of melting beneath mid-ocean ridges. Earth Planet. Sci. Letts., 166, 15-30, 1999.

Seitz, H.-M., Altherr, R., Ludwig, T., Partitioning of transition elements between orthopyroxene and clinopyroxene in peridotitic and websteritic xenoliths; new empirical geothermometers, Geochim. Cosmochim. Acta., 63 (23-24), 3967-3982, 1999.

Sharp, W. D. and Renne, P. R., $^{40}Ar/^{39}Ar$ dating of core recovered by the Hawaii Scientific Drilling Project (Phase 2) Hilo, Hawaii, Geochem. Geophys. Geosyst. 6, Q04G17, doi:10.1029/2004GC000846, 2005.

Shinozaki, K., Ren, Z.-Y., Takahashi, E., Geochemical and petrological characteristics of Nuuanu and Wailau landslide blocks, in Hawaiian volcanoes; deep underwater perspectives, Geophysical Monograph Series, vol. 128, (eds, Takahashi, E., Lipman, P. W., Garcia, M. O., Naka, J., Aramaki, S), 297-310, 2002.

Sobolev, A.V., Hofmann, A.W., and Nikogosian, I. K., Recycled oceanic crust observed in ghost plagioclase within the source of Mauna Loa lavas, Nature 404, 986-990, 2000.

Sobolev, A. V., Hofmann, A. W., Sobolev, S. V., Nikogosian, I. K., An olivine free mantle source of Hawaiian shield basalts, submitted to Nature.

Stolper, E., Sherman, S., Garcia, M., Baker, M. and Seaman, C., Glass in the submarine section of the HSDP2 drill core, Hilo, Hawaii, Geochem. Geophys. Geosys, 5, Q07G15, doi:10.1029/2003GC000553, 2004.

Takahashi, E., Nakajima, K. and Wright, T. L., Origin of the Columbia River basalts; melting model of a heterogeneous plume head, Earth Planet Sci Letts., 162, 63-80, 1998.

Takahashi, E., and Nakajima, K., Melting process in the Hawaiian Plume; an experimental study, in Hawaiian volcanoes; deep underwater perspectives, Geophysical Monograph Series, vol. 128, (eds, Takahashi, E., Lipman, P. W., Garcia, M. O., Naka, J., Aramaki, S), 403-418, 2002.

Tanaka, R., Nakamura, E., Takahashi, E., Geochemical evolution of Koolau Volcano, Hawaii, in Hawaiian volcanoes; deep underwater perspectives, Geophysical Monograph Series, vol. 128, (eds, Takahashi, E., Lipman, P. W., Garcia, M. O., Naka, J., Aramaki, S), 311-332, 2002.

Thompson, G., Humphris, S. E., Schroeder, B., Sulanowska, M. and Rona, P. A., Active vents and massive sulfides at 26°N (TAG) and 23°N (Snakepit) on the mid-Atlantic ridge, Can. Mineral., 26, 697-711, 1988.

Tu, G., Zhao, Z. and Qiu, Y., Evolution of Precambrian REE mineralization, Precam. Res., 27, 131-151, 1985.

van Westrenen, W., Blundy, J. and Wood, B., Crystal-chemical controls on trace element partitioning between garnet and anhydrous silicate melt, Am. Mineral., 84, 838-847, 1999.

van Westrenen, W., Blundy, J. D., Wood, B. J., High field strength element/rare earth element fractionation during partial melting in the presence of garnet; implications for identification of mantle heterogeneities, Geochem. Geophys., Geosys, 2(7), doi:10.1029/2000GC000133, 2001.

Wagner, T. P., and Grove, T. L., Melt/harzburgite reaction in the petrogenesis of tholeiitic magma from Kilauea Volcano, Hawaii, Contrib. Mineral. Petrol., 131 (1), 1-12, 1998.

Walter, M. J., Melting of garnet peridotite and the origin of komatiite and depleted lithosphere, J. Petrol., 39 (1), 29-60, 1998.

Yaxley G. M. and Green, D. H., Reactions between eclogite and peridotite: mantle refertilisation by subduction of oceanic crust, Schweiz. Mineral. Petrogr. Mitt. 78, 243-255, 1998.

Yogodzinski, G. M., Kay, R. W., Volynets, O. N., Koloskov, A. V., Kay, S. M., Magnesian andesite in the western Aleutian Komandorsky region; implications for slab melting and processes in the mantle wedge, Geol. Soc. Am. Bull., 107 (5), 505-519, 1995.

Zhong, S. and Watts, A. B., Constraints on the dynamics of mantle plumes from uplift of the Hawaiian Islands, Earth Planet Sci Letts., 203, 105-116, 2002.

Figure Caption:

Fig. 1. Th abundance vs selected incompatible element abundances (in ppm). All data are obtained using ICP-MS at MIT (Table 1).

In this figure and all subsequent figures, all KSDP core samples are designated as Kalihi-stage lavas. The Kalihi-stage to Makapuu-stage transition is inferred to be within the overlying rotary drilled interval (see Fig. 10 of Haskins and Garcia, 2004). Most notable are the higher La/Th and Sr/Th of Makapuu-stage lavas. In **panels c** and **d**, the greater scatter of Rb and Sr reflects post-magmatic alteration as indicated by altered lavas; unaltered lavas are defined as lavas with $2.2>K_2O/P_2O_5>1.2$ and Loss on Ignition (L.O.I.) <0.8% (Haskins and Garcia (2004).

Fig. 2. Primitive mantle normalized trace element abundances in Makapuu-stage and Kahili-stage lavas. Primitive mantle values are from Hofmann (1988).

Measured incompatible element abundances in lavas with $2.2>K_2O/P_2O_5>1.2$ and MgO>6.5% were adjusted by adding or subtracting equilibrium olivine until the whole rock Fe/Mg ratio was in equilibrium with Fo_{90} olivine (0.1% increments using $(Fe/Mg)_{olivine}/(Fe/Mg)_{melt}=0.30$).

Fig. 3. Depth profiles of Al_2O_3/CaO, La/Nb, Sr/Nb and La/Yb for KSDP drill hole.

(2σ analytical uncertainties for La/Nb, Sr/Nb and La/Yb are from Appendix of Huang and Frey (2003), and 2σ analytical uncertainty for Al_2O_3/CaO is less than the symbol size (Rhodes, 1996)).

All lavas from the KSDP core were classified as Kalihi-stage lavas by Haskins and Garcia (2004). The Makapuu/Kalihi-stage compositional boundary, vertical dashed lines, is taken as $Al_2O_3/CaO = 1.45$ (Haskins and Garcia, 2004), La/Nb = 1.09 and Sr/Nb = 39.4 (lowest values in Makapuu-stage lavas; Fig. 4). Several lavas with geochemical characteristics similar to Makapuu-stage lavas, e.g., high Al_2O_3/CaO, La/Nb and Sr/Nb, occur in the interval of 304 to 336 m. In addition, a few altered lavas at ~550 m have some geochemical characteristics similar to Makapuu-stage lavas. See Fig. 1 caption for definition of altered and unaltered lavas.

There is considerable structure in these depth profiles. Al_2O_3/CaO, La/Nb and Sr/Nb generally increase upwards from an elevation of ~470 m below sea level, but there are superimposed high frequency variations. The depth profiles of Sr/Nb and La/Yb are highlighted by thick gray lines (defined by running means for every 5 samples). The former contains several cycles and a secular trend of increasing Sr/Nb with decreasing depth. The latter contains several cycles, but lacks a secular trend. These cycles are discussed in **Section 3.8**.

Fig. 4. Sr/Nb vs La/Nb, and MgO (%) vs Sr/Nb for Makapuu-stage and Kalihi-stage lavas.

Following Haskins and Garcia (2004), only relatively unaltered lavas (Kalihi-stage, Makapuu-stage and Mauna Loa lavas) with $2.2>K_2O/P_2O_5>1.2$ and L.O.I.<0.8% are plotted. The squares are ICP-MS data for Makapuu-stage lavas and open circles are data for Kalihi-stage lavas obtained in this study.

In **panel a**, Kalihi-stage lavas are not similar to subaerially exposed Makapuu-stage lavas, but they are within the field defined by Mauna Loa lavas. Specifically, compared with Makapuu-stage lavas, Kalihi-stage lavas have lower La/Nb and Sr/Nb. These differences are not related to MgO content (**panel b**); consequently, the high Sr/Nb in Makapuu-stage lavas is not a result of plagioclase accumulation.

Major element data are from Frey et al. (1994) (Makapuu) and Haskins and Garcia (2004) (KSDP), respectively. Fields labeled as "Makapuu-stage Lavas" are defined by XRF and INAA data from Frey et al. (1994). Mauna Loa data are from Garcia et al. (1995a), Rhodes (1995; 1996), Rhodes and Hart (1995), Cohen et al. (1996), Rhodes and Vollinger (2004), our unpublished INAA data for Mauna Loa section of HSDP2.

Fig. 5 La/Nb and Th/La vs $^{143}Nd/^{144}Nd$, $^{176}Hf/^{177}Hf$ and $^{208}Pb^*/^{206}Pb^*$ for Makapuu-stage and Kalihi-stage lavas.

$^{208}Pb^*/^{206}Pb^*$ represents the time-integrated $^{232}Th/^{238}U$ since the Earth formation, and is defined as $[(^{208}Pb/^{204}Pb)_{sample}-29.475]/[(^{206}Pb/^{204}Pb)_{sample}-9.307]$ (Galer and O'Nions, 1985).

Kalihi-stage lavas overlap with the field defined by Mauna Loa lavas in **panels a** and **c**. The linear trends in these panels imply that the transition from Kalihi-stage composition to Makapuu-stage composition reflects an increasing role of a component with high La/Nb, $^{208}Pb^*/^{206}Pb^*$ and low Th/La, $^{143}Nd/^{144}Nd$ and $^{176}Hf/^{177}Hf$. Kalihi-stage Units 6 and 9 near the top of the KSDP core are transitional (i.e., relatively low Th/La and high La/Nb) to Makapuu-stage characteristics. Labeled Kalihi-stage Units 8 and 71 also have relatively low Th/La (Unit 71 also has relatively high La/Nb), but their isotopic ratios do

not trend to the Makapuu-stage field. Unit 8 was not analyzed for Pb isotopic ratios; consequently, it is not plotted in **panel f**.

Isotopic data for Kalihi-stage lavas are from Salters et al. (in prep.) and Fekiacova et al. (in prep.). Isotopic data for Makapuu-stage lavas are from Roden et al. (1994), Lassiter and Hauri (1998) and Blichert-Toft et al. (1999).

Mauna Loa data are from Rhodes (1995; 1996), Rhodes and Hart (1995), Cohen et al. (1996), Blichert-Toft et al. (2003) and our unpublished INAA data for Mauna Loa section of HSDP 2.

Fig. 6 CaO (%) vs Th/La and Sr/Nb, and Al_2O_3/P_2O_5 vs Th/La for different marine sediment sections. Arrows show sediments with Th/La<0.05 and Sr/Nb>55, similar to extreme Makapuu-stage ratios (Figs. 4 and 5). Such sediments are CaO- and P_2O_5-rich sediments or hydrothermally-derived clays, such as those from the Tonga trench.

Data are from Plank and Langmuir (1998), Patino et al. (2000) and Plank et al. (2002).

Fig. 7 ε_{Nd} vs ε_{Hf} for Hawaiian lavas. Field for Hawaiian shield lavas is from Fig. 2 of Blichert-Toft et al. (1999); data for KSDP lavas are from Salters et al. (in prep.). The solid triangle is calculated by adding 3% of 2 Ga recycled phosphate-bearing carbonate-rich sediment to 97% primitive mantle (see Table 2 for details). The open triangle is calculated by adding 0.25% of 2 Ga recycled hydrothermal clay to 99.75% primitive mantle (see Table 2 for details). These mixtures are appropriate as an end-member component for Makapuu-stage lavas.

Fig. 8 Ce/Pb vs La/Nb, Th/La and Ba/Th for Koolau glasses (shaded field), as well as relatively unaltered whole rocks (with $2.2>K_2O/P_2O_5>1.2$ and L.O.I.<0.8%). Except for Sample 500-3B from Norman et al. (2004), Koolau glasses form trends in these panels, requiring a component with low Ce/Pb, Th/La and high La/Nb, Ba/Th. These geochemical characteristics are consistent with phosphate-bearing carbonate-rich or hydrothermal sediment as a source component for Koolau lavas (see text for details). In contrast, the whole rocks do not form trends in these panels, implying that Ce/Pb and Ba/Th were affected by post-magmatic processes even in relatively unaltered whole rocks.

Glass data are from Haskins and Garcia (2004) and Norman et al. (2004).

Fig. 9. La/Nb vs Sr/Nb, $^{143}Nd/^{144}Nd$ and $^{208}Pb^*/^{206}Pb^*$ for samples from Koolau shield and Nuuanu landslide blocks studied by Tanaka et al. (2002). Legend indicates stratigraphic sequence inferred in Fig. 2 of Tanaka et al. (2002). Fields labeled as "Makapuu-stage", "Kalihi-stage" and "Mauna Loa" in **panel a** are the same as these in Fig 4; Kalihi-stage (KSDP) field in **panels b** and **c** is defined by KSDP lavas (this study; Salters et al., in prep.; Fekiacova et al., in prep.); and Makapuu field in **panels b** and **c** is from Fig. 5.

Fig. 10. MgO (%) vs Sc, Yb, Y and Ni (all in ppm) for Makapuu-stage and Kalihi-stage lavas.

Fields for Mauna Kea, Mauna Loa and Kilauea lavas are plotted for comparison. Relative to Kalihi-stage, Mauna Loa, Mauna Kea and Kilauea lavas, Makapuu-stage lavas have

lower Sc, Y and Yb and higher Ni abundances. For Ni also see Garcia (2002) and Fig. 1 of Sobolev et al. (in press).

In **panels a, b** and **d**, only our ICP-MS data for Koolau (Makapuu-stage and Kalihi-stage) and Mauna Kea lavas are plotted. Since there are negligible systematic differences between Sc and Yb abundances determined by INAA and ICP-MS at MIT (e.g., Fig. A5 of Huang and Frey., 2003), **panels a** and **b** also show a field for Mauna Loa lavas (Sc and Yb abundances determined by INAA). However, there is a significant interlab difference in Y abundance determined by ICP-MS at MIT and XRF at University of Massachusetts (Fig. A4 of Huang and Frey., 2003); therefore, **panel c** shows Y data obtained by XRF and **panel d** shows Y data obtained by ICP-MS. **Panel e**: Ni abundances in Koolau, Mauna Kea, Mauna Loa and Kilauea lavas were obtained by XRF from University of Massachusetts.

Data sources: Kalihi-stage lavas: MgO, Ni and Y (XRF) from Haskins and Garcia (2004); Sc-Y(ICP-MS)-Yb: this study.

Makapuu-stage lavas: MgO, Ni and Y (XRF) from Frey et al. (1994); Sc-Y(ICP-MS)-Yb: this study.

Mauna Kea: MgO, Ni and Y(XRF) from Rhodes (1996) and Rhodes and Vollinger (2004); Sc-Y(ICP-MS)-Yb from Huang and Frey (2003).

Mauna Loa: from Garcia et al. (1995a), Rhodes (1995; 1996), Rhodes and Hart (1995), Cohen et al. (1996), Rhodes and Vollinger (2004).

Kilauea: Garcia et al., (2000).

Fig. 11. La/Yb vs Sc/Y, Zr/Yb and Tb/Yb for Makapuu-stage and Kalihi-stage lavas.

Fields for Mauna Loa and Makapuu-stage lavas defined by XRF and INAA data are also shown for comparison. Since Tb data obtained by INAA are not very precise (Fig. A5 of Huang and Frey, 2003), the fields for Makapuu-stage lavas and Mauna Loa lavas defined by INAA data are not plotted in **panel c**. Only lavas with $2.2>K_2O/P_2O_5>1.2$ and L.O.I.<0.8% are plotted.

As discussed in the text, the source of Makapuu-stage lavas included a recycled sedimentary component. We consider this complexity in modeling. First, we calculate the trends formed by Makapuu-stage and Kalihi-stage lavas using a common garnet peridotite source; i.e., with the same Sc/Y, La/Yb and Zr/Yb ratios. These are the melting trajectories labeled as "original source". Input values for the calculation are in Table 3. Then we add 3% carbonate sediment to this "original source" (Table 3). The melting trajectories labeled as "original source + 3% sediment" are calculated using this sediment enriched source. Less than 3% sediment is sufficient to explain the distinctive features of Makapuu-stage lavas, such as high Sr/Nb, low Th/La and their Nd-Hf isotopic ratios. The effect of adding 0.25% hydrothermal clay to the "original source" is similar to that of adding 3% carbonate sediment (Table 3); consequently, we do not show modeling trends for this case.

Fig. 12. Sm/Yb vs Zr/Hf for Makapuu-stage and Kalihi-stage lavas. Melting trajectories of eclogite are taken from Fig. 10 of Pertermann et al. (2004). Melting trajectories for garnet peridotite with variable initial clinopyroxene/garnet ratios use the input parameters in Table 3, with Zr/Hf and Sm/Yb equal to primitive mantle values (Hofmann, 1988). That is, the proportions of olivine and orthopyroxene in garnet peridotite are fixed, and

the proportions of clinopyroxene and garnet are variable. The melting trajectories are labeled with % melting and initial clinopyroxene/garnet ratios. Pertermann et al. (2004) noted that the steep trajectories for melting of eclogite (high clinopyroxene/garnet ratio of 82/18 and 75/25) contrast with the nearly horizontal trend for melting of garnet peridotite with clinopyroxene/garnet ~1. They concluded that some Koolau lavas are consistent with partial melting of garnet-poor eclogite. This conclusion obviously depends upon the clinopyroxene/garnet ratio of the garnet peridotite.

It is important that Makapuu-stage and Kalihi-stage lavas may form different trends, but the whole range of Zr/Hf in Koolau lavas is barely beyond analytical uncertainty. The 2σ analytical uncertainties for Zr/Hf and Sm/Yb are from Huang and Frey (2003).

Fig. 13. Olivine adjusted SiO_2 (%) vs $^{208}Pb^*/^{206}Pb^*$, $^{143}Nd/^{144}Nd$ and $^{176}Hf/^{177}Hf$ for Makapuu-stage and Kalihi-stage lavas.

These linear trends show that variations in olivine adjusted major element contents are not artifacts of olivine adjustment, but reflect source heterogeneity in major element composition. Surprisingly, Makapuu-stage and Kalihi-stage lavas form subparallel trends in these panels.

Averages of stratigraphic sections from different Hawaiian shields (excluding the Loihi alkalic section) from Table 1 of Hauri (1996) are shown in **panel b**. Interestingly, these averages largely overlap with Koolau (Makapuu-stage and Kalihi-stage) lavas, implying that the geochemical heterogeneity of Koolau source mimics that seen in all Hawaiian shields.

Data source: See captions of Figs. 5 and 10.

Fig. 14 MgO vs SiO_2 and CaO (%); and SiO_2 vs Na_2O+K_2O (%).

Makapuu-stage (squares) and Kalihi-stage (open circles) lavas (with $2.2>K_2O/P_2O_5>1.2$ and MgO>6.5%) are adjusted to be in equilibrium with Fo_{90} olivine. The Hawaiian shield field is defined by olivine adjusted (to be in equilibrium with Fo_{90} olivine) compositions (only lavas with $K_2O/P_2O_5>1.2$ and MgO>6.5% are included.). The three mixing endmembers of Hauri (1996) are shown as grey solid circles. Note that his high SiO_2 component differs from 2-3 GPa partial melts of eclogite (triangles, Takahashi et al., 1998; Yaxley and Green, 1998; Takahashi and Nakajima, 2002; Pertermann and Hirschmann, 2003).

a. In the MgO-SiO_2 plot, Hawaiian shield lavas define a negative trend with Makapuu-stage lavas as one extreme endmember. Clearly, the negative trend defined by Koolau (Makapuu-stage and Kalihi-stage) lavas points towards low temperature partial melts of eclogite.

b. In the MgO-CaO plot, lavas from all Hawaiian shields do not form a single trend, but the positive trend formed by Makapuu-stage and Kalihi-stage lavas also points towards low temperature partial melts of eclogite.

c. Partial melts of eclogite form a positive trend in a SiO_2-(Na_2O+K_2O) plot. Interestingly, olivine adjusted SiO_2 and (Na_2O+K_2O) contents of Koolau lavas plot on the lower extension of this trend. Compared with Kalihi-stage lavas, Makapuu-stage lavas have higher SiO_2 and (Na_2O+K_2O) contents. We interpret this trend as a mixing line between a low SiO_2-(Na_2O+K_2O) picrite melt and a high SiO_2-(Na_2O+K_2O) dacite melt.

Hawaiian shield data used in this figure are: Koolau (Frey et al., 1994; Haskins and Garcia, 2004); Mauna Loa (Garcia et al., 1995a; Rhodes, 1995; 1996; Rhodes and Hart, 1995; Rhodes and Vollinger, 2004); Mauna Kea (Rhodes, 1996; Rhodes and Vollinger, 2004; Stolper et al., 2004); Kilauea (Chen et al., 1996; Garcia et al., 2000; Quane et al., 2000); Loihi (Frey and Clague, 1983; Garcia et al., 1993; 1995b; 1998; Norman and Garcia, 1999); Kahoolawe (Fodor et al., 1992; Leeman et al., 1994; our unpublished data).

Fig. 16 Lomb normalized periodograms of Al_2O_3/CaO, Th/La, Sr/Nb, La/Nb, La/Yb and Tb/Yb for KSDP lavas. Only unaltered lavas ($1.2<K_2O/P_2O_5<2.2$ and L.O.I.<0.8) are included in the analysis. Two confidence level lines (at 50% and 95%) are shown for comparison.

The procedure is given by Press et al. (pp575-579, 1992), and Matlab® script Lomb.m (http://mathforum.org/epigone/comp.soft-sys.matlab/hangdiher/34CED3BF.B95E25AF@spectral-imaging.com) was used.

In **Panel e**, the long-term secular trend in Al_2O_3/CaO was removed before we applied the analysis; that is, the Al_2O_3/CaO vs time trend was fitted using a polynomial function (n=2), and this trend was subtracted from the measured Al_2O_3/CaO values. This step removes the very low frequency peak observed in **Panel a** without affecting the peak at ~21 times resurfacing time. In addition, this peak is not sensitive to the procedure used for removing the secular trend; e.g., the peak is also present if a n=5 polynomial function is used to remove the secular trend (not shown).

Table 1a. Trace Element Abundances (in ppm) in KSDP Lavas determined by ICP-MS.

UNIT	Elev. (m)	rock type	Sc	Rb	Sr	Y	Zr	Nb	Ba	La	Ce	Pr	Nd	Sm	Eu	Gd	Tb	Dy	Ho	Er	Tm	Yb	Lu	Hf	Ta	Pb	Th	U
1	-303.8	picrite	23.3	3.16	249	19.4	95	7.06	69.1	7.18	17.6	2.68	12.8	3.56	1.22	3.87	0.623	3.55	0.698	1.78	0.259	1.49	0.216	2.47	0.474	0.976	0.497	0.136
2	-308.4	picrite	22.2	1.85	225	17.3	85	6.15	60.7	6.17	15.3	2.36	11.2	3.15	1.09	3.45	0.555	3.10	0.617	1.55	0.227	1.34	0.190	2.19	0.410	1.14	0.434	0.123
3	-308.9	picrite	22.6	3.44	250	19.9	98	7.14	66.1	7.53	18.9	2.78	13.1	3.72	1.31	4.05	0.653	3.69	0.705	1.91	0.261	1.54	0.218	2.63	0.489	1.12	0.524	0.152
4	-312.3	ol basalt	25.8	2.38	318	22.8	121	7.61	73.8	8.31	20.6	3.23	15.4	4.40	1.58	4.73	0.755	4.20	0.814	2.07	0.295	1.73	0.246	3.05	0.520	0.936	0.573	0.165
5	-314.4	picrite	22.4	2.71	259	18.9	98	6.29	72.9	6.68	17.4	2.55	12.6	3.60	1.29	3.93	0.636	3.56	0.689	1.78	0.254	1.50	0.210	2.56	0.422	0.828	0.465	0.143
6	-316.6	picrite	21.0	3.55	261	18.9	97	6.28	66.1	6.81	16.8	2.66	12.8	3.66	1.29	3.90	0.623	3.50	0.678	1.75	0.241	1.44	0.203	2.53	0.430	0.795	0.455	0.140
7	-325.0	ol basalt	27.9	4.66	301	23.9	126	8.35	76.6	8.50	21.4	3.36	16.0	4.52	1.59	4.80	0.792	4.33	0.838	2.16	0.301	1.78	0.247	3.25	0.560	1.58	0.571	0.171
8	-329.0	ol basalt	26.6	5.15	304	24.6	125	8.52	79.1	8.78	21.9	3.43	16.4	4.59	1.59	4.98	0.796	4.48	0.868	2.22	0.308	1.80	0.256	3.21	0.558	1.04	0.555	0.173
9	-332.4	ol basalt	26.9	3.46	267	23.4	104	6.85	59.0	7.04	17.3	2.72	13.3	3.96	1.43	4.44	0.726	4.19	0.830	2.12	0.300	1.79	0.257	2.74	0.465	0.744	0.465	0.146
10	-334.2	basalt	27.1	2.25	271	22.7	103	6.98	69.8	6.99	18.1	2.73	13.1	3.93	1.40	4.37	0.736	4.17	0.811	2.07	0.294	1.75	0.252	2.68	0.472	0.836	0.486	0.137
12	-336.0	basalt	26.2	3.59	274	23.3	108	7.27	67.7	7.13	17.9	2.76	13.4	4.00	1.42	4.45	0.728	4.14	0.814	2.08	0.300	1.74	0.248	2.77	0.477	1.06	0.467	0.138
13	-338.0	basalt	29.9	7.15	378	27.8	158	11.4	106	12.1	29.9	4.50	21.2	5.62	1.92	5.81	0.920	5.13	0.970	2.43	0.346	2.02	0.286	3.96	0.729	1.23	0.814	0.247
14	-341.9	ol basalt	30.2	7.03	371	27.1	151	10.8	101	11.7	30.1	4.29	20.4	5.46	1.86	5.70	0.886	4.93	0.957	2.47	0.341	1.99	0.278	3.84	0.701	1.23	0.794	0.241
15	-343.8	ol basalt	27.2	5.30	301	25.0	123	9.69	82.6	9.29	24.0	3.54	16.6	4.63	1.64	5.03	0.823	4.57	0.885	2.30	0.319	1.87	0.270	3.21	0.658	1.23	0.678	0.201
16	-345.5	basalt	30.0	6.79	380	27.5	156	11.9	107	11.9	30.4	4.43	21.6	5.63	1.92	5.82	0.931	5.13	0.990	2.52	0.351	2.01	0.283	4.00	0.801	1.30	0.793	0.243
17	-350.4	basalt	30.0	5.90	346	26.8	142	10.6	91.1	10.2	25.7	3.91	18.5	5.10	1.78	5.51	0.892	5.06	0.976	2.56	0.363	1.99	0.296	3.62	0.727	1.17	0.725	0.220
18	-355.6	ol basalt	29.7	5.95	375	28.1	155	11.4	93.0	11.2	28.8	4.25	20.4	5.56	1.91	5.82	0.935	5.14	0.987	2.52	0.350	2.02	0.287	3.87	0.748	1.17	0.785	0.228
19	-357.8	basalt	30.1	6.43	372	28.0	154	11.5	100	11.4	29.2	4.25	20.9	5.57	1.92	5.83	0.940	5.17	0.992	2.53	0.352	2.06	0.280	3.91	0.761	1.20	0.781	0.239
20	-359.2	picrite	26.1	5.63	312	23.3	129	10.2	90.4	9.74	24.4	3.64	17.1	4.61	1.56	4.84	0.775	4.37	0.818	2.16	0.293	1.71	0.241	3.32	0.671	1.06	0.692	0.203
21	-362.5	basalt	29.0	1.94	340	25.9	147	10.7	93.9	9.70	23.9	3.77	18.1	5.12	1.77	5.33	0.875	4.87	0.927	2.34	0.326	1.93	0.275	3.74	0.707	1.14	0.694	0.209
22	-363.9	basalt	30.0	5.13	346	25.7	135	9.68	82.2	9.10	24.4	3.56	17.5	4.90	1.69	5.14	0.825	4.67	0.910	2.33	0.331	1.90	0.275	3.43	0.643	0.993	0.635	0.198
23	-367.3	basalt	29.2	4.87	339	27.6	140	9.94	92.6	10.3	27.7	3.99	18.9	5.29	1.84	5.67	0.898	5.05	0.967	2.42	0.340	1.98	0.286	3.50	0.652	1.05	0.644	0.200
24	-370.6	basalt	28.5	4.68	330	26.1	133	9.54	81.2	9.62	25.1	3.71	17.8	5.03	1.78	5.40	0.879	4.88	0.948	2.41	0.332	1.94	0.274	3.51	0.640	0.957	0.635	0.197
25	-372.5	basalt	29.3	4.12	335	26.3	137	9.58	83.6	9.47	23.8	3.74	18.0	5.03	1.70	5.37	0.869	4.80	0.936	2.42	0.348	1.94	0.270	3.47	0.630	0.996	0.622	0.197
26	-376.1	basalt	28.8	5.44	336	26.9	141	10.1	82.9	10.2	26.3	4.02	18.9	5.24	1.83	5.63	0.904	5.02	0.954	2.48	0.331	1.99	0.286	3.70	0.673	1.36	0.668	0.210
27	-379.5	basalt	30.6	4.51	355	28.0	147	10.3	93.5	10.4	25.6	4.01	19.3	5.26	1.82	5.67	0.904	5.04	0.974	2.51	0.343	2.01	0.288	3.72	0.674	1.15	0.700	0.217
28	-379.8	basalt	29.7	6.16	342	26.7	145	10.3	92.9	10.2	26.2	3.98	19.1	5.30	1.81	5.60	0.893	5.01	0.967	2.49	0.351	2.02	0.289	3.73	0.682	1.08	0.731	0.230
29	-381.3	picrite	24.6	3.76	289	22.8	121	8.50	88.5	8.78	21.7	3.38	16.2	4.41	1.54	4.65	0.743	4.28	0.804	2.08	0.287	1.68	0.239	3.08	0.567	1.07	0.577	0.182

UNIT	Elev. (m)	rock type	Sc	Rb	Sr	Y	Zr	Nb	Ba	La	Ce	Pr	Nd	Sm	Eu	Gd	Tb	Dy	Ho	Er	Tm	Yb	Lu	Hf	Ta	Pb	Th	U
30	-383.0	basalt	27.6	4.58	306	25.2	128	9.07	93.9	9.36	23.1	3.61	17.2	4.73	1.57	5.06	0.805	4.62	0.878	2.28	0.317	1.84	0.263	3.24	0.590	1.13	0.669	0.209
31	-387.6	picrite	21.6	2.57	248	18.3	100	7.08	64.4	6.97	17.9	2.72	12.9	3.56	1.24	3.77	0.611	3.38	0.643	1.66	0.226	1.35	0.201	2.54	0.468	0.771	0.493	0.147
32	-388.2	picrite	26.7	2.49	298	22.5	123	8.73	83.2	8.71	21.9	3.42	16.4	4.49	1.54	4.72	0.762	4.24	0.816	2.10	0.292	1.69	0.239	3.15	0.575	0.989	0.602	0.170
33	-390.0	nd	30.8	4.22	325	26.5	143	10.4	95.8	9.46	24.4	3.78	17.9	5.00	1.76	5.36	0.860	4.87	0.929	2.43	0.337	2.00	0.280	3.63	0.679	1.20	0.700	0.210
34	-391.4	ol basalt	28.7	3.79	320	25.7	132	9.43	72.6	8.82	23.4	3.57	17.4	4.79	1.69	5.22	0.856	4.74	0.918	2.34	0.326	1.89	0.273	3.42	0.654	0.943	0.627	0.198
35	-392.0	ol basalt	30.4	3.31	323	28.3	141	10.2	87.0	9.50	25.5	3.78	18.1	5.13	1.77	5.49	0.897	5.09	0.985	2.61	0.354	2.08	0.293	3.67	0.672	1.08	0.674	0.219
36	-394.4	ol basalt	29.0	3.12	304	24.8	132	9.40	82.1	8.67	22.1	3.48	16.7	4.65	1.61	5.02	0.795	4.57	0.879	2.25	0.312	1.88	0.265	3.37	0.627	0.966	0.607	0.176
37	-395.8	basalt	30.8	4.68	327	27.0	140	10.2	90.4	9.52	24.3	3.80	18.0	5.06	1.77	5.48	0.880	4.89	0.962	2.43	0.346	1.99	0.286	3.61	0.676	1.22	0.658	0.194
38	-398.6	basalt	30.8	5.02	337	27.1	143	10.6	91.9	9.87	24.5	3.91	18.7	5.17	1.81	5.55	0.893	5.01	0.964	2.49	0.336	2.07	0.287	3.73	0.715	1.10	0.714	0.226
39	-403.9	basalt	31.6	4.74	348	28.2	152	11.1	90.6	9.87	27.0	3.93	19.4	5.42	1.87	5.74	0.917	5.16	1.01	2.57	0.358	2.09	0.294	3.82	0.731	1.14	0.708	0.221
40	-407.6	basalt	31.5	5.10	332	27.9	147	10.8	86.8	10.0	25.4	4.00	19.1	5.22	1.79	5.62	0.916	5.15	0.984	2.52	0.355	2.09	0.289	3.79	0.719	1.63	0.691	0.225
41	-408.8	basalt	31.6	4.70	339	29.8	153	11.0	97.9	10.6	25.5	4.21	20.2	5.63	1.87	6.04	0.974	5.47	1.07	2.75	0.390	2.21	0.316	3.98	0.739	1.12	0.725	0.228
44	-411.2	basalt	31.7	5.19	340	28.3	149	10.8	94.3	10.1	25.9	4.08	19.2	5.37	1.82	5.79	0.928	5.23	1.02	2.62	0.369	2.13	0.308	3.86	0.732	1.14	0.718	0.219
45	-412.3	basalt	27.9	4.80	308	24.9	131	9.25	83.5	9.10	23.1	3.63	17.5	4.72	1.64	5.08	0.819	4.59	0.890	2.30	0.322	1.86	0.257	3.38	0.636	1.01	0.615	0.190
46	-413.6	basalt	29.2	5.21	340	26.1	143	10.3	99.4	10.0	24.9	3.89	18.4	5.07	1.75	5.35	0.859	4.79	0.913	2.40	0.336	1.91	0.277	3.59	0.675	1.16	0.683	0.206
47	-418.8	basalt	31.1	5.37	342	26.5	142	10.3	86.8	9.99	25.0	3.87	18.5	5.10	1.70	5.31	0.856	4.78	0.929	2.42	0.337	1.95	0.277	3.61	0.677	1.10	0.673	0.204
48	-422.7	basalt	30.3	5.70	354	27.1	143	10.7	97.2	10.7	27.7	3.97	19.4	5.27	1.82	5.53	0.889	4.90	0.965	2.46	0.335	1.99	0.273	3.66	0.699	1.21	0.714	0.209
49	-426.1	basalt	32.0	4.71	329	26.1	136	9.77	78.0	9.00	23.3	3.60	17.4	4.84	1.68	5.17	0.839	4.71	0.898	2.33	0.323	1.88	0.278	3.50	0.645	0.979	0.652	0.195
50	-429.7	basalt	27.0	5.05	350	24.0	139	10.5	108	10.4	24.9	3.95	18.6	5.03	1.73	5.17	0.820	4.52	0.853	2.16	0.309	1.78	0.253	3.52	0.685	1.20	0.712	0.208
51	-433.4	basalt	31.6	4.94	350	26.9	143	9.71	90.8	9.77	24.2	3.87	18.6	5.14	1.81	5.51	0.884	4.90	0.937	2.44	0.328	1.96	0.279	3.60	0.647	1.02	0.642	0.199
52	-438.9	ol basalt	27.2	4.67	315	24.3	130	9.81	88.8	9.56	24.0	3.64	17.0	4.73	1.60	5.05	0.795	4.53	0.888	2.24	0.318	1.82	0.264	3.34	0.671	1.07	0.691	0.195
53	-440.4	ol basalt	25.8	5.37	299	23.0	124	9.57	93.4	8.84	22.3	3.31	15.9	4.41	1.55	4.74	0.753	4.30	0.831	2.12	0.295	1.75	0.249	3.21	0.640	1.10	0.656	0.193
54	-443.7	basalt	29.7	5.65	362	28.0	152	12.1	106	11.9	27.9	4.42	20.5	5.48	1.89	5.84	0.909	5.14	0.970	2.49	0.350	1.99	0.283	3.90	0.791	1.20	0.818	0.231
55	-445.7	basalt	31.9	3.17	372	27.5	158	12.8	109	11.1	28.4	4.38	20.7	5.62	1.96	5.89	0.928	5.20	0.987	2.44	0.356	2.06	0.290	4.01	0.828	1.23	0.867	0.221
56	-448.8	basalt	30.3	4.62	368	27.3	148	11.9	99.8	11.1	27.8	4.21	19.9	5.36	1.86	5.57	0.893	4.94	0.963	2.42	0.341	1.98	0.283	3.78	0.766	1.11	0.809	0.230
57	-453.2	basalt	29.5	5.06	353	27.4	153	12.2	108	11.1	27.9	4.28	20.2	5.45	1.90	5.68	0.930	5.03	0.972	2.50	0.342	2.02	0.285	3.90	0.799	1.16	0.830	0.221
59	-456.1	basalt	30.0	6.71	353	27.6	151	12.3	109	11.1	27.9	4.23	19.9	5.47	1.91	5.67	0.929	5.06	0.987	2.47	0.351	2.07	0.291	3.83	0.788	1.19	0.823	0.251
60	-464.6	basalt	30.6	2.78	366	30.3	165	13.6	115	12.2	29.7	4.54	21.5	5.77	1.96	6.20	0.998	5.50	1.07	2.75	0.382	2.18	0.315	4.10	0.878	1.19	0.876	0.191
61	-469.3	basalt	29.3	6.12	350	27.9	144	12.0	101	10.6	27.7	4.05	18.8	5.20	1.80	5.57	0.897	5.04	0.969	2.49	0.348	2.02	0.286	3.67	0.786	1.12	0.796	0.226
62	-476.4	basalt	28.9	5.71	324	25.2	130	11.04	97.3	9.61	25.0	3.65	17.1	4.66	1.63	5.02	0.817	4.61	0.889	2.33	0.323	1.85	0.261	3.27	0.700	0.991	0.698	0.199

UNIT	Elev. (m)	rock type	Sc	Rb	Sr	Y	Zr	Nb	Ba	La	Ce	Pr	Nd	Sm	Eu	Gd	Tb	Dy	Ho	Er	Tm	Yb	Lu	Hf	Ta	Pb	Th	U
63	-482.1	basalt	30.2	7.06	338	28.0	146	12.3	105	10.9	27.0	4.10	19.0	5.20	1.76	5.63	0.906	5.07	0.990	2.57	0.363	2.09	0.304	3.71	0.809	1.14	0.835	0.249
64	-493.4	ol basalt	26.3	3.45	252	21.6	99	6.87	61.3	6.59	17.3	2.57	12.6	3.69	1.32	4.13	0.669	3.92	0.748	2.01	0.276	1.63	0.236	2.56	0.463	0.802	0.444	0.132
65	-495.9	basalt	27.5	4.98	293	24.6	123	8.61	74.6	8.28	21.2	3.32	16.0	4.51	1.60	4.90	0.785	4.45	0.870	2.27	0.310	1.83	0.271	3.14	0.567	0.862	0.547	0.171
66	-506.9	basalt	29.3	5.73	318	25.0	131	9.98	82.7	9.20	23.3	3.60	17.1	4.68	1.64	5.11	0.804	4.54	0.892	2.27	0.324	1.88	0.267	3.37	0.656	1.05	0.630	0.191
67	-511.1	ol basalt	26.7	4.26	286	23.4	118	8.27	66.0	7.74	19.8	3.10	14.7	4.24	1.49	4.66	0.741	4.32	0.832	2.14	0.299	1.77	0.251	3.00	0.551	0.803	0.522	0.150
68	-514.2	ol basalt	28.1	3.53	316	24.5	128	8.86	73.8	8.78	22.5	3.41	16.1	4.54	1.58	5.00	0.800	4.56	0.869	2.26	0.314	1.79	0.255	3.26	0.599	0.951	0.607	0.172
69	-521.8	basalt	28.5	4.69	304	26.7	126	8.78	80.5	8.84	20.5	3.41	16.6	4.75	1.68	5.33	0.865	4.81	0.924	2.38	0.333	1.93	0.280	3.29	0.579	0.886	0.553	0.172
70	-526.0	basalt	29.0	2.70	300	24.1	124	8.61	185	8.20	19.0	3.16	15.3	4.48	1.60	4.84	0.787	4.40	0.848	2.15	0.305	1.77	0.248	3.15	0.555	0.885	0.552	0.190
71	-526.5	basalt	29.5	4.36	314	26.4	131	9.17	85.3	9.63	20.1	3.63	17.6	4.90	1.75	5.37	0.853	4.74	0.910	2.28	0.316	1.84	0.269	3.32	0.595	1.01	0.588	0.175
72	-533.7	basalt	30.0	3.81	322	27.0	135	9.65	80.9	9.34	23.9	3.61	17.5	4.82	1.70	5.36	0.880	4.85	0.951	2.45	0.339	1.94	0.279	3.41	0.648	1.06	0.608	0.182
73	-535.2	basalt	30.0	3.60	335	28.5	143	9.87	104	10.8	25.2	4.09	19.5	5.36	1.86	5.83	0.926	5.13	0.999	2.51	0.359	1.97	0.283	3.59	0.661	1.09	0.649	0.181
74	-537.9	basalt	29.8	4.11	320	26.5	133	9.24	95.6	9.20	22.6	3.50	17.0	4.76	1.69	5.21	0.839	4.69	0.907	2.34	0.314	1.88	0.264	3.45	0.613	1.00	0.638	0.172
75	-544.9	basalt	29.1	5.43	311	26.9	139	9.52	81.7	9.42	23.9	3.72	18.0	5.04	1.76	5.48	0.891	4.96	0.976	2.48	0.353	2.03	0.291	3.59	0.643	0.984	0.643	0.203
76	-550.3	basalt	32.0	2.40	305	24.8	140	9.68	84.0	8.72	22.4	3.74	18.3	5.13	1.82	5.38	0.849	4.70	0.898	2.23	0.307	1.78	0.255	3.64	0.669	0.948	0.609	0.186
81	-556.4	basalt	30.6	5.69	318	27.7	141	9.88	133	11.1	23.2	4.25	20.1	5.46	1.88	5.81	0.926	5.11	0.966	2.41	0.346	1.96	0.284	3.54	0.654	1.09	0.620	0.383
82	-558.7	basalt	31.8	2.38	325	29.5	144	10.2	73.3	10.5	24.9	4.11	19.7	5.38	1.88	5.88	0.952	5.27	1.03	2.63	0.374	2.14	0.300	3.72	0.684	1.00	0.648	0.180
83	-562.0	basalt	29.9	2.91	323	28.8	141	9.96	68.4	9.98	24.4	3.83	18.4	5.19	1.82	5.64	0.916	5.14	1.01	2.58	0.362	2.11	0.311	3.61	0.685	0.990	0.640	0.259
85	-564.8	ol basalt	29.0	3.12	283	27.1	135	11.3	114	11.5	26.8	4.22	19.6	5.09	1.73	5.47	0.858	4.93	0.946	2.48	0.344	1.97	0.286	3.36	0.734	1.59	0.748	0.213
87	-566.2	basalt	31.9	8.22	171	24.7	148	12.6	267	9.23	27.8	3.53	16.1	4.46	1.56	4.75	0.805	4.50	0.875	2.22	0.327	1.90	0.267	3.77	0.817	1.74	0.843	0.223
88	-569.4	ol basalt	24.9	2.42	212	21.4	104	8.68	81.6	8.72	21.1	3.15	14.5	3.92	1.37	4.24	0.685	3.87	0.753	1.95	0.274	1.64	0.233	2.73	0.589	0.947	0.631	0.117
91	-573.7	basalt	31.3	2.87	357	28.0	163	14.3	128	14.8	37.1	5.06	22.4	5.72	1.95	5.82	0.933	5.18	0.991	2.58	0.351	2.05	0.291	4.13	0.954	1.59	1.09	0.252
92	-581.7	picrite	21.5	2.10	191	18.7	94	7.89	207	7.40	18.0	2.71	12.8	3.46	1.16	3.77	0.604	3.43	0.650	1.66	0.231	1.33	0.189	2.38	0.531	1.08	0.486	0.122
93	-586.4	basalt	31.3	2.16	324	27.4	140	9.97	90.0	9.28	24.2	3.79	18.5	5.18	1.80	5.61	0.896	5.16	0.990	2.57	0.358	2.08	0.297	3.63	0.684	1.14	0.629	0.186
94	-590.4	basalt	30.3	1.44	330	27.3	129	8.86	68.0	9.04	22.5	3.55	17.3	4.88	1.72	5.37	0.854	4.81	0.943	2.41	0.337	1.98	0.282	3.30	0.604	1.05	0.544	0.157
95	-593.7	basalt	29.9	1.75	317	25.5	129	9.10	64.6	8.62	21.9	3.47	16.8	4.79	1.69	5.18	0.862	4.76	0.917	2.33	0.325	1.95	0.275	3.33	0.612	0.882	0.572	0.168
96	-596.0	basalt	30.3	1.40	316	24.1	116	8.23	64.3	7.92	19.8	3.14	15.3	4.34	1.55	4.70	0.762	4.27	0.832	2.13	0.309	1.79	0.256	2.99	0.545	1.12	0.510	0.160
97	-597.7	picrite	27.3	2.24	236	23.5	121	9.91	84.2	8.62	22.9	3.37	16.2	4.43	1.54	4.82	0.777	4.28	0.830	2.14	0.294	1.72	0.241	3.20	0.671	0.872	0.602	0.171
98	-600.3	basalt	31.8	2.07	294	27.4	134	10.8	83.9	9.05	23.4	3.65	17.5	4.95	1.75	5.51	0.891	5.01	0.989	2.51	0.359	2.06	0.292	3.54	0.720	0.989	0.638	0.158
100	-606.3	basalt	32.6	3.70	308	28.3	141	10.4	64.7	9.22	23.9	3.73	17.8	5.02	1.78	5.54	0.911	5.06	1.00	2.59	0.361	2.05	0.294	3.61	0.684	1.08	0.668	0.220
101	-622.3	basalt	30.6	3.03	295	24.0	120	8.97	49.5	8.23	21.3	3.29	15.7	4.23	1.48	4.72	0.752	4.33	0.841	2.19	0.305	1.74	0.254	3.05	0.607	0.835	0.539	0.162
102	-625.5	ol basalt	30.8	3.86	289	25.3	124	9.66	60.3	8.69	23.5	3.48	16.4	4.52	1.60	5.01	0.821	4.59	0.912	2.34	0.327	1.89	0.272	3.29	0.649	0.869	0.589	0.196
103	-627.8	basalt	32.5	3.32	311	28.0	135	10.3	66.3	9.53	25.7	3.70	17.5	4.87	1.68	5.38	0.892	4.96	0.982	2.53	0.354	2.07	0.293	3.47	0.686	0.925	0.641	0.203

Table 1b. Trace Element Abundances (in ppm) in Makapuu-stage Lavas.

Sample [1]	Sc	Rb	Sr	Y	Zr	Nb	Ba	La	Ce	Pr	Nd	Sm	Eu	Tb	Dy	Ho	Er	Tm	Yb	Lu	Hf	Ta	Pb	Th	U
KOO-1	26.5	5.79	416	24.0	151	8.13	83.8	10.7	26.2	4.15	19.6	5.21	1.74	0.803	4.42	0.831	2.11	0.304	1.67	0.240	3.56	0.560	1.20	0.611	0.181
KOO-7	25.7	6.24	411	25.5	139	9.05	81.5	10.3	25.0	4.25	20.0	5.27	1.77	0.847	4.69	0.891	2.31	0.340	1.85	0.263	3.73	0.633	1.16	0.592	0.175
KOO-8	24.9	7.17	480	25.5	154	9.42	112	12.1	30.7	4.48	21.0	5.35	1.78	0.822	4.51	0.853	2.20	0.312	1.72	0.238	3.62	0.628	1.28	0.674	0.200
KOO-9	22.7	2.10	280	22.2	99	5.06	49.5	6.00	15.5	2.36	12.0	3.79	1.34	0.682	3.94	0.751	1.99	0.297	1.61	0.233	2.52	0.351	0.709	0.362	0.102
KOO-10	23.1	3.07	340	21.0	117	6.80	61.7	7.88	20.0	3.06	15.1	4.27	1.45	0.687	3.83	0.730	1.87	0.274	1.50	0.218	2.90	0.469	0.968	0.474	0.125
KOO-15	25.5	1.50	377	28.4	148	8.71	103	12.2	27.9	4.48	21.3	5.53	1.85	0.885	4.98	0.975	2.46	0.354	2.00	0.278	3.64	0.579	1.10	0.662	0.146
KOO-16	25.9	0.74	372	29.0	140	8.65	67.8	10.3	25.5	3.96	19.2	5.36	1.84	0.923	5.21	0.999	2.58	0.382	2.05	0.287	3.57	0.609	1.06	0.600	0.139
KOO-17A	19.2	0.23	276	19.5	101	5.64	40.3	7.72	18.2	2.85	13.3	3.39	1.13	0.538	3.00	0.597	1.55	0.225	1.23	0.173	2.36	0.387	0.743	0.388	0.075
KOO-20	28.8	7.26	454	26.4	171	10.7	110	13.2	33.3	4.90	23.2	5.96	1.95	0.916	5.03	0.954	2.42	0.350	1.96	0.275	4.09	0.713	1.43	0.756	0.194
KOO-26	26.6	1.87	345	25.0	115	6.80	61.8	8.44	20.6	3.14	15.2	4.29	1.49	0.747	4.29	0.841	2.16	0.317	1.76	0.247	2.87	0.465	0.954	0.497	0.125
KOO-29	26.5	3.10	440	26.2	161	9.08	75.1	10.9	26.8	4.30	20.8	5.62	1.88	0.887	4.89	0.926	2.34	0.341	1.89	0.269	3.78	0.610	1.19	0.679	0.141
KOO-30	25.2	3.13	438	23.5	152	10.3	73.9	16.3	39.6	5.46	23.4	5.42	1.73	0.779	4.25	0.814	2.06	0.297	1.65	0.232	3.67	0.667	1.91	0.881	0.164
KOO-31	-	2.99	409	24.0	152	8.80	71.0	10.7	27.8	4.10	19.7	5.25	1.75	0.815	4.50	0.855	2.14	0.309	1.74	0.243	3.55	0.577	0.951	0.543	0.133
KOO-48	25.5	4.81	435	27.0	142	9.86	103	11.9	30.4	4.62	21.5	5.54	1.85	0.872	4.85	0.923	2.39	0.348	1.90	0.268	3.63	0.658	1.21	0.673	0.168
KOO-50	26.1	0.20	398	29.3	144	9.44	78.4	12.2	27.3	4.44	20.9	5.48	1.87	0.901	5.03	0.993	2.56	0.370	2.02	0.283	3.45	0.607	1.15	0.660	0.123

(1) For sample locations see Frey et al. (1994).

Table 2a. Mixing of Aged, Recycled Phosphate-Bearing Carbonate-Rich Sediment and Primitive Mantle

Estimated Phosphate-Bearing Carbonate-Rich Sediment @ 2 Ga[1]

$^{143}Nd/^{144}Nd$	$^{176}Hf/^{177}Hf$	Sm/Nd	Lu/Hf	Nd (ppm)	Hf (ppm)
0.509941	0.281490	0.25	1.4	10.13	0.17

Calculated Phosphate-Bearing Carbonate-Rich Sediment after 2 Ga of Aging

$^{143}Nd/^{144}Nd$	$^{176}Hf/^{177}Hf$
0.511972	0.289299

Present Primitive Mantle

$^{143}Nd/^{144}Nd$	$^{176}Hf/^{177}Hf$	Nd (ppm)[2]	Hf (ppm)[2]
0.512638	0.282843	1.19	0.27

Mixture of 3% 2 Ga Recycled Carbonate and Apatite-Rich Sediment and 97% Primitive Mantle

$^{143}Nd/^{144}Nd$	$^{176}Hf/^{177}Hf$	epsilon Nd	epsilon Hf
0.512499	0.282967	-2.71	4.40

Table 2b. Mixing of Aged, Recycled Hydrothermal Clay-Rich Sediment and Primitive Mantle

Estimated Hydrothermal Clay-Rich Sediment @ 2 Ga[3]

$^{143}Nd/^{144}Nd$	$^{176}Hf/^{177}Hf$	Sm/Nd	Lu/Hf	Nd (ppm)	Hf (ppm)
0.509941	0.281490	0.20	0.47	124	4.59

Calculated Hydrothermal Clay-Rich Sediment after 2 Ga of Aging

$^{143}Nd/^{144}Nd$	$^{176}Hf/^{177}Hf$
0.511972	0.289299

Mixture of 0.25% 2 Ga Recycled Hydrothermal Clay-Rich Sediment and 99.75% Primitive Mantle

$^{143}Nd/^{144}Nd$	$^{176}Hf/^{177}Hf$	epsilon Nd	epsilon Hf
0.512423	0.282895	-4.19	1.83

(1) Isotopic ratios are assumed to be primitive mantle values at 2Ga, and trace element abundances are from carbonate section at Guatemala (Table 1 of Plank and Langmuir, 1998).

(2) from Hofmann (1988).

(3) Isotopic ratios are assumed to be primitive mantle values at 2Ga, and trace element abundances are from hydrothermal clay at Tonga (Table 1 of Plank and Langmuir, 1998).

Table 3. Input Parameters for Peridotite Melting Model

	Mineral Proportions			
	Olivine	orthopyroxene	clinopyroxene	garnet
Source Mode[1]	0.53	0.04	0.38	0.05
Melting Reaction[1]	0.05	-0.49	1.31	0.13

	Partition Coefficients			
	olivine[2]	orthopyroxene[3]	clinopyroxene[4]	garnet[4]
La	0	0.002	0.008[5]	0.023[5]
Zr	0	0.017	0.027	0.411
Hf	0	0.036	0.049	0.517
Tb[6]	0	0.046	0.119	1.72
Yb	0	0.092	0.174	5.17
Y	0	0.060	0.165	2.37
Sc	0.14[7]	0.27[7]	1.4 [8]	5.17[9]

	source compositions (abundance in ppm)															
	La	Nb	Zr	Tb	Yb	Y	Sc	Sr	Th	Th/La	La/Nb	Sr/Nb	La/Yb	Zr/Yb	Sc/Y	Tb/Yb
original source [10]	0.67	0.71	10	0.085	0.28	3.9	10.8	25	0.047	0.070	0.95	35	2.4	36	2.8	0.30
Guatemala Carbonate Section [11]	14	0.79	5.9	0.47 [12]	1.6	32	4.8	1504	0.29	0.020	18	1904	9.1	3.8	0.15	0.29
adding 3% carbonate-rich sediment into original source	1.1	0.71	10	0.096	0.32	4.7	11	69	0.05	0.050	1.5	98	3.4	31	2.3	0.30
Tonga Hydrothermal Clay [11]	134	2.4	161	4.5 [12]	14	154	13	822	3.6	0.027	56	347	9.4	11	0.08	0.31
adding 0.25% hydrothermal sediment into original source	1.0	0.71	10	0.096	0.31	4.2	11	27	0.06	0.056	1.4	38	3.2	33	2.6	0.30

(1) from Table 2 of Salters (1996)

(2) $D^{olivine/melt}$ is assumed to be zero, except for Sc.

(3) sample TM 295-5 (2.8GPa and 1540°C) from Salters and Longhi, 1999

(4) sample TM 694-6 (2.8GPa and 1537°C) from Salters and Longhi, 1999

(5) $D_{La}^{clinopyroxene/melt} = D_{Nb}^{clinopyroxene/melt}$ and $D_{La}^{garnet/melt} = D_{Nb}^{garnet/melt}$ are assumed.

(6) $D_{Tb} = (D_{Sm}+D_{Er})/2$.

(7) $D_{Sc}^{olivine/melt}$ and $D_{Sc}^{orthopyroxene/melt}$ are calculated using mineral and melt composition of Sample TM 295-5 (2.8GPa and 1540°C) and Equation 39 of Beattie et al. (1991).

(8) $D_{Sc}^{clinopyroxene/melt}$ ranges from 0.8 to 3.2 (e.g., Hart and Dunn, 1993; Hauri et al., 1994a; Blundy et al., 1998).

We use $D_{Sc}^{clinopyroxene/melt} = 1.4$ in our modeling.

(9) $D_{Sc}^{garnet/melt} = D_{Yb}^{garnet/melt}$ is assumed (e.g., van Westrenen et al., 1999).

(10) Y abundance is taken as the primitive mantle value, and Y/Yb is assumed equal to the ratio in both Makapuu- and Kalihi-stage lavas (13.6+/-0.8).
Other ratios are chosen to fit the trends, and abundances of La, Nb, Tb, Zr and Sc are calculated based on these ratios and abundances of Y and Yb.

(11) from Table 1 of Plank and Langmuir, 1998. Sediment column at this trench is carbonate-rich.

(12) Tb abundance is calculated assuming $Tb_{PM}=(Gd_{PM}+Dy_{PM})/2$. Primitive mantle values are from Hofmann (1988).

Table 4. Average Compositions (in %) of Olivine Adjusted Makapuu-Stage Lavas.

	SiO	TiO_2	Al_2O_3	FeO	MnO	MgO	CaO	Na_2O	K_2O	P_2O_5
unaltered	50.3	1.67	11.1	10.9	0.13	15.70	7.43	2.29	0.37	0.2
Hauri 's average	49.98	1.65	11.3	10.8	0.14	15.6	7.60	2.28	0.36	0.2

"Unaltered" includes only Makapuu-stage lavas with K_2O/P_2O_5>1.2 and MgO>6.5% (Frey et al., 1994).

"Hauri's average" is taken from Hauri (1996), and includes Makapuu-stage lavas with MgO>6.5%.

Both groups are adjusted to be in equilibrium with olivine $Fo_{90.5}$. These averages are similar; hence, including altered lavas does not have major effect on the average compositions of Makapuu-stage lavas.

Fig. 1

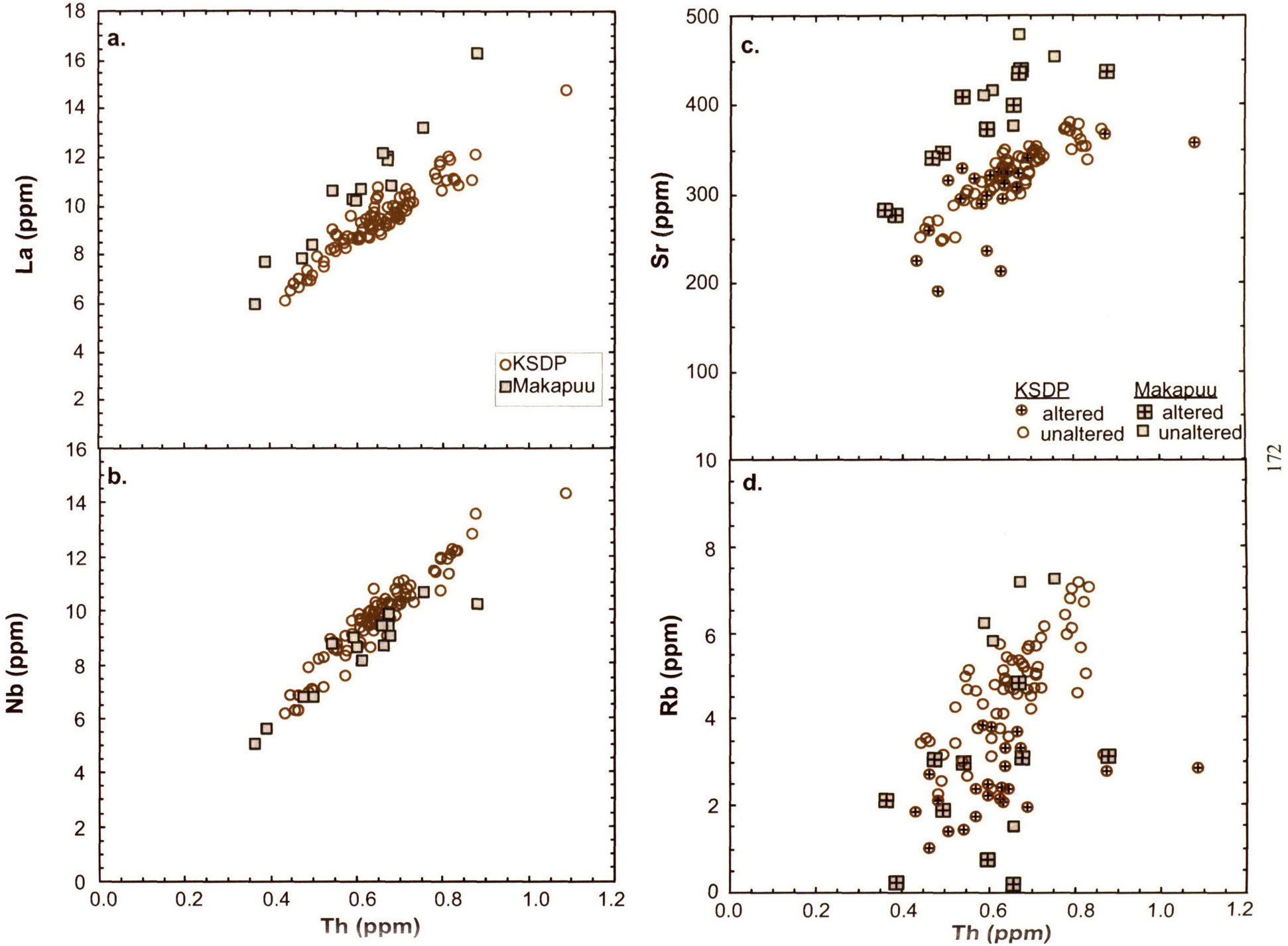
a.
La (ppm)
KSDP
Makapuu
b.
Nb (ppm)
Th (ppm)
c.
Sr (ppm)
KSDP
altered
unaltered
Makapuu
altered
unaltered
d.
Rb (ppm)
Th (ppm)

Fig. 2

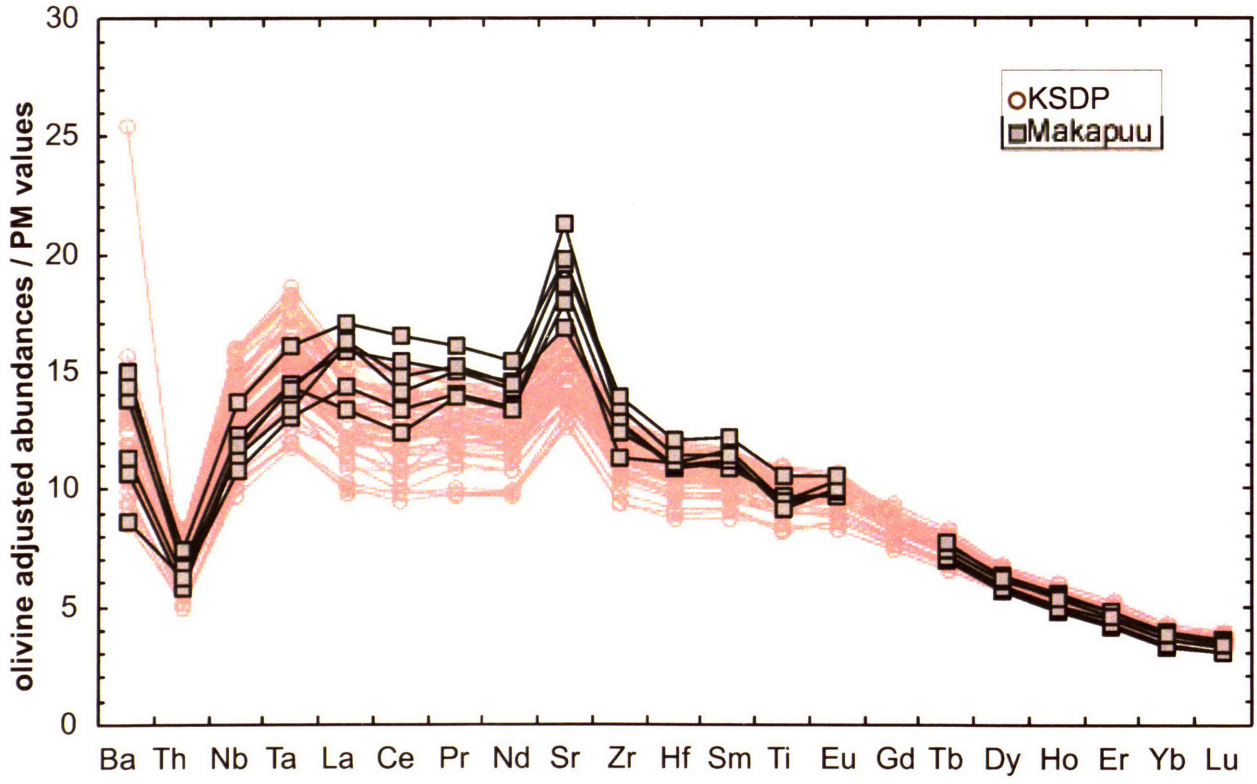
olivine adjusted abundances / PM values
30
25
20
15
10
5
0
KSDP
Makapuu
Ba Th Nb Ta La Ce Pr Nd Sr Zr Hf Sm Ti Eu Gd Tb Dy Ho Er Yb Lu

Fig. 3

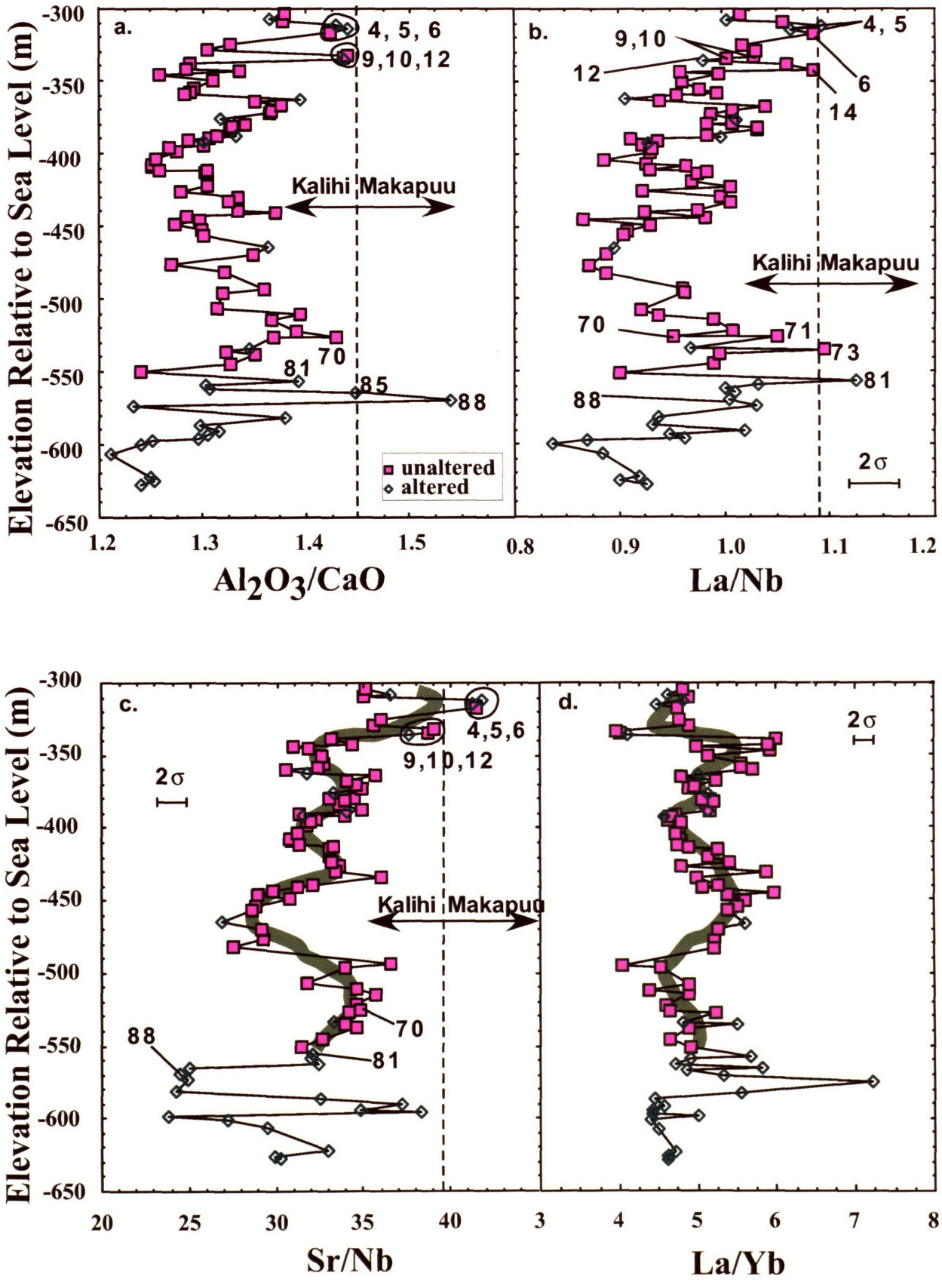
a.
b.
c.
d.
4, 5, 6
9,10,12
Kalihi
Makapuu
70
81
85
88
unaltered
altered
2σ
Elevation Relative to Sea Level (m)
-300
-350
-400
-450
-500
-550
-600
-650
1.2
1.3
1.4
1.5
0.8
0.9
1.0
1.1
1.2
Al2O3/CaO
La/Nb
9,10
12
4, 5
6
14
71
73
4,5,6
9,10,12
20
25
30
35
40
3
4
5
6
7
8
Sr/Nb
La/Yb

Fig. 4

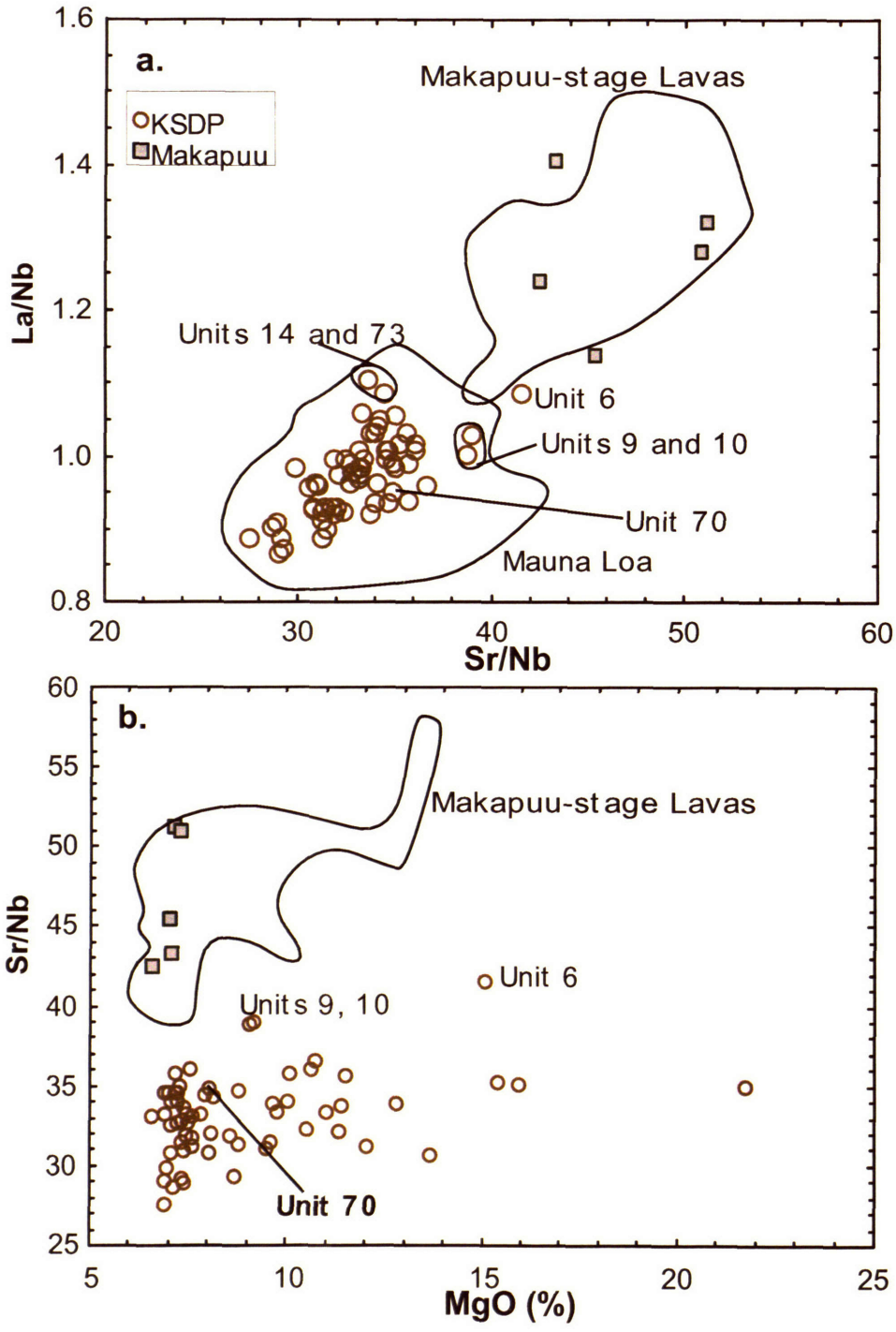
a.
KSDP
Makapuu
Makapuu-stage Lavas
Units 14 and 73
Unit 6
Units 9 and 10
Unit 70
Mauna Loa
La/Nb
Sr/Nb
b.
Makapuu-stage Lavas
Unit 6
Units 9, 10
Unit 70
Sr/Nb
MgO (%)

Fig. 5

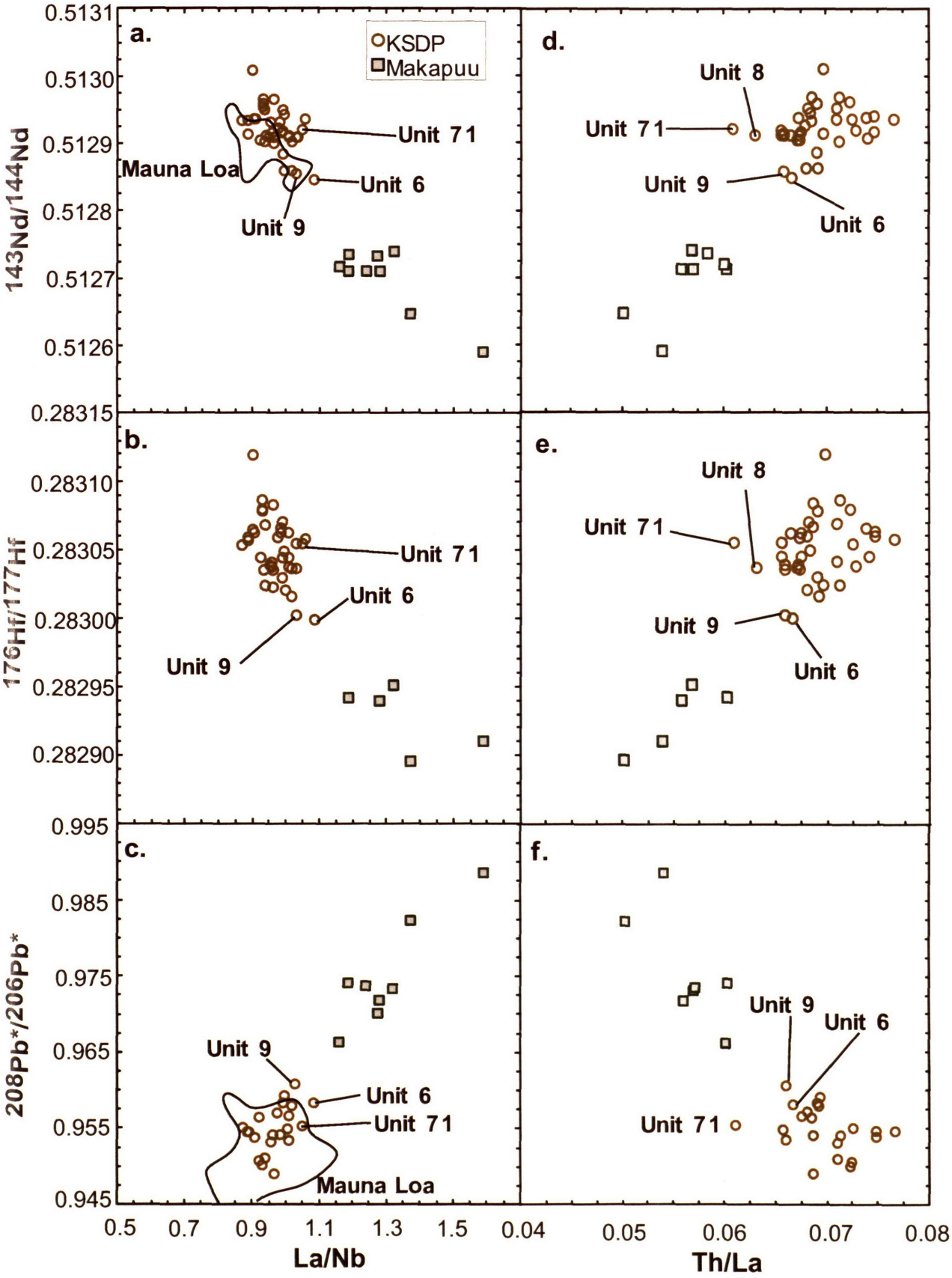
a.
KSDP
Makapuu
Unit 71
Mauna Loa
Unit 6
Unit 9
d.
Unit 8
Unit 71
Unit 9
Unit 6
b.
Unit 71
Unit 6
Unit 9
e.
Unit 8
Unit 71
Unit 9
Unit 6
c.
Unit 9
Unit 6
Unit 71
Mauna Loa
f.
Unit 9
Unit 6
Unit 71
143Nd/144Nd
176Hf/177Hf
208Pb*/206Pb*
La/Nb
Th/La
0.5131
0.5130
0.5129
0.5128
0.5127
0.5126
0.28315
0.28310
0.28305
0.28300
0.28295
0.28290
0.995
0.985
0.975
0.965
0.955
0.945
0.5
0.7
0.9
1.1
1.3
1.5
0.04
0.05
0.06
0.07
0.08

Fig. 6

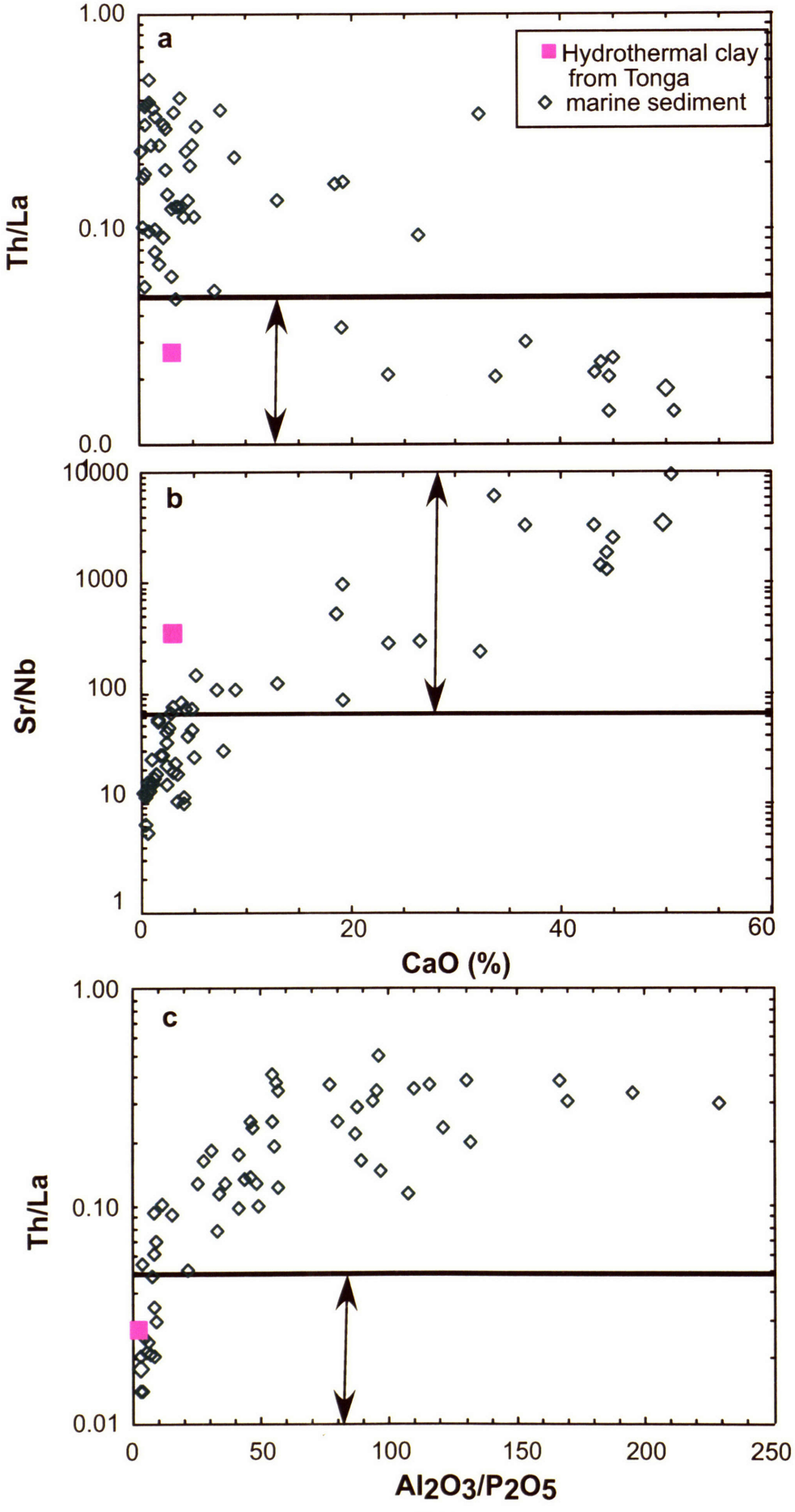
a
Hydrothermal clay from Tonga
marine sediment
Th/La
1.00
0.10
0.0
b
Sr/Nb
10000
1000
100
10
1
0
20
40
60
CaO (%)
c
Th/La
1.00
0.10
0.01
0
50
100
150
200
250
Al2O3/P2O5

Fig. 7

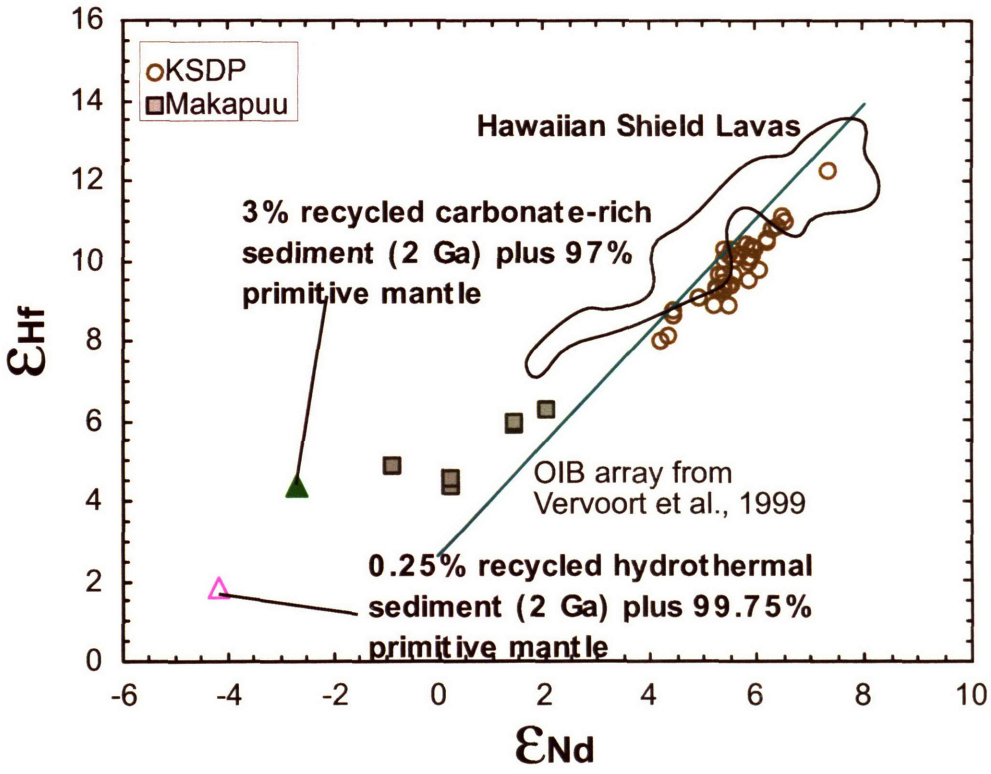
KSDP
Makapuu
Hawaiian Shield Lavas
3% recycled carbonate-rich sediment (2 Ga) plus 97% primitive mantle
OIB array from Vervoort et al., 1999
0.25% recycled hydrothermal sediment (2 Ga) plus 99.75% primitive mantle
εHf
εNd
16
14
12
10
8
6
4
2
0
-6
-4
-2
0
2
4
6
8
10

Fig. 8

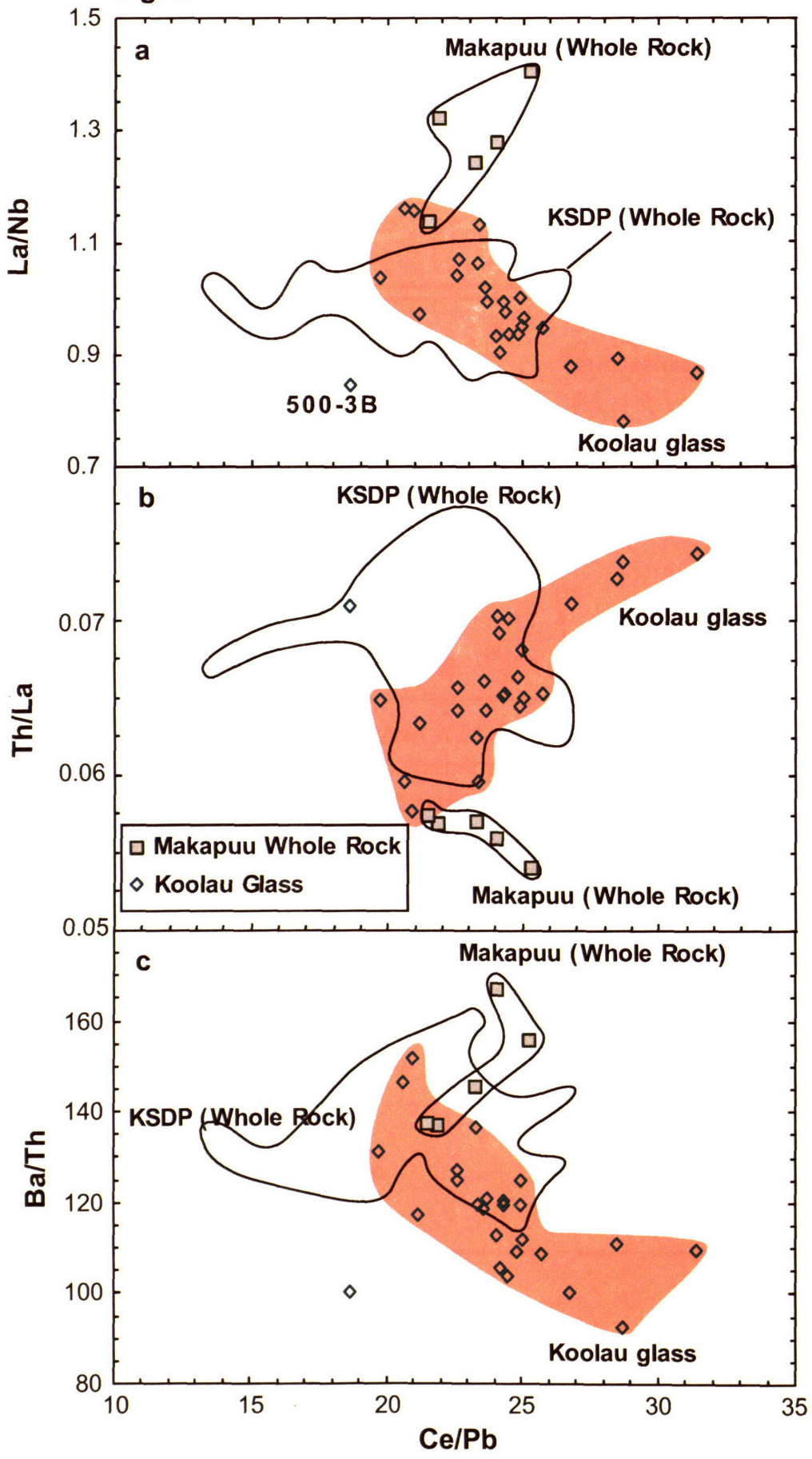
a
Makapuu (Whole Rock)
KSDP (Whole Rock)
500-3B
Koolau glass
La/Nb
1.5
1.3
1.1
0.9
0.7
b
KSDP (Whole Rock)
Koolau glass
Makapuu (Whole Rock)
Makapuu Whole Rock
Koolau Glass
Th/La
0.07
0.06
0.05
c
Makapuu (Whole Rock)
KSDP (Whole Rock)
Koolau glass
Ba/Th
160
140
120
100
80
10
15
20
25
30
35
Ce/Pb

Fig. 9

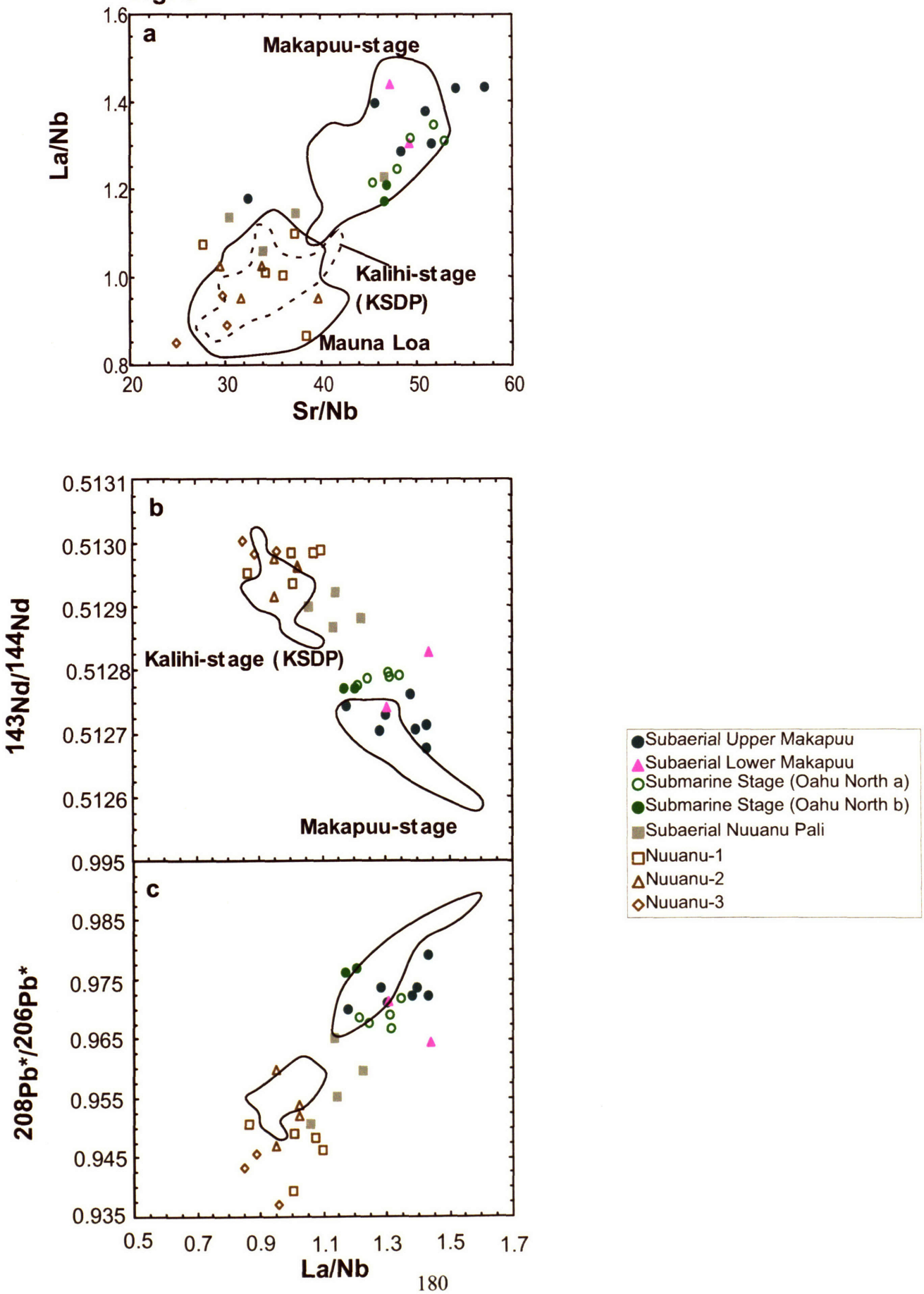
a
Makapuu-stage
Kalihi-stage
(KSDP)
Mauna Loa
La/Nb
Sr/Nb
b
Kalihi-stage (KSDP)
Makapuu-stage
143Nd/144Nd
c
208Pb*/206Pb*
La/Nb
Subaerial Upper Makapuu
Subaerial Lower Makapuu
Submarine Stage (Oahu North a)
Submarine Stage (Oahu North b)
Subaerial Nuuanu Pali
Nuuanu-1
Nuuanu-2
Nuuanu-3

Fig. 10

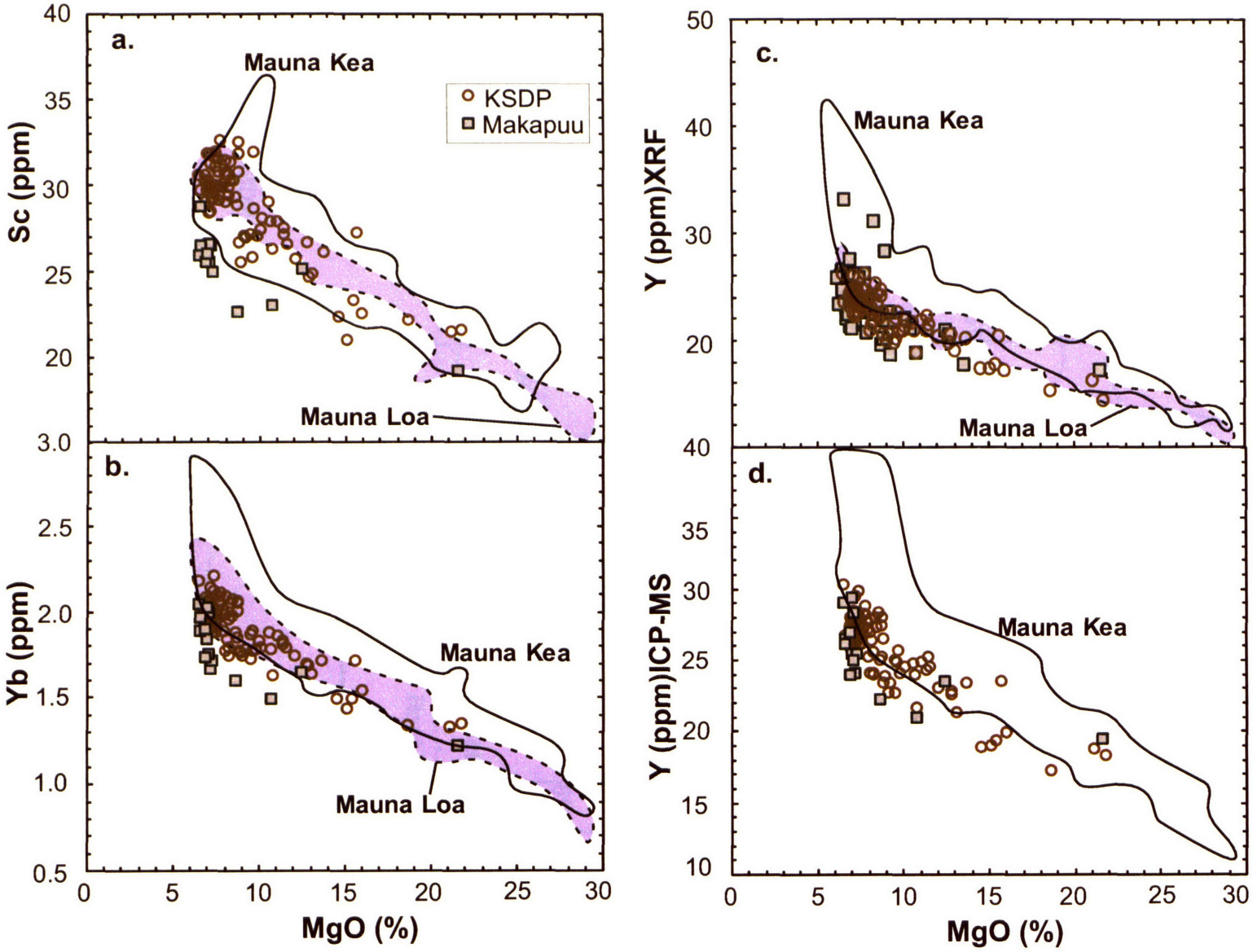
a.
Mauna Kea
KSDP
Makapuu
Mauna Loa
Sc (ppm)
b.
Mauna Kea
Mauna Loa
Yb (ppm)
MgO (%)
c.
Mauna Kea
Mauna Loa
Y (ppm)XRF
d.
Mauna Kea
Y (ppm)ICP-MS
MgO (%)

Fig. 10e

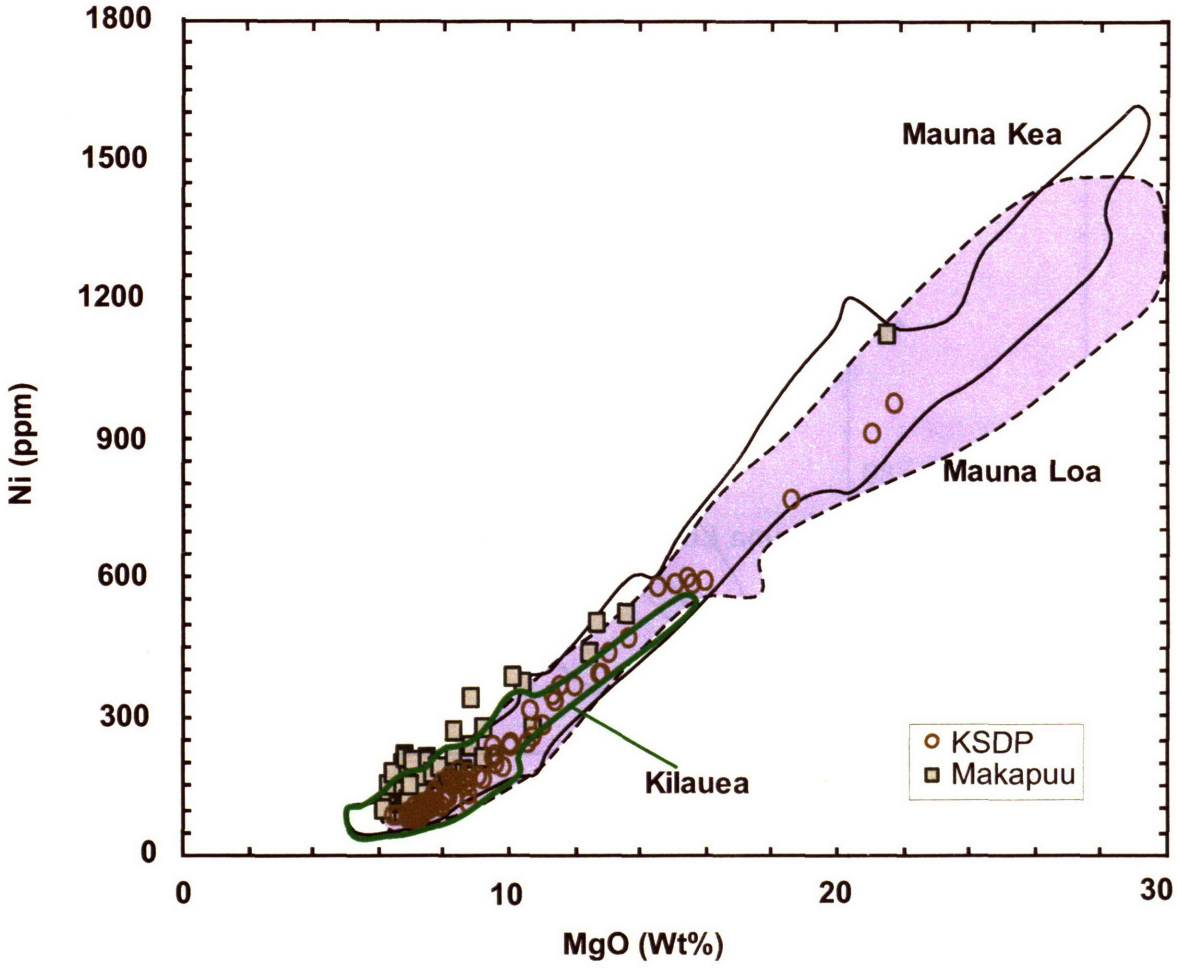
1800
1500
1200
900
600
300
0
Ni (ppm)
0
10
20
30
MgO (Wt%)
Mauna Kea
Mauna Loa
Kilauea
KSDP
Makapuu

Fig. 11

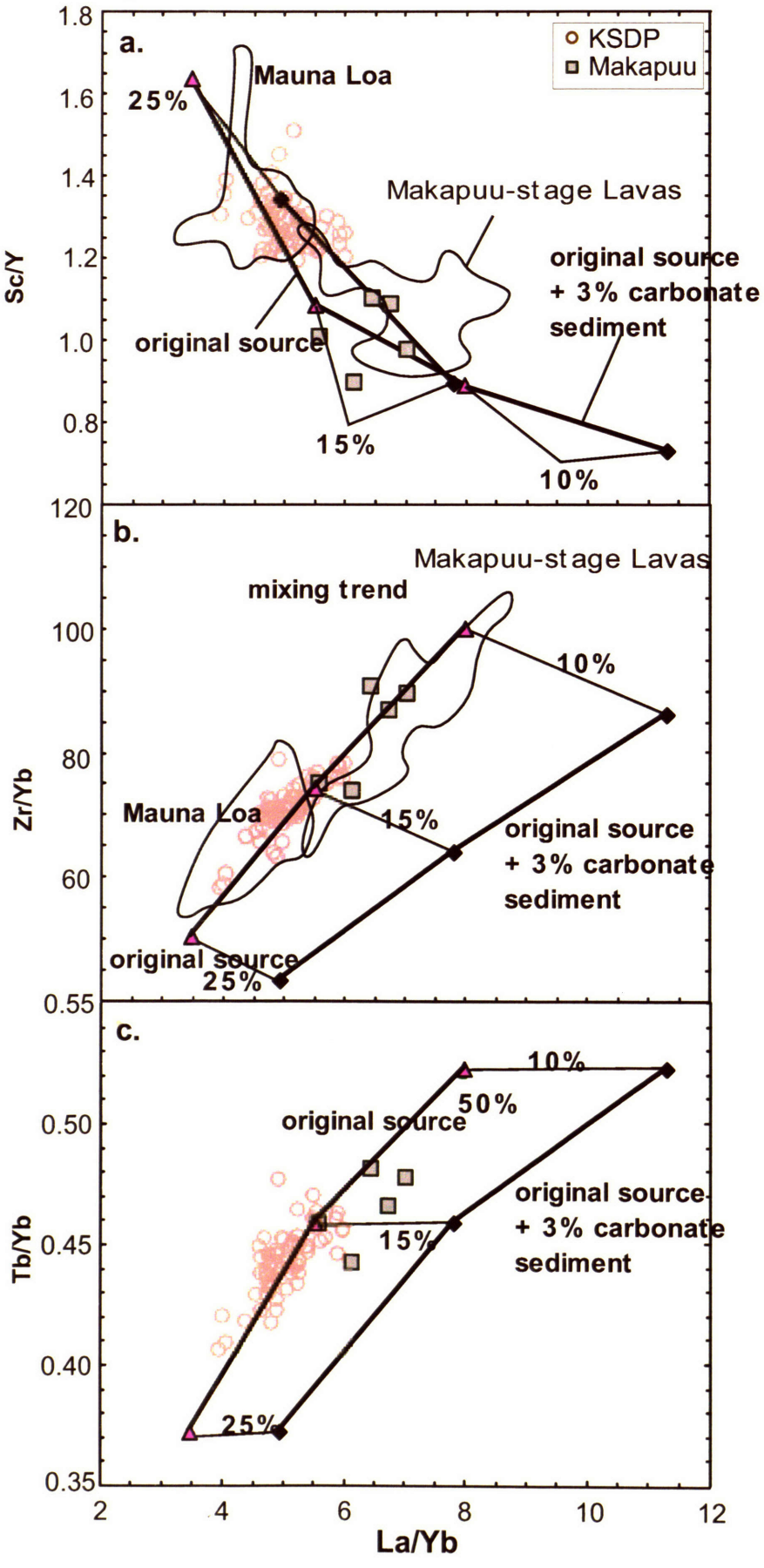
a.
KSDP
Makapuu
Mauna Loa
25%
Makapuu-stage Lavas
original source
+ 3% carbonate
sediment
original source
15%
10%
Sc/Y
1.8
1.6
1.4
1.2
1.0
0.8
b.
Makapuu-stage Lavas
mixing trend
10%
Mauna Loa
15%
original source
+ 3% carbonate
sediment
original source
25%
Zr/Yb
120
100
80
60
c.
10%
50%
original source
original source
+ 3% carbonate
sediment
15%
25%
Tb/Yb
0.55
0.50
0.45
0.40
0.35
2
4
6
8
10
12
La/Yb

Fig. 12

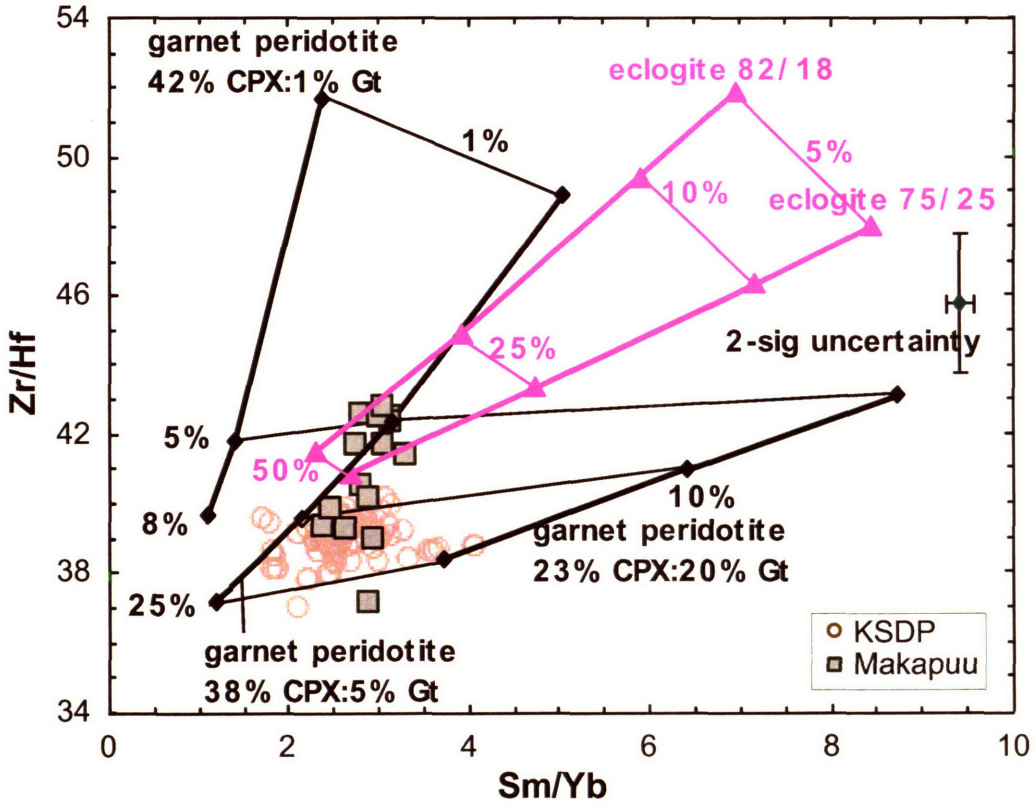
garnet peridotite
42% CPX:1% Gt
1%
eclogite 82/18
5%
10%
eclogite 75/25
25%
2-sig uncertainty
5%
50%
8%
10%
garnet peridotite
23% CPX:20% Gt
25%
garnet peridotite
38% CPX:5% Gt
KSDP
Makapuu
Zr/Hf
Sm/Yb
54
50
46
42
38
34
0
2
4
6
8
10

Fig. 13

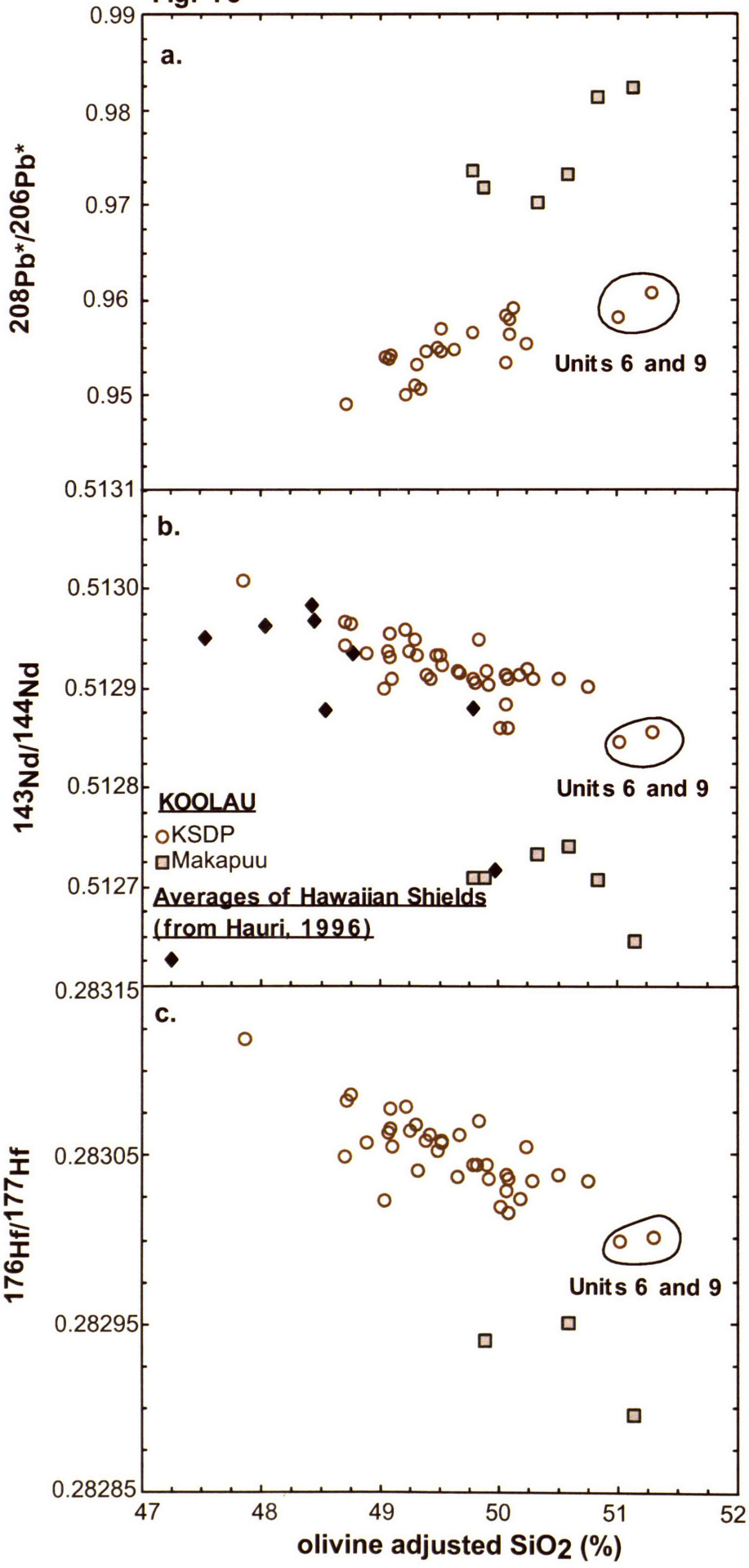
a.
b.
c.
208Pb*/206Pb*
143Nd/144Nd
176Hf/177Hf
olivine adjusted SiO2 (%)
Units 6 and 9
KOOLAU
KSDP
Makapuu
Averages of Hawaiian Shields
(from Hauri, 1996)
0.99
0.98
0.97
0.96
0.95
0.5131
0.5130
0.5129
0.5128
0.5127
0.28315
0.28305
0.28295
0.28285
47
48
49
50
51
52

Fig. 14a

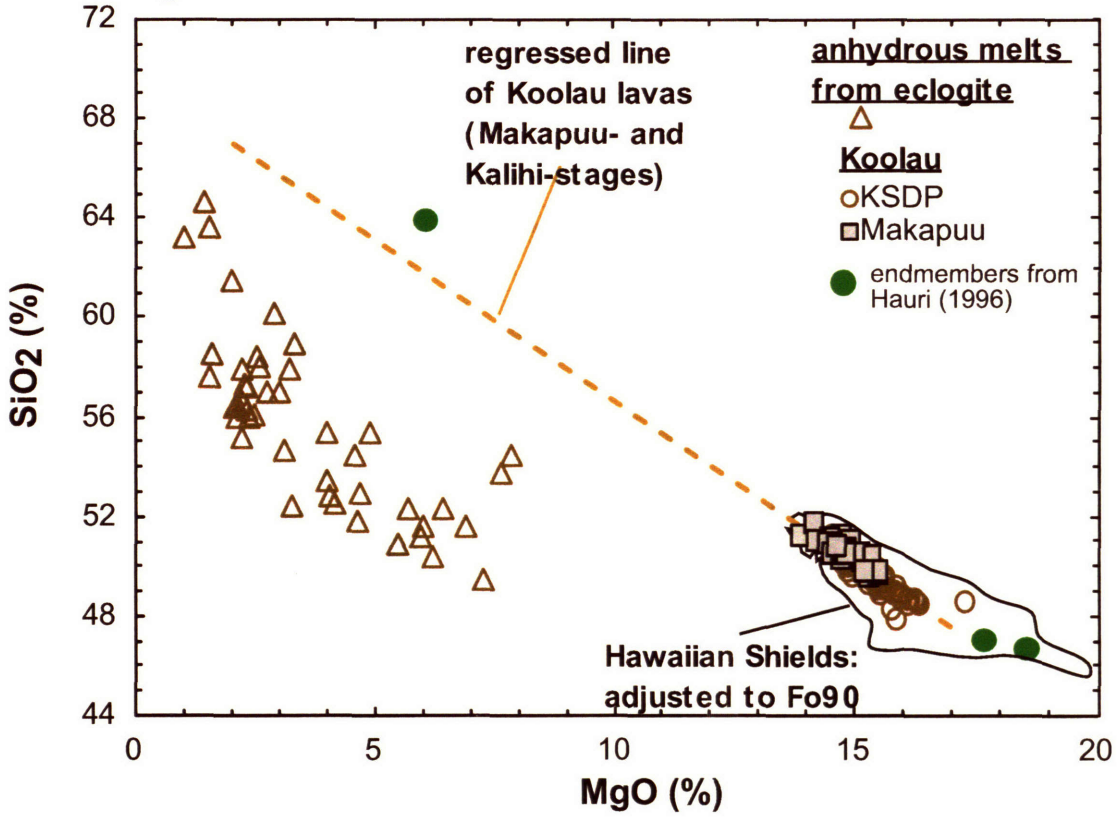

Fig. 14b

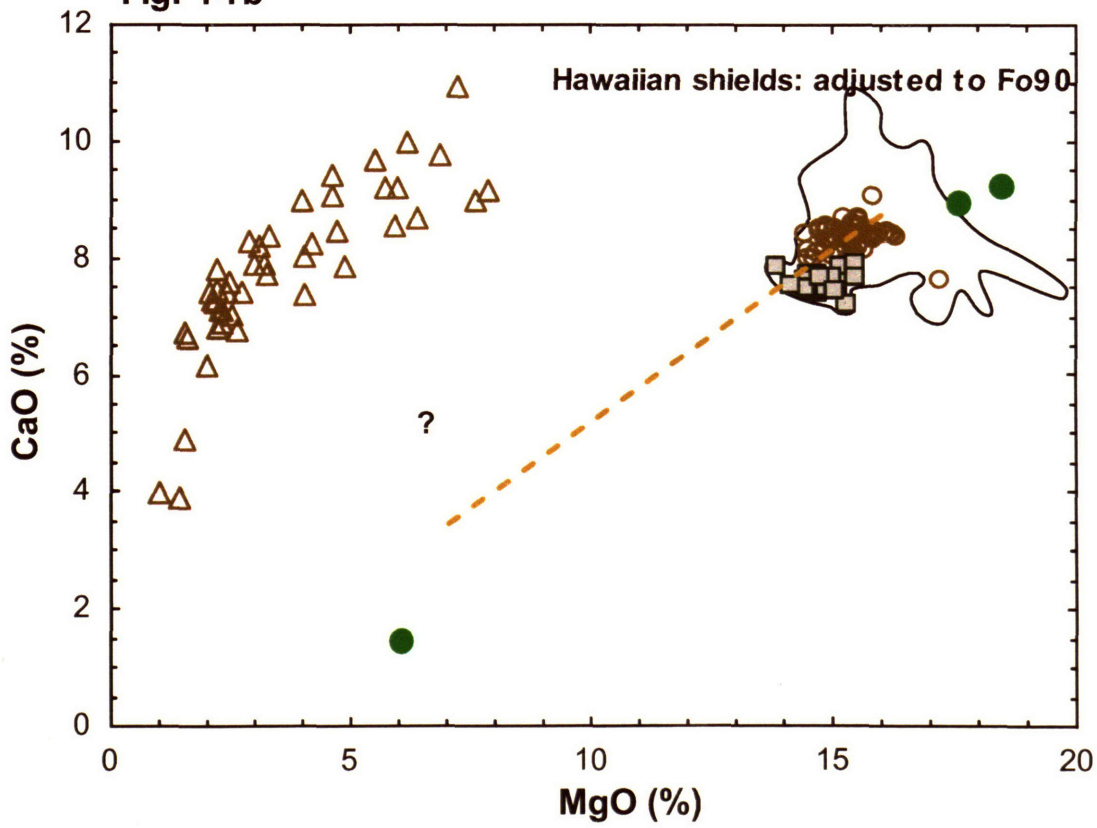

Fig. 14c

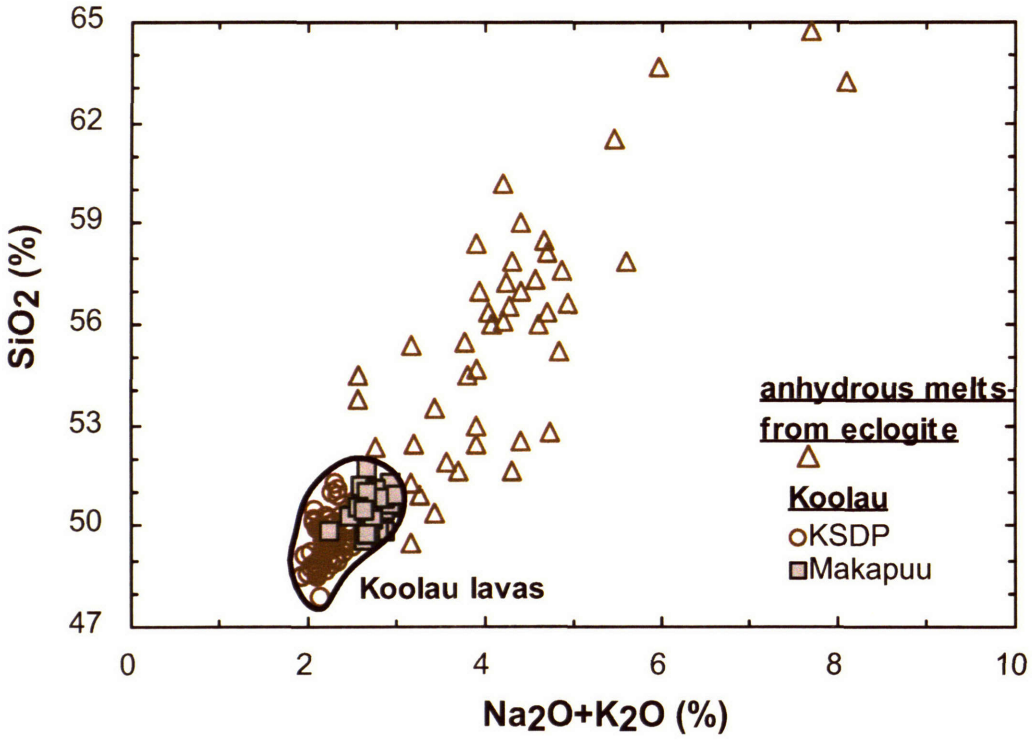
65
62
59
56
53
50
47
SiO2 (%)
0
2
4
6
8
10
Na2O+K2O (%)
anhydrous melts
from eclogite
Koolau
KSDP
Makapuu
Koolau lavas

Fig. 15

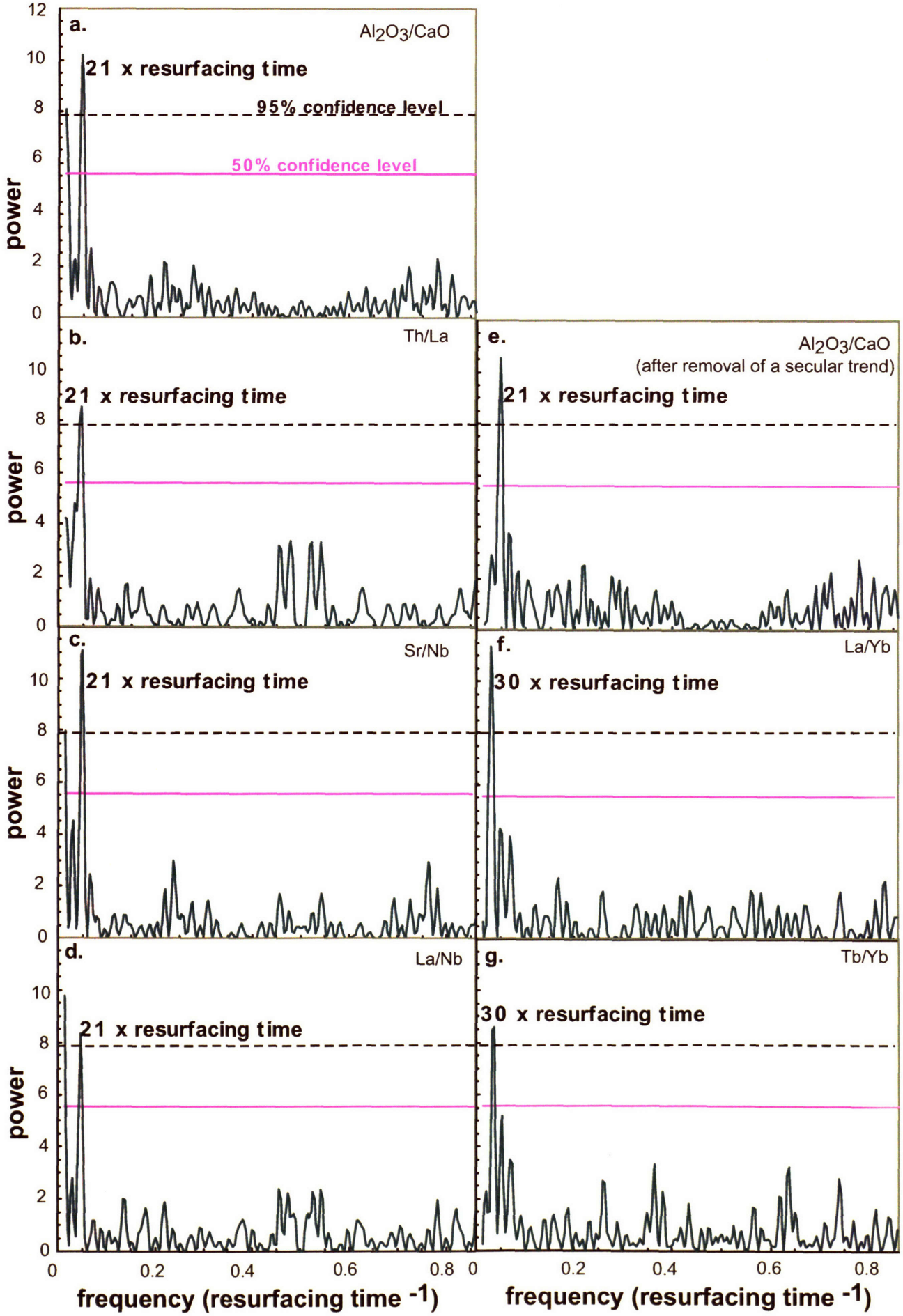
a.
Al_2O_3/CaO
21 x resurfacing time
95% confidence level
50% confidence level
b.
Th/La
21 x resurfacing time
e.
Al_2O_3/CaO
(after removal of a secular trend)
21 x resurfacing time
c.
Sr/Nb
21 x resurfacing time
f.
La/Yb
30 x resurfacing time
d.
La/Nb
21 x resurfacing time
g.
Tb/Yb
30 x resurfacing time
power
0
2
4
6
8
10
12
0
0.2
0.4
0.6
0.8
frequency (resurfacing time $^{-1}$)

CHAPTER 3: ENRICHED COMPONENTS IN THE HAWAIIAN PLUME: EVIDENCE FROM KAHOOLAWE VOLCANO, HAWAII.

Abstract:

The geochemical differences between individual Hawaiian shields provide clues to the magma source components in the Hawaiian plume. Lavas from Koolau (Makapuu-stage) and Kahoolawe volcanoes define the enriched, i.e. relatively high $^{87}Sr/^{86}Sr$ and low $^{143}Nd/^{144}Nd$, extreme for Hawaiian shield lavas. There are, however, important geochemical differences between these shields; Kahoolawe lavas lack the relatively high SiO_2, low CaO and high Sr/Nb and La/Nb that are characteristic of Makapuu-stage Koolau lavas, and they are offset from other Hawaiian shield lavas to high $^{87}Sr/^{86}Sr$ at a given $^{143}Nd/^{144}Nd$. Consequently, a varying role for recycled plagioclase-rich gabbro is inferred; in particular, lower amounts of low $^{87}Sr/^{86}Sr$ component in Kahoolawe lavas. Also, lavas from Loa-trend volcanoes, such as Kahoolawe, define trends ranging toward high $^{208}Pb^*/^{206}Pb^*$ and $^{87}Sr/^{86}Sr$, and low $^{143}Nd/^{144}Nd$ and $^{176}Hf/^{177}Hf$. Such trends are consistent with variable amounts of recycled sediment in the source of Loa-trend volcanoes, with the largest proportion in Makapuu-stage Koolau lavas. Therefore, the enriched component in the Hawaiian plume, the **Koolau** component, is recycled oceanic crust, which is heterogeneous because of varying proportions of sediment, basalt and gabbro.

Hawaiian shield-stage lavas range widely in $^{87}Sr/^{86}Sr$, $^{143}Nd/^{144}Nd$, $^{176}Hf/^{177}Hf$ and $^{206}Pb/^{204}Pb$, but they have similar ratios of Sr/Nd, Nd/Hf and Hf/Pb, each varying by a factor of <3 among the Hawaiian shields. This observation has important consequences. Namely, the similar Hf/Pb ratios are inconsistent with a two-component (i.e., **Kea** and **Koolau**) mixing model for explaining the hyperbolic trend of $^{176}Hf/^{177}Hf$ vs $^{206}Pb/^{204}Pb$ defined by shield lavas. Such a model requires end-members with very different Hf/Pb (a

factor of 15 to 40), but this is not observed; therefore, a third component must be involved. Based on trends of $^{208}Pb^*/^{206}Pb^*$ vs $^{87}Sr/^{86}Sr$, $^{143}Nd/^{144}Nd$ and $^{176}Hf/^{177}Hf$, I infer that Loa and Kea trend shield lavas contain variable amounts of the **Loihi** source component.

1. Introduction

Radiogenic isotope ratios of Sr, Nd, Hf, Pb and Os are quite variable in Hawaiian shield lavas. Clearly their source, dominantly the Hawaiian plume, is geochemically heterogeneous. Among Hawaiian shields, lavas from the surface of the Koolau shield (Makapuu-stage) define an extreme in geochemical characteristics. Specifically, Makapuu-stage Koolau lavas have the highest $^{87}Sr/^{86}Sr$, La/Nb and SiO_2 content, and the lowest $^{143}Nd/^{144}Nd$, $^{176}Hf/^{177}Hf$ and $^{206}Pb/^{204}Pb$ coupled with low CaO and total iron content. These extreme geochemical characteristics are inferred to reflect small amounts of ancient recycled oceanic crust in the Hawaiian plume (e.g., *Frey et al., 1994; Roden et al., 1994; Hauri, 1996; Lassiter and Hauri, 1998; Blichert-Toft et al., 1999; Jackson et al., 1999; Huang and Frey, 2005*). Lavas from two other Hawaiian volcanoes, Kahoolawe and Lanai, share some but not all of these distinctive geochemical characteristics (e.g., *West et al., 1987; Frey et al., 1994; Basu and Faggart, 1996*).

Radiogenic isotope data for Kahoolawe lavas have been reported by *West et al.* (*1987*, Sr, Nd and Pb), *Blichert-Toft et al.* (*1999*, Hf) and *Abouchami et al.* (*2005*, high precision Pb). *West et al.* (*1987*) showed that Kahoolawe lavas range more widely in Sr, Nd and Pb isotopic ratios than most other Hawaiian shields, and that Kahoolawe lavas range to the high $^{87}Sr/^{86}Sr$, and low $^{143}Nd/^{144}Nd$ and $^{206}Pb/^{204}Pb$ that define the end-member Makapuu-stage Koolau lavas. *Abouchami et al.* (*2005*) confirmed that

Kahoolawe lavas range widely in Pb isotopic ratios, e.g., $^{206}Pb/^{204}Pb$ from 17.95 to 18.40, but in detail the Kahoolawe $^{208}Pb/^{204}Pb$ vs $^{206}Pb/^{204}Pb$ trend differs from Makapuu-stage Koolau lavas. *Leeman et al.* (*1994*) in a further study of the Kahoolawe samples studied by *West et al.* (*1987*) used complex trends between ratios of highly incompatible elements, e.g., Th/Ta, and Sr, Nd and Pb isotopic ratios to argue for three source components contributing to Kahoolawe lavas, i.e., plume, asthenosphere and lithospheric mantle. *Blichert-Toft et al.* (*1999*) found that in a $^{143}Nd/^{144}Nd$ vs $^{176}Hf/^{177}Hf$ plot, Kahoolawe lavas lie on the Hawaiian shield trend, but that Kahoolawe lavas are not as extreme as Makapuu-stage Koolau lavas.

In this paper, I report major and trace element abundances for 25 shield stage and 2 caldera filling lavas from Kahoolawe Volcano (Table 1); one shield stage lava, KAH-73, has a K-Ar age of 1.25±0.15 My (Fodor et al., 1992). Isotopic ratios for Sr, Nd, Hf and Pb are reported for a subset of 13 shield stage and 1 caldera filling lavas (Table 2). Our objective is to define and use the geochemical similarities and differences between Kahoolawe and other Hawaiian shield lavas to understand the origin and processes that created the enriched components in the Hawaiian plume. Important results are: **1.** an ancient recycled plagioclase-rich gabbroic crust component, characterized by low $^{87}Sr/^{86}Sr$, is present in the Hawaiian plume; compared with other Hawaiian shield lavas, Kahoolawe lavas contain lesser amounts of this component; **2.** Kahoolawe volcano is a Loa-trend volcano (Fig. 1). Lavas from Loa-trend volcanoes range to high $^{208}Pb^*/^{206}Pb^*$ and $^{87}Sr/^{86}Sr$ coupled with low $^{143}Nd/^{144}Nd$ and $^{176}Hf/^{177}Hf$; consequently, I infer that Loa-trend lavas contain variable amounts of a recycled sedimentary component that is not

present in Kea-trend lavas; **3.** all Hawaiian shield lavas contain the **Loihi** source component.

2. Samples and Analytical Procedures:

Twenty five shield stage samples and two caldera-filling lavas were collected by R. V. Fodor and G. R. Bauer (*Fodor et al., 1992*) from three stratigraphic sections on Kahoolawe Island, Hawaii, which was originally mapped by *Stearns* (*1940*) (Fig. 1). Major element contents were determined by X-ray fluorescence analysis at the University of Massachusetts at Amherst following the procedure described in *Rhodes* (*1996*). Trace element abundances were determined by ICP-MS at MIT following the procedure described in *Huang and Frey* (*2003*). Sr-Nd-Pb isotopic ratios were obtained on acid-leached powders at MIT following the procedures described in *Huang et al.* (*2005*). Hf isotopic ratios were obtained on unleached powders in Lyon following the procedure described in *Blichert-Toft et al.* (*1997*). $^{176}Hf/^{177}Hf$ was normalized for mass fractionation relative to $^{179}Hf/^{177}Hf$=0.7325 and $^{176}Hf/^{177}Hf$ of the JMC-475 Hf standard averaged 0.282160±0.000010 (2 sigma). The Hf standard was run systematically after every two samples. Hf total procedural blanks were less than 25 pg.

3. Results:

3.1 Major Elements:

Kahoolawe shield and caldera-filling lavas are tholeiitic basalt. Among Hawaiian shield lavas, tholeiitic basalt forming the Makapuu-stage of the Koolau shield is distinctive because of its relatively high SiO_2 and low CaO content (Fig. 2); these are features attributed to a dacitic melt component derived from recycled oceanic crust (*Hauri, 1996; Huang and Frey, 2005*). Consistent with the conclusions of *Frey et al.*

(*1994*), Kahoolawe lavas do not have the distinctively high SiO_2 and low CaO contents that distinguish Makapuu-stage Koolau lavas from other Hawaiian shield lavas; after applying a $K_2O/P_2O_5>1$ alteration filter to reject samples whose compositions have been affected by low-temperature alteration (e.g., *Huang and Frey, 2003*), the SiO_2 and CaO contents of Kahoolawe shield and caldera-filling lavas scatter widely (Fig. 2).

3.2 Trace Elements

Relative to primitive mantle compositions, tholeiitic basalt forming Hawaiian shields, is characterized by increasing relative enrichment as the incompatibility of the element increases; typical highly incompatible elements, such as Ba, La and Ce, are enriched by factors of >9 whereas less incompatible elements, such as heavy rare earth elements (REE), are enriched by factors of 3 to 5 (Fig. 3). In a primitive-mantle normalized multi-element diagram, tholeiitic basalts from Kahoolawe have trace element abundances similar to Makapuu-stage Koolau lavas, and range to higher incompatible element abundances than Mauna Loa lavas (Fig. 3).

Also, some abundance ratios, such as Ba/Th, distinguish Hawaiian shield lavas from mid-ocean ridge basalts (MORB) and most other ocean island basalts (OIB) (e.g., *Hofmann and Jochum, 1996; Yang et al., 2003*). Consistent with this result, $(Ba/Th)_{PM}$ in Kahoolawe lavas (with $K_2O/P_2O_5>1$) ranges from 1.5 to 3.0. Other ratios, such as La/Nb, in Hawaiian shield lavas are variable and correlated with radiogenic isotopic ratios (e.g., Fig. 14 of *Huang and Frey, 2003*). Among Hawaiian shield lavas, Makapuu-stage Koolau lavas have the highest La/Nb and Sr/Nb; such ratios are inferred to reflect a recycled sedimentary component in the source of Makapuu-stage lavas (*Jackson et al., 1999; Huang and Frey, 2005*). In contrast, Kahoolawe shield and caldera-filling lavas have

lower La/Nb and Sr/Nb and largely overlap the field for Mauna Loa lavas (Fig. 4). The difference between Makapuu-stage Koolau lavas and Kahoolawe lavas is especially clear for Sr/Nb. Since Kahoolawe caldera-filling lavas have similar geochemical compositions as Kahoolawe shield lavas (e.g., Figs. 2, 4), I do not distinguish them in the following discussion and figures.

3.3 Sr-Nd-Hf-Pb Isotopic Ratios

Our data for $^{87}Sr/^{86}Sr$ and $^{143}Nd/^{144}Nd$ in Kahoolawe lavas define an inverse trend with considerably less scatter than previously published data (Fig. 5). In part, this is a result of higher precision, but most importantly, except for 3 of the 11 shield lavas, the isotopic data for Kahoolawe lavas reported by *West et al.* (*1987*) were obtained on powders that were not acid-leached. It is now recognized that $^{87}Sr/^{86}Sr$ of Hawaiian lavas can be significantly modified, typically increased, by residence in the tropical marine environment of Hawaii (e.g., *Roden et al., 1994*). Nevertheless, the new data confirm that Kahoolawe lavas, like Makapuu-stage Koolau lavas, range to relatively high $^{87}Sr/^{86}Sr$ and low $^{143}Nd/^{144}Nd$; most importantly, relative to Makapuu-stage Koolau lavas, Kahoolawe lavas are offset to high $^{87}Sr/^{86}Sr$ at a given $^{143}Nd/^{144}Nd$ (Fig. 5).

In an ε_{Hf} vs ε_{Nd} plot, *Blichert-Toft et al.* (*1999*) showed that Hawaiian shield lavas define a shallower trend than the OIB array. Specifically, they found that Makapuu-stage Koolau lavas are at the extreme of the Hawaiian trend with relatively high ε_{Hf} at a given ε_{Nd} (Fig. 6). They also found that the Kahoolawe sample, KW-19, with the lowest ε_{Nd} is offset to relatively high ε_{Hf}. In contrast, our Kahoolawe data do not deviate from the OIB array; Sample KAH-24 with the lowest ε_{Hf} is on the OIB array (Fig. 6). I are confident that these differences are not analytical artifacts because the low ε_{Nd} of KW-19 is

consistent with its relatively high $^{87}Sr/^{86}Sr$ (Fig. 5), and ε_{Hf} for KAH-24 and KW-19 were determined in the same laboratory and are within analytical uncertainty.

In Pb-Pb isotopic plots, Kahoolawe lavas range to the low $^{206}Pb/^{204}Pb$ end of the array defined by Hawaiian shield lavas (Fig. 7). As expected for a Loa-trend volcano, Kahoolawe lavas have relatively high $^{208}Pb/^{204}Pb$ at a given $^{206}Pb/^{204}Pb$ (*Abouchami et al., 2005*). However, unlike Makapuu-stage Koolau lavas, the Pb-Pb trends for Kahoolawe lavas are parallel to those for other Hawaiian shields (Fig. 7).

An important feature of Kahoolawe lavas is their wide range in isotopic ratios. There are no systematic geochemical variations within or between the three stratigraphic sections of shield lavas. The isotopic extremes are represented by samples studied by *West et al. (1987)*; KW-19 from a Kanapou Bay section has the highest $^{87}Sr/^{86}Sr$ and lowest $^{143}Nd/^{144}Nd$ (Fig. 5), whereas samples KW-5 and KW-7 from the Northeast shore have the lowest $^{87}Sr/^{86}Sr$, highest $^{143}Nd/^{144}Nd$ and ε_{Hf}, and the most radiogenic Pb isotopic ratios (Figs. 5-7). Most importantly, isotopic heterogeneity is expressed on a very local scale, in terms of location and eruption age; i.e., sample KW-6 is stratigraphically situated between samples KW-5 and KW-7 (Fig. 1; Fig. 2 of *Leeman et al., 1994*), but does not have extreme isotopic ratios (Figs. 5-7). Among our samples, KAH-24 from Kanapou Bay has the highest $^{87}Sr/^{86}Sr$ and lowest ε_{Nd} and ε_{Hf}, and the least radiogenic Pb isotopic ratios (Figs. 5-7).

4. Discussion:

4.1 Source Components Contributing to Hawaiian Shield Lavas:

Among Hawaiian shield lavas, the extremes in radiogenic isotopic ratios are manifested in lavas from specific volcanoes. Lavas from Loihi and Kauai are

characterized by the highest $^{3}He/^{4}He$ (*Kurz et al., 1983; Mukhopadhyay et al., 2003*). Lavas from Mauna Kea, Kilauea and Kauai are characterized by the lowest $^{87}Sr/^{86}Sr$ and highest $^{143}Nd/^{144}Nd$, $^{176}Hf/^{177}Hf$ and Pb isotopic ratios (e.g., *Lassiter et al., 1996; Blichert-Toft et al., 1999; Abouchami et al., 2000*). In contrast, lavas from the Makapuu-stage of Koolau, Lanai and Kahoolawe range to the highest $^{87}Sr/^{86}Sr$ and lowest $^{143}Nd/^{144}Nd$, $^{176}Hf/^{177}Hf$ and Pb isotopic ratios (e.g., *West et al., 1987; Roden et al., 1994*). The enriched end-member, i.e., highest $^{87}Sr/^{86}Sr$ and lowest $^{143}Nd/^{144}Nd$, in Hawaiian shield lavas is defined by lavas from the Makapuu-stage of the Koolau shield (*Frey et al., 1994; Roden et al., 1994; Hauri, 1996; Lassiter and Hauri, 1998; Blichert-Toft et al., 1999; Jackson et al., 1999; Huang and Frey, 2005*). Although an enriched component also contributed to lavas from the Lanai and Kahoolawe shields (*West et al., 1987; Basu and Faggart, 1996*), I find that Kahoolawe shield lavas differ from Makapuu-stage Koolau lavas. Compared with Makapuu-stage Koolau lavas, Kahoolawe lavas are offset to higher $^{87}Sr/^{86}Sr$ at a given $^{143}Nd/^{144}Nd$ (Fig. 5). Also, they lack the distinctive major and trace element characteristics of Makapuu-stage Koolau lavas; i.e., high SiO_2 and low CaO contents attributed to a dacite melt derived from partial melting of eclogite, and high La/Nb and Sr/Nb attributed to recycled sediment (*Huang and Frey, 2005*). Such differences provide insights for understanding the origin of enriched components in the Hawaiian plume.

4.2 Mixing Among Different Source Components:

The diversity of isotopic ratios in Hawaiian shield lavas is commonly explained by variable mixing proportions of source components known as the **Koolau**, **Loihi** and **Kea** components (e.g., *Eiler et al., 1996, 1998; Lassiter and Hauri, 1998; Blichert-Toft et*

al., 1999). Based on isotopic data for Kauai lavas, *Mukhopadhyay et al.* (*2003*) proposed that a fourth component **DM** (depleted mantle as represented by rejuvenated-stage lavas) is necessary. Four components are also required by the Pb-Pb isotopic trends defined by Hawaiian shield lavas (*Abouchami et al., 2005*). With four source components, it is surprising that some isotopic trends defined by Hawaiian shield lavas are near-linear, e.g., $^{87}Sr/^{86}Sr$ vs $^{143}Nd/^{144}Nd$ (Fig. 5) and $^{143}Nd/^{144}Nd$ vs $^{176}Hf/^{177}Hf$ (Fig. 6). Therefore, one approach to modeling the mixing process is to assume that different source components have similar trace element abundance ratios (i.e., Sr/Nd and Nd/Hf) and, in some cases, similar trace element abundances (e.g., *Eiler et al., 1996, 1998; Mukhopadhyay et al., 2003*). The observation that Hawaiian shield lavas have similar ratios (within a factor of 3) of Sr/Nd and Nd/Hf at a given MgO content (Fig. 8) is consistent with the assumptions made by *Eiler et al.* (*1996, 1998*) and *Mukhopadhyay et al.* (*2003*) who successfully reproduced the isotopic variations in Hawaiian shield lavas using three or four source components. However, similar Sr/Nd and Nd/Hf in isotopically distinct source components is surprising if these components were created by diverse processes, ranging from partial melting to formation of different types of sediments. A possible explanation is that the "source components" in the mixing models are mixtures of different mantle reservoirs rather than independent source components created by different processes. The mixing lines involving different mantle reservoirs may be highly curved, i.e., they have very different element abundance ratios (such as Sr/Nd), but if the mixing proportions of different mantle reservoirs vary over a small range, it is possible that the mixing lines are close to linear. As an example, the sources of Koolau lavas contain variable, but small amounts (<3%) of recycled sediment (*Huang and Frey, 2005*).

Other isotopic ratio trends defined by Hawaiian shield lavas, most notably $^{206}Pb/^{204}Pb$ vs $^{176}Hf/^{177}Hf$ (Fig. 9), are highly curved and very different Hf/Pb are inferred for the proposed mixing end-members (*Blichert-Toft et al., 1999*). Although *Blichert-Toft et al.* (*1999*) proposed that the end-members for the **Koolau** and **Kea** components differ by a factor of 40 in Hf/Pb, I find the trend of Hawaiian shield lavas is consistent with $(Hf/Pb)_{\mathbf{Kea/Koolau}} = 15$ (Fig. 9). A mixing calculation using $(Hf/Pb)_{\mathbf{Kea/Koolau}} = 15$ implies that Hf/Pb in Mauna Kea and Makapuu-stage Koolau lavas differs by a factor of 5 (8.0/1.6) (Fig. 9). In detail, other shield lava trends, such as $^{206}Pb/^{204}Pb$ vs $^{87}Sr/^{86}Sr$ and $^{143}Nd/^{144}Nd$, are also best fitted by Sr/Pb and Nd/Pb that differ by factors of ~5 in the **Koolau** and **Kea** components (Fig. 10).

Given the non-linearity of trends involving $^{206}Pb/^{204}Pb$ (Figs. 9, 10), it is surprising that Hawaiian shield lavas with >7% MgO have Sr/Pb, Nd/Pb and Hf/Pb that differ by factors less than 3 (Fig. 8). If these ratios in the lavas are representative of those in the sources, a consequence is that mixing of end-members, e.g., Mauna Kea (**Kea**) and the Makapuu-stage of Koolau (**Koolau**), yields near-linear trends which do not adequately explain the curvature defined by lavas from Hawaiian shields (Figs. 9, 10). For example, the curvature in the $^{206}Pb/^{204}Pb$ vs $^{176}Hf/^{177}Hf$ plot requires that $(Hf/Pb)_{\mathbf{Kea/Koolau}} = 15$ (Fig. 9), but such a difference is not observed (Fig. 8). How can this contradiction be resolved? One potential problem is our assumption that Hf/Pb in lavas represents the source value. Could solid sources have quite different Hf/Pb but magmas resulting from the partial melting process have similar Hf/Pb? I evaluate this possibility.

We assume that a garnet peridotite contains 10% garnet and 15% clinopyroxene, a melting reaction of 40% garnet + 40% clinopyroxene + 10% olivine + 10%

orthopyroxene = 100% melt, and that 10% partial melting is required to generate tholeiitic lavas (e.g., *Feigenson et al., 2003*). During partial melting of peridotite, Pb partitioning is similar to Ce or Nd (e.g., *Hofmann, 1997*); since these elements are highly incompatible in these minerals, D_{Pb} is assumed to be 0. Also, I assume that $D_{Hf}^{garnet/melt}$=0.5, $D_{Hf}^{clinopyroxene/melt}$=0.2, and that Hf is very incompatible in orthopyroxene and olivine. These partition coefficients are on the high end of published values (e.g., *Salters and Longhi, 1999; Pertermann et al., 2004*); therefore our calculations maximize the effect of partial melting on Hf/Pb. I find that Hf/Pb in melt generated by 10% partial melting is about 0.7 times that in the original source. Therefore, it is reasonable to assume that Hf/Pb in Hawaiian shield lavas approximates their source.

However, Hawaiian shield lavas may be saturated with sulfide (e.g., *Lassiter, 2003; Norman et al., 2004*). *Norman et al.* (*2004*) showed that there is no correlation between Pb and S abundances in basaltic glasses from Hawaiian shields; consequently, it is unlikely that Pb abundance was affected by S devolatilization. Based on abundances of platinum group elements in Hawaiian shield lavas, *Lassiter* (*2003*) argued that the source of Hawaiian shield lavas may contain small amounts of sulfide, which may significantly affect the partition coefficient of Pb. Is it reasonable to assume D_{Pb}=0? I use a Pb-Hf abundance plot to investigate their relative incompatibility during the partial melting process (Fig. 11). The large dataset for Mauna Kea lavas shows that Pb and Hf abundances are positively correlated, with alkalic lavas having the highest Pb and Hf abundances (Fig. 11). Undoubtedly, this trend in part represents olivine accumulation and fractionation, but I infer that the large range, factor of 3, was dominantly controlled by variable extents of melting. Moreover, since the regressed line intercepts the Hf axis (Fig.

11), I infer that during the partial melting process, Pb was more incompatible than Hf. Therefore, I conclude that it is reasonable to assume that Hf/Pb in Hawaiian shield lavas reflects source ratios within 30%.

If Hf/Pb in the lavas reflect those of the sources, a possible explanation is that the curvature of the isotopic-isotopic trends in Figs. 9 and 10 reflects the involvement of a third component. Supporting evidence for this inference arises from plots of $^{208}Pb^*/^{206}Pb^*$ vs Hf, Sr and Nd isotopic ratios for Hawaiian shield lavas (Fig. 12). It is well known that the spatial arrangement of recent Hawaiian volcanoes form two offset trends, i.e., the Kea and Loa trends (e.g., *Lassiter et al.,* 1996; Fig. 1). There are important geochemical differences between Loa and Kea trend lavas (e.g., *Lassiter et al., 1996*). Many of these differences are source related; e.g., Loa and Kea shield lavas define distinct arrays in $^{206}Pb/^{204}Pb$ vs $^{208}Pb/^{204}Pb$ (Fig. 7), thereby requiring four components with different Pb isotopic ratios (*Abouchami et al., 2005*). In Fig. 12 I show that Kea and Loa lavas form two linear trends in plots of $^{208}Pb^*/^{206}Pb^*$ vs Hf, Sr and Nd isotopic ratios, with Loihi lavas at the intersection of the Kea and Loa trends. Specifically, lavas from Kea trend volcanoes have variable $^{208}Pb^*/^{206}Pb^*$ but relatively constant $^{176}Hf/^{177}Hf$, $^{87}Sr/^{86}Sr$ and $^{143}Nd/^{144}Nd$; consequently, they form a near-horizontal trend. In contrast, lavas from Loa trend volcanoes form a steep trend. The extremes of the Kea and Loa trends at relatively low and high $^{208}Pb^*/^{206}Pb^*$, i.e., the **Kea** and **Koolau** components respectively, are consistent with Loa trend sources containing a small and variable recycled sedimentary component characterized by relatively high $^{87}Sr/^{86}Sr$ and $^{208}Pb^*/^{206}Pb^*$ coupled with low $^{143}Nd/^{144}Nd$ and $^{176}Hf/^{177}Hf$, i.e., the **Koolau** component. The **Koolau** component is absent in Kea trend lavas, and the **Kea** component is absent in

Loa trend lavas. In addition to the Kea and Loa extremes, a third component is required. This third component is best manifested by Loihi lavas; that is, the field for Loihi lavas is at the intersection of the straight lines that define the Loa and Kea trends in Figs. 9, 10 and 12.

Random sampling of three isotopically distinct source components, i.e., **Koolau**, **Kea** and **Loihi**, should result in a triangle in 2-D isotopic plots. *Douglass and Schilling (2000)* showed that under certain conditions mixing between three components can result in linear trends in isotopic ratio space, i.e., a pseudo-binary mixing array. The formation of a pseudo-binary mixing array requires that: "**1.** the mass fraction of at least two of the three endmembers (source components) must co-vary linearly, and **2.** the elemental enrichment of the different isotopes in a given endmember relative to the third endmember must be the same" (*Douglass and Schilling, 2000*). The second requirement is necessary only if the mixing array is linear. If only the first requirement is satisfied, mixing of three source components may result in a linear or curved trend (e.g., Fig. 3 of *Douglass and Schilling, 2000*), similar to Figs. 6 and 9.

What are the physical conditions that lead to pseudo-binary mixing arrays? A possible explanation is that sampling of the proposed source components is controlled by their different solidi. Consider upwelling mantle consisting of several different lithologies; since heat diffuses much faster than atoms, it is possible that this geochemically heterogeneous mantle is in thermal equilibrium throughout the upwelling process (*Phipps Morgan, 2001*). Consequently, during upwelling the melting extent of each lithology is determined by its solidus, the potential temperature of this geochemically heterogeneous mantle and the final depth where upwelling terminates (see

Fig. 9 of *Phipps Morgan, 2001*). The effect of this process on the isotopic compositions of pooled magmas is discussed by *Ito and Mahoney* (*2005*).

For Hawaii, the **Koolau** component defined by Makapuu-stage Koolau lavas has been proposed to be an eclogitic component formed from recycled oceanic crust including sediments (see *Hauri, 1996; Huang and Frey, 2005* for a detailed discussion). Consequently, the **Koolau** component has a lower solidus temperature than mantle peridotites. I infer that the **Kea** and **Loihi** components are peridotites. The **Loihi** component may have higher H_2O content than the **Kea** component based on the volatile contents of Mauna Kea glasses (*Seaman et al., 2004*). Specifically, a subset of submarine Mauna Kea glasses have Pb and He isotopic signatures similar to Loihi lavas. They also have higher water content and H_2O/K_2O than typical Mauna Kea glasses. This difference is inferred to be a source signature. Consequently, I speculate that the **Loihi** component may have a higher water content than the **Kea** component; therefore the **Loihi** component has a lower solidus temperature than the **Kea** component.

We propose that the Hawaiian plume contains three geochemically distinct source components: **Koolau, Kea and Loihi**. During upwelling of the Hawaiian plume, the **Koolau** component, having the lowest solidus, begins to melt at the greatest depth. Consequently, initial partial melts from the geochemically heterogeneous source have the isotopic characteristics of the **Koolau** component. Then, with further upwelling to a shallower depth, the **Loihi** component begins to melt. Consequently, partial melts from this geochemically heterogeneous source reflect two lithologies, the **Koolau** and **Loihi** components; i.e., the isotopic ratios of partial melts trend from the **Koolau** component to the **Loihi** component. Finally, with further upwelling, the **Kea** component begins to melt.

The isotopic ratios of these low-pressure partial melts trend toward the **Kea** component isotopic composition. Consequently, partial melts from different depths of a geochemically heterogeneous mantle may form trends rather than triangles in isotopic ratio plots.

A further complication that may be important is that during progressive melting of a given lithology, the solidus temperature increases (e.g., *Phipps Morgan, 2001*). Therefore, it is possible that at the depth where the **Kea** component begins to melt, the **Koolau** component becomes too refractory to melt. The consequence is that partial melts from this geochemically heterogeneous mantle generated at high pressure sample only the **Koolau** and **Loihi** components, whereas those generated at shallower depths sample only the **Loihi** and **Kea** components. The net result is that partial melts of a three-component mantle may form a trend in isotopic ratio space.

4.3 Source Components Contributing to Kahoolawe Lavas

Leeman et al. (*1994*) found that some abundance ratios involving only highly incompatible elements are highly variable in Kahoolawe lavas, e.g., Nb/Th=9-24 and Th/Ta=0.5-1.2. Using Th/Ta vs isotopic ratios of Sr, Nd and Pb, they argued for three source components contributing to Kahoolawe lavas. However, our new data for Kahoolawe lavas do not show such variability; in fact, Th/Ta in Hawaiian and Emperor Seamount shield lavas (over 300 samples) ranges only from 0.7 to 1.1, much less than the Th/Ta range for 11 Kahoolawe tholeiitic lavas analyzed by *Leeman et al.* (*1994*) (Fig. 13). Therefore, I conclude that the three source components proposed by *Leeman et al.* (*1994*) for Kahoolawe lavas are not plausible. In particular, I note that their component with anomalously low Th/Ta of 0.5 is defined by two MgO-rich, picritic lavas (Fig. 13);

their low Th abundances, ~0.3 ppm, determined by instrumental neutron activation analysis may not be accurate.

In addition to the commonly proposed **Koolau**, **Kea** and **Loihi** components for Hawaiian lavas, *Mukhopadhyay et al.* (*2003*) showed that isotopic data for Kauai shield lavas and perhaps all Hawaiian shield lavas require a fourth component (**DM**), namely the depleted component that controls the isotopic characteristics of rejuvenated-stage lavas. In addition, *Mukhopadhyay et al.* (*2003*) assumed that these four components have the same Sr/Nd, Sr/Pb and He/Pb. The validity of assuming similar trace element abundance ratios for these source components with such diverse origins can be questioned, especially the He/Pb. Nevertheless, the limited variations of Sr/Nd and Sr/Pb in Hawaiian shield lavas shown in Fig. 8 are consistent with this assumption. In detail, the calculation of component proportions in Fig. 14 of *Mukhopadhyay et al.* (*2003*) also assumed uniform Sr, Nd, Pb and He abundances in these four source components. This assumption, however, is not needed to assess the suitability of the four chosen source components to explain the observed isotopic variations. Since Kahoolawe lavas were not considered by *Mukhopadhyay et al.* (*2003*), I ask whether their model can explain the isotopic variations in Kahoolawe lavas. The four source components are close to a line in a $^{87}Sr/^{86}Sr$ vs $^{143}Nd/^{144}Nd$ plot (see the inset in Fig. 5). Since most Hawaiian shield lavas, except for Kahoolawe lavas, form a near-linear trend in a $^{87}Sr/^{86}Sr$-$^{143}Nd/^{144}Nd$ plot, these source components are consistent with most data (Fig. 5). Kahoolawe lavas, however, cannot be modeled as mixtures of these four source components. Although the $^{87}Sr/^{86}Sr$ vs $^{143}Nd/^{144}Nd$ trend of Kahoolawe lavas can be reproduced by a curved mixing line between the **Koolau** and **Kea** components, the curvature requires that Sr/Nd of the

Koolau component is ~8 times that of the **Kea** component (inset in Fig. 5); this inference is inconsistent with the similar Sr/Nd in Hawaiian shield lavas (Fig. 8a). Therefore, the range in $^{87}Sr/^{86}Sr$ at a given $^{143}Nd/^{144}Nd$ in Hawaiian shield lavas, especially Kahoolawe vs Makapuu-stage Koolau lavas (Fig. 5), can be explained either by introducing an additional source component in the Hawaiian plume, or as I argue later, $^{87}Sr/^{86}Sr$ heterogeneity in the **Koolau** component.

Additional evidence for this complexity arises from correlations between highly incompatible element abundance ratios and isotopic ratios. Comparisons of Hawaiian shields show that some abundance ratios involving only highly incompatible elements, such as La/Nb, are correlated with isotopic ratios (*Roden et al., 1994; Huang and Frey, 2003; 2005;* Fig. 14). The $^{87}Sr/^{86}Sr$ of Kahoolawe lavas is not highly correlated with La/Nb; ~50% of these lavas deviate from the intershield trend to high $^{87}Sr/^{86}Sr$ (Fig. 14a). As with $^{87}Sr/^{86}Sr$ vs $^{143}Nd/^{144}Nd$ (Fig. 5), a curved mixing line can be postulated, but a Sr/Nb range of 10 is required to encompass Kahoolawe lavas with high $^{87}Sr/^{86}Sr$ and relatively low La/Nb (Fig. 14a). However, the range of Sr/Nb in all Hawaiian shield lavas (with MgO>7%) is less than 4 (Fig. 4b).

In summary, in most plots involving isotopic ratios and isotopic ratios versus a highly incompatible element abundance ratio, Kahoolawe lavas fall on the trends defined by other Hawaiian shield lavas (Figs. 6, 7, 9, 10b, 14c, 14d). However, in plots involving $^{87}Sr/^{86}Sr$, Kahoolawe lavas are offset from the trends of other Hawaiian shield lavas toward higher $^{87}Sr/^{86}Sr$ (Figs. 5, 10a, 14a). This offset requires a component that only affects $^{87}Sr/^{86}Sr$.

4.4 Nature of the $^{87}Sr/^{86}Sr$ Heterogeneity in the Koolau Component

In the previous section, I showed that Kahoolawe lavas are offset from other Hawaiian shield lavas only in plots involving $^{87}Sr/^{86}Sr$. This offset may be explained by introducing an additional source component in the Hawaiian plume. I infer that this source component is characterized by very high Sr/X (where X designates incompatible elements such as Nb, REE, Hf, Pb); this component is a spike source of Sr. Is it necessary to introduce an additional mantle reservoir to explain this source component and, if so, what is its nature? Previous studies of Hawaiian shield lavas have inferred ancient recycled oceanic lithosphere, including carbonate-rich or hydrothermal sediment, basaltic crust, gabbroic crust and lithospheric mantle, as components in the Hawaiian plume (*Hauri, 1996; Lassiter and Hauri, 1998; Blichert-Toft et al., 1999; Jackson et al., 1999; Sobolev et al., 2000; Frey et al., 2005; Huang and Frey, 2005*).

Because of the distinctive geochemical characteristics in Makapuu-stage lavas, such as high Sr/Nb and La/Nb, *Huang and Frey* (*2005*) argued that their source contained a recycled carbonate-rich or hydrothermal sedimentary component. Strontium is compatible in calcium carbonate and sulphate phases, which are abundant in carbonate-rich and hydrothermal sediments, respectively. Consequently, they are characterized by high Sr/X (e.g., *Plank and Langmuir, 1998; Chavagnac et al., 2005*). In order to explain the rare Sr-enriched melt inclusions in Mauna Loa olivine phenocrysts, *Sobolev et al.* (*2000*) proposed that recycled plagioclase-rich gabbroic crust is present in the Hawaiian plume. Sr is highly compatible in plagioclase (e.g., *Blundy and Wood, 1991*); consequently, recycled gabbro with cumulate plagioclase is characterized by extremely high Sr/X (e.g., *Zimmer et al., 1995*).

Since recycled carbonate-rich and hydrothermal sediments and plagioclase-rich gabbros have high Sr/X, they can act as a spike source of Sr. However, recycled carbonate-rich and hydrothermal sediments and plagioclase-rich gabbros have very different $^{87}Sr/^{86}Sr$. Since $^{87}Sr/^{86}Sr$ in ancient (2Ga) seawater was ~0.705 (Fig. 3 of *Ray et al., 2002*), ancient carbonate-rich and hydrothermal sediments, which inherited $^{87}Sr/^{86}Sr$ from seawater, are characterized by initially high $^{87}Sr/^{86}Sr$ that was further increased by ingrowth during aging. In contrast, recycled plagioclase-rich gabbro has the very low $^{87}Sr/^{86}Sr$ of ancient oceanic crust and because of its very low Rb/Sr, there is insignificant ingrowth during aging (e.g., *Zimmer et al., 1995*).

In Fig. 15, I plot $^{87}Sr/^{86}Sr$ vs Ce/Sr for Hawaiian shield lavas with MgO>7% and $K_2O/P_2O_5>1$; Hawaiian lavas with MgO>7% typically have not fractionated plagioclase (e.g., *Huang and Frey, 2003*). Since only tholeiitic lavas are plotted, it is reasonable to assume that Ce/Sr in these lavas was not fractionated by the partial melting process. The Hawaiian shields, the Makapuu-stage of Koolau, Mauna Loa and Mauna Kea, define a negative trend on this plot, and most Kahoolawe lavas are offset from this trend toward higher Ce/Sr. In detail, Kahoolawe lavas have $^{87}Sr/^{86}Sr$ similar to Makapuu-stage Koolau lavas, but most Kahoolawe lavas have higher Ce/Sr. A possible, but speculative interpretation is that Hawaiian shield lavas generally sampled an ancient plagioclase-rich gabbroic component, whereas Kahoolawe lavas sampled comparatively less of this component (Figs. 5, 10c, 14b and 15); i.e., Kahoolawe lavas do not contain an additional component, but rather they contain less of a low Ce/Sr and low $^{87}Sr/^{86}Sr$ component.

We present a simple calculation to test this idea. Following the approach used by many researchers (e.g., *Hauri, 1996; Mukhopadhyay et al., 2003*), I assume that sources

of Hawaiian shield lavas are mixtures of several end-member source components, and that partial melting does not significantly change incompatible element abundance ratios (Sr/Nd, Hf/Pb, Sr/Nb ...). In Figs. 5, 10c, 14b and 15, the green line shows mixtures between average Mauna Loa source composition and Makapuu-stage Koolau source composition. If 1% recycled gabbro (Table 3) is subtracted from mixtures of average Mauna Loa source composition and Makapuu-stage Koolau source composition, this trend (the solid red line in Figs. 5, 10c, 14b and 15) passes through the field of Kahoolawe lavas. That is, compared with Kahoolawe lavas, Mauna Loa and Makapuu-stage Koolau lavas sampled more of a recycled gabbroic component.

We emphasize that source components are not equivalent to mantle reservoirs. For example, I propose that the **Koolau** component is eclogite formed from a mixture of recycled oceanic basaltic crust with associated sediment and plagioclase-rich gabbroic lower crust (see also *Hauri, 1996; Huang and Frey, 2005*). However, Loa trend volcanoes sample a **Koolau** component containing variable proportions of sediment, basalt and gabbro. For example, the **Koolau** component in Kahoolawe lavas contains lesser amounts of gabbroic crust. Kahoolawe lavas also lack the trace element signatures of recycled sediment, i.e., the high Sr/Nb and La/Nb that is characteristic of Makapuu-stage Koolau lavas (Fig. 4). The negative trend formed by lavas from Koolau, Mauna Loa and Mauna Kea in a plot of $^{87}Sr/^{86}Sr$ vs Ce/Sr (Fig. 15) reflects sampling various amounts of the **Koolau** component with constant proportions of recycled oceanic basaltic crust, sediment and plagioclase-rich gabbroic lower crust. Although these three lithologies have very different $^{87}Sr/^{86}Sr$ and Ce/Sr, their mixture (the **Koolau** component) is characterized

by relatively high $^{87}Sr/^{86}Sr$ and low Ce/Sr. Most Kahoolawe lavas deviate from this trend (Fig. 15) because they have a lower proportion of low $^{87}Sr/^{86}Sr$ gabbroic crust.

A direct consequence of our hypothesis is that a recycled gabbroic component is generally present in Hawaiian shield lavas. Is there any evidence supporting this argument? The most direct evidence is the Sr-enriched melt inclusions in Mauna Loa olivine phenocrysts (*Sobolev et al., 2000*). In addition, both Mauna Loa and Koolau (Makapuu-stage and Kalihi-stage) lavas show a positive Sr anomaly in a primitive mantle normalized multiple element diagram (Fig. 2 of *Huang and Frey, 2005*; Fig. 3). Since only high-MgO lavas are plotted (MgO>7 for Fig. 3 and MgO>6.5 for Fig. 2 of *Huang and Frey, 2005*), the Sr-enrichment in these lavas should be a source characteristic, a result consistent with a recycled plagioclase-rich gabbroic component in the sources of these lavas. In detail, *Huang and Frey* (*2005*) argue that high Sr/Nb in Makapuu-stage Koolau lavas reflects a recycled carbonate-rich or hydrothermal sedimentary component. That is, the Sr-enrichment in Hawaiian shield lavas may have two origins: recycled carbonate-rich or hydrothermal sediment and recycled plagioclase-rich gabbro. In detail, some atypical Kahoolawe lavas, such as KW-5 (Figs. 5, 7), are also characterized by Sr-enrichment (Fig. 3), and KW-5 is within the Mauna Loa field in Fig. 15. Like other Hawaiian shield lavas, KW-5 may also sample a recycled plagioclase-rich gabbroic component. The relatively high SiO_2 content in several Loa-trend shields, including Mauna Loa and Makapuu-stage Koolau lavas (e.g., Fig. 2 of *Hauri, 1996*), is inferred to be a result of sampling a dacitic magma generated from partial melting of an eclogite component that formed from recycled oceanic crust (*Hauri, 1996; Huang and Frey,*

2005). This inference is also consistent with a recycled plagioclase-rich gabbroic lower crust component in the Hawaiian plume.

5. Summary:

1) Like Makapuu-stage Koolau lavas, Kahoolawe shield lavas range widely in radiogenic isotope ratios, and among Hawaiian shield lavas they extend to high $^{87}Sr/^{86}Sr$ with low $^{143}Nd/^{144}Nd$, $^{176}Hf/^{177}Hf$ and $^{206}Pb/^{204}Pb$. However, the enriched component in the source of Kahoolawe lavas differs from that sampled by Makapuu-stage Koolau lavas (*Huang and Frey, 2005*). Specifically, Kahoolawe lavas are offset to high $^{87}Sr/^{86}Sr$ from the trends of Hawaiian shield lavas. I interpret this offset as a result of varying proportions of a recycled plagioclase-rich gabbroic lower crust in the Hawaiian plume; that is, Kahoolawe lavas sampled a lower proportion of this low $^{87}Sr/^{86}Sr$ component. I conclude that the enriched component in the Hawaiian plume is derived from ancient recycled oceanic crust, but that Koolau (Makapuu-stage) and Kahoolawe lavas sampled different proportions of recycled sediment, basalt and gabbro.
2) Shield lavas from Loa and Kea trend volcanoes define intersecting linear trends in plots of $^{208}Pb^*/^{206}Pb^*$ vs $^{87}Sr/^{86}Sr$, $^{143}Nd/^{144}Nd$ and $^{176}Hf/^{177}Hf$; they converge at the field defined by Loihi lavas, implying that all Hawaiian shield lavas sample the **Loihi** component. The trend of Loa lavas to high $^{208}Pb^*/^{206}Pb^*$ and $^{87}Sr/^{86}Sr$ and low $^{143}Nd/^{144}Nd$ and $^{176}Hf/^{177}Hf$ is consistent with variable amounts of a recycled sedimentary component that is not present in Kea-trend lavas.
3) Hawaiian shield lavas range widely in radiogenic isotopic ratios of Sr, Nd, Hf and Pb, but they have similar abundance ratios, within a factor of three, of Sr/Nd,

Sr/Pb and Hf/Pb. A consequence is that the hyperbolic trend of $^{206}Pb/^{204}Pb$ versus $^{176}Hf/^{177}Hf$ defined by Hawaiian shield lavas requires three component mixing rather than mixing of two components with very different Hf/Pb. It is, however, surprising that isotopically distinct mantle reservoirs, presumably created by very different processes, have similar Sr/Nd, Sr/Pb and Hf/Pb. I postulate that source components inferred from trends defined by isotopic ratios, e.g., $^{87}Sr/^{86}Sr$ vs. $^{143}Nd/^{144}Nd$, are mixtures of reservoirs with very different Sr/Nd, Sr/Pb and Hf/Pb ratios, but that limited ranges of mixing proportions yield mixtures with similar ratios.

4) Despite evidence for more than two isotopically distinct source components contributing to Hawaiian shield lavas, these lavas commonly define trends in two dimensional isotopic ratio plots (e.g., Figs. 9, 10, 12). This observation can be explained if the isotopically different source components have significantly different solidus temperatures.

Figure Captions:

Fig. 1 Map of Kahoolawe Island showing sample locations. Location for samples KW-5, KW-6 and KW-7 from Leeman et al. (1994) is also shown. The inset shows Loa and Kea volcano trends; Kahoolawe Volcano is a Loa-trend volcano.

Fig. 2 MgO vs SiO_2 and CaO (all in %) for Kahoolawe shield and caldera-filling lavas. Since SiO_2 and CaO are sensitive to post-magmatic alteration, only relatively unaltered lavas with $K_2O/P_2O_5>1$ are plotted. Kahoolawe lavas scatter widely; most are not in the field for Makapuu-stage Koolau lavas (~40 samples) . Data sources: Kahoolawe: Fodor et al., 1992, Leeman et al., 1994, this study; Mauna Kea: Rhodes, 1996, Rhodes and Vollinger, 2004; Mauna Loa: Garcia et al., 1995a, Rhodes, 1995, 1996, Rhodes and Hart, 1995, Rhodes and Vollinger, 2004; Koolau (Makapuu-stage): Frey et al., 1994.

Fig. 3 Primitive mantle value normalized incompatible element abundances in Kahoolawe lavas. Fields for Mauna Loa and Makapuu-stage Koolau lavas are shown for comparison. Only lavas with 7%<MgO<10% and $K_2O/P_2O_5>1$ are shown. Only Sample KW-5 from Leeman et al. (1994) satisfies these criteria; it is important because among Kahoolawe lavas it has the largest relative Sr enrichment. Our samples crushed in a WC shatter box were contaminated with Ta (see Table 1 footnote); consequently, Ta abundances are not shown for these samples. Data sources: Mauna Loa: Rhodes, 1995, 1996, Cohen et al., 1996, Rhodes and Hart, 1995, Rhodes and Vollinger, 2004, our unpublished instrumental neutron activation analysis data for the Mauna Loa section of

the Hawaii Scientific Drilling Project Phase 2 drill core. Primitive mantle values are from Hofmann, 1988; Makapuu-stage of Koolau: Frey et al., 1994; Huang and Frey, 2005.

Fig. 4 MgO vs La/Nb and Sr/Nb for Kahoolawe shield and caldera-filling lavas. Fields for Loa-trend shields (Makapuu-stage of Koolau and Mauna Loa) and a Kea-trend shield (Mauna Kea) are shown for comparison. These ratios are not correlated with MgO content. The important result is that most Kahoolawe lavas lack the high La/Nb and Sr/Nb that distinguishes Makapuu-stage Koolau lavas. Data sources: Kahoolawe: Fodor et al., 1992, Leeman et al., 1994, this study; Makapuu-stage Koolau and Mauna Loa: see Figs. 2 and 3 captions; Mauna Kea: Rhodes, 1996, Yang et al., 1996, Huang and Frey, 2003, Rhodes and Vollinger, 2004.

Fig. 5 $^{87}Sr/^{86}Sr$ vs $^{143}Nd/^{144}Nd$ for Kahoolawe shield lavas. Shield lavas KW-5, KW-7 and KW-19 define the extremes for Kahoolawe lavas. Fields for other Hawaiian shields, rejuvenated stage lavas and MORB are shown for comparison. Most notable is the large range for Kahoolawe, and Makapuu-stage Koolau lavas, and the offset of Kahoolawe lavas to high $^{87}Sr/^{86}Sr$ at a given $^{143}Nd/^{144}Nd$. The inset shows the fields for Hawaiian shields, rejuvenated stage lavas and MORB, along with the four "source components" (red dots) of Mukhopadhyay et al. (2003). Note that these four "source components" define a near-linear trend; Kahoolawe lavas are offset from this trend. The blue line is a mixing line between source components "**Kea**" and "**Koolau**", and Sr/Nd of these two components are the average values of Mauna Kea and the Makapuu-stage Koolau lavas, 15 and 21, respectively. Note that I assume that partial melting does not significantly

change Sr/Nd; consequently, Sr/Nd in the lavas reflect their source values. The red dashed line is also a mixing line between source components "**Kea**" and "**Koolau**", using Sr/Nd of 15 and 126 for these two components, respectively. This large difference in Sr/Nd is required for the mixing line to include Kahoolawe lavas. In the large figure, two model mixing lines are also shown: the green line represents mixing between average Mauna Loa source composition and average Makapuu-stage Koolau source composition. The red line which passes through the Kahoolawe data reflects 1% subtraction of recycled gabbro from the mixtures of average Mauna Loa source and average Makapuu-stage Koolau source. Increments on the mixing lines are 20%. Modeling details are given in Table 3. Data sources: Kahoolawe lavas: West et al., 1987, this study; Koolau (Makapuu): Roden et al., 1984, 1994; Mauna Kea: Lassiter et al., 1996, Bryce et al., submitted; Mauna Loa: Cohen et al., 1996, Kurz et al., 1995; Kauai: Mukhopadhyay et al., 2003; Loihi: Garcia et al., 1993, 1995b, 1998; rejuvenated stage lavas: Stille et al., 1983, Roden et al., 1984, Chen and Frey, 1985, Tatsumoto et al., 1987, West et al., 1987, Frey et al., 2000 and Lassiter et al., 2000; EPR MORB: Niu et al., 1999, Regelous et al., 1999, Castillo et al., 2000).

Fig. 6 Nd-Hf isotopic correlation. $\varepsilon_{Hf} = (((^{176}Hf/^{177}Hf)_{sample}/(^{176}Hf/^{177}Hf)_{CHUR}-1)x10000$ and $\varepsilon_{Nd} = (((^{143}Nd/^{144}Nd)_{sample}/(^{143}Nd/^{144}Nd)_{CHUR}-1)x10000$ with $(^{176}Hf/^{177}Hf)_{CHUR}=0.282772$ and $(^{143}Nd/^{144}Nd)_{CHUR}=0.512638$. Data sources: Blichert-Toft et al., 1999 for the Hawaiian shield field, Kahoolawe data points (triangles), Mauna Loa and Koolau (Makapuu-stage) fields; Salters et al., in prep. for Koolau (KSDP); this

study for additional Kahoolawe data (diamonds). The OIB array is shown for comparison (Vervoort et al., 1999).

Fig. 7 Pb-Pb isotopic ratios for Kahoolawe shield lavas. Five Kahoolawe lavas previously analyzed by West et al. (1987) were re-analyzed by Abouchami et al. (2005) and are connected by brown lines. Generally, lavas from Loa trend volcanoes have higher $^{208}Pb/^{204}Pb$ at a given $^{206}Pb/^{204}Pb$ than lavas from Kea trend volcanoes, and the thick pink line in **Panel b** marks the boundary between Loa and Kea lavas (see Abouchami et al., 2005 for a detailed discussion). Data sources: Kahoolawe lavas: West et al., 1987, Abouchami et al., 2004, this study; Koolau (Makapuu): Roden et al., 1994, Abouchami et al., 2004; Koolau (Koolau Scientific Drilling Project (KSDP)): Fekiacova et al., in prep.; Mauna Kea: Abouchami et al., 2000, Blichert-Toft et al., 2003, Eisler et al., 2003; Mauna Loa: Cohen et al., 1996, Kurz et al., 1995, Abouchami et al., 2000; Kauai: Mukhopadhyay et al., 2003; Loihi: Garcia et al., 1993, 1995b, 1998.

Fig. 8 MgO (%) vs Sr/Nd, Nd/Hf, Hf/Pb and Sr/Pb for Hawaiian shield lavas that define the isotopic endmembers for Hawaiian shields (i.e., Mauna Kea, Loihi and the Makapuu-stage of Koolau). It is surprising that these abundance ratios vary by less than a factor of 3 (at MgO>7%). Even the alkalic, rejuvenated stage lavas of the Honolulu Volcanics derived by low extents of partial melting (e.g., Yang et al., 2003) have Sr/Nd and Sr/Pb overlapping the shield fields. In contrast, Nd/Hf and Hf/Pb for the Honolulu lavas do not overlap the shield fields because Hf was controlled by residual oxides (Clague and Frey, 1982; Yang et al., 2003). Data sources: See Fig. 2-4 captions, plus Loihi data from Frey

and Clague, 1983, Garcia et al., 1993, 1995b, 1998, Norman and Garcia, 1999; and Honolulu Volcanics data from Clague and Frey, 1982, Yang et al., 2003.

Fig. 9 $^{206}Pb/^{204}Pb$-ε_{Hf}. The isotopic ratios of the two source components, "**Kea**" and "**Koolau**", are from Blichert-Toft et al. (1999) who inferred that the highly curved trend of Hawaiian shield lavas represents a mixing line between two components with very different Hf/Pb (a ratio of 40 shown by the dashed purple line). The Hawaiian trend can be fitted using $(Hf/Pb)_{Kea/Koolau}$=15. For simplicity, I assume that these two components have the same Pb abundance, and I let Hf/Pb = x in the "**Koolau**" component. The red line with ticks shows the mixing line between these two components with $(Hf/Pb)_{Kea/Koolau}$=15. The proportions of the "**Kea**" component and Hf/Pb in the mixtures are labeled. This two-source component model implies that Hf/Pb in Mauna Kea lavas (8.0x) is ~5 times that in Makapuu-stage Koolau lavas (1.6x). The blue line in the inset shows the mixing line between average Mauna Kea source composition (Hf/Pb=4.0) and Makapuu-stage Koolau source composition (Hf/Pb=3.0). Clearly, this mixing line cannot explain the highly curved Hawaiian trend. Data sources: Blichert-Toft et al., 1999, Frey et al., 2005, Salters et al., in prep., this study.

Fig. 10 $^{206}Pb/^{204}Pb$ vs $^{87}Sr/^{86}Sr$ and $^{143}Nd/^{144}Nd$ for Hawaiian shield lavas. As in **Fig. 9**, Hawaiian shield lavas define curved trends in plots of $^{206}Pb/^{204}Pb$ vs $^{87}Sr/^{86}Sr$ and $^{143}Nd/^{144}Nd$. The blue solid lines in **panels a** and **b** show the mixing lines between average Mauna Kea source composition and Makapuu-stage Koolau source composition, with $(Sr/Pb)_{Koolau/Kea}$ = 1.1 and $(Nd/Pb)_{Koolau/Kea}$ = 0.82. The pink dashed lines in **panels a**

and **b** show mixing lines between two source components with the same isotopic ratios as those of average Mauna Kea and Makapuu-stage Koolau lavas, and $(Sr/Pb)_{Koolau/Kea}$ = 0.22 and $(Nd/Pb)_{Koolau/Kea}$ = 0.16, which are 5 times lower than those of average Mauna Kea and Makapuu-stage Koolau lavas. The curved trends of Hawaiian shield lavas, excluding the Kahoolawe lavas in the plot of $^{206}Pb/^{204}Pb$ vs $^{87}Sr/^{86}Sr$, can be explained by such mixing lines, but they are not consistent with the observed similarity of Sr/Pb and Nd/Pb in Hawaiian shield lavas. In **panel c** (same axes as **panel a**), two model mixing lines are shown: the green line represents mixing between average Mauna Loa source composition and average Makapuu-stage Koolau source composition. The red line represents subtraction of 1% recycled gabbro (see text) from the mixtures of average Mauna Loa source and average Makapuu-stage Koolau source composition (the green line). The offset of Kahoolawe lavas can be explained by the red line. Increments on the mixing lines are 20%. Modeling details are in Table 3. Data sources are in Fig. 5 and 7 captions.

Fig. 11 Pb vs Hf abundances (in ppm) for Mauna Kea (HSDP2) lavas. Samples with >20% MgO are not plotted because their low Pb contents are especially sensitive to contamination during sample preparation (e.g., Eisele et al., 2003; Huang and Frey, 2003). The regression line intercepts the Hf axis, implying that Pb is more incompatible than Hf during partial melting generating Mauna Kea lavas.

Fig. 12 $^{208}Pb^*/^{206}Pb^*$ vs $^{176}Hf/^{177}Hf$, $^{87}Sr/^{86}Sr$ and $^{143}Nd/^{144}Nd$ for Hawaiian shield lavas. $^{208}Pb^*/^{206}Pb^*$ represents the time-integrated $^{232}Th/^{238}U$ since the Earth's formation and is

defined as $[(^{208}Pb/^{204}Pb)_{sample}-29.475]/[(^{206}Pb/^{204}Pb)_{sample}-9.307]$ (Galer and O'Nions, 1985). Lavas from Loa and Kea trend volcanoes define different trends in these plots. Lavas from the Kea trend have relatively constant $^{176}Hf/^{177}Hf$, $^{87}Sr/^{86}Sr$ and $^{143}Nd/^{144}Nd$, and, consequently, they define near-horizontal trends. In contrast, lavas from the Loa trend define a steep trend. Loihi lavas, highlighted by blue fields, are at the intersection of Loa and Kea trend lavas, and define the **Loihi** component. The **Koolau** and **Kea** components (open circles) are also labeled in the figure. Data sources are in Fig. 5 and 7 captions.

Fig. 13 MgO (%) vs Th/Ta for Kahoolawe shield lavas. The field is for lavas from several Hawaiian shields and Detroit Seamount which were analyzed in our lab by ICP-MS. The Th/Ta range in 11 Kahoolawe tholeiitic lavas analyzed by Leeman et al. (1994) exceeds that of over 300 samples that define the field. For unknown reasons, sample KOO-30 from Koolau has anomalously high Th/Ta (Huang and Frey, 2005). Because of the possible fractionation by Fe-Ti oxides, highly fractionated lavas, e.g., hawaiite, are excluded from this plot. Data sources: Leeman et al., 1994, this study; Yang et al., 1996, Huang and Frey, 2003, 2005; Huang et al., 2005; Xu et al., 2005.

Fig. 14 La/Nb vs $^{87}Sr/^{86}Sr$, $^{143}Nd/^{144}Nd$ and $^{208}Pb^*/^{206}Pb^*$ for Hawaiian shield lavas. Generally, Hawaiian shields form linear trends in these plots, with the extreme defined by Makapuu-stage Koolau lavas (see Huang and Frey, 2005 for a detailed discussion). Kahoolawe lavas are offset from the shield trend to higher $^{87}Sr/^{86}Sr$ in **panel a**. The blue solid line in **panel a** represents mixing between average Mauna Kea source composition

and Makapuu-stage Koolau source composition with $(Sr/Nb)_{Koolau/Kea}$ = 2.3. The pink dashed line is a mixing line between two source components which have La/Nb and $^{87}Sr/^{86}Sr$ equal to average Mauna Kea and Makapuu-stage Koolau lavas, but have $(Sr/Nb)_{Koolau/Kea}$ = 10. In **panel b**, two model mixing lines are shown: the green line is a mixing line between average Mauna Loa source composition and average Makapuu-stage Koolau source composition. The red line represents subtraction of 1% recycled gabbro from the mixtures of average Mauna Loa source composition and average Makapuu-stage Koolau source composition (the green line). The offset of Kahoolawe lavas can be explained by the red line. Increments on the mixing lines are 20%. Modeling details are given in Table 3. Data sources are in Fig. 4, 5 and 7 captions. La/Nb from Garcia et al. (1993, 1995b) are adjusted using reported BHVO data in Garcia et al. (1993) and Huang and Frey (2005).

Fig. 15 Ce/Sr vs $^{87}Sr/^{86}Sr$. I plot Ce/Sr instead of Nd/Sr because Nd data are less abundant in Leeman et al. (1994). To minimize the effects of plagioclase fractionation and alteration on Ce/Sr, only lavas with MgO>7% and K_2O/P_2O_5>1 are plotted. Two model mixing lines are shown: the green line represents mixing between average Mauna Loa source composition and average Makapuu-stage Koolau source composition. The red line, which passes through most Kahoolawe data, reflects 1% subtraction of recycled gabbro from the mixtures of average Mauna Loa source composition and average Makapuu-stage Koolau source composition (the green line). Note that KW-5, with the lowest $^{87}Sr/^{86}Sr$ among analyzed Kahoolawe lavas (Fig. 5), is within the Mauna Loa field; KW-7, which has the second-lowest $^{87}Sr/^{86}Sr$, has MgO<7% and is not plotted in

this diagram. Increments on the mixing lines are 20%. Except for average Makapuu-stage Koolau lavas, modeling details are given in Table 3. In this figure, the average of Makapuu-stage Koolau source composition ($^{87}Sr/^{86}Sr$=0.704120, [Sr]=36 ppm and [Ce]=2.3 ppm) is calculated for lavas with MgO>7% and K_2O/P_2O_5>1. The primitive mantle value of Ce/Sr is shown for comparison (Hofmann, 1988). Data sources: Hawaiian shields (see Fig. 4, 5 and 7 captions); gabbro (Table 3); carbonate-rich and hydrothermal sediments: Ce/Sr from Plank and Langmuir, 1998 and Chavagnac et al. 2005, respectively, and $^{87}Sr/^{86}Sr$ is assumed to be 0.705 (see text for details).

Reference:

Abouchami, A., Hofmann, A. W., Galer, S. J. G., Frey, F. A., Eisele, J. and Feigenson, M., Lead isotopes reveal bilateral asymmetry and vertical continuity in the Hawaiian mantle plume, Nature, in press.

Basu, A. R. and Faggart, B. E., Temporal isotopic variations in the Hawaiian Mantle Plume: The Lanai anomaly, the Molokai fracture zone and a seawater-altered lithospheric component in Hawaiian volcanism, in: A. Basu, S. Hart (Eds.), Earth Processes: Reading the Isotopic Code, *AGU Geophys. Monogr. 95 149–159*, 1996.

Blichert-Toft, J., Chauvel, C., Albarede, F., Separation of Hf and Lu for high-precision isotope analysis of rock samples by magnetic sector-multiple collector ICP-MS, *Contrib. Mineral. Petrol, 127 (3), 248-260,* 1997.

Blichert-Toft, J., Frey, F. A., and Albarede, F., Hf isotope evidence for pelagic sediments in the source of Hawaiian basalts, *Science, 285 (5429), 879-882,* 1999.

Blichert-Toft, J., Weis, D., Maerschalk, C., Agranier, A., and Albarède, F., Hawaiian hot spot dynamics as inferred from the Hf and Pb isotope evolution of Mauna Kea volcano, *Geochem. Geophys. Geosyst., 4(2), 8704, doi:10.1029/2002GC000340,* 2003.

Blundy, J. D., Wood, B. J., Crystal-chemical controls on the partitioning of Sr and Ba between plagioclase feldspar, silicate melts, and hydrothermal solutions, *Geochim. Cosmochim. Acta., 55 (1), 193-209,* 1991.

Carmichael, I. S. E., Turner, F. J. and Verhoogen, F., Igneous Petrology, McGraw-Hill, New York, 1974.

Castillo, P. R., Klein, E., Bender, J., Langmuir, C., Shirey, S., Batiza, R., and White, W., 2000. Petrology and Sr, Nd, and Pb isotope geochemistry of mid-ocean ridge basalt glasses from the 11°45′N to 15°00′N segment of the East Pacific Rise, *Geochem. Geophys. Geosyst., 1, doi:10.1029/1999GC000024,* 2000.

Chen, C.-Y. and Frey, F.A., Trace element and isotope geochemistry of lavas from Haleakala Volcano, East Maui: Implications for the origin of Hawaiian basalts, *J. Geophys. Res., 90, B10, 8743-8768,* 1985.

Chavagnac, V., German, C. R., Milton, J. A. and Palmer, M. R., Sources of REE in sediment cores from the Rainbow vent site (36°14'N, MAR), *Chem. Geol., 216, 329-352,* 2005.

Clague, D. A. and Frey, F.A., Petrology and trace element geochemistry of the Honolulu Volcanics, Oahu: implications for the oceanic mantle below Hawaii, *J. Petrol* , 23, 447-504, 1982.

Cohen, A. S., O'Nions, R. K., and Kurz, M. D., Chemical and isotopic variations in Mauna Loa tholeiites, *Earth Planet. Sci. Lett., 143, 111-124,* 1996.

Douglass, J. and Schilling, J.-G., Systematics of three-component, pseudo-binary mixing lines in 2D isotope ratio space representations and implications for mantle plume-ridge interaction, *Chem. Geol.,163, 1-23,* 2000.

Eiler, J. M., Farley, K. A., Valley, J. W., Hofmann, Albrecht W., Stolper, Edward M., Oxygen isotope constraints on the sources of Hawaiian volcanism, *Earth Planet Sci Letts., 144 (3-4), 453-468,* 1996.

Eiler, J. M., Farley, K. A., Stolper, E. M., Correlated helium and lead isotope variations in Hawaiian lavas, *Geochim. Cosmochim. Acta., 62 (11), 1977-1984,* 1998.

Eisele, J., Abouchami, W., Galer, S.J.G. and Hofmann, A.W., The 320 kyr Pb isotope evolution of Mauna Kea lavas recorded in the HSDP-2 drill core, *Geochem. Geophys. Geosyst.*, *4*(5), *8710, doi:10.1029/2002GC000339,* 2003.

Fodor, R. V., Malta, D. P., Bauer, G. R. and Jacobs, R. S., Microbeam analyses of rare-earth element phosphate in basalt from Kahoolawe Island, Hawaii, in: *Russell P. E. (ed) Proceedings of the 24th Annual Conf. Microbeam Analyt Soc, San Francisco Press, San Francisco, 554-558;* 1989.

Fodor, R. V., Frey, F. A., Bauer, G. R., Clague, D. A., Ages, rare-earth element enrichment, and petrogenesis of tholeiitic and alkalic basalts from Kahoolawe Island, Hawaii, *Contrib. Mineral. Petrol., 110, 442-462,* 1992.

Frey, F. A. and Clague, D. A., Geochemistry of diverse basalt types from Loihi Seamount, Hawaii; petrogenetic implications. *Earth Planet. Sci. Lett., 66, 337-355,* 1983.

Frey, F. A., Wise, W. S., Garcia, M. O., West, H., Kwon, S. T., Kennedy, A., Evolution of Mauna Kea Volcano, Hawaii; petrologic and geochemical constraints on postshield volcanism, *J. Geophys. Res., 95 (2), 1271-1300,* 1990.

Frey, F. A., Garcia, M. O., Wise, W. S., Kennedy, A., Gurriet, P., Albarede, F., The evolution of Mauna Kea volcano, Hawaii: Petrogenesis of tholeiitic and alkalic basalts, *J. Geophys. Res., 96, 14,347-14,375,* 1991.

Frey, F. A., Garcia, M. O., and Roden, M. F., Geochemical characteristics of Koolau Volcano: Implications of intershield geochemical differences among Hawaiian volcanoes. *Geochim. Cosmochim. Acta., 58, 1441-1462,* 1994.

Frey, F.A., Clague, D., Mahoney, J.J., Sinton, J.M., Volcanism at the edge of the Hawaiian plume; petrogenesis of submarine alkalic lavas from the North Arch volcanic field, *Jour. Petrol., 41(5), 667-691,* 2000.

Frey, F.A., Huang, S., Blichert-Toft, J., Regelous, M. and Boyet, M., Origin of depleted components in basalt related to the Hawaiian hot spot: Evidence from isotopic and incompatible element ratios, *Geochem. Geophys., Geosys, doi: 10.1029/2004GC000757,* 2005.

Garcia, M. O., Jorgenson, B. A., Mahoney, J. J., Ito E., and Irving, A. J., An evaluation of temporal geochemical evolution of Loihii summit lavas: Results from Alvin submersible dives. *J. Geophys. Res. 98, 535-550,* 1993.

Garcia, M. O., Foss, D. J. P., West, H. B. and Mahoney, J. J., Geochemical and isotopic evolution of Loihi Volcano, Hawaii, *J. Petrol., 36, 1647-1644,* 1995b.

Garcia, M. O., Hulsebosch, T. P., Rhodes, J. M., Olivine-rich submarine basalts from the southwest rift zone of Mauna Loa Volcano; implications for magmatic processes and geochemical evolution, in *Mauna Loa Revealed, Geophysical Monograph Series, vol. 92, (eds, J.M. Rhodes and J.P. Lockwood) 219-239, AGU, Washington, D.C.,* 1995a.

Garcia, M. O., Rubin, K. H., Norman, M. D., Rhodes, J. M., Graham, D. W., Muenow, D W., Spencer, K., Petrology and geochronology of basalt breccia from the 1996 earthquake swarm of Loihi Seamount, Hawaii; magmatic history of its 1996 eruption, *Bull. Volcan., 59, 577-592,* 1998.

Galer, S. J. G., and O'Nions, R. K., Residence time of thorium, uranium and lead in the mantle with implications for mantle convection, *Nature, 316 (6031), 778-782,* 1985.

Hauri, E. H., Major-element variability in the Hawaiian mantle plume, *Nature 382, 415-419,* 1996.

Hofmann, A. W., Chemical differentiation of the earth: the relationship between mantle, continental crust, and oceanic crust, *Earth Planet. Sci. Lett. 90, 297-314,* 1988.

Hofmann, A. W. and Jochum, K. P., Source characteristics derived from very incompatible trace elements in Mauna Loa and Mauna Kea basalts, Hawaii Scientific Drilling Project, *J. Geophys. Res., 101, 11,831-11,839,* 1996.

Holcomb, R. T., Eruptive history and long-term behavior of Kilauea Volcano, in *Volcanism in Hawaii, (eds, Decker, R. W., Wright, T. L. and Stauffer, P. H.) U. S. Geological Survey Professional Paper, P 1350, p. 261-350,* 1987.

Huang, S. and Frey, F.A., Trace element abundances of Mauna Kea basalt from Phase 2 of the Hawaiian Scientific Drilling Project: Petrogenetic implications of correlations with major element content and isotopic ratios, *Geochem. Geophys., Geosys, 4(6), 8711, doi, 1029/2002 GC000322,* 2003.

Huang, S., Regelous, M., Thordarson, T. and Frey, F. A., Petrogenesis of lavas from Detroit Seamount: Geochemical differences between Emperor Chain and Hawaiian volcanoes, *Geochem. Geophys., Geosys, 6(1), Q01L06, doi, 1029/2004GC000756,* 2005.

Huang, S. and Frey, F. A., Recycled Oceanic Crust in the Hawaiian Plume: Evidence from Temporal Geochemical Variations Within the Koolau Shield. *Contributions to Mineralogy and Petrology*, 2005.

Ito and Mahoney, Flow and melting of a heterogeneous mantle: 1. Method and importance to the geochemistry of ocean island and mid-ocean ridge basalts. *Earth Planet Sci Letts., 230, 29-46,* 2005.

Jackson, M. C., Wilmoth, R. A., and Frey, F. A., Geology and petrology of basaltic lavas and dikes of the Koolau Volcano in the Trans-Koolau exploratory tunnels, Oahu, Hawaii. *Bull. Volcan. 60, 381-401,* 1999.

Kurz, M.D., W.J. Jenkins, S. Hart, and D. Clague, Helium isotopic variations in Loihi Seamount and the island of Hawaii. *Earth Planet. Sci. Lett., 66, 388-406,* 1983.

Kurz, M.D., Kenna, T.C., Kammer, D.P., Rhodes, J.M., and Garcia, M.O., Isotopic evolution of Mauna Loa volcano: a view from the submarine southwest rift Mauna Loa: A Decade Volcano. in Mauna Loa Revealed, *Geophysical Monograph Series*, vol. 92, edited by J.M. Rhodes and J.P. Lockwood, . 289-306, AGU, Washington, D.C., 1995.

Kurz, M. D., J. Curtice, D. E. Lott III, and A. Solow, Rapid helium isotopic variability in Mauna Kea shield lavas from the Hawaiian Scientific Drilling Project, *Geochem. Geophys. Geosyst., 5, Q04G14, doi:10.1029/2002GC000439,* 2004

Lassiter, J.C., DePaolo, D.J., and Tatsumoto, M., Isotopic evolution of Mauna Kea volcano: Results from the initial phase of the Hawaiian Scientific Drilling Project. *J. Geophys. Res. 101, 11,769-11,780,* 1996.

Lassiter, J. C. and Hauri, E. H., Osmium-iosotope variations in Hawaiian lavas: Evidence for recycled oceanic lithosphere in the Hawaiian plume. *Earth Planet Sci Letts., 164, 483-496,* 1998.

Lassiter, J.C., Hauri, E.H., Reiners, P.W., Garcia, M.O., Generation of Hawaiian post-erosional lavas by melting of a mixed lherzolite/pyroxenite source, *Earth Planet Sci Letts., 178(3-4), 269-284,* 2000.

Leeman, W. P., Gerlach, D. C., Garcia, M. O., West, H. B., Geochemical variations in lavas from Kahoolawe volcano, Hawaii: evidence for open system evolution of plume-derived magmas, *Contrib. Mineral. Petrol., 116, 62-77,* 1994.

Macdonald, G. A. and Katsura, T., Chemical composition of Hawaiian lavas, *Journ. Petrol., 5(1), 82-133,* 1964.

Mukhopadhyay, S., Lassiter, J.L., Farley, K.A., and Bogue, S.W., Geochemistry of Kauai shield-stage lavas: Implications for the chemical evolution of the Hawaiian plume. *Geochem. Geophys. Geosyst.*, 4(1), 1009,doi: 10.1029/2002GC 000342, 2003.

Niu, Y., Collerson, K.D., Batiza, R., Wendt, J.I., Regelous, M., Origin of enriched-type mid-ocean ridge basalt at ridges far from mantle plumes; the East Pacific Rise at 11 degrees 20'N, *J. Geophys. Res., 104(4), 7067-7087,* 1999.

Norman, M. D. and Garcia, M. O., Primitive magmas and source characteristics of the Hawaiian Plume; petrology and geochemistry of shield picrites, *Earth Planet. Sci. Lett., 168 (1-2), 27-44,* 1999.

Regelous, M., Niu, Y., Wendt, J.I., Batiza, R., Greig, A., Collerson, K.D., Variations in the geochemistry of magmatism on the East Pacific Rise at 10 degrees 30'N since 800 ka, *Earth Planet. Sci. Lett., 168(1-2), 45-63,* 1999.

Pertermann, M., Hirschmann, M. M., Hametner, K., Gunther, D., Schmidt, M. W., Experimental determination of trace element partitioning between garnet and silica-rich liquid during anhydrous partial melting of MORB-like eclogite, *Geochem. Geophys, Geosyst, 5, Q05A01, doi:10.1029/2003GC000638,* 2004.

Phipps Morgan, J., Thermodynamics of pressure release melting of a veined plum pudding mantle, *Geochem. Geophys. Geosyst., 2 (4), doi:10.1029/2000GC000049,* 2001.

Plank, T., and Langmuir, C. H., The chemical composition of subducting sediment and its consequences for the crust and mantle, *Chem. Geol., 145 (3-4), 325-394,* 1998.

Ray, J. S., Martin, M. W., Veizer, J. and Bowring, S. A., U-Pb zircon dating and Sr isotope systematics of the Vindhyan Supergroup, India, *Geology, 30(2), 131-134,* 2002.

Rhodes, J. M. and Hart, S. R., Episodic trace element and isotopic variation in historical Mauna Loa lavas, in *Mauna Loa Revealed, Geophysical Monograph Series, vol. 92, (eds, J.M. Rhodes and J.P. Lockwood) 263-288, AGU, Washington, D.C.,* 1995.

Rhodes, J. M., Geochemical stratigraphy of lava flows sampled by the Hawaii Scientific Drilling Project, *J. Geophys. Res. 101, 11,729-11,746,* 1996.

Rhodes, J. M., and M. J. Vollinger, Composition of basaltic lavas sampled by phase-2 of the Hawaii Scientific Drilling Project: Geochemical stratigraphy and magma types, *Geochem. Geophys. Geosyst., 5, Q03G13, doi:10.1029/2002GC000434,* 2004.

Roden, M. F., Frey, F. A., Clague, D. A., Geochemistry of tholeiitic and alkalic lavas from the Koolau Range, Oahu, Hawaii; implications for Hawaiian volcanism, *Earth Planet. Sci. Lett., 69(1), 141-158,* 1984.

Roden, M. F., Trull, T., Hart, S. R., and Frey, F. A., New He, Sr, Nd and Pb isotopic constraints on the constitution of the Hawaiian plume: Results from Koolau Volcano, Oahu, Hawaii. *Geochim. Cosmochim. Acta., 58, 1431-1440,* 1994.

Salters, V. J. M. and Longhi, J., Trace element partitioning during the initial stages of melting beneath mid-ocean ridges. *Earth Planet. Sci. Letts., 166, 15-30,* 1999.

Sobolev, A.V., Hofmann, A.W., and Nikogosian, I. K., Recycled oceanic crust observed in ghost plagioclase within the source of Mauna Loa lavas, *Nature 404, 986-990,* 2000.

Stearns, H. T., Geology and Ground-Water Resources of the Islands of Lanai and Kahoolawe, Hawaii. Hawaii (Territory): Division of Hydrography. 177p. 1940.

Stille, P., Unruh, D.M., Tatsumoto, M., Pb, Sr, Nd and Hf isotopic evidence of multiple sources for Oahu, Hawaii basalts, *Nature, 304(5921), 25-29,* 1983.

Tanaka, R., Nakamura, E., Takahashi, E., Geochemical evolution of Koolau Volcano, Hawaii, in *Hawaiian volcanoes; deep underwater perspectives, Geophysical Monograph Series, vol. 128, (eds, Takahashi, E., Lipman, P. W., Garcia, M. O., Naka, J., Aramaki, S), 311-332,* 2002.

Tatsumoto, M., Hegner, E., Unruh, D.M., Origin of the West Maui volcanic rocks inferred from Pb, Sr, and Nd isotopes and a multicomponent model for oceanic basalt, in Decker, R.W., Wright, T.L., and Stauffer, P.H., eds., Volcanism in Hawaii: *U.S. Geological Survey Professional Paper 1350, II, 723-744,* 1987.

Vervoort, J. D., Patchett, P. J., Blichert-Toft, J. and Albarede, F., Relationships between Lu-Hf and Sm-Nd isotopic systems in the global sedimentary system. *Earth Planet. Sci. Lett., 168, 79-99,* 1999.

West, H. B., Gerlach, D. C., Leeman, William P., Garcia, Michael O., Isotopic constraints on the origin of Hawaiian lavas from the Maui volcanic complex, Hawaii, *Nature, 330 (6145), 216-220,* 1987.

Xu, G., Frey, F. A., Clague, D. A., Weis, D. and Beeson, M. H., East Molokai and other Kea-trend volcanoes: Magmatic processes and sources as they migrate away from the Hawaiian hot spot, *Geochem. Geophys. Geosyst., doi:10.1029/2004GC000830,* 2005.

Yang, H.-J., Frey, F. A., Rhodes, J. M., and Garcia, M. O., Evolution of Mauna Kea volcano: Inferences from lava compositions recovered in the Hawaii Scientific Drilling Project, *J. Geophys. Res. 101, 11,747-11,767,* 1996

Yang, H. J., Frey, F. A., Clague, D. A., Constraints on the source components of lavas forming the Hawaiian North Arch and Honolulu volcanics, *J. Petrol., 44 (4), 603-627,* 2003.

Zimmer, M., Kroener, A., Jochum, K. P., Reischmann, T., Todt, W., The Gabal Gerf Complex; a Precambrian N-MORB ophiolite in the Nubian Shield, NE Africa, *Chem. Geol., 123 (1-4), 29-51,* 1995.

Table 1. Major and Trace Element Abundance in Kahoolawe Shield and Caldera Filling Lavas [1]

Sample	KAH 13	KAH 13	KAH 14 [2]	KAH 16 [2]	KAH 18 [2]	KAH 21	KAH 23 [2]	KAH 24	KAH 24
shatter box [3]	WC	agate	WC	WC	WC	agate	WC	agate	WC
Location	Kanapou bay	Kanapou bay	Kanapou bay	Kanapou bay	Kanapou bay	Kanapou bay	Kanapou bay	Kanapou bay	Kanapou bay
Elevation (m)	215	215	192	171	143	113	98	90	90
SiO_2		51.8	50.7	49.1	51.2		50.1	50.1	
TiO_2		2.62	2.52	2.54	2.25		2.60	1.52	
Al_2O_3		13.6	15.4	14.0	12.8		14.1	11.8	
Fe_2O_3		12.9	13.2	13.1	12.2		13.2	12.2	
MnO		0.18	0.18	0.17	0.16		0.18	0.17	
MgO		6.14	6.17	8.30	9.06		6.32	13.9	
CaO		10.0	9.3	10.1	9.1		10.6	8.18	
Na_2O		2.15	2.08	2.35	2.21		2.38	1.65	
K_2O		0.40	0.17	0.11	0.61		0.18	0.18	
P_2O_5		0.29	0.27	0.31	0.34		0.36	0.16	
TOTAL		100.1						99.8	
LOI [4]		0.83	1.94	1.64	1.11		1.07	0.75	
Sc	33	33	32	31	29	33	34	23	15
Rb	5.3	5.2	0.38	0.26	9.4	0.35	1.20	3.0	2.5
Sr	306	304	295	376	409	331	360	208	193
Y	32.3	31.6	32.1	31.7	28.1	32.4	33.5	20.6	19.7
Zr	162	161	155	161	159	143	172	95	94
Nb	11.4	11.2	11.1	13.6	13.4	10.2	14.0	6.34	6.25
Ba	98.4	98.5	94.3	105	190	79.9	67.2	71.2	70.3
La	11.8	11.6	13.6	14.7	13.5	12.1	13.3	6.70	6.61
Ce	27.9	27.6	29.5	33.4	30.2	26.5	33.2	16.7	16.6
Pr	4.5	4.4	4.5	5.1	4.7	4.6	5.0	2.5	2.5
Nd	21.2	21.3	21.4	23.7	22.1	21.8	22.9	12.1	11.3
Sm	6.1	5.9	5.9	6.2	5.8	6.1	6.2	3.4	3.3
Eu	1.97	1.97	1.98	2.05	1.94	2.05	2.04	1.17	1.15
Tb	1.01	1.00	0.992	1.03	0.91	1.07	1.05	0.64	0.61
Gd	6.3	6.2	6.3	6.4	6.1	6.7	6.7	3.8	3.8
Dy	5.8	5.7	5.5	5.6	5.0	6.0	6.1	3.6	3.5
Ho	1.12	1.11	1.08	1.10	0.95	1.16	1.20	0.71	0.69
Er	2.95	2.88	2.79	2.74	2.44	2.99	3.04	1.90	1.83
Tm	0.41	0.40	0.40	0.40	0.35	0.45	0.45	0.28	0.26
Yb	2.35	2.33	2.26	2.15	1.94	2.47	2.54	1.62	1.57
Lu		0.332	0.296	0.275	0.245	0.315	0.328	0.234	0.217
Hf	4.1	4.1	3.9	4.0	3.8	3.6	4.4	2.4	2.4
Ta	0.76	0.74	1.32	2.93	3.4	0.66	3.6	0.42	0.41
Pb	1.40	1.33	5.10	3.37	2.66	1.36	4.63	1.33	1.35
Th	0.74	0.72	0.78	0.90	0.85	0.70	0.93	0.43	0.40
U	0.213	0.196	0.171	0.134	0.256	0.163	0.175	0.138	0.136

(1) Major element contents are reported in %, and trace element abundances are reported in ppm.

(2) Taken from Fodor et al. (1992) by converting FeO to Fe_2O_3. Major element contents are re-normalized to 100% after converting FeO to Fe_2O_3.

(3) Sample powders prepared by Fodor et al. (1992) were crushed in a WC shatter box. To avoid the possible Ta and Pb contamination arising from using a WC shatter box, most of the samples that we analyzed were crushed in an agate shatter box. Two samples (KAH-13 and -24) were prepared in both WC and agate shatter boxes; trace element abundances agree within 10%, even for Ta and Pb! However, Nb/Ta in six other samples prepared in WC shatter box have low Nb/Ta (2.5-8.5) and Ce/Pb (2.2-11.3), relative to the Nb/Ta (14.2-15.5) and Ce/Pb (12.5-29.0) in 21 samples crushed in agate shatter box.

(4) LOI: Loss on ignition. ~0.2g samples were ignited at 1000 °C for over 8 hours. LOI was calculated using (weight loss during ignition/weight before ignition)*100%.

Table 1 (continued)

Sample	**KAH 25**	**KAH 26**	**KAH 28**	**KAH 31**	**KAH 65**	**KAH 67**	**KAH 68**	**KAH 71**
shatter box [3]	agate	agate	agate	agate	agate	agate	agate	agate
Location	Kanapou bay	Kanapou bay	Kanapou bay	Kanapou bay	Waikahalulu bay	Waikahalulu bay	Waikahalulu bay	Waikahalulu bay
Elevation (m)	86	68	47	30	8	20	26	39
SiO_2	48.5	50.2	48.9		51.9	50.5	50.3	49.9
TiO_2	2.08	2.35	3.18		2.38	2.33	2.28	2.50
Al_2O_3	12.6	14.4	14.3		13.7	13.9	14.0	14.3
Fe_2O_3	13.05	12.82	14.75		12.3	12.5	12.6	12.4
MnO	0.18	0.18	0.21		0.18	0.16	0.19	0.20
MgO	12.2	7.76	5.52		6.71	7.24	7.20	6.87
CaO	9.44	9.71	9.99		10.5	11.0	11.0	11.0
Na_2O	1.79	2.14	2.59		1.98	2.08	2.22	2.33
K_2O	0.09	0.22	0.28		0.26	0.18	0.13	0.17
P_2O_5	0.12	0.26	0.36		0.23	0.22	0.22	0.26
TOTAL	100.0	99.9	100.0		100.1	100.2	100.1	99.9
LOI [4]	1.15	1.61	0.61		0.49	0.02	0.26	0.41
Sc	23	30	31	34	33	34	34	21
Rb	0.232	0.70	3.1	2.90	2.69	2.15	1.17	0.62
Sr	247	300	394	320	282	288	288	273
Y	19.2	30.5	37.2	31.1	29.3	28.1	27.7	27.4
Zr	123	146	204	149	136	132	128	139
Nb	8.93	9.84	16.7	10.7	10.5	10.4	9.62	10.9
Ba	39	72	103	64	74	62	53	137
La	6.50	10.2	16.5	12.1	9.44	9.27	8.83	9.67
Ce	14.1	24.2	40.5	28.9	23.3	24.0	22.7	25.6
Pr	2.7	4.1	5.9	4.6	3.7	3.5	3.5	3.9
Nd	13.2	20.1	27.3	21.5	17.8	17.0	16.8	18.5
Sm	3.9	5.7	7.0	6.0	4.9	5.0	4.6	5.3
Eu	1.38	1.91	2.32	2.16	1.66	1.67	1.62	1.79
Tb	0.67	0.98	1.18	1.03	0.89	0.88	0.88	0.92
Gd	4.0	6.1	7.3	6.4	5.4	5.4	5.3	5.7
Dy	3.8	5.5	6.6	5.8	5.0	5.1	4.9	5.2
Ho	0.73	1.09	1.26	1.11	1.00	1.00	0.97	1.00
Er	1.86	2.79	3.32	2.82	2.60	2.62	2.54	2.53
Tm	0.27	0.40	0.46	0.40	0.37	0.40	0.37	0.36
Yb	1.52	2.31	2.71	2.29	2.16	2.21	2.14	2.06
Lu	0.219	0.327	0.379	0.292	0.309	0.283	0.277	0.293
Hf	3.1	3.7	5.1	3.9	3.5	3.4	3.4	3.6
Ta	0.59	0.66	1.11	0.72	0.70	0.73	0.66	0.77
Pb	0.81	1.05	2.23	1.48	0.843	0.827	1.03	1.21
Th	0.53	0.64	1.19	0.71	0.62	0.64	0.59	0.64
U	0.105	0.154	0.166	0.159	0.172	0.159	0.142	0.141

Table 1 (continued)

Sample	**KAH 73**	**KAH 75**	**KAH 178**	**KAH 179**	**KAH 180**	**KAH 181**	**KAH 182**
shatter box [3]	agate	agate	agate	agate	agate	agate	agate
Location	Waikahalulu bay	Waikahalulu bay	Southeast shore	Southeast shore	Southeast shore	Southeast shore	Southeast shore
Elevation (m)	60	67	14	15	37	43	45
SiO_2	50.6	48.8	51.1	51.7	51.8	48.8	49.6
TiO_2	2.51	2.42	2.29	2.24	2.24	2.45	2.30
Al_2O_3	13.9	14.4	14.0	13.9	13.9	14.5	13.6
Fe_2O_3	12.8	12.7	12.4	12.1	12.2	13.7	12.6
MnO	0.19	0.19	0.18	0.18	0.17	0.19	0.18
MgO	6.37	6.94	7.15	6.82	7.12	8.86	9.09
CaO	10.8	11.8	10.2	10.2	9.83	8.68	9.79
Na_2O	2.25	2.11	2.12	2.18	2.21	2.37	2.24
K_2O	0.37	0.10	0.20	0.35	0.36	0.15	0.18
P_2O_5	0.30	0.27	0.27	0.26	0.26	0.25	0.27
TOTAL	100.1	99.8	100.0	99.9	100.1	100.0	99.9
LOI [4]	0.49	1.29	0.50	0.25	0.81	3.07	0.05
Sc	32	34	19	29	30	25	26
Rb	5.3	0.46	0.94	2.68	3.7	0.38	1.46
Sr	345	324	259	323	310	311	331
Y	31.3	30.0	27.1	28.5	29.0	32.0	29.0
Zr	166	150	142	141	142	154	148
Nb	12.6	10.8	10.1	9.94	10.1	9.55	9.11
Ba	95	126	89	106	118	75	104
La	12.6	10.7	10.0	10.5	10.4	11.0	10.2
Ce	31.4	26.6	25.2	25.8	25.4	26.5	26.4
Pr	4.7	4.0	3.8	3.9	3.9	4.3	4.1
Nd	21.8	19.1	18.1	18.7	18.5	20.7	19.6
Sm	6.0	5.4	5.0	5.1	5.1	5.7	5.7
Eu	1.92	1.81	1.71	1.77	1.73	1.88	1.83
Tb	0.99	0.90	0.89	0.90	0.89	0.98	0.93
Gd	6.2	5.8	5.5	5.5	5.5	6.2	5.8
Dy	5.6	5.2	5.0	5.1	5.0	5.5	5.2
Ho	1.12	1.05	0.98	0.99	0.98	1.05	1.00
Er	2.85	2.73	2.56	2.53	2.52	2.70	2.49
Tm	0.42	0.39	0.36	0.37	0.36	0.38	0.36
Yb	2.35	2.23	2.00	2.08	2.12	2.17	2.05
Lu	0.295	0.291	0.287	0.294	0.300	0.319	0.299
Hf	4.1	3.9	3.6	3.6	3.6	3.9	3.8
Ta	0.84	0.72	0.67	0.66	0.66	0.64	0.62
Pb	1.22	0.94	1.09	1.05	1.05	1.10	1.05
Th	0.86	0.71	0.62	0.67	0.69	0.67	0.63
U	0.197	0.172	0.173	0.192	0.201	0.145	0.110

Table 1 (continued)

Sample	**KAH 183**	**KAH 184**	**KAH 185**	**KAH 34** [2]	**KAH 36** [2]
shatter box [3]	agate	agate	agate	WC	WC
Location	Southeast shore	Southeast shore	Southeast shore	Caldera fill	Caldera fill
Elevation (m)	50	60	67		
SiO_2	50.1	49.9	50.7	49.0	51.1
TiO_2	2.47	2.21	2.34	2.91	2.08
Al_2O_3	14.7	14.6	13.6	14.7	14.2
Fe_2O_3	13.0	12.2	12.1	13.0	11.5
MnO	0.18	0.18	0.18	0.17	0.17
MgO	7.09	7.03	7.14	5.84	7.20
CaO	9.77	11.1	10.7	11.0	11.1
Na_2O	2.28	2.21	2.33	2.73	2.26
K_2O	0.13	0.13	0.29	0.23	0.25
P_2O_5	0.27	0.26	0.27	0.42	0.24
TOTAL	100.0	99.8	99.7		
LOI [4]	2.31	0.44	0.55	0.76	1.04
Sc	30	34	31	33	33
Rb	0.39	0.43	3.9	1.45	3.4
Sr	329	385	368	394	311
Y	28.9	27.8	27.8	35.2	26.4
Zr	154	142	150	205	129
Nb	10.1	10.3	11.7	17.4	11.1
Ba	86	97	99	113	76
La	10.7	11.3	11.4	17.4	9.84
Ce	27.2	27.4	28.9	37.4	23.8
Pr		4.2	4.2	5.7	3.6
Nd	20.2	19.2	20.0	26.1	16.8
Sm	5.5	5.1	5.3	7.1	4.6
Eu	1.83	1.75	1.76	2.36	1.63
Tb	0.95	0.85	0.89	1.11	0.82
Gd	5.9	5.4	5.6	7.3	5.1
Dy	5.3	4.8	5.0	6.5	4.7
Ho	0.99	0.94	0.96	1.24	0.92
Er	3.54	2.45	2.45	3.21	2.40
Tm	0.36	0.34	0.35	0.47	0.36
Yb	2.09	1.97	2.05	2.62	1.99
Lu	0.292	0.279	0.303	0.323	0.253
Hf	3.8	3.5	3.8		3.3
Ta	0.66	0.66	0.79	5.5	4.5
Pb	1.08	1.13	1.05	4.49	11.0
Th	0.68	0.72	0.77	1.12	0.66
U	0.120	0.158	0.193	0.205	0.169

Table 2. Sr, Nd, Pb and Hf isotopic Ratios in Kahoolawe Shield and Caldera Filling Lavas

Sample	$^{87}Sr/^{86}Sr$	2 sigma	$^{143}Nd/^{144}Nd$	2 sigma	$^{206}Pb/^{204}Pb$	2 sigma	$^{207}Pb/^{204}Pb$	2 sigma	$^{208}Pb/^{204}Pb$	2 sigma	$^{176}Hf/^{177}Hf$	2 sigma
KAH 13	0.704049	0.000008	0.512873	0.000008	18.009	0.001	15.438	0.001	37.797	0.002	0.283046	0.000007
KAH 14	0.704226	0.000008	0.512819	0.000012	18.004	0.001	15.426	0.001	37.785	0.002	0.283001	0.000006
KAH 21	0.704161	0.000010	0.512834	0.000007	17.999	0.001	15.429	0.001	37.780	0.002	0.283008	0.000006
KAH 24	0.704300	0.000008	0.512796	0.000008	17.867	0.001	15.414	0.001	37.685	0.003	0.282968	0.000009
KAH 25	0.704091	0.000008	0.512862	0.000006	18.060	0.001	15.436	0.001	37.817	0.002	0.283015	0.000007
KAH 28	0.704090	0.000008	0.512828	0.000007	17.998	0.001	15.424	0.001	37.778	0.002	0.283002	0.000008
KAH 31	0.704073	0.000007	0.512863	0.000007	18.021	0.001	15.438	0.001	37.808	0.002	0.283004	0.000006
KAH 36	0.704167	0.000011	0.512821	0.000007	17.992	0.001	15.427	0.001	37.791	0.002	0.283010	0.000006
KAH 67	0.704093	0.000008			18.095	0.001	15.439	0.001	37.888	0.002	0.283010	0.000008
KAH 71	0.703937	0.000010	0.512902	0.000007	18.109	0.001	15.426	0.001	37.838	0.001	0.283050	0.000009
KAH 75	0.704160	0.000010	0.512855	0.000010	18.028	0.001	15.423	0.001	37.829	0.002	0.282988	0.000006
KAH 181	0.704139	0.000008	0.512852	0.000008	17.945	0.001	15.423	0.001	37.760	0.002	0.283002	0.000007
KAH 182	0.704139	0.000008	0.512860	0.000009	17.952	0.001	15.427	0.001	37.758	0.002	0.282990	0.000006
KAH 185	0.704190	0.000008	0.512832	0.000022	18.029	0.001	15.448	0.001	37.908	0.002	0.282981	0.000007

Table 3. Input Parameters for Mixing Lines in Figs. 5, 10, 14 and 15 [1]

	$^{87}Sr/^{86}Sr$	$^{143}Nd/^{144}Nd$	$^{206}Pb/^{204}Pb$	[Sr]	[Nd]	[Pb]	[La]	[Ce]	[Nb]	[Th]
average Koolau Lavas (Makapuu) [2]	0.704226	0.512680	17.868	384	18.3	1.1	10.3	25.8	8.1	0.58
average source composition of Koolau (Makapuu) [3]	0.704226	0.512680	17.868	38.4	1.83	0.11	1.03	2.58	0.81	0.058
average Mauna Loa Lavas [4]	0.703767	0.512904	18.162	272	14.2	0.85	7.5	19.9	8.0	0.50
average source composition of Mauna Loa [3]	0.703767	0.512904	18.162	27.2	1.42	0.085	0.75	1.99	0.80	0.050
average Gabbro [5]	0.702596	0.512936	17.523	562	2.75	0.31	1.43	3.81	0.87	0.046

(1) Since we argue that Loa-trend volcanoes do not sample the **Kea** component (e.g., Fig. 12), we compare Kahoolawe lavas with mixtures between two other Loa-trend volcanoes, Makapuu-stage of Koolau and Mauna Loa.
(2) Isotopic ratios are from Roden et al., 1994; Lassiter and Hauri, 1998 and Abouchami et al., 2004. Trace element data (ppm) are from Huang and Frey, 2005.
(3) Trace element abundances in source are inferred assuming solid/melt partition coefficients are << 0.1 and 10% partial melting. Although Hawaiian shield lavas form by variable extents of melting, assuming a constant melting extent does not change the mixing lines in Figs. 5, 10, 14,15). Variable extents of melting only change the relative proportions of different sources (Mauna Loa vs Makapuu-stage of Koolau).
(4) Isotopic ratios are from Kurz et al., 1995, Cohen et al., 1996, Abouchami et al., 2000 and Blichert-Toft et al., 2003.
Trace element data (ppm) are from Cohen et al., 1996 with Nb data from Kurz et al., 1995.
(5) Data source: Gabbros from Zimmer et al., 1995.

Fig. 1

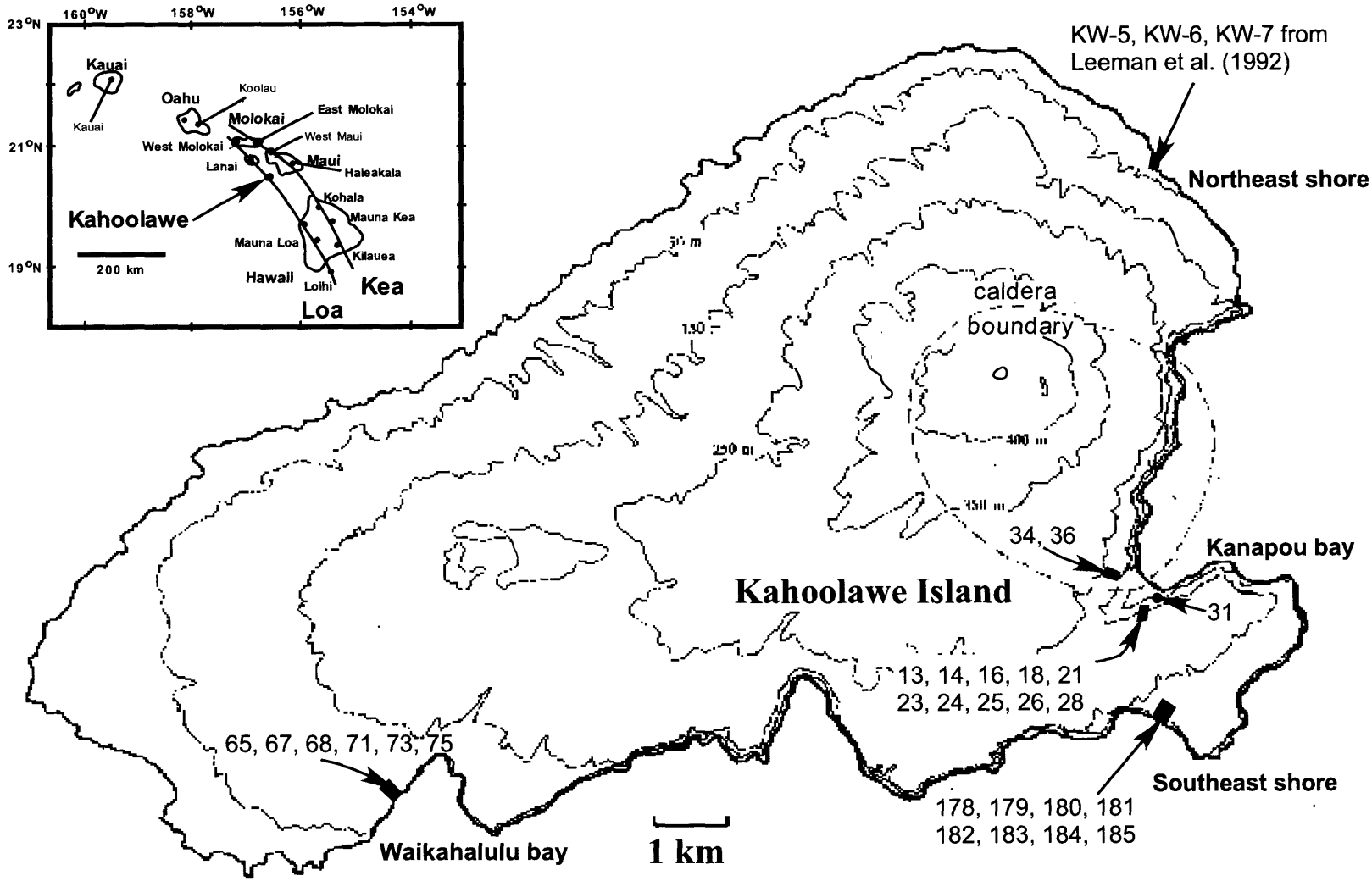
160°W
158°W
156°W
154°W
23°N
21°N
19°N
Kauai
Oahu
Koolau
Molokai
East Molokai
West Molokai
West Maui
Lanai
Maui
Haleakala
Kohala
Mauna Kea
Mauna Loa
Kilauea
Hawaii
Loihi
Kea
Loa
Kahoolawe
200 km
KW-5, KW-6, KW-7 from
Leeman et al. (1992)
Northeast shore
caldera
boundary
34, 36
Kanapou bay
Kahoolawe Island
31
13, 14, 16, 18, 21
23, 24, 25, 26, 28
65, 67, 68, 71, 73, 75
Southeast shore
178, 179, 180, 181
182, 183, 184, 185
Waikahalulu bay
1 km

Fig. 2a

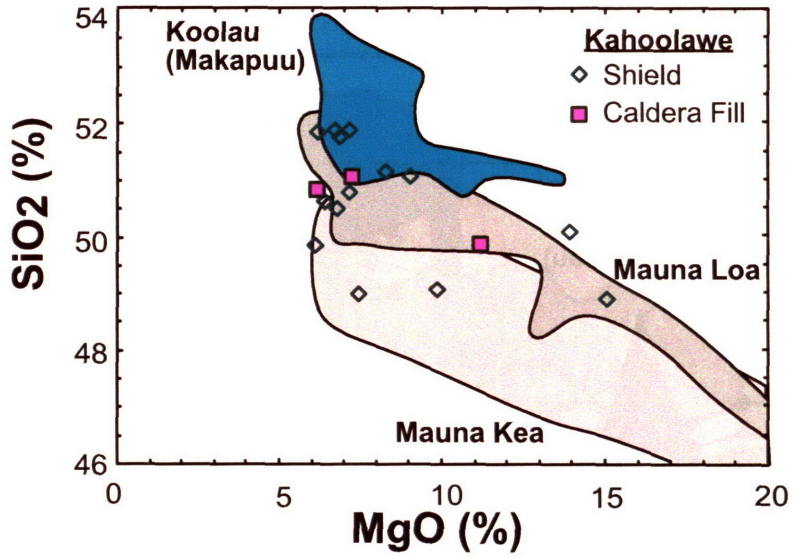
Koolau
(Makapuu)
Kahoolawe
Shield
Caldera Fill
Mauna Loa
Mauna Kea
SiO2 (%)
MgO (%)
54
52
50
48
46
0
5
10
15
20

Fig. 2b

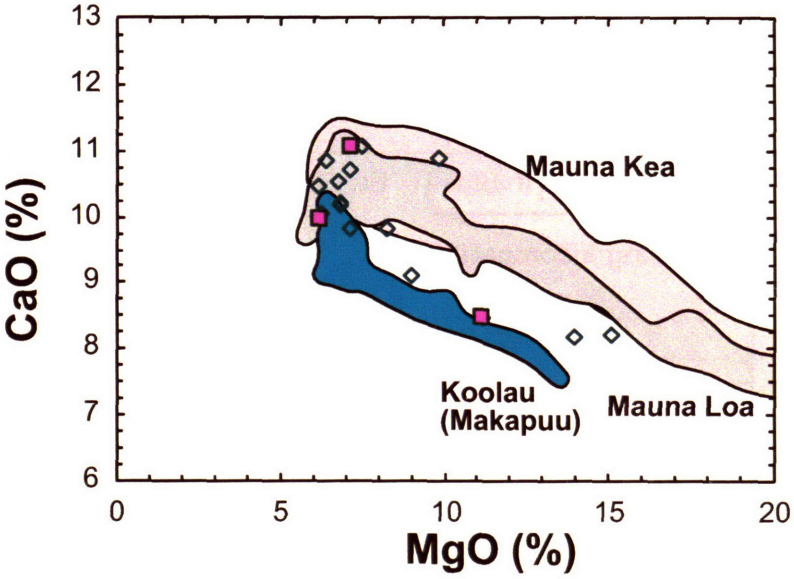
Mauna Kea
Koolau
(Makapuu)
Mauna Loa
CaO (%)
MgO (%)
13
12
11
10
9
8
7
6
0
5
10
15
20

Fig. 3

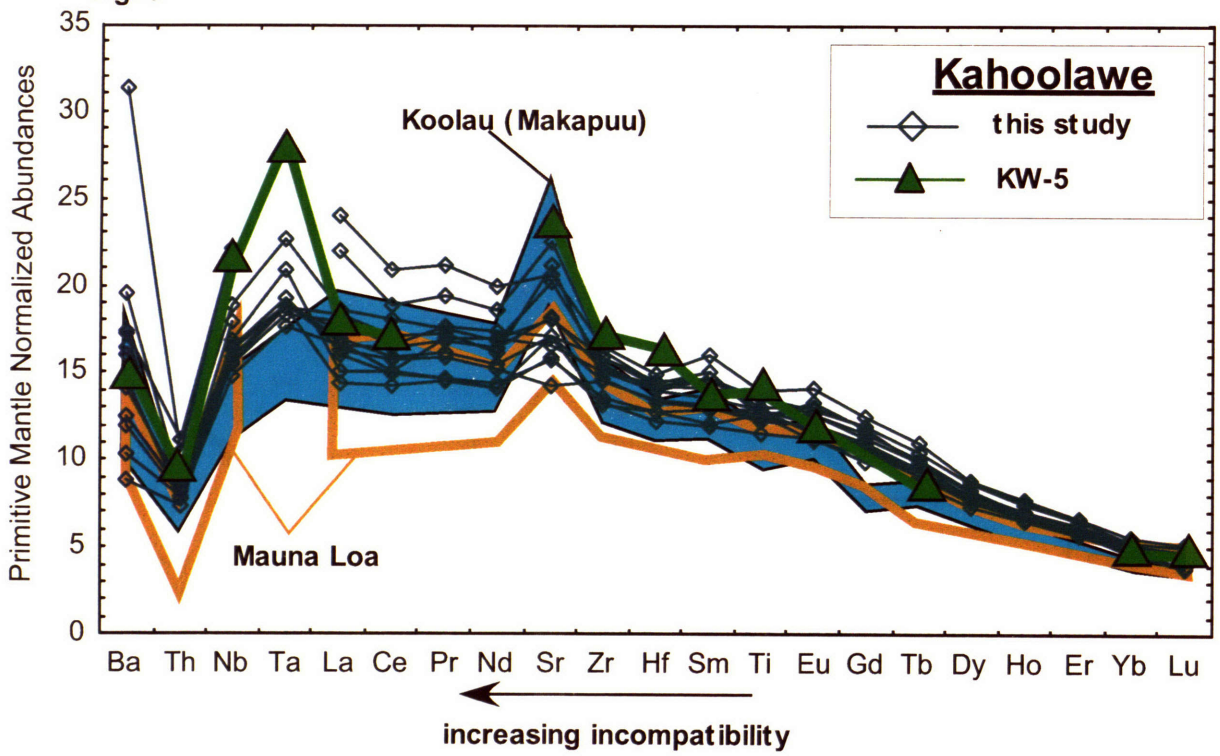
Kahoolawe
this study
KW-5
Koolau (Makapuu)
Mauna Loa
Primitive Mantle Normalized Abundances
0
5
10
15
20
25
30
35
Ba Th Nb Ta La Ce Pr Nd Sr Zr Hf Sm Ti Eu Gd Tb Dy Ho Er Yb Lu
increasing incompatibility

Fig. 4

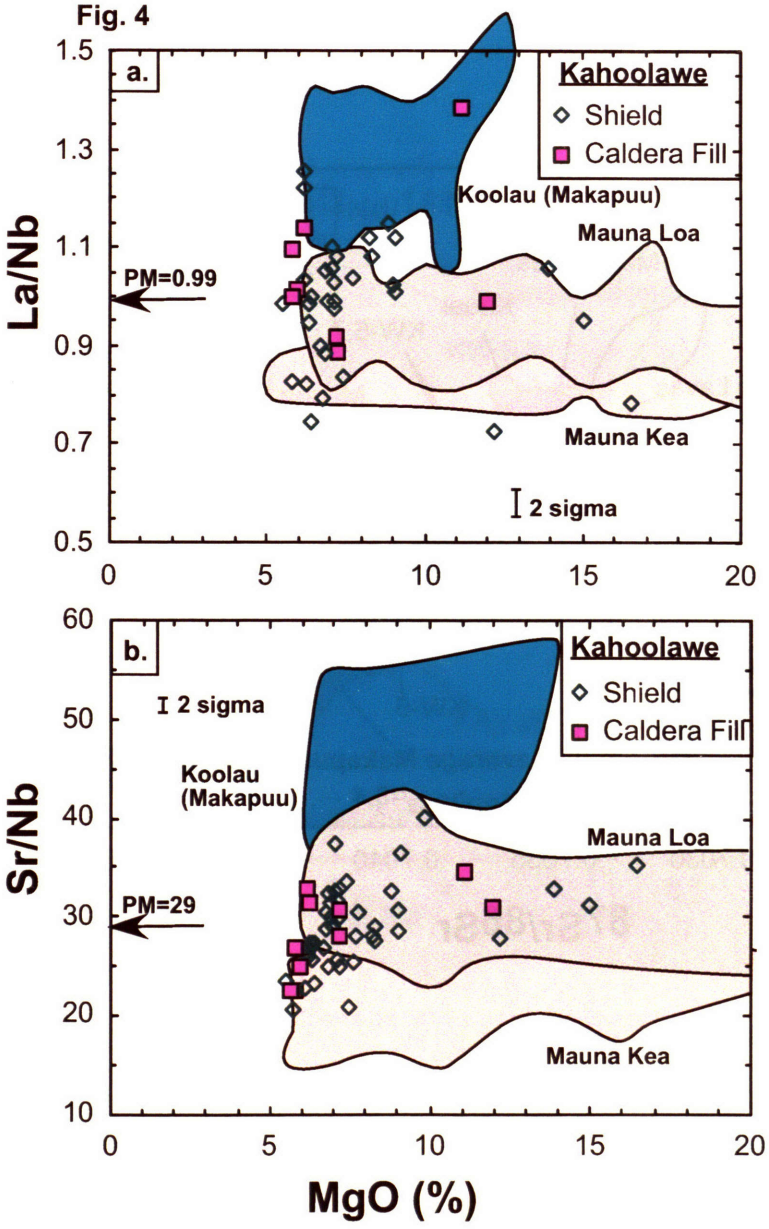
a.
Kahoolawe
Shield
Caldera Fill
Koolau (Makapuu)
Mauna Loa
Mauna Kea
PM=0.99
2 sigma
La/Nb
b.
Kahoolawe
Shield
Caldera Fill
2 sigma
Koolau (Makapuu)
Mauna Loa
Mauna Kea
PM=29
Sr/Nb
MgO (%)

Fig. 5

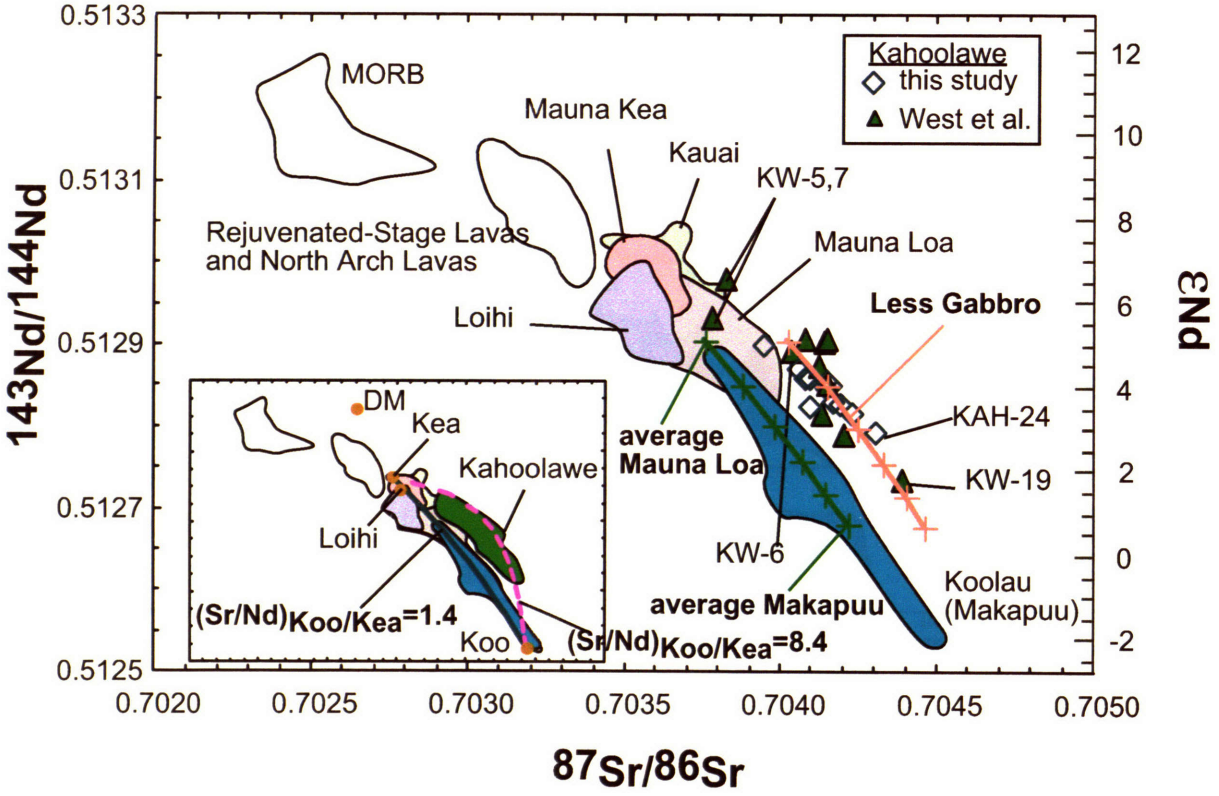
0.5133
0.5131
0.5129
0.5127
0.5125
143Nd/144Nd
0.7020
0.7025
0.7030
0.7035
0.7040
0.7045
0.7050
87Sr/86Sr
12
10
8
6
4
2
0
-2
pN3
MORB
Mauna Kea
Kauai
KW-5,7
Mauna Loa
Rejuvenated-Stage Lavas
and North Arch Lavas
Loihi
Less Gabbro
KAH-24
KW-19
KW-6
average
Mauna Loa
average Makapuu
Koolau
(Makapuu)
Kahoolawe
this study
West et al.
DM
Kea
Kahoolawe
Loihi
(Sr/Nd)Koo/Kea=1.4
Koo
(Sr/Nd)Koo/Kea=8.4

Fig. 6

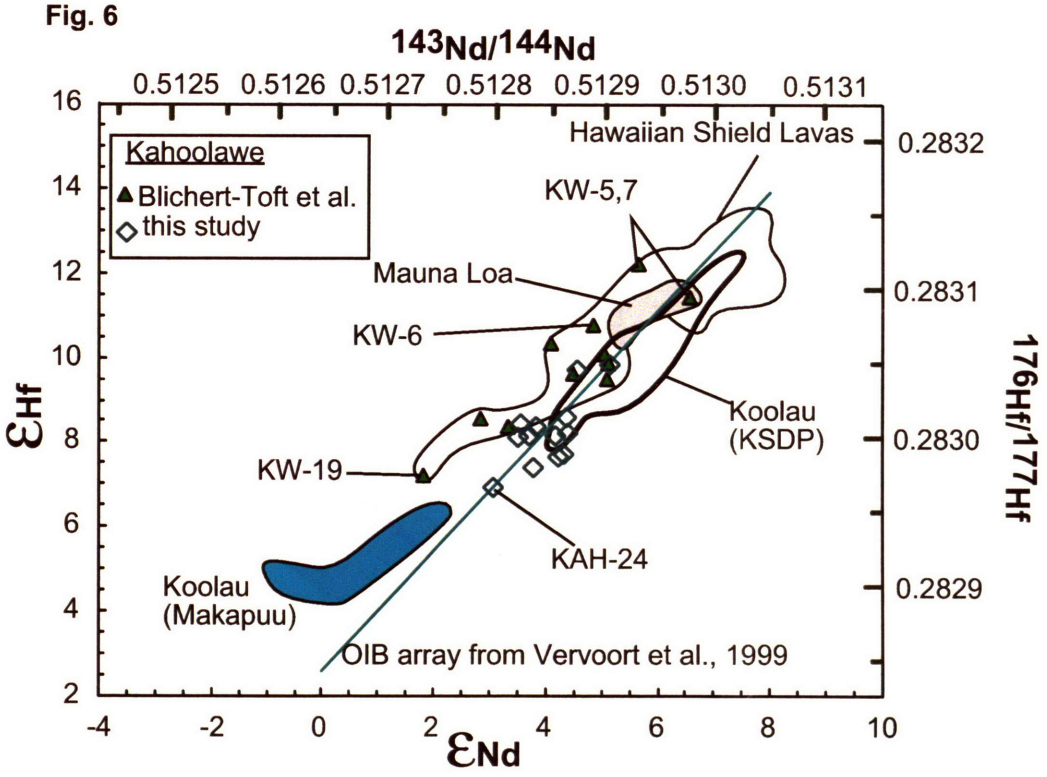
143Nd/144Nd
0.5125 0.5126 0.5127 0.5128 0.5129 0.5130 0.5131
εHf
16 14 12 10 8 6 4 2
εNd
-4 -2 0 2 4 6 8 10
176Hf/177Hf
0.2832 0.2831 0.2830 0.2829
Kahoolawe
Blichert-Toft et al.
this study
Hawaiian Shield Lavas
KW-5,7
Mauna Loa
KW-6
Koolau
(KSDP)
KW-19
KAH-24
Koolau
(Makapuu)
OIB array from Vervoort et al., 1999

Fig. 7

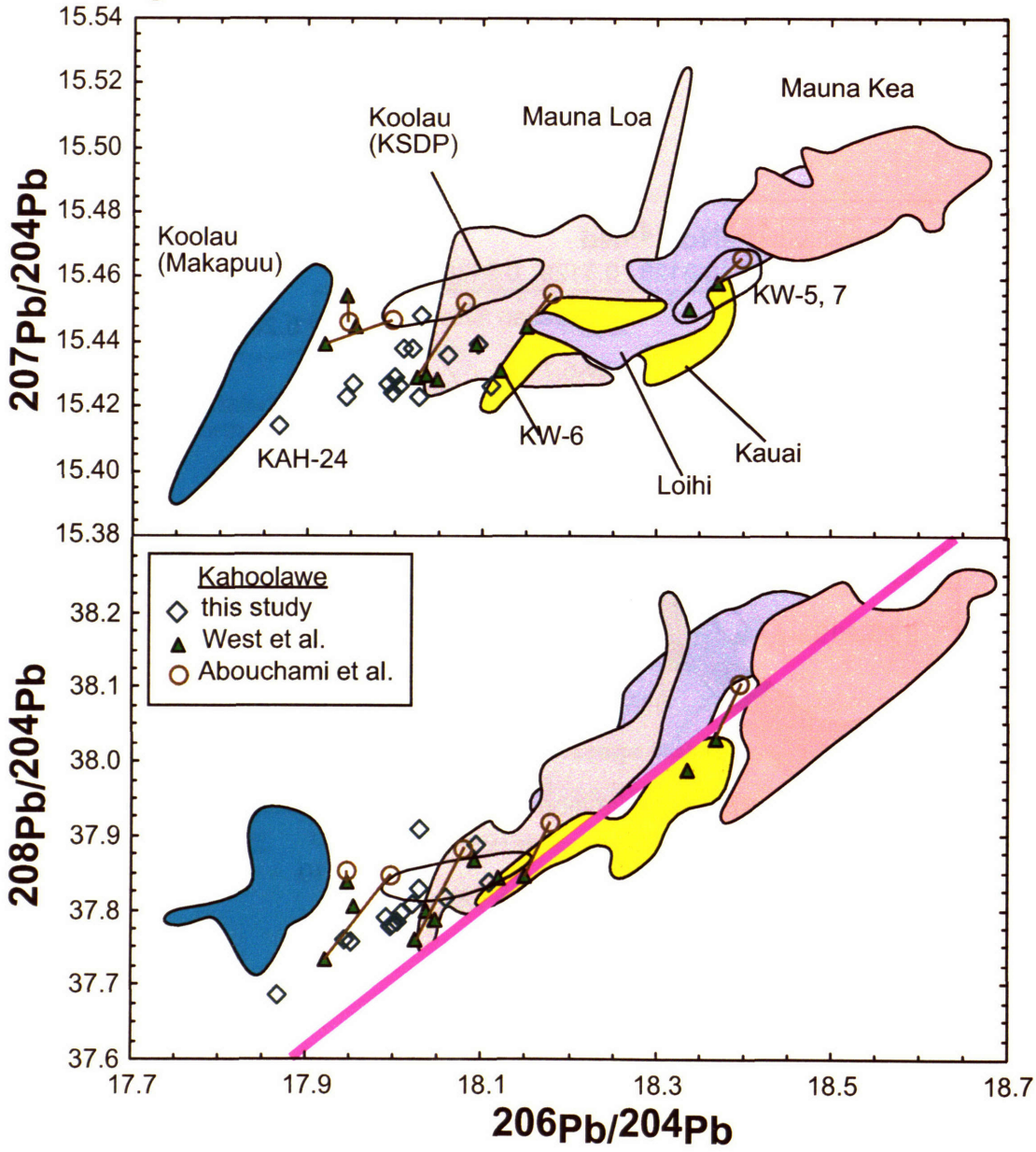
15.54
15.52
15.50
15.48
15.46
15.44
15.42
15.40
15.38
207Pb/204Pb
Koolau
(KSDP)
Mauna Loa
Mauna Kea
Koolau
(Makapuu)
KW-5, 7
KAH-24
KW-6
Kauai
Loihi
Kahoolawe
this study
West et al.
Abouchami et al.
38.2
38.1
38.0
37.9
37.8
37.7
37.6
208Pb/204Pb
17.7
17.9
18.1
18.3
18.5
18.7
206Pb/204Pb

Fig. 8

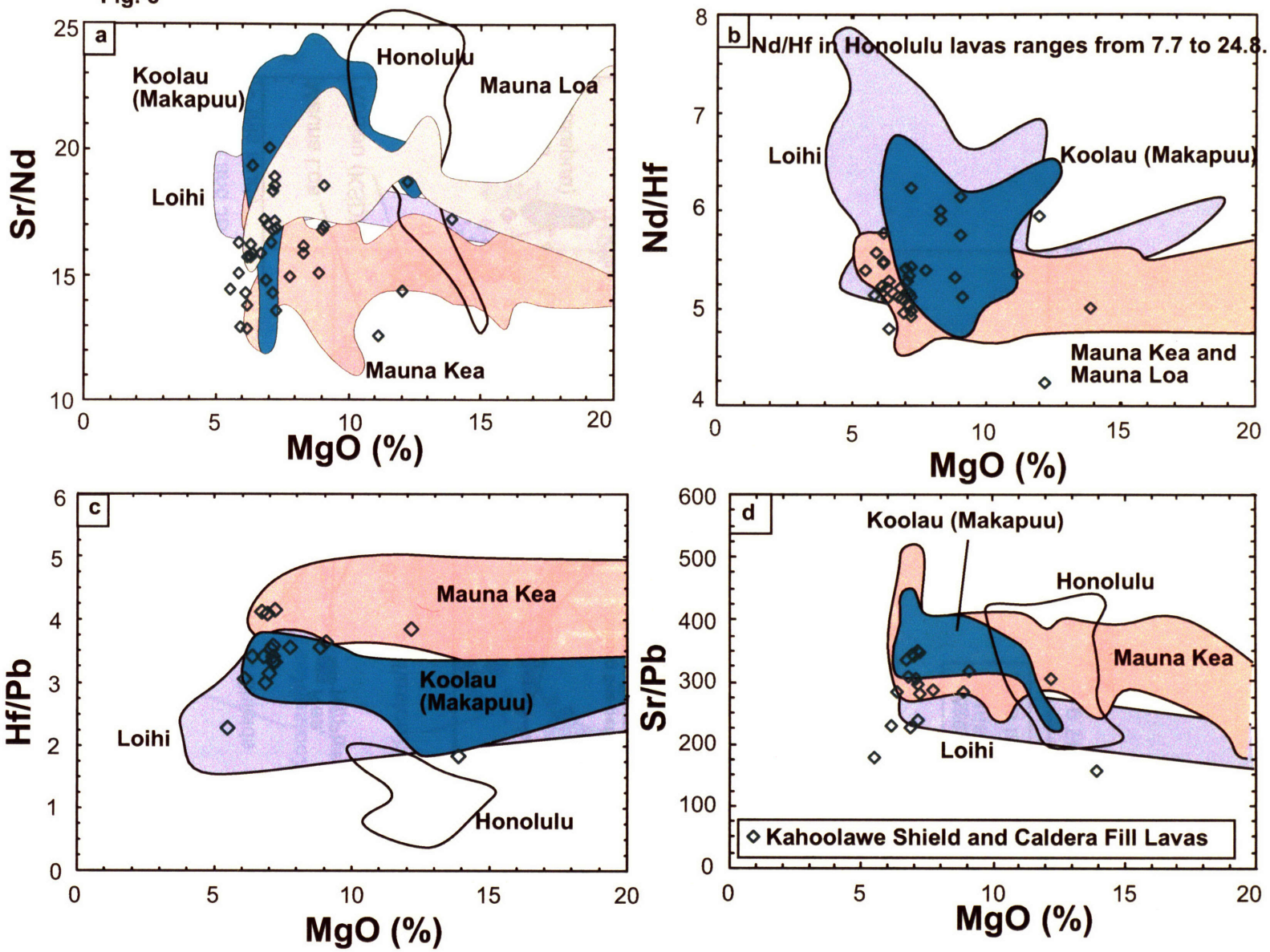
a
Sr/Nd
MgO (%)
Koolau (Makapuu)
Honolulu
Mauna Loa
Loihi
Mauna Kea
b
Nd/Hf in Honolulu lavas ranges from 7.7 to 24.8.
Nd/Hf
MgO (%)
Loihi
Koolau (Makapuu)
Mauna Kea and Mauna Loa
c
Hf/Pb
MgO (%)
Mauna Kea
Koolau (Makapuu)
Loihi
Honolulu
d
Sr/Pb
MgO (%)
Koolau (Makapuu)
Honolulu
Mauna Kea
Loihi
Kahoolawe Shield and Caldera Fill Lavas

Fig. 9

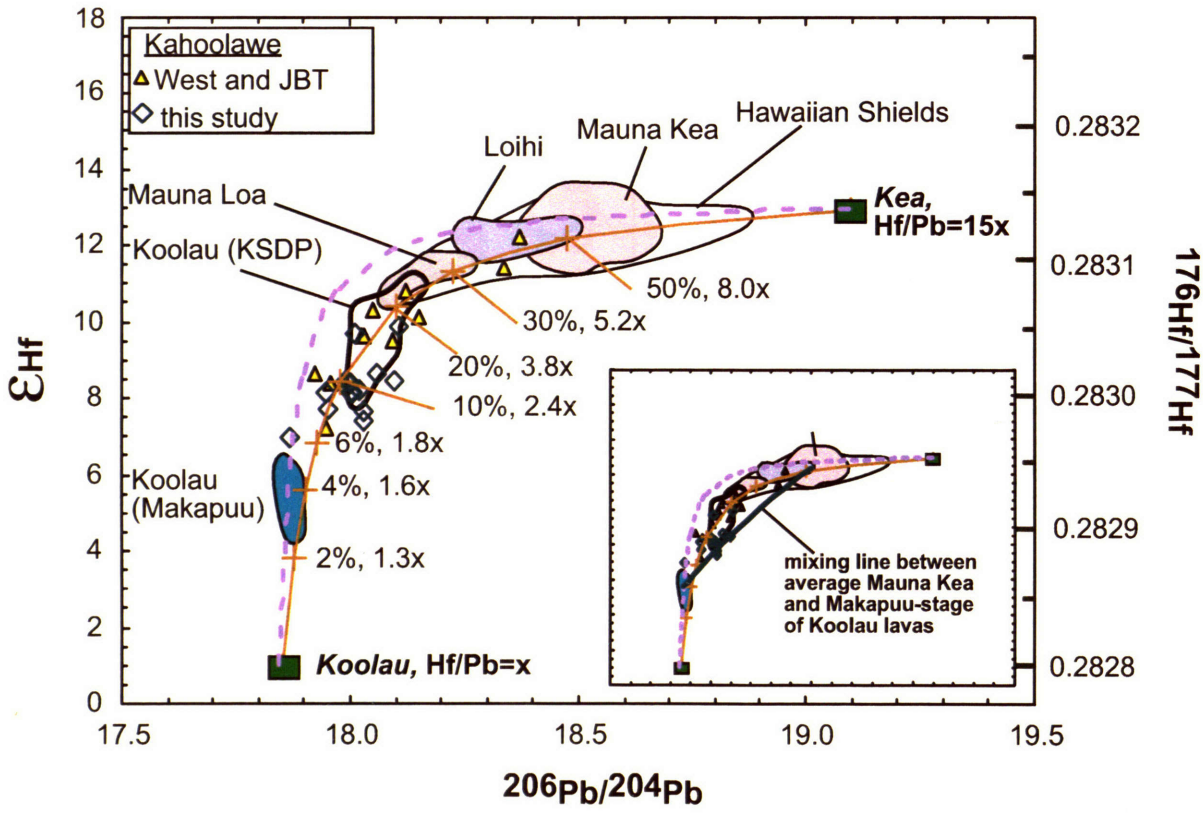
Kahoolawe
West and JBT
this study
Hawaiian Shields
Mauna Kea
Loihi
Mauna Loa
Koolau (KSDP)
Kea, Hf/Pb=15x
50%, 8.0x
30%, 5.2x
20%, 3.8x
10%, 2.4x
6%, 1.8x
4%, 1.6x
2%, 1.3x
Koolau (Makapuu)
Koolau, Hf/Pb=x
mixing line between average Mauna Kea and Makapuu-stage of Koolau lavas
εHf
176Hf/177Hf
206Pb/204Pb
0
2
4
6
8
10
12
14
16
18
17.5
18.0
18.5
19.0
19.5
0.2828
0.2829
0.2830
0.2831
0.2832

Fig. 10

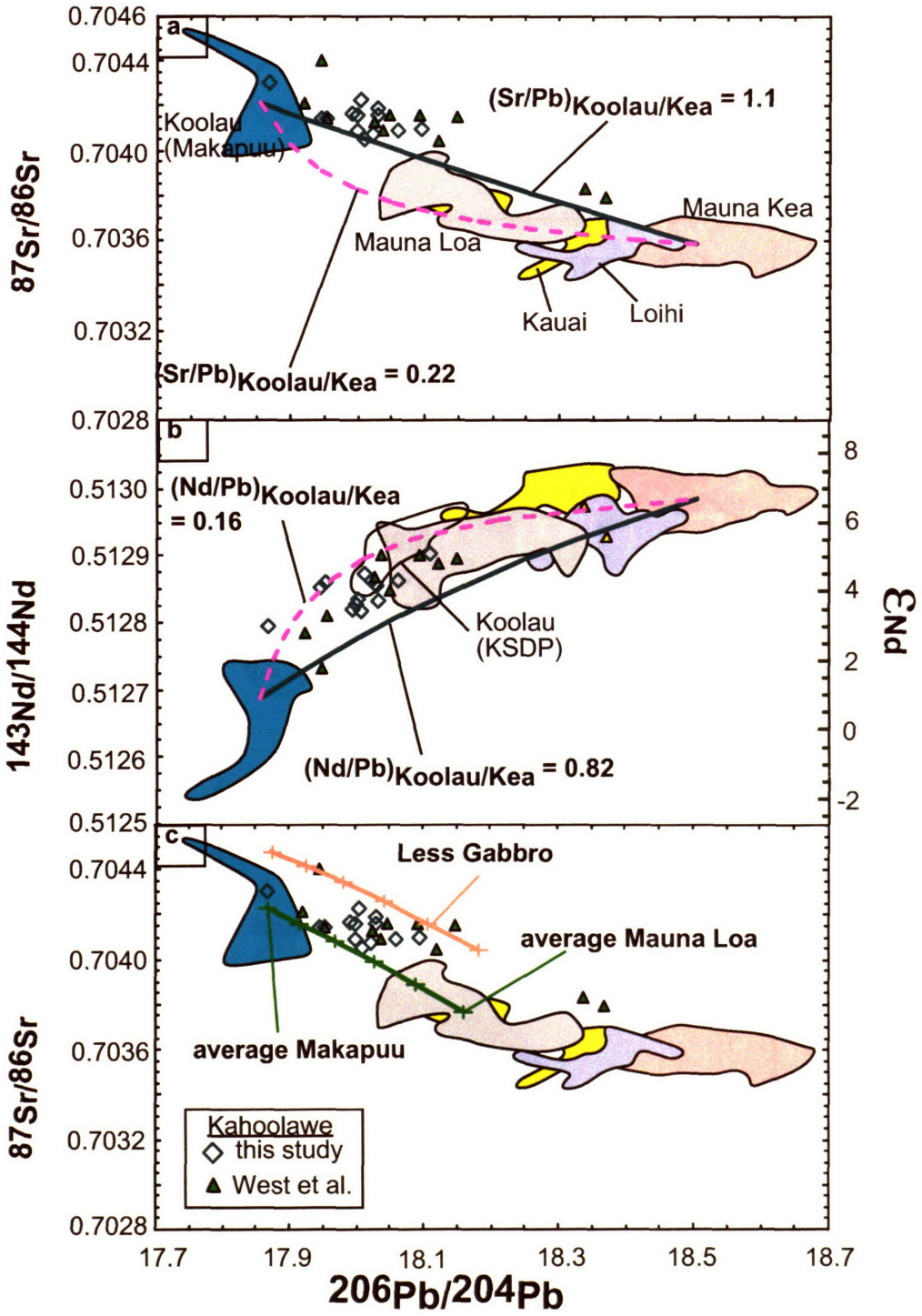
a
b
c
Koolau
(Makapuu)
(Sr/Pb)Koolau/Kea = 1.1
(Sr/Pb)Koolau/Kea = 0.22
Mauna Kea
Mauna Loa
Kauai
Loihi
(Nd/Pb)Koolau/Kea
= 0.16
(Nd/Pb)Koolau/Kea = 0.82
Koolau
(KSDP)
Less Gabbro
average Mauna Loa
average Makapuu
Kahoolawe
this study
West et al.
87Sr/86Sr
143Nd/144Nd
εNd
206Pb/204Pb
0.7046
0.7044
0.7040
0.7036
0.7032
0.7028
0.5130
0.5129
0.5128
0.5127
0.5126
0.5125
8
6
4
2
0
-2
17.7
17.9
18.1
18.3
18.5
18.7

Fig. 11

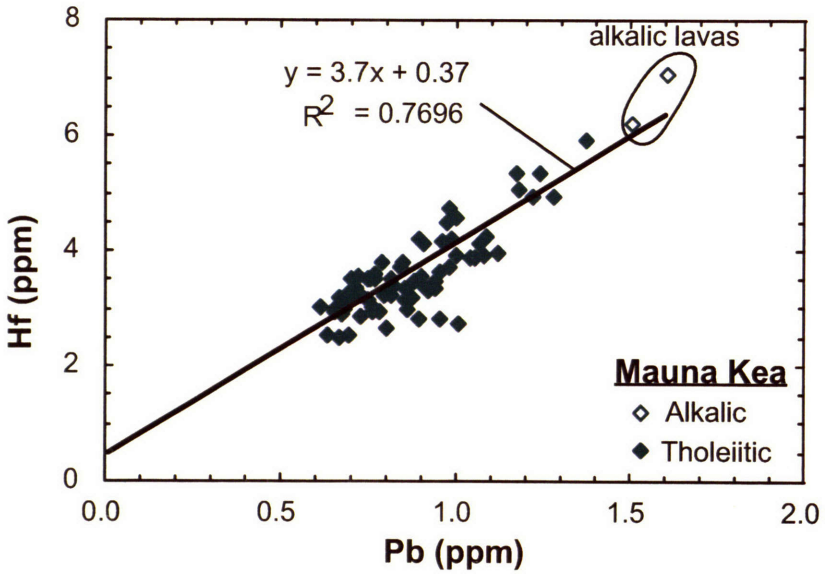
alkalic lavas
y = 3.7x + 0.37
R2 = 0.7696
Mauna Kea
Alkalic
Tholeiitic
Hf (ppm)
Pb (ppm)
0
2
4
6
8
0.0
0.5
1.0
1.5
2.0

Fig. 12

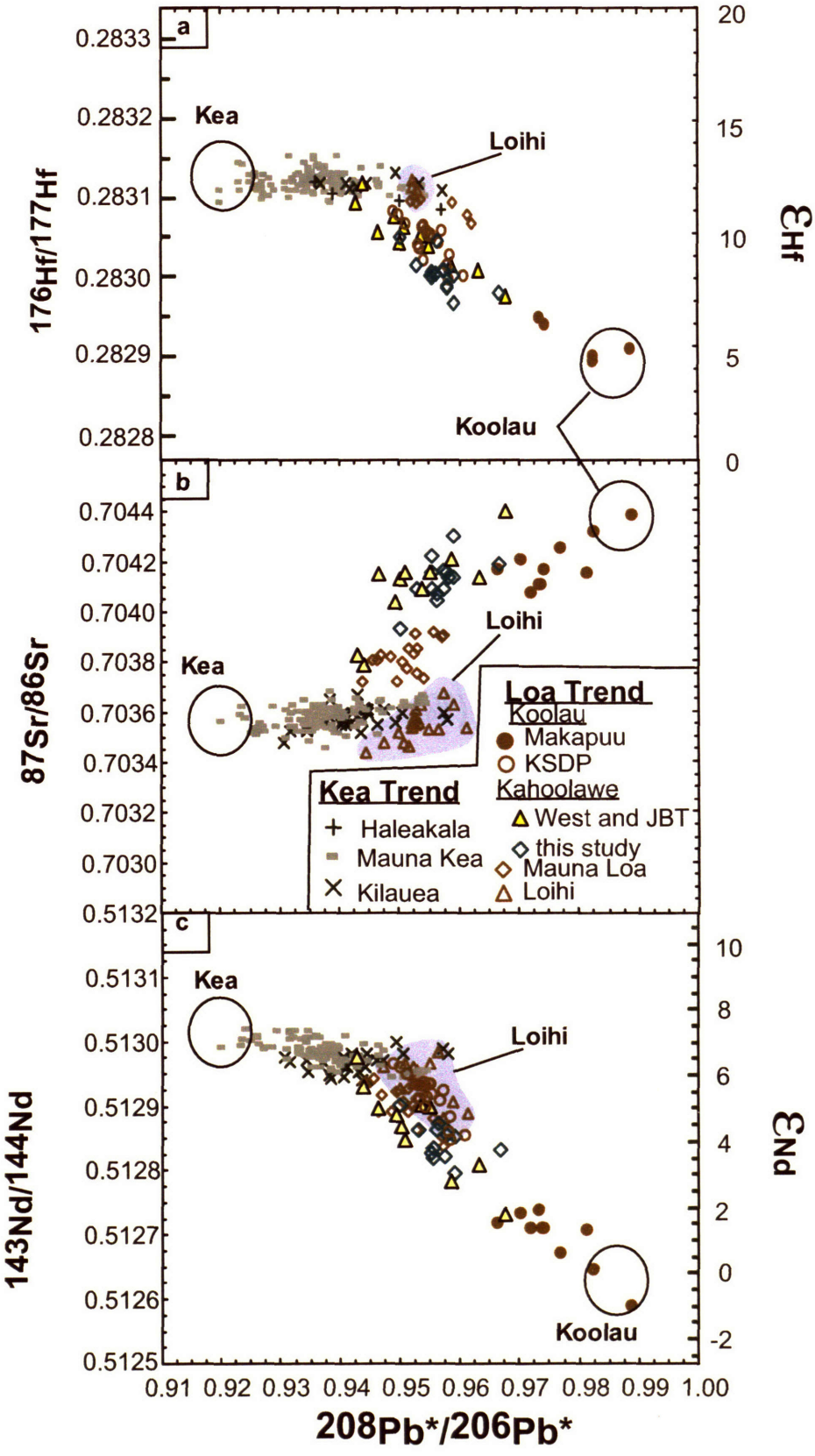
a
b
c
Kea
Loihi
Koolau
176Hf/177Hf
εHf
87Sr/86Sr
143Nd/144Nd
εNd
208Pb*/206Pb*
Loa Trend
Koolau
Makapuu
KSDP
Kahoolawe
West and JBT
this study
Mauna Loa
Loihi
Kea Trend
Haleakala
Mauna Kea
Kilauea

Fig. 13

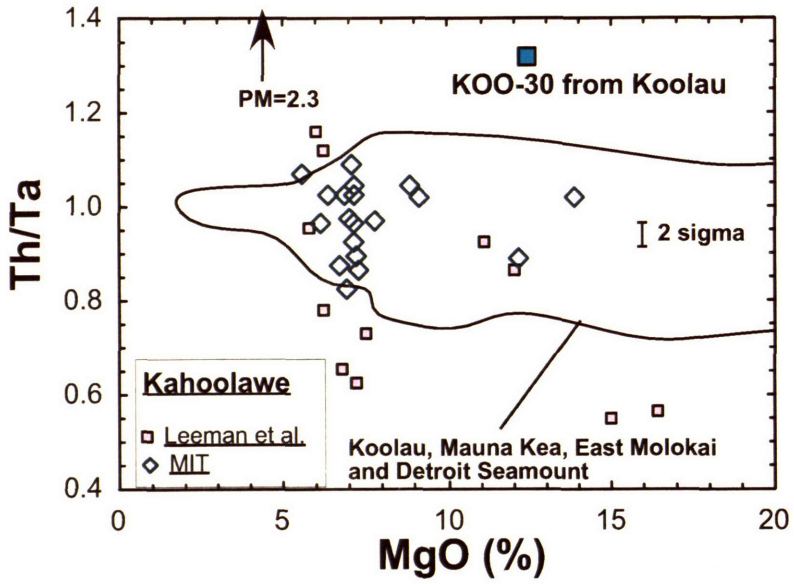
PM=2.3
KOO-30 from Koolau
2 sigma
Kahoolawe
Leeman et al.
MIT
Koolau, Mauna Kea, East Molokai
and Detroit Seamount
Th/Ta
MgO (%)
1.4
1.2
1.0
0.8
0.6
0.4
0
5
10
15
20

Fig. 14

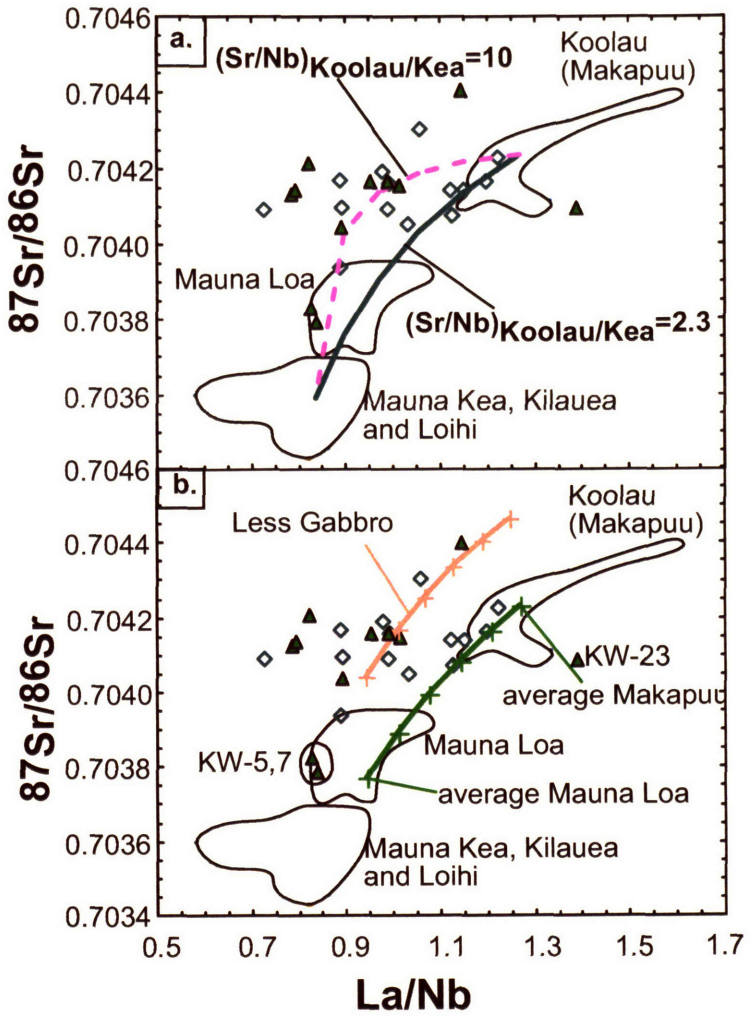
a.
(Sr/Nb)Koolau/Kea=10
Koolau (Makapuu)
Mauna Loa
(Sr/Nb)Koolau/Kea=2.3
Mauna Kea, Kilauea and Loihi
b.
Less Gabbro
Koolau (Makapuu)
KW-23
average Makapuu
Mauna Loa
KW-5,7
average Mauna Loa
Mauna Kea, Kilauea and Loihi
87Sr/86Sr
0.7046
0.7044
0.7042
0.7040
0.7038
0.7036
0.7034
0.5
0.7
0.9
1.1
1.3
1.5
1.7
La/Nb

Fig. 13

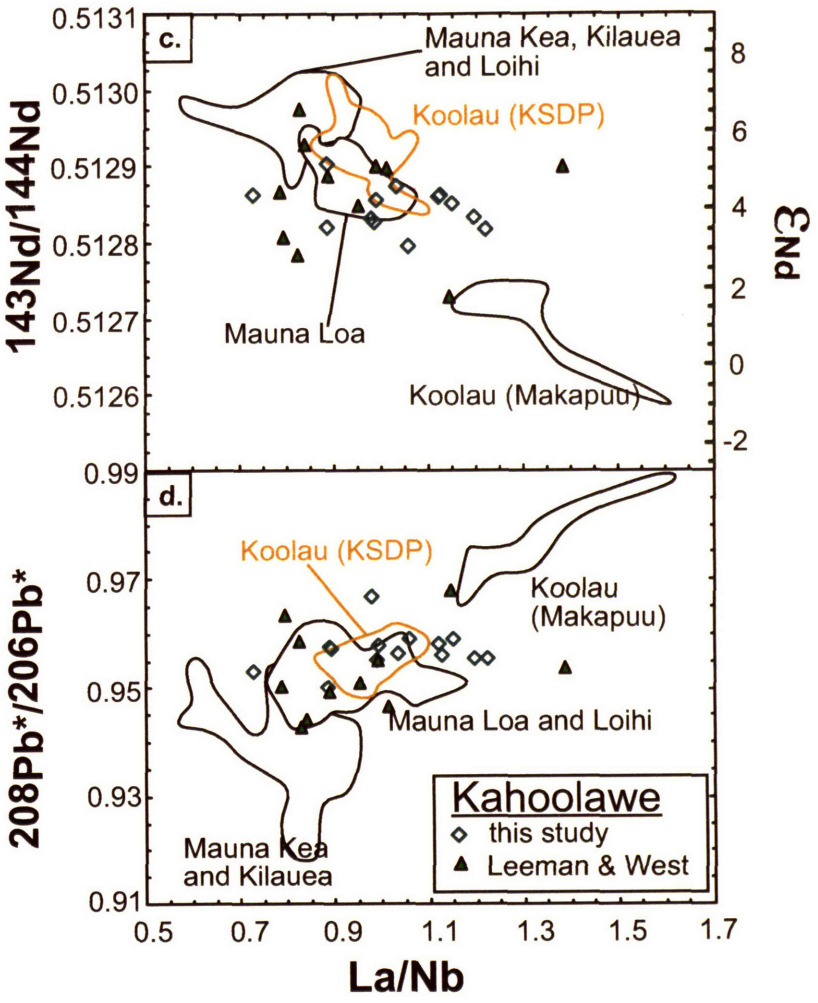
c.
Mauna Kea, Kilauea and Loihi
Koolau (KSDP)
Mauna Loa
Koolau (Makapuu)
143Nd/144Nd
0.5131
0.5130
0.5129
0.5128
0.5127
0.5126
εNd
8
6
4
2
0
-2
d.
Koolau (KSDP)
Koolau (Makapuu)
Mauna Loa and Loihi
Kahoolawe
this study
Leeman & West
Mauna Kea and Kilauea
208Pb*/206Pb*
0.99
0.97
0.95
0.93
0.91
0.5
0.7
0.9
1.1
1.3
1.5
1.7
La/Nb

Fig. 15

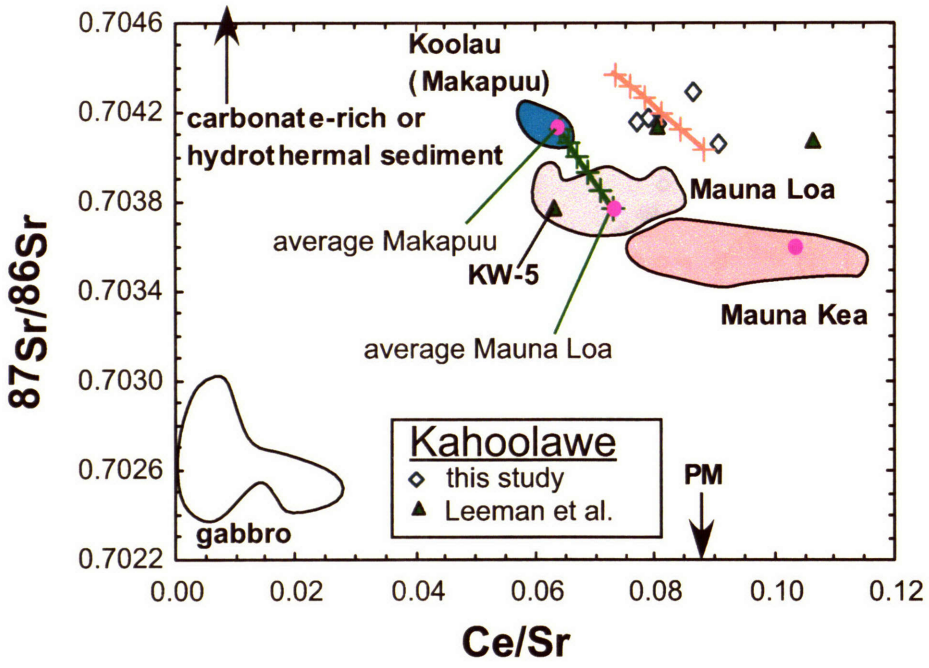
0.7046
0.7042
0.7038
0.7034
0.7030
0.7026
0.7022
87Sr/86Sr
0.00
0.02
0.04
0.06
0.08
0.10
0.12
Ce/Sr
Koolau
(Makapuu)
carbonate-rich or
hydrothermal sediment
Mauna Loa
average Makapuu
KW-5
Mauna Kea
average Mauna Loa
gabbro
Kahoolawe
this study
Leeman et al.
PM

CHAPTER 4: PETROGENESIS OF LAVAS FROM DETROIT SEAMOUNT: GEOCHEMICAL DIFFERENCES BETWEEN EMPEROR CHAIN AND HAWAIIAN VOLCANOES.

ABSTRACT

The Hawaiian Ridge and Emperor Seamount Chain define a hotspot track that provides an 80 Myr record of Hawaiian magmatism. Detroit Seamount (~76 to 81 Ma) is one of the oldest Emperor Seamounts. Volcanic rocks forming this seamount have been cored by the Ocean Drilling Program at six locations. Only tholeiitic basalt occurs at Site 884 on the eastern flank and only alkalic basalt, probably post-shield lavas, occurs at Sites 883 and 1204 on the summit plateau. However, at Site 1203 the basement core (453m penetration) includes four thick flows of pahoehoe alkalic basalt underlying ~300 m of volcaniclastic rocks interbedded with submarine erupted tholeiitic basalt. The geochemical characteristics of these alkalic lavas indicate that phlogopite was important in their petrogenesis; they may represent pre-shield stage volcanism. The surprising upwards transition from subaerial to submarine eruptives implies rapid subsidence of the volcano, which can be explained by the inferred near ridge axis setting of the seamount at ~80 Ma. A near ridge axis setting with thin lithosphere is also consistent with a shallow depth of melt segregation for Detroit Seamount magmas relative to Hawaiian magmas, and the significant role for plagioclase fractionation as the Detroit Seamount magmas evolved in the crust.

An important long-term trend along the hotspot track is that $^{87}Sr/^{86}Sr$ decreases in lavas erupted from ~40 to 80 Ma. Tholeiitic basalt at Site 884 on Detroit Seamount is the extreme and overlaps with the $^{87}Sr/^{86}Sr$-$^{143}Nd/^{144}Nd$ field of Pacific MORB. Complementary evidence for a depleted component in Detroit Seamount lavas is that relative to Hawaiian basalt, Detroit Seamount lavas have lower abundances of incompatible elements at a given MgO content. These lavas, especially from Sites 883 and 884, trend to extremely unradiogenic Pb isotopic ratios which are unlike MORB

erupted at the East Pacific Rise. A component with relatively low $^{87}Sr/^{86}Sr$ and $^{206}Pb/^{204}Pb$ is required. Lavas erupted from a spreading center in the Garrett transform fault, 13°28'S on the East Pacific Rise, have this characteristic. A plausible hypothesis is mixing of a plume-related component with a component similar to that expressed in lavas from the Garrett transform fault. However, basaltic glasses from Detroit Seamount also have relatively high Ba/Th, a distinctive characteristic of Hawaiian lavas. I argue that all Detroit Seamount lavas, including those from Site 884, are related to Hawaiian hotspot. Rejuvenated stage Hawaiian lavas also have high Ba/Th and define a trend to low $^{87}Sr/^{86}Sr$ and $^{206}Pb/^{204}Pb$. I speculate that rejuvenated stage lavas and Detroit Seamount lavas sample a depleted mantle component, intrinsic to the plume, over the past 80 Myr.

1. INTRODUCTION

The linear intra-plate Hawaiian Ridge and Emperor Seamount Chain define an approximately 6000 km long, age-progressive hotspot track (Wilson, 1963), ranging from active volcanoes at the southeastern end of the Hawaiian Ridge to >80 Myr old extinct volcanoes at the northern end of the Emperor Seamount Chain (Fig. 1a). Hawaiian volcanoes are predominantly constructed by eruptions of basaltic magma with major and trace element compositions and radiogenic isotopic ratios that distinguish them from mid-ocean ridge basalt (MORB) (e.g., B.V.S.P., 1981). An understanding of the origin and evolution of Hawaiian magmatism requires documentation and understanding of geochemical variations in hotspot-derived lavas on both short-term (< 1Myr) and long-term (> 10 Myr) time scales. On a time scale of ~1 Myr, volcanoes forming the Hawaiian islands evolve through a sequence of growth stages, characterized by the transition from alkalic to tholeiitic and back to alkalic magmatism (e.g., Clague and Dalrymple, 1987). These transitions are consistent with passage of the Pacific plate over the hotspot (e.g., Chen and Frey, 1985). Although there have been numerous studies of young volcanoes exposed on the Hawaiian Islands (e.g., Rhodes and Lockwood, 1995; Theme of Hawaii Scientific Drilling Project in Geochem. Geophys. Geosyst. 2003), much less is known about the geochemistry of lavas forming the older volcanoes of the submarine Emperor Seamount Chain. Are lavas forming the Emperor Seamounts geochemically similar to lavas forming Hawaiian volcanoes, and did these old volcanoes evolve through a similar sequence of growth stages?

Detailed study of lavas forming the Emperor Seamounts requires drilling to penetrate the thick sedimentary cover and to obtain samples whose relative ages are known. The first detailed sampling of the Emperor Seamounts was during Deep Sea Drilling Project Leg 55, which penetrated 387 m of basalt at Suiko Seamount (Fig. 1a). Dalrymple et al. (1980) and Sharp and Clague (2002) reported ages of 64.7±1.1 Ma and 61.3±0.5 Ma, respectively, for Suiko Seamount lavas. Important results are that: (1) like Hawaiian volcanoes, Suiko Seamount has shield stage lavas of tholeiitic basalt overlain by alkalic basalt (Kirkpatrick et al., 1980); (2) Initial $^{87}Sr/^{86}Sr$ ratios of tholeiitic basalt decrease from Daikakuji Seamount at the Hawaiian-Emperor bend to Suiko Seamount, which represent over 20 Myr of hotspot activity (~42-61 Ma, Fig. 1) (Lanphere et al., 1980).

More recently, the Ocean Drilling Program (ODP) Leg 145 drilled and cored the older Detroit Seamount (~76-81 Ma, Table 1, Fig. 1a) (Keller et al., 1995; Duncan and Keller, 2004). The basaltic core from Site 883 and especially Site 884 of ODP Leg 145 yielded surprising results. Relative to primitive mantle and tholeiitic basalt from younger volcanoes on the Hawaiian Ridge-Emperor Seamount Chain, the ~81 Ma basalt from Site 884 has lower ratios of highly to moderately incompatible elements, lower initial $^{87}Sr/^{86}Sr$ and higher initial $^{143}Nd/^{144}Nd$ ratios; in fact, Site 884 lavas are similar to MORB (Keller et al., 2000; Regelous et al., 2003). These results have led to two contrasting interpretations for the origin and evolution of magma forming Detroit Seamount. Keller et al. (2000) noted that at ~80 Ma, the Hawaiian hotspot was located near an active mid-ocean ridge (see Fig. 5c of Cottrell and Tarduno, 2003). They suggest that the MORB-like isotopic signature of Detroit Seamount lavas from Site 884 resulted from entrainment

of MORB-related upper mantle (i.e., hot low viscosity asthenosphere and hot thin lithosphere) by the rising mantle plume. In contrast, Regelous et al. (2003) propose that the depleted characteristics of Site 884 lavas reflect sampling of a depleted and refractory plume component by unusually high extents of mantle melting beneath young and thin oceanic lithosphere.

During ODP Leg 197 three additional cores with basement penetrations of 41 to 453 m were recovered from Detroit Seamount (Table 1, Tarduno, J. A., Duncan, R. A., Scholl, D. W., et al., 2002). Lavas from Site 1203 yield ^{40}Ar-^{39}Ar ages of 76±1 Ma (Duncan and Keller, 2004). In this paper, I report major and trace element abundances for basaltic whole rocks recovered during ODP Leg 197 and basaltic glasses recovered during ODP Legs 197 and 145. In addition, Sr, Nd and Pb isotopic ratios are reported for whole rock samples from Leg 197. I use these geochemical data, along with the petrographic and volcanological information to constrain the magmatic evolution at Detroit Seamount and to evaluate the two alternative hypotheses for the origin of its magmas.

Important results are that: (1) alkalic basalt at Sites 883 and 1204 may reflect post-shield stage lavas, but the upwards transition from intercalated alkalic and tholeiitic basalt to solely tholeiitic basalt at Hole 1203A may reflect the pre-shield to shield stage transition; (2) compared with Hawaiian shield stage lavas, tholeiitic basalt magmas erupted at Detroit Seamount segregated at a lower mean pressure; (3) Detroit Seamount lavas sampled a depleted component (i.e., low $^{87}Sr/^{86}Sr$, Pb isotopic ratios and high $^{143}Nd/^{144}Nd$, Ba/Th) that is not present in Hawaiian shield stage lavas or East Pacific Rise (EPR) MORB. It is also present in Hawaiian rejuvenated-stage and North Arch lavas

(Frey et al., in revision). I speculate that this depleted component has been associated with the Hawaiian hotspot for ~80 Myr.

2. DETROIT SEAMOUNT

2.1 Bathymetry

A region of shallow seafloor, depths of 2400 to 3000m, centered at 51°N in the northern part of the Emperor Seamount Chain has been referred to as Detroit Tablemount or Detroit Plateau (Lonsdale et al., 1993). I refer to this region as Detroit Seamount (Fig. 1). The area, 10,000 km^2, of the Detroit Seamount is similar to the subaerial part of the Big Island of Hawaii (Fig. 1b). Like the Big Island, Detroit Seamount probably represents several coalesced volcanic shields (Duncan and Keller, 2004). Three peaks, Detroit, Windsor and Wayne, reach shallower depths, up to 1388m (Fig. 1b). Dredging of the northerly peak recovered lapilli hyalotuffs that included nepheline and perovskite-bearing lava fragments that were interpreted as rejuvenated-stage volcanism, analogous to the highly alkalic rejuvenated-stage of some Hawaiian volcanoes (Lonsdale et al., 1993). These unsedimented peaks were avoided during ODP drilling whose objective was to sample lavas erupted during the shield construction stage; such lavas are buried beneath 460 to 850 m of sediment.

2.2. Stratigraphy and Petrography

2.2.1 Hole 1203A

Hole 1203A, located in a valley on the eastern flank of Detroit Seamount, penetrated 452.6 m into basement, and recovered parts of 18 lava flow units (Figs. 1b and 2). Five samples from four tholeiitic units (Units 11, 14, 16 and 24) have been dated using the ^{40}Ar-^{39}Ar technique, and yield an age of 76±1 Ma (Duncan and Keller, 2004).

From top to bottom, these lava flow units range from dominantly non-vesicular pillow lavas to dominantly vesicular compound pahoehoe lavas. Glassy lobe margins are present in all lava units except for Units 6 and 24 whose lobe margins were not recovered. Unaltered glass occurs in the lobe margins throughout the upper pillow lava units; but only altered glass occurs in the lower pahoehoe lava units. Vesicles are variably filled with secondary minerals, such as carbonate, zeolites and sulfides. The vesicular compound pahoehoe lavas are inferred to have been erupted subaerially, whereas the upper non-vesicular pillow lavas and some of the associated volcaniclastic rocks (Fig. 2) are inferred to be submarine eruptives (Shipboard Scientific Party, Site 1203, 2002; Fig. 3). Volatile analyses of glasses from lobe margins of these pillow lavas indicate that they were erupted at variable water depths. In detail, uppermost pillow lavas, Units 3 and 8, are undegassed; hence, they were erupted in water depths greater than 500 m. In contrast, the deeper pillow lavas, Units 14 and 18, are partially degassed, and inferred eruption water depths are less than 500 m (Thordarson et al., in prep.).

The subsidence indicated by the upwards transition from subaerial to submarine eruptives differs from that of a typical Hawaiian volcano. For example, submarine lavas underlie subaerial lavas in the drill core for Mauna Kea volcano recovered by the Hawaii Scientific Drilling Project (HSDP) (DePaolo et al., 1999). That is, the accumulation rate, 9 to 18 mm/yr (Sharp and Renne, 2005), for the HSDP drill core from Mauna Kea was greater than subsidence rate of the Big Island, ~2.4 mm/yr (Moore, 1987). The dominance of subsidence rate over accumulation rate at Detroit Seamount can be explained by a lower accumulation rate and the proximity of the seamount to an active spreading center at ~ 80 Ma (Rea and Dixon, 1983; Mammerickx and Sharman, 1988;

Cottrell and Tarduno, 2003). The relatively thin and weak oceanic lithosphere close to a spreading center subsides rapidly (e.g., Parsons and Sclater, 1977; Stein and Stein, 1992), so it is possible that during the growth of Detroit Seamount the subsidence rate was greater than the volcano accumulation rate.

Lava flows from Hole 1203A are aphyric to olivine-and/or-plagioclase-phyric basalt (Table 2). Plagioclase and olivine phenocrysts commonly occur as glomerocrysts. Large plagioclase phenocrysts/glomerocrysts, up to 1.3 cm in length, occur in Units 14 and 31. Trace amounts (<5%) of clinopyroxene phenocrysts occur in several units (Table 2). Some plagioclase phenocrysts have rounded or embayed margins, which suggests that they are not in equilibrium with surrounding groundmass. Olivine rich zones, containing >10% olivine by volume, occur in Units 11 and 16. Some olivine phenocrysts are unaltered, but many are altered to clay, iddingsite, Fe-oxyhydroxide and carbonate, and they are recognized by their equant form and characteristic fracture patterns. The groundmass of these lavas consists of plagioclase, clinopyroxene, opaque minerals (mostly titanomagnetite) and glass (usually devitrified).

2.2.2 Holes 883E, 883F, 1204A and 1204B

Site 1204 is ~27 km north of Site 1203, and within ~0.5 km of Site 883. Both sites are located on the edge of a summit plateau (Fig. 1b). Holes 1204A and 1204B were drilled within ~100 m of each other. Five samples from Site 1204 and two from Site 883 yield no reliable ^{40}Ar-^{39}Ar ages (Keller et al., 1995; Duncan and Keller, 2004). However, nannofossils in the sediment overlying and intercalated within the basalt from Site 1204 imply a minimal age of 71-76 Ma (cc22-23; Shipboard Scientific Party, Site 1204, 2002). At Hole 1204A the basement penetration was 60.8 m, but a clogged bit limited recovery

to 38.4 m of one vesicular pillow lava flow unit (Table 1; Fig. 2). Hole 1204B penetrated 140.5 m into basement, and recovered 3 lava flow units; Unit 2 is ~77 m thick (Fig. 2). These lava flow units, except for subunit 2B, are multi-lobed vesicular pillow lavas, and unaltered glass was recovered from several glassy margins. Subunit 2B is composed of coarse grained (up to 6 mm) diabase: From the upper and lower margins toward the center of this subunit, grain size ranges from highly vesicular aphanitic to fine-grained to sparsely vesicular medium-grained with ophitic to subophitic texture. This subunit may be a submarine sheet lobe or it may represent an internal transport system that fed an active flow front (Fig. 3; Thordarson et al., in prep.). Based on their high vesicularity, Site 1204 lavas, and nearby Site 883 lavas, were classified as subaerially erupted pahoehoe flows in Shipboard Scientific Party, Site 1204 (2002). However, volatile analyses of glasses associated with these lavas indicate that these lavas were only partially degassed upon eruption. They probably erupted at relatively shallow water depths (<500 – 1000 m) (Fig. 3; Thordarson et al., in prep.).

The four lava flow units from Site 1204 are nearly aphyric, with some units containing trace amounts (< 5%) of plagioclase phenocrysts and olivine and plagioclase microphenocrysts. These lava flows range from highly vesicular (up to 30% close to lobe margins) to non-vesicular (in diabase). Vesicles are variably filled with secondary minerals, such as carbonate, zeolites, sulfides and green clay. Olivine, in groundmass or as microphenocrysts, is altered to Fe-oxyhydroxide, iddingsite and carbonate. Glass in groundmass is altered to green and brown clays and Fe-oxyhydroxide.

2.2.3 Hole 884E

In contrast to the relatively shallow water depth of Sites 1203, 1204 and 883 (2370-2593 m), Site 884 is located in deeper water (3284 m) on the northeastern flank of Detroit Seamount (Fig. 1b). Only one of three samples from this drill site yields a meaningful ^{40}Ar-^{39}Ar plateau age: 81±1 Ma (Keller et al., 1995). Hole 884E was drilled 87 m into basement and recovered 13 cooling units (Shipboard Scientific Party, Site 884, 1993). From top to bottom, these lava flow units range from variably vesicular (0-30%) pahoehoe lavas to non-vesicular pillow lavas. Unaltered glass only occurs in the lobe margins of lower pillow lavas, and their volatile contents require eruption at deep water depth (>500m) (Fig. 3; Thordarson et al., in prep.). No volcaniclastic rock was recovered from Hole 884E.

At Site 884 the upper pahoehoe lavas range from aphyric to highly plagioclase-phyric to megaphyric basalt. Lower pillow lavas range from highly plagioclase-phyric to megaphyric to highly plagioclase-olivine basalt (Shipboard Scientific Party, Site 884, 1993). The compositional zonation of cm-size plagioclase reflects magma mixing (Kinman and Neal, 2002).

3. SAMPLES AND SAMPLE PREPARATION

All lava flow units recovered from Detroit Seamount during ODP Leg 197 were sampled and multiple samples were collected from thick units. Table 2a shows the unit number, name and thickness, basalt type, lava flow type and phenocryst proportions for each sample. Unaltered glass was obtained from 12 units at Sites 883, 884, 1203 and 1204 (Table 2b).

Highly altered regions, such as amygdules and veins, were removed from all samples selected for whole rock analysis. The trimmed whole rock samples were wrapped in plastic and crushed with a hammer into small pieces (<0.5 cm). Again, pieces containing filled vesicles and/or veins were removed. The remaining chips were rinsed with deionized water several times before pulverizing in an agate shatter box. Fragments of unaltered glass were hand-picked using a binocular microscope. To remove alteration phases, these fragments were leached in a 1:1 mixture of 2N HCl and H_2O_2 for 10 minutes.

4. ANALYTICAL PROCEDURES

4.1 Major and Trace Element Analyses

4.1.1 Whole-Rock Samples

Abundance of major and some trace elements (Table 3a) were analyzed by X-ray fluorescence analysis at the University of Massachusetts at Amherst following the procedure described in Rhodes (1996). Other trace elements (Table 3a) were analyzed by inductively coupled plasma mass spectrometry (ICP-MS) at Massachusetts Institute of Technology using the procedure described in Huang and Frey (2003). Whole rocks from Sites 883 and 884 have been studied by Regelous et al. (2003). For comparison of their data with our data on Sites 1203 and 1204 lavas, their data have been normalized using BHVO standard values reported in Regelous et al. (2003) and Huang and Frey (2003).

4.1.2 Glass Samples

Major element compositions of glasses were obtained at the University of Bristol (UB) using a JEOL 8600 electron microprobe with 15keV accelerating voltage, a 10nA

beam current and 5-10μm spot size. The results reported in Table 3b are averages of 4 to 10 analyses for each glass.

In-situ laser ablation ICP-MS trace element analyses were obtained at UB using a VG Elemental PlasmaQuad 3+ S-option instrument equipped with a 266nm Nd-YAG laser (VG Microprobe II). The laser beam diameter at the sample surface was ~50μm, and the laser repetition rate was set to 10Hz. This choice of laser beam conditions reflected the need to obtain good sensitivity in order to achieve low detection limits. Helium gas and then an argon/helium mixture carried the ablated material from the sample cell to the plasma torch. All measurements were made using Thermo Elemental PlasmaLab 'time-resolved analysis' data acquisition software with a total acquisition time of 100s per analysis (50s for a gas blank and 50s for laser ablation). The data reduction algorithm is that of Longerich et al. (1996). NIST 610 glass was used for calibration and NIST 612 glass was used to check on instrument linearity. Analyses of the NIST glass standards bracketed the analysis of unknowns in order to correct for instrument drift. The glass standards BCR-2g, BHVO-2g, BIR-1g were analysed as unknowns as a check of accuracy. Ca was used as internal standard to correct for variations in ablation yield between and during individual analyses of both standards and samples. Data in Table 3b represent averages of a minimum of 6 analyses of each glass fragment, and for comparison with whole rock data, the glass data have been normalized to the values of BHVO-2 obtained from solution ICP-MS by Huang and Frey (2003).

4.2 Isotopic Analyses

Sr-Nd-Pb isotopic ratios were determined in seventeen whole rock samples (Table 4a). Because isotopic ratios and parent/daughter ratios were likely affected by post-

magmatic alteration processes (Regelous et al., 2003), Sr, Nd and Pb isotopic ratios and their parent/daughter ratios were determined on acid leached whole-rock powders.

Whole rock powders were strongly acid-leached before being digested in HF-HNO_3 for Sr-Nd-Pb isotopic analyses. Specifically, ~0.3 to 0.4 g whole rock powder was weighed into a pre-cleaned Teflon® beaker, and ~10 ml 6N HCl was added. This beaker was placed in an ultra-sonic bath and the HCl was changed every 30 minutes until the acid was colorless or pale yellow. For most samples, 6 to 9 leaching steps were required. The residue was soaked in deionized H_2O for 30 minutes, rinsed twice, and dried. The weight loss after acid leaching was between 28 to 80% (Table 4a). Electron microprobe analyses of several residual assemblages showed that only plagioclase, pyroxene and olivine were present.

The leached sample powders were digested in HF-HNO_3. Three separate dissolutions were prepared for: 1) Pb isotope analyses by Thermal Ionization Mass Spectrometry (TIMS); 2) Sr-Nd isotope analyses by TIMS; and 3) parent/daughter abundance ratio determination by ICP-MS. Pb was separated from the sample matrix by anion exchange technique in HBr acid. Sr and Nd were separated by cation exchange technique in HNO_3 and HCl, respectively. Detailed TIMS analytical procedures are described in Schmitz and Bowring (2003). Parent/daughter abundance ratios in the leached powder (Table 4a) were analyzed by ICP-MS using the procedure described in Huang and Frey (2003). Initial Sr-Nd-Pb isotopic ratios in Detroit Seamount lavas are reported in Table 4b.

4.3 Effects of Acid Leaching on Isotopic Ratios

In order to assess the effects of alteration on isotopic ratios, I carried out a nine step-leaching experiment on one sample, 1203A 32R4W 76-80 (Table 4a). I prepared a series of pre-cleaned centrifuge tubes labeled as LE-A through LE-I, and ~0.4 g sample 1203A 32R4W 76-80 was weighed into each tube; 10 ml 6N HCl was added to each tube, and the tubes were shaken. Then the tubes were placed in an ultra-sonic bath. After 30 minutes, the acid was decanted from each tube. For Tube LE-A, the leaching step was followed by two steps of rinsing with 10 ml deionized H_2O. Tube LE-B was subjected to two leaching steps, Tube LE-C to three leaching steps, etc. for Tubes LE-D to LE-I with Tube LE-I experiencing nine leaching steps. The color of HCl was colorless after six leaching steps. Sr-Nd-Pb isotopic compositions and Rb/Sr, Sm/Nd, Th/U and U/Pb ratios in this series of unleached and leached powders are reported in Table 4a. As indicated in Fig 4, these isotopic ratios and parent/daughter ratios are relatively constant after two (or three for Rb/Sr and Th/Pb) acid leaching steps. The higher Sm/Nd but lower Rb/Sr, Th/Pb and U/Pb ratios in the leached powders reflect removal of fine-grained groundmass and alteration phases during acid leaching (Fig. 4). I assume that the parent/daughter ratios of the leached powders are those of the unaltered mineral assemblage and use them for age correction. After age-correction to 76 Ma, the unleached sample and sample LE I have similar (within 2 σ uncertainty) initial $^{143}Nd/^{144}Nd$, $^{206}Pb/^{204}Pb$ and $^{207}Pb/^{204}Pb$ ratios, but significantly different $^{87}Sr/^{86}Sr$ and $^{208}Pb/^{204}Pb$ ratios (Table 4b; Fig. 4).

The similar initial $^{143}Nd/^{144}Nd$ ratios in leached and unleached powders is consistent with the immobility of REE during post-magmatic alteration. The different initial $^{87}Sr/^{86}Sr$ and $^{208}Pb/^{204}Pb$ ratios in leached and unleached powders clearly reflect the

disturbance of the Rb-Sr and Th-Pb systems during post-magmatic alteration (Table 4b). Given the evidence for Pb mobility (e.g., Bach et al., 2003; Regelous et al., 2003), the difference in initial $^{208}Pb/^{204}Pb$ probably reflects loss of Pb (and consequently high Th/Pb) during post-magmatic alteration. However, it is surprising that leached and unleached powders have similar initial $^{206}Pb/^{204}Pb$ and $^{207}Pb/^{204}Pb$ ratios (Table 4b; Fig. 4c). Since the Th/Pb ratio in leached and unleached powders changed by more than a factor of 2, but U/Pb ratio changed by only a factor of ~ 1.5 (Fig. 4c, 4d), it is possible that both Pb and U were mobile during alteration, but that the U/Pb ratio was not changed dramatically.

5. RESULTS

5.1 Classification of Basalt Type

The whole rock samples are altered to variable extent as indicated by their Loss on Ignition (L.O.I.) (Table 3a), and the presence of secondary minerals. Among the 69 analyzed whole rock samples, 54 samples have L.O.I. > 2% (hereafter described as strongly altered samples), and 15 samples have 0.4% < L.O.I. < 2% (hereafter described as moderately altered samples). In contrast, the sums of major elements in the 36 glass samples are greater than 97.9%, and 24 samples have sums greater than 99% (Table 3b, Thordarson et al., in prep.). This confirms the visual inspections that these glasses are unaltered. Rock classification using the total alkalis–silica criteria can be unreliable for altered rocks, because of the mobility of Na and K during post-emplacement alteration (Fig. 5a). However, the composition of unaltered glasses enables unambiguous alkali-silica classification for 7 of the 22 cooling units recovered at Detroit Seamount during ODP Leg 197 and 5 flow units recovered during ODP Leg 145 (Fig. 3b). Out of 29 whole

rock samples from Site 1204 and 6 from the nearby Site 883 (data from Regelous et al., 2003), 30 samples are within the alkalic field (Fig. 5a). The remaining 5 samples are in the tholeiitic field close to the Macdonald-Katsura line. They include 3 samples from Hole 1204B (2 from Unit 2 and 1 from Unit 1) and 2 from Unit 2 at Hole 1204A. However, glasses from Units 1 and 2 at Hole 1204B are within the alkalic field (Table 3b, Fig. 5b). Therefore, I infer that the three whole rock samples from Hole 1204B in the tholeiitic field lost alkalis during post magmatic alteration. Although no glass is available from Unit 2 at Hole 1204A, 7 of the 9 Unit 2 whole rock samples are within the alkalic field. Therefore, I classify all lavas from Sites 1204 and 883 as alkalic basalt.

In contrast, glasses from Sites 884 and 1203, whole rocks from Site 884 and moderately altered (L.O.I. < 2%) whole rocks from Site 1203 are tholeiitic basalt. Highly altered (L.O.I. > 2%) whole rocks from Site 1203 range from the tholeiitic to the alkalic field. Three highly altered whole rock samples from Site 1203 Unit 20 (L.O.I. ranges from 5-11%) are within alkalic field (Fig. 5c); however the two glass samples from this unit are within the tholeiitic field (Fig. 5c). In addition, whole rock and glass samples from this unit have incompatible element abundances similar to other tholeiitic basalts (Table 3). I classify Unit 20 as tholeiitic basalt.

Whole rock samples from the thick compound pahoehoe Units 23, 26, 29 and 30 at Site 1203 (Fig. 2) lie within the alkalic field or are close to alkalic-tholeiitic boundary line (Fig. 5d). No unaltered glass is available from these units, but whole rock samples from these units have high abundances of incompatible elements, such as Ti and Zr (Table 3a); hence, I conclude that they represent alkalic basalt underlying the main tholeiitic basalt succession in Hole 1203A (Fig 2).

5.2. Compositional Effects of Alteration

Our objectives are to understand the magmatic evolution of lavas forming Detroit Seamount. Because these lavas are ~76-81 Myr old, the igneous geochemical characteristics of the whole rocks have been affected by post-magmatic processes. For submarine erupted lavas, these are submarine alteration processes. For now submerged but subaerially erupted lavas, both subaerial and submarine alteration processes have occurred. In this section, I discuss the effect of alteration on whole rock chemical compositions.

A direct approach to evaluate compositional changes of whole rocks caused by post-magmatic alteration is comparison of unaltered glass and whole rock compositions. Our discussion begins with elements that are known to be mobile, e.g., K and Rb, but also Ba and P, and concludes with assessment of changes in ratios of highly incompatible elements.

K (as K_2O) and Rb are incompatible elements, and their abundance in unaltered tholeiitic and alkalic basalt glasses are positively correlated with Th abundance (Fig. 6a, 6b). However, whole rock samples do not define linear trends in Th-K_2O and Th-Rb diagrams, which is best explained as the result of K and Rb mobility during alteration. Most Site 1204 whole rock samples are from oxidizing zones defined in Shipboard Scientific Party, Site 1204 (2002), and they have higher K_2O and Rb content than the unaltered glass samples at a given Th abundance (Figs 6a, 6b). In contrast, tholeiitic whole rock samples from Site 1203 range to higher and lower K_2O and Rb contents than unaltered glass samples at a given Th abundance (Figs 6a, 6b). For example, three whole rock samples from Unit 20 at Site 1203 deviate from the trend formed by unaltered

glasses to higher K_2O and Rb content. Their L.O.I. varies from 5% to 11%. Hence, I conclude that K_2O and Rb were added during alteration. Two samples from Unit 19 at Site 1203 exhibit contrasting alteration trends. Sample 1203A 42R1W 88-92 deviates from the glass trends to higher K_2O and Rb content, and sample 1203A 42R5W 40-44 trends to lower K_2O and Rb content (Figs 6a, 6b). Their L.O.I. are 5% and 4%, respectively (Table 3a). I infer that K_2O and Rb were added to sample 1203A 42R1W 88-92, and lost from sample 1203A 42R5W 40-44 during alteration.

Among the four alkalic, incompatible element-enriched units at the bottom of Hole 1203A, Units 29 and 30 have higher contents of K_2O and Rb than Units 23 and 26 (Figs 6a, 6b). K_2O/P_2O_5 is sensitive to alteration, and unaltered Hawaiian lavas have $K_2O/P_2O_5 > 1$ (e.g., Huang and Frey, 2003). Therefore, the low and variable K_2O/P_2O_5 in Units 23 and 26 (8 of 9 samples range from 0.24 to 0.92) compared to that of Units 29 and 30 (2.3 to 2.9) indicate that K_2O and Rb were removed from Units 23 and 26 during post-magmatic alteration. This inference is important in subsequent evaluation of the role of phlogopite during the petrogenesis of these alkalic lavas.

P is an incompatible element, and its content (as P_2O_5) in unaltered glasses is positively correlated with Th abundance (Fig. 6c). Most whole rock samples form a positive trend in Th vs P_2O_5 diagram which overlaps with the trend formed by the unaltered glasses. Six whole rock samples (labeled in Fig. 6c) deviate from the trend to higher P_2O_5 content. Their P_2O_5 contents, 0.5 to 0.7%, could be explained by secondary apatite, up to 1 wt %.

Mobility of Ba has been observed in altered oceanic crust (e.g., Staudigel et al., 1995). Most whole rocks from Detroit Seamount form a positive trend in a Th-Ba plot,

overlapping with the trend formed by unaltered glasses (Fig. 6d). However, several whole rock samples deviate from the trend to high Ba abundance (Fig. 6d). The high Ba abundance in Sample 1204B 14R1W 87-91 has been confirmed by both ICP-MS and XRF analyses (Table 3a). This sample is highly altered and contains large irregular domains of clay after glass.

Ce/Pb and Ba/Th ratios are not readily changed by most magmatic processes; consequently, Ce/Pb and Ba/Th ratios are relatively uniform in unaltered oceanic basalt (e.g., Hofmann and White, 1983; Hofmann, 1986). However, due to the mobility of Pb and Ba during alteration processes, these ratios may vary significantly in altered whole rocks. Comparison of unaltered glasses and whole rocks shows that each of these ratios are quite variable in the whole rock samples, even among samples from the same unit, but relatively uniform in the unaltered glasses (Fig. 7). For example, the average value of Ce/Pb in unaltered glasses from Detroit Seamount is 31±6, which is close to the average value of oceanic basalt (25±5) (Hofmann, 1986) and that of Mauna Kea lavas (29±8) (Huang and Frey, 2003). The highly variable Ce/Pb ratio (6-66) in the whole rock samples (Fig. 7a) most likely results from the mobility of Pb during alteration. The Ba/Th ratio in unaltered glasses from Detroit Seamount is 98±17, but the Ba/Th ratio ranges widely (50-257) in the whole rock samples, reflecting Ba mobility during alteration (Fig. 7b). Primitive mantle values of 74 and 82 are reported by Hofmann (1988) and Sun and McDonough (1989), respectively.

5.3 Major Elements: Comparison with Hawaiian Lavas and MORB

I use MgO variation plots to compare and contrast the composition of the basalt from the four ODP drill sites at Detroit Seamount as well as to compare with mid-ocean

basalt (MORB) from the East Pacific Rise (EPR) and basalt from Mauna Kea Volcano and Loihi Seamount, which have well studied shield to post-shield and pre-shield to shield transitions, respectively. Our principal objective is to use the well known differences in major element composition between MORB and Hawaiian magmas (e.g., Albarede, 1992) to determine the affinities of the magmas erupted at Detroit Seamount.

5.3.1 SiO_2

For whole rocks and glasses with 5-10% MgO, SiO_2 contents increase from Mauna Kea and Loihi alkalic basalt (post- and pre-shield stages, respectively) to Mauna Kea (low SiO_2 group) and Loihi tholeiitic basalt (shield stages). The highest SiO_2 contents (>50%) are in EPR MORB and the high SiO_2 group lavas of Mauna Kea Shield lavas (Fig. 8a). In contrast to the negative MgO-SiO_2 trend defined by Hawaiian tholeiitic shield lavas, a trend reflecting olivine addition, subtraction and fractionation (e.g., Yang et al., 1996; Rhodes and Vollinger, 2004), most Detroit Seamount lavas define a broad positive trend (Fig. 8a). Only the olivine-rich samples from Units 11 and 16 at Site 1203 fall on an olivine-control trend. Alkalic basalt, whole rocks and glasses, from Sites 883 and 1204 has relatively low SiO_2 content that overlaps the range of alkalic post-shield lavas from Mauna Kea and pre-shield stage lavas from Loihi. Tholeiitic glasses from Sites 884 and 1203 overlap with the low-SiO_2 tholeiitic shield lavas from Mauna Kea volcano (Fig. 8a).

5.3.2 Total Iron as FeO*

For whole-rocks with 7-10% MgO, the trend of increasing FeO* contents is opposite to that for SiO_2; i.e., EPR N-MORB have the lowest FeO* abundances and Hawaiian tholeiitic basalt generally has lower FeO* abundance than Hawaiian alkalic

basalt. For Detroit Seamount lavas, the whole-rock data for FeO* are scattered widely. The FeO* content of tholeiitic basalt from Sites 1203 and 884 varies from ~ 7% to 13% which is similar to EPR N-MORB. The olivine-rich units 11 and 16 at Site 1203 overlap with Mauna Kea shield stage tholeiitic basalt (Fig. 8b). The alkalic lavas from Sites 883, 1203 and 1204 overlap with the Mauna Kea tholeiitic field but a few samples range to high FeO* (>13%) and are within the field of Mauna Kea alkalic basalt. A negative MgO-FeO* trend is well defined by Detroit Seamount glasses with the highest FeO* in alkalic basalt from Sites 883 and 1204. This trend parallels the trends for EPR N-MORB and Mauna Kea glasses (Fig. 8b).

5.3.3 Al_2O_3

In the context of the MORB-related versus Hawaiian plume-related alternatives proposed for Detroit Seamount lavas (Keller et al., 2000; Regelous et al., 2003), MgO vs Al_2O_3 is especially important because the parental magmas for N-MORB and Hawaiian shield lavas differ significantly in Al_2O_3. For MgO >8%, the Al_2O_3 content of MORB exceeds that for Hawaiian shield lavas (e.g., Fig. 8c; see also Fig. 2 in Albarede, 1992). Unfortunately, this distinction diminishes as MgO content decreases, because at ~7% MgO the positive Al_2O_3-MgO trend of MORB caused by plagioclase fractionation intersects the negative trend of Hawaiian shield lavas caused by olivine fractionation (Fig. 8c). The ~5.8 to 8.0% MgO glasses from Detroit Seamount are in the region of overlap between the Mauna Kea and EPR N-MORB fields. However, the positive MgO-Al_2O_3 trend for Detroit Seamount glasses is similar to the plagioclase fractionation trend of N-MORB. In contrast, the three high MgO (olivine-rich) samples from Units 11 and

16 at Site 1203 define a negative trend that is intermediate between the Mauna Kea shield and EPR MORB fields.

The five lavas with atypically high Al_2O_3 at ~5.7 to 7.2 % MgO (Site 1203, Units 14 and 31 and samples 145-10 and 145-11 from Site 884, Fig. 8c) are rich (>7 vol. %) in plagioclase phenocrysts (Table 2; Regelous et al., 2003; Shipboard Scientific Party, Site 1203, 2002).

5.3.4 TiO_2

It is well known that the primary magmas for Hawaiian tholeiitic lavas contain higher abundances of TiO_2 (and incompatible trace elements) than primary magmas for N-MORB (e.g., Frey and Roden, 1987; Albarede, 1992). For Detroit Seamount lavas, there is a range in TiO_2 at a given MgO content: TiO_2 content increases in the order Site 884 < Site 1203 (tholeiitic) < Site 1204 ~ Site 883 < Site 1203 (alkalic) (Fig. 8d). Tholeiitic lavas from Sites 884 and 1203 overlap with the N-MORB field. Note that the alkalic lavas from Site 1203 have lower TiO_2 content than alkalic lavas from Mauna Kea (Fig. 8d).

5.3.5 Summary

Alkalic basalt with relatively low SiO_2 content and high contents of FeO* and TiO_2 at Detroit Seamount is consistent with the tholeiitic to alkalic basalt transition that is characteristic of the late shield and post-shield stages of Hawaiian volcanoes (e.g., Frey et al., 1990, 1991). On the other hand, Site 884 lavas with low TiO_2 and P_2O_5 contents are similar to MORB. Although MORB and Hawaiian shield stage lavas with >8% MgO content differ significantly in Al_2O_3 (Albarede, 1992), evolved MORB and Hawaiian lavas with ~6-8% MgO have similar Al_2O_3 content. Therefore, I cannot use Al_2O_3

content to establish a MORB or Hawaiian affinity for the glasses from Detroit Seamount which have ~6-8% MgO. However, as in MORB, plagioclase fractionation was an important process controlling the compositions of Detroit Seamount lavas.

5.4 Incompatible Elements

In both whole rocks and glasses, abundances of incompatible elements that are immobile during alteration, such as Nb, Zr and TiO_2, are positively correlated with Th abundance (Fig. 9a-c). Generally, the lowest abundance of these incompatible elements are in Site 884 lavas and the three high MgO lavas from Site 1203 (from Units 11 and 16) (Table 3a, 3b). Alkalic lavas from Sites 1204 and 883 have incompatible element abundance intermediate between tholeiitic lavas from Sites 1203 and 884 and alkalic lavas from Site 1203. The highest abundances are in the 4 thick compound pahoehoe units, Units 23, 26, 29 and 30, in the lower part of the Site 1203 core (Fig. 2). The combination of high incompatible element abundances and their location within the alkalic field or straddling the alkalic-tholeiitic boundary line in Fig. 5d shows that these lavas are alkalic basalt. These 4 alkalic basalt units define two separate trends in the Zr and TiO_2 vs Th plots (e.g., Fig 9b,c). The Ti/Zr ratio in most lavas from Detroit Seamount ranges from 86-109, which is close to the primitive mantle value of 116 (Sun and McDonough, 1989); however, alkalic Units 23 and 26 from Site 1203 have a lower Ti/Zr ratio (67-72). Also Zr/Hf in Units 23 and 26 (44-45) differ from those in Units 29 and 30 (40-41) (Table 5).

Abundance of other moderately incompatible elements, such as Na (as Na_2O) and Lu, versus Th abundance define more complex trends (Fig 9d,e). Except for the three high MgO lavas (from Site 1203 Units 11 and 16), which have the lowest Th, Lu and

Na_2O abundance, tholeiitic lavas (glasses and whole-rocks) from Sites 1203 and 884 have similar Lu and Na_2O abundance. This result is surprising because Site 884 lavas have the lowest abundance of highly incompatible elements. Also, whole rock data for Site 884 tholeiitic lavas and Site 1203 alkalic lavas overlap in Na_2O content. However, alkalic glasses from Sites 883 and 1204 have higher Na_2O content than tholeiitic glasses from Sites 884 and 1203.

Trends defined by Ba and Sr versus Th abundance are also complex (Fig. 6d, 9f). Site 1203 alkalic lavas have variable Th abundances but relatively uniform Sr and Ba abundances. The Sr data for glasses show that Sr abundances are similar in alkalic glasses from Sites 883 and 1204 and tholeiitic glasses from Site 1203 (Fig. 9f). This is a surprising result given the relative enrichment of other incompatible elements in these alkalic glasses.

In a primitive mantle normalized trace element diagram, the relative enrichment in highly incompatible elements decreases in the order Mauna Kea alkalic lavas > Site 1203 alkalic lavas > Sites 1204 and 883 alkalic lavas (Fig. 10a). Also relative to alkalic basalt from Mauna Kea, Detroit Seamount alkalic basalt has more pronounced depletion in Sr and flatter patterns. For tholeiitic lavas, incompatible element abundance decrease in the order Mauna Kea tholeiitic lavas > Site 1203 tholeiitic lavas > Site 884 tholeiitic lavas (Fig. 10b). As pointed out by Regelous et al. (2003), the Site 884 tholeiitic lavas, both whole rocks and glasses, form convex upward trends which are similar to average MORB (Fig. 10b). However, the relative depletion in Sr that is characteristic of average MORB does not occur in Mauna Kea or Detroit Seamount lavas.

5.5 First Series Transition Metals: Ni and Sc

Abundance of Ni is positively correlated with MgO content in the glasses; tholeiitic glasses from Sites 884 and 1203 typically have higher Ni abundance than alkalic glasses from Sites 883 and 1204 (Fig. 11a). The highest Ni abundances are in the three olivine-rich whole rock samples from Units 11 and 16 at Site 1203.

An inverse MgO-Sc trend reflecting olivine control is typical of Hawaiian shield lavas (e.g., Frey et al., 1994; Huang and Frey, 2003). The three MgO-rich samples from Units 11 and 16 at Site 1203 show this trend (Fig. 11b). Most importantly, at a given MgO content, the Sc abundance in EPR N-MORB exceeds that of Hawaiian lavas. The majority of Detroit Seamount samples (whole rocks and glasses) have >35 ppm Sc; hence, they are within the MORB field (Fig. 11b).

5.6 Summary: Incompatible Elements and First Series Transition Metals

The abundance of highly incompatible, relatively immobile elements, such as Nb, La, and Th are highly correlated in Detroit Seamount lavas. There is, however, a large range from Site 884 tholeiitic basalt which are MORB-like to moderately incompatible element-rich alkalic basalt in the lower part of the Hole 1203A core. For a given lava type, tholeiitic or alkalic, lavas from Detroit Seamount are less enriched in highly incompatible elements than Mauna Kea lavas. In detail, the alkalic lavas from Site 1203 have several characteristics, relative depletion in Ba and Sr and two groups of Ti/Zr and Zr/Hf ratios, which reflect a distinctive petrogenesis. Finally, at a given MgO content, Sc abundances distinguish MORB and Hawaiian tholeiitic basalt. Lavas from Detroit Seamount have relatively high Sc abundance which overlaps with the MORB field.

5.7 Sr-Nd-Pb Isotopic Ratios

Initial Sr-Nd-Pb isotopic ratios in Detroit Seamount lavas are reported in Table 4b. Because of low Rb/Sr ratios in the leached residues, which are plagioclase, pyroxene and olivine, the age correction on $^{87}Sr/^{86}Sr$ in most samples is very small (Table 4). Correction for $^{143}Nd/^{144}Nd$ are significant but the variability is similar for unleached and leached samples (Table 4). In contrast, the scatter of Pb isotopic ratios, especially $^{206}Pb/^{204}Pb$, decreases after age-correction (Table 4).

In a Sr-Nd diagram, Sites 883, 884 and 1204 lavas plot close to the age-corrected EPR MORB field (Fig. 12a). Among Detroit Seamount lavas, Site 884 lavas have the highest $^{143}Nd/^{144}Nd$ and lowest $^{87}Sr/^{86}Sr$ ratios, and overlap with the 76 Ma MORB field. In contrast, Site 1203 tholeiitic and alkalic lavas are similar and overlap with the age-corrected Hawaiian rejuvenated stage lava and North Arch lava field which is intermediate between the EPR MORB and Mauna Kea shield fields (Fig. 12a).

In Pb isotopic diagrams, Site 883, 1203 and 1204 lavas scatter around the Hawaiian shield field defined by lavas from Mauna Kea and Mauna Loa (Fig. 12b). Compared with Site 1203 tholeiitic lavas, Site 1203 alkalic lavas are offset to higher $^{208}Pb/^{204}Pb$ ratio at a given $^{206}Pb/^{204}Pb$ ratio. In detail, Units 23 and 26 lie on an extension of the pre-shield stage Loihi field, which has higher $^{208}Pb/^{204}Pb$ ratio at a given $^{206}Pb/^{204}Pb$ ratio than the Mauna Kea field; Units 29 and 30 have even higher $^{208}Pb/^{204}Pb$ ratio at a given $^{206}Pb/^{204}Pb$ ratio (Fig. 12b). It is important to point out that Sample 1203A 65R4W 9-13 from Unit 29 at Site 1203, which has the highest age-corrected $^{208}Pb/^{204}Pb$ ratio, has been carefully analyzed with two separate analyses for the isotopic ratios and three separate analyses for parent/daughter ratios. These multiple analyses yield similar

Pb isotopic ratios and parent/daughter ratios (Table 4a). Compared with Site 1204 lavas, Site 883 lavas are offset to slightly lower $^{207}Pb/^{204}Pb$ ratio at a given $^{206}Pb/^{204}Pb$ ratio.

Site 884 lavas are offset from the Hawaiian shield field to lower $^{207}Pb/^{204}Pb$ and $^{208}Pb/^{204}Pb$ ratios at a given $^{206}Pb/^{204}Pb$ ratio (Fig. 12b). Relative to the EPR MORB field defined by data obtained by the triple spike technique, Site 884 lavas clearly have lower $^{207}Pb/^{204}Pb$ and trend to lower $^{206}Pb/^{204}Pb$ and $^{208}Pb/^{204}Pb$. Consequently, Regelous et al., (2003) concluded that Site 884 lavas are not similar to EPR MORB or Hawaiian shield stage lavas. However, as indicated in Fig. 12b, Detroit Seamount lavas form trends pointing to the field defined by Garrett transform fault lavas, which have low Pb isotopic ratios (Wendt et al., 1999). The positive trend of Detroit Seamount in a $^{206}Pb/^{204}Pb$ vs $^{87}Sr/^{86}Sr$ diagram is unlike the negative trend defined by Hawaiian shield stage lavas, and it extrapolates towards the field defined by Garrett transform fault lavas (Fig. 12c).

In summary, lavas recovered from 4 drill sites are characterized by different age-corrected isotopic ratios. Even in the same drill hole, Hole 1203A, alkalic lavas and tholeiitic lavas have different age-corrected $^{208}Pb/^{204}Pb$ ratios. Compared with modern Hawaiian shields, Detroit Seamount lavas have lower $^{87}Sr/^{86}Sr$ and higher $^{143}Nd/^{144}Nd$ ratios, that range from MORB-like to similar to that in Hawaiian rejuvenated stage lavas and North Arch lavas. Trends of Detroit Seamount lavas in $^{206}Pb/^{204}Pb$ vs $^{208}Pb/^{204}Pb$ and, especially, $^{207}Pb/^{204}Pb$ extend to lower ratios than typical of EPR MORB, but they extend toward the field defined by Garrett transform fault lavas which have $^{206}Pb/^{204}Pb$ less than 18.

6. Discussion

6.1 Role of Crystal Fractionation

Although the isotopic heterogeneity (Fig. 12) and compositional changes caused by post-magmatic alteration preclude definition of liquid lines of descent, some geochemical trends provide compelling evidence that olivine and plagioclase fractionation and accumulation were significant processes during the evolution of lavas forming Detroit Seamount. For example, olivine fractionation is shown by the MgO-Ni correlation (Fig. 11a) and plagioclase fractionation is indicated by the positive MgO-Al_2O_3 correlation for glasses (Fig. 8c), the hyperbolic trend of Th-Sr for whole rocks and glasses (Fig. 9f) and the positive Eu/Eu*-Sr/Nd correlation (Fig. 13). This is a significant result because the compositions of Hawaiian shield lavas are dominantly controlled by olivine fractionation with a relatively minor role for plagioclase and clinopyroxene (e.g., Huang and Frey, 2003; Rhodes and Vollinger, 2004). In contrast, like Detroit Seamount lavas, MORB compositions are typically controlled by plagioclase and olivine (e.g., Langmuir et al., 1992).

6.2 Significance of Alkalic Basalt Deep in the Hole 1203A Core

6.2.1 Pre-Shield or Post-Shield Stage Alkalic Lavas?

In Hole 1203A, there is an upward change from intercalated alkalic and tholeiitic basalt to solely tholeiitic basalt (Fig. 2). Specifically, four thick, ranging from 8 to 63 m, subaerially erupted compound pahoehoe alkalic flow units underlie a ~300 m thick sequence of submarine erupted tholeiitic lava flows interbedded with volcaniclastic rocks. Although this alkalic to tholeiitic transition is expected in the pre-shield to shield transition at a single volcano, it could also reflect interfingering of lavas from two

adjacent volcanoes at different growth stages. For example, shield stage tholeiitic lavas from Mauna Loa volcano overlie late-shield to post-shield stage alkalic lavas from Mauna Kea volcano in the drill cores recovered by the Hawaii Scientific Drilling Project (HSDP) (Rhodes, 1996; Rhodes and Vollinger, 2004). Did alkalic and tholeiitic lavas at Site 1203 erupt from the same volcano? Although there are erosional contacts between some units, such as Units 5 and 6, Units 23 and 24, Units 27 and 28, I cannot confidently use the contact relations in the non-continuous core containing numerous volcaniclastic units to determine if there is a regional uncomformity between the alkalic and overlying tholeiitic lavas. Therefore, I evaluate isotopic differences between these units. The tholeiitic lavas from Mauna Loa in the HSDP core are clearly isotopically distinct from the underlying alkalic to transitional Mauna Kea lavas (e.g., Fig. 6 of Lassiter et al., 1996). Therefore, the similar age-corrected $^{87}Sr/^{86}Sr$ and $^{143}Nd/^{144}Nd$ ratios of the Site 1203 alkalic and tholeiitic lavas (Fig. 12a) are evidence against the hypothesis of interfingering between two adjacent volcanoes at different growth stages. I cannot preclude the possibility that lavas from two adjacent volcanoes were similar in Sr and Nd isotopic ratios (e.g., Kilauea and Mauna Kea in Fig. 6 of Lassiter et al., 1996), but the subtle isotopic differences between alkalic and tholeiitic lavas at Site 1203 (Figs 12a, 12b) are typical of isotopic differences found in lavas from a single volcano (e.g., Lassiter et al., 1996 and Blichert-Toft et al., 2003 for Mauna Kea). Particularly interesting, these alkalic lavas have high $^{208}Pb/^{204}Pb$ at a given $^{206}Pb/^{204}Pb$ (Fig. 12b), which is a distinct characteristic of pre-shield stage Loihi lavas (e.g., Garcia et al., 1993; 1995).

Could these alkalic lava flows represent pre-shield stage lavas of Detroit Seamount? There are two examples of pre-shield stage lavas among Hawaiian volcanoes: Loihi Seamount and the submarine part of Kilauea volcano (Garcia et al., 1993; 1995; Lipman et al., 2002; Sisson et al., 2002). In contrast to these submarine eruptives, the four alkalic flow units at Hole 1203A are subaerially erupted compound pahoehoe lavas. However, modern Hawaiian volcanoes are built on Cretaceous oceanic crust with a water depth of ~4 km; in contrast, the near-ridge setting of Detroit Seamount at ~80 Ma indicates that the seamount initiated in a shallow water depth environment. This inference is consistent with the inferred eruption environment of Site 1203 lavas (Fig. 3). Since the maximum thickness of Loihi Seamount is ~ 3.5 km, and the alkalic to tholeiitic transition occurs within the top several hundred meters (Garcia et al., 1995), it is possible that the pre-shield stage includes 2-3 km of alkalic basalt. The average water depth of zero age oceanic crust is less than 3 km in both North Pacific and North Atlantic oceans (e.g., Parsons and Sclater, 1977; Stein and Stein, 1992). Therefore, if Detroit Seamount grew rapidly relative to subsidence of the young oceanic lithosphere, it is possible that its pre-shield stage included a subaerial growth stage. However, as discussed earlier, the upward transition from subaerial to submarine eruptives at Hole 1203A requires a subsequent decrease in accumulation rate relative to subsidence rate as the volcano aged.

6.2.2 Petrogenesis of Alkalic Lavas at Site 1203

The four alkalic units form two compositional groups whose differences provide keys to understanding their petrogenesis. Specifically, relative to lavas from Units 29 and 30, lavas from Units 23 and 26 have lower K_2O and Rb abundances (Fig. 6a, 6b), lower Ba/Th, Ti/Zr and higher Zr/Hf ratio (Table 5). Common phenocryst phases, such as

plagioclase and olivine, do not affect these ratios, but phlogopite, a mineral that fractionates Ba/Th, Ti/Zr and Zr/Hf (Table 5), occurs in pre-shield stage alkalic Kilauea lavas (Sisson et al., 2002). For these Site 1203 alkalic lavas, a difficulty with inferring a petrogenetic role for phlogopite as a residual or fractionating mineral is that phlogopite is not a phenocryst phase, presumably because of the low K_2O contents (<1.8%) (Table 3a). Melts saturated with phlogopite typically have more than 2% K_2O (Table 5b); however, Mengel and Green (1986) infer that only 1.6% K_2O is required to saturate a SiO_2-undersaturated nephelinite with phlogopite. The K_2O content in Units 29 and 30 ranges from ~1.5 to 1.8%, but is less than 1% in Units 23 and 26 (Fig. 6a; Table 3a). As discussed in **Section 5.2**, the low K_2O content in Units 23 and 26 reflects K_2O loss during alteration. If I assume that K_2O contents of Units 29 and 30 reflect magmatic ratios (K_2O/P_2O_5 = 2.3–2.9, with K_2O = 1.5-1.8%), it is possible that phlogopite was a residual phase during partial melting. Although phlogopite may not be stable during the high temperature melting typically inferred for a plume environment (Class and Goldstein, 1997; Sisson et al., 2002), the presence of fluorine increases the thermal stability of phlogopite (e.g., Foley et al., 1986).

A specific scenario was postulated by Sisson et al. (2002) to explain the generation of submarine nephelinite to basanite lavas at Kilauea Volcano. They suggested that these alkalic lavas formed by low degree melting of phlogopite-bearing garnet pyroxenite cumulates formed during high pressure solidification of plume-derived magmas. If these melts bearing a residual phlogopite signature, i.e., relatively low Ti/Zr and Ba/Th and high Zr/Hf, interact with peridotite or mix with a peridotite-derived melt, their high K_2O content would be diminished. Hence, they would no longer be phlogopite-

saturated, but they could retain the trace element signature of residual phlogopite. This hypothesis is consistent with the geochemical data for the alkalic lavas from Site 1203.

6.3 Melt Segregation Pressure of Detroit Seamount Lavas

Based on plate reconstruction Mammerickx and Sharman (1988) and Lonsdale (1988) suggested that Detroit Seamount was built on a relatively young and thin lithosphere (Fig. 1a). The paleolatitude (Tarduno et al., 2003) and the oceanic paleodepth of Detroit Seamount (Caplan-Auerbach et al., 2000) are consistent with this inference. Therefore during formation of Detroit Seamount decompression melting is likely to have continued to a shallower depth and the mean pressure of melt segregation was lower than that during formation of modern Hawaiian volcanoes which are constructed on thick (~100-110 km, Li et al., 2004) Cretaceous oceanic lithosphere (Fig. 14). Are the compositional data for Detroit Seamount lavas consistent with this interpretation? If the mean pressure of melt segregation increases from MORB to Detroit Seamount lavas to Mauna Kea lavas (Fig. 14), these lava groups should show systematic differences in compositional parameters sensitive to pressure.

6.3.1 SiO_2 and Total Iron

The SiO_2 and FeO contents of partial melts of peridotite are a function of melt segregation pressure and extent of melting (e.g., Walter, 1998; Fig. 13 of Stolper et al., 2003). Regelous et al. (2003) noted that compared to young Emperor Seamounts, whole rock tholeiitic basalt compositions from Detroit Seamount are offset to lower total iron at a given MgO content; consequently, they inferred that melt segregation at Detroit Seamount occurred at relatively low pressure beneath thin lithosphere. Consistent with this inference, whole rock FeO and SiO_2 contents for tholeiitic basalt from Detroit

Seamount overlap with MORB field, but inexplicably, the SiO_2 content of the associated glasses do not (Figs 8a, b).

There is also evidence that the depth of melt segregation changes during growth of a Hawaiian volcano. Compared with tholeiitic shield stage lavas from Mauna Kea, post-shield stage alkalic lavas from Mauna Kea have higher total iron content but lower SiO_2 content (Fig. 8a, b). This result was used to infer that these alkalic lavas were generated by lower extent of partial melting at higher pressure (e.g., Yang et al., 1996). Similarly, at Detroit Seamount, the alkalic lavas have higher FeO* and lower SiO_2 contents than tholeiitic lavas (Figs 8a, b). Hence, I infer that compared with tholeiitic lavas from Detroit Seamount, the alkalic lavas were generated by a lower degree of melting at higher pressure.

6.3.2 Sc

Sc is compatible in garnet and clinopyroxene (e.g., Irving and Frey 1978; Hart and Dunn, 1993; Blundy et al., 1995; 1998; van Westrenen et al., 1999). Hawaiian lavas have lower Sc abundance than MORB at a given MgO content (Frey et al., 1994; Fig. 11b). If the source of Hawaiian lavas has a Sc abundance similar to the source of MORB, the lower Sc abundances in Hawaiian shield lavas can be explained as a result of more residual garnet (Frey et al., 1994). At a certain MgO content, Detroit Seamount lavas have higher Sc abundance than Mauna Kea and Koolau lavas (Fig. 11b), which implies less residual garnet for Detroit Seamount lavas. This result is consistent with the hypothesis that Detroit Seamount lavas segregated at lower mean pressure than Hawaiian shield stage lavas.

The similar Sc abundance of alkalic and tholeiitic basalt (Fig. 11b) from Detroit Seamount is inconsistent with the inferred higher pressure of melt segregation for the alkalic basalt based on SiO_2 and total iron contents. However, Sc is an incompatible element during melting of peridotite; therefore, the unexpectedly high Sc abundance of the alkalic basalt may reflect the combination of a lower extent of melting and higher pressure of melt segregation. In fact, alkalic and tholeiitic basalt from Mauna Kea Volcano also have similar Sc abundances (see Fig. 5e of Huang and Frey, 2003).

6.3.3 Na_2O/TiO_2 and Tb/Yb

During mantle melting, the partition coefficient of sodium (as Na_2O) between clinopyroxene and melt increases with increasing pressure (e.g., Kinzler, 1997; Putirka, 1999; Longhi, 2002); that is, the proportion of jadeite component in clinopyroxene increases with increasing pressure. In contrast, the partition coefficient of titanium (as TiO_2) is not strongly dependent on pressure; it may decrease slightly with increasing pressure (e.g., Longhi, 2002). Therefore, the Na_2O/TiO_2 ratio yields information on the pressure of melt segregation with relatively lower Na_2O/TiO_2 ratio indicating higher mean pressure of melt segregation (e.g., Fig. 5 of Putirka, 1999). The ratio of Tb/Yb in a melt can also be used as an indicator for pressure of melt segregation because $(D_{Tb}/D_{Yb})^{garnet/melt} << (D_{Tb}/D_{Yb})^{clinopyroxene/melt}$ (e.g., van Westrenen et al., 1999). Hence, a higher proportion of residual garnet results in higher Tb/Yb ratio due to the compatibility of Yb in garnet.

Compared with EPR N-MORB, Mauna Kea lavas have lower Na_2O/TiO_2 but higher Tb/Yb ratios at a certain MgO content (Fig. 15). These differences in Na_2O/TiO_2 and Tb/Yb ratios show that relative to EPR N-MORB, Mauna Kea lavas segregated at a

higher pressure, although source heterogeneity in these ratios may also contribute to this difference. As indicated in Fig. 15, Na_2O/TiO_2 decreases and Tb/Yb increases from Site 884 tholeiitic lavas to Site 1203 tholeiitic lavas and Site 883 and 1204 alkalic lavas to Site 1203 alkalic lavas. Site 884 lavas are distinct and overlap with the low pressure end of the EPR N-MORB field. All other Detroit Seamount lavas overlap with the low Na_2O/TiO_2 and high Tb/Yb (relatively high pressure) end of the MORB field. This observation is consistent with the hypothesis that the mean pressure of melt segregation decreases from Mauna Kea lavas to Detroit Seamount lavas to MORB. The lower Na_2O/TiO_2 and higher Tb/Yb ratios in Site 1203 alkalic lavas relative to Site 1203 tholeiitic lavas indicate that the former segregated at higher pressure.

6.3.4 Summary

In summary, compositional indicators of mean pressure of melt segregation, such as Sc abundance and ratios of Na_2O/TiO_2 and Tb/Yb, show that tholeiitic lavas from Detroit Seamount are more similar to MORB than young Hawaiian shield lavas. This similarity to MORB is inferred to reflect segregation of Detroit Seamount lavas at low pressure beneath thin lithosphere. The extremes are expressed in Site 884 lavas (lowest pressure) and Site 1203 alkalic lavas (highest pressure).

6.4 Did Detroit Seamount Lavas Sample a Depleted MORB-Related Component or a Depleted Plume Component?

6.4.1 Controversy about the Origin of Detroit Seamount Lavas

Studies of lavas recovered from Site 883 and 884 during ODP Leg 145 have led to two different interpretations for the depleted component found in Detroit Seamount lavas. Keller et al. (2000) used age-corrected Sr-Nd-Pb isotopic ratios in Detroit

Seamount lavas, especially Site 884 lavas, to conclude that lavas forming Detroit Seamount are "indistinguishable from mid-ocean ridge basalt". Hence, they proposed that the Hawaiian plume interacted with young and hot lithosphere and "entrained enough of the isotopically depleted upper mantle to overwhelm the chemical characteristics of the plume itself". In contrast, using a high precision triple spike technique, Regelous et al. (2003) argued that the Pb isotopic compositions of Site 884 lavas are not similar to either EPR MORB or modern Hawaiian shield stage lavas (Fig. 6 of Regelous et al., 2003; Fig. 12b). They argued that the Site 884 lavas were derived from a depleted plume component that is not sampled by modern Hawaiian volcanoes. Based on Nd-Hf isotopic correlation, Kempton et al. (2002), Thompson et al. (2002) and Frey et al. (2005) also suggest that Detroit Seamount lavas sampled a depleted plume component. With additional data for lavas from Detroit Seamount, our objective is to evaluate these alternative hypotheses.

6.4.2 Constraints from Sr-Nd Isotopes

Age-corrected Sr and Nd isotopic ratios of basalt from 3 of the 4 drill sites on Detroit Seamount (Sites 883, 884 and 1204) overlap with the field calculated for 76 Ma EPR MORB (Fig. 12a). A new observation is that both tholeiitic (Site 884) and alkalic basalt (Sites 883 and 1204) overlap with the MORB field, but alkalic basalt has slightly higher $^{87}Sr/^{86}Sr$ and lower $^{143}Nd/^{144}Nd$ than tholeiitic basalt. The simplest interpretation is that a depleted MORB-like component, perhaps slightly heterogeneous in $^{87}Sr/^{86}Sr$ and $^{143}Nd/^{144}Nd$, was melted to various extents to form Detroit Seamount lavas.

6.4.3 Constraints from Pb Isotopes

In plots of Pb isotopic ratios, our new data for Sites 1203 and 1204 basalt confirm the observation by Regelous et al. (2003) that for a given $^{206}Pb/^{204}Pb$ ratio, most lavas

from Detroit Seamount have lower $^{207}Pb/^{204}Pb$ ratios than EPR MORB data obtained using the triple-spike technique (Fig. 12b). Regelous et al. (2003) noted that measured $^{207}Pb/^{204}Pb$ in Site 884 lavas, ranging from 15.43 to 15.46, are lower than data for most EPR MORB. Consequently, the difference in $^{207}Pb/^{204}Pb$ between Site 884 lavas and EPR MORB is not a result of an inaccurate age-correction. In addition, as emphasized by Regelous et al. (2003) the $^{206}Pb/^{204}Pb$ for lavas from Site 883 and 884 extend to considerably lower ratios (<18) than the EPR MORB field defined by data obtained using the triple-spike technique.

Is the field defined by triple-spike data representative of young Pacific MORB? In order to answer this question, I used the web database Pet DB (http://petdb.ldeo.columbia.edu/petdb/Default.htm). Three important results arise from assessing Pb isotopic ratios for the 996 samples (Fig. 16). (1) The EPR MORB field defined by data obtained by the triple-spike technique is representative of the Pacific MORB database, but it does not include the extremes. (2) Although the database for old Pacific MORB (distant from active spreading centers) is sparse, Pb isotopic ratios of such lavas are similar to young Pacific MORB (Fig. 16). (3) Pacific MORB with $^{206}Pb/^{204}Pb <$ 18 are very unusual. The majority of Pacific MORB with low $^{206}Pb/^{204}Pb$ (<18) erupted at a spreading center in the Garrett transform fault (Fig. 16). Wendt et al. (1999) proposed that Garrett transform fault lavas reflect two-stage melting of a MORB source; i.e., initial melting at the EPR axis followed by melting of the residue to generate the incompatible element-depleted Garrett transform fault lavas. Therefore, if the low $^{206}Pb/^{204}Pb$ (<18) component in Detroit Seamount lavas is a MORB-related component, as suggested by Keller et al. (2000), it is not typical Pacific MORB. Sampling of this atypical component

may occur only at high extents of melting, such as achieved in the two-stage melting scenario proposed for lavas erupted in the Garrett transform fault (Wendt et al., 1999), and when the Hawaiian plume was near a ridge axis, such as Detroit Seamount at ~80 Ma (Keller et al., 2000).

6.4.4 Constraints From Incompatible Element Abundance Ratios

In both MORB and Hawaiian tholeiitic basalt many incompatible trace element ratios are correlated with radiogenic isotopic ratios (e.g., Niu et al., 2002, Huang and Frey, 2003). Among Hawaiian shield lavas, La/Nb is positively correlated with $^{87}Sr/^{86}Sr$ and negatively correlated with $^{143}Nd/^{144}Nd$; Detroit Seamount tholeiites, like EPR MORB, define opposite correlations (Figs 17a, b). Obviously, Detroit Seamount lavas sampled a depleted, low $^{87}Sr/^{86}Sr$, $^{206}Pb/^{204}Pb$ and high $^{143}Nd/^{144}Nd$, La/Nb component that was not sampled by Hawaiian shield stage lavas. Is this depleted component similar to that sampled by Garrett transform fault lavas (Fig. 17), as argued on the basis of isotope compositions?

As discussed earlier, tholeiitic basalt from Site 884 has MORB-like incompatible element patterns (Fig. 10). There is, however, an important difference between Site 884 lavas and MORB. Relative to MORB, Hawaiian lavas have high Ba/Th (>100) (Hofmann and Jochum, 1996; Huang and Frey, 2003; Yang et al., 2003); such ratios are interpreted as characteristic of recycled oceanic lithosphere in the Hawaiian plume (Hofmann and Jochum, 1996; Huang et al., 2000; Sobolev et al., 2000). High Ba/Th ratios are also characteristic of Detroit Seamount glasses, and Site 884 glasses are at the high end of the Ba/Th range in Detroit Seamount lavas (85-113) (Fig. 17c). In contrast, Garrett transform fault lavas have low Ba/Th (35-57) which overlap with those of N-MORB (Wendt et al.,

1999; Fig. 17c). I therefore speculate that the depleted component sampled by Site 884 lavas has high Ba/Th (>100), and is unrelated to the low $^{87}Sr/^{86}Sr$ and $^{206}Pb/^{204}Pb$ source of Garrett transform fault lavas. Rather, it is an intrinsic component of the plume.

Young Hawaiian rejuvenated-stage lavas also contain a component with low $^{87}Sr/^{86}Sr$, $^{206}Pb/^{204}Pb$ and high $^{143}Nd/^{144}Nd$ and Ba/Th. Such lavas have relatively high incompatible trace element concentrations, and are thought to represent small degrees of melting of plume mantle mixed with melts of a depleted source (e.g. Yang et al. 2003). Frey et al. (2005) argue that the low $^{87}Sr/^{86}Sr$ component in these lavas is the same as that present in Detroit lavas, i.e. it is intrinsic to the plume, and is sampled during a later stage of melting of the Hawaiian plume that previously melted to produce the tholeiitic shields. If this interpretation is correct, it implies that the depleted component has been an integral part of the Hawaiian plume for at least 80 Ma.

6.4.5 Summary

1) I agree with Regelous et al. (2003) that the Pb isotopic data, especially $^{206}Pb/^{204}Pb$ (<18), for Detroit Seamount lavas reflect a depleted component that is not commonly present in either ancient or recent Pacific MORB. Such a component is present in lavas erupted from a spreading center in the Garrett transform fault. Therefore if the depleted component arises from a MORB source, it is only sampled under unusual conditions such as the two-stage melting proposed for Garrett transform fault lavas (Wendt et al., 1999) or the proximity of the Hawaiian plume to a ridge axis (Detroit Seamount).
2) The occurrence at Sites 883 and 1204 of alkalic lavas that have depleted isotopic characteristics shows that the depleted component is not restricted to

tholeiitic basalt. In the context of the Regelous et al. (2003) hypothesis the depleted plume component with a high solidus temperature was melted to varying extents.

3) High Ba/Th is a characteristic feature of Hawaiian lavas and even the most depleted lavas from Detroit Seamount have Ba/Th ratios exceeding those of MORB (Fig. 17c). Their high Ba/Th implies that their source is also characterized by high Ba/Th. Consequently, this source is unlike the source of Garrett transform fault lavas in terms of Ba/Th.

4) Support for the hypothesis of Regelous et al. (2003) that the depleted component is plume related arises from rejuvenated-stage Hawaiian lavas. Their Pb isotopic ratios also extend to low $^{206}Pb/^{204}Pb$ ratios (Fedicova and Abouchami, 2003; Frey et al., 2005), and they have high Ba/Th (Yang et al., 2003). Therefore a depleted plume component may be sampled by rejuvenated-stage lavas during a second stage of plume melting (Ribe and Christensen, 1999) and during ascent of the plume beneath young and thin oceanic lithosphere, i.e., at Detroit Seamount.

6.5 A hypothesis for the Geochemical and Age Differences between Lavas from Site 884 and Site 1203

The age of Site 884 lavas is ~81±1 Ma based on ^{40}Ar-^{39}Ar data for a reverse polarity, tholeiitic basalt (Keller et al., 1995). At Site 1203, Duncan and Keller (2004) obtained an average age of ~76±1 Ma for five normal polarity, tholeiitic lavas. Based on its large area (Fig. 1b), it is likely that Detroit Seamount consists of several coalesced shields, much like the Big Island of Hawaii. However, an age difference of 5 Myr

between Site 1203 and Site 884 is much larger than that for the five shields on the Big Island of Hawaii which all formed over the past 1 Myr. What is the explanation for an age difference of 5 Myr for tholeiitic lavas erupted at sites separated by only 48 km?

It is well-established that near-axis plumes interact with the spreading ridge axis. Using the Galapagos Platform as an analogy, plume-related volcanism in a near-ridge environment is more dispersed and long-lived (e.g., Sinton et al., 1996) than at an intraplate location, such as Hawaii. I propose a scenario that can explain both the old age of Site 884 lavas and their relatively shallow, MORB-like, melt segregation depths (Fig. 15). Sleep (2002) noted that "off-axis hot spots appear to shut off at the time that an on-axis hot spot becomes active along an axis-approaching track"; i.e., there is a time when volcanism ceases above the hotspot and partial melting of plume material does not occur until ascent at the spreading center (Fig. 18a). If the plate moved faster than the plume motion, at some later time the plume was overlain by plume-related lithosphere created at the spreading center (Fig. 18b). Perhaps at ~76 Ma, the Hawaiian plume was distant from the spreading center, and intra-plate volcanism represented by lavas from Site 883, 1203 and 1204 erupted in close proximity to older Site 884 lavas which erupted at the spreading center (Fig. 18c). Melting to a shallow depth at a spreading center for Site 884 lavas implies a large melting extent, and consequently Site 884 magmas sampled a depleted and refractory component with low $^{206}Pb/^{204}Pb$.

7. Conclusions:

Based on studies of drill cores from four drill sites at Detroit Seamount and the comparisons with EPR N-MORB and Mauna Kea lavas, our major conclusions are:

1. The rapid subsidence rates inferred for Detroit Seamount support the view that this seamount formed on young and thin oceanic lithosphere close to a spreading ridge axis. Also consistent with this inference, major and trace element compositions of Detroit Seamount lavas show that their parental magmas were segregated at a lower pressure than Hawaiian lavas which formed under old and thick oceanic lithosphere.
2. The upwards transition from intercalated alkalic and tholeiitic basalt to solely tholeiitic basalt at Site 1203 may reflect the pre-shield to shield stage transition, whereas alkalic basalts from Sites 883 and 1204 probably represent post-shield stage lavas. Like pre-shield stage alkalic Kilauea lavas, phlogopite appears to have played an important role in generating the pre-shield stage alkalic lavas at Site 1203. Also, similar to pre-shield stage Loihi lavas, Site 1203 alkalic lavas are characterized by high $^{208}Pb/^{204}Pb$ at a given $^{206}Pb/^{204}Pb$.
3. Both tholeiitic and alkalic Detroit Seamount lavas have lower concentrations of highly incompatible elements, lower $^{87}Sr/^{86}Sr$ and higher $^{143}Nd/^{144}Nd$ than the corresponding lava types from young Hawaiian volcanoes. Also Detroit Seamount lavas contain a component with unradiogenic Pb that is not present in Hawaiian shield stage lavas or EPR MORB. Such a component is present in lavas erupted from a spreading center within the Garrett transform fault. However, Site 884 lavas with the most depleted isotopic characteristics have high Ba/Th unlike those of MORB and Garrett transform fault

lavas. If the depleted component has high Ba/Th, it is plume-related. Hawaiian rejuvenated-stage lavas also have high Ba/Th and define a trend to low $^{87}Sr/^{86}Sr$ and $^{206}Pb/^{204}Pb$, similar to the trend of Detroit lavas (Fig. 12c). Rejuvenated-stage melts have been proposed as second-stage melts of the Hawaiian plume (Ribe and Christensen, 1999). Therefore this depleted component may be a refractory component of the plume that is only sampled at high degrees of melting, such as occurred at ~81 Ma when the plume was near a spreading center.

4. The surprisingly large age difference (~81 and 76 Ma) between lavas at two drill sites on Detroit Seamount may reflect the complexity of plume-related volcanism in a near ridge axis environment.

Reference

Abouchami, W., W., Galer, S. J. G., and Hofmann, A. W., High precision lead isotope systematics of lavas from the Hawaiian Scientific Drilling Project. Chem. Geol., 169, 187-209, 2000.

Adam, J., Green, T. H. and Sie, S. H., Proton microprobe determined partitioning of Rb, Sr, Ba, Y, Zr, Nb and Ta between experimentally produced amphiboles and silicate melts with variable F content, Chem. Geol., 109, 29-49, 1993.

Albarede, F., How deep do common basaltic magmas form and differentiate?, J. Geophys. Res., 97 (7), 10,997-11,009, 1992.

Bach, W., B. Peucker-Ehrenbrink, S. R. Hart, and J. S. Blusztajn, Geochemistry of hydrothermally altered oceanic crust: DSDP/ODP Hole 504B – Implications for seawater-crust exchange budgets and Sr- and Pb-isotopic evolution of the mantle, Geochem. Geophys. Geosyst., 4(3), 8904, doi:10.1029/2002GC000419, 2003.

Barrett T. J., Strontium and Lead-isotope composition of some basalts from Deep Sea Drilling Project Hole 504B, Costa Rica Rift, Legs 69 and 70, in Cann, J. R., Langseth, M. G., Honnorez, J, Von Herzen, R. P., White, S. M., et al., Init. Repts. DSDP, Washington (U.S. Govt. Printing Office), 69: 643-650, 1983.

Basaltic Volcanism Study Project, Basaltic Volcanism on the Terrestrial Planets. Pergamon Press, Inc., New York. 1286 pp. 1981.

Bass, M. N., Moberly, R., Rhodes, J. M., Shih, C. and Church, S. E., Volcanic rocks cored in the Central Pacific, Leg 17 Deep Sea Drilling Project, in Init. Repts. DSDP, Washington (U.S. Govt. Printing Office), 17: 429-504, 1973.

Blichert-Toft, J., D. Weis, C. Maerschalk, A. Agranier, and F. Albarède, Hawaiian hot spot dynamics as inferred from the Hf and Pb isotope evolution of Mauna Kea volcano, Geochem. Geophys. Geosyst., 4(2), 8704, doi:10.1029/2002GC000340, 2003.

Blundy, J. D., Falloon, T. J., Wood, B. J., Dalton, J. A., Sodium partitioning between clinopyroxene and silicate melts, J. Geophys. Res., 100 (8), 15,501-15,515, 1995.

Blundy, J. D., Robinson, J. A. C., and Wood, B. J., Heavy REE are compatible in clinopyroxene on the spinel lherzolite solidus. Earth Planet. Sci. Lett., 160, 493-504, 1998.

Bryce, J. G., DePaolo, D. J. and Lassiter, J. C., Sr, Nd and Os isotopes in a 2.84 km section of Mauna Kea Volcano: Implications for the geochemical structure of the Hawaiian plume, submitted to Geochem. Geophys. Geosyst.

Caplan-Auerbach, J., Duennebier, F., Ito, G., Origin of intraplate volcanoes from guyot heights and oceanic paleodepth, J. Geophys. Res., 105(2), 2679-2698, 2000.

Carmichael, I. S. E., Turner, F. J. and Verhoogen, F., Igneous Petrology, McGraw-Hill, New York, 1974.

Castillo, P. R., Carlson, R. W., Batiza, R., Origin of Nauru Basin igneous complex; Sr, Nd and Pb isotope and REE constraints, Earth Planet Sci Letts., 103(1-4), 200-213, 1991.

Castillo, P. R., Floyd, P. A. and France-Lanord, C., Isotope geochemistry of Leg 129 basalts: Implications for the origin of the widespread Cretaceous volcanic event in the Pacific, in Proc. Ocean Drill. Program, Sci. Results, 129, 405-513, 1992.

Castillo, P. R., Pringle, M. S., Carlson, R. W., East Mariana Basin tholeiites; Cretaceous intraplate basalts or rift basalts related to the Ontong Java plume?, Earth Planet Sci Letts., 123(1-4), 139-154, 1994.

Castillo, P. R., Natland, J. H., Niu, Y. and Lonsdale, P. F., Sr, Nd and Pb isotopic variation along the Pacific-Antarctic risecrest, 53-57 degrees S; implications for the composition and dynamics of the South Pacific upper mantle, Earth Planet Sci Letts., 154 (1-4), 109-125, 1998.

Castillo, P. R., E. Klein, J. Bender, C. Langmuir, S. Shirey, R. Batiza, and W. White, 2000. Petrology and Sr, Nd, and Pb isotope geochemistry of mid-ocean ridge basalt glasses from the 11°45′N to 15°00′N segment of the East Pacific Rise, Geochem. Geophys. Geosyst., 1, doi:10.1029/1999GC000024, 2000.

Chen, C.-Y. and Frey, F.A., Trace element and isotope geochemistry of lavas from Haleakala Volcano, East Maui: Implications for the origin of Hawaiian basalts, J. Geophys. Res., 90, B10, 8743-8768, 1985.

Clague, D. A. and Dalrymple, G. B., The Hawaiian-Emperor volcanic chain; Part I, Geologic evolution, in Volcanism in Hawaii, (eds, Decker, R. W., Wright, T. L. and Stauffer, P. H.) U. S. Geological Survey Professional Paper, P 1350, p. 5-73, 1987..

Class, C. and Goldstein, S. L., Plume-lithosphere interactions in the ocean basins; constraints from the source mineralogy, Earth Planet Sci Letts., 150 (3-4), 245-260, 1997.

Cottrell, R. D. and Tarduno, J. A., A Late cretaceous pole for the Pacific plate: implications for apparent and true polar wander and the drift of hotspots, Tectonphys. 362, 321-333, 2003.

Dalrymple, G. B., Lanphere, M. A., Clague, D. A., Conventional and $^{40}Ar/^{39}Ar$ K-Ar ages of volcanic rocks from Ojin (Site 430), Nintoku (Site 432), and Suiko (Site 433) seamounts and the chronology of volcanic propagation along the Hawaiian-Emperor

chain, in Jackson, E. D., Koizumi, I., et al. (eds), Initial Reports of the Deep Sea Drilling Project, 55, Washington, D.C.: U.S. Government Printing Office, 659-676, 1980.

DePaolo, D. J., Stolper, E. M., Thomas, D. M. and Garcia, M. O., Hawaii Scientific Drilling Project: Core logs and summarizing data, rep, Calif. Inst. of Technol., Pasadena, 1999.

Duncan, R. A., and Keller, R. A., Radiometric ages for basement rocks from the Emperor Seamounts, ODP Leg 197, Geochem. Geophys. Geosystems, 5, Q08L03, doi:10.1029/2004GC000704, 2004..

Eisele, J., Abouchami, W., Galer, S. J. G. and Hofmann, A. W., The 320 kyr Pb isotope evolution of Mauna Kea lavas recorded in the HSDP-2 drill core, Geochem. Geophys. Geosyst., 4(5), 8710, doi:10.1029/2002GC000339, 2003.

Fekiacova, Z. and Abouchami, W., Pb isotopic evolution of Koolau volcano (Oahu, Hawaii), Eos Trans. AGU, 84 (46) Fall Meet. Suppl., Abstract V32A-0991, F1557, 2003.

Foley, S. F., Taylor, W. R. and Green, D. H., The role of fluorine and oxygen fugacity in the genesis of the ultrapotassic rocks, Contrib. Mineral. Petrol., 94 (2), 183-192, 1986.

Foley, S. F., Jackson, S. E., Fryer, B. J., Greenough, J. D. and Jenner, G. A., Trace element partition coefficients for clinopyroxene and phlogopite in an alkaline lamprophyre from Newfoundland by LAM-ICP-MS, Geochim. Cosmochim. Acta., 60(4), 629-638, 1996.

Fornari, D. J., Perfit, M. R., Allan, J. F., Batiza, R., Haymon, R. M., Barone, A. M., Ryan, W. B. F., Terri, S., Simkin, T., Luckman, M. A., Geochemical and structural studies of the Lamont Seamounts; seamounts as indicators of mantle processes, Earth Planet. Sci. Lett., 89(1), 63-83, 1988.

Frey, F. A. and Roden, M. F., The mantle source for the Hawaiian Islands: Constraints from the lavas and ultramafic inclusions, in Mantle Metasomatism, 423-463, Academic Press, 1987.

Frey, F. A., Wise, W. S., Garcia, West, H., Kwon, S. T., and Kennedy, A., Evolution of Mauna Kea volcano, Hawaii: Petrologic and geochemical constraints on postshield volcanism, J. Geophys. Res., 95, 1271-1300, 1990.

Frey, F. A., Garcia, M. O., Wise, W. S., Kennedy, A., Gurriet, P., Albarede, F., The evolution of Mauna Kea volcano, Hawaii: Petrogenesis of tholeiitic and alkalic basalts, J. Geophys. Res., 96, 14,347-14,375, 1991.

Frey, F. A., Garcia, M. O., and Roden, M. F., Geochemical characteristics of Koolau Volcano: Implications of intershield geochemical differences among Hawaiian volcanoes. Geochim. Cosmochim. Acta., 58, 1441-1462, 1994.

Frey, F. A., Clague, D., Mahoney, J. J., Sinton, J. M., Volcanism at the edge of the Hawaiian plume; petrogenesis of submarine alkalic lavas from the North Arch volcanic field, Jour. Petrol., 41(5), 667-691, 2000.

Frey, F. A., Huang, S., Blichert-Toft, J., Regelous, M. and Boyet, M., Origin of Depleted Components in Lavas Related to the Hawaiian Hotspot: Evidence From Hf Isotope Data, Geochem. Geophys., Geosys, 6(2), doi:10.1029/2004GC000757, 2005.

Galer, S. J. G., Abouchami, W. and Macdougall, J. D., East Pacific Rise MORB through the Pb isotope looking-glass, Eos Trans. AGU, 80 Fall Meet. Suppl., F1086, 1999.

Garcia, M. O., Jorgenson, B. A., Mahoney, J. J., Ito E., and Irving, A. J., An evaluation of temporal geochemical evolution of Loihii summit lavas: Results from Alvin submersible dives. J. Geophys. Res. 98, 535-550, 1993.

Garcia, M. O., Foss, D. J. P., West, H. B. and Mahoney, J. J., Geochemical and isotopic evolution of Loihi Volcano, Hawaii, Journal of Petrology, 36, 1647-1644, 1995.

Garcia, M. O., Rubin, K. H., Norman, M. D., Rhodes, J. M., Graham, D. W., Muenow, D W., Spencer, K., Petrology and geochronology of basalt breccia from the 1996 earthquake swarm of Loihi Seamount, Hawaii; magmatic history of its 1996 eruption, Bulletin of Volcanology., 59, 577-592, 1998.

Green, T. H., Blundy, J. D., Adam, J. and Yaxley, G. M., SIMS determination of trace element partition coefficients between garnet, clinopyroxene and hydrous basaltic liquids at 2-7.5 GPa and 1080-1200°C, Lithos, 53, 165-187, 2000.

Haase, Karsten M., Geochemical constraints on magma sources and mixing processes in Easter Microplate MORB (SE Pacific); a case study of plume-ridge interaction, Chem. Geol., 182 (2-4), 335-355, 2002.

Hanan, B. B. and Schilling, J.-G., Easter Microplate evolution; Pb isotope evidence, J. Geophys. Res., 94(6), 7432-7448, 1989.

Hart, S. R. and Dunn, T., Experimental clinopyroxene/melt partitioning for 24 trace elements. Contrib. Mineral. Petrol., 113(1), 1-8, 1993.

Hickey-Vargas, R., Isotope characteristics of submarine lavas from the Philippine Sea; implications for the origin of arc and basin magmas of the Philippine tectonic plate, Earth Planet. Sci. Lett., 107(2), 290-304, 1991.

Hofmann, A. W. and White, W. M., Ba, Rb and Cs in the Earth's mantle, Z. Naturforssch 38a, 258-266, 1983.

Hofmann, A. W., Nb in Hawaiian magmas; constraints on source composition and evolution, Chem. Geol. 57, 17-30, 1986.

Hofmann, A. W., Chemical differentiation of the earth: the relationship between mantle, continental crust, and oceanic crust, Earth Planet. Sci. Lett. 90, 297-314, 1988.

Hofmann, A. W. and Jochum, K. P., Source characteristics derived from very incompatible trace elements in Mauna Loa and Mauna Kea basalts (Hawaiian Scientific Drilling Project), J. Geophys. Res. 101, 11,831-11,839, 1996.

Huang, S., Yang, H.-J. and Frey, F. A., Understanding the anomalous Ba/Th ratio in Hawaiian shield lavas, Eos Trans. AGU, 81(48) Fall Meet. Suppl., Abstract V11D-06, F1342, 2000.

Huang, S. and Frey, F. A., Trace element abundances of Mauna Kea basalt from Phase 2 of the Hawaiian Scientific Drilling Project: Petrogenetic implications of correlations with major element content and isotopic ratios, Geochem. Geophys., Geosys, 4(6), 8711, doi, 1029/2002 GC000322, 2003.

Huang, S. and Frey, F. A., Temporal geochemical variation within the Koolau shield: A trace element perspective, submitted.

Irving, A. F. and Frey F. A., Distribution of trace elements between garnet megacrysts and host volcanic liquids of kimberlitic to rhyolite composition, Geochim. Cosmochim. Acta., 42, 771-787, 1978.

Janney, P. E. and Castillo, P. R., Geochemistry of Mesozoic Pacific mid-ocean ridge basalt; constraints on melt generation and the evolution of the Pacific upper mantle, J. Geophys. Res., 102(3), 5207-5229, 1997.

Keller, R. A., Duncan, R. A., and Fisk, M. R., Geochemistry and $^{40}Ar/^{39}Ar$ geochronology of basalt from ODP Leg 45 (North Pacific Transect), in Rea, D. K., Basov, I. A., Scholl, D. W., Allan, J. A., (eds) Proceedings of the Ocean Drilling Program, Scientific Result, 145. College Station, TX: Ocean Drilling Program, 333-343, 1995.

Keller, R.A., Fish, M.R. and White, W.M., Isotopic evidence for Late Cretaceous plume-ridge interaction at the Hawaiian hotspot, Nature, 405, 673-676, 2000.

Kempton, P. D., Thompson, P. M. E. and Saunders, A. D., Did the ancestral Hawaiian plume interact with a mid-ocean ridge? The isotopic evidence. Geochim. Cosmochim. Acta., 66(15A): A392-A392 Suppl. 2002.

Kinman, W. S. and Neal, C. R., The influence of MORB on a plume-generated seamount: The story told by plagioclase phenocrysts from Detroit Seamount lavas, Emperor

Seamount Chain, EOS. Trans. AGU, 83(47), Fall Meet. Suppl., Abstract T61C-10, F1283, 2002.

Kinzler, R. J., Melting of mantle peridotite at pressures approaching the spinel to garnet transition; application to mid-ocean ridge basalt petrogenesis, J. Geophys. Res., 102 (1), 853-874, 1997.

Kirkpatrick, R.J., Clague, D., and Freisen, W., Petrology and geochemistry of volcanic rocks, DSDP Leg 55, Emperor Seamount Chain, in: Jackson, E.D., Kosumi, I. et al. (eds.), Initial Reports of the Deep Sea Drilling Project, 55, Washington, D.C.: U.S. Government Printing Office, 509-557, 1980.

Langmuir , C. H., Klein, E. M. and Plank, T., Petrological systematics of mid-ocean ridge basalt: Constraints on melt generation beneath ocean ridges, in Mantle Flow and Melt Generation at Mid-Ocean Ridges, Geophysical Monograph, 128, 71, 183-280, 1992.

Lanphere, M.A., Dalrymple, G.B. and Clague, D.A., Rb-Sr systematics of basalts from the Hawaiian-Emperor volcanic chain, in: Jackson, E.D., Kosumi, I. et al. (eds.), Initial Reports of the Deep Sea Drilling Project, 55, Washington, D.C.: U.S. Government Printing Office, 695-706, 1980.

Lassiter, J. C., DePaolo, D. J., and Tatsumoto, M., Isotopic evolution of Mauna Kea volcano: Results from the initial phase of the Hawaiian Scientific Drilling Project. J. Geophys. Res. 101, 11,769-11,780, 1996.

Lassiter, J. C. and Hauri, E. H., Osmium-iosotope variations in Hawaiian lavas: Evidence for recycled oceanic lithosphere in the Hawaiian plume. Earth Planet Sci Letts., 164, 483-496, 1998.

Lassiter, J. C., Hauri, E. H., Reiners, P. W., Garcia, M. O., Generation of Hawaiian post-erosional lavas by melting of a mixed lherzolite/pyroxenite source, Earth Planet Sci Letts., 178(3-4), 269-284, 2000.

LaTourrett, T., Hervig, R. L. and Holloway, J. R., Trace element partitioning between amphibole, phlogopite, and basanite melt, Earth Planet Sci Letts., 135, 13-30, 1995.

Li, X., Kind, R., Yuan, X., Wölbern I. and Hanka, W., Rejuvenation of the lithosphere by the Hawaiian plume, Nature 427, 827-829 doi:10.1038/nature02349, 2004.

Lipman, P. W., Sisson, T. W., Ui, T., Naka, J. and Smith, D. K., Ancestral submarine growth of kilauea volcano and instability of its South flank, in Hawaiian Volcanoes: Deep underwater perspectives (eds. Takahashi, E., Lipman, P.W. Garcia, M. O., Naka, J and Aramaki, S.), Geophysical Monograph, 128, 161-192, 2002.

Longerich, H. P., Jackson, S. E. and Günther, D., Laser ablation inductively coupled plasma mass spectrometric transient signal data acquisition and analyte concentration calculation, Journal of Atomic Analytical Spectrometry 11, 899-904, 1996.

Longhi, J., Some phase equilibrium systematics of lherzolite melting: I, Geochem. Geophys. Geosyst., 3(3), 1020, doi:10.1029/2001GC000204, 2002.

Lonsdale, P., Paleogene history of the Kula Plate: offshore evidence and onshore implications, Geological Society of America Bulletin, 100, 733-754, 1988.

Lonsdale, P., Dieu, J. and Natland, J., Posterosional volcanism in the Cretaceous part of the Hawaiian hotspot trail, J. Geophys. Res., 98, 4081-4898, 1993.

Macdonald, G. A. and Katsura, T., Chemical composition of Hawaiian lavas, Journ. Petrol., 5(1), 82-133, 1964.

Mammerickx, J. and Sharman, G. F., Tectonic evolution of the North Pacific during the Cretaceous Quiet Period, J. Geophys. Res., 93, 3009-3024, 1988.

Mengel, K. and Green, D. H., Stability of amphibole and phlogopite in metasomatized peridotite under water-saturated and water-undersaturated conditions, in Proceedings of the fourth international kimberlite conference (eds, Ross, J., Jaques, A. L., Ferguson, J., Green, D. H., O'Reilly, Danchin, R. V., Janse, A. J. A.), 1, 571-581, 1986.

Moore, J. G., Subsidence of the Hawaiian Ridge, in Decker, R.W., Wright, T.L., and Stauffer, P.H., eds., Volcanism in Hawaii: U.S. Geological Survey Professional Paper 1350, II, 85-100, 1987.

Mueller, R. D., Roest, W. R., Royer, J.-Y., Gahagan, L. M., Sclater, J. G., Digital isochrons of the world's ocean floor, J. Geophys. Res., 102 (2), 3211-3214, 1997.

Niu, Y. and Batiza, R., Trace element evidence from seamounts for recycled oceanic crust in the eastern Pacific mantle, Earth Planet. Sci. Lett., 148(3-4), 471-483, 1997.

Niu, Y., Collerson, K. D., Batiza, R., Wendt, J. I., Regelous, M., Origin of enriched-type mid-ocean ridge basalt at ridges far from mantle plumes; the East Pacific Rise at 11 degrees 20'N, J. Geophys. Res., 104(4), 7067-7087, 1999.

Niu, Y., Regelous, M., Wendt, I. J., Batiza, R., O'Hara, M. J., Geochemistry of near-EPR seamounts; importance of source vs. process and the origin of enriched mantle component, Earth Planet. Sci. Lett., 199(3-4), 327-345, 2002.

Norman, M. D. and Garcia, M. O., Primitive magmas and source characteristics of the Hawaiian Plume; petrology and geochemistry of shield picrites, Earth Planet. Sci. Lett., 168 (1-2), 27-44, 1999.

Parsons, B. and Sclater, J. G., An analysis of the variation of ocean floor bathymetry and heat flow with age, J. Geophys. Res., 82(5), 803-827, 1977.

Paster, T. P., Schauwecker, D. S., Haskin, L. A., The behavior of some trace elements during solidification of the Skaergaard layered series, Geochim. Cosmochim. Acta., 38 (10), 1549-1577, 1974.

Putirka, K., Melting depths and mantle heterogeneity beneath Hawaii and the East Pacific Rise; constraints from Na/Ti and rare earth element ratios, J. Geophys. Res., 104(2), 2817-2829, 1999.

Rea, D. K. and Dixon, J. M., Late Cretaceous and Paleogene tectonic evolution of the North Pacific Ocean, Earth Planet. Sci. Lett., 65, 145-166, 1983.

Regelous, M., Niu, Y., Wendt, J. I., Batiza, R., Greig, A., Collerson, K. D., Variations in the geochemistry of magmatism on the East Pacific Rise at 10 degrees 30'N since 800 ka, Earth Planet. Sci. Lett., 168(1-2), 45-63, 1999.

Regelous, M., Hofmann, A.W., Abouchami, W. and Galer, S.J.G., Geochemistry of lavas from the Emperor Seamounts, and the geochemical evolution of Hawaiian magmatism from 85 to 42 Ma. Journ. Petrol., 44, 113-140, 2003.

Rhodes J.M. and LockwooMauna J.P., Loa Revealed, Geophysical Monograph Series, vol. 92, AGU, Washington, D.C., 1995.

Rhodes, J. M., Geochemical stratigraphy of lava flows sampled by the Hawaii Scientific Drilling Project, J. Geophys. Res., 101, 11,729-11,746, 1996.

Rhodes, J. M., and M. J. Vollinger, Composition of basaltic lavas sampled by phase-2 of the Hawaii Scientific Drilling Project: Geochemical stratigraphy and magma types, Geochem. Geophys. Geosyst., 5, Q03G13, doi:10.1029/2002GC000434, 2004.

Ribe, N. M. and Christensen, U. R., The dynamical origin of Hawaiian volcanism, Earth Planet. Sci. Lett., 171(4), 517-531, 1999.

Roden, M. F., Frey, F. A., Clague, D. A., Geochemistry of tholeiitic and alkalic lavas from the Koolau Range, Oahu, Hawaii; implications for Hawaiian volcanism, Earth Planet. Sci. Lett., 69(1), 141-158, 1984.

Roden, M. F., Trull, T., Hart, S. R., and Frey, F. A., New He, Sr, Nd and Pb isotopic constraints on the constitution of the Hawaiian plume: Results from Koolau Volcano, Oahu, Hawaii. Geochim. Cosmochim. Acta., 58, 1431-1440, 1994.

Schmidt, K. H., Bottazzi, P., Vannucci, R. and Mengel, K., Trace element partitioning between phlogopite, clinopyroxene and leucite lamproite melt, Earth Planet Sci Letts., 168, 287-299, 1999.

Schmitz, M. D. and Bowring, S. A., Ultrahigh-temperature metamorphism in the lower crust during Neoarchean Ventersdorp rifting and magmatism, Kaapvaal Craton, southern Africa: Geological Society of America Bulletin, 115: 533-548, 2003

Sharp, W. D., and Clague, D. A., An older, slower Hawaii-Emperor bend, EOS. Trans. AGU, 83(47), Fall Meet. Suppl., Abstract T61C-04, F1282, 2002.

Shipboard Scientific Party, Site 884, in Rea, Basov, Janecek, Palmer-Julson, et al., Proc. ODP, Init. Repts., 145, Ocean Drilling Program, Texas A&M University, College Station TX 77845-9547, USA, 1993.

Shipboard Scientific Party, Site 1203, in Tarduno, J. A., Duncan, R. A., School, D. W., et al., Proc. ODP, Init. Repts, 197, 1-171 [CD-ROM]. Available from: Ocean Drilling Program, Texas A&M University, College Station TX 77845-9547, USA, 2002.

Shipboard Scientific Party, Site 1204, in Tarduno, J. A., Duncan, R. A., School, D. W., et al., Proc. ODP, Init. Repts, 197, 1-125 [CD-ROM]. Available from: Ocean Drilling Program, Texas A&M University, College Station TX 77845-9547, USA, 2002.

Sinton, C. W., Christie, D. M., Duncan, R. A., Geochronology of Galapagos seamounts, J. Geophys. Res., 101 (6), 13,689-13,700, 1996.

Sisson, T., Lipman, P. W. and Naka, J., Submarine alkalic through tholeiitic shield-stage development of Kilauea volcano, in Hawaiian Volcanoes: Deep underwater perspectives (eds. Takahashi, E., Lipman, P.W. Garcia, M. O., Naka, J and Aramaki, S.), Geophysical Monograph, 128, 193-220, 2002.

Sleep, N. H., Ridge-crossing mantle plumes and gaps in tracks, Geochem. Geophys. Geosyst., 3(12), 8505, doi:10.1029/2001GC000290, 2002.

Sobolev, A.V., Hofmann, A.W., and Nikogosian, I. K., Recycled oceanic crust observed in ghost plagioclase within the source of Mauna Loa lavas, Nature 404, 986-990, 2000.

Staudigel, H., Davies, G.R., Hart, S.R., Marchant, K.M. and Smith, B.M., Large scale isotopic Sr, Nd and O isotopic anatomy of altered oceanic crust: DSDP/ODP sites 417/418, Earth Planet. Sci. Lett., 130, 169-185, 1995.

Stein, C. A. and Stein, S., A model for the global variation in oceanic depth and heat flow with lithospheric age, Nature 359(6391), 123-129, 1992.

Stille, P., Unruh, D. M., Tatsumoto, M., Pb, Sr, Nd and Hf isotopic evidence of multiple sources for Oahu, Hawaii basalts, Nature, 304(5921), 25-29, 1983.

Stolper, E., Sherman, S., Garcia, M., Baker, M. and Seaman, C., Glass in the submarine section of the HSDP2 drill core, Hilo, Hawaii, Geochem. Geophys. Geosys., 5, Q07G15, doi:10.1029/2003GC000553, 2004.

Sturm, M. E., Klein, E. M., Graham, D. W., Karsten, J., Age constraints on crustal recycling to the mantle beneath the southern Chile Ridge; He-Pb-Sr-Nd isotope systematics, J. Geophys. Res., 104(3), 5097-5114, 1999.

Sun, S.-S. and McDonough, W. F., Chemical and isotopic systematics of oceanic basalts: implications for mantle composition and processes. In Magmatism in the Ocean Basins, Vol. 42 (ed. A. D. Saunders and M. J. Norry), 313-345, 1989.

Tarduno, J. A., Duncan, R. A., School, D. W., et al., Proc. ODP, Init. Repts, 197, 1-171 [CD-ROM]. Available from: Ocean Drilling Program, Texas A&M University, College Station TX 77845-9547, USA, 2002.

Tarduno, J. A., Duncan, R. A., Scholl, D. W., Cottrell, R. D., Steinberger, B., Thordarson, T., Kerr, B. C., Neal, C. R., Frey, F. A., Torii, M., Carvallo, C., The Emperor Seamounts; southward motion of the Hawaiian Hotspot plume in Earth's mantle, Science, 301 (5636), 1064-1069, 2003.

Tatsumoto, M., Hegner, E., Unruh, D. M., Origin of the West Maui volcanic rocks inferred from Pb, Sr, and Nd isotopes and a multicomponent model for oceanic basalt, in Decker, R.W., Wright, T.L., and Stauffer, P.H., eds., Volcanism in Hawaii: U.S. Geological Survey Professional Paper 1350, II, 723-744, 1987.

Thompson, P. M. E., Kempton, P. D., Saunders, A. D., The 48 Ma Koko Guyot: Early indications of temporal changes in the composition of the Hawaiian plume, EOS. Trans. AGU, 83(47), Fall Meet. Suppl., Abstract T61C-09, F1283, 2002.

Thordarson, T. et al., Physical volcanology of the Leg 197 basement sections: A synthesis of volcanism at Detroit, Nintoku, and Koko seamounts and comparison with present day activity at the Big Island of Hawaii, in prep.

van Westrenen, W., Blundy, J., and Wood, B., Crystal-chemical controls on trace element partitioning between garnet and anhydrous silicate melt. Am. Mineral., 84, 838-847, 1999.

Villemant, B., Jaffrezic, H., Joron, J.-L. and Treuil, M., Distribution coefficients of major and trace elements; fractional crystallization in the alkali basalt series of Chaine des Puys (Massif Central, France), Geochim. Cosmochim. Acta., 45, 1997-2016, 1981.

Walter, M. J., Melting of garnet peridotite and the origin of komatiite and depleted lithosphere, Jour. Petrol., 39(1), 29-60, 1998.

Wendt, J. I., Regelous, M., Niu, Y., Hekinian, R. and Collerson, K. D., Geochemistry of lavas from the Garrett Transform Fault: insights into mantle heterogeneity beneath the eastern Pacific, Earth Planet. Sci. Lett., 173, 271-284, 1999.

White, W. M., Hofmann, A. W. and Puchelt, H., Isotope geochemistry of Pacific mid-ocean ridge basalt, J. Geophys. Res., 92, 4881-4893, 1987.

Wilson, J. T., A possible origin of the Hawaiian Islands, Can. J. Phys., 21, 863-870, 1963.

Yang, H.-J., Frey, F. A., Rhodes, J. M., and Garcia, M. O., Evolution of Mauna Kea volcano: Inferences from lava compositions recovered in the Hawaii Scientific Drilling Project, J. Geophys. Res. 101, 11,747-11,767, 1996

Yang, H.-J., Frey, F. A. and Clague, D. A., Constraints on the source components of lavas forming the Hawaiian North Arch and Honolulu Volcanoes, J. Petrol., 44, 603-627, 2003.

Figure Caption:

Fig. 1a. The Hawaii-Emperor Seamount Chain and the location of Detroit Seamount. Modified from Tarduno et al. (2003) by adding new ^{40}Ar-^{39}Ar ages for Detroit Seamount, Nintoku Seamount and Koko Seamount from Duncan and Keller (2004), and for Suiko Seamount from Sharp and Clague (2002). Magnetic-anomaly identifications are following Mueller et al. (1997).

Fig. 1b. Bathymetry of Detroit Seamount and drillsite locations. Detroit Seamount refers to the region north of the red dashed line. Also shown is the outline of the Big Island of Hawaii (thick green line).

Fig. 2. Stratigraphy of basement core at Holes 1203A, 1204A and 1204B. Unit boundaries, rock types, presence of glass and phenocryst abundance are indicated. Modified from Tarduno, Duncan, Scholl, et al. (2002).

Fig. 3. Inferred volcanic environment of four drillsites at Detroit Seamount. Modified from Thordarson et al. (in prep.). See text for details.

Fig 4a-c. Sr-Nd-Pb isotopic ratios and parent/daughter ratios in samples from different leaching steps. See **Section 4.3** text for details. The important result is that these isotopic and parent/daughter ratios are relatively constant after three acid leaching steps. The isotope data reported in Table 4 were obtained on rock powders that were subjected to 6-9 leaching steps.

Fig. 5. Na_2O+K_2O versus SiO_2 (all in wt%)

The broken line shows the alkalic-tholeiitic boundary of Macdonald and Katsura (1964), using the equation: total alkalis = $0.37SiO_2$–14.43 (Carmichael et al., 1974). The

Macdonald-Katsura line is based on data for total iron measured as FeO and Fe_2O_3; consequently, for our analyses total iron is assumed to be 10% Fe^{3+} and 90% Fe^{2+}.

a. Whole-rock data.

All the Detroit Seamount lavas with low L.O.I. (<2%) are within the tholeiitic field, and those with high L.O.I. (>2%) range from tholeiitic to alkalic basalt. See text for details. Shown for comparison is the field (shaded) for late shield to post shield stage lavas from Mauna Kea (Frey et al., 1990, 1991). Whole rock field for Sites 883 and 884 are from Regelous et al. (2003).

b. Glass data.

Compositions of unaltered glasses (Table 3b) clearly show that all lavas from Sites 883 and 1204 are alkalic basalt, whereas lavas from Site 884 are tholeiitic. Glasses are available in several units (Units 1, 3, 8, 18 and 20) at Site 1203, and they are also tholeiitic. Detroit Seamount glass data are from this study and Thordarson et al. (in prep.).

c. Whole rock-glass pairs from submarine lava flow units at Site 1203.

Except for the three samples from Unit 20, which are highly altered (L.O.I. ranges from 5-11%), the other whole rock samples (three highly altered and three moderately altered) are within the tholeiitic field. As discussed in the text, I classify Unit 20 as a tholeiitic unit (see Panel b), and conclude that the high total alkali contents in Unit 20 whole-rocks are a result of alteration.

d. The subaerial lava flows Units 23, 26, 29 and 30 at Site 1203 are highly altered (L.O.I. > 2%), and are within alkalic field or straddle the alkalic-tholeiitic boundary line. No

unaltered glass is available from these units; however, based on their high abundances of incompatible elements, they are classified as alkalic basalt (see text).

Fig. 6. Th (ppm) vs **a.** K_2O (wt. %); **b.** Rb (ppm); **c.** P_2O_5 (wt. %); **d.** Ba (ppm) in glasses and whole rocks.

Fig. 7. Highly incompatible element ratios: Ce/Pb and Ba/Th. Blue diamond: whole rock data. Pink square: glass data. Site 883 and 884 data are normalized using the BHVO standard values reported in Regelous et al. (2003) and Huang and Frey (2003). The pink fields show the glass range. Data for primitive mantle (Hofmann, 1988; Sun and McDonough, 1989), average oceanic basalt (Hofmann, 1986), Garrett transform fault lavas (Wendt et al., 1999) and Mauna Kea shield lavas (Huang and Frey, 2003) are shown for comparison.

Fig. 8. MgO content vs other oxide contents (all in wt.%). For each element, there are two panels: whole rock data and glass data. Only samples with L.O.I. less than 7% are plotted. Whole rock data are plotted after converting Fe_2O_3 to FeO.

Data sources are: Detroit Seamount whole rocks (Sites 1203 and 1203: this study; Sites 883 and 884: Regelous et al., 2003); Detroit Seamount glasses (this study and Thordarson et al., in prep.); EPR N-MORB whole rock (downloaded data from PET DB); EPR N-MORB glass (Niu and Batiza, 1997, Niu et al., 1999; Regelous et al., 1999); Loihi glass (Garcia et al., 1993, 1995, 1998); Mauna Kea whole rock (Rhodes, 1996; Rhodes and Vollinger, 2004) and Mauna Kea glass (Stolper et al., 2004). In the SiO_2 panels the Mauna Kea fields are divided into Low and High SiO_2 groups; these groups are combined in other panels.

Fig. 9. Th abundance (in ppm) vs selected incompatible element abundances (in ppm or %). For each element, there are two panels: whole rock data and glass data. Only samples with L.O.I. less than 7% are plotted. Whole rock trace element abundances have been adjusted using: plotted value = measured value/(1-L.O.I.). Whole rock fields are shown in glass panels for comparison. Site 883 and 884 whole rock data are from Regelous et al. (2003).

Fig. 10. Primitive mantle normalized incompatible element abundances for lavas from Detroit Seamount. **a.** Alkalic lavas; **b.** Tholeiitic lavas. In order to minimize the effect of crystal fractionation, only lavas with 6% < MgO < 9% are plotted, except for Site 883 glass samples whose MgO contents are ~ 5.8%. Both glass and whole rock data are plotted. In each group, glass data overlap with whole rock data.

Mauna Kea data are from Huang and Frey (2003). Primitive mantle values are from Hofmann (1988). Average N-MORB data are from Hofmann (1988) and Sun and McDonough (1989).

Fig. 11. MgO content (in wt %) vs Ni and Sc abundances (in ppm). For each element, there are two panels: whole rock data and glass data. Only samples with L.O.I. less than 7% are plotted. Whole rock fields are shown in glass panels for comparison. As shown, three samples contain large proportion of olivine phenocryst (>15 vol. %), and the positive trend in the **panel a** is a result of olivine addition.

See Fig 8 caption for other data sources. Koolau data are from Frey et al. (1994).

Fig 12a. Sr-Nd isotopic ratios for Detroit Seamount lavas.

12b. Pb-Pb isotopic ratios for Detroit Seamount lavas.

12c. $^{206}Pb/^{204}Pb$ vs $^{87}Sr/^{86}Sr$ for Detroit Seamount lavas.

For comparison, fields are shown for EPR MORB, Garrett transform fault lavas, two extreme Hawaiian shields (Mauna Kea and Koolau) and Hawaiian rejuvenated stage lavas.

All data points and fields have been age-corrected to 76 Ma, except for Site 884 lavas which have been age-corrected to 81 Ma. A 2-sigma error bar is indicated unless the symbol is larger than the error bar. For the relatively young Hawaiian shield stage lavas and EPR MORB, parent/daughter ratios for age corrections should be those of the magma source. As a crude estimate of these ratios for tholeiitic basalt, I use average parent/daughter ratios in unaltered lavas (see table below). For the Sr and Pb isotopic systems, this approach leads to over-estimates for the age correction and for the Nd isotopic system, the age corrections are under-estimates. Parent/daughter ratios in Koolau and Mauna Kea lavas are average values of relatively unaltered samples (K_2O/P_2O_5 > 1.3) from Frey et al. (1994) and Huang and Frey (2003). Parent/ daughter ratios in Mauna Loa are average values of relatively unaltered samples (K_2O/P_2O_5 > 1.3) from Hofmann and Jochum (1996). Parent/daughter ratios in EPR-MORB are average N-MORB values from Sun and McDonough (1989). Parent/daughter ratios in Garrett transform fault lavas are average values of lavas with $^{206}Pb/^{204}Pb$ < 18 (Wendt et al., 1999). Because rejuvenated-stage and North Arch alkalic basalt were formed by low extents of melting (e.g., Yang et al., 2003) which may lead to significant changes in parent/daughter ratios, I used two sets of parent/daughter ratios for Hawaiian Rejuvenated Stage lavas: N-MORB values for the orange solid line, and Mauna Kea values for the black dash line.

Parent/daughter ratios are:

	Koolau	Mauna Kea	Mauna Loa	Loihi	EPR-MORB	GTF*
Rb/Sr	0.015	0.021	--	--	0.0062	0.0040
Sm/Nd	0.26	0.27	--	--	0.36	0.39
Th/Pb	0.52	0.97	0.55	0.80	0.40	0.22
U/Pb	0.15	0.31	0.17	0.27	0.16	0.15

*: Garrett transform fault lavas

Our selection of U/Pb and Th/Pb ratios in EPR MORB results in $^{238}U/^{204}Pb$ and $^{232}Th/^{204}Pb$ values of 10 and 26, respectively, which are about 2 times the values used by Regelous et al. (2003).

Data sources: Koolau (Roden et al., 1994; Lassiter and Hauri, 1998); Mauna Kea (Bryce et al., submitted; Lassiter et al., 1996; Abouchami et al., 2000; Eisele et al., 2003); Mauna Loa (Abouchami et al., 2000); Loihi (Garcia et al., 1993, 1995, 1998; Norman and Garcia, 1999); EPR MORB (Niu et al., 1999; Regelous et al., 1999; Castillo et al., 2000); Hawaiian rejuvenated stage and North Arch lavas (Stille et al., 1983; Roden et al., 1984; Tatsumoto et al., 1987; Chen and Frey, 1985; Lassiter et al., 2000; Frey et al., 2000); Garrett transform fault lavas (Wendt et al., 1999); Site 883 and 884 lavas (Keller et al., 2000; Regelous et al., 2003); EPR MORB fields in Pb-Pb plots are taken from Regelous et al. (2003).

Fig. 13. $(Sr/Nd)_{PM}$ vs Eu/Eu* for Detroit Seamount lavas (whole rocks). Eu/Eu* = $2*[Eu]_{PM}/([Gd]_{PM}+[Sm]_{PM})$. Subscript PM indicates normalization to primitive mantle values from Sun and McDonough (1989). These ratios are sensitive to plagioclase fractionation, and the range from >1 to <1 indicates accumulation and loss of plagioclase, respectively. Because Gd abundance for glasses are not reported, glasses are not

included. The labeled units with high $(Sr/Nd)_{PM}$ also have anomalously high Al_2O_3 (Fig. 8c).

Fig. 14 Schematic diagram showing melting column length for EPR MORB, Detroit Seamount and Mauna Kea, i.e., the depth interval from onset of melting to the lithosphere. The mean pressure of melt segregation increases from MORB to Detroit Seamount lavas to Mauna Kea lavas.

Fig. 15 a. MgO vs. Na_2O/TiO_2 and **b.** Tb/Yb. Both whole rock and glass data from Detroit Seamount are plotted. See Figs 8 and 10 caption for data sources.

Fig. 16 Pb isotopic plots for Pacific MORB. Data are downloaded from PeT DB. The red field with dots is the EPR MORB field defined by data obtained using the triple-spike technique (Galer et al., 1999). The low $^{206}Pb/^{204}Pb$ (<18) end of the Pacific MORB field is defined by Garrett transform fault lavas (Wendt et al., 1999). Pacific MORB with $^{206}Pb/^{204}Pb < 18$ are also reported in Barrett (1983), White et al. (1987), Fornari et al. (1988), Hanan and Schilling (1989), Castillo et al. (1998), Sturm et al. (1999) and Haase (2002). Old Pacific MORB are shown for comparison, and they do not differ from young Pacific MORB. Data sources: Bass et al., 1973; Hickey-Vargas, 1991; Castillo et al., 1991; 1992; 1994; Janney and Castillo, 1997.

Fig. 17a, b La/Nb vs $^{87}Sr/^{86}Sr$ and $^{143}Nd/^{144}Nd$ for Detroit Seamount lavas (whole rocks). Unit 31, a plagioclase-rich unit (Table 2), at Site 1203 has high La/Nb ratio, which has been confirmed by three ICP-MS analyses (1.06, 1.07 and 1.10). Note that Hawaiian shield lavas and Detroit Seamount lavas define opposing slopes in the Sr and Nd panels.

Fig. 17c La/Nb vs Ba/Th for Detroit Seamount glasses. Only Detroit Seamount glass data are plotted to avoid the alteration effect on whole rock Ba data. The important point is that in this panel, Site 884 data do not overlap with the EPR MORB field.

Data sources: Koolau: Frey et al., 1994; Roden et al., 1994; Lassiter and Hauri, 1998; Huang and Frey, submitted; Mauna Kea: Bryce et al., submitted; Eisele et al., 2003; Huang and Frey, 2003; Garrett transform fault: Wendt et al., 1999; EPR N-MORB: Niu et al., 1999; Regelous et al., 1999. The fields for Hawaiian shields are from Huang and Frey (2003).

Fig. 18. Plume-ridge interactions (adapted from Sleep, 2002). Panel **a.** shows that when a plume is near a ridge axis, the plume material flows toward the ridge axis where it melts upon ascent. This scenario may be appropriate for 81 Ma lavas at Site 884. Panel **b.** shows the situation where both the plume and lithospheric plate are moving in the same direction, but the plate is migrating faster than the plume. In this case, panel **c.** shows that eventually plume-related magmas and lithosphere created at the ridge axis (panel **a.**) may override the plume and young (76 Ma lavas at Site 1203) lavas may erupt in proximity to old (81 Ma) lavas.

Table 1. Sampling of Detroit Seamount

Hole	Penetration into basement (m)	basement recovery (%)
883E	37.8	63
883F	26.7	41
884E	87	76
1203A	452.6	56.5
1204A	60.8*	52*
1204B	140.5	37.9

*: The penetration of basement was 60.8 m at Hole 1204A. However, there was no recovery in the lower 22.4 m due to a clogged bit. The basement recovery is based on the upper 38.4 m. See shipboard Scientific Party, Site 1204 for details.

Table 2a. Whole Rock Sample Info.

Sample Name	UNIT	UNIT NAME[1]	Basalt Type[2]	Lava flow type[1]	Unit thickness (m)[1]	depth (mbsf)[1]	Phenocryst (%)[3]		
							PLAG	OL	CPX
1203A 17R4W 43-47	1	Highly Plagioclase-Olivine-Phyric Basalt	Tholeiitic	pillow lava	7.95	457.99	10	4	0
1203A 18R3W 116-119	3	Highly Plagioclase-Olivine-Phyric Basalt	Tholeiitic	pillow lava	24.60	467.96	10	3	1[4]
1203A 20R3W 10-14	3			pillow lava		486.1	9	4	9
1203A 25R1W 37-41	5	Moderately Plagioclase-Olivine-Phyric Basalt	Tholeiitic	sheet lobe	1.94	531.47	0	0	0
1203A 26R2W 5-9	6	Sparsely Plagioclase-Phyric Basalt	Tholeiitic	sheet lobe	4.78	535.84	0	0	0
1203A 26R3W 97-101	6			sheet lobe		537.4	0	0	0
1203A 30R1W 108-112	8	Highly Plagioclase-Olivine-Phyric Basalt	Tholeiitic	pillow lava	18.70	570.88	2	0.5	0
1203A 31R1W 46-50	8			pillow lava		579.86	5	1	0
1203A 32R2W 32-36	11	Plagioclase-Olivine-Phyric Basalt	Tholeiitic	sheet lobe	4.58	590.6	2	2	0
1203A 32R3W 58-62	11			sheet lobe		592.36	25	35	5
1203A 32R4W 76-80	11			sheet lobe		593.82	20	15	0
1203A 32R5W 60-64	11			sheet lobe		594.77	3	0.5	0
1203A 36R3W 25-29	14	Moderately Plagioclase-Phyric Basalt	Tholeiitic	vesicular pillow lava	9.49	620.55	7	0	0
1203A 36R6W 18-22	14			vesicular pillow lava		624.18	8	0	0
1203A 37R2W 87-91	16	Aphyric to Highly-Olivine-Phyric Basalt	Tholeiitic	sheet lobe	10.37	629.87	0.5	16	0
1203A 37R3W 103-107	16			sheet lobe		631.53	0.5	45	0
1203A 38R1W 123-126	16			sheet lobe		638.33	1	4	0
1203A 39R5W 98-102	18	Moderately Plagioclase-Olivine-Phyric Basalt	Tholeiitic	vesicular pillow lava	14.57	653.14	5	3	0
1203A 42R1W 88-92	19	Vesicular Moderately Olivine-Phyric Basalt	Tholeiitic	compound pahoehoe	19.63	676.38	10	7	1
1203A 42R5W 40-44	19			compound pahoehoe		681.59	17	11	2
1203A 44R1W 75-79	20	Moderately Olivine-Phyric Basalt	Tholeiitic	vesicular pillow lava	36.73	695.45	1	5	0
1203A 45R1W 35-39	20			vesicular pillow lava		703.45	1	5	0
1203A 46R4W 50-54	20			vesicular pillow lava		717.48	1	2	0
1203A 47R3W 50-54	21	Moderately Olivine-Phyric Basalt	Tholeiitic	vesicular pillow lava	19.05	725.48	2	2	0
1203A 48R2W 96-100	21			vesicular pillow lava		729.4	2	0	0
1203A 49R3W 50-54	21			vesicular pillow lava		735.05	0	0	0
1203A 52R 6W 23-27	23	Vesicular Sparsely Olivine-Plagioclase-Phyric to Aphyric Basalt	Alkalic	compound pahoehoe	63.39	768.09	4	1	0
1203A 53R6W 123-127	23			compound pahoehoe		779.13	2	1	0
1203A 54R4W 74-78	23			compound pahoehoe		785.09	2	1	0
1203A 55R1W 109-113	23			compound pahoehoe		790.79	2	trace	0[5]
1203A 58R2W 94-98	23			compound pahoehoe		816.95	3	1	1
1203A 58R4W 37-41	24	Vesicular Aphyric Basalt	Tholeiitic	pahoehoe sheet lobe	3.38	819.24	1	0.5	0
1203A 59R2W 69-73	24			pahoehoe sheet lobe		820.55	0.5	0	0
1203A 62R1W 101-105	26	Vesicular Aphyric Basalt	Alkalic	compound pahoehoe	40.55	848.41	0	0	0
1203A 62R2W 88-92	26			compound pahoehoe		849.78	trace	0	0
1203A 63R4W 19-22	26			compound pahoehoe		861.65	0	0	0
1203A 65R4W 9-13	29	Vesicular Aphyric Basalt	Alkalic	compound pahoehoe	8.38	880.03	2	1	0
1203A 66R2W 8-10	30	Vesicular, Sparsely Plagioclase-Phyric Basalt	Alkalic	compound pahoehoe	23.76	887.38	1	4	0
1203A 67R4W 10-14	30			compound pahoehoe		899.9	0.5	0.5	0
1203A 68R4W 40-43	31b	Highly Plagioclase-Phyric Basalt	Tholeiitic	pillow lava	>>0.2	909.86	15	0.5	0
1204A 7R3W 12-16	2	Aphyric Basalt	Alkalic	vesicular pillow lava	35.49	822.44	0.5	0	0
1204A 8R1W 73-77	2			vesicular pillow lava		829.73	0.5	0	0
1204A 9R2W 55-59	2			vesicular pillow lava		840.65	0	0	0
1204A 9R2W 76-80	2			vesicular pillow lava		840.86	0.5	0	0
1204A 9R3W 25-27	2			vesicular pillow lava		841.85	0	0	0
1204A 10R2W 89-93	2			vesicular pillow lava		850.66	0	trace	0
1204A 10R2W 108-112	2			vesicular pillow lava		850.85	0	trace	0
1204A 10R3W 77-81	2			vesicular pillow lava		851.68	0	0	0
1204A 10R5W 44-48	2			vesicular pillow lava		854.26	0.5	0.5	0
1204B 1R4W 51-53	1	Aphyric Basalt	Alkalic	vesicular pillow lava	27.07	815.26	<1	0	0
1204B 2R2W 76-80	1			vesicular pillow lava		822.36	<1	0	0
1204B 2R4W 102-105	1			vesicular pillow lava		824.82	<1	0	0
1204B 2R5W 11-15	1			vesicular pillow lava		825.26	<1	0	0
1204B 3R2W 41-44	1			vesicular pillow lava		831.76	<1	0	0
1204B 4R2W 49-53	2A	Aphyric Basalt	Alkalic	vesicular pillow lava	30.53	841.59	0	0	0
1204B 6R1W 44-47	2A			vesicular pillow lava		859.04	0	0	0
1204B 7R2W 39-43	2A			vesicular pillow lava		870.06	0	0	0
1204B 7R3W 68-72	2A			vesicular pillow lava		871.85	0	0	0
1204B 8R2W 85-89	2B	Diabase	Alkalic	sheet lobe/internal pathway	46.22	880.15	0	0	0
1204B 9R3W 28-32	2B			sheet lobe/internal pathway		888.97	0	0	0
1204B 10R1W 11-14	2B			sheet lobe/internal pathway		888.91	0	0	0
1204B 10R2W 50-54	2B			sheet lobe/internal pathway		890.8	0	0	0
1204B 10R4W 43-47	2B			sheet lobe/internal pathway		892.79	0	0	0
1204B 12R1W 65-69	2B			sheet lobe/internal pathway		906.95	0	0	0
1204B 13R1W 118-122	2B			sheet lobe/internal pathway		909.48	0	0	0
1204B 14R1W 18-22	2B			sheet lobe/internal pathway		916.08	0	0	0
1204B 14R1W 87-91	2B			sheet lobe/internal pathway		916.77	0	0	0
1204B 17R1W 107-110	3	Aphyric Basalt	Alkalic	vesicular pillow lava	2.33	945.97	0	0	0
1204B 17R2W 11-15	3			vesicular pillow lava		946.19	0	0	0

1. Taken from Tarduno, J. A , Duncan, R. A., School, D. W., et al. (2002) with modification.
2. See Section 5.1 for details.
3. Phenocryst content is estimated in volume %.
4. Phenocrysts are low first order yellow to gray and biaxial. They may be orthopyroxene.
5. This sample contains a single clinopyroxene phenocryst (2.5 mm in diameter), which is attached to a plagioclase phenocryst.

2b. Glass Sample Info.

Sample Name	Unit[1]	Depth mbsf
1203A 18R-2 17-21	1f: base of Unit 1 overlying sediment	465.47
1203A 18R-2 21-27	1f: glass at the top of Unit 2 sediment	465.51
1203A 19R-2 38-42	3k: glass in middle of lobe 3k	475.28
1203A 20R-1 106-107	3x: base of lobe, overlying 3y	484.06
1203A 20R-2 58-61	3ab top of lobe	485.08
1203A 31R-1 105-108	8k: glass in middle of lobe	580.45
1203A 31R-2 1-6	8m top of lobe	580.91
1203A 39R-6 57-63	18f top of lobe	653.97
1203A 40R-1 0-3	18h top of lobe	656.2
1203A 40R-1 65-70	18h bottom of lobe	656.85
1203A 40R-2 102-105	18i base of lobe	657.92
1203A 40R-2 142-146	18j base of lobe	658.32
1203A 40R-4 57-65	18n top of lobe	660.29
1203A 40R-4 80-90	18o top/side of lobe	660.52
1203A 45R-2 32-35	20s top of lobe	704.92
1203A 46R-4 0-4	20aj top of lobe	716.98
1204B 1R-3 69-81	Unit 1 glass fragments	814.39
1204B 3R-2 97-100	Unit 1 lobe boundary	832.2
1204B 3R-2 100-106	Unit 1 lobe boundary	832.35
1204B 3R-2 106-110	Unit 1 lobe boundary	832.41
1204B 15R-1 112-116	Unit 2c lobe margin	926.72
883E 20R-5 46-50	Unit 8 top	
883E 22R-2 105-110	Unit 17 lobe margin	
883E 22R-4 112-120	Unit 19-20 boundary	
884E 10R-5 59-62	Unit 11 top	
884E 10R-6 38-40	Unit 11 base	
884E 10R-6 118-121	Unit 13 top	

(1) Most units are multi-lobed, and are divided into subunits. Letters after numbers refer to subunits. See Tarduno, J. A., Duncan, R. A., School, D. W., et al. (2002) for a detailed documentation of subunits.

Table 3a. Whole Rock Analyses [1]

Sample Name	UNIT	UNIT NAME	depth(mbsf)	LOI [2]	SiO_2	TiO_2	Al_2O_3	Fe_2O_3* [3]	MnO	MgO	CaO	Na_2O	K_2O	P_2O_5	Total[4]
1203A 17R4W 43-47	1	Highly Plagioclase-Olivine-Phyric Basalt	457.99	2.13	49.4	1.99	16.0	11.0	0.16	6.01	12.1	2.36	0.56	0.21	99.7
1203A 18R3W 116-119	3	Highly Plagioclase-Olivine-Phyric Basalt	467.96	2.18	48.6	1.95	15.3	12.7	0.17	5.90	11.7	2.39	0.64	0.20	99.5
1203A 20R3W 10-14	3	Highly Plagioclase-Olivine-Phyric Basalt	486.1	1.39	49.3	1.95	15.6	11.3	0.16	7.00	11.9	2.10	0.17	0.19	99.7
1203A 25R1W 37-41	5	Moderately Plagioclase-Olivine-Phyric Basalt	531.47	3.18	48.1	2.04	16.1	12.4	0.17	8.71	9.12	2.67	0.33	0.22	99.9
1203A 26R2W 5-9	6	Sparsely Plagioclase-Phyric Basalt	535.84	4.49	47.7	2.00	16.1	12.4	0.18	10.0	8.26	2.32	0.27	0.21	99.4
1203A 26R3W 97-101	6	Sparsely Plagioclase-Phyric Basalt	537.4	4.13	47.9	1.91	15.7	12.5	0.21	9.99	8.45	2.38	0.36	0.23	99.7
1203A 30R1W 108-112	8	Highly Plagioclase-Olivine-Phyric Basalt	570.88	0.370	49.0	1.95	15.6	12.2	0.21	5.63	12.5	2.17	0.27	0.20	99.8
1203A 31R1W 46-50	8	Highly Plagioclase-Olivine-Phyric Basalt	579.86	1.55	49.5	1.94	15.9	10.3	0.24	6.46	12.3	2.51	0.25	0.19	99.6
1203A 32R2W 32-36	11	Plagioclase-Olivine-Phyric Basalt	590.6	2.32	50.1	2.01	15.7	11.3	0.12	8.59	8.22	3.05	0.37	0.20	99.7
1203A 32R3W 58-62	11	Plagioclase-Olivine-Phyric Basalt	592.36	1.56	44.7	0.94	9.94	13.3	0.20	21.9	7.15	1.06	0.14	0.10	99.5
1203A 32R4W 76-80	11	Plagioclase-Olivine-Phyric Basalt	593.82	1.99	48.4	1.54	16.3	11.7	0.15	7.89	11.5	2.06	0.15	0.16	99.8
1203A 32R5W 60-64	11	Plagioclase-Olivine-Phyric Basalt	594.77	2.27	49.3	1.89	15.7	11.3	0.13	8.11	9.87	2.80	0.29	0.17	99.5
1203A 36R3W 25-29	14	Moderately Plagioclase-Phyric Basalt	620.55	1.52	48.9	1.68	17.9	9.80	0.17	5.74	12.9	2.37	0.10	0.16	99.7
1203A 36R6W 18-22	14	Moderately Plagioclase-Phyric Basalt	624.18	1.37	49.8	1.77	18.0	9.10	0.13	6.11	11.8	2.71	0.15	0.17	99.7
1203A 37R2W 87-91	16	Aphyric to Highly-Olivine-Phyric Basalt	629.87	3.23	47.3	1.23	14.4	11.8	0.16	13.3	9.68	1.34	0.10	0.10	99.5
1203A 37R3W 103-107	16	Aphyric to Highly-Olivine-Phyric Basalt	631.53	1.51	43.8	0.72	7.78	12.4	0.18	28.4	5.41	0.86	0.08	0.06	99.7
1203A 38R1W 123-126	16	Aphyric to Highly-Olivine-Phyric Basalt	638.33	1.78	48.7	1.44	15.4	12.1	0.17	8.31	11.3	1.74	0.16	0.12	99.4
1203A 39R5W 98-102	18	Moderately Plagioclase-Olivine-Phyric Basalt	653.14	3.08	48.4	1.74	15.9	11.0	0.24	6.58	13.3	2.20	0.27	0.19	99.8
1203A 42R1W 88-92	19	Vesicular Moderately Olivine-Phyric Basalt	676.38	5.35	47.9	1.56	15.5	11.0	0.17	8.49	11.9	2.02	1.14	0.14	99.7
1203A 42R5W 40-44	19	Vesicular Moderately Olivine-Phyric Basalt	681.59	3.59	47.9	1.54	15.3	11.0	0.19	9.89	11.4	2.50	0.08	0.15	100.0
1203A 44R1W 75-79	20	Moderately Olivine-Phyric Basalt	695.45	5.23	47.3	2.17	15.2	11.8	0.21	6.26	13.0	2.19	1.25	0.20	99.5
1203A 45R1W 35-39	20	Moderately Olivine-Phyric Basalt	703.45	8.01	45.6	2.13	16.1	14.6	0.22	3.10	11.5	4.05	2.19	0.35	99.8
1203A 46R4W 50-54	20	Moderately Olivine-Phyric Basalt	717.48	10.9	44.3	2.21	15.2	12.5	0.30	3.65	16.2	3.26	1.67	0.27	99.5
1203A 47R3W 50-54	21	Moderately Olivine-Phyric Basalt	725.48	3.28	49.1	2.21	15.9	11.9	0.20	9.43	8.51	2.25	0.31	0.20	100.0
1203A 48R2W 96-100	21	Moderately Olivine-Phyric Basalt	729.4	2.93	48.1	2.17	15.4	13.3	0.19	8.33	9.50	2.47	0.25	0.20	99.8
1203A 49R3W 50-54	21	Moderately Olivine-Phyric Basalt	735.05	1.83	47.8	2.19	14.9	13.5	0.20	8.34	10.3	2.07	0.08	0.20	99.6
1203A 52R 6W 23-27	23	Vesicular Sparsely Olivine-Plagioclase-Phyric to Aphyric Basalt	768.09	3.02	48.2	2.59	16.0	11.6	0.18	8.01	8.98	3.19	0.30	0.47	99.5
1203A 53R6W 123-127	23	Vesicular Sparsely Olivine-Plagioclase-Phyric to Aphyric Basalt	779.13	2.52	47.6	2.58	15.3	12.7	0.19	6.90	10.8	2.90	0.18	0.48	99.6
1203A 54R4W 74-78	23	Vesicular Sparsely Olivine-Plagioclase-Phyric to Aphyric Basalt	785.09	1.48	48.1	2.88	15.7	12.4	0.19	5.98	11.1	2.94	0.13	0.54	99.9
1203A 55R1W 109-113	23	Vesicular Sparsely Olivine-Plagioclase-Phyric to Aphyric Basalt	790.79	1.98	47.5	2.69	15.5	12.6	0.20	6.42	10.8	2.76	0.40	0.51	99.4
1203A 58R2W 94-98	23	Vesicular Sparsely Olivine-Plagioclase-Phyric to Aphyric Basalt	816.95	1.96	47.8	2.66	15.0	13.1	0.25	7.02	10.4	2.54	0.45	0.49	99.7
1203A 58R4W 37-41	24	Vesicular Aphyric Basalt	819.24	1.83	49.0	1.72	15.5	11.8	0.18	7.75	11.2	2.63	0.24	0.17	100.1
1203A 59R2W 69-73	24	Vesicular Aphyric Basalt	820.55	1.98	48.5	1.76	15.5	11.9	0.15	7.56	11.5	2.41	0.09	0.17	99.5
1203A 62R1W 101-105	26	Vesicular Aphyric Basalt	848.41	4.85	45.2	3.30	13.7	13.1	0.30	5.45	14.4	2.53	1.00	0.68	99.7
1203A 62R2W 88-92	26	Vesicular Aphyric Basalt	849.78	3.97	47.4	2.93	15.1	12.5	0.19	9.16	8.21	3.12	0.36	0.56	99.4
1203A 63R4W 19-22	26	Vesicular Aphyric Basalt	861.65	3.23	49.0	3.05	15.6	11.8	0.16	9.28	7.16	3.28	0.35	0.58	100.2
1203A 65R4W 9-13	29	Vesicular Aphyric Basalt	880.03	3.79	47.6	3.60	15.1	14.0	0.18	6.77	7.62	2.75	1.51	0.65	99.8
1203A 66R2W 8-10	30	Vesicular, Sparsely Plagioclase-Phyric Basalt	887.38	4.83	46.5	3.44	14.8	15.4	0.15	7.56	6.76	2.74	1.79	0.63	99.7
1203A 67R4W 10-14	30	Vesicular, Sparsely Plagioclase-Phyric Basalt	899.9	3.62	47.5	3.19	14.6	13.4	0.16	6.06	9.94	2.62	1.50	0.51	99.5
1203A 68R4W 40-43	31b	Highly Plagioclase-Phyric Basalt	909.86	3.22	48.8	1.40	19.3	10.4	0.10	5.72	10.8	2.09	1.05	0.10	99.8

(1) Major oxide contents are in %, and trace element abundances are in ppm.

(2) L.O.I.: Loss on ignition. ~0.2 g samples were ignited at 1000°C for over 8 hours. L.O.I. was calculated using (weight loss during ingition/weight before ignition)*100%.

(3) Samples were oxidized prior to analyses,so all iron is reported as Fe^{3+}, i.e., Fe_2O_3.

(4) Total is sum of oxides measured after ignition and oxidation.

continued	UNIT	UNIT NAME	depth(mbsf)	LOI	SiO_2	TiO_2	Al_2O_3	Fe_2O_3*	MnO	MgO	CaO	Na_2O	K_2O	P_2O_5	Total
1204A 7R3W 12-16	2	Aphyric Basalt	822.44	8.17	44.1	2.29	15.1	10.2	0.16	3.58	20.5	2.79	0.79	0.30	99.8
1204A 8R1W 73-77	2	Aphyric Basalt	829.73	8.99	42.9	2.32	14.9	10.2	0.15	3.42	22.1	2.81	0.84	0.30	99.9
1204A 9R2W 55-59	2	Aphyric Basalt	840.65	8.39	42.0	2.19	14.6	13.4	0.20	3.64	20.1	2.64	0.75	0.28	99.8
1204A 9R2W 76-80	2	Aphyric Basalt	840.86	3.43	46.8	2.19	15.0	13.9	0.18	6.84	10.5	2.92	0.97	0.24	99.6
1204A 9R3W 25-27	2	Aphyric Basalt	841.85	6.02	45.1	2.53	14.0	12.5	0.23	4.73	16.4	2.65	0.92	0.26	99.4
1204A 10R2W 89-93	2	Aphyric Basalt	850.66	3.85	47.5	2.33	16.2	12.3	0.17	7.55	10.2	2.99	0.62	0.26	100.2
1204A 10R2W 108-112	2	Aphyric Basalt	850.85	3.44	48.3	2.19	16.7	11.7	0.14	9.09	8.15	3.05	0.40	0.24	99.9
1204A 10R3W 77-81	2	Aphyric Basalt	851.68	3.11	47.6	2.34	15.8	13.7	0.16	8.68	7.71	2.81	0.45	0.30	99.5
1204A 10R5W 44-48	2	Aphyric Basalt	854.26	3.91	47.5	2.41	15.4	13.1	0.19	8.09	9.30	3.07	0.72	0.26	100.0
1204B 1R4W 51-53	1	Aphyric Basalt	815.26	4.06	46.3	2.33	17.4	12.9	0.15	2.76	14.4	2.77	0.72	0.28	100.0
1204B 2R2W 76-80	1	Aphyric Basalt	822.36	6.80	44.3	2.33	15.8	11.6	0.17	3.44	18.6	2.54	0.56	0.27	99.7
1204B 2R4W 102-105	1	Aphyric Basalt	824.82	3.62	45.9	2.56	17.9	13.8	0.20	2.14	12.5	3.08	1.06	0.56	99.8
1204B 2R5W 11-15	1	Aphyric Basalt	825.26	3.16	45.7	2.40	16.5	14.8	0.23	3.01	12.5	2.93	1.16	0.34	99.6
1204B 3R2W 41-44	1	Aphyric Basalt	831.76	2.63	46.0	2.50	17.7	14.5	0.19	2.30	11.6	3.54	1.17	0.71	100.2
1204B 4R2W 49-53	2A	Aphyric Basalt	841.59	5.18	46.6	2.27	15.7	12.7	0.16	3.44	14.1	2.91	1.22	0.33	99.4
1204B 6R1W 44-47	2A	Aphyric Basalt	859.04	4.67	46.6	2.36	15.9	13.0	0.12	3.80	13.5	3.01	1.17	0.33	99.8
1204B 7R2W 39-43	2A	Aphyric Basalt	870.06	4.45	46.5	2.58	14.4	13.0	0.18	5.57	13.4	2.87	0.99	0.31	99.8
1204B 7R3W 68-72	2A	Aphyric Basalt	871.85	2.67	47.6	2.26	16.0	13.1	0.19	6.25	10.1	2.66	1.51	0.36	100.1
1204B 8R2W 85-89	2B	Diabase	880.15	4.05	47.0	2.39	15.4	12.9	0.17	6.17	11.7	2.21	1.13	0.32	99.4
1204B 9R3W 28-32	2B	Diabase	888.97	2.87	47.4	2.20	15.5	13.3	0.17	8.74	8.98	2.63	0.39	0.25	99.6
1204B 10R1W 11-14	2B	Diabase	888.91	2.59	47.8	2.29	15.9	13.0	0.15	8.35	9.08	2.74	0.38	0.25	99.9
1204B 10R2W 50-54	2B	Diabase	890.8	3.20	47.3	2.27	15.3	13.4	0.16	7.41	9.77	3.01	1.09	0.27	99.9
1204B 10R4W 43-47	2B	Diabase	892.79	2.17	47.7	2.24	15.5	12.7	0.18	7.73	9.88	2.80	0.43	0.31	99.4
1204B 12R1W 65-69	2B	Diabase	906.95	3.10	47.6	2.46	15.0	13.5	0.20	6.61	10.6	3.10	0.93	0.31	100.2
1204B 13R1W 118-122	2B	Diabase	909.48	3.15	47.5	2.44	15.1	13.6	0.19	6.06	11.0	2.91	0.99	0.33	100.0
1204B 14R1W 18-22	2B	Diabase	916.08	3.33	47.5	2.25	16.0	12.1	0.17	8.34	10.0	2.92	0.51	0.25	100.1
1204B 14R1W 87-91	2B	Diabase	916.77	3.76	45.6	2.16	14.5	16.1	0.25	7.18	9.80	2.73	1.08	0.24	99.6
1204B 17R1W 107-110	3	Aphyric Basalt	945.97	4.56	47.4	2.20	15.3	12.7	0.19	5.56	12.3	2.82	1.25	0.26	99.9
1204B 17R2W 11-15	3	Aphyric Basalt	946.19	6.27	46.1	2.36	15.4	12.2	0.20	4.59	15.0	2.79	1.07	0.31	100.0

continued	UNIT	XRF	Nb	Zr	Y	Sr	Rb	Zn	Ni	Cr	V	ICP-MS	Sc	Rb	Sr	Y	Zr	Nb	Ba	La	Ce	Pr	Nd
1203A 17R4W 43-47	1		8.2	124	27.3	249	9.0	108	80	271	265		40.6	9.21	244	30.9	124	8.69	41.0	7.41	19.4	3.08	14.3
1203A 18R3W 116-11	3		8.1	123	26.2	238	11.6	109	71	247	297		38.8	11.4	229	29.2	120	8.69	35.2	7.02	18.4	2.95	14.0
1203A 20R3W 10-14	3		8.0	122	26.5	246	0.4	113	98	236	305		39.8	0.731	232	29.0	118	8.60	30.1	6.80	18.4	2.90	13.8
1203A 25R1W 37-41	5		8.2	129	24.9	231	3.8	88	130	232	257		35.1	3.81	227	28.2	128	9.02	54.9	7.40	19.4	3.07	14.6
1203A 26R2W 5-9	6		7.7	123	24.2	227	1.3	85	133	259	244		33.8	1.46	214	26.9	122	8.52	51.9	6.97	18.3	2.95	13.8
1203A 26R3W 97-101	6		8.1	128	25.6	215	2.8	84	150	238	215		30.9	2.98	201	28.1	127	8.98	55.0	7.47	20.0	3.05	14.6
1203A 30R1W 108-11	8		7.5	117	26.2	243	3.2	111	89	260	298		40.1	3.53	230	28.9	112	8.03	25.0	6.65	17.5	2.84	13.5
1203A 31R1W 46-50	8		7.4	117	26.5	253	1.0	110	97	250	303		43.4	1.22	252	29.5	114	8.15	37.9	6.67	17.7	2.81	13.5
1203A 32R2W 32-36	11		7.4	117	25.2	238	3.4	109	76	290	304		43.2	3.44	232	28.4	115	8.35	48.4	6.95	18.0	2.90	13.7
1203A 32R3W 58-62	11		3.4	55	12.8	164	1.7	86	812	651	140		21.1	1.87	150	13.7	54	3.91	23.5	3.25	8.2	1.36	6.5
1203A 32R4W 76-80	11		5.9	92	20.7	235	1.2	81	120	264	200		33.1	1.31	223	22.5	89	6.26	29.9	5.25	14.0	2.24	10.6
1203A 32R5W 60-64	11		6.8	107	22.0	229	1.6	106	76	262	298		40.7	1.62	217	24.0	104	7.47	40.6	5.95	15.7	2.54	12.1
1203A 36R3W 25-29	14		6.4	97	22.3	266	0.3	87	77	272	263		36.9	0.390	257	24.3	94	6.76	27.1	5.69	14.7	2.43	11.7
1203A 36R6W 18-22	14		6.7	103	22.1	271	0.4	79	81	306	284		38.1	0.689	257	24.3	100	7.24	36.5	6.10	15.9	2.53	12.1
1203A 37R2W 87-91	16		3.0	65	17.5	155	1.1	84	376	895	187		31.1	1.21	144	18.9	65	3.43	17.3	3.11	8.55	1.47	7.39
1203A 37R3W 103-10	16		1.9	41	10.7	90	1.2	85	1322	1442	124		20.0	0.990	83	11.7	41	2.09	11.5	1.95	5.29	0.914	4.67
1203A 38R1W 123-12	16		4.0	81	21.1	195	1.3	89	164	353	232		34.5	1.51	186	23.5	80	4.34	25.4	4.04	10.9	1.87	9.33
1203A 39R5W 98-102	18		6.8	103	23.2	260	5.3	89	112	268	249		34.7	5.15	240	24.8	101	7.33	26.5	6.15	16.1	2.56	12.2
1203A 42R1W 88-92	19		5.3	85	20.0	201	16.6	85	174	372	203		31.9	16.8	197	22.5	84	5.73	27.5	4.84	12.8	2.13	10.1
1203A 42R5W 40-44	19		5.3	85	20.3	242	0.6	84	212	487	231		32.7	0.794	233	22.4	85	5.67	16.1	4.85	12.5	2.03	10.0
1203A 44R1W 75-79	20		7.2	119	28.2	208	15.9	105	119	247	297		44.8	17.3	222	33.7	126	8.24	37.3	6.52	17.6	2.91	14.1
1203A 45R1W 35-39	20		6.7	113	27.7	244	27.4	97	99	245	339		48.2	30.9	272	35.3	125	8.15	51.9	6.79	17.6	2.86	13.8
1203A 46R4W 50-54	20		6.7	113	27.3	324	20.6	105	93	277	336		47.0	23.2	356	34.3	122	7.89	48.4	6.45	16.9	2.80	13.7
1203A 47R3W 50-54	21		7.3	122	27.6	191	1.2	102	114	242	306		46.8	1.23	206	34.1	132	8.67	33.0	6.60	18.3	2.95	14.5
1203A 48R2W 96-100	21		7.3	121	29.2	189	2.3	102	102	238	296		47.4	2.80	198	35.5	129	8.39	43.5	6.74	17.8	2.90	14.1
1203A 49R3W 50-54	21		7.1	121	29.4	197	0.0	97	115	273	299		49.7	0.302	206	35.8	128	8.33	27.7	6.64	17.9	2.93	14.3
1203A 52R 6W 23-27	23		13.6	214	35.4	235	0.8	112	104	183	299		44.0	0.844	250	43.4	229	15.4	46.4	12.3	32.9	4.98	23.6
1203A 53R6W 123-12	23		13.9	216	39.7	232	0.0	126	92	183	295		42.8	0.481	244	48.3	232	15.6	47.0	12.7	34.5	5.29	25.2
1203A 54R4W 74-78	23		15.5	244	45.3	254	0.0	137	85	200	328		49.2	0.343	260	54.8	256	17.3	52.2	14.4	38.3	5.88	28.0
1203A 55R1W 109-11	23		14.6	228	41.8	237	3.7	131	94	187	305		44.0	4.36	245	50.6	239	16.1	46.4	13.6	36.1	5.52	26.6
1203A 58R2W 94-98	23		14.1	222	40.1	228	0.5	121	82	180	298		38.1	1.28	229	46.8	225	15.5	50.2	12.8	34.7	5.34	25.4
1203A 58R4W 37-41	24		5.8	103	24.2	221	2.8	84	107	267	238		38.5	3.02	211	27.0	100	6.38	44.0	5.67	14.9	2.46	11.9
1203A 59R2W 69-73	24		5.9	107	24.8	233	0.0	86	106	249	239		36.9	0.386	219	27.1	103	6.53	32.6	5.63	15.3	2.51	12.0
1203A 62R1W 101-10	26		18.5	284	54.1	219	8.0	137	66	129	335		38.1	8.01	210	62.3	283	19.4	62.3	17.6	46.1	6.94	33.1
1203A 62R2W 88-92	26		15.9	246	41.6	225	0.5	120	86	136	310		33.7	0.913	216	46.7	245	16.8	55.2	14.4	38.1	5.68	26.8
1203A 63R4W 19-22	26		16.7	255	38.1	239	0.8	108	95	145	331		34.0	0.893	225	42.9	257	17.8	61.3	14.9	39.2	5.87	27.3
1203A 65R4W 9-13	29		15.8	211	41.2	236	17.8	150	75	179	363		39.0	17.8	230	46.1	203	16.2	62.7	14.0	37.2	5.61	26.8
1203A 66R2W 8-10	30		14.9	199	38.3	225	24.1	142	63	167	384		35.1	23.0	211	42.1	192	15.0	57.6	13.4	34.8	5.19	24.6
1203A 67R4W 10-14	30		14.0	185	36.9	234	9.4	140	92	160	337		36.5	9.37	226	41.8	185	15.0	58.4	12.3	32.7	5.09	24.4
1203A 68R4W 40-43	31b		4.6	79	19.9	218	27.4	93	72	277	217		31.3	27.7	212	21.8	76	4.83	28.9	5.19	13.3	2.18	10.6

continued	UNIT	XRF	Nb	Zr	Y	Sr	Rb	Zn	Ni	Cr	V	ICP-MS	Sc	Rb	Sr	Y	Zr	Nb	Ba	La	Ce	Pr	Nd
1204A 7R3W 12-16	2		8.2	134	30.7	243	11.0	95	40	144	283		35.9	10.5	226	32.8	129	8.58	69.9	7.78	20.2	3.23	15.8
1204A 8R1W 73-77	2		8.5	132	29.9	230	8.6	95	40	153	295		37.6	8.31	216	32.0	123	8.71	66.0	7.65	20.6	3.26	15.7
1204A 9R2W 55-59	2		8.0	135	29.3	248	17.2	88	51	138	300		35.3	16.4	236	32.5	132	8.63	74.5	7.57	19.6	3.14	15.2
1204A 9R2W 76-80	2		8.1	135	29.3	189	21.8	92	86	185	264		39.4	20.9	181	32.9	133	8.69	65.8	7.52	20.0	3.17	15.4
1204A 9R3W 25-27	2		8.4	143	33.0	224	62.0	99	40	174	352		44.1	61.5	211	36.8	141	9.27	88.7	8.15	21.1	3.42	16.6
1204A 10R2W 89-93	2		8.5	142	31.0	206	9.3	87	75	414	278		36.9	8.99	192	33.9	137	9.19	66.0	7.86	21.0	3.35	16.1
1204A 10R2W 108-11:	2		8.1	136	28.3	205	3.6	89	95	154	299		35.6	3.51	194	31.2	131	8.55	59.3	7.55	20.0	3.11	14.9
1204A 10R3W 77-81	2		10.2	164	35.2	193	3.5	100	79	127	283		34.6	3.54	182	39.0	161	10.8	70.3	9.49	25.2	3.89	18.7
1204A 10R5W 44-48	2		8.9	147	32.5	196	21.9	94	75	284	296		41.0	21.5	184	36.9	148	9.69	89.0	8.43	22.3	3.56	17.1
1204B 1R4W 51-53	1		9.1	147	32.2	284	9.3	106	62	166	325		37.5	9.17	266	35.7	141	9.46	67.3	8.26	21.9	3.48	16.9
1204B 2R2W 76-80	1		8.6	145	32.3	287	7.8	99	74	160	288		38.9	7.44	277	35.3	138	9.16	57.9	7.92	21.5	3.35	16.1
1204B 2R4W 102-105	1		9.8	159	35.4	291	14.1	139	70	148	373		40.5	13.7	277	39.2	155	10.3	115	9.24	24.4	3.88	18.6
1204B 2R5W 11-15	1		9.2	154	31.8	253	19.0	126	79	164	380		41.1	18.4	241	35.7	152	9.79	92.6	8.53	22.8	3.56	17.3
1204B 3R2W 41-44	1		9.7	157	36.8	286	13.6	142	72	155	400		42.2	13.1	267	40.7	151	9.96	97.9	9.36	23.5	3.71	18.1
1204B 4R2W 49-53	2A		8.9	145	31.0	239	30.2	172	64	149	272		37.0	30.2	233	34.9	142	9.51	80.3	8.20	21.6	3.42	16.4
1204B 6R1W 44-47	2A		9.1	149	32.3	239	22.7	167	55	154	305		38.4	22.4	229	35.6	143	9.63	75.6	8.29	21.9	3.46	16.8
1204B 7R2W 39-43	2A		10.0	165	36.3	209	36.8	125	63	148	331		42.6	36.6	197	40.6	161	10.6	81.1	9.22	24.4	3.83	18.6
1204B 7R3W 68-72	2A		8.3	142	32.6	222	56.0	177	111	182	334		40.0	54.2	204	35.9	137	9.12	78.2	8.22	20.8	3.39	16.4
1204B 8R2W 85-89	2B		8.7	145	32.5	209	34.2	166	145	128	304		35.4	32.9	195	35.9	142	9.52	76.6	8.44	22.6	3.56	17.3
1204B 9R3W 28-32	2B		8.5	141	30.2	194	3.5	88	85	149	285		36.7	3.47	172	32.8	136	8.95	58.5	7.76	20.7	3.27	15.9
1204B 10R1W 11-14	2B		8.5	143	30.3	203	3.5	90	94	149	292		38.5	3.51	186	33.9	138	9.12	60.3	7.99	21.1	3.35	16.2
1204B 10R2W 50-54	2B		8.5	143	30.0	191	25.2	210	140	162	299		37.2	24.3	177	32.8	140	9.32	66.6	7.79	21.1	3.34	16.2
1204B 10R4W 43-47	2B		9.9	160	33.6	202	3.8	99	105	146	285		36.4	3.62	184	36.5	153	10.1	65.3	8.75	23.6	3.75	18.2
1204B 12R1W 65-69	2B		10.1	169	35.8	198	20.0	107	81	176	334		38.4	19.3	186	39.8	160	10.8	97.8	9.41	25.3	3.93	18.9
1204B 13R1W 118-12:	2B		10.1	168	37.0	211	30.9	134	79	148	293		36.9	29.1	192	40.2	163	11.0	84.8	9.86	26.1	4.11	19.8
1204B 14R1W 18-22	2B		8.6	142	31.4	197	3.6	95	96	151	285		37.5	3.46	184	34.0	138	9.08	62.1	7.93	21.0	3.34	16.0
1204B 14R1W 87-91	2B		8.0	135	29.8	181	23.4	80	77	150	267		37.5	22.5	170	32.8	133	8.69	151	7.46	19.8	3.12	15.1
1204B 17R1W 107-11(	3		8.4	139	29.4	215	72.5	148	179	139	283		36.8	73.6	209	33.5	138	8.91	85.2	7.84	20.7	3.32	15.7
1204B 17R2W 11-15	3		8.9	147	31.4	239	40.8	140	67	146	274		38.2	42.5	242	35.5	142	9.57	80.4	8.17	22.1	3.45	16.3

continued	Unit	ICP-MS	Sm	Eu	Gd	Tb	Dy	Ho	Er	Tm	Yb	Lu	Hf	Ta	Pb	Th	U
1203A 17R4W 43-47	1		4.25	1.55	5.05	0.881	5.30	1.09	2.94	0.428	2.65	0.386	3.13	0.609	0.834	0.560	0.769
1203A 18R3W 116-119	3		4.13	1.51	4.89	0.845	5.05	1.05	2.85	0.425	2.54	0.361	3.12	0.613	0.708	0.552	0.286
1203A 20R3W 10-14	3		4.00	1.46	4.84	0.826	5.00	1.02	2.78	0.409	2.51	0.374	3.01	0.589	0.814	0.542	0.149
1203A 25R1W 37-41	5		4.15	1.52	4.77	0.823	4.90	1.00	2.76	0.412	2.51	0.359	3.14	0.590	0.674	0.555	0.182
1203A 26R2W 5-9	6		3.98	1.47	4.60	0.787	4.71	0.974	2.67	0.390	2.42	0.352	3.08	0.553	0.633	0.527	0.172
1203A 26R3W 97-101	6		4.13	1.49	4.80	0.819	4.88	1.00	2.73	0.419	2.45	0.363	3.15	0.575	0.937	0.561	0.182
1203A 30R1W 108-112	8		4.07	1.50	4.87	0.845	5.10	1.05	2.91	0.423	2.58	0.371	3.00	0.551	0.726	0.512	0.183
1203A 31R1W 46-50	8		3.98	1.47	4.69	0.812	4.90	1.01	2.80	0.399	2.52	0.357	2.90	0.521	0.690	0.496	0.266
1203A 32R2W 32-36	11		4.03	1.50	4.88	0.843	5.08	1.02	2.86	0.430	2.57	0.374	3.01	0.599	0.991	0.521	0.179
1203A 32R3W 58-62	11		1.88	0.710	2.29	0.399	2.41	0.500	1.34	0.202	1.25	0.185	1.41	0.273	0.336	0.241	0.0809
1203A 32R4W 76-80	11		3.12	1.18	3.74	0.647	3.90	0.799	2.20	0.328	1.99	0.288	2.28	0.437	0.603	0.394	0.134
1203A 32R5W 60-64	11		3.57	1.36	4.25	0.726	4.41	0.889	2.41	0.367	2.22	0.323	2.77	0.526	0.602	0.467	0.548
1203A 36R3W 25-29	14		3.45	1.32	4.06	0.709	4.22	0.876	2.41	0.346	2.12	0.303	2.49	0.495	0.576	0.449	0.164
1203A 36R6W 18-22	14		3.51	1.35	4.20	0.714	4.26	0.888	2.40	0.366	2.15	0.312	2.59	0.526	0.646	0.469	0.236
1203A 37R2W 87-91	16		2.39	0.937	3.04	0.533	3.32	0.691	1.88	0.281	1.72	0.250	1.73	0.244	0.702	0.205	0.0726
1203A 37R3W 103-107	16		1.45	0.580	1.85	0.331	2.06	0.428	1.20	0.175	1.08	0.160	1.07	0.262	0.295	0.124	0.0460
1203A 38R1W 123-126	16		2.98	1.16	3.76	0.660	4.02	0.835	2.30	0.349	2.06	0.303	2.16	0.335	0.482	0.257	0.0902
1203A 39R5W 98-102	18		3.57	1.34	4.19	0.725	4.36	0.908	2.46	0.370	2.20	0.325	2.56	0.505	0.597	0.469	0.241
1203A 42R1W 88-92	19		3.10	1.18	3.74	0.646	4.02	0.830	2.26	0.329	2.04	0.300	2.29	0.397	0.480	0.369	0.234
1203A 42R5W 40-44	19		3.01	1.17	3.65	0.645	3.87	0.810	2.21	0.323	1.98	0.290	2.17	0.468	0.796	0.351	0.146
1203A 44R1W 75-79	20		4.22	1.56	5.27	0.912	5.54	1.17	3.20	0.474	2.93	0.432	3.20	0.580	0.677	0.525	0.266
1203A 45R1W 35-39	20		4.27	1.55	5.20	0.902	5.52	1.17	3.24	0.482	2.97	0.439	3.12	0.640	0.626	0.505	0.394
1203A 46R4W 50-54	20		4.10	1.53	5.07	0.892	5.39	1.13	3.08	0.466	2.88	0.431	3.02	0.566	0.545	0.485	0.233
1203A 47R3W 50-54	21		4.40	1.61	5.29	0.925	5.60	1.18	3.26	0.481	2.95	0.437	3.36	0.584	0.825	0.547	0.185
1203A 48R2W 96-100	21		4.34	1.62	5.32	0.937	5.64	1.18	3.30	0.503	2.97	0.448	3.23	0.542	1.21	0.521	0.172
1203A 49R3W 50-54	21		4.38	1.60	5.38	0.942	5.76	1.19	3.29	0.493	2.99	0.446	3.21	0.566	0.591	0.518	0.174
1203A 52R 6W 23-27	23		6.53	2.23	7.32	1.22	7.22	1.48	4.04	0.602	3.64	0.531	5.12	0.961	0.895	0.891	0.451
1203A 53R6W 123-127	23		6.95	2.36	8.03	1.34	7.80	1.60	4.39	0.646	3.86	0.579	5.20	0.988	0.947	0.923	0.318
1203A 54R4W 74-78	23		7.77	2.63	8.97	1.49	8.82	1.83	4.93	0.719	4.40	0.636	5.70	1.08	1.02	0.990	0.380
1203A 55R1W 109-113	23		7.28	2.46	8.37	1.40	8.32	1.72	4.68	0.675	4.03	0.603	5.42	1.03	0.977	0.948	0.409
1203A 58R2W 94-98	23		6.98	2.37	8.10	1.35	7.93	1.64	4.44	0.648	3.89	0.572	5.18	0.988	0.877	0.893	0.353
1203A 58R4W 37-41	24		3.55	1.34	4.36	0.749	4.56	0.932	2.57	0.387	2.37	0.353	2.64	0.427	1.23	0.393	0.131
1203A 59R2W 69-73	24		3.64	1.36	4.45	0.765	4.57	0.960	2.66	0.394	2.40	0.345	2.69	0.440	0.573	0.396	0.134
1203A 62R1W 101-105	26		8.99	2.96	10.5	1.73	10.3	2.12	5.76	0.838	4.96	0.739	6.49	1.27	1.59	1.15	1.13
1203A 62R2W 88-92	26		7.28	2.44	8.23	1.37	8.07	1.65	4.46	0.658	4.01	0.597	5.57	1.10	0.958	1.00	0.467
1203A 63R4W 19-22	26		7.28	2.46	8.03	1.36	7.84	1.61	4.42	0.659	4.04	0.586	5.91	1.16	1.04	1.07	0.635
1203A 65R4W 9-13	29		7.42	2.58	8.50	1.41	8.25	1.66	4.51	0.637	3.86	0.568	5.08	1.10	1.06	0.977	0.460
1203A 66R2W 8-10	30		6.75	2.38	7.65	1.28	7.50	1.53	4.11	0.609	3.63	0.532	4.69	1.03	0.940	0.893	0.453
1203A 67R4W 10-14	30		6.75	2.37	7.65	1.29	7.44	1.53	4.17	0.582	3.58	0.504	4.60	1.01	0.953	0.880	0.628
1203A 68R4W 40-43	31b		3.17	1.23	3.82	0.655	3.88	0.810	2.13	0.321	1.88	0.278	2.01	0.347	0.612	0.295	0.280

continued	Unit	ICP-MS	Sm	Eu	Gd	Tb	Dy	Ho	Er	Tm	Yb	Lu	Hf	Ta	Pb	Th	U
1204A 7R3W 12-16	2		4.65	1.69	5.44	0.942	5.73	1.21	3.32	0.497	2.97	0.454	3.36	0.606	0.903	0.581	0.394
1204A 8R1W 73-77	2		4.53	1.63	5.35	0.917	5.59	1.16	3.15	0.475	2.93	0.429	3.34	0.618	1.24	0.601	0.262
1204A 9R2W 55-59	2		4.44	1.61	5.29	0.913	5.55	1.17	3.22	0.492	3.00	0.439	3.24	0.583	0.747	0.577	0.351
1204A 9R2W 76-80	2		4.54	1.62	5.44	0.925	5.56	1.18	3.19	0.482	2.93	0.433	3.38	0.593	0.787	0.588	0.176
1204A 9R3W 25-27	2		4.88	1.77	5.87	1.03	6.17	1.31	3.62	0.535	3.24	0.484	3.62	0.624	0.869	0.613	1.06
1204A 10R2W 89-93	2		4.69	1.71	5.54	0.952	5.79	1.22	3.33	0.506	3.10	0.462	3.53	0.637	0.634	0.604	0.218
1204A 10R2W 108-112	2		4.32	1.59	5.04	0.873	5.32	1.13	3.10	0.472	2.89	0.418	3.32	0.587	0.480	0.587	0.233
1204A 10R3W 77-81	2		5.39	1.91	6.36	1.08	6.62	1.39	3.76	0.566	3.52	0.519	3.92	0.732	0.522	0.743	0.222
1204A 10R5W 44-48	2		5.00	1.81	5.97	1.04	6.24	1.32	3.65	0.540	3.28	0.485	3.74	0.628	0.726	0.632	0.241
1204B 1R4W 51-53	1		4.94	1.79	5.89	1.02	6.06	1.29	3.50	0.529	3.18	0.481	3.63	0.640	0.775	0.637	0.522
1204B 2R2W 76-80	1		4.70	1.72	5.57	0.980	5.77	1.22	3.40	0.506	3.06	0.458	3.51	0.617	0.781	0.620	1.79
1204B 2R4W 102-105	1		5.43	1.98	6.47	1.13	6.65	1.40	3.89	0.585	3.51	0.528	4.02	0.696	0.934	0.701	0.583
1204B 2R5W 11-15	1		5.07	1.84	6.01	1.03	6.11	1.29	3.46	0.525	3.16	0.468	3.85	0.672	0.899	0.652	0.385
1204B 3R2W 41-44	1		5.23	1.90	6.30	1.09	6.48	1.39	3.83	0.584	3.52	0.527	3.90	0.690	0.978	0.681	0.608
1204B 4R2W 49-53	2A		4.80	1.72	5.70	0.977	5.90	1.23	3.39	0.512	3.07	0.458	3.54	0.636	0.852	0.622	0.321
1204B 6R1W 44-47	2A		4.90	1.78	5.79	1.01	6.02	1.27	3.44	0.530	3.17	0.479	3.63	0.650	0.966	0.648	0.318
1204B 7R2W 39-43	2A		5.50	1.94	6.47	1.12	6.71	1.41	3.90	0.583	3.54	0.535	4.03	0.701	1.07	0.689	0.705
1204B 7R3W 68-72	2A		4.73	1.73	5.78	1.00	5.97	1.28	3.51	0.537	3.22	0.481	3.54	0.614	0.423	0.612	0.671
1204B 8R2W 85-89	2B		5.08	1.85	6.03	1.05	6.20	1.32	3.57	0.538	3.24	0.497	3.63	0.631	0.411	0.643	1.40
1204B 9R3W 28-32	2B		4.62	1.69	5.44	0.956	5.74	1.19	3.26	0.494	3.00	0.452	3.47	0.597	0.834	0.605	0.184
1204B 10R1W 11-14	2B		4.68	1.72	5.56	0.962	5.81	1.22	3.39	0.500	3.11	0.459	3.54	0.610	0.665	0.599	0.194
1204B 10R2W 50-54	2B		4.68	1.70	5.63	0.961	5.83	1.22	3.29	0.500	2.99	0.442	3.60	0.640	1.25	0.624	0.357
1204B 10R4W 43-47	2B		5.26	1.87	6.26	1.07	6.34	1.33	3.60	0.545	3.32	0.495	3.81	0.676	0.957	0.699	0.178
1204B 12R1W 65-69	2B		5.47	1.91	6.51	1.12	6.78	1.41	3.96	0.603	3.64	0.531	4.07	0.725	1.30	0.742	0.372
1204B 13R1W 118-122	2B		5.66	2.00	6.71	1.17	6.93	1.46	4.01	0.603	3.67	0.541	4.10	0.740	1.33	0.747	0.487
1204B 14R1W 18-22	2B		4.72	1.73	5.57	0.980	5.84	1.22	3.32	0.503	3.02	0.448	3.46	0.602	1.14	0.603	0.199
1204B 14R1W 87-91	2B		4.45	1.61	5.29	0.919	5.47	1.16	3.17	0.481	2.89	0.431	3.33	0.589	0.624	0.579	0.160
1204B 17R1W 107-110	3		4.56	1.67	5.49	0.962	5.65	1.19	3.26	0.492	2.98	0.439	3.41	0.591	0.812	0.605	0.263
1204B 17R2W 11-15	3		4.77	1.74	5.66	0.979	5.91	1.24	3.42	0.513	3.15	0.459	3.59	0.648	0.862	0.642	0.633

Table 3b Glass Analyses [1]

sample #	interval	Depth mbsf	Unit[2]	SiO_2	TiO_2	Al_2O_3	FeO	MnO	MgO	Cr_2O_3	CaO	Na_2O	K_2O	P_2O_5	Total
1203A-1	1203A 18R-2 17-21	465.47	1f: base of Unit 1 overlying sediment	49.5	2.21	13.6	13.1	0.22	6.21	0.05	11.2	2.97	0.33	0.19	99.5
1203A-2	1203A 18R-2 21-27	465.51	1f: glass at top of Unit 2 sediment	49.0	2.19	13.6	13.3	0.16	6.18	0.06	11.1	2.97	0.34	0.21	99.1
1203A-3	1203A 19R-2 38-42	475.28	3k: glass in middle of lobe 3k	49.0	2.20	13.6	13.2	0.19	6.17	0.06	11.1	3.00	0.34	0.28	99.1
1203A-4	1203A 20R-1 106-107	484.06	3x: base of lobe, overlying 3y	48.6	2.19	13.3	13.3	0.17	6.20	0.05	11.1	2.92	0.33	0.23	98.4
1203A-4r				48.5	2.20	13.3	13.3	0.14	6.25	0.05	11.0	2.94	0.34	0.27	98.3
1203A-5	1203A 20R-2 58-61	485.08	3ab top of lobe	48.1	1.90	14.8	11.4	0.19	7.12	0.05	11.7	2.94	0.27	0.22	98.7
1203A-6	1203A 31R-1 105-108	580.45	8k: glass in middle of lobe	48.0	1.90	14.8	11.4	0.21	7.17	0.06	11.7	2.95	0.27	0.21	98.7
1203A-7	1203A 31R-2 1-6	580.91	8m top of lobe	49.2	1.97	14.1	12.6	0.23	6.74	0.02	11.3	2.97	0.30	0.26	99.8
1203A-8	1203A 39R-6 57-63	653.97	18f top of lobe	49.0	1.93	14.1	12.8	0.19	6.67	0.06	11.3	2.94	0.30	0.18	99.6
1203A-9	1203A 40R-1 0-3	656.2	18h top of lobe	48.9	2.21	13.5	13.5	0.19	6.22	0.03	11.1	2.98	0.33	0.22	99.1
1203A-10	1203A 40R-1 65-70	656.85	18h bottom of lobe	48.6	1.91	14.9	11.3	0.13	7.21	0.01	11.7	3.01	0.28	0.21	99.3
1203A-11	1203A 40R-2 102-105	657.92	18i base of lobe	48.6	1.88	14.9	11.4	0.17	7.26	0.05	11.8	2.90	0.26	0.19	99.4
1203A-12	1203A 40R-2 142-146	658.32	18j base of lobe	48.7	1.92	15.1	11.4	0.21	7.39	0.10	11.7	2.91	0.29	0.28	100.0
1203A-13	1203A 40R-4 57-65	660.29	18n top of lobe	48.7	1.87	15.0	11.4	0.19	7.26	0.08	11.7	2.97	0.28	0.18	99.7
1203A-14	1203A 40R-4 80-90	660.52	18o top/side of lobe	48.7	1.89	15.0	11.5	0.18	7.28	0.06	11.7	2.94	0.28	0.20	99.7
1203A-15	1203A 45R-2 32-35	704.92	20s top of lobe	47.9	2.39	14.6	12.6	0.29	6.58	0.03	10.9	3.01	0.28	0.24	98.8
1203A-16	1203A 46R-4 0-4	716.98	20aj top of lobe	47.6	2.38	14.4	12.9	0.21	6.52	0.06	10.9	2.99	0.28	0.24	98.5
1204B-1	1204B 1R-3 69-81	814.39	Unit 1 glass fragments	47.0	2.47	15.1	13.1	0.23	6.31	0.03	11.1	3.44	0.39	0.25	99.4
1204B-2	1204B 3R-2 97-100	832.2	Unit 1 lobe boundary	47.2	2.62	14.4	13.8	0.19	6.04	0.02	11.2	3.45	0.44	0.34	99.6
1204B-3	1204B 3R-2 100-106	832.35	Unit 1 lobe boundary	46.8	2.40	15.2	13.1	0.24	6.48	0.04	11.0	3.42	0.40	0.26	99.3
1204B-4	1204B 3R-2 106-110	832.41	Unit 1 lobe boundary	46.2	2.43	14.7	13.1	0.20	6.23	0.07	11.0	3.33	0.40	0.31	97.9
1204B-4r				46.1	2.46	14.6	13.4	0.18	6.20	0.03	11.0	3.35	0.38	0.25	98.0
1204B-5	1204B 15R-1 112-116	926.72	Unit 2c lobe margin	46.6	2.42	14.9	13.2	0.18	6.36	0.02	11.0	3.36	0.38	0.31	98.7
883-1	883E 20R-5 46-50		Unit 8 top	46.6	2.74	14.0	14.1	0.23	5.85	0.03	11.1	3.43	0.43	0.29	98.8
883-2	883E 22R-2 105-110		Unit 17 lobe margin	46.7	2.72	14.1	14.0	0.19	5.84	0.02	11.1	3.41	0.43	0.34	98.8
883-3	883E 22R-4 112-120		Unit 19-20 boundary	46.9	2.74	14.0	14.1	0.22	5.80	0.04	11.2	3.42	0.44	0.33	99.1
884-1	884E 10R-5 59-62		Unit 11 top	48.2	1.33	14.7	10.8	0.19	7.77	0.05	12.7	3.03	0.12	0.15	99.2
884-2	884E 10R-6 38-40		Unit 11 base	48.1	1.38	14.8	10.7	0.16	7.80	0.07	12.7	2.93	0.12	0.13	98.9
884-3	884E 10R-6 118-121		Unit 13 top	48.3	1.37	14.9	10.7	0.21	7.78	0.04	12.7	2.95	0.12	0.12	99.2

(1) Major oxides were analyzed by electron microprobe, and are reported in %. Trace elements were analyzed by LA-ICP-MS, and are reported in ppm.
(2) See footnote of Table 2b.

continued	Sc	Cr	Co	Ni	Rb	Sr	Y	Zr	Nb	Ba	La	Ce	Pr	Nd	Sm	Eu	Gd	Tb	Dy	Ho	Er	Tm	Yb
1203A-1	39.6	159	49.9	61.1	3.91	220	33.5	137	9.45	58.6	8.34	21.1	3.37	15.7	4.64	1.54	5.48	0.919	5.79	1.25	3.36	0.531	3.14
1203A-2	39.8	182	49.7	59.0	3.83	220	32.8	138	9.59	58.5	8.31	20.7	3.28	15.9	4.51	1.53	5.33	0.922	5.55	1.19	3.33	0.523	3.11
1203A-3	39.2	179	49.3	58.9	3.94	220	33.3	139	9.68	59.1	8.40	20.9	3.33	15.9	4.49	1.57	5.26	0.897	5.45	1.17	3.34	0.478	2.85
1203A-4	38.3	198	50.6	56.1	4.12	220	31.9	134	9.59	59.9	8.21	21.5	3.34	15.6	4.59	1.53	5.33	0.897	5.45	1.18	3.24	0.470	2.90
1203A-5	39.2	226	46.5	78.0	2.85	231	30.9	124	7.97	47.7	7.48	18.0	2.93	14.3	4.29	1.38	5.04	0.885	5.18	1.16	3.16	0.479	2.79
1203A-6	37.9	247	49.9	81.6	3.00	221	28.0	115	7.89	46.1	6.85	17.2	2.74	12.8	3.66	1.31	4.48	0.765	4.49	0.980	2.78	0.410	2.48
1203A-7	37.4	221	51.2	60.0	3.32	213	28.3	115	7.50	49.5	6.81	16.6	2.67	12.6	3.78	1.30	4.64	0.779	4.55	1.00	2.71	0.418	2.43
1203A-8	37.7	221	49.9	62.2	3.22	212	28.4	114	7.56	49.9	6.66	17.0	2.67	12.9	3.46	1.31	4.48	0.789	4.71	0.976	2.75	0.430	2.48
1203A-9	37.4	182	49.8	58.4	3.90	209	31.5	132	8.98	55.2	7.75	19.7	3.13	14.8	4.17	1.43	5.06	0.856	5.10	1.11	3.04	0.476	2.70
1203A-10	37.9	247	49.7	80.6	3.33	221	27.8	115	7.72	44.5	6.74	17.1	2.72	12.9	3.76	1.30	4.35	0.762	4.50	1.02	2.81	0.423	2.48
1203A-11	37.5	237	46.0	79.3	2.88	217	28.3	118	7.70	44.4	6.76	16.5	2.68	12.6	3.64	1.27	4.42	0.779	4.80	1.03	2.80	0.442	2.56
1203A-12	38.1	248	49.0	82.9	2.94	217	28.6	116	7.74	40.6	6.58	16.6	2.55	12.5	3.91	1.26	4.51	0.760	4.39	1.00	2.69	0.378	2.32
1203A-13	37.5	247	48.8	84.7	3.00	219	28.2	114	7.78	41.4	6.44	16.4	2.55	12.8	3.43	1.24	4.27	0.714	4.53	0.993	2.71	0.367	2.30
1203A-14	38.0	244	46.9	79.6	2.77	216	28.4	116	7.49	39.9	6.51	16.5	2.63	12.5	3.68	1.19	4.47	0.747	4.63	1.00	2.70	0.422	2.43
1203A-15	36.8	202	49.3	89.8	3.20	193	34.7	132	8.39	42.2	6.87	18.7	2.97	13.9	4.12	1.43	5.12	0.861	5.53	1.12	3.49	0.500	3.07
1203A-16	38.6	203	49.2	77.6	3.20	194	34.2	132	8.36	42.6	6.95	18.8	2.94	13.6	4.19	1.47	5.04	0.846	5.63	1.23	3.38	0.490	3.04
1204B-1	39.4	161	49.2	63.2	4.26	214	39.0	162	10.2	63.0	8.60	21.8	3.56	17.2	4.87	1.62	5.58	0.996	6.28	1.31	3.55	0.561	3.38
1204B-2	42.4	162	50.0	50.0	4.63	211	41.8	174	10.9	67.5	9.14	23.9	3.76	18.2	5.11	1.74	5.96	1.07	6.52	1.43	3.93	0.593	3.48
1204B-3	40.3	148	46.1	59.1	3.80	218	41.3	169	9.88	60.8	8.98	21.2	3.49	17.5	5.00	1.69	6.30	1.06	6.37	1.40	3.88	0.615	3.54
1204B-4	39.1	154	46.3	68.0	4.00	217	40.9	165	9.79	62.6	8.83	21.9	3.60	17.4	5.12	1.70	5.92	1.03	6.29	1.40	3.93	0.592	3.39
1204B-5	38.9	157	47.9	63.9	4.08	217	39.8	161	9.77	62.5	8.83	21.8	3.47	17.5	5.31	1.65	5.79	0.998	6.16	1.34	3.89	0.549	3.29
883-1	41.6	145	45.4	41.0	4.61	204	41.6	174	10.7	66.1	9.20	23.7	3.70	17.6	5.35	1.74	6.00	1.06	6.50	1.42	4.12	0.605	3.77
883-2	41.9	150	46.1	45.2	4.54	206	41.5	174	10.7	67.0	9.33	24.1	3.80	18.5	5.42	1.72	6.35	1.07	6.77	1.40	3.99	0.612	3.72
883-3	42.3	151	48.4	46.7	4.71	205	41.5	176	10.8	65.0	9.15	23.8	3.72	18.5	5.36	1.74	6.41	1.08	6.43	1.44	4.03	0.620	3.71
884-1	46.8	307	49.3	75.3	1.21	132	31.5	79	2.98	20.3	2.66	7.62	1.37	7.50	2.65	0.898	3.91	0.646	4.57	1.00	3.09	0.465	2.73
884-2	46.4	301	49.3	83.9	1.39	131	31.7	78	3.11	20.4	2.79	7.79	1.45	7.93	2.83	0.948	4.23	0.694	4.94	1.06	3.29	0.493	2.94
884-3	44.8	294	49.2	80.5	1.26	132	31.4	79	3.01	20.4	2.89	8.46	1.53	8.24	2.82	0.971	4.22	0.692	4.91	1.05	3.29	0.487	3.03

continued	Lu	Hf	Ta	Pb	Th	U
1203A-1	0.432	3.47	0.649	0.653	0.638	0.181
1203A-2	0.433	3.37	0.665	0.659	0.564	0.187
1203A-3	0.408	3.45	0.617	0.658	0.638	0.193
1203A-4	0.384	3.41	0.607	0.763	0.579	0.205
1203A-5	0.410	3.04	0.520	0.543	0.557	0.136
1203A-6	0.383	2.69	0.492	0.517	0.455	0.144
1203A-7	0.351	2.73	0.463	0.542	0.458	0.139
1203A-8	0.367	2.70	0.495	0.536	0.469	0.136
1203A-9	0.375	3.12	0.573	0.775	0.567	0.187
1203A-10	0.340	2.76	0.541	0.514	0.499	0.162
1203A-11	0.374	2.73	0.476	0.459	0.486	0.142
1203A-12	0.350	2.70	0.480	0.516	0.448	0.139
1203A-13	0.333	2.64	0.445	0.556	0.490	0.133
1203A-14	0.359	2.72	0.463	0.489	0.432	0.139
1203A-15	0.424	3.09	0.528	0.552	0.488	0.141
1203A-16	0.426	3.22	0.545	0.542	0.505	0.166
1204B-1	0.501	3.73	0.619	0.699	0.647	0.171
1204B-2	0.515	3.90	0.721	0.808	0.602	0.197
1204B-3	0.543	4.03	0.661	0.644	0.631	0.162
1204B-4	0.527	3.91	0.671	0.715	0.643	0.163
1204B-5	0.464	3.60	0.681	0.663	0.639	0.186
883-1	0.515	3.64	0.658	0.664	0.615	0.196
883-2	0.519	3.90	0.709	0.709	0.697	0.215
883-3	0.522	3.88	0.639	0.718	0.697	0.199
884-1	0.401	2.07	0.229	0.297	0.176	0.0473
884-2	0.444	2.19	0.226	0.302	0.191	0.0497
884-3	0.432	2.06	0.244	0.342	0.197	0.0593

Table 4a. Sr-Nd-Pb Isotopic Ratios and Parent/Daughter Ratios

Sample	Unit	Weight Loss (%)[1]	$^{143}Nd/^{144}Nd$	± 2 sigma	$^{87}Sr/^{86}Sr$	± 2 sigma	$^{206}Pb/^{204}Pb$	± 2 sigma	$^{207}Pb/^{204}Pb$	± 2 sigma	$^{208}Pb/^{204}Pb$	± 2 sigma	in leached residue				in unleached whole-rock			
													Sm/Nd	Rb/Sr	U/Pb	Th/Pb	Sm/Nd	Rb/Sr	U/Pb	Th/Pb
1203A 17 R4W 43-47	1	48	0.513080	0.000006	0.703218	0.000023	18.721	0.003	15.473	0.002	37.947	0.005	0.41	0.0046	0.33	0.14	0.30	0.038	0.92	0.67
1203A 20 R3W 10-14	3	37	0.513079	0.000006	0.703198	0.000013	18.362	0.004	15.487	0.004	37.986	0.010	0.41	0.00096	0.057	0.075	0.29	0.003	0.18	0.67
1203A 31 R1W 46-50	8	28	0.513085	0.000006	0.703105	0.000010	18.312	0.002	15.476	0.002	37.927	0.004	0.39	0.0025	0.13	0.13	0.30	0.005	0.39	0.72
1203A 32 R4W 76-80	11	36	0.513077	0.000007	0.703102	0.000008	18.266	0.004	15.462	0.003	37.838	0.008	0.40	0.0016	0.16	0.27	0.29	0.0059	0.22	0.65
1203A 38 R1W 123-126	16	36	0.513112	0.000006	0.703035	0.000011	18.177	0.002	15.454	0.002	37.733	0.004	0.42	0.0034	0.14	0.15	0.32	0.008	0.19	0.53
1203A 49 R3W 50-54	21	38	0.513078	0.000010	0.703046	0.000008	18.299	0.002	15.469	0.002	37.903	0.005	0.40	0.00053	0.088	0.10	0.31	0.0010	0.29	0.88
1203A 54 R4W 74-78	23	40	0.513047	0.000006	0.703162	0.000008	18.590	0.002	15.484	0.002	38.130	0.005	0.36	0.00069	0.24	0.14	0.28	0.0010	0.37	0.97
1203A 59 R2W 69-73	24	33	0.513093	0.000007	0.703113	0.000008	18.206	0.002	15.467	0.002	37.784	0.004	0.43	0.00054	0.077	0.11	0.30	0.0020	0.23	0.69
1203A 63 R4W 19-22	26	54	0.513065	0.000009	0.703085	0.000008	18.629	0.008	15.468	0.006	38.023	0.014	0.33	0.004	0.46	0.10	0.27	0.0040	0.61	1.02
1203A 65 R4W 9-13[2]	29	60	0.513045	0.000006	0.703188	0.000010	19.073	0.003	15.515	0.002	38.380	0.005	0.32	0.031	1.19	0.26	0.28	0.077	0.43	0.92
1203A 66 R2W 8-10	30	80	0.513047	0.000008	0.703202	0.000015	18.775	0.002	15.490	0.002	38.140	0.005	0.33	0.032	0.72	0.079	0.27	0.109	0.48	0.95
1203A 68 R4W 40-43	31	50	0.513079	0.000005	0.703146	0.000008	19.111	0.003	15.534	0.002	38.196	0.006	0.33	0.00002	0.91	0.79	0.30	0.131	0.46	0.48
1204A 10 R2W 108-112	2	44	0.513096	0.000006	0.702915	0.000007	18.261	0.004	15.457	0.004	37.823	0.008	0.35	0.013	0.28	0.56	0.29	0.018	0.49	1.22
1204B 3 R2W 41-44	1	40	0.513101	0.000005	0.702853	0.000008	18.231	0.003	15.448	0.003	37.847	0.007	0.37	0.016	0.12	0.26	0.29	0.049	0.62	0.70
1204B 7 R3W 68-72	2A	40	0.513090	0.000007	0.702999	0.000010	18.328	0.003	15.476	0.002	37.871	0.005	0.38	0.054	0.34	0.69	0.29	0.27	1.59	1.45
1204B 10 R4W 43-47	2B	39	0.513078	0.000006	0.702910	0.000008	18.162	0.001	15.457	0.001	37.793	0.003	0.34	0.009	0.13	0.14	0.29	0.02	0.19	0.73
1204B 17 R1W 107-110	3	52	0.513093	0.000007	0.702940	0.000013	18.318	0.003	15.447	0.002	37.928	0.006	0.35	0.025	0.10	0.25	0.29	0.353	0.32	0.75
LE Unleached			0.513036	0.000006	0.703205	0.000008	18.308	0.002	15.469	0.002	37.905	0.005	0.29	0.0059	0.22	0.65				
LE A					0.703114	0.000007	18.285	0.008	15.472	0.006	37.881	0.017	0.40	0.0027	0.15	0.30				
LE B			0.513077	0.000007	0.703117	0.000018							0.40	0.0022	0.16	0.29				
LE C					0.703124	0.000010	18.271	0.003	15.454	0.003	37.819	0.007	0.39	0.0018	0.15	0.26				
LE D					0.703118	0.000018	18.271	0.003	15.457	0.002	37.827	0.006								
LE E					0.703120	0.000007														
LE F					0.703124	0.000007							0.40	0.0016	0.16	0.27				
LE G					0.703109	0.000007														
LE H					0.703115	0.000007														
LE I			0.513077	0.000007	0.703113	0.000008	18.266	0.004	15.462	0.003	37.838	0.008	0.40	0.0016	0.16	0.27				
standard sample values[3]																				
MIT			0.511856		0.710265		16.937		15.493		36.713									
from Keller et al.			0.511876		0.710248		16.937		15.493		36.705									
from Regelous et al.			0.511872		0.710223		16.9403		15.4974		36.7246									

1: Weight loss during acid leaching.

2: Pb isotopic ratios in this sample are average of two independent analyses, and U/Pb and Th/Pb ratios are average of three independent analyses:

Measured $^{206}Pb/^{204}Pb$, $^{207}Pb/^{204}Pb$ and $^{208}Pb/^{204}Pb$ are 19.072, 15.530, 38.415 and 19.074, 15.500, 38.345, respectively.

Measured U/Pb ratios in residue are 1.04, 1.30 and 1.23, and Th/Pb ratios are 0.24, 0.25 and 0.29.

3: Values are reported for standard samples: La Jolla Nd standard (for Nd), NBS-987 (for Sr) and NBS-981 (for Pb).

Because each laboratory obtained similar values for standard samples, no correction was made in the following figures involving isotopic ratios.

Table 4b. Age-corrected (to 76 Ma) Sr-Nd-Pb Isotopic Ratios

Sample	Unit	$^{143}Nd/^{144}Nd$	± 2 sigma	$^{87}Sr/^{86}Sr$	± 2 sigma	$^{206}Pb/^{204}Pb$	± 2 sigma	$^{207}Pb/^{204}Pb$	± 2 sigma	$^{208}Pb/^{204}Pb$	± 2 sigma
1203A 17 R4W 43-47	1	0.512953	0.000009	0.703204	0.000023	18.477	0.013	15.461	0.002	37.913	0.005
1203A 20 R3W 10-14	3	0.512952	0.000009	0.703195	0.000013	18.320	0.005	15.485	0.004	37.968	0.010
1203A 31 R1W 46-50	8	0.512964	0.000009	0.703097	0.00001	18.216	0.005	15.471	0.002	37.896	0.004
1203A 32 R4W 76-80	11	0.512950	0.000015	0.703097	0.000008	18.152	0.007	15.457	0.003	37.774	0.009
1203A 38 R1W 123-126	16	0.512982	0.000009	0.703025	0.000011	18.075	0.005	15.449	0.002	37.697	0.004
1203A 49 R3W 50-54	21	0.512955	0.000012	0.703044	0.000008	18.233	0.004	15.466	0.002	37.879	0.005
1203A 54 R4W 74-78	23	0.512936	0.000008	0.703160	0.000008	18.412	0.009	15.476	0.002	38.096	0.005
1203A 59 R2W 69-73	24	0.512960	0.000010	0.703111	0.000008	18.147	0.004	15.464	0.002	37.758	0.004
1203A 63 R4W 19-22	26	0.512963	0.000011	0.703073	0.000008	18.289	0.019	15.452	0.006	37.999	0.014
1203A 65 R4W 9-13	29	0.512946	0.000008	0.703095	0.000011	18.183	0.045	15.473	0.003	38.316	0.006
1203A 66 R2W 8-10	30	0.512945	0.000010	0.703106	0.000016	18.241	0.027	15.465	0.002	38.121	0.005
1203A 68 R4W 40-43	31	0.512976	0.000007	0.703146	0.000008	18.432	0.034	15.502	0.003	38.002	0.011
1204A 10 R2W 108-112	2	0.512988	0.000008	0.702876	0.000007	18.056	0.011	15.447	0.004	37.688	0.010
1204B 3 R2W 41-44	1	0.512986	0.000008	0.702805	0.000008	18.143	0.005	15.444	0.003	37.784	0.008
1204B 7 R3W 68-72	2A	0.512972	0.000009	0.702837	0.000013	18.078	0.013	15.464	0.002	37.705	0.010
1204B 10 R4W 43-47	2B	0.512972	0.000008	0.702883	0.000008	18.067	0.005	15.452	0.001	37.759	0.003
1204B 17 R1W 107-110	3	0.512984	0.000009	0.702865	0.000014	18.244	0.005	15.444	0.002	37.868	0.007
LE Unleached		0.512945	0.000011	0.703187	0.000009	18.145	0.008	15.461	0.002	37.747	0.009
LE I		0.512950	0.000015	0.703097	0.000008	18.152	0.007	15.457	0.003	37.774	0.009

The 2 sigma uncertainity in parent/daughter ratios is taken to be 5%.

The 2 sigma uncertainity in age-corrected isotopic ratios is estimated considering both uncertainity in TIMS analyses and uncertainity in parent/daught ratio analyses.

Table 5a. Ti/Zr, Ba/Th and Zr/Hf in Alkalic Lavas at Site 1203

unit	Sample	Ti/Zr	Ba/Th	Zr/Hf
23	1203A 52R 6W 23-27	68.7	51.5	44.4
23	1203A 53R6W 123-127	66.7	51.2	45.0
23	1203A 54R4W 74-78	67.2	52.2	45.4
23	1203A 55R1W 109-113	67.5	48.1	44.4
23	1203A 58R2W 94-98	70.9	55.2	43.5
26	1203A 62R1W 101-105	69.9	53.9	43.6
26	1203A 62R2W 88-92	72.0	54.9	43.7
26	1203A 63R4W 19-22	71.2	57.6	43.5
29	1203A 65R4W 9-13	105.3	63.5	40.2
30	1203A 66R2W 8-10	107.4	64.5	40.9
30	1203A 67R4W 10-14	103.4	67.5	40.5

Table 5b. Partition coefficients of selected elements between phlogopite and melt

											K_2O (%)	
reference	melt type	Ba	Th	Zr	Hf	Ti	Sr	La	Ce	Y	in melt	in phlogopite
Villemant et al., 1981	trachyte	10.0		2.5	1.8		0.7					
Adam er al., 1993	basanite	2.9		0.13			0.22			<1	2.74	7.28
LaTourrette et al., 1995	basanite	3.68	0.0014	0.017	0.19	1.768	0.159	0.028		0.018	2.15	7.91
Foley et al., 1996	alkaline lamprophyre	3.48	0.0145	0.023			0.183		0.0078	0.007	2.5	8.87
Schmidt et al., 1999	lamproite	1.03	0.00002	0.012		0.87	0.038		0.00002		8.7	9.9
	lamproite	1.61	0.000005	0.017		0.92	0.058		0.00002		9	9.8
	lamproite	0.56	0.0002	0.009		0.827	0.016		0.0002		8.6	9.7
Green et al., 2000	basanite	3.34		0.008	0.09	0.7	0.21	0.007		0.018	2.15	9.16

Fig. 1a

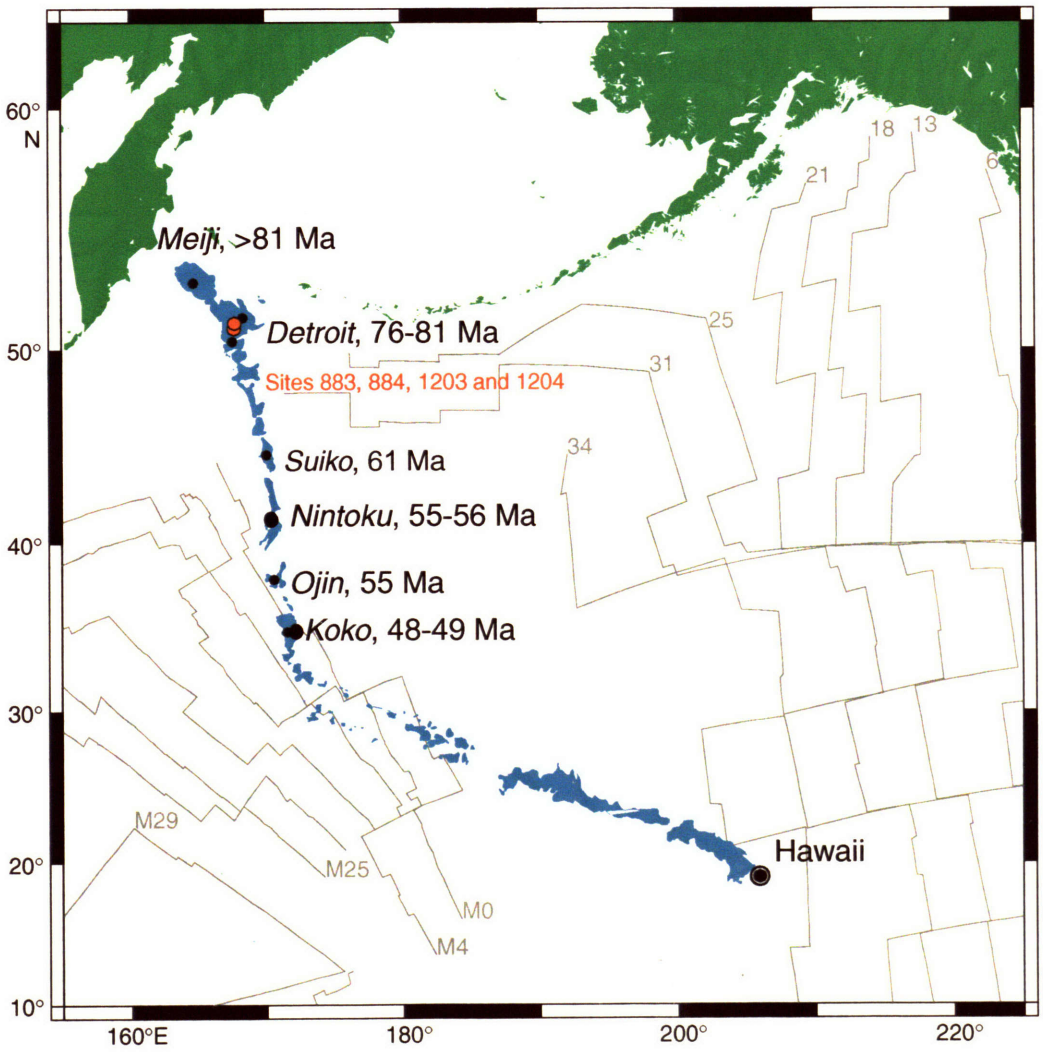
60° N
50°
40°
30°
20°
10°
160°E
180°
200°
220°
Meiji, >81 Ma
Detroit, 76-81 Ma
Sites 883, 884, 1203 and 1204
Suiko, 61 Ma
Nintoku, 55-56 Ma
Ojin, 55 Ma
Koko, 48-49 Ma
Hawaii
18
13
6
21
25
31
34
M29
M25
M0
M4

Fig. 1b

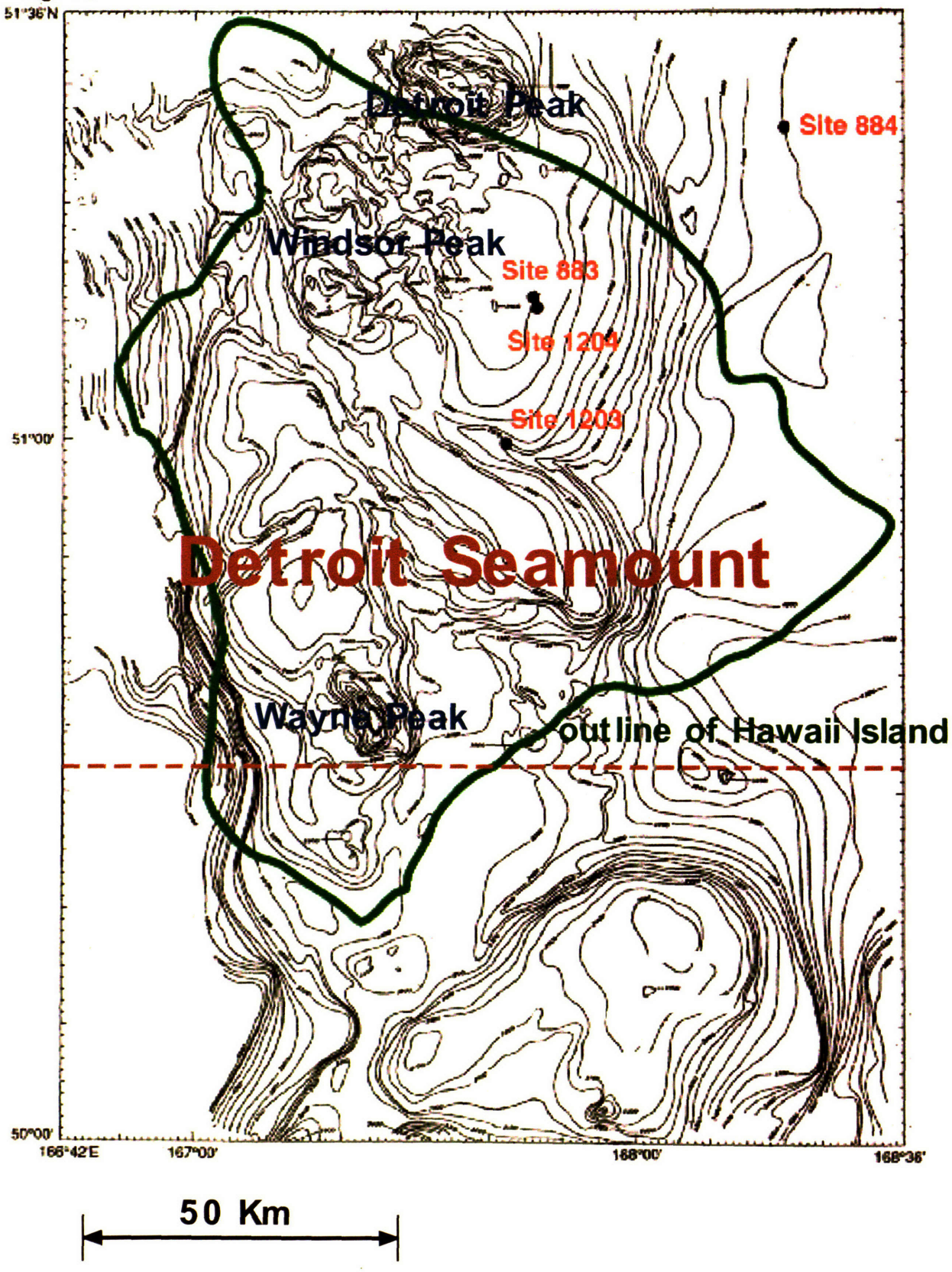
51°36'N
Detroit Peak
Site 884
Windsor Peak
Site 883
Site 1204
Site 1203
51°00'
Detroit Seamount
Wayne Peak
outline of Hawaii Island
50°00'
166°42'E
167°00'
168°00'
168°36'
50 Km

Fig. 2

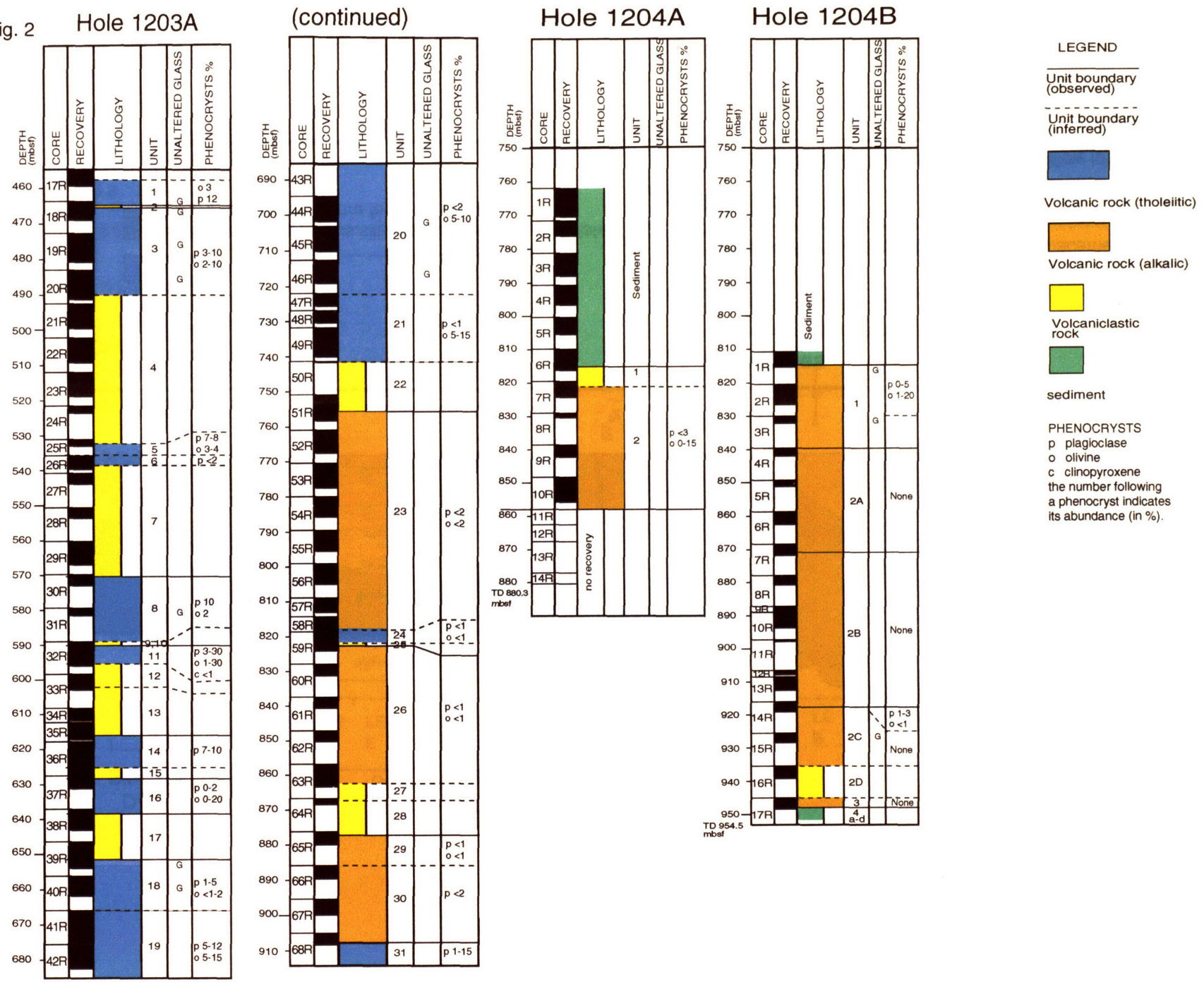
Hole 1203A
(continued)
Hole 1204A
Hole 1204B
DEPTH (mbsf)
CORE
RECOVERY
LITHOLOGY
UNIT
UNALTERED GLASS
PHENOCRYSTS %
TD 880.3 mbsf
TD 954.5 mbsf
no recovery
Sediment
LEGEND
Unit boundary (observed)
Unit boundary (inferred)
Volcanic rock (tholeiitic)
Volcanic rock (alkalic)
Volcaniclastic rock
sediment
PHENOCRYSTS
p plagioclase
o olivine
c clinopyroxene
the number following a phenocryst indicates its abundance (in %).

Fig. 3

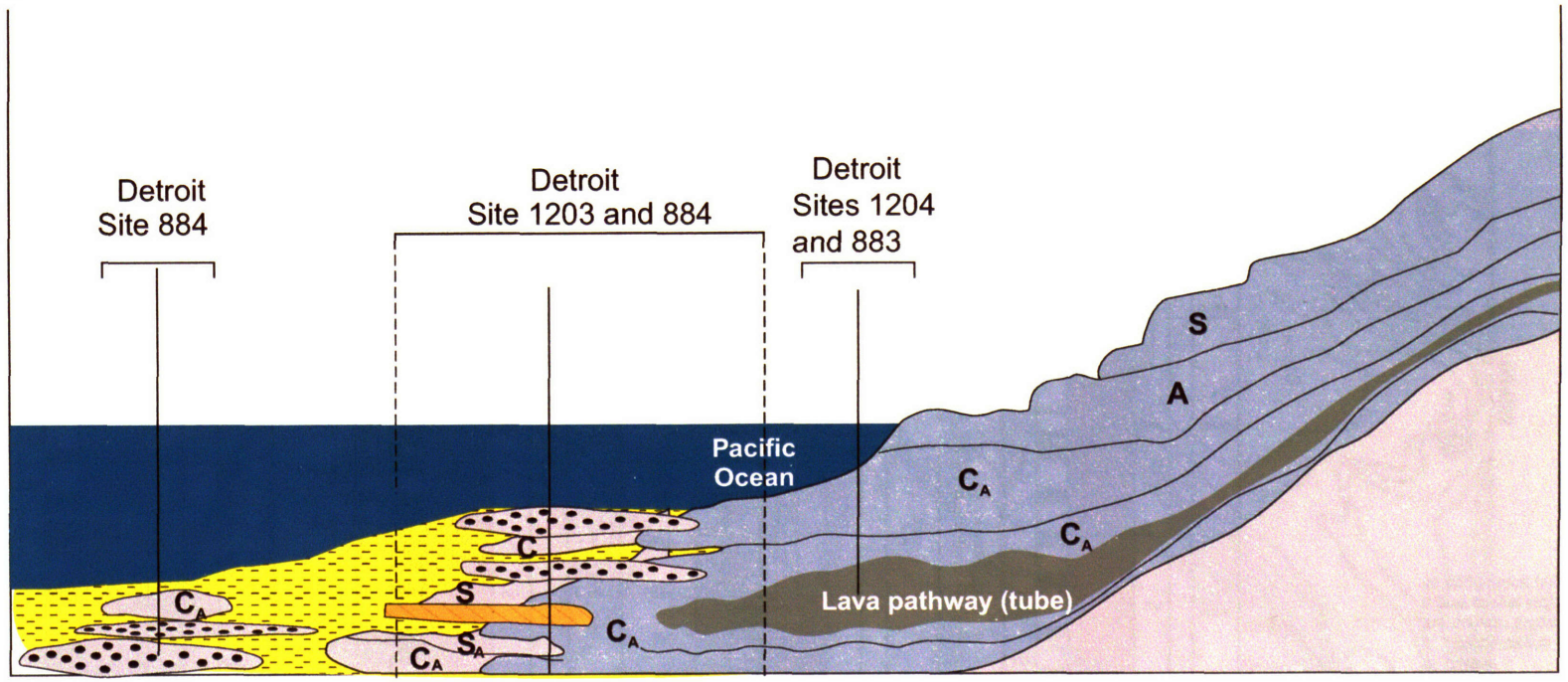

KEY

Lithologies

- Tholeiite basalt
- Alkali basalt
- Bedded calcerous silt- and sandtones intercalated with primary tephra fall deposits

Flow types

C, compound pahoehoe

S, simple pahoehoe

A, a'a

Subscript "A" indicates subaerial lava emplacement

- pillow lava
- lava delta (flow foot breccia and pillow lobes)

Fig 4a

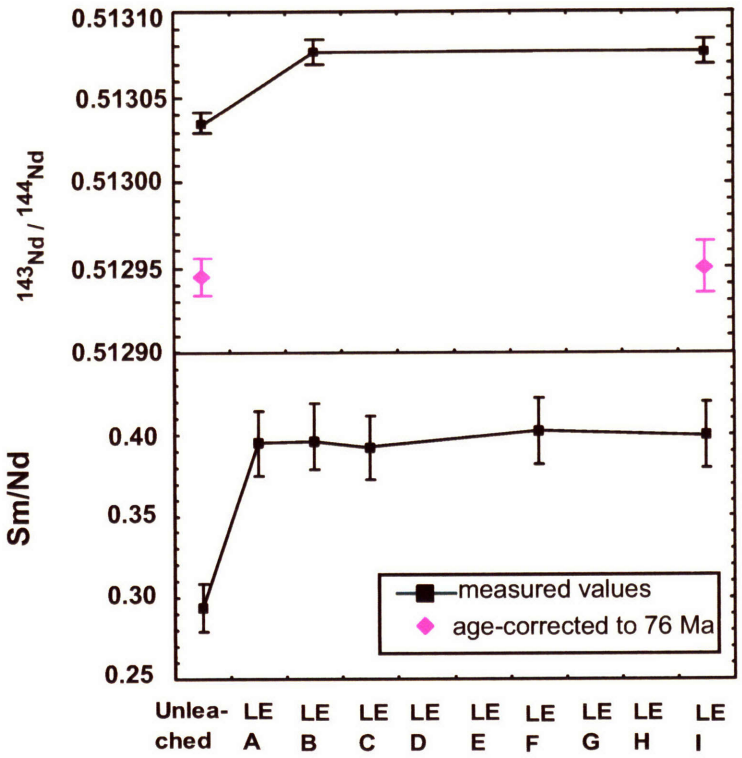
0.51310
0.51305
0.51300
0.51295
0.51290
143Nd / 144Nd
0.40
0.35
0.30
0.25
Sm/Nd
measured values
age-corrected to 76 Ma
Unlea-ched
LE A
LE B
LE C
LE D
LE E
LE F
LE G
LE H
LE I

Fig 4b

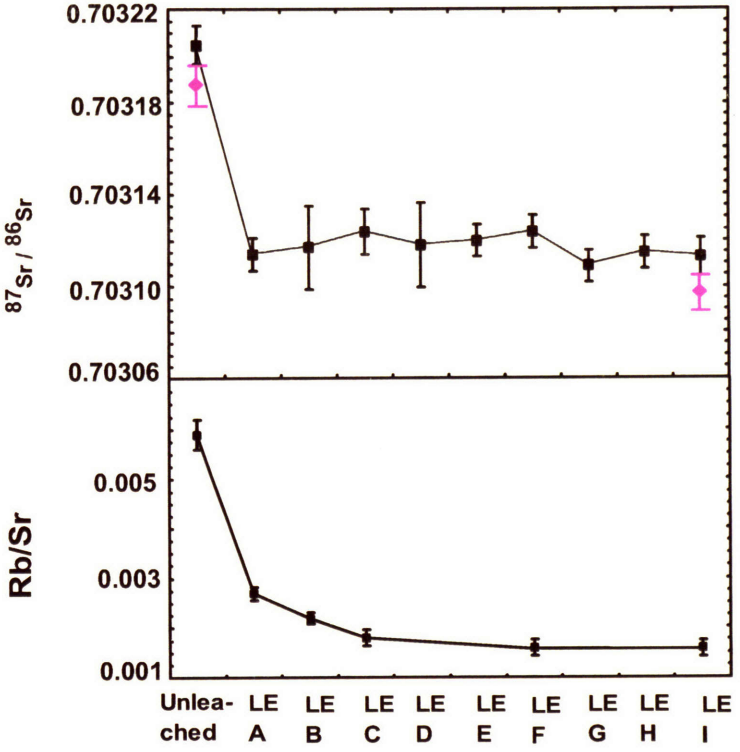
0.70322
0.70318
0.70314
0.70310
0.70306
87Sr / 86Sr
0.005
0.003
0.001
Rb/Sr
Unlea-ched
LE A
LE B
LE C
LE D
LE E
LE F
LE G
LE H
LE I

Fig 4c

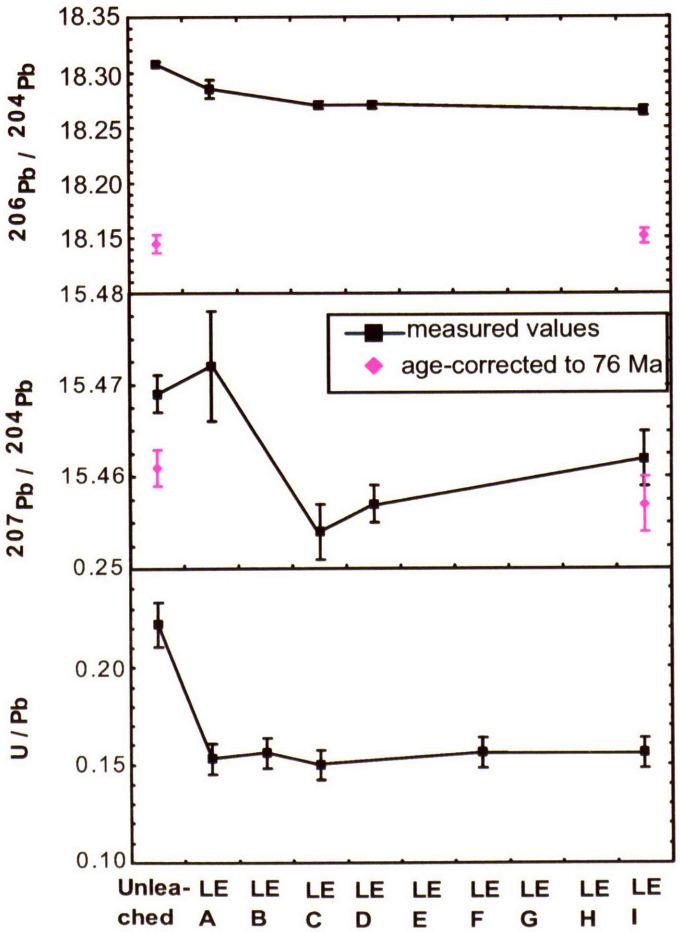
18.35
18.30
18.25
18.20
18.15
206Pb / 204Pb
15.48
15.47
15.46
207Pb / 204Pb
measured values
age-corrected to 76 Ma
0.25
0.20
0.15
0.10
U / Pb
Unlea-ched
LE A
LE B
LE C
LE D
LE E
LE F
LE G
LE H
LE I

Fig 4d

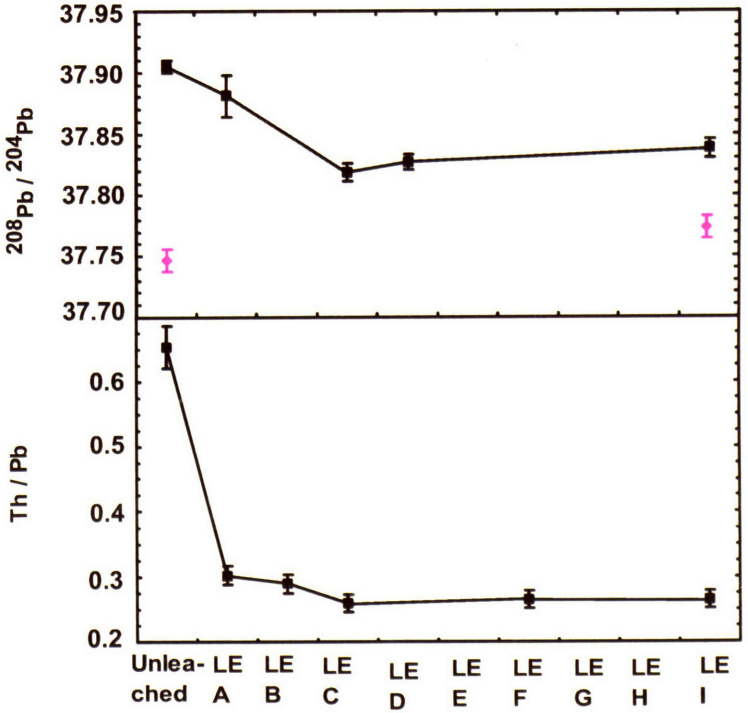
37.95
37.90
37.85
37.80
37.75
37.70
208Pb / 204Pb
0.6
0.5
0.4
0.3
0.2
Th / Pb
Unlea-ched
LE A
LE B
LE C
LE D
LE E
LE F
LE G
LE H
LE I

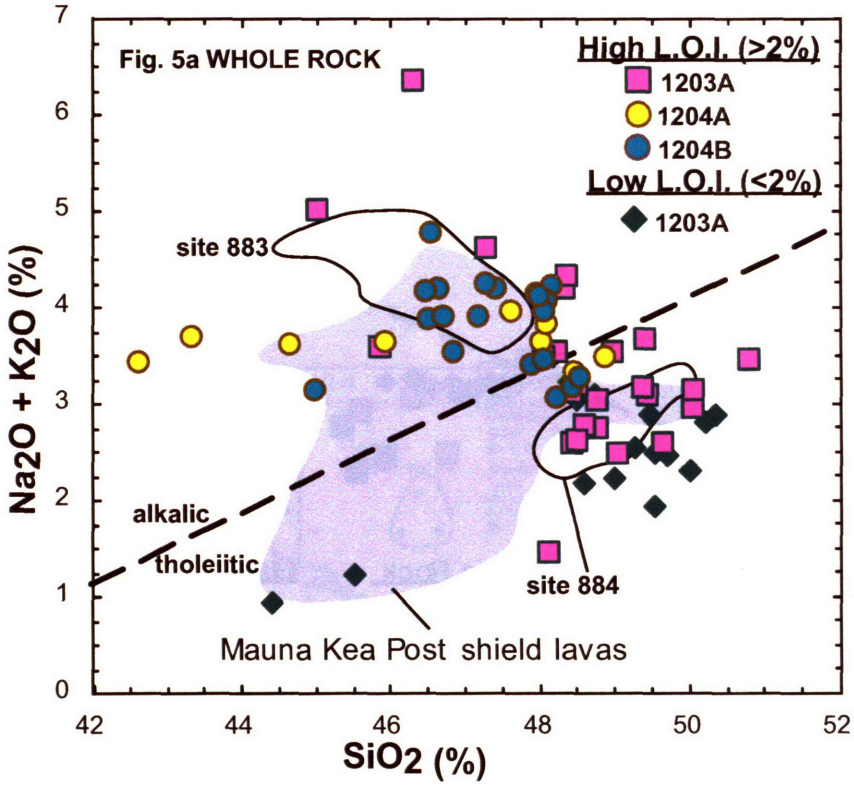
Fig. 5a WHOLE ROCK
High L.O.I. (>2%)
1203A
1204A
1204B
Low L.O.I. (<2%)
1203A
site 883
alkalic
tholeiitic
site 884
Mauna Kea Post shield lavas
Na2O + K2O (%)
SiO2 (%)
0
1
2
3
4
5
6
7
42
44
46
48
50
52

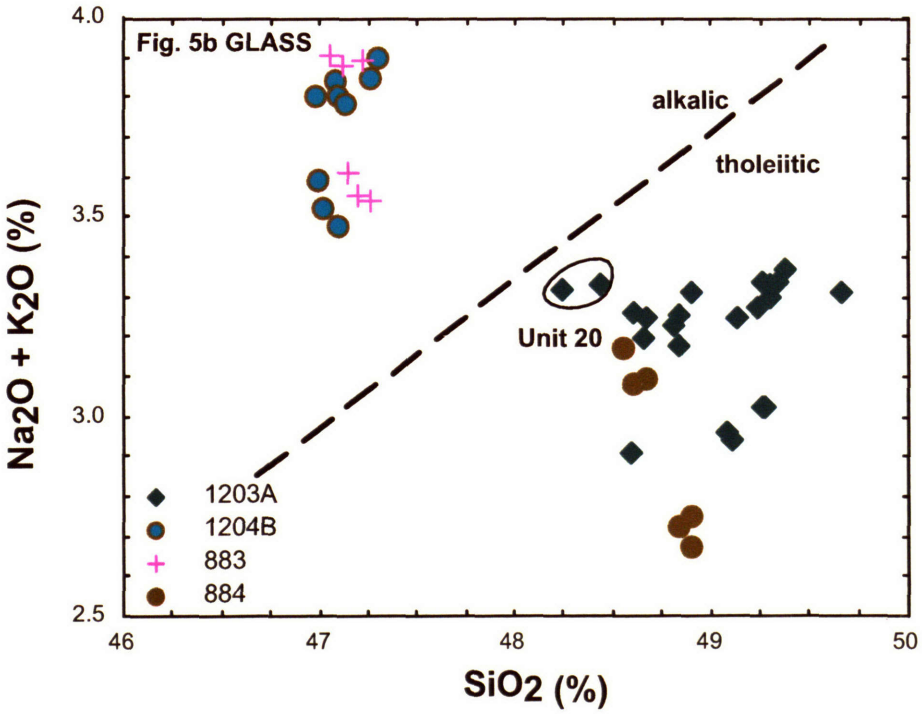
Fig. 5b GLASS
alkalic
tholeiitic
Unit 20
1203A
1204B
883
884
Na2O + K2O (%)
SiO2 (%)
2.5
3.0
3.5
4.0
46
47
48
49
50

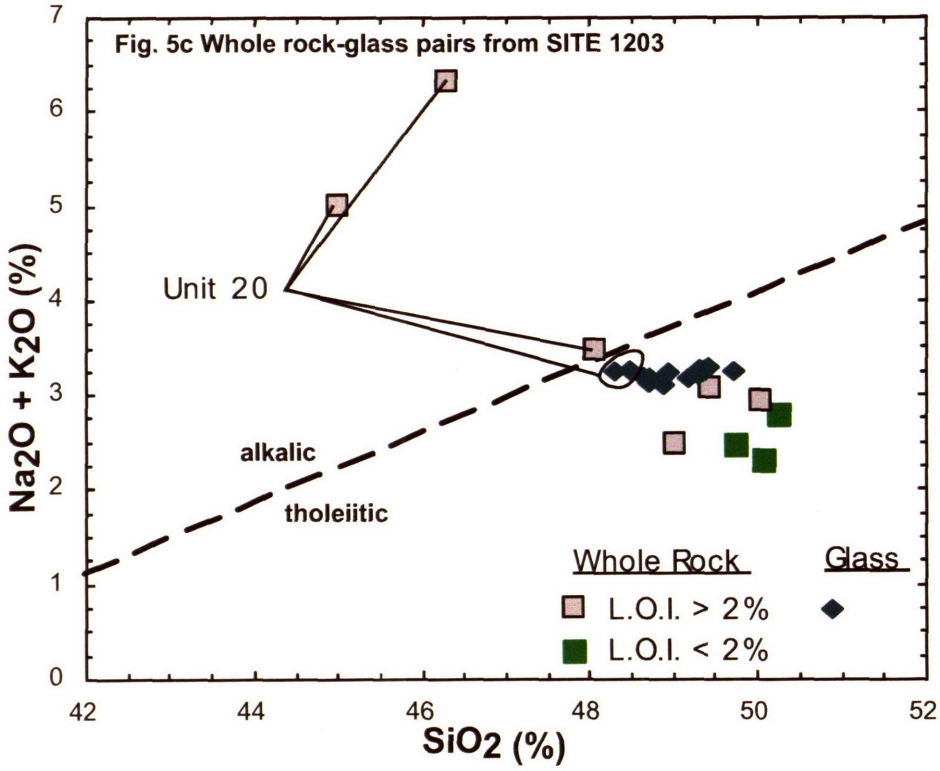
Fig. 5c Whole rock-glass pairs from SITE 1203
Unit 20
alkalic
tholeiitic
Whole Rock
Glass
L.O.I. > 2%
L.O.I. < 2%
Na2O + K2O (%)
SiO2 (%)
0
1
2
3
4
5
6
7
42
44
46
48
50
52

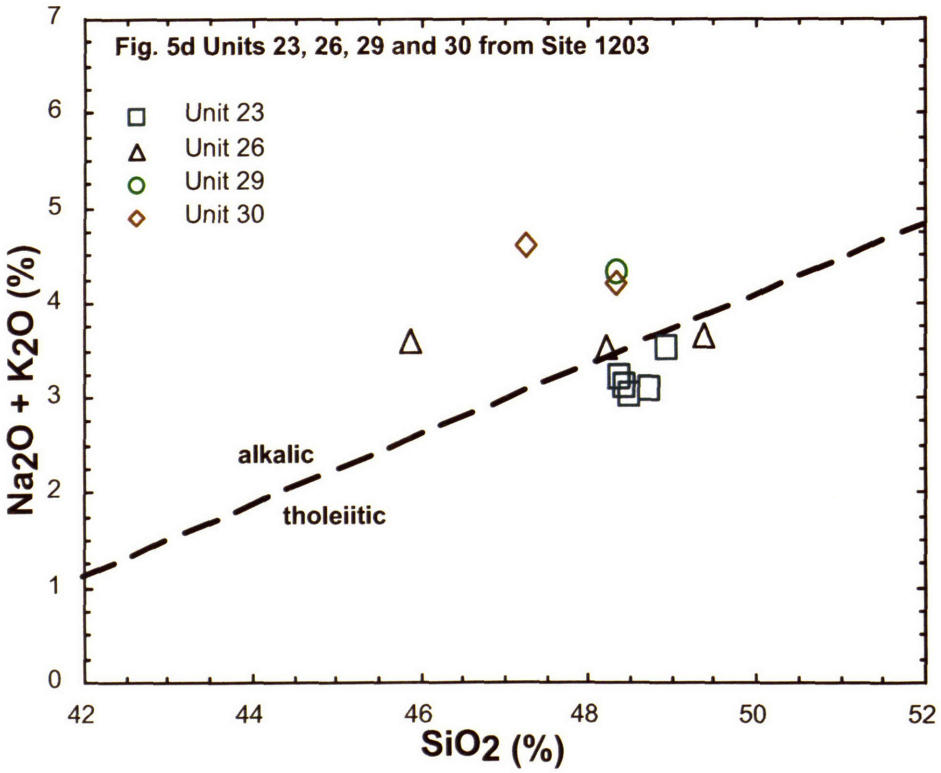
Fig. 5d Units 23, 26, 29 and 30 from Site 1203
Unit 23
Unit 26
Unit 29
Unit 30
alkalic
tholeiitic
Na2O + K2O (%)
SiO2 (%)
0
1
2
3
4
5
6
7
42
44
46
48
50
52

Fig. 6

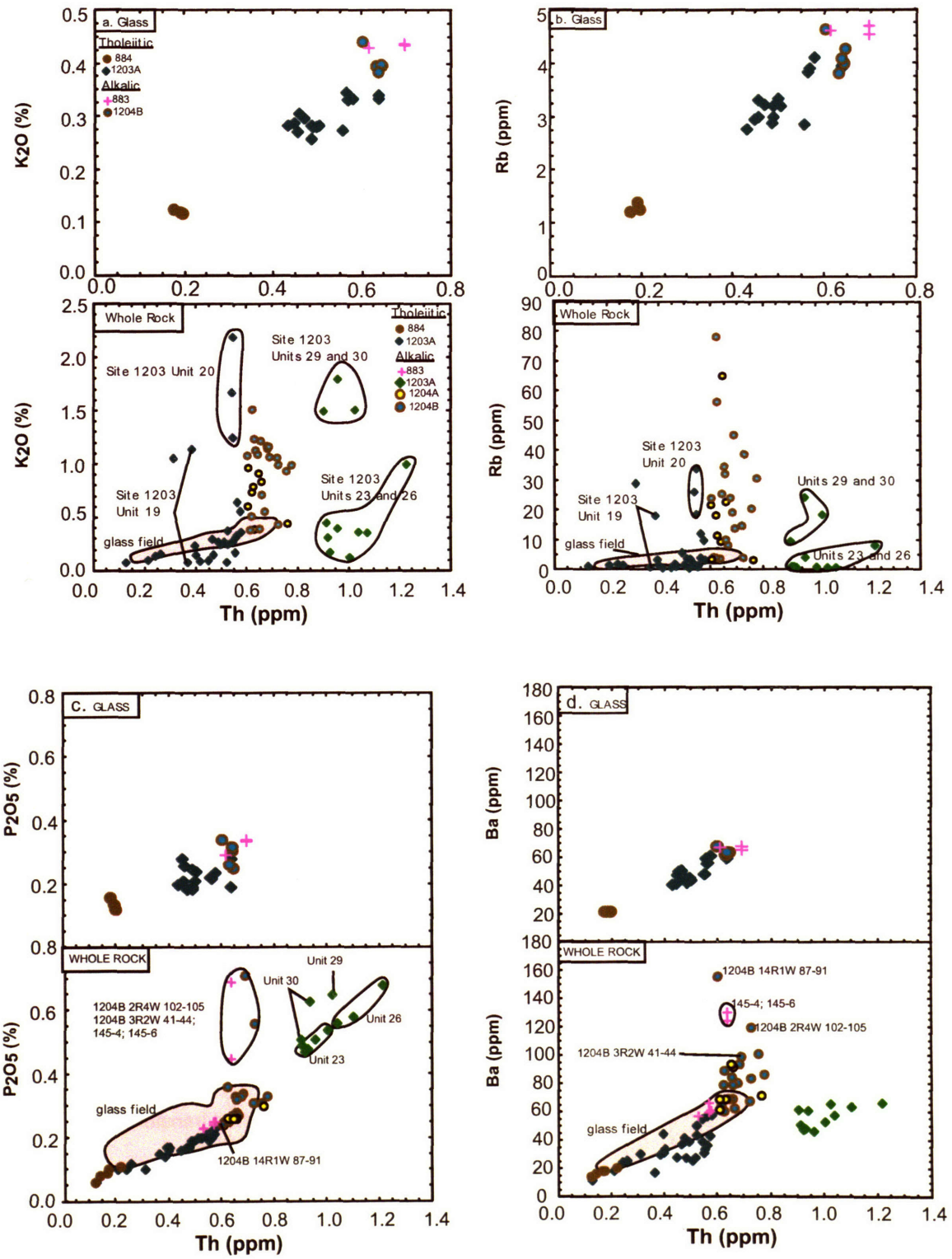
a. Glass
Tholeiitic
884
1203A
Alkalic
883
1204B
K2O (%)
Whole Rock
Site 1203 Unit 20
Site 1203 Units 29 and 30
Site 1203 Unit 19
Site 1203 Units 23 and 26
glass field
1204A
Th (ppm)
b. Glass
Rb (ppm)
c. GLASS
P2O5 (%)
WHOLE ROCK
1204B 2R4W 102-105
1204B 3R2W 41-44;
145-4; 145-6
Unit 29
Unit 30
Unit 26
Unit 23
1204B 14R1W 87-91
d. GLASS
Ba (ppm)

Fig 7

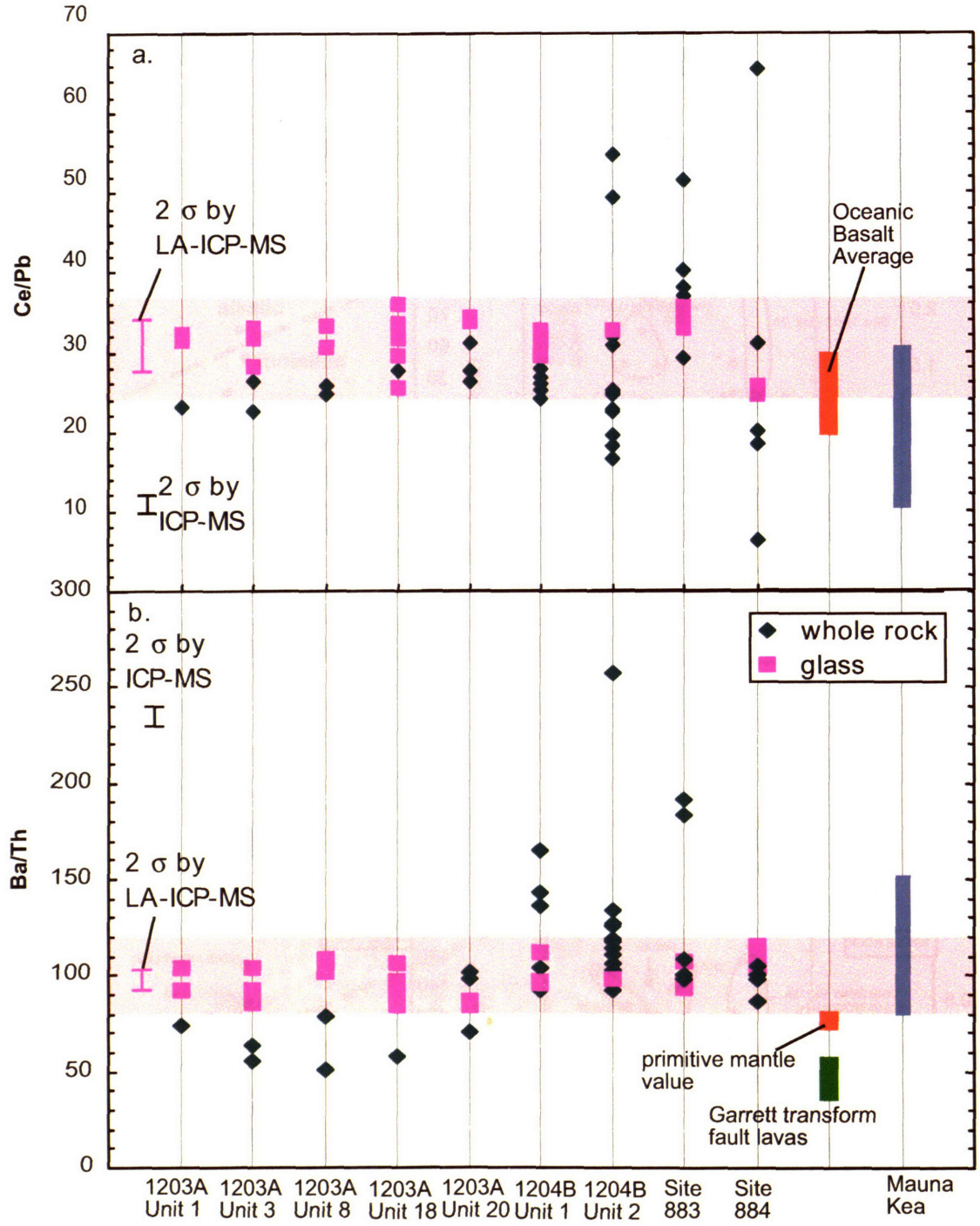
a.
Ce/Pb
70
60
50
40
30
20
10
2 σ by
LA-ICP-MS
2 σ by
ICP-MS
Oceanic
Basalt
Average
b.
Ba/Th
300
250
200
150
100
50
0
2 σ by
ICP-MS
2 σ by
LA-ICP-MS
whole rock
glass
primitive mantle
value
Garrett transform
fault lavas
1203A
Unit 1
1203A
Unit 3
1203A
Unit 8
1203A
Unit 18
1203A
Unit 20
1204B
Unit 1
1204B
Unit 2
Site
883
Site
884
Mauna
Kea

Fig. 8a

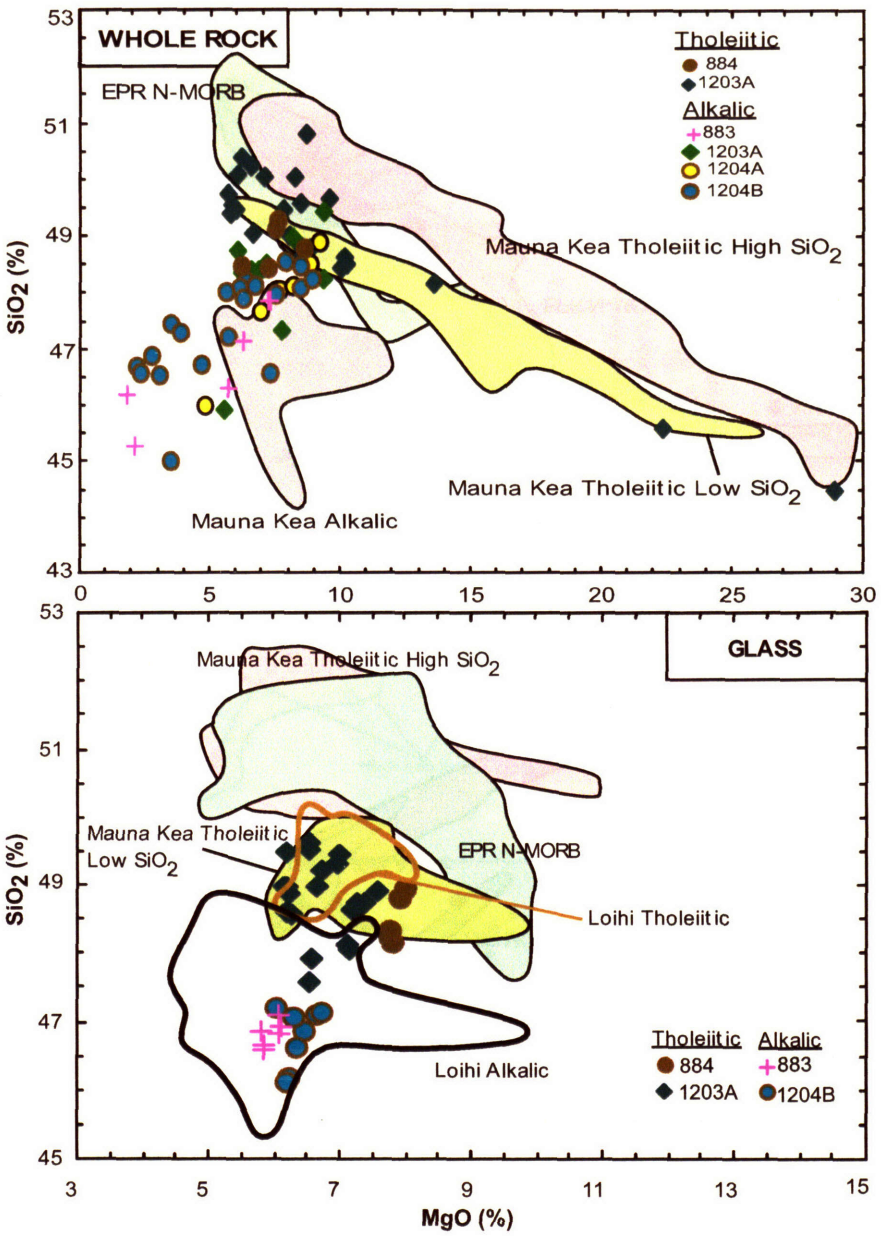
WHOLE ROCK
EPR N-MORB
Tholeiitic
884
1203A
Alkalic
883
1203A
1204A
1204B
Mauna Kea Tholeiitic High SiO2
Mauna Kea Tholeiitic Low SiO2
Mauna Kea Alkalic
SiO2 (%)
GLASS
Mauna Kea Tholeiitic High SiO2
Mauna Kea Tholeiitic Low SiO2
EPR N-MORB
Loihi Tholeiitic
Loihi Alkalic
Tholeiitic
884
1203A
Alkalic
883
1204B
MgO (%)

Fig. 8b

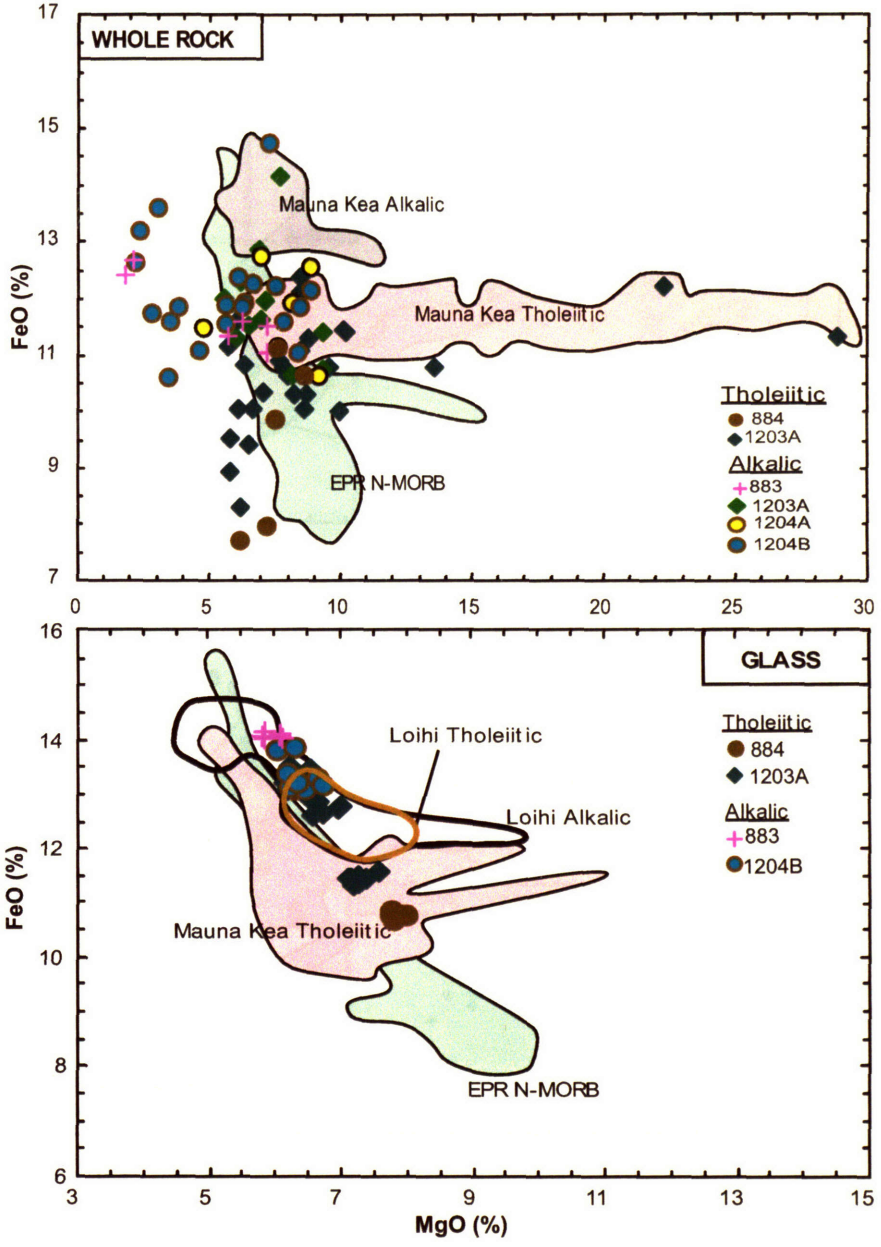
WHOLE ROCK
Mauna Kea Alkalic
Mauna Kea Tholeiitic
EPR N-MORB
Tholeiitic
884
1203A
Alkalic
883
1203A
1204A
1204B
FeO (%)
GLASS
Loihi Tholeiitic
Loihi Alkalic
Mauna Kea Tholeiitic
EPR N-MORB
Tholeiitic
884
1203A
Alkalic
883
1204B
MgO (%)

Fig.8c

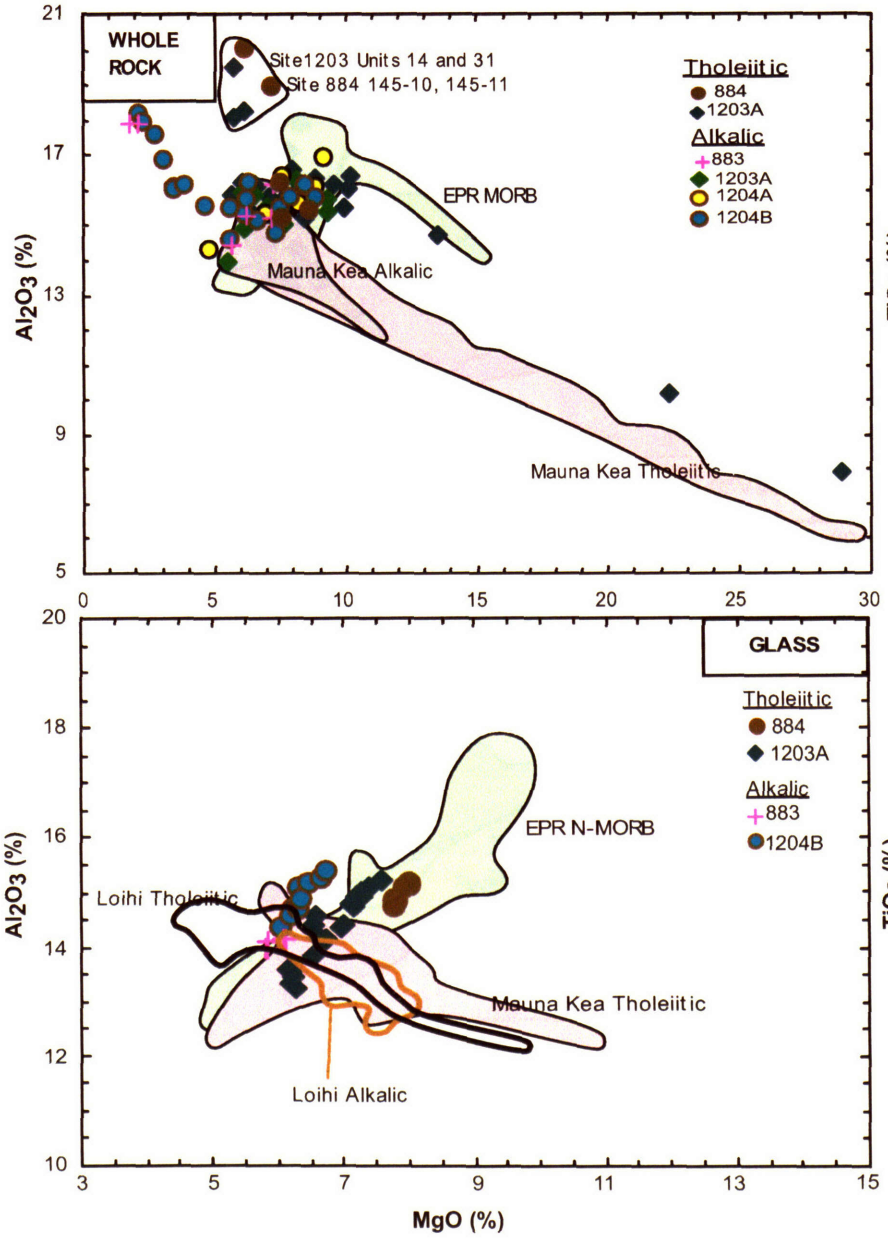
WHOLE ROCK
Site1203 Units 14 and 31
Site 884 145-10, 145-11
Tholeiitic
884
1203A
Alkalic
883
1203A
1204A
1204B
EPR MORB
Mauna Kea Alkalic
Mauna Kea Tholeiitic
Al2O3 (%)
GLASS
Tholeiitic
884
1203A
Alkalic
883
1204B
EPR N-MORB
Loihi Tholeiitic
Mauna Kea Tholeiitic
Loihi Alkalic
Al2O3 (%)
MgO (%)

Fig. 8d

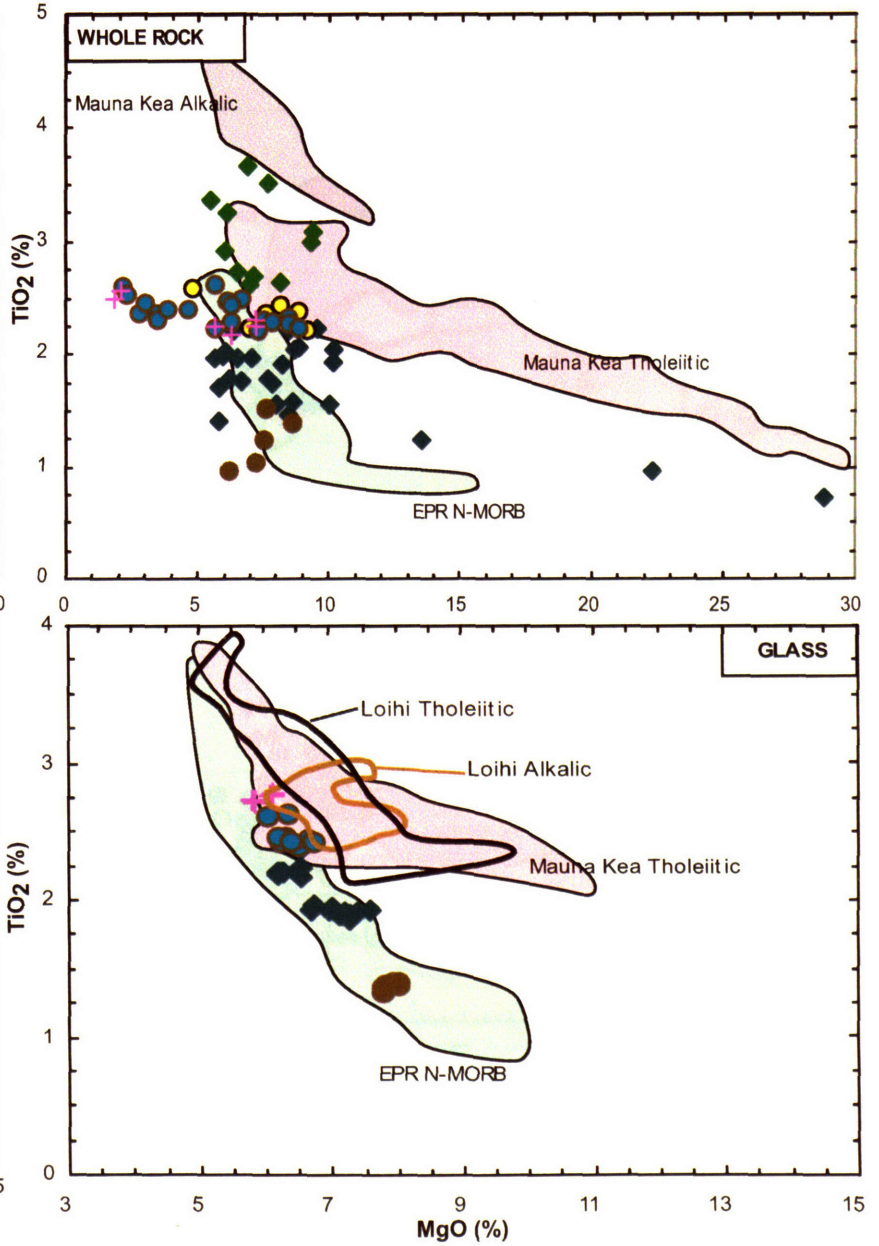
WHOLE ROCK
Mauna Kea Alkalic
Mauna Kea Tholeiitic
EPR N-MORB
TiO2 (%)
GLASS
Loihi Tholeiitic
Loihi Alkalic
Mauna Kea Tholeiitic
EPR N-MORB
TiO2 (%)
MgO (%)

Fig. 9

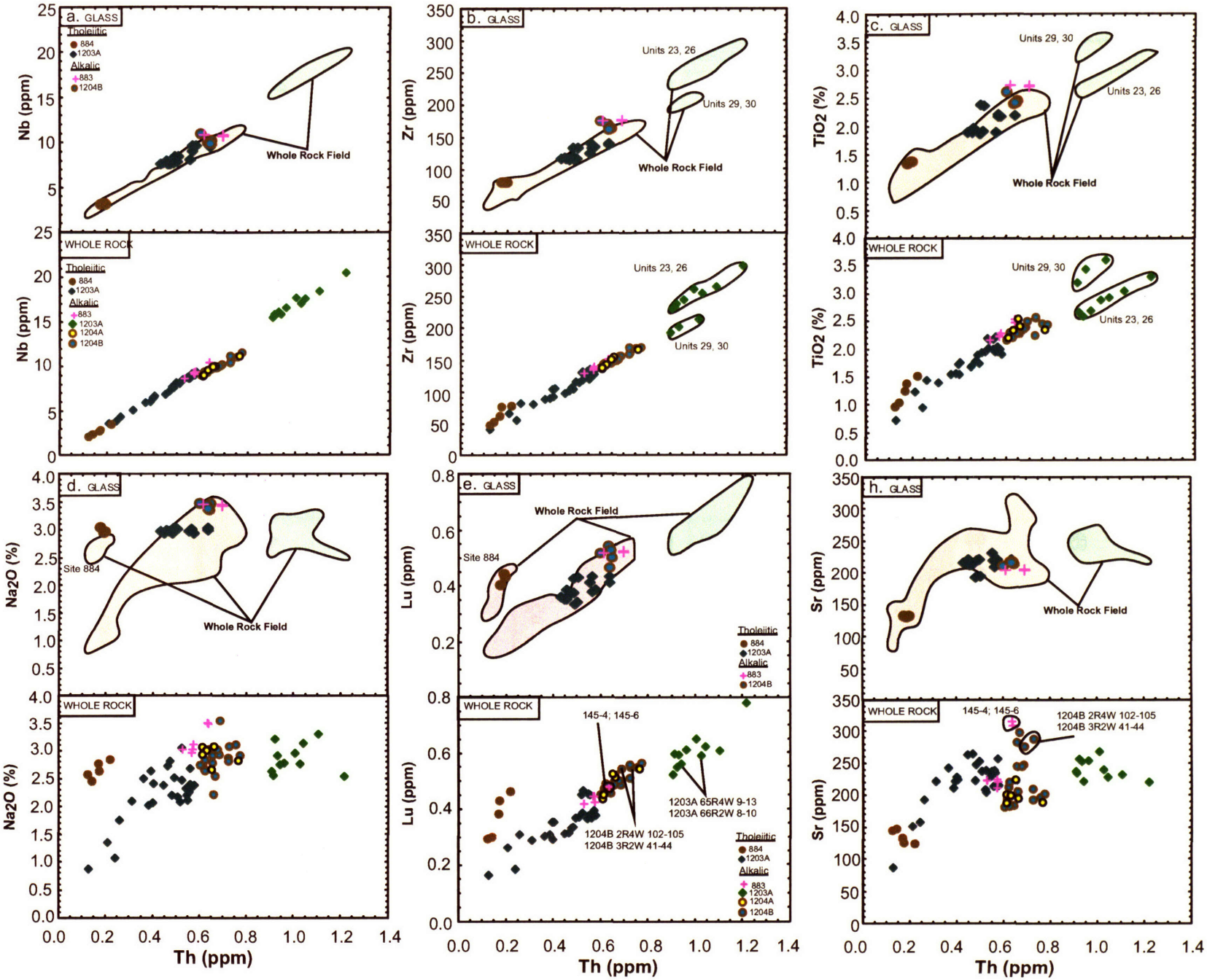
a. GLASS
Tholeiitic
884
1203A
Alkalic
883
1204B
Whole Rock Field
WHOLE ROCK
Tholeiitic
884
1203A
Alkalic
883
1203A
1204A
1204B
Nb (ppm)
b. GLASS
Units 23, 26
Units 29, 30
Whole Rock Field
WHOLE ROCK
Zr (ppm)
c. GLASS
Units 29, 30
Units 23, 26
Whole Rock Field
WHOLE ROCK
TiO2 (%)
d. GLASS
Site 884
Whole Rock Field
WHOLE ROCK
Na2O (%)
e. GLASS
Whole Rock Field
Site 884
WHOLE ROCK
145-4; 145-6
1204B 2R4W 102-105
1204B 3R2W 41-44
1203A 65R4W 9-13
1203A 66R2W 8-10
Lu (ppm)
h. GLASS
Whole Rock Field
WHOLE ROCK
145-4; 145-6
1204B 2R4W 102-105
1204B 3R2W 41-44
Sr (ppm)
Th (ppm)

Fig. 10

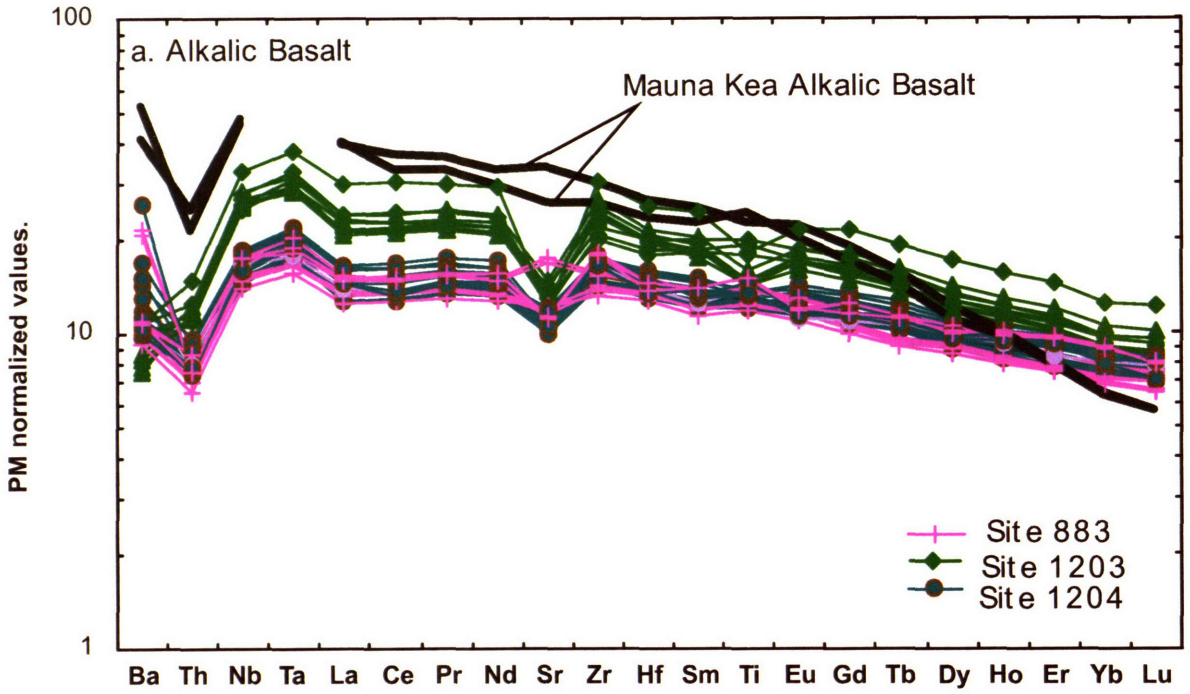
a. Alkalic Basalt
Mauna Kea Alkalic Basalt
Site 883
Site 1203
Site 1204
PM normalized values.
100
10
1
Ba Th Nb Ta La Ce Pr Nd Sr Zr Hf Sm Ti Eu Gd Tb Dy Ho Er Yb Lu

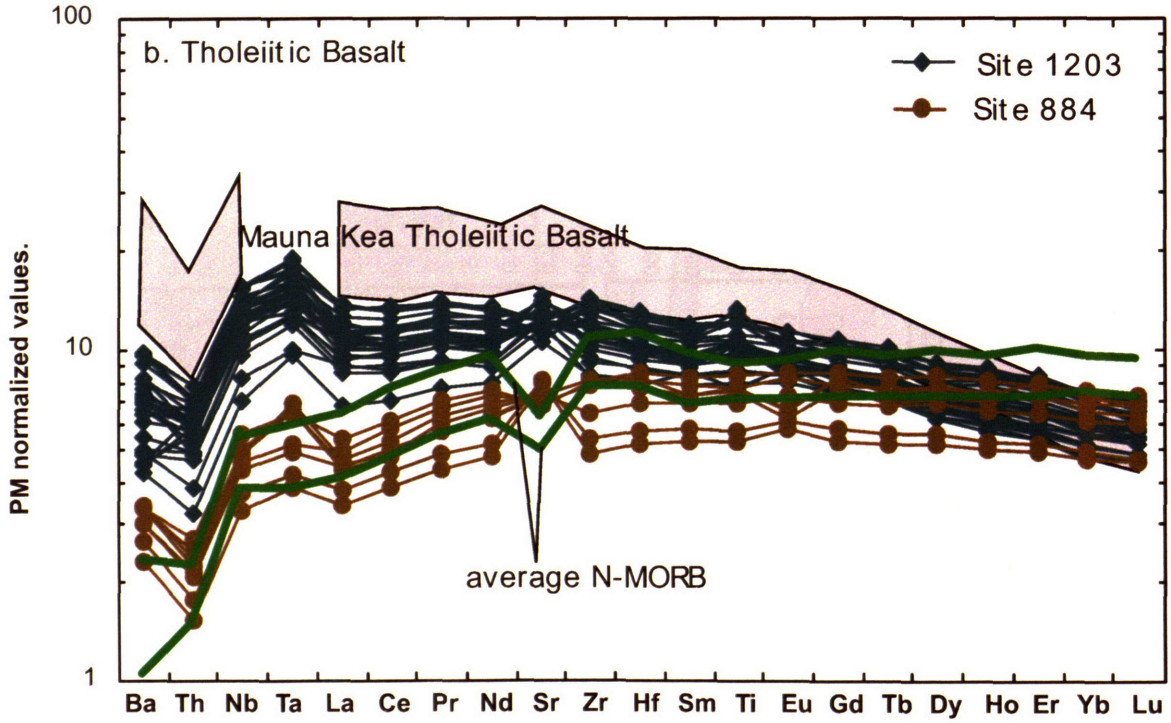
b. Tholeiitic Basalt
Site 1203
Site 884
Mauna Kea Tholeiitic Basalt
average N-MORB
PM normalized values.
100
10
1
Ba Th Nb Ta La Ce Pr Nd Sr Zr Hf Sm Ti Eu Gd Tb Dy Ho Er Yb Lu

Fig. 11a

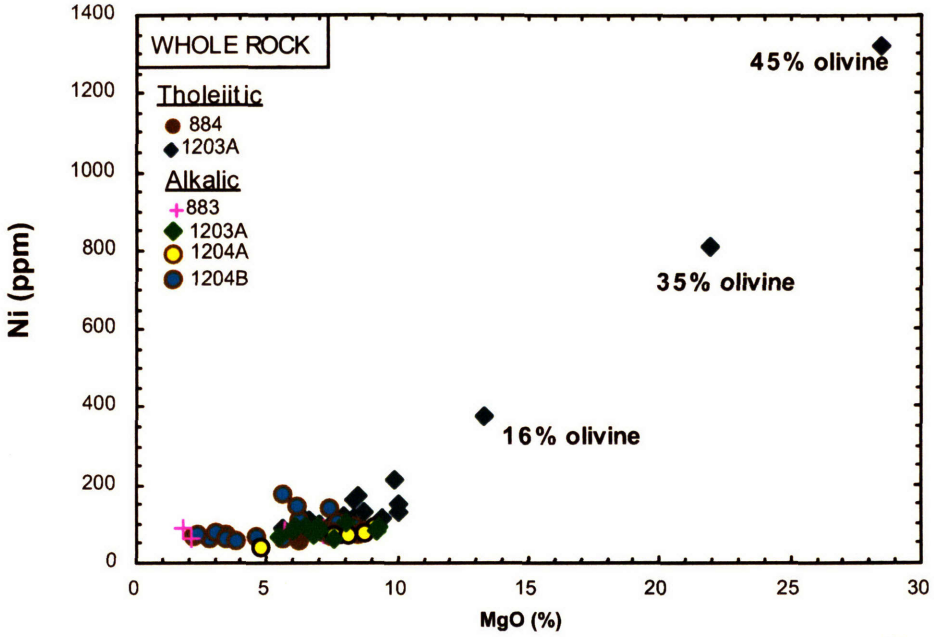

Fig. 11b

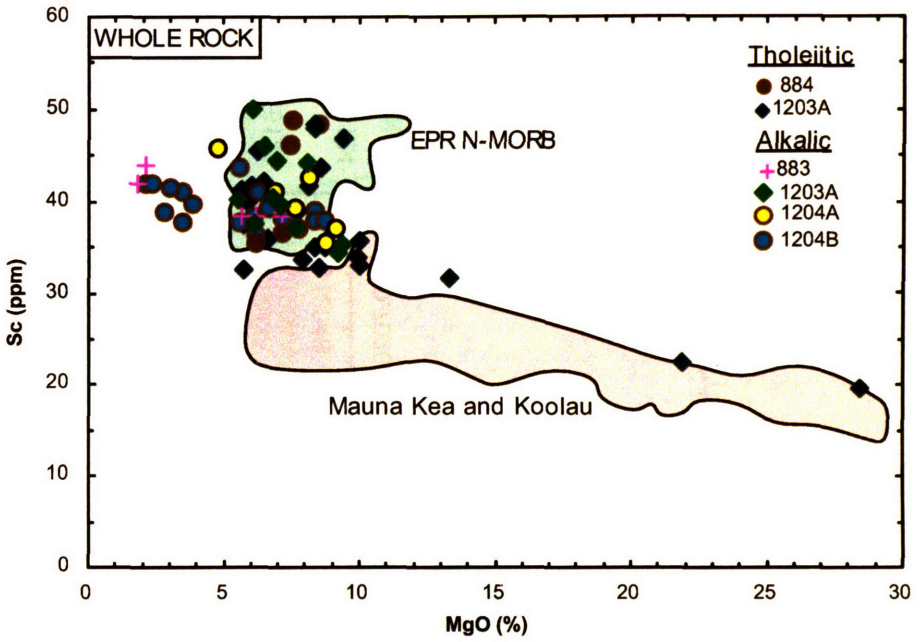

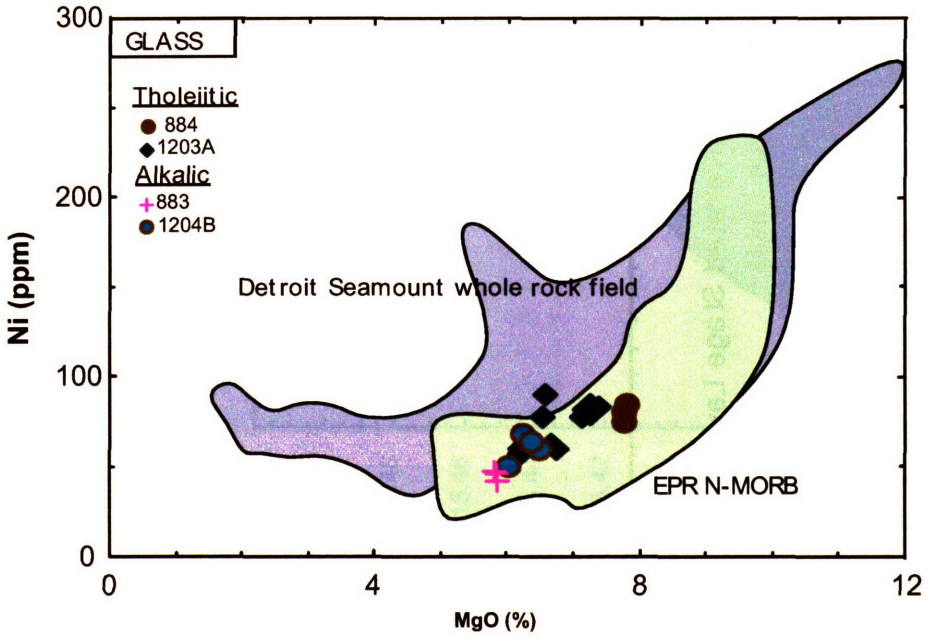

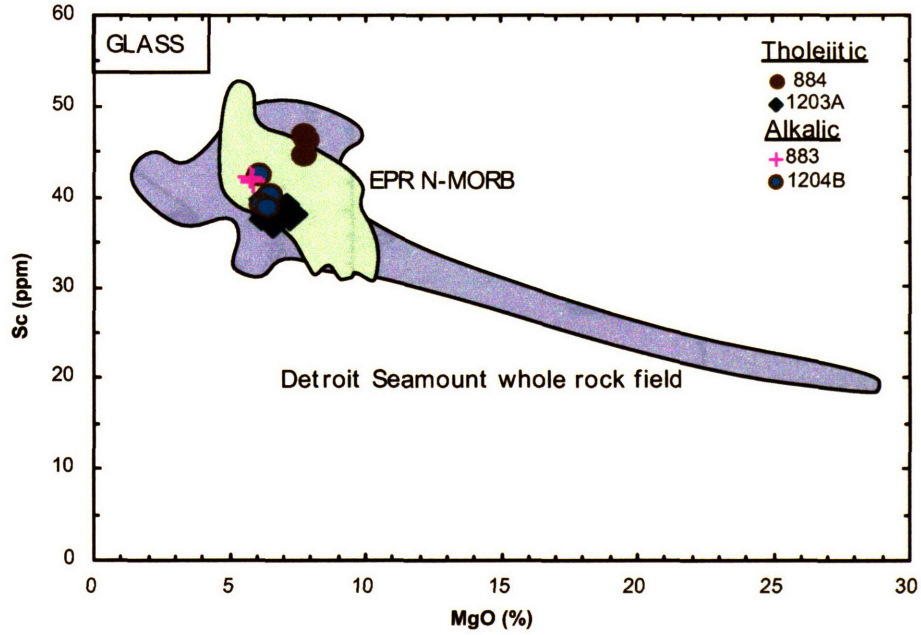

Fig 12a

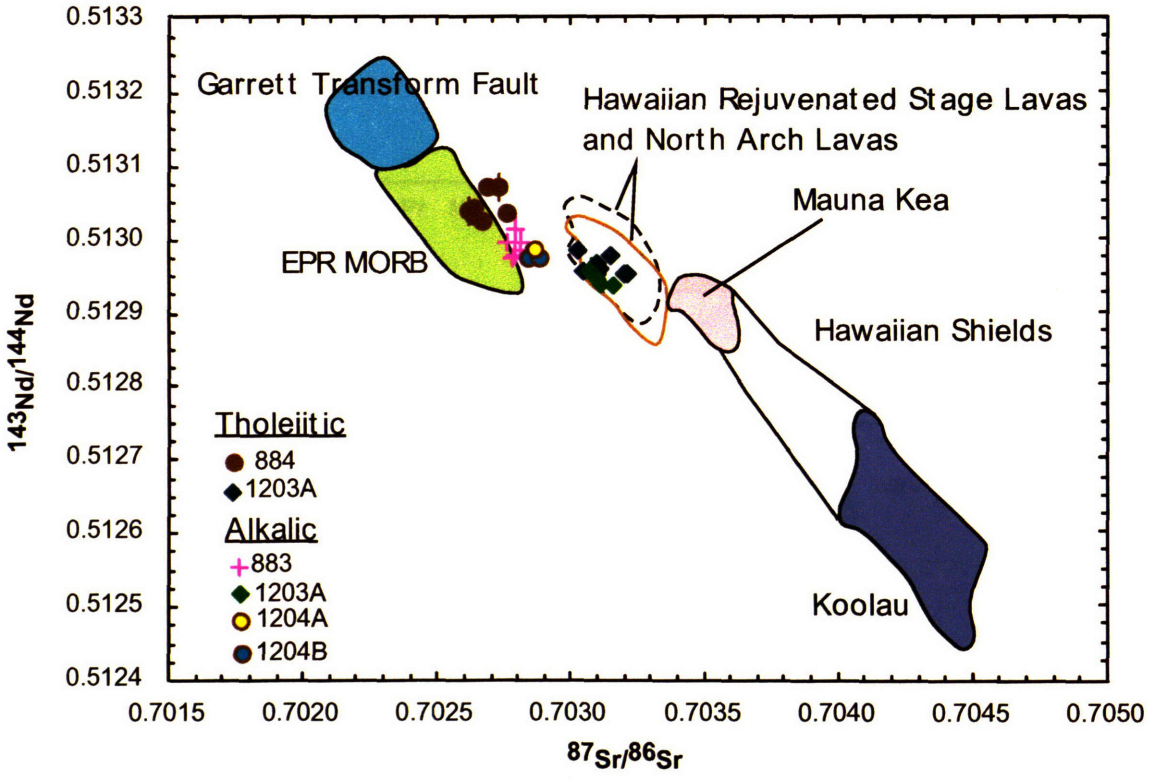
0.5133
0.5132
0.5131
0.5130
0.5129
0.5128
0.5127
0.5126
0.5125
0.5124
143Nd/144Nd
0.7015
0.7020
0.7025
0.7030
0.7035
0.7040
0.7045
0.7050
87Sr/86Sr
Garrett Transform Fault
Hawaiian Rejuvenated Stage Lavas
and North Arch Lavas
Mauna Kea
EPR MORB
Hawaiian Shields
Koolau
Tholeiitic
884
1203A
Alkalic
883
1203A
1204A
1204B

Fig 12b

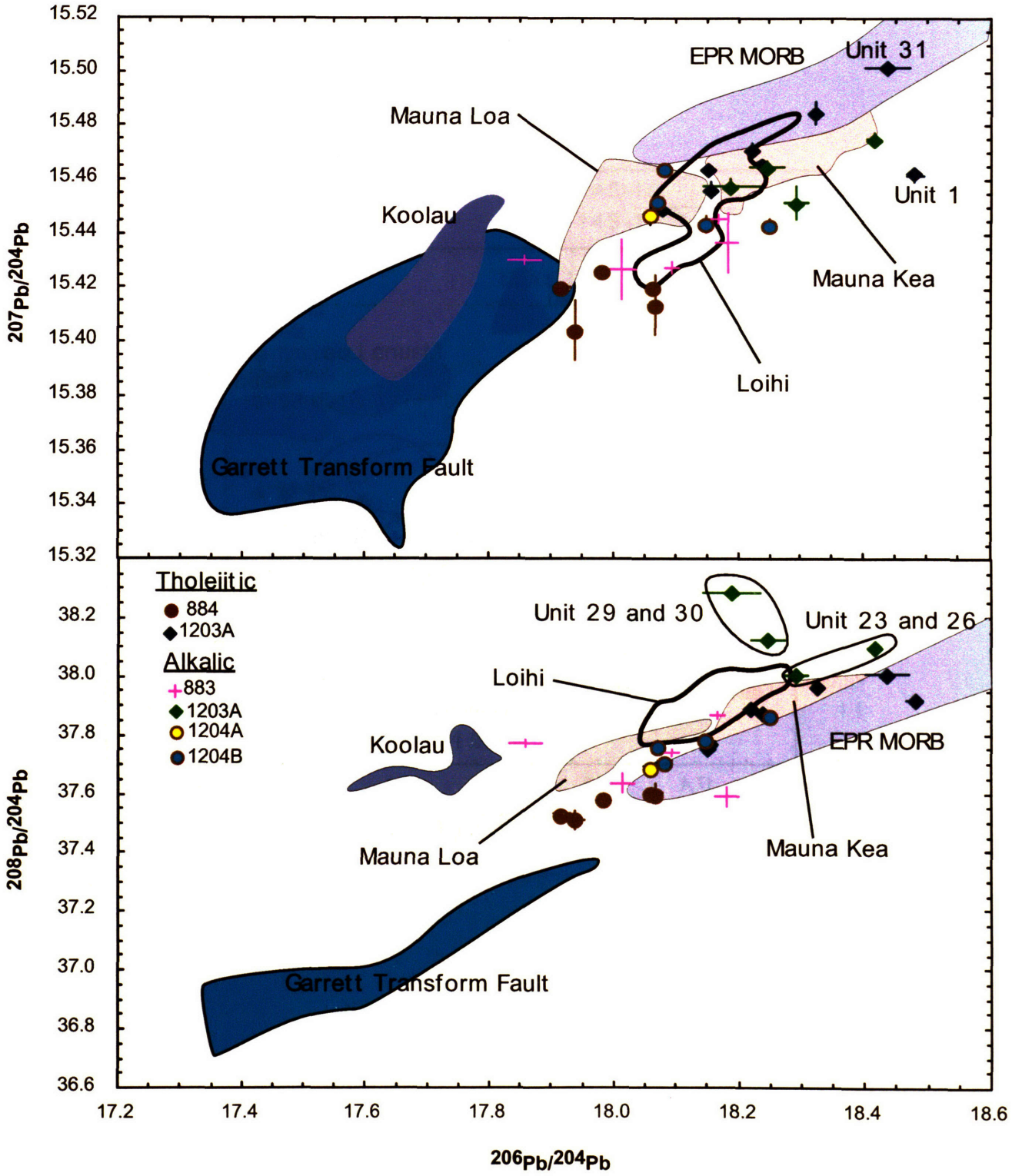
EPR MORB
Unit 31
Mauna Loa
Unit 1
Koolau
Mauna Kea
Loihi
Garrett Transform Fault
Tholeiitic
884
1203A
Alkalic
883
1203A
1204A
1204B
Unit 29 and 30
Unit 23 and 26
Loihi
Koolau
EPR MORB
Mauna Loa
Mauna Kea
Garrett Transform Fault
207Pb/204Pb
208Pb/204Pb
206Pb/204Pb
15.52
15.50
15.48
15.46
15.44
15.42
15.40
15.38
15.36
15.34
15.32
38.2
38.0
37.8
37.6
37.4
37.2
37.0
36.8
36.6
17.2
17.4
17.6
17.8
18.0
18.2
18.4
18.6

Fig 12c

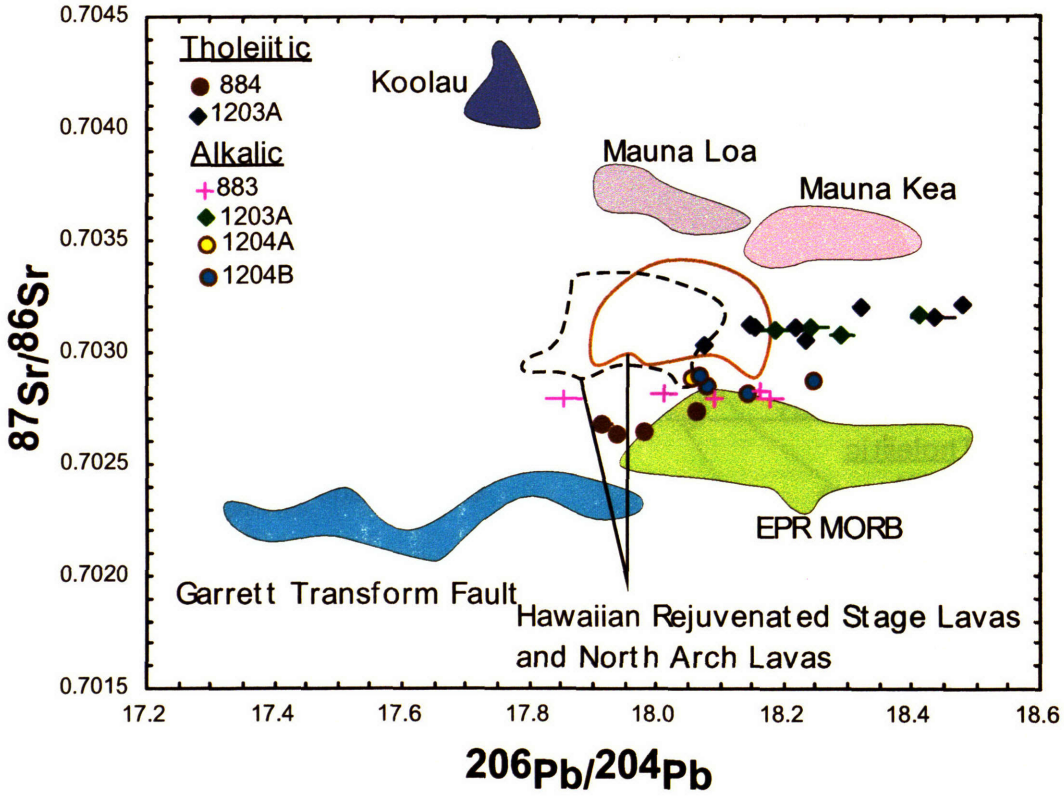
Tholeiitic
884
1203A
Alkalic
883
1203A
1204A
1204B
Koolau
Mauna Loa
Mauna Kea
EPR MORB
Garrett Transform Fault
Hawaiian Rejuvenated Stage Lavas
and North Arch Lavas
0.7045
0.7040
0.7035
0.7030
0.7025
0.7020
0.7015
87Sr/86Sr
17.2
17.4
17.6
17.8
18.0
18.2
18.4
18.6
206Pb/204Pb

Fig. 13

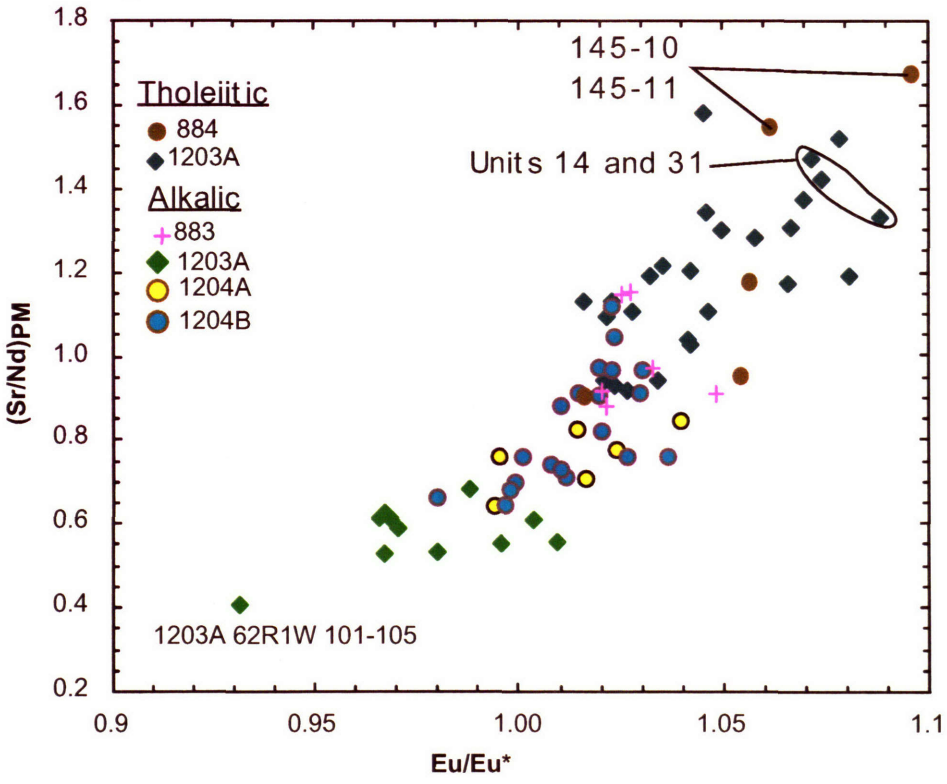
Tholeiitic
884
1203A
Alkalic
883
1203A
1204A
1204B
145-10
145-11
Units 14 and 31
1203A 62R1W 101-105
(Sr/Nd)PM
Eu/Eu*
1.8
1.6
1.4
1.2
1.0
0.8
0.6
0.4
0.2
0.9
0.95
1.00
1.05
1.1

Fig.14

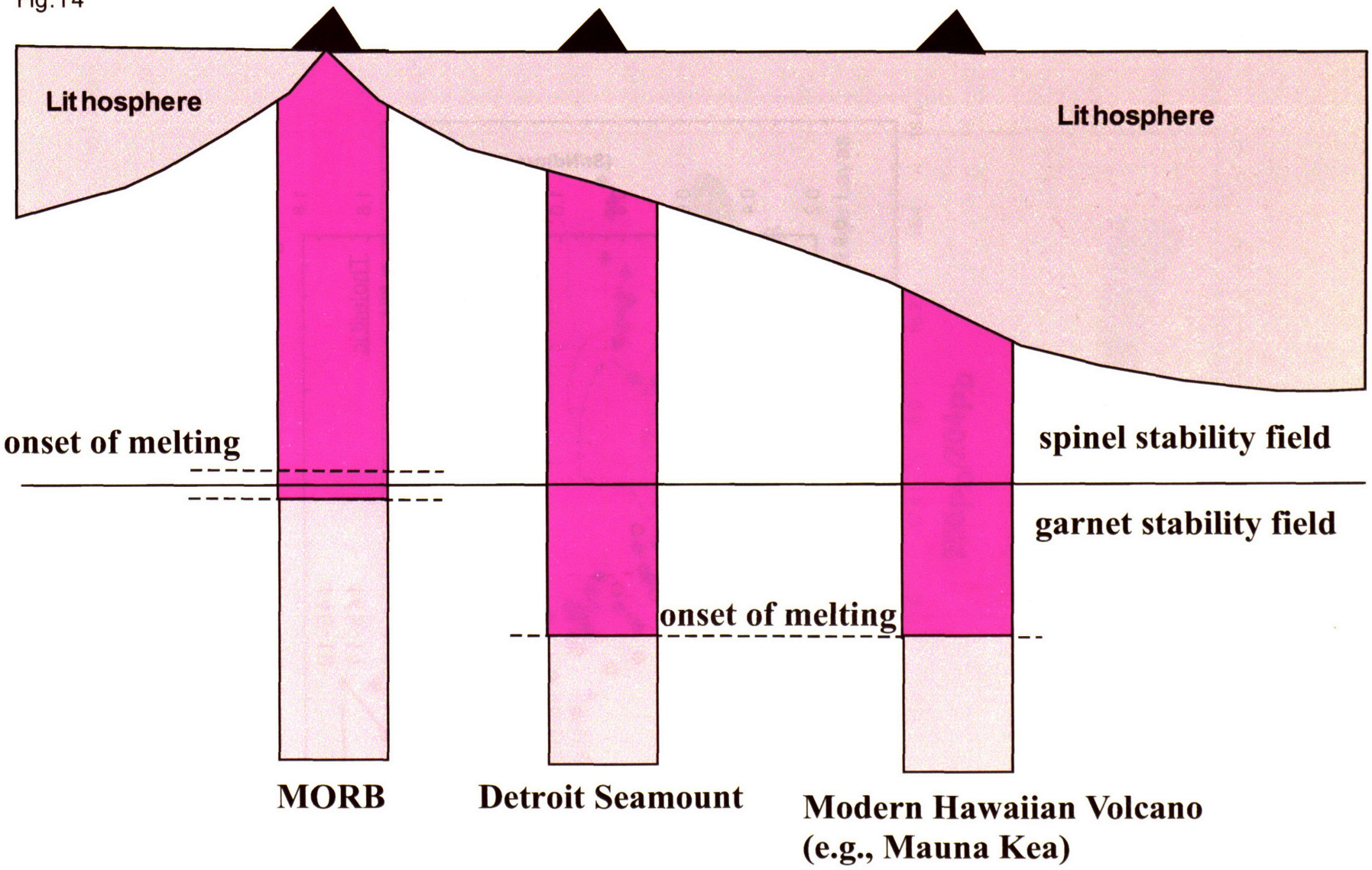
Lithosphere
Lithosphere
onset of melting
spinel stability field
garnet stability field
onset of melting
MORB
Detroit Seamount
Modern Hawaiian Volcano
(e.g., Mauna Kea)

Fig. 15

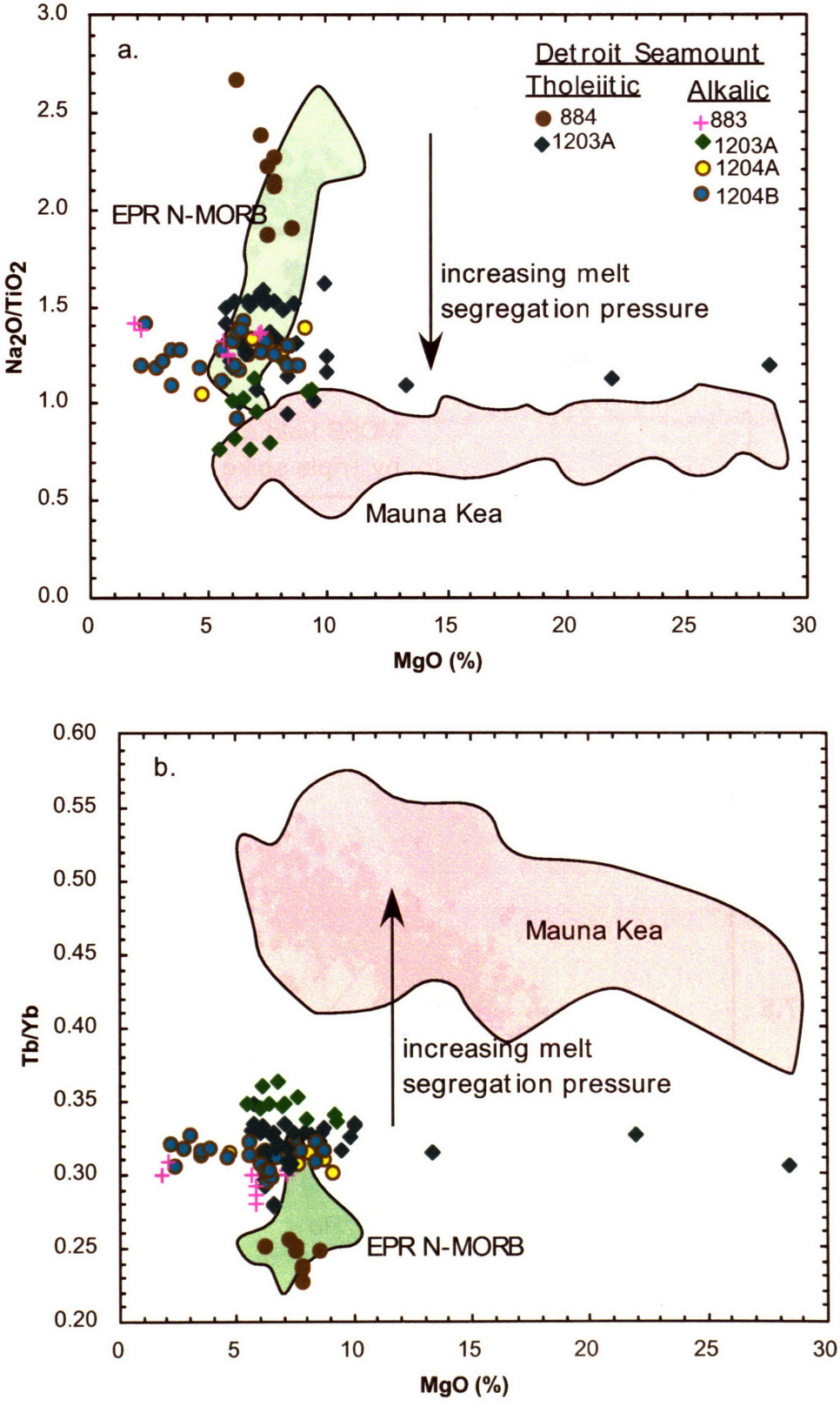
a.
Detroit Seamount
Tholeiitic
884
1203A
Alkalic
883
1203A
1204A
1204B
EPR N-MORB
increasing melt
segregation pressure
Mauna Kea
Na2O/TiO2
MgO (%)
b.
Mauna Kea
increasing melt
segregation pressure
EPR N-MORB
Tb/Yb
MgO (%)

Fig. 16

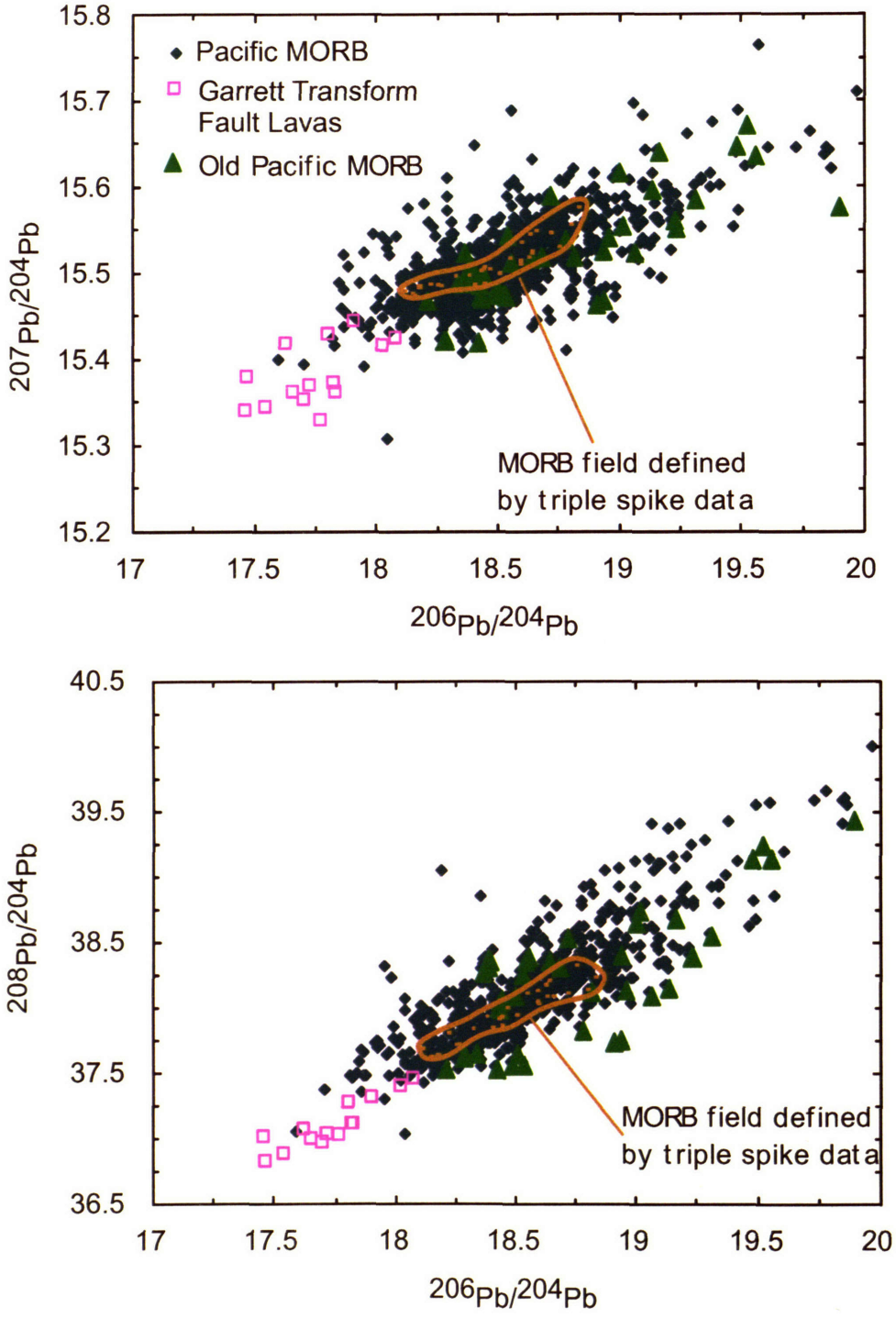
Pacific MORB
Garrett Transform Fault Lavas
Old Pacific MORB
MORB field defined by triple spike data
$^{207}Pb/^{204}Pb$
$^{206}Pb/^{204}Pb$
15.8
15.7
15.6
15.5
15.4
15.3
15.2
17
17.5
18
18.5
19
19.5
20
$^{208}Pb/^{204}Pb$
40.5
39.5
38.5
37.5
36.5

Fig. 17

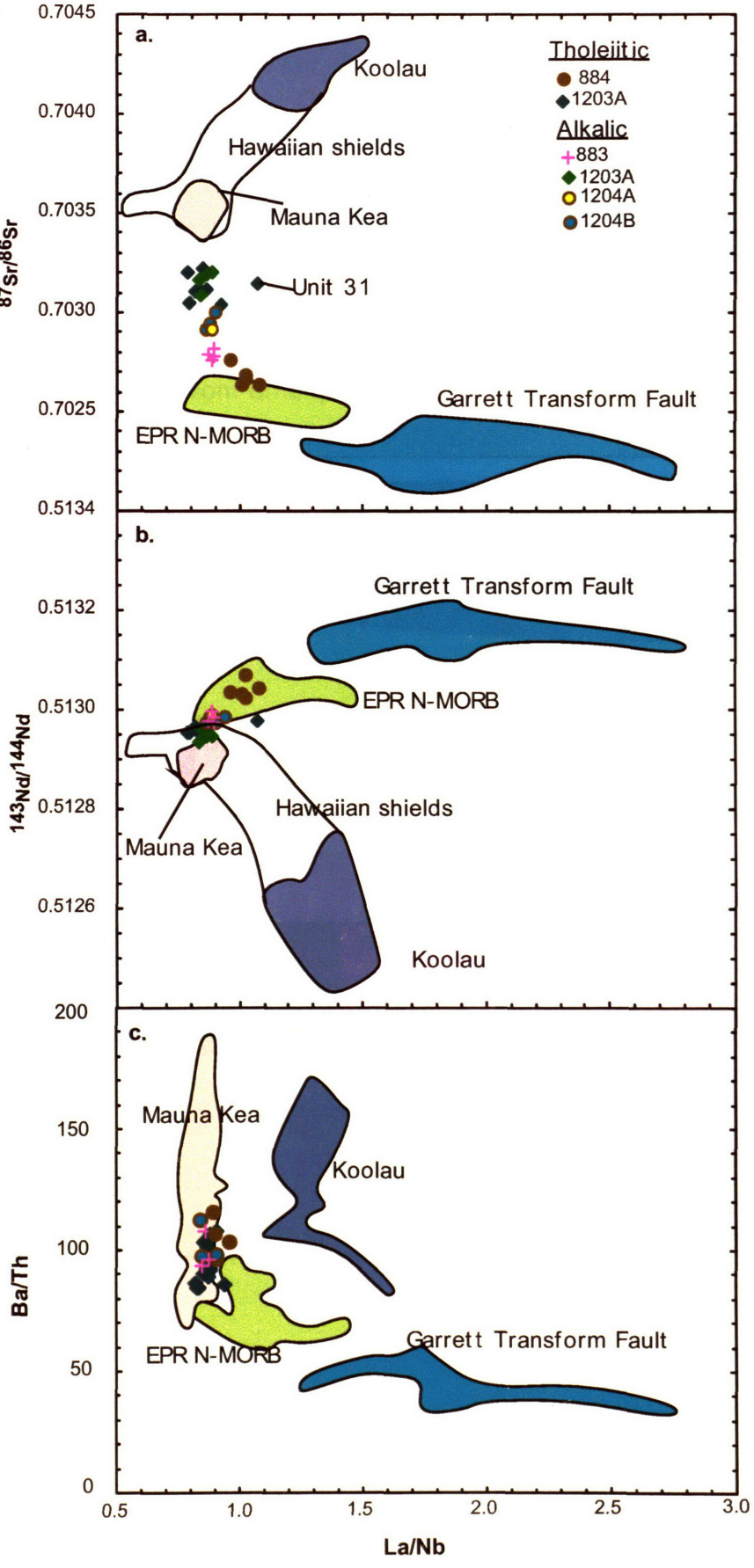
a.
Koolau
Hawaiian shields
Mauna Kea
Unit 31
Garrett Transform Fault
EPR N-MORB
Tholeiitic
884
1203A
Alkalic
883
1203A
1204A
1204B
$^{87}Sr/^{86}Sr$
0.7045
0.7040
0.7035
0.7030
0.7025
0.5134
b.
Garrett Transform Fault
EPR N-MORB
Hawaiian shields
Mauna Kea
Koolau
$^{143}Nd/^{144}Nd$
0.5132
0.5130
0.5128
0.5126
200
c.
Mauna Kea
Koolau
Garrett Transform Fault
EPR N-MORB
Ba/Th
150
100
50
0
0.5
1.0
1.5
2.0
2.5
3.0
La/Nb

Fig. 18

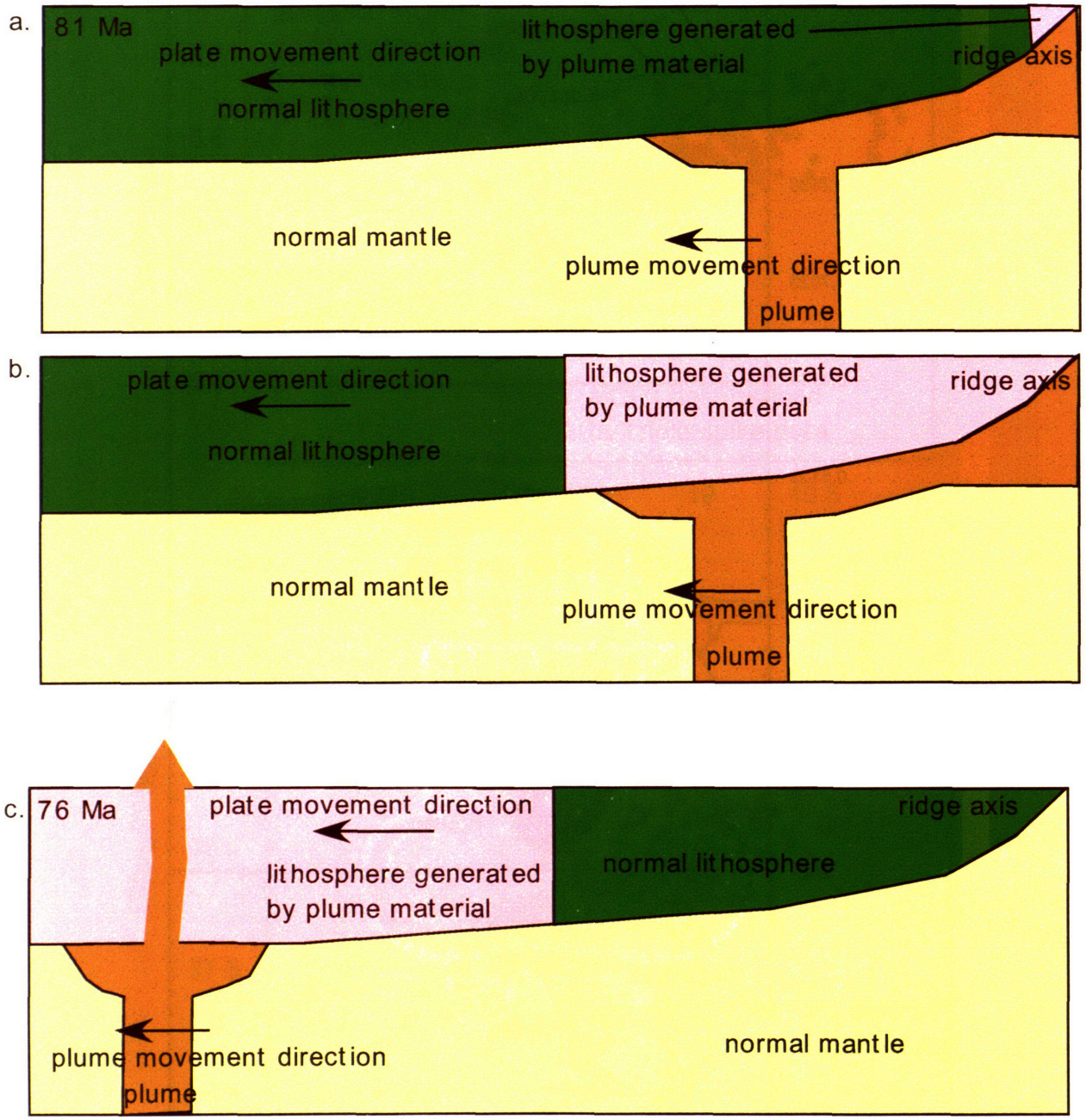
a.
81 Ma
plate movement direction
normal lithosphere
lithosphere generated
by plume material
ridge axis
normal mantle
plume movement direction
plume
b.
plate movement direction
normal lithosphere
lithosphere generated
by plume material
ridge axis
normal mantle
plume movement direction
plume
c.
76 Ma
plate movement direction
lithosphere generated
by plume material
ridge axis
normal lithosphere
plume movement direction
plume
normal mantle

CHAPTER 5: TESTING THE PLUME HYPOTHESIS: EVIDENCE FROM VOLCANISM ALONG THE HAWAII-EMPEROR CHAIN

1. Is There A Mantle Plume Beneath Hawaii-Emperor Chain?

1.1 What is a mantle plume?

There are three types of linear volcanism: mid-ocean ridge, arc volcanism and intra-plate volcanism, such as the Hawaii-Emperor Chain. In the first two, concurrent volcanism occurs along the plate boundaries. In contrast, intra-plate linear volcanism, such as the Hawaii-Emperor Chain, is characterized by age propagation (e.g., Duncan and Keller, 2004). The linear Hawaii-Emperor Chain (Fig. 1) is attributed to the passage of the Pacific plate over a relatively fixed mantle source of magma (hotspot), perhaps a mantle plume (e.g., Wilson, 1963; Morgan, 1971). The mantle plume concept developed from the study of the Hawaii-Emperor Chain, as well as other oceanic islands, such as Iceland. A mantle plume is described as a hot, active upwelling mantle flow originating in the lower mantle (Morgan, 1971). Plume-related volcanism is characterized by volume and geochemical characteristics different from that of MORB. The buoyancy of a mantle plume is attributed to its excess potential temperature (Morgan, 1971); consequently, a mantle plume is inferred to originate from a thermal boundary within the Earth. There are debates on whether mantle plumes exist (e.g., Anderson, 2000). In the following sections, I particularly address if a mantle plume generated the Hawaii-Emperor Chain.

1.2 Evidence Supporting a Hawaiian Plume

1.2.1 Five Criteria from Courtillot et al. (2003)

If a mantle plume originates from the deep mantle, there are important geophysical and geochemical consequences. Courtillot et al. (2003) inferred that, if a mantle plume originates from the deep mantle, it should have the following five characteristics: **1.** a long lived, age-progressive track; **2.** a large igneous province (LIP) at its initiation; **3.** a

buoyancy flux value > 10^3 Kg/S; **4.** high $^3He/^4He$ relative to MORB and **5.** Slow seismic wave velocity anomaly at 500 km depth. Courtillot et al. (2003) noted that the Hawaii-Emperor Chain satisfies four of these criteria.

The first two criteria are based on the results of fluid and numerical experiments, in which hot plume material is assumed to be much less viscous than the ambient mantle; in this case the plume may have a large spherical head followed by a thin tail (Fig. 2a; Korenaga, 2005). The large spherical plume head is assumed to generate a LIP, and the plume tail generates the age-progressive volcanic trend (e.g., Richards et al., 1989). The 6000 km long, age progressive Hawaii-Emperor Chain (Fig. 1) satisfies the first criterion. This volcanic trend is best explained as a result of movement of the Pacific Plate over a plume tail.

The Hawaii-Emperor Chain lacks an associated LIP; however, the LIP may have been subducted, or a mantle plume may not necessarily generate a LIP (Farnetani and Samuel, 2005; Korenaga, 2005). Geodynamic models of thermo-chemical plumes imply that a spherical plume head may be absent in some cases (Farnetani and Samuel, 2005). Specifically, in their numerical approach, Farnetani and Samuel (2005) modeled thermo-chemical plumes in a mantle wind caused by plate motion. The plumes are generated by heating a dense layer at the base of the mantle. There is complex internal convection within this dense layer, and when it starts to ascend its shape may or may not involve a spherical plume head (Fig. 1 of Farnetani and Samuel, 2005). A mantle plume without a spherical head is also obtained in the numerical model of Korenaga (2005). Specifically, Korenaga (2005) assumed that hotter mantle is more viscous than colder mantle, an assumption that is opposite to the traditional view. However, Korenaga (2005) argued

that mantle deformation may be controlled by diffusion creep (Solomatov, 1996, 2001), which is sensitive to grain size and temperature. Higher temperature has a direct effect (decrease) on viscosity. However, higher temperature also increases the grain size, which in turn increases the viscosity. It is possible that the effect of increasing grain size is greater than that of increasing temperature. That is, a hotter plume is more viscous than ambient mantle. Under this circumstance, Korenaga (2005) showed that a plume head and tail structure is not developed (Fig. 2b).

The third criterion is a volumetric argument. Albers and Christensen (1996) argued that a deep mantle plume must have a large mass flux (> 1000 kg s^{-1}) so that it does not lose too much heat as it rises, and melting continues to the base of the lithosphere. Based on the mass anomaly associated with the Hawaiian swell and the Pacific plate motion velocity, the estimated buoyancy flux of the Hawaii-Emperor Chain is 6-9,000 kg s^{-1} (Davies, 1988; Sleep, 1990).

The fourth criterion, high $^3He/^4He$, is a geochemical argument. Generally, compared with the shallow MORB source mantle, the deep mantle is believed to be less degassed; consequently, it is characterized by higher $^3He/^4He$ than the depleted upper mantle which is sampled by MORB (e.g., Farley and Neroda, 1998). Therefore, a deep mantle plume should be characterized by high $^3He/^4He$. Shield lavas from Hawaii-Emperor Chain generally have higher $^3He/^4He$ (>10Ra) than MORB (Fig. 4; Keller et al., 2004a; Kurz et al., 2004).

The last criterion is a seismic argument. A hot mantle plume is characterized by lower seismic velocity. Because plume tails may not be resolved in the lower mantle using seismic waves, Courtillot et al. (2003) restricted the seismic criterion to

identification of low velocity structure at a depth of 500 km. The newly-developed finite-frequency tomography technique shows that the low velocity structure beneath the Hawaiian Island continues to at least 2300 km deep (Fig. 3; Montelli et al., 2004).

1.2.2 Evolution of a Single Hawaiian Volcano

The temporal variation at a single volcano also supports a Hawaiian plume beneath Hawaiian volcanoes. Generally, Hawaiian volcanoes systematically evolve through four growth stages: pre-shield, shield, post-shield and rejuvenated stages (Fig. 5). Among the first three growth stages, there is systematic compositional variation. That is, the lava type changes from alkalic to tholeiitic and back to alkalic basalt. This transition is consistent with a volcano forming as the plate approaches, over-rides and leaves the plume (e.g., Fig. 6; Chen and Frey, 1985; Clague and Dalrymple, 1987). As a volcano begins, it samples the edge of the Hawaiian plume where temperature is low. Consequently, melting extent is low and alkalic lavas are generated. As the volcano overrides the center of the Hawaiian plume where temperature is high, melting extent is larger and tholeiitic lavas are generated. As the volcano movers away from the Hawaiian plume, it samples the edge of the Hawaiian plume where alkalic lavas are generated because of lower temperature.

1.2.3 Geochemical Differences Between Hawaiian Lavas and MORB

All lavas from the Hawaii-Emperor Chain have geochemical characteristics different from MORB; these include differences in radiogenic isotopic ratios and abundances of major and trace elements. The implication is that that lavas from the Hawaii-Emperor Chain sampled source components that are not represented in MORB. Specifically, **1**. Hawaiian-Emperor lavas have higher $^{87}Sr/^{86}Sr$, range to lower $^{143}Nd/^{144}Nd$ and

$^{176}Hf/^{177}Hf$, and define different Pb isotopic fields (e.g., Fig. 7; Hofmann, 2003); **2.** at MgO>8%, Hawaiian shield lavas have lower Al_2O_3 than MORB (Fig. 8; Albarede, 1992); **3.** in addition, lavas from Hawaii-Emperor Seamount, except for Site 884 lavas at Detroit Seamount (see Huang et al., 2005 for a detailed discussion), are enriched in highly incompatible elements (e.g., Fig. 9; Hofmann, 1997; Regelous et al., 2003; Huang et al., 2005; Shafer et al., 2005). In contrast, N-MORB are depleted in highly incompatible elements (Fig. 9; Hofmann, 1988). Although the enrichment of highly incompatible elements in Hawaii-Emperor lavas can be a result of lower melting extents, the sources of these lavas are inferred to be enriched in incompatible elements relative to the MORB source (e.g., Feigenson et al., 2003); **4.** lavas from modern Hawaiian volcanoes, both shield and rejuvenated stage lavas, are characterized by high Ba/Th (>100), a feature that is characteristic of the source (Fig. 10; Hofmann and Jochum, 1996; Huang and Frey, 2003; Yang et al., 2003). Huang et al. (2005) noted that lavas recovered from Detroit Seamount (~76-81 Ma), which is on the northern end of the Hawaii-Emperor Chain (Fig. 1), are also characterized by high Ba/Th; thereby providing evidence for the longevity of these MORB-Hawaiian geochemical differences; **5.** modern Hawaiian shield lavas are generally characterized by high $^{3}He/^{4}He$ (Fig. 4; Kurz et al., 2004). Keller et al. (2004) noted that lavas from the Emperor Seamounts also have higher $^{3}He/^{4}He$ (>10) than MORB values, again documenting that the MORB-Hawaiian geochemical differences persisted for ~80 Myr.

1.3 Arguments Against a Hawaiian Plume

Despite the success of the plume hypothesis in explaining the geophysical and geochemical characteristics of the Hawaii-Emperor Chain, some researchers argue against a Hawaiian plume. In this section, I review these arguments.

1.3.1 Excess Temperature

Intra-plate volcanism is generally believed to be caused by excess temperature or excess water content, or both (e.g., Morgan, 1971; Schilling et al., 1980). Hawaiian shield lavas have higher water content than MORB; however, this was explained as a consequence of lower partial melting extent (Dixon and Clague, 2001). Rather, based on H_2O/Ce which is insensitive to the partial melting and crystal fractionation, Dixon and Clague (2001) argued that, compared with MORB source, the source of Hawaiian shield lavas is relatively depleted in H_2O.

Is Hawaiian volcanism caused by excess temperature? Based on olivine-melt equilibria, Green et al. (2001) argued that Hawaiian shield lavas and MORB were generated at similar temperature; they inferred that the Hawaiian plume is not hot. However, Green et al. (2001) ignored the pressure effect on Fe-Mg exchange between olivine and melt, and the fact that Hawaiian shield lavas are enriched in FeO. Using a similar dataset, Putirka (2005) argued that the potential temperature of the Hawaiian plume is 213-235°C hotter than the ambient mantle, which is consistent with a thermally driven Hawaiian plume.

1.3.2 No Excess Heat Flow Anomaly Across the Hawaiian Swell

As a consequence of a thermally driven Hawaiian plume, excess heat flow across the Hawaiian swell is expected. However, this is not observed (e.g., Stein and Stein,

1993). Stein and Stein (2003, www.mantleplumes.org/Heatflow.html) proposed that the heat effect of a mantle plume is concentrated at the base of the lithosphere, and it takes tens of millions of years to conduct to the surface. Consequently, it is implied that heat flow anomaly may be detected in old Hawaiian volcanoes. However, von Herzen et al. (1989) measured the heat flow along a 1230-km-long profile across the axis of the Hawaiian Swell about 700 km ESE of Midway Island, and no anomalous high heat flow was measured. Similarly, there is no heat flow anomaly observed for the Icelandic plume (Stein and Stein, 2003). The lack of heat flow anomaly associated with mantle plumes remains as a puzzle for the plume hypothesis.

1.3.3 No Isolated Plume Sources

As discussed above, Hawaiian-Emperor lavas are geochemically different from MORB. Such differences, especially in isotopic ratios, are inferred to reflect source differences. In the plume hypothesis, the Hawaiian plume originates from the deep mantle. Consequently, source differences are inferred to reflect sampling of different mantle reservoirs, e.g., lower mantle vs upper mantle. However, Meibom and Anderson (2003) and Ito and Mahoney (2005) showed that MORB and OIB in general may sample a common source by different processes. Specifically, Ito and Mahoney (2005) proposed that the geochemical difference between MORB and OIB is a result of process. In Ito and Mahoney's model, MORB and OIB sample a common mantle source which contains several geochemically distinct source components with different solidus temperatures. These mantle source components are assumed to be in thermal equilibrium throughout an upwelling process. Therefore, different source components begin to melt at different depths. In their model, MORB are generated by passive mantle flow driven by the

spreading plates, whereas OIB are generated by active upwelling mantle flows, i.e., mantle plumes. Consequently, beneath a mid-ocean ridge, the horizontal mantle flow velocity is relatively constant at different depth (Fig. 11). In contrast, beneath a plume-related volcano, the horizontal mantle flow velocity increases with increasing depth (Fig. 11), i.e., partial melting generating OIB mainly occurs at greater depth. That is, the mean magma segregation pressure of OIB is greater than that of MORB. Consequently, OIB sample more of the source components with lower solidus temperatures, and MORB sample more of these source components with higher solidus temperatures. That is, in Ito and Mahoney's model, the geochemical differences between MORB and OIB are explained as a result of process. Although Ito and Mahoney's model can to a first order explain some geochemical (Sr-Nd-Pb isotopic ratios) differences between MORB and OIB, this model needs to be evaluated with Helium isotopic ratios and ratios of highly incompatible elements. However, even if MORB and OIB sample a common source, this result can be used to argue against a layered mantle model (Fig. 12); it is not an argument against plume hypothesis.

Phipps Morgan and Morgan (1999) proposed a two-stage melting model to explain the geochemical differences between MORB and OIB (Fig. 13). In this model, the rising mantle plume first melts beneath thick lithosphere to generate plume-related volcanism. Then, the melting residues which form the asthenosphere upwell again at mid-ocean ridge and melt again to generate MORB. Similar to the Ito and Mahoney's model, Phipps Morgan and Morgan (1999) also assumed that mantle contains several geochemically distinct source components with different solidus temperatures. Consequently, during the first melting stage, OIB sample most of the source components

with lower solidus temperatures, and the melting residues are depleted in these easy-melting source components. During the second melting stage, MORB sample most of the source components with higher solidus temperatures. As with the Ito and Mahoney's hypothesis, this model does not preclude the existence of mantle plumes.

2. At what depth does the Hawaiian plume originate? – Is It From the Core-Mantle Boundary?

At what depth does the Hawaiian plume originate? Is it from the core-mantle boundary? There are difficulties imaging a mantle plume, especially the Hawaiian plume, using seismic waves (see a detailed discussion in Keller et al., 2000b). The Hawaiian volcanoes are located in the center of the Pacific Plate, and are far from plate boundaries where many earthquakes occur. Also, the central-ocean location of the Hawaiian volcanoes limits the distributions of seismic stations which are used to collect seismic data. Consequently, similar to the Iceland example discussed in Keller et al. (2000b), the ray paths of the collected seismic waves are nearly vertical, and vertical resolution is low. Even with the newly-developed finite-frequency tomography technique, there is no resolution below 2300 km (Montelli et al., 2004). Given these difficulties, at the present stage, existing seismic studies may not uniquely answer the question -- At what depth does the Hawaiian plume originate?

What constraints can geochemists provide? Some studies argue that core signatures, such as high $^{186}Os/^{188}Os$, which measures time-integrated Pt/Os (Brandon et al., 1999), and high Fe/Mn (Humayun et al., 2004), are present in Hawaiian shield lavas. Consequently, they inferred that Hawaiian shield lavas sampled a core component; therefore the Hawaiian plume originates from the core-mantle boundary.

2.1 $^{186}Os/^{188}Os$ vs $^{187}Os/^{188}Os$

Brandon et al. (1999) noted that Hawaiian picrites, except for Koolau lavas, form a positive trend in a plot of $^{186}Os/^{188}Os$ vs γ_{Os} ($\gamma_{Os}=[(^{187}Os/^{188}Os_{sample(t)}/ ^{187}Os/^{188}Os_{chondrite(t)})-1]x100$) (Fig. 14; Fig. 2 of Brandon et al., 1999). Consequently, a source component with high $^{186}Os/^{188}Os$ (up to 0.11987) and γ_{Os}, i.e., time integrated high (superchondritic) Pt/Os and Re/Os, is inferred. In addition, the slope of this trend requires high (superchondritic) Pt/Re (88-100). As reviewed in Brandon and Walker (2005), recent experiments on solid metal-liquid metal partitioning of Re, Os and Pt indicate that $D_{Os}>D_{Re}>D_{Pt}$ (Lauer and Jones, 1998; Fleet et al., 1999; Walker, 2000; Chabot et al., 2003). Such results are also consistent with that inferred from the observed fractionation in asteroidal cores (e.g., Morgan et al., 1995). Consequently, Brandon and Walker (2005) inferred that, because of the crystallization of the inner core, the Earth's outer core is likely characterized by high (superchondritic) Pt/Os, Re/Os and Pt/Re. The positively correlated $^{186}Os/^{188}Os$-γ_{Os} trend of Hawaiian picrites is interpreted as a result of sampling small (<0.5 wt %) amount of the Earth's outer core.

2.2 Fe/Mn

Humayun et al. (2004) showed that Hawaiian lavas generally have high Fe/Mn (>65); in contrast, MORB and Icelandic lavas have Fe/Mn<62 (Fig. 15a; Fig. 1 of Humayun et al., 2004). At a given MgO, Hawaiian lavas have higher Fe/Mn than MORB (Fig. 15a). Although Fe/Mn in whole rocks is affected by olivine fractionation, this effect is relatively insignificant (Fig. 15b). Consequently, the high Fe/Mn in Hawaiian lavas is not a result of crystal fractionation. Since $D_{Fe}>D_{Mn}$ in olivine, and $D_{Fe}<D_{Mn}$ in clinopyroxene, orthopyroxene and garnet (Fig. 3 of Humayun et al., 2004), Humayun et

al. (2004) argued that partial melting of a peridotite does not significantly fractionate Fe from Mn; in contrast, partial melting of eclogite which is olivine-free can fractionate Fe/Mn. Humayun et al. (2004) inferred that partial melts from eclogite may not be important to Hawaiian shield lavas, because they did not find any Fe/Mn difference between Koolau lavas, which are inferred to sample up to 20-30% partial melts from eclogite (Hauri, 1996; Lassiter and Hauri, 1998; Huang and Frey, 2005), and other Hawaiian shield lavas. Consequently, the observed high Fe/Mn is inferred to be a source signature, which may originate from the Earth's core (Humayun et al., 2004).

If high $^{186}Os/^{188}Os$, γ_{Os} and Fe/Mn are core signatures, one expects correlations among these ratios. However, such correlations are not observed (Fig. 2 of Humayun et al., 2004). Brandon and Walker (2005) argued that "the process of core-mantle interaction and later partial melting of the source" may decouple Os isotopic ratios and Fe/Mn. Specifically, Humayun et al. (2004) inferred that the liquid outer core (liquid Fe-FeS-FeO) reacts with lower mantle (Mg perovskite and ferropericlase) and generates liquid Fe-FeS, Mg perovskite and ferropericlase. The net result is to increase the FeO content of the lower mantle. The liquid Fe-FeS either returns back to the core or crystallizes within the lower mantle as Fe-FeS veins. Consequently, the interaction between lower mantle and liquid outer core results in an elevated FeO (high Fe/Mn) content and unevenly distributed Fe-FeS veins, which contain radiogenic Os inherited from the outer core, in the lower mantle. Consequently, partial melting of such metasomatised mantle does not generate coupled Fe/Mn and Os isotopic ratios.

Since this model predicts no correlation, it is not testable. In addition, since partial melts of eclogite may be generally present in Hawaiian shield lavas (Hauri, 1996; Huang

and Frey, 2005), the high Fe/Mn in Hawaiian shield lavas may have two origins: partial melts of eclogite and a core component. Therefore, it is necessary to address the effect of partial melts of eclogite on Fe/Mn in Hawaiian shield lavas. As discussed in Hauri (1996) and Huang and Frey (2005), partial melts of eclogite contributing to Hawaiian shield lavas are characterized by high SiO_2 content, $^{87}Sr/^{86}Sr$ and La/Nb and low CaO content, $^{143}Nd/^{144}Nd$, $^{176}Hf/^{177}Hf$, $^{206}Pb/^{204}Pb$, Th/La. An ongoing research is to investigate correlations of Fe/Mn with isotopic ratios (Humayun, personnel communication).

2.3 ^{182}W

^{182}Hf decays into ^{182}W with a half life of ~9 Ma (Lee and Halliday, 1995). Consequently, W isotopic heterogeneity in the Earth was generated within the first 50 Ma. Since Hf is absent from the metallic core, Hf/W in the core is ~0. Consequently, the core is depleted in ^{182}W, and has ε_W=-2.1 to -2.2 (ε_W measures the enrichment or depletion of ^{182}W relative to a terrestrial standard in parts per 10,000) for different core formation models and mass balance (Schersten et al., 2004; Halliday, 2004). Consequently, if the Hawaiian plume originates from the core mantle boundary, low ε_W is expected in Hawaiian shield lavas. However, Hawaiian lavas with elevated $^{186}Os/^{188}Os$ and γ_{Os}, which were interpreted as a core signature, have ε_W around 0, i.e., the expected low ε_W is not observed (Schersten et al., 2004). Consequently, Schersten et al. (2004) suggested that the observed elevated $^{186}Os/^{188}Os$ and γ_{Os} are caused by recycled Mn-nodules, 2-3% in the source of Hawaiian lavas, which are characterized by high Re/Os, Pt/Os and Pt/Re. However, involving large amounts of Mn-nodules significantly increases (5-9 times) the Mn abundance and decreases the Fe/Mn in the source (Schersten et al., 2004). This inference is inconsistent with the observed relatively high Fe/Mn in

Hawaiian shield lavas (Humayun et al., 2004). Brandon and Walker (2005) suggested that the lack of low ε_W in Hawaiian lavas may be a result of sampling recycled oceanic crust. Since W is as incompatible as U during partial melting of the mantle, oceanic and continental crust is enriched in W (~1100 ppb) (Newsom et al., 1996). Pelagic sediments have even higher W (1500 to 2700 ppb) (Gao et al., 1998; Strekopytov, 1998). In contrast, the estimated W abundance in the outer core is 490 ppb (Schersten et al., 2004). Consequently, if Hawaiian lavas sampled even small amount of recycled oceanic crust component, including sediments, the recycled crust component will mask any ε_W anomaly arising from the outer core. Brandon and Walker (2005) concluded that the present level of analytical resolution for W isotopes is not sufficient to unambiguously identify the presence of a core component.

3. Geochemical Components in the Hawaiian Plume

3.1 Did Hawaiian- Emperor Lavas Sample A MORB-Related Source Component?

The large isotopic variation in Hawaiian-Emperor lavas (e.g., Figs. 4, 7, 16, 17) reflects multiple source components in the Hawaiian plume. What is the nature of these isotopically distinctive source components? That is, what causes the isotopic heterogeneity in the Hawaiian plume? There are debates on whether Hawaiian shield lavas sampled a MORB-related source component (West et al., 1987; Basu and Faggart, 1996; Lassiter et al., 1996; Lassiter and Hauri, 1998; Abouchami et al., 2000; Keller et al., 2000a; Blichert-Toft et al., 2003; Regelous et al., 2003; Frey et al., 2005; Huang et al., 2005). In this section, I discuss observations used to argue against a MORB-related component in Hawaiian shield lavas. Some of these arguments are still valid, but others are weakened by new data.

3.1.1 Observations Previously Used to Argue Against a MORB-Related Component That Have Been Weakened by New Data

a. $^{87}Sr/^{86}Sr$ vs $^{143}Nd/^{144}Nd$

Hawaiian shield lavas form an inverse $^{87}Sr/^{86}Sr$ vs $^{143}Nd/^{144}Nd$ trend which ranges from near bulk earth values, Makapuu-stage of Koolau shield, to values for Mauna Kea lavas which nearly reach the MORB field (Fig. 16). Basu and Faggart (1996) and Lassiter and Hauri (1998) argued against a role for MORB-related component because the extrapolated $^{87}Sr/^{86}Sr$ vs $^{143}Nd/^{144}Nd$ trend of Hawaiian shield lavas, excluding Kahoolawe lavas, does not intersect the MORB field (e.g., Fig. 1 of Lassiter and Hauri, 1998; Fig. 16). That is, compared with MORB, the low $^{87}Sr/^{86}Sr$-high $^{143}Nd/^{144}Nd$ end (**Kea** component) of the Hawaiian trend has similar $^{143}Nd/^{144}Nd$ but higher $^{87}Sr/^{86}Sr$. However, this conclusion is not compelling. Because Kahoolawe lavas were not included in the discussion of Basu and Faggart (1996) and Lassiter and Hauri (1998), the slope of the Hawaiian trend in a $^{87}Sr/^{86}Sr$ vs $^{143}Nd/^{144}Nd$ plot is mostly controlled by Makapuu-stage Koolau lavas (Fig. 16). This is a consequence of the large $^{87}Sr/^{86}Sr$ and $^{143}Nd/^{144}Nd$ variations in Makapuu-stage Koolau lavas which define the high $^{87}Sr/^{86}Sr$ and low $^{143}Nd/^{144}Nd$ end of the Hawaiian shield trend (Fig. 16). However, with the recognition of multiple $^{87}Sr/^{86}Sr$ vs $^{143}Nd/^{144}Nd$ trends defined by different Hawaiian shields, e.g., Koolau compared with Kahoolawe (Fig. 16), the $^{87}Sr/^{86}Sr$ vs $^{143}Nd/^{144}Nd$ trend for Hawaiian shield lavas cannot be used to preclude a role of MORB-related component.

b. $\delta^{18}O$

Olivines from subaerially-erupted Mauna Kea lavas recovered by Phase 1 of Hawaii Scientific Drilling Project have $\delta^{18}O$ of 4.6 to 5.0‰ (Eiler et al., 1996), which are

distinctively lower than olivines from upper mantle peridotites (5.1 to 5.5‰, e.g., Mattey et. al., 1994; Chazot et al., 1997). Such observation was used by Eiler et al. (1996) and Lassiter and Hauri (1996) to argue against a MORB-related source component in Mauna Kea lavas. However, analyses of deep (submarine) lavas of Mauna Kea Volcano recovered by Phase 2 of the Hawaii Scientific Drilling Project show that olivines from old Mauna Kea lavas have $\delta^{18}O$ of 4.8 to 5.3‰, similar to that in upper mantle peridotites (Wang et al., 2003).

c. $^{206}Pb/^{204}Pb$ vs $^{176}Hf/^{177}Hf$

Hawaiian shield lavas form a hyperbolic trend in a $^{206}Pb/^{204}Pb$ vs ε_{Hf} plot (Blichert-Toft et al., 1999; 2003; Fig. 17a), which was explained as a mixing line between two source components (**Koolau** and **Kea**) with very different Hf/Pb ($(Hf/Pb)_{Kea/Koolau}$=40) (Blichert-Toft et al., 1999). Consequently, a source component with ε_{Hf}=12.9 is inferred for **Kea** component (Fig. 17a, Blichert-Toft et al., 1999). Although this value is within the Pacific MORB values, Blichert-Toft et al. (2003) showed that Pacific MORB with such low ε_{Hf} are rare (Fig. 17b); consequently, the inferred **Kea** component is not MORB-related.

Hf/Pb is not effectively fractionated by partial melting. I assume a garnet peridotite contains 10% garnet and 15% clinopyroxene, a melting reaction of 50% garnet + 50% clinopyroxene = 100% melt, and that 10% partial melting extent is required to generate tholeiitic lavas (e.g., Feigenson et al., 2003). During partial melting of peridotite, Pb partitioning is similar to Ce or Nd (e.g., Hofmann, 1997); consequently, D_{Pb} is assumed to be 0. Also, I assume that $D_{Hf}^{garnet/melt}$=0.5, $D_{Hf}^{clinopyroxene/melt}$=0.2, and that Hf is perfect incompatible in orthopyroxene and olivine; these partition coefficients

are on the high end of published values (e.g., Salters and Longhi, 1999; Pertermann et al., 2004). Consequently, Hf/Pb in melt generated by 10% partial melting is about 0.7 times that in the original source. Therefore, it is reasonable to assume that Hf/Pb in Hawaiian shield lavas reflects its source ratios.

There are concerns that Hawaiian shield lavas may be saturated by sulfide (e.g., Lassiter, 2003; Norman et al., 2004); consequently, Pb abundance may be affected by S devolatilization. However, Norman et al. (2004) showed that there is no correlation between abundances of Pb and S in basaltic glasses from Hawaiian shields; consequently, it is unlikely that Pb abundance is affected by S devolatilization. Based on abundances of platinum group elements in Hawaiian shield lavas, Lassiter (2003) argued that the source of Hawaiian shield lavas may contain small amounts of sulfide, which may significantly affect the partition coefficient of Pb. However, Huang and Frey (2003) inferred that Pb is more incompatible than Hf in generating Mauna Kea lavas (Fig. 3 of Huang and Frey, 2003). Consequently, my estimate, $(Hf/Pb)_{melt}=0.7\ (Hf/Pb)_{source}$, which is based on $D_{Pb}=0$, is a minimum estimate.

A consequence of the Blichert-Toft et al. (1999) model is that Hf/Pb in Hawaiian shield lavas should be highly variable. Blichert-Toft et al. (1999) proposed that $(Hf/Pb)_{Kea/Koolau}=40$, Huang et al. (submitted) found that the trend of Hawaiian shield lavas is consistent with $(Hf/Pb)_{Kea/Koolau}=15$ (Fig. 17a). A mixing calculation using $(Hf/Pb)_{Kea/Koolau} = 15$ requires an average Mauna Kea/Koolau lava ratio of 5 for Hf/Pb (Fig. 17a). However, such a large range in Hf/Pb is not observed; Hf/Pb in Hawaiian shield lavas ranges less than a factor of 3 (Fig. 18). In fact, the mixing line of average compositions of Mauna Kea and Koolau (Makapuu-stage) lavas is near-linear, and cannot

explain the highly curved Hawaiian trend (the inset in Fig. 17a). Consequently, Huang et al. (submitted) inferred that the curvature of the $^{206}Pb/^{204}Pb$ vs ε_{Hf} trend reflects the involvement of a third component. Consequently, I argue that Blichert-Toft et al.'s argument against a MORB-related component in Hawaiian shield lavas is not valid.

3.1.2 Observations Previously Used to Argue Against a MORB-Related Component That Remain Valid

a. $^{187}Os/^{188}Os$ vs Sr-Nd-Pb Isotopic Ratios

Lassiter and Hauri (1998) noted that Hawaiian shield lavas form a positive trend in plot of $^{187}Os/^{188}Os$ vs $^{87}Sr/^{86}Sr$ (Fig. 19), and negative trends in plots of $^{187}Os/^{188}Os$ vs $^{143}Nd/^{144}Nd$ and $^{206}Pb/^{204}Pb$. Gabbroic xenoliths recovered from the Honolulu Volcanics, representing the middle to lower oceanic crust beneath Hawaiian volcanoes, have much higher $^{187}Os/^{188}Os$ (0.225-0.539) than Hawaiian shield lavas, which reflects the in-situ growth of ^{187}Os since the formation of the Pacific oceanic crust (Lassiter and Hauri, 1998). Consequently, these gabbros are offset from the Hawaiian shield trends in plots of $^{187}Os/^{188}Os$ vs $^{87}Sr/^{86}Sr$, $^{143}Nd/^{144}Nd$ and $^{206}Pb/^{204}Pb$ (Lassiter and Hauri, 1998; Fig. 19). Therefore, Lassiter and Hauri (1998) inferred that Hawaiian shield lavas do not sample the underlying oceanic crust. A similar argument can be used to argue against a depleted MORB source component in Hawaiian shield lavas. The depleted MORB-related mantle is characterized by relatively low $^{187}Os/^{188}Os$ (0.12 to 0.13) (Roy-Barman and Allègre, 1994; Snow and Reisberg, 1995; Standish et al., 2002). In conjunction with its low $^{87}Sr/^{86}Sr$, high $^{143}Nd/^{144}Nd$ and large range in $^{206}Pb/^{204}Pb$, the depleted MORB-related mantle does not locate on the extension of the Hawaiian shield trend (e.g., Fig. 19).

b. Pb-Pb Isotopic Correlation

Using triple-spiked Pb isotopic data for Mauna Kea and Mauna Loa lavas and EPR MORB, Abouchami et al. (2000) noted that the trends formed by Hawaiian shield lavas do not point toward the field defined by EPR MORB in a $^{206}Pb/^{204}Pb$ vs $^{207}Pb/^{204}Pb$ plot (Fig. 20; Fig. 11 of Abouchami et al., 2000; Fig. 7 of Eisele et al., 2003). Specifically, compared with MORB, Hawaiian shield lavas have lower $^{207}Pb/^{204}Pb$ and higher $^{208}Pb/^{204}Pb$ at a given $^{206}Pb/^{204}Pb$. Consequently, they inferred that Hawaiian shield lavas do not sample a depleted MORB mantle source. This argument is based on the limited EPR MORB dataset analyzed at Max-Planck using triple-spike technique, which contains ~30 samples (Fig. 11 of Abouchami et al., 2000). It is questionable that such a limited MORB dataset is representative of Pacific MORB. However, by comparison between the published Pacific MORB Pb data and EPR MORB triple-spike Pb data from Max-Planck, Frey et al. (2005) and Huang et al. (2005) concluded that the triple-spike Pb data on ~30 EPR MORB from Max-Planck are representative of the Pacific MORB data (Fig. 21). Consequently, the argument of Abouchami et al. (2000) and Eisele et al. (2003) is valid.

c. Low $^{206}Pb/^{204}Pb$ in Detroit Lavas and Hawaiian Rejuvenated Stage Lavas

Frey et al. (2005) and Huang et al. (2005) noted the isotopic similarity between Hawaiian rejuvenated stage lavas and shield lavas from Detroit Seamount. Specifically, both lava suites have relatively low $^{87}Sr/^{86}Sr$ and high $^{143}Nd/^{144}Nd$ and trend to low $^{206}Pb/^{204}Pb$ (<18) (Fig. 7). Consequently, it is inferred that both Detroit Seamount lavas and Hawaii rejuvenated stage lavas sampled a common depleted component with $^{206}Pb/^{204}Pb<18$. Pacific MORB with $^{206}Pb/^{204}Pb<18$ are rare, and are dominated by lavas from the spreading center within Garrett transform fault (Frey et al., 2005; Huang et al.,

2005; Fig. 21). However, these lavas do not have high Ba/Th which is a definitive geochemical characteristic of lavas from the Hawaii-Emperor Chain (Hofmann and Jochum, 1996; Yang et al., 2003; Huang et al., 2005). Consequently, the depleted component, characterized by low $^{87}Sr/^{86}Sr$ and $^{206}Pb/^{204}Pb$ (<18) and high $^{143}Nd/^{144}Nd$, in Detroit Seamount lavas and Hawaiian rejuvenated stage lavas is not MORB-related (Frey et al., 2005; Huang et al., 2005).

3.2. Recycled Oceanic Lithosphere in the Hawaiian Plume

Generally, there are three ways to generate mantle heterogeneity: mantle metasomatism (Frey and Green, 1974), recycling of oceanic lithosphere including sediments (Hofmann and White, 1982) and delamination of lower continental crust (McKenzie and O'Nions, 1983). The geochemical heterogeneity of the Hawaiian plume is consistent with the hypothesis of recycling oceanic lithosphere. Below I summarize geochemical evidence consistent with recycled oceanic lithosphere in the source of Hawaiian lavas, i.e., the Hawaiian plume.

3.2.1 Ancient Recycled Sediments

Evidence for a recycled sedimentary component in Hawaiian shield lavas arises from assessment of geochemical data of Koolau lavas (Hauri et al., 1996; Lassiter and Hauri, 1998; Blichert-Toft et al., 1999; Jackson et al., 1999; Huang and Frey, 2003; 2005). Below I list the geochemical arguments in favor of an ancient recycled sedimentary component in the Hawaiian plume.

a. Low $^{206}Pb/^{204}Pb$ and High $^{208}Pb^*/^{206}Pb^*$

Makapuu-stage Koolau lavas are characterized by low $^{206}Pb/^{204}Pb$ (Fig. 17a), which implies a source with time-integrated low U/Pb. In addition, the linear correlations

of $^{208}Pb^*/^{206}Pb^*$, which measures the time-integrated Th/U, vs Sr, Nd and Hf isotopic ratios, La/Nb and Th/La for Koolau lavas imply these lavas also sampled a source component with high $^{208}Pb^*/^{206}Pb^*$, i.e., time-integrated high Th/U (Figs. 22, 23). Since marine sediments are generally characterized by low U/Pb and high Th/U (e.g., Ben Othman et al., 1989), the low $^{206}Pb/^{204}Pb$ and high $^{208}Pb^*/^{206}Pb^*$ in Koolau, especially Makapuu-stage of Koolau, lavas are interpreted as a result of sampling an ancient recycled sedimentary component (Weaver et al., 1991; Hauri et al., 1996; Lassiter and Hauri, 1998; Blichert-Toft et al., 1999; Huang and Frey, 2005).

Recycled sediment is also proposed to explain the low $^{206}Pb/^{204}Pb$ in Pitcairn lavas (e.g., Eisele et al., 2002) and the DUPAL anomaly of Indian ocean MORB (e.g., Rehkämper and Hofmann, 1997). However, these inferences have been questioned (e.g., Douglass and Schilling, 2000; Escrig et al., 2004), because recycled sediments, characterized by low U/Pb, are always associated with oceanic basaltic crust, characterized by high U/Pb. Douglass and Schilling (2000) and Escrig et al. (2004) argued that aged mixtures of low U/Pb sediment and high U/Pb basalt with reasonable proportions (sediment/basalt<10/90), cannot generate the very low $^{206}Pb/^{204}Pb$ (<17) observed in Indian MORB. Rather, they favor recycled lower continental crust, which is also characterized by low U/Pb (e.g., Rudnick and Fountain, 1995), to explain the observed low $^{206}Pb/^{204}Pb$. However, since the Pb abundances and isotopic ratios in recycled sediments and basalt are highly variable, it is possible to generate low $^{206}Pb/^{204}Pb$ (<17) in a recycled oceanic crust. For example, a calculated recycled, 1.8 Ga oceanic crust with a sediment/basalt = 3/97 has $^{206}Pb/^{204}Pb$ = 17.4 (Fig. 2 of Lassiter and Hauri, 1998). Slightly increasing the sediment/basalt ratio to 5/95 results in $^{206}Pb/^{204}Pb$ =

16.9 in the recycled oceanic crust. Therefore, the arguments by Douglass and Schilling (2000) and Escrig et al. (2004) are not valid.

b. Shallow Slope of ε_{Nd}-ε_{Hf} Trend

It is well established that OIB form a positive trend in an ε_{Nd} vs ε_{Hf} plot (e.g., Vervoort et al., 1999). Hawaiian shield lavas also form a positive trend in this plot, but compared with the OIB trend, the Hawaiian trend has a shallower slope (Fig. 24; Blichert-Toft et al., 1999). Consequently, Blichert-Toft et al. (1999) inferred that Hawaiian shield lavas, especially Makapuu-stage Koolau lavas, sampled a source component characterized by high ε_{Hf} at a given ε_{Nd}. Because pelagic sediments are generally characterized by relatively high Lu/Hf (e.g., Plank and Langmuir, 1998; Vervoort et al., 1999), they inferred that Hawaiian shield lavas, especially Makapuu-stage Koolau lavas, sampled an ancient recycled sedimentary component. However, modern pelagic sediments are also characterized by high ε_{Hf} at a given ε_{Nd} (Fig. 24; Fig. 1 of Blichert-Toft et al., 1999). Consequently, the shallow slope of the Hawaiian trend in an ε_{Nd}-ε_{Hf} plot cannot distinguish between modern and ancient sediments. It is the low $^{206}Pb/^{204}Pb$ in Makapuu-stage Koolau lavas that requires an ancient sedimentary component in the Hawaiian plume.

c. High $\delta^{18}O$ and $^{187}Os/^{188}Os$

Lassiter and Hauri (1998) noted that Hawaiian shield lavas form a positive trend in a $\delta^{18}O$ vs $^{187}Os/^{188}Os$ plot, with Makapuu-stage Koolau lavas define the high $\delta^{18}O$-$^{187}Os/^{188}Os$ end (Fig. 25). Since high temperature magmatic processes do not effectively fractionate oxygen isotopes, the high $\delta^{18}O$ (up to 6.0‰) in Makapuu-stage Koolau lavas reflects a low temperature alteration signature (Lassiter and Hauri, 1998). Based on

correlations of $^{187}Os/^{188}Os$ vs Sr-Nd-Pb isotopic ratios of Hawaiian shield lavas, Lassiter and Hauri (1998) argued that Hawaiian shield lavas did not significantly assimilate the aged underlying Pacific MORB. Consequently, it is unlikely that the high $\delta^{18}O$ in Makapuu-stage Koolau lavas is a result of assimilation of local altered Pacific MORB. Rather, in conjunction with other isotopic characteristics, such as low $^{206}Pb/^{204}Pb$ and high $^{187}Os/^{188}Os$, Lassiter and Hauri (1998) inferred that the high $\delta^{18}O$ in Makapuu-stage Koolau lavas reflects sampling an ancient recycled altered oceanic crust, including sediment. Note that, neither recycled sediment nor recycled basaltic crust alone can explain the distinctive Makapuu-stage Koolau lavas. Specifically, recycled basaltic crust is characterized by high $^{206}Pb/^{204}Pb$ because of its high U/Pb, which is inconsistent with the low $^{206}Pb/^{204}Pb$ in Makapuu-stage Koolau lavas. Recycled sediment has high Pb/Os; consequently, involving small amount of recycled sediment will decrease $^{206}Pb/^{204}Pb$ significantly with little effect on $^{187}Os/^{188}Os$ (Fig. 2 of Lassiter and Hauri, 1998). A mixture of recycled sediment (Pb/Os) and basalt (low Pb/Os) is required to explain the distinctive Makapuu-stage signatures.

d. High La/Nb, Sr/Nb and Low Th/La

The linear correlations of La/Nb and Th/La with Sr/Nb, $^{143}Nd/^{144}Nd$ and $^{208}Pb^*/^{206}Pb^*$ in Koolau lavas (Figs. 23, 26) imply that Koolau lavas sampled a source component with high La/Nb (>1.6), Sr/Nb (>55) and low Th/La (<0.05). The high La/Nb and Sr/Nb in Makapuu-stage Koolau lavas were explained as a result of Nb depletion, a characteristic of marine sediments (Frey et al., 1994; Jackson et al., 1999; Huang and Frey, 2003). However, given the relatively constant Nb/Th in Koolau lavas, Huang and Frey (2005) suggest that the distinctive geochemical characteristics of Makapuu-stage

Koolau lavas, high La/Nb, Sr/Nb and low Th/La, reflect enrichment of La and Sr rather than Nb depletion. Marine sediments have highly variable La/Nb, Sr/Nb and Th/La (Plank, 2005), and phosphate-bearing carbonate-rich and hydrothermal sediments are enriched in La and Sr compared with Th and Nb (Thompson et al., 1988; Plank and Langmuir, 1998; Honnorez et al., 1999; Patino et al., 2000; Plank et al., 2002; Chavagnac et al., 2005). Although modern carbonate-rich sediments are associated with biological activity, such as nannofossil and foram deposits that did not exist at 2Ga, Proterozoic marine carbonates, such as phosphorites and carbonates associated with banded iron formations, have high rare earth element abundance and are widely distributed (e.g., Tu et al., 1985). These sediments are likely to have low Th/La accompanied by high La/Nb and Sr/Nb.

Alternatively, carbonate-bearing hydrothermal sediments also have relatively high La/Nb and Sr/Nb (Thompson et al., 1988; Plank and Langmuir, 1998; Honnorez et al., 1999; Chavagnac et al., 2005). In this case, hydrothermal alteration leaches Ca from MORB (e.g., Bach et al., 2003), and carbonates are precipitated from the Ca-rich hydrothermal fluids.

There is debate on whether carbonates can survive subduction processes and be returned into deep mantle (see Schmidt and Poli, 2003 for a detailed discussion). Schmidt and Poli (2003) inferred that, at subduction zone, the upward-migrating aqueous fluid, produced by dehydration of the subducting serpentinite and basalt, can totally dissolve the carbonates in the overlying sedimentary layer. However, they argued that if the migration of the aqueous fluid is efficiently channeled, only a very small fraction of carbonates will be affected by the fluid-carbonate reaction. Schmidt and Poli (2003)

inferred that ">90% of the carbonates may survive complete dehydration of the underlying oceanic lithosphere. In this case, these carbonates will be subducted to depths of the transition zone". Based on experimental results on partial melting of carbonated eclogite, Dasgupta et al. (2004) inferred that "elimination of carbonate from eclogite requires temperatures ~100 °C hotter than any plausible subduction geotherm".

3.2.2 Recycled Basaltic Oceanic Crust

a. Evidence Supporting Recycled Basaltic Oceanic Crust in the Hawaiian Plume

Although trace element characteristics, such as the relatively uniform abundance of heavy rare earth elements, of Hawaiian shield lavas require garnet as an important residual mineral (e.g., Hofmann et al., 1984), the estimated primary magma compositions of Hawaiian shield lavas (Eggins, 1992; Wagner and Grove, 1998), especially Makapuu-stage Koolau lavas (Hauri, 1996), are not in equilibrium with garnet peridotite. In detail, the estimated primary magma compositions of Hawaiian shield lavas are too enriched in SiO_2. Among Hawaiian shield lavas, Makapuu-stage Koolau lavas are characterized by the highest SiO_2 and lowest CaO content (Frey et al., 1994; Hauri, 1996; Haskins and Garcia, 2004; Huang and Frey, 2005). Within Koolau lavas, SiO_2 content (after adjusted to be in equilibrium with Fo_{90} olivine) is correlated with Nd-Hf-Pb isotopic ratios (Fig. 27). In detail, Makapuu-stage Koolau lavas and Kalihi-stage Koolau lavas form subparallel trends in Fig. 27. A possible explanation is that both Makapuu-stage and Kalihi-stage (KSDP) Koolau lavas sampled varying amounts of a SiO_2-rich component but that the Makapuu-stage lavas contain more of an isotopically distinctive sedimentary component, i.e., high $^{208}Pb^*/^{206}Pb^*$ and low $^{143}Nd/^{144}Nd$ and $^{176}Hf/^{177}Hf$. The SiO_2-rich component in Koolau lavas is inferred to be a dacitic magma generated by low extent

partial melting of an imbedded eclogitic body in the Hawaiian plume. The low CaO content in Makapuu-stage lavas is also consistent with this interpretation (Hauri, 1996; Huang and Frey, 2005). Consequently, the source of Hawaiian shield lavas is a mixture of peridotite and eclogite (see Huang and Frey, 2005 for a detailed discussion). The coupled distinctive isotopic and trace element characteristics, e.g., low $^{206}Pb/^{204}Pb$ and high $^{208}Pb^*/^{206}Pb^*$, with a high-SiO_2, low-CaO dacitic component in Koolau lavas strongly suggest an ancient recycled basaltic oceanic crust, including sediment, in the Hawaiian plume.

Since dacitic melts are characterized by very high FeO/MgO (e.g., Yaxley and Green, 1998; Pertermann et al., 2004), the assumption that the primary magmas of Hawaiian shield lavas are equilibrium with Fo_{90} olivine can be questioned. However, dacitic melts have much lower FeO and MgO contents than picritic melts. Consequently, adding a large amount (up to 30%) of dacitic melt to picritic melt does not significantly change the FeO/MgO in the picritic melt (Table 1). Therefore, it is reasonable to assume that the primary magmas of all Hawaiian shield lavas are equilibrium with a common olivine composition (Fo_{90}).

b. Argument Against Recycled Basaltic Oceanic Crust in the Source of OIB

Niu and O'Hara (2003) argued against the presence of recycled oceanic basaltic crust in the source of OIB. Below are their arguments (in bold text) and my comments (in plain text):

1. **melting of subducted oceanic crust is unable to produce high-magnesian OIB melts.** Sources of OIB contain both eclogite formed from recycled oceanic crust and

peridotite. The high MgO melt is from partial melting of peridotite (e.g., Hauri, 1996; Lassiter and Lassiter, 1998; Huang and Frey, 2005).

2. **ancient oceanic crust is isotopically too depleted to yield OIB.** Obviously, they did not include sediments in their calculation. In fact, Lassiter and Hauri (1998) successfully modeled the isotopic variation of Hawaiian shield lavas using recycled oceanic crust, including sediment.
3. **OIB lack subduction zone dehydration signatures.** They claimed that OIB lack both trace element and isotopic signatures of subduction zone dehydration effect on subducted MORB. However, since OIB sample several mantle source components including recycled oceanic crust, it is possible that the dehydration signatures are diluted by other mantle source components. In fact, in the model calculation of Lassiter and Hauri (1998), Pb/Os in recycled the oceanic crust is decreased by subduction processes (see their Fig. 2).
4. **subducted oceanic crusts are too dense in the lower mantle to rise to the upper mantle.** As I discussed above, the source of OIB is a mixture of recycled oceanic crust and peridotite, and it is possible that the recycled oceanic crust is only a small proportion of the OIB source (e.g., Hauri, 1996; Lassiter and Hauri, 1998; Huang and Frey, 2005); consequently, because of its high temperature, a mantle plume, mixture of recycled oceanic crust and peridotite, may be less dense than the ambient mantle.

3.2.3 Recycled Gabbroic Crust

Since ancient recycled basaltic oceanic crust and the associated sediments are inferred to be present in the Hawaiian plume, it is logical to ask – Is the lower part of the recycled oceanic crust, i.e., the gabbroic crust, also present in the Hawaiian plume?

Sobolev et al. (2000) found unusually Sr-enriched melt inclusion compositions in olivine phenocrysts from Mauna Loa lavas. Consequently, they inferred that the Sr-enrichment in these melt inclusions reflect sampling of an ancient recycled plagioclase-rich gabbroic crust, which act as a spike source of Sr. In addition, by comparing isotopic data for Kahoolawe lavas and other Hawaiian shield lavas, Huang et al. (submitted) noted that a relative absence of this spike source of Sr is required to explain the $^{87}Sr/^{86}Sr$ offset of Kahoolawe lavas from other Hawaiian shield lavas. See Chapter 3 for a detailed discussion.

4. The Structure of the Hawaiian Plume: Concentrically Zoned vs Bilateral?

In previous sections, I discussed the geochemical heterogeneity in Hawaiian shield lavas, and their possible mantle source components. The inter-shield geochemical heterogeneity has been used to infer the structure of the Hawaiian plume (e.g., Lassiter et al., 1996; DePaolo et al., 2001; Kurz et al., 2004; Abouchami et al., 2005). It is well known that the spatial arrangement of recent Hawaiian volcanoes form two offset trends, i.e., the Kea and Loa trends (e.g., Lassiter et al., 1996; Fig. 1). Lavas from these trends have important geochemical differences (e.g., Lassiter et al., 1996; Abouchami et al., 2005). For example, Loa and Kea trend lavas form different trends in $^{87}Sr/^{86}Sr$ and $^{208}Pb^*/^{206}Pb^*$ vs $^{3}He/^{4}He$ plot (e.g., Lassiter et al., 1996; Kurz et al., 2004; Figs. 28, 29). Abouchami et al. (2005) noted that, compared with Kea trend lavas, Loa trend lavas have relatively higher $^{208}Pb/^{204}Pb$ at a given $^{206}Pb/^{204}Pb$ (Fig. 30a), i.e., Loa trend lavas have higher $^{208}Pb^*/^{206}Pb^*$. Kea and Loa trend lavas also form different trends in plots of $^{208}Pb^*/^{206}Pb^*$ vs Hf, Sr and Nd isotopic ratios (Fig. 22). An important observation is that Loihi lavas are located in the conjunction of Loa and Kea trends (Figs. 22, 28, 29);

implying that the Loihi component (high $^{3}He/^{4}He$) is a common source component for Loa and Kea trend volcanoes.

There are, however, exceptions; e.g., there are two examples of Kea trend lavas having Loa trend characteristics: **1.** the Low-SiO_2 group lavas from Mauna Kea volcano recovered by Phase 2 of Hawaii Scientific Drilling Project. This group of lavas form a trend toward high $^{208}Pb^{*}/^{206}Pb^{*}$ and $^{3}He/^{4}He$, and was argued to sample a Loihi-like source component (Eiler et al., 2003; Huang and Frey; 2003; Kurz et al., 2004; Rhodes and Vollinger, 2004); **2.** Ren et al. (in press) argued that there is a transition in geochemical compositions from Kilauea-like to Mauna Loa-like at Haleakala Volcano.

The geochemical differences between Loa and Kea trend lavas are inferred to reflect source characteristics. Two different models for the structure of the Hawaiian plume have been proposed (Lassiter et al., 1996; Abouchami et al., 2005). Lassiter et al. (1996) proposed a zoned plume model (Fig. 31a), where Loa trend volcanoes pass over the central part of the plume and Kea trend volcanoes pass over the edge of the plume. Consequently, the geochemical differences between Loa and Kea trend lavas reflect different source components in the center and the edge of the Hawaiian plume. This plume structure is supported by fluid dynamic experiments of Hauri et al. (1994). Specifically, an upwelling mantle plume may be concentrically zoned because it entrains ambient mantle as it rises. That is, the Hawaiian plume has a core of plume material which is surrounded by entrained mantle material (Lassiter et al., 1996; Fig. 31a). Based on the temporal variations of geochemical compositions of shield lavas from several Hawaiian shields, such as Mauna Kea, Koolau and Haleakala, Kurz et al. (2004) and Ren

et al. (submitted) proposed that although the plume is grossly zoned, there are Kea- and Loa-type sources present throughout the plume (Fig. 31b).

Alternatively, Abouchami et al. (2005) proposed a bilaterally assymmetric plume model (Fig. 31c). They inferred that the geochemical differences between Loa and Kea trend lavas reflect different geochemical compositions in the two parts of the Hawaiian plume. In addition, Abouchami et al. (2005) noted the long-term geochemical similarity within Loa and Kea trend lavas, respectively. That is, in the $^{206}Pb/^{204}Pb$ vs $^{208}Pb/^{204}Pb$ plot, all Kea trend lavas sampled two common source components, and all Loa trend lavas sampled another two common source components (Abouchami et al., 2005; Fig. 30a). Consequently, they inferred that "the Hawaiian plume contains relatively narrow compositional streaks ("spaghetti") that are drawn out by laminar flow in the conduit over a significant part of the vertical extent of the plume". Using a 3D numerical model in Cartesian geometry, Farnetani et al. (2002) and Farnetani and Samuel (2005) showed that heterogeneities initially located in a thermal boundary where a mantle plume rises will be stretched and folded to form narrow filaments in the plume tail (Fig. 32). This result is consistent with the "spaghetti" model proposed by Eisele et al. (2003).

There are important similarities between these two types of models: **1.** both assume no vertical isotopic variation in the Hawaiian plume (e.g., DePaolo et al., 2001; Eisele et al., 2003); **2.** both assume that the observed isotopic variations in the shield lavas accurately reflect the isotopic characteristics of their source, i.e., a 1:1 "map"; **3.** finally, the postshield stage lavas are not considered in their discussion. In fact, as noted by Xu et al. (2005), postshield stage lavas from Kea trend volcanoes (Mauna Kea, Kohala and West Maui) largely overlap with the Kea trend shield lavas in a $^{206}Pb/^{204}Pb$ vs

$^{208}Pb/^{204}Pb$ plot; whereas, postshield stage lavas from Hualalai (a Loa trend volcano) overlap with the Loa trend shield lavas in such a plot (Fig. 30b). That is, the Loa-Kea geochemical difference may continue to postshield stage lavas. This result argues against a concentrically zoned plume model. Since postshield stage volcanism samples the edge of the Hawaiian plume (Fig. 6), if the Hawaiian plume is concentrically zoned (Fig. 31a), postshield stage lavas from both Loa and Kea trend volcanoes should sample the same source components.

Both types of models, concentrically zoned versus bilateral, can be tested. However, I first question the assumption that the observed isotopic variations in the shield lavas reflect exactly the isotopic variations in their source. Is it possible to generate the Loa and Kea trend lavas from a common mantle source? Below I evaluate this possibility.

I propose a simple model based on the work of Ito and Mahoney (2005). Also since Kilauea Volcano, a Kea trend volcano, is presently the most active volcano, I propose that Kea trend volcanoes pass over the center of the Hawaiian plume with higher temperature, and Loa trend volcanoes pass over the edge of the Hawaiian plume with lower temperature (Fig. 31d). This spatial arrangement contrasts with that proposed by Kurz et al. (2004), but their assumption is not compelling. Specifically, Kurz et al. (2004) noted that $^{3}He/^{4}He$ decreases as a Hawaiian volcano moves away from the center toward the edge of the Hawaiian plume, i.e., from shield stage to postshield stage. Consequently, Kurz et al. (2004) inferred that the center of the Hawaiian plume is characterized by high $^{3}He/^{4}He$. Because Loihi lavas have the highest $^{3}He/^{4}He$ among Hawaiian lavas, Kurz et al. (2004) argued that the present center of the Hawaiian plume is beneath Loihi

Seamount. However, this argument can be questioned. Loihi Seamount erupts intercalated alkalic and tholeiitic lavas, and is proposed to be in transition from the preshield stage to shield stage (Garcia et al., 1993; 1995). Therefore, it is unlikely that Loihi Seamount is above the center of the Hawaiian plume.

In my model, I assume that Loa and Kea volcanoes sampled a common mantle source with imbedded geochemical heterogeneities. I propose that there are three source components in the Hawaiian plume, M1, M2 and M3 as shown in Figs. 22, 28, 29. M1 is mainly defined by Makapuu-stage Koolau lavas, characterized by high $^{208}Pb^*/^{206}Pb^*$, $^{87}Sr/^{86}Sr$ and SiO_2, and low $^{206}Pb/^{204}Pb$, $^{143}Nd/^{144}Nd$, $^{176}Hf/^{177}Hf$ and CaO. Such a component is variably sampled by Loa trend lavas, but is absent in Kea trend lavas. This source component is inferred to be an eclogitic component formed from recycled oceanic crust; consequently, it has a lower solidus temperature than mantle peridotites. It is not abundant in the Hawaiian plume (Hauri, 1996; Lassiter and Hauri, 1998; Blichert-Toft et al., 1999; Huang and Frey, 2005). In addition, I speculate that solidus temperatures increase from M1 to M2 to M3. Because heat diffuses much faster than atoms, it is possible that these three isotopically heterogeneous source components are in thermal equilibrium throughout the upwelling process (Phipps Morgan, 2001; Ito and Mahoney, 2005). In the case of Loa trend volcanoes, they sample the edge of the Hawaiian plume where temperature is low (Fig. 31d). Consequently, partial melting does not occur until shallow depth. M1 begins to melt first because of its low solidus temperature. At a shallower depth, M2 begins to melt. Because of the low temperature, M3 with the highest solidus temperature may not melt throughout the whole upwelling process forming Loa trend volcanoes. Consequently, the pooled magmas in this case only sample M1 and M2.

Because Kea trend volcanoes sample the center of the Hawaiian plume, partial melting initiates at greater depth and M1 may be totally melted. Although the melting extent of M1 is large (100%), because of its low abundance, its geochemical signal is diluted in the pooled magmas by the more abundant partial melts from M2 and M3. Consequently, the pooled magmas for Kea trend volcanoes only reflect varying proportion of M2 and M3. These scenarios were discussed in detail in Ito and Mahoney (2005).

In summary, I speculate that the Loa-Kea geochemical differences reflect the temperature difference between Loa and Kea trend volcanoes rather than a source difference. Such a simple model can to a first order explain the Loa-Kea geochemical differences manifested in shield stage lavas. In addition, it can also explain the intra-shield transition from Kea-like (M3) composition to Loa-like (M2) composition at Haleakala Volcano (Ren et al., in press) and the transition from Kea-like (M3) composition to Loa-like (M2) composition to Makapuu-stage Koolau (M1) composition at Koolau Volcano (Tanaka et al., 2002; Huang and Frey, 2005). I infer that such transitions reflect a temperature decrease as a volcano moves away from the center of the Hawaiian plume.

Loa trend lavas form highly curved trends in plots of $^{87}Sr/^{86}Sr$ and $^{208}Pb^*/^{206}Pb^*$ vs $^{3}He/^{4}He$ (Figs. 28, 29); implying that M1, mostly defined by Makapuu-stage Koolau lavas, has much higher He/Pb and He/Sr than M2, mostly defined by Loihi lavas. This inference can be tested. An apparent problem is that Helium abundance is highly affected by degassing, which makes it difficult to infer magmatic He/Pb and He/Sr from whole rock data. Submarine glasses may not be degassed (e.g., Dixon and Clague, 2001), which

can be used for testing my model. An alternative way is to analyze melt inclusions which may not be degassed (e.g., Hauri, 2002).

Similar to Lassiter et al. (1996) and Abouchami et al. (2005) models, I do not involve postshield stage lavas in my model. The common source model cannot explain the geochemical transition from shield to postshield volcanism. Detailed studies on Kea-trend volcanoes indicate that the transition from shield to postshield volcanism is characterized by decrease in $^{87}Sr/^{86}Sr$ and Pb isotopic ratios and increase in $^{143}Nd/^{144}Nd$ (e.g., Chen and Frey, 1985; Frey et al., 1990; 1991; Yang et al., 1996; Huang et al., 2003). Such a transition cannot be explained as a result of decrease in temperature only. Rather, a source component with low $^{87}Sr/^{86}Sr$ and Pb isotopic ratios and high $^{143}Nd/^{144}Nd$ must be present in the edge of the Hawaiian plume. At this stage, it is unclear whether the Loa-Kea geochemical differences continue to postshield stage lavas (Xu et al., 2005); if they do my model needs refinement.

5. Summary

Major conclusions are:

1. Long-term geochemical similarities in lavas erupted along the age-progressive Hawaii-Emperor Chain strongly argue for a long-lived mantle source contributing to Hawaiian-Emperor volcanism. Consequently, a mantle plume is inferred.
2. At present there are geochemical hints indicating that the Hawaiian plume may originate from the core-mantle boundary, but this inference requires further geophysical and geochemical tests.
3. It is unlikely that Hawaiian-Emperor lavas include a depleted MORB-related component.

4. The large variations in major and trace element compositions and isotopic ratios in Hawaiian shield lavas are consistent with the presence of ancient recycled oceanic crust, including sediment, in the Hawaiian plume.
5. Based on the Loa-Kea geochemical differences, two plume models, concentrically zoned and bilateral, have been proposed for the Hawaiian plume. However, I propose that the observed geochemical differences in Loa and Kea trend lavas may not necessarily be attributed to source differences. Rather, they may reflect a temperature difference between Loa and Kea trend volcanoes that reflects their distance from the hot plume core.

Reference:

Abouchami, W., W., Galer, S. J. G., and Hofmann, A. W., High precision lead isotope systematics of lavas from the Hawaiian Scientific Drilling Project, Chem. Geol., 169, 187-209, 2000.

Abouchami, W., Hofmann, A. W., Galer, S. J. G., Frey, F. A., Eisele, J., Feigenson, M., Lead isotopes reveal bilateral asymmetry and vertical continuity in the Hawaiian mantle plume, Nature, 434, 851-856, doi:10.1038/nature03402, 2005.

Albarede, F., How deep do common basaltic magmas form and differentiate?, J. Geophys. Res., 97 (7), 10,997-11,009, 1992.

Albers, M. and Christensen, U., The excess temperature of plumes rising from the core mantle boundary, Geophys. Res. Lett. , 23 , 3567-3570, 1996.

Anderson, D. L., Thermal State of the Upper Mantle; No Role for Mantle Plumes, Geophys. Res. Lett., 27 (22) 3623-3626, 2000.

Appora, I., J. M. Eiler, A. Matthews, and E. M. Stolper, Experimental determination of oxygen isotope fractionations between CO_2 and soda-melilite melt, Geochim. Cosmochim. Acta., 67, 459-471, 2002.

Bach, W., B. Peucker-Ehrenbrink, S. R. Hart, and J. S. Blusztajn, Geochemistry of hydrothermally altered oceanic crust: DSDP/ODP Hole 504B – Implications for seawater-crust exchange budgets and Sr- and Pb-isotopic evolution of the mantle, Geochem. Geophys. Geosyst., 4(3), 8904, doi:10.1029/2002GC000419, 2003.

Basu, A. R. and Faggart, B. E., Temporal isotopic variations in the Hawaiian Mantle Plume: The Lanai anomaly, the Molokai fracture zone and a seawater-altered lithospheric component in Hawaiian volcanism, in: A. Basu, S. Hart (Eds.), Earth Processes: Reading the Isotopic Code, AGU Monogr. 95 149–159, 1996.

Blichert-Toft, J., Frey, F. A., and Albarede, F., Hf isotope evidence for pelagic sediments in the source of Hawaiian basalts, Science, 285 (5429), 879-882, 1999.

Blichert-Toft, J., D. Weis, C. Maerschalk, A. Agranier, and F. Albarède, Hawaiian hot spot dynamics as inferred from the Hf and Pb isotope evolution of Mauna Kea volcano, Geochem. Geophys. Geosyst., 4(2), 8704, doi:10.1029/2002GC000340, 2003.

Brandon A. D., Norman M. D., Walker R. J. and Morgan J. W., ^{186}Os-^{187}Os systematics of Hawaiian picrites, Earth Planet. Sci. Lett. **172** , 25-42, 1999.

Brandon A. D. and M. D., Walker R. J., The debate over core–mantle interaction, Earth Planet. Sci. Lett., 232, 211-225, doi:10.1016/j.epsl.2005.01.034, 2005.

Chabot, N. L., Campbell, A. J., Jones, J. H., Humayun, M. and Agee, C. B., An experimental test of Henry's law in solid metal–liquid metal systems with implications to iron meteorites, Meteorit. Planet. Sci., 38, 181–196, 2003.

Chavagnac, V., German, C. R., Milton, J. A. and Palmer, M. R., Sources of REE in sediment cores from the Rainbow vent site (36°14'N, MAR), Chem. Geol., 216, 329-352, doi:10.1016/j.chemgeo.2004.11.015, 2005.

Chazot, G., Lowry, D., Menzies, M. and Mattey, D., Oxygen isotopic composition of hydrous and anhydrous mantle peridotite, Geochim. Cosmochim. Acta., 61, 161–169, 1997.

Chen, C.-Y. and Frey, F.A., Trace element and isotope geochemistry of lavas from Haleakala Volcano, East Maui: Implications for the origin of Hawaiian basalts, J. Geophys. Res., 90, B10, 8743-8768, 1985.

Clague, D. A., Hawaiian alkaline volcanism, Geol. Soc. Am. Spec. Publ., 30: 227-252, 1987.

Clague, D. A., and Dalrymple, B. G., The Hawaiian-Emperor volcanic chain; Part I, Geologic evolution, in Decker, R. W. (editor), Wright, T. L. (editor), Stauffer, P. H. (editor), Volcanism in Hawaii, U. S. Geological Survey Professional Paper, P 1350, 5-73, 1987.

Courtillot, V., A. Davaille, J. Besse and J. Stock, Three distinct types of hotspot in the Earth's mantle, Earth Planet. Sci. Lett., 205, 295-308, 2003.

Dasgupta, R., Hirschmann, M. M. and Withers, A. C., Deep Global Cycling of Carbon Constrained by the Solidus of Anhydrous, Carbonated Eclogite under Upper Mantle Conditions, Earth Planet. Sci. Lett., 227, 73-85, doi:10.1016/j.epsl.2004.08.004, 2004.

Davies, G. F., Ocean bathymetry and mantle convection 1. large-scale flow and hotspots, J. Geophys. Res., 93, 10,467–10,480, 1988.

DePaolo, D. J., Bryce, J. G., Dodson, A., Shuster, D. L., Kennedy, B. M., Isotopic evolution of Mauna Loa and the chemical structure of the Hawaiian plume, Geochem. Geophys. Geosyst. 2 paper number 2000GC000139, 2001.

Dixon, J. E. and Clague, D. A., Volatiles in basaltic glasses from Loihi Seamount: Evidence for a relatively dry plume component, Jour. Petrol., 42(3), 627-654, 2001.

Douglass, J. and Schilling, J.G., Systematics of three-component, pseudo-binary mixing lines in 2D isotope ratio space representations and implications for mantle plume-ridge interaction, Chem. Geol., 163, 1–23, 2000.

Duncan, R. A., and Keller, R. A., Radiometric ages for basement rocks from the Emperor Seamounts, ODP Leg 197, Geochem. Geophys. Geosystems, 5, Q08L03, doi:10.1029/2004GC000704, 2004.

Eggins, S. M., Petrogenesis of Hawaiian tholeiites; 1, Phase equilibria constraints, Contrib. Mineral. Petrol., 110 (2-3), 387-397, 1992.

Eiler, J. M., Valley, J. W. and Stolper, E. M., Oxygen isotope ratios in olivine from the Hawaii Scientific Drilling Project. J. Geophys. Res. 101, 11807–11813, 1996.

Eiler, J. M., K. A. Farley, J. W. Valley, E. Hauri, H. Craig, S. R. Hart, and E. M. Stolper, Oxygen isotope variations in ocean island basalt phenocrysts, Geochim. Cosmochim. Acta, 61, 2281–2293, 1997.

Eiler, J. M., Oxygen isotope variations of basaltic lavas and upper mantle rocks, in Stable Isotope Geochemistry, edited by J. W. Valley and D. R. Cole, Rev. Mineral., 43, 319–364, 2001.

Eisele, J., Sharma, M. Galer, S. J. G., Blichert-Toft, J., Devey, C. W., Hofmann, A. W., The role of sediment recycling in EM-1 inferred from Os, Pb, Hf, Nd, Sr isotope and trace element systematics of the Pitcairn hotspot. Earth Planet. Sci. Lett. 196, 197-212, 2002.

Eisele, J., Abouchami, W., Galer, S. J. G. and Hofmann, A. W., The 320 kyr Pb isotope evolution of Mauna Kea lavas recorded in the HSDP-2 drill core, Geochem. Geophys. Geosyst., 4(5), 8710, doi:10.1029/2002GC000339, 2003.

Escrig, S., Capmas, F., Dupré, B. and Allègre, C. J., Osmium isotopic constraints on the nature of the DUPAL anomaly from Indian mid-ocean-ridge basalts, nature, 431, 59-63, doi:10.1038/nature02904, 2004.

Farley, K. A. and Neroda, E., Noble gases in the Earth's mantle, Ann. Rev. Earth Planet. Sci., 26, 189-218, 1998.

Farnetani, C. G., Legras, B., Tackley, P. J., Mixing and deformations in mantle plumes, Earth Planet Sci Letts., 196 (1-2), 1-15, 2002.

Farnetani, C. G. and Samuel, H., Beyond the thermal plume paradigm, Geophys. Res. Lett. Vol. 32, L07311, doi:10.1029/2005GL022360, 2005.

Feigenson, M. D., L. L. Bolge, M. J. Carr, and C. T. Herzberg, REE inverse modeling of HSDP2 basalts: Evidence for multiple sources in the Hawaiian plume, Geochem. Geophys. Geosyst., 4(2), 8706, doi:10.1029/2001GC000271, 2003.

Fleet, M. E., Liu, M. and Crocket, J. H., Partitioning of trace amounts of highly siderophile elements in the Fe–Ni–S system and their fractionation in nature, Geochim. Cosmochim. Acta., 63, 2611–2622, 1999.

Frey, F. A. and Green, D. H., The mineralogy, geochemistry and origin of lherzolite inclusions in Victorian basanites, Geochim. Cosmochim. Acta., 38 (7), 1023-1059, 1974.

Frey, F. A., Wise, W. S., Garcia, West, H., Kwon, S. T., and Kennedy, A., Evolution of Mauna Kea volcano, Hawaii: Petrologic and geochemical constraints on postshield volcanism, J. Geophys. Res., 95, 1271-1300, 1990.

Frey, F. A., Garcia, M. O., Wise, W. S., Kennedy, A., Gurriet, P., Albarede, F., The evolution of Mauna Kea volcano, Hawaii: Petrogenesis of tholeiitic and alkalic basalts, J. Geophys. Res., 96, 14,347-14,375, 1991.

Frey, F. A., Garcia, M. O., and Roden, M. F., Geochemical characteristics of Koolau Volcano: Implications of intershield geochemical differences among Hawaiian volcanoes. Geochim. Cosmochim. Acta., 58, 1441-1462, 1994.

Frey, F. A., Huang, S., Blichert-Toft, J., Regelous, M. and Boyet, M., Origin of Depleted Components in Lavas Related to the Hawaiian Hotspot: Evidence From Hf Isotope Data, Geochem. Geophys., Geosys, 6(2), doi:10.1029/2004GC000757, 2005.

Galer, S. J. G., Abouchami, W. and Macdougall, J. D., East Pacific Rise MORB through the Pb isotope looking-glass, Eos Trans. AGU, 80 Fall Meet. Suppl., F1086, 1999.

Gao, S., Luo, T.-C., Zhang, B.-R., Zhang, H.-F., Han, Y.-W., Zhao Z.-D. and Hu, Y.-K., Chemical composition of the continental crust as revealed by studies in East China, Geochim. Cosmochim. Acta., 62, 1959–1975, 1998.

Garcia, M. O., Jorgenson, B. A., Mahoney, J. J., Ito E., and Irving, A. J., An evaluation of temporal geochemical evolution of Loihii summit lavas: Results from Alvin submersible dives. J. Geophys. Res. 98, 535-550, 1993.

Garcia, M. O., Foss, D. J. P., West, H. B. and Mahoney, J. J., Geochemical and isotopic evolution of Loihi Volcano, Hawaii, Journal of Petrology, 36, 1647-1644, 1995.

Green, D. H., T. J. Falloon, S. M. Eggins, and G. M. Yaxley, Primary magmas and mantle temperatures, Eur. J. Mineral., 13, 437–451, 2001.

Halliday, A. N., Mixing, volatile loss and compositional change during impact-driven accretion of the earth, Nature 427, 505–509, 2004.

Haskins, E. R., and Garcia M. O., Scientific drilling reveals geochemical heterogeneity within the Ko'olau shield, Hawai'i, Contrib. Mineral. Petrol., 147, 162-188, 2004.

Hauri, E. H., Whitehead, J. A. and Hart, S. R., Fluid dynamic and geochemical aspects of entrainment in mantle plumes, J. Geophys. Res., 99(12), 24,275-24,300, 1994.

Hauri, E. H., Major-element variability in the Hawaiian mantle plume, Nature 382, 415-419, 1996.

Hauri, E. H., SIMS investigations of volatiles in silicate glasses 2: abundances and isotopes in Hawaiian melt inclusions, Chem. Geol. 183, 115-141, 2002.

Hofmann, A. W. and White, W. M., Mantle plumes from ancient oceanic crust. Earth Planet. Sci. Lett., 57, 421-436, 1982.

Hofmann, A. W., Feigenson, M. D., Raczek, I., Case studies on the origin of basalt; III, Petrogenesis of the Mauna Ulu eruption, Kilauea, 1969-1971, Contrib. Mineral. Petrol., 88 (1-2), 24-35, 1984.

Hofmann, A. W. and Jochum, K. P., Source characteristics derived from very incompatible trace elements in Mauna Loa and Mauna Kea basalts (Hawaiian Scientific Drilling Project), J. Geophys. Res. 101, 11,831-11,839, 1996.

Hofmann, A. W., Mantle geochemistry: the message from oceanic volcanism, Nature 385, 219-229, 1997.

Hofmann, A.W., Sampling mantle heterogeneity through oceanic basalts: Isotopes and trace elements, 61-101. In The Mantle and Core (ed. R.W. Carlson) Vol. 2, Treatise on Geochemistry (eds. H. Holland and K. K. Turekian), Elsevier-Pergamon, Oxford, 2003.

Honnorez, J., Mevel, C., Honnerez-Guerstein, B. M. and Tomschi, H. P., Mineralogy and chemistry of sulfide deposits drilled from hydrothermal mound of the snake pit active field, MAR, in Detrick, R., Honnorez. J., Bryan, W. B., Juteau, T., et al., Proceedings of the Ocean Drilling Program, Scientific Results, Vol. 106/109: 145-162, Washington, D.C.: U.S. Government Printing Office. 1990.

Huang, S. and Frey, F. A., Trace element abundances of Mauna Kea basalt from Phase 2 of the Hawaiian Scientific Drilling Project: Petrogenetic implications of correlations with major element content and isotopic ratios, Geochem. Geophys., Geosys, 4(6), 8711, doi, 1029/2002 GC000322, 2003.

Huang, S. and Frey, F. A., Recycled Oceanic Crust in the Hawaiian Plume: Evidence from Temporal Geochemical Variations Within the Koolau Shield. Contrib. Mineral. Petrol. 2005.

Huang, S., Regelous, M., Thordarson, T. and Frey, F. A., Petrogenesis of Lavas from Detroit Seamount: Geochemical Differences Between Emperor Chain and Hawaiian Volcanoes. Geochem. Geophys. Geosystem. 6(1), Q01L06, doi:10.1029/2004GC000756, 2005.

Huang, S., Frey, F. A., Blichert-Toft, J., Fodor, R. V., Bauer, G. R. and Xu, G., Enriched Components in the Hawaiian Plume: Evidence from Kahoolawe Volcano, Hawaii, submitted to Geochem. Geophys. Geosystem.

Humayun, M., Qin, L. and Norman, M. D., Geochemical evidence for excess iron in the mantle beneath Hawaii, Science, 306, 91-94, 2004.

Ito, G. and J. J. Mahoney, Flow and melting of a heterogeneous mantle: 2. Implications for a chemically non-layered mantle, Earth Planet. Sci. Lett., 230, 47-63, 2005.

Jackson, M. C., Wilmoth, R. A., and Frey, F. A., Geology and petrology of basaltic lavas and dikes of the Koolau Volcano in the Trans-Koolau exploratory tunnels, Oahu, Hawaii. Bull. Volcan. 60, 381-401, 1999.

Keller, R. A., D. W. Graham, K. A. Farley, R. A. Duncan, and J. E. Lupton, Cretaceous-to-recent record of elevated $^{3}He/^{4}He$ along the Hawaiian-Emperor volcanic chain, Geochem. Geophys. Geosyst., 5, Q12L05, doi:10.1029/2004GC000739, 2004a.

Keller, W., D. Anderson, and R. Clayton, Resolution of tomographic models of the mantle beneath Iceland, Geophys. Res. Lett., 27(24), 3993-3996, 2000b.

Korenaga, J., Firm mantle plumes and the nature of the core-mantle boundary region, Earth Planet. Sci. Lett., 232, 29-37, 2005.

Kurz, M. D., Curtice, J., Lott III, D. E. and Solow, A., Rapid helium isotopic variability in Mauna Kea shield lavas from the Hawaiian Scientific Drilling Project, Geochem. Geophys. Geosyst., 5, Q04G14, doi:10.1029/2002GC000439, 2004.

Lassiter, J.C., DePaolo, D.J., and Tatsumoto, M., Isotopic evolution of Mauna Kea volcano: Results from the initial phase of the Hawaiian Scientific Drilling Project. J. Geophys. Res. 101, 11,769-11,780, 1996.

Lassiter, J. C. and Hauri, E. H., Osmium-iosotope variations in Hawaiian lavas: Evidence for recycled oceanic lithosphere in the Hawaiian plume, Earth Planet Sci Letts., 164, 483-496, 1998.

Lassiter, J. C., Platinum-Group Element Variations in Hawaiian Lavas: Constraints on the Role of Sulfides during Melt Generation and Fractional Crystallization, EOS. Trans. AGU, 84(46) Fall Meeting Suppl. Abstract, V42C-0371, F1598, 2003.

Lauer H. V. and Jones, J. H., Partitioning of Pt and Os between solid and liquid metal in the iron–nickel–sulfur system, Proc. Lunar Planet. Sci. Conf. **XXIX,** p. 1796, 1998.

Lee D.-C. and Halliday, A. N., Hafnium–tungsten chronometry and the timing of terrestrial core formation, Nature 378, 771–774, 1995.

McKenzie, D. and O'Nions, R. K., Mantle reservoirs and ocean island basalts, Nature, 301 (5897), 229-231, 1983.

Mattey, D., Lowry, D. and Macpherson, C., Oxygen isotope composition of mantle peridotite, Earth Planet. Sci. Lett. 128, 231–241, 1994.

Meibom, A. and Anderson, D. L., The Statistical Upper Mantle Assemblage, Earth Planet. Sci. Lett., 217, 123-139, 2003.

Montelli, R., Nolet, G., Dahlen, F.A., Masters, G., Engdahl, E.R, Hung, S., Finite-Frequency Tomography Reveals a Variety of Plumes in the Mantle, Science. 303, 338-343, 2004.

Morgan, J. W., Horan, M. F., Walker, R. J. and Grossman, J. N., Rhenium–osmium concentration and isotope systematics in group IIAB iron meteorites, Geochim. Cosmochim. Acta., 59, 2331–2344, 1995.

Morgan, W. J., Convection plumes in the lower mantle, Nature (London), 230 (5288), 42-43, 1971.

Mukhopadhyay, S., Lassiter, J.L., Farley, K.A., and Bogue, S.W., Geochemistry of Kauai shield-stage lavas: Implications for the chemical evolution of the Hawaiian plume. Geochem. Geophys. Geosyst., 4(1), 1009,doi: 10.1029/2002GC 000342, 2003.

Newsom, H. E., Sims, K. W. W., Noll, P. D., Jaeger, W. L., Maehr, S. A. and Beserra, T. B., The depletion of tungsten in the bulk silicate earth: constraints on core formation, Geochim. Cosmochim. Acta., 60, 1155–1169, 1996.

Niu, Y. and O'Hara, M. J., The origin of ocean island basalts (OIB): A new perspective from petrology, geochemistry and mineral physics considerations, J. Geophys. Res., 108, 10.1029/2002JB002048, 2003.

Norman, M. D., Garcia, M.O. and Bennett, V.C., Rhenium and chalcophile elements in basaltic glasses from Ko'olau and Moloka'i volcanoes: Magmatic outgassing and composition of the Hawaiian plume, Geochim. Cosmochim. Acta., 68, 3761-3777, 2004.

Patino, L, C., Carr, M. J. and Feigenson, M. D., Local and regional variations in Central American arc lavas controlled by variations in subducted sediment input, Contrib. Mineral. Petrol., 138(3), 265-283, 2000.

Pertermann, M., Hirschmann, M. M., Hametner, K., Gunther, D., Schmidt, M. W., Experimental determination of trace element partitioning between garnet and silica-rich liquid during anhydrous partial melting of MORB-like eclogite, Geochem. Geophys, Geosyst, 5, Q05A01, doi:10.1029/2003GC000638, 2004.

Phipps Morgan, J. and W. Jason Morgan, Two-stage melting and the geochemical evolution of the mantle: A recipe for mantle plum-pudding, Earth Planet Sci. Lett., 170, 215-239, 1999.

Phipps Morgan, J., Thermodynamics of pressure release melting of a veined plum pudding mantle, Geochem. Geophys. Geosyst., 2 (4), doi:10.1029/2000GC000049, 2001.

Plank, T., and Langmuir, C. H., The chemical composition of subducting sediment and its consequences for the crust and mantle, Chem. Geol., 145 (3-4), 325-394, 1998.

Plank, T., Balzer, V. and Carr, M., Nicaraguan volcanoes record paleoceanographic changes accompanying closure of the Panama gateway, Geology, 30(12), 1087-1090, 2002.

Putirka, K. D., Mantle potential temperatures at Hawaii, Iceland, and the mid-ocean ridge system, as inferred from olivine phenocrysts: Evidence for thermally driven mantle plumes, Geochem. Geophys. Geosyst., 6, Q05L08, doi:10.1029/2005GC000915, 2005.

Regelous, M., Hofmann, A.W., Abouchami, W. and Galer, S.J.G., Geochemistry of lavas from the Emperor Seamounts, and the geochemical evolution of Hawaiian magmatism from 85 to 42 Ma. J. Petrol., 44, 113-140, 2003.

Rehkämper, M. and Hofmann, A. W., Recycled ocean crust and sediment in Indian Ocean MORB, Earth Planet Sci. Lett., 147(1-4), 93-106, 1997.

Ren, Z.-Y., T. Shibata, M. Yoshikawa, K. T. M. Johnson, and E. Takahashi, Isotope compositions of the submarine Hana Ridge lavas, Haleakala volcano, Hawaii: Implications for source compositions, melting process and the structure of Hawaiian plume, J. Petrol., in press.

Ren, Z.-Y., Ingle, S., Takahashi, E., Hirano, N and Hirata, T., The chemical structure of the Hawaiian mantle plume, submitted to Nature.

Rhodes, J. M., and M. J. Vollinger, Composition of basaltic lavas sampled by phase-2 of the Hawaii Scientific Drilling Project: Geochemical stratigraphy and magma types, Geochem. Geophys. Geosyst., 5, Q03G13, doi:10.1029/2002GC000434, 2004.

Richards, M. A., R. A. Duncan, and V. E. Courtillot, Flood basalts and hotspot tracks: Plume heads and tails, Science, 246, 103-107, 1989.

Roy-Barman M. and Allègre, C. J., $^{187}Os/^{186}Os$ ratios of mid-ocean ridge basalts and abyssal peridotites. Geochim. Cosmochim. Acta., 58, 5043–5054, 1994.

Rudnick, R. L. and Fountain, D. M., Nature and composition of the continental crust: A lower crustal perspective, Rev. Geophys., 33, 267-309, 1995,

Salters, V. J. M. and Longhi, J., Trace element partitioning during the initial stages of melting beneath mid-ocean ridges. Earth Planet. Sci. Letts., 166, 15-30, 1999.

Schersten, A., Elliott, T., Hawkesworth, C. and Norman, M., Tungsten isotope evidence that mantle plumes contain no contribution from the Earth's core, Nature 427, 234–237, 2004.

Schilling, J.-G., Bergeron, M. B. and Evans, R., Halogens in the mantle beneath the North Atlantic, Phil. Trans. R. Soc. Lond. A 297, 147-178, 1980.

Schmidt, M. W. and Poli, S., Generation of mobile components during subduction of oceanic crust, 567-588, in The Crust (ed. R. L. Rudnick) Vol. 3, Treatise on Geochemistry (eds. H. Holland and K. K. Turekian), Elsevier-Pergamon, Oxford, 2003.

Shafer, J. T., C. R. Neal, and M. Regelous, Petrogenesis of Hawaiian postshield lavas: Evidence from Nintoku Seamount, Emperor Seamount Chain, Geochem. Geophys. Geosyst., 6, Q05L09, doi:10.1029/2004GC000875, 2005.

Sleep, N. H., Hotspots and mantle plumes: Some phenomenology, J. Geophys. Res., 95, 6715–6736, 1990.

Snow, J. E. and Reisberg, L., Os isotopic systematics of the MORB mantle: results from altered abyssal peridotites". Earth Planet. Sci. Lett. 136, 723–733, 1995.

Sobolev, A.V., Hofmann, A.W., and Nikogosian, I. K., Recycled oceanic crust observed in ghost plagioclase within the source of Mauna Loa lavas, Nature 404, 986-990, 2000.

Solomatov, V. S., Can hotter mantle have a larger viscosity? Geophys. Res. Lett. 23, 937–940, 1996.

Solomatov, V. S., Grain size-dependent viscosity convection and the thermal evolution of the Earth, Earth Planet. Sci. Lett. 191, 203– 212, 2001.

Standish, J. J., S. R. Hart, J. Blusztajn, H. J. B. Dick, and K. L. Lee, Abyssal peridotite osmium isotopic compositions from Cr-spinel, Geochem. Geophys. Geosyst., 3(01), 1004, doi:10.1029/2001GC000161, 2002.

Stein, C.A., and S. Stein, Constraints on Pacific midplate swells from global depth-age and heat flow-age models, in The Mesozoic Pacific: Geology, Tectonics, and Volcanism, pp. 53-76, American Geophysical Union, Washington, D.C., 1993.

Stein, C. and S. Stein, Mantle plumes: heat flow near Iceland, Astronomy and Geophysics, 44, 8-10, 2003.

Strekopytov, S. V., Molybdenum and tungsten in oceanic sediments and nodules, Geochem. Int. 36, 838–845, 1998.

Tanaka, R., Nakamura, E., Takahashi, E., Geochemical evolution of Koolau Volcano, Hawaii, in Hawaiian volcanoes; deep underwater perspectives, Geophysical Monograph Series, vol. 128, (eds, Takahashi, E., Lipman, P. W., Garcia, M. O., Naka, J., Aramaki, S), 311-332, 2002.

Thompson, G., Humphris, S. E., Schroeder, B., Sulanowska, M. and Rona, P. A., Active vents and massive sulfides at 26°N (TAG) and 23°N (Snakepit) on the mid-Atlantic ridge, Can. Mineral., 26, 697-711, 1988.

Tu, G., Zhao, Z. and Qiu, Y., Evolution of Precambrian REE mineralization, Precam. Res., 27, 131-151, 1985.

Vervoort, J. D., Patchett, P. J., Blichert-Toft, J., Albarede, F., Relationships between Lu-Hf and Sm-Nd isotopic systems in the global sedimentary system, Earth Planet. Sci. Lett., 168 (1-2), 79-99, 1999.

von Herzen, R.P., M.J. Cordery, R.S. Detrick, and C. Fang, Heat-flow and the thermal origin of hot spot swells - the hawaiian swell revisited, J. geophys. Res., 94, 13,783-13,799, 1989.

Wagner, T. P., and Grove, T. L., Melt/harzburgite reaction in the petrogenesis of tholeiitic magma from Kilauea Volcano, Hawaii, Contrib. Mineral. Petrol., 131 (1), 1-12, 1998.

Walker, D., Core participation in mantle geochemistry, Geochim. Cosmochim. Acta., 64, 2897–2911, 2000.

Wang, Z., Kitchen, N. E. and Eiler, J. M., Oxygen isotope geochemistry of the second HSDP core, Geochem. Geophys. Geosyst., 4(8), 8712, doi:10.1029/2002GC000406, 2003.

Weaver, B. L., Trace element evidence for the origin of ocean-island basalts, Geology, 19 (2), 123-126, 1991.

West, H. B., Gerlach, D. C., Leeman, William P., Garcia, Michael O., Isotopic constraints on the origin of Hawaiian lavas from the Maui volcanic complex, Hawaii, Nature, 330 (6145), 216-220, 1987.

Wilson, T. J., A possible origin of the Hawaiian Islands, Canadian Journal of Physics, 41 (6), 863-870, 1963.

Workman, R. K., S. R. Hart, M. Jackson, M. Regelous, K. A. Farley, J. Blusztajn, M. Kurz, and H. Staudigel, Recycled metasomatized lithosphere as the origin of the Enriched Mantle II (EM2) end-member: Evidence from the Samoan Volcanic Chain, Geochem. Geophys. Geosyst., 5, Q04008, doi:10.1029/2003GC000623, 2004.

Xu, G., Frey, F. A., Clague, D. A., Weis, D. and Beeson, M. H., East Molokai and other Kea-trend volcanoes: Magmatic processes and sources as they migrate away from the Hawaiian hot spot, Geochem. Geophys. Geosyst., doi:10.1029/2004GC000830, 2005.

Yang, H.-J., Frey, F. A., Rhodes, J. M., and Garcia, M. O., Evolution of Mauna Kea volcano: Inferences from lava compositions recovered in the Hawaii Scientific Drilling Project, J. Geophys. Res. 101, 11,747-11,767, 1996

Yang, H.-J., Frey, F. A. and Clague, D. A., Constraints on the source components of lavas forming the Hawaiian North Arch and Honolulu Volcanoes, J. Petrol., 44, 603-627, 2003.

Figure Captions:

Fig. 1 Map shows volcanoes along the Emperor Seamount Chain (eruption ages within parenthesis). Inset shows the Hawaiian Islands (green), Loa and Kea trend shields (blue and black, respectively) and rejuvenated stage volcanism (red) and North Arch volcanic field.

Fig. 2 Two different shapes of mantle plume. **a.** If the plume is less viscous than ambient mantle, it can have a large spherical head followed by a thin plume tail. **b.** If the plume is more viscous than ambient mantle, a plume head-tail structure is not developed. Figure is taken from Korenaga (2005).

Fig. 3 Three-dimensional view of the Hawaiian plume obtained using newly-developed finite-frequency tomography technique. Different colors represent P wave velocity perturbation. Map is 40° by 40°. The lack of low velocity anomaly at great depth (>2350 km) results from lack of resolution. Figure is taken from Montelli et al. (2004).

Fig. 4 $^{3}He/^{4}He$ vs age for Hawaiian and Emperor lavas. Hawaiian and Emperor lavas generally have higher $^{3}He/^{4}He$ (>10 R/R_A) than MORB. R_A represents atmospheric $^{3}He/^{4}He$. Question marks in the figure indicate lack of data. Figure is taken from Keller et al. (2004).

Fig. 5 Cross-section through a hypothetical Hawaiian Volcano adopted from Clague (1987).

Fig. 6 In some Hawaiian volcano models (e.g., DePaolo and Stolper, 1996; Ribe and Christensen, 1999), it is assumed that a Hawaiian volcano captures magma generated over a circular area, which is termed as magma capture area. As a Hawaiian volcano approaches the Hawaiian plume, i.e., preshield stage growth, its magma capture area samples magmas generated at the edge of the plume with relatively low temperature. As a volcano overrides the Hawaiian plume, i.e., shield stage growth, its magma capture area samples magmas generated at the center of the plume with relatively high temperature. Finally, as a volcano moves away from the Hawaiian plume, i.e., postshield stage growth, its magma capture area samples magmas generated at the edge of the plume with relatively low temperature.

Fig. 7 $^{87}Sr/^{86}Sr$ vs $^{143}Nd/^{144}Nd$ and $^{206}Pb/^{204}Pb$ vs $^{87}Sr/^{86}Sr$ for Detroit Seamount lavas. Figure is taken from Huang et al. (2005). For comparison, fields are shown for EPR MORB, Garrett transform fault lavas, two extreme Hawaiian shields (Mauna Kea and Koolau) and Hawaiian rejuvenated stage lavas. All data points and fields have been age-corrected to 76 Ma, except for Site 884 lavas which have been age-corrected to 81 Ma. A 2-sigma error bar is indicated unless the symbol is larger than the error bar. Because rejuvenated-stage and North Arch alkalic basalt were formed by low extents of melting (e.g., Yang et al., 2003) which may lead to significant changes in parent/daughter ratios, two sets of parent/daughter ratios were used for Hawaiian Rejuvenated Stage lavas: N-MORB values for the orange solid line, and Mauna Kea values for the black dash line. Figure is taken from Huang et al. (2005).

Fig. 8 MgO vs Al_2O_3 (%) for Mauna Kea lavas and MORB. Mauna Kea Volcano is the best sampled and studied Hawaiian volcano; consequently, I use Mauna Kea volcano as a representative of Hawaiian shields in Figs. 8 and 9.. At a given MgO content, MORB have higher Al_2O_3 content than Hawaiian shield lavas. However, because of plagioclase fractionation, this difference diminishes at low MgO content. Figure is modified after Huang et al. (2005).

Fig. 9 Primitive mantle normalized multiple element diagrams for tholeiitic lavas from Mauna Kea Volcano and average MORB. In contrast to MORB, shield stage lavas from the Hawaii-Emperor Chain are generally enriched in highly incompatible elements. Figure is modified after Huang et al. (2005).

Fig. 10 Ba/Th vs Sr/Nd for Hawaiian lavas and other OIB. Primitive mantle and N-MORB values are plotted for comparison. Compared with other OIB (excluding Icelandic lavas) and MORB, Hawaiian lavas have high Ba/Th and Sr/Nd. Figure is taken from Yang et al. (2003).

Fig. 11 Cartoons showing mantle flows (streamlines) and melting of a heterogeneous mantle for mid-ocean ridge melting and plume melting. Ovals represent enriched mantle (EM) and rectangles represent pyroxenite, imbedded in a matrix of depleted mantle (DM). Solidus temperatures of there three mantle lithologies increase in the order of EM<pyroxenite<DM. Consequently, EM begins to melt at the greatest depth and DM

begins to melt at the shallowest depth. Shading of each material increases with increasing partial melting extent. **(a)** Mantle flow beneath a mid-ocean ridge is passively driven by the spreading plates, and generates a nearly uniformly wide "residual mantle column"; **(b)** Active plume flow generates a "residual mantle cylinder" (RMC) that widens with depth. Consequently, compared with MORB, OIB sample a larger proportions of EM and pyroxenite, which begin to melt at greater depths. Figure is taken from Ito and Mahoney (2005b).

Fig. 12 Layered mantle convection (**a**) vs whole mantle convection (**b**). Mantle plume is proposed to originate from deep mantle, probably the lower mantle. In contrast, the mid-ocean ridge basalt samples the upper mantle. The 660-discontinuity is a barrier separating the upper and lower mantle. Consequently, the upper and lower mantle may have different geochemical compositions. Such an argument is used to explain the geochemical differences between MORB and OIB. In contrast, whole mantle convection does not require geochemical differences between the upper and lower mantle.

Fig. 13 Two-stage plume-ridge melting model. Upwelling mantle plume first melts to generate OIB, and its residues upwells again and melts a second time beneath a mid-ocean ridge. Figure is taken from Phipps Morgan and Morgan (1999).

Fig. 14 $^{186}Os/^{188}Os$ vs γ_{Os} ($\gamma_{Os}=[(^{187}Os/^{188}Os_{sample(t)}/\ ^{187}Os/^{188}Os_{chondrite(t)})-1]x100$) for mantle-derived materials. Regression lines for the Gorgona komatiites and all Hawaiian picrites, except for the two Koolau samples, are shown with calculated r-squares. The two

regression lines converge at $^{186}Os/^{188}Os$=0.11987 and γ_{Os}=+17.5, which is considered to be a common Os (COs) end-member for the different sample suites. This COs is argued to represent an outer core component. Figure is taken from Brandon and Walker (2005).

Fig. 15 MgO (%) vs Fe/Mn. **a.** Diamonds are Hawaiian lavas, circles are Icelandic lavas and squares are MORB. At a given MgO content, Hawaiian lavas have higher Fe/Mn. **b.** Different symbols represent lavas from different Hawaiian shields. Although Fe/Mn is affected by olivine fractionation, such effect is relatively insignificant compared with the Fe/Mn difference between Hawaiian lavas and other OIB and MORB (panel **a**). The thick gray line band represents possible MgO contents of the parental magmas for Hawaiian shield lavas. Figure is taken from Humayun et al. (2004).

Fig. 16 $^{87}Sr/^{86}Sr$ vs $^{143}Nd/^{144}Nd$ for Kahoolawe lavas. Fields for other Hawaiian shields, rejuvenated stage lavas and MORB are shown for comparison. Most notable is the large range for Kahoolawe and Makapuu-stage Koolau lavas, and the offset of Kahoolawe lavas to high $^{87}Sr/^{86}Sr$ at a given $^{143}Nd/^{144}Nd$. Figure is adopted from Huang et al. (submitted).

Fig. 17a $^{206}Pb/^{204}Pb$-ε_{Hf}. The isotopic ratios of the two source components, "**Kea**" and "**Koolau**", are from Blichert-Toft et al. (1999) who infer that the highly curved trend of Hawaiian shield lavas represents a mixing line between two components with very different Hf/Pb (a ratio of 40 shown by the dashed purple line). The Hawaiian trend can be fitted using $(Hf/Pb)_{Kea/Koolau}$=15. For simplicity, we assume that these two components

have the same Pb abundance, and Hf/Pb = x in "**Koolau**" component. The red line with ticks shows the mixing line between these two components with $(Hf/Pb)_{Kea/Koolau}$=15. The proportions of "**Kea**" component and Hf/Pb in the mixtures are labeled. This two source component model implies that Hf/Pb in Mauna Kea lavas (8.0x) is ~5 times that in Makapuu-stage of Koolau lavas (1.6x). The blue line in the inset shows the mixing line between average Mauna Kea (Hf/Pb=4.0) and Makapuu-stage Koolau lavas (Hf/Pb=3.0). Clearly, this mixing line cannot explain the highly curved Hawaiian trend. Figure is taken from Huang et al. (submitted).

Fig. 17b Histogram of ε_{Hf} in Pacific MORB and Mauna Kea lavas. Figure is modified from Blichert-Toft et al. (2003).

Fig. 18 MgO (%) vs Hf/Pb for Hawaiian shield lavas that define the isotopic endmembers for Hawaiian shields (i.e., Mauna Kea, Loihi and Makapuu-stage of Koolau). It is surprising that these abundance ratios vary by less than a factor of 3 (at MgO>7%). Figure is taken from Huang et al. (submitted).

Fig. 19 $^{187}Os/^{188}Os$ vs $^{87}Sr/^{86}Sr$ for Hawaiian shield lavas. MORB-related gabbroic xenoliths recovered from Hualalai Volcano have $^{187}Os/^{188}Os$ of 0.23-0.54 and $^{87}Sr/^{86}Sr$ of 0.7207-0.7028; they are offset from the Hawaiian shield trend. The depleted upper mantle has $^{187}Os/^{188}Os$ of 0.12 to 0.13 and $^{87}Sr/^{86}Sr < 0.7028$, and is not located on the extension of the Hawaiian trend. Figure is modified from Lassiter and Hauri (1998).

Fig. 20 Pb isotopic ratios for Hawaiian shield lavas, EPR MORB and Pacific MORB. Data were obtained at Max-Planck using triple-spike techniques. Compared with Pacific MORB, Hawaiian shield lavas have high $^{208}Pb/^{204}Pb$ and lower $^{206}Pb/^{204}Pb$ at a given $^{207}Pb/^{204}Pb$. Consequently, Abouchami et al. (2000) and Eisele et al. (2003) argued that Hawaiian shield lavas do not sample a MORB-related component.

Fig. 21 $^{206}Pb/^{204}Pb$ vs $^{207}Pb/^{204}Pb$ for Pacific MORB. Data are downloaded from PeT DB. The red field with dots is the EPR MORB field defined by data obtained using the triple-spike technique at Max-Planck (Galer et al., 1999). The low $^{206}Pb/^{204}Pb$ (<18) end of the Pacific MORB field is defined by Garrett transform fault lavas (Wendt et al., 1999). Figure is taken from Huang et al. (2005).

Fig. 22 $^{208}Pb^*/^{206}Pb^*$ vs $^{176}Hf/^{177}Hf$, $^{87}Sr/^{86}Sr$ and $^{143}Nd/^{144}Nd$ for Hawaiian shield lavas. $^{208}Pb^*/^{206}Pb^*$ represents the time-integrated $^{232}Th/^{238}U$ since the Earth formation, and is defined as $[(^{208}Pb/^{204}Pb)_{sample}-29.475]/[(^{206}Pb/^{204}Pb)_{sample}-9.307]$ (Galer and O'Nions, 1985). Lavas from Loa and Kea trend volcanoes define different trends in these plots. Lavas from Kea trend have relatively constant $^{176}Hf/^{177}Hf$, $^{87}Sr/^{86}Sr$ and $^{143}Nd/^{144}Nd$, and consequently, they define near-horizontal trends. In contrast, lavas from the Loa trend define a steep trend. M1, M2 and M3 represent different source components contributing to Hawaiian shield lavas. See text for a detailed discussion. Figure is taken from Huang et al. (submitted).

Fig. 23 La/Nb and Th/La vs $^{143}Nd/^{144}Nd$ and $^{208}Pb^*/^{206}Pb^*$ for Makapuu- and Kalihi-stage lavas. Kalihi-stage lavas overlap with the field defined by Mauna Loa lavas in **panels a** and **c**. The linear trends in these panels imply that the transition from Kalihi-stage composition to Makapuu-stage composition reflects an increasing role of a component with high La/Nb and $^{208}Pb^*/^{206}Pb^*$ coupled with low $^{143}Nd/^{144}Nd$ and Th/La. Since $^{176}Hf/^{177}Hf$ is positively correlated with $^{143}Nd/^{144}Nd$ (Salters et al., in prep.), the distinctive component in Makapuu-stage lavas also has relatively low $^{176}Hf/^{177}Hf$. Figure is taken from Huang and Frey (2005).

Fig. 24 Nd-Hf isotopic correlation. $\varepsilon_{Hf} = (((^{176}Hf/^{177}Hf)_{sample}/(^{176}Hf/^{177}Hf)_{CHUR}-1)x10000$ and $\varepsilon_{Nd} = ((^{143}Nd/^{144}Nd)_{sample}/(^{143}Nd/^{144}Nd)_{CHUR}-1)x10000$ with $(^{176}Hf/^{177}Hf)_{CHUR}=0.282772$ and $(^{143}Nd/^{144}Nd)_{CHUR}=0.512638$. Figure is taken from Huang et al (submitted).

Fig. 25 $\delta^{18}O$ vs $^{187}Os/^{188}Os$ for Hawaiian shield lavas. $\delta^{18}O$ is obtained on olivines and $^{187}Os/^{188}Os$ is obtained on whole rocks. They form a positive trend, implying an endmember with high $\delta^{18}O$ and $^{187}Os/^{188}Os$. The mixing endmembers are **Kea** component with [Os]=3.1 ppb, $^{187}Os/^{188}Os=0.129$ and $\delta^{18}O_{olivine}=4.6‰$, and a mixture of recycled sediment and oceanic crust (3:97). Recycled sediment has [Os]=200 ppb, $^{187}Os/^{188}Os=0.64$ and $\delta^{18}O=20‰$, and recycled oceanic crust has [Os]=50 ppb, $^{187}Os/^{188}Os=2.74$ and $\delta^{18}O=9‰$. Figure is taken from Lassiter and Hauri (1998).

Fig. 26 Sr/Nb vs La/Nb for Koolau (Makapuu- and Kalihi-stage) lavas. Field for Mauna Loa lavas is shown for comparison. Only relatively unaltered lavas (Kalihi-stage, Makapuu-stage and Mauna Loa lavas) with $2.2>K_2O/P_2O_5>1.2$ and L.O.I.<0.8% are plotted. Field labeled as "Makapuu-stage Lavas" is defined by XRF and INAA data from Frey et al. (1994). Figure is taken from Huang and Frey (2005).

Fig. 27 Olivine adjusted SiO_2 (%) vs $^{208}Pb^*/^{206}Pb^*$, $^{143}Nd/^{144}Nd$ and $^{176}Hf/^{177}Hf$ for Makapuu-stage and Kalihi-stage (KSDP) lavas. These linear trends show that variations in olivine adjusted major element contents are not artifacts of olivine adjustment, but reflect source heterogeneity in major element composition. Surprisingly, Makapuu-stage and Kalihi-stage lavas form subparallel trends in these panels. Figure is taken from Huang and Frey (2005).

Fig. 28 $^{87}Sr/^{86}Sr$ vs $^{3}He/^{4}He$ for Hawaiian shield lavas. Figure is modified from Mukhopadhyay et al. (2003) and Kurz et al. (2004). Loa and Kea trend lavas form different trends in this plot. M1, M2 and M3 represent different source components contributing to Hawaiian shield lavas. See text for a detailed discussion.

Fig. 29 $^{208}Pb^*/^{206}Pb^*$ vs $^{3}He/^{4}He$ for Hawaiian shield lavas. M1, M2 and M3 represent different source components contributing to Hawaiian shield lavas. See text for a detailed discussion.

Fig. 30a $^{208}Pb/^{204}Pb$ vs $^{206}Pb/^{204}Pb$ for Hawaiian lavas. Loa trend lavas have higher $^{208}Pb/^{204}Pb$ at a given $^{206}Pb/^{204}Pb$ than Kea trend lavas. Figure is taken from Abouchami et al. (2005).

Fig. 30b $^{208}Pb/^{204}Pb$ vs $^{206}Pb/^{204}Pb$ for Hawaiian postshield lavas. The pink line is taken from Abouchami et al. (2005) separating Loa and Kea shield lavas. Postshield stage lavas from Kea trend volcanoes (Mauna Kea, Kohala and West Maui) largely overlap with the Kea trend shield lavas; whereas, postshield stage lavas from Hualalai (a Loa trend volcano) overlap with the Loa trend shield. That is, the Loa and Kea geochemical difference may continue to postshield stage volcanism. Figure is taken from Xu et al. (2005).

Fig. 31 A concentric plume (**panel a**), a grossly zoned plume (**panel b**) vs a bilateral plume (**panel c**). Under the concentric plume model (**panel a**), the plume is concentrically zoned (different color implies different geochemical characteristics). That is, the center of the plume has different geochemical characteristics from the edge of the plume. The geochemical difference between Loa and Kea trend lavas reflect sampling central part (Loa trend) and peripheral part (Kea trend) of the plume. In the concentric plume model (**panel a**), the plume is zoned but there may be Kea- and Loa-type sources present throughout the plume (**panel b**). In the bilateral plume model (**panel c**), the plume is bilaterally zoned. Consequently, the geochemical difference between Loa and Kea trend lavas reflect sampling the left and right parts of the plume. **Panel d** shows an alternative model. The small colored circles represent different source components, M1, M2 and M3. These geochemical heterogeneities are homogeneously distributed within

the Hawaiian plume. The varying color, white to orange, in the big circle, which represents the Hawaiian plume, reflects temperature. See text for a detailed discussion.

Fig. 33 Cartoon shows the "spaghetti" plume model. Geochemical heterogeneities within a mantle plume are sheared into long-lasting and distinct filaments ("spaghetti") which are sampled successively by different plume-related volcanoes. The Loa-Kea geochemical differences are proposed to represent sampling different "spaghettis" (Abouchami et al., 2005).

Table 1. Mixing dacitic melt and picritic melt [1]

	SiO_2	TiO_2	Al_2O_3	FeO	MnO	MgO	CaO	Na_2O	K_2O	P_2O_5	total	Fe/Mg in melt	equilibrium olivine Fo
dacite [2]	64.7	2.7	14.7	4.2	0.0	1.4	3.9	4.1	3.6	0.8	100.1	1.667	0.67
picrite [3]	44.9	1.5	10.6	11.6	0.1	19.2	9.4	2	0.3	0.3	99.9	0.336	0.91
30% dacite + 70% picrite	50.8	1.9	11.8	9.4	0.1	13.9	7.8	2.6	1.3	0.5	100.0	0.376	0.90

(1) Major oxide contents are in %. Fe/Mg in melt is molar ratio.

(2) Dacitic melt composition of experiment C338 from Yaxley and Green (1998).

(3) Picritic melt composition of experiment C327 from Yaxley and Green (1998).

Fig 1

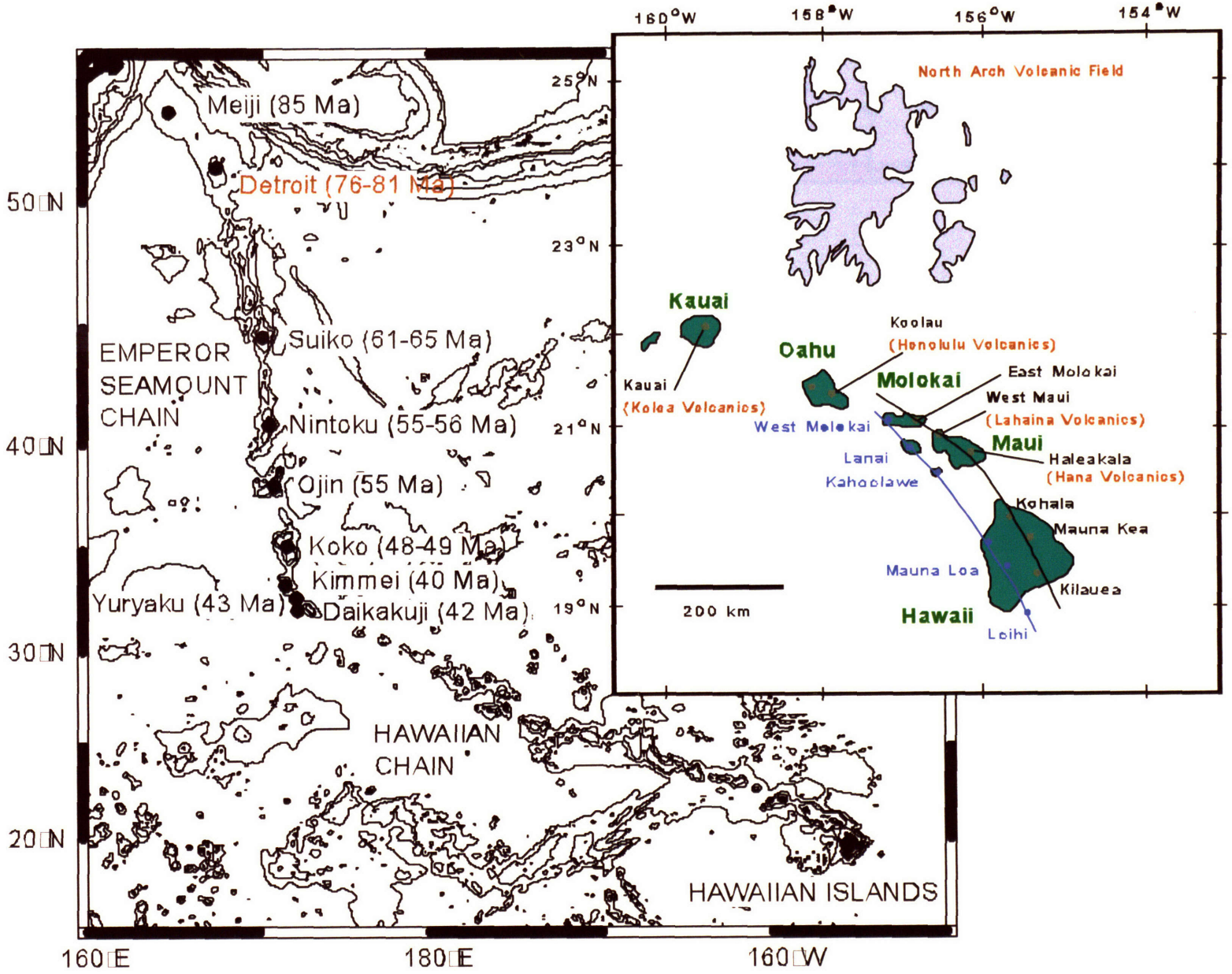
160°W
158°W
156°W
154°W
25°N
23°N
21°N
19°N
North Arch Volcanic Field
Kauai
Koolau
(Honolulu Volcanics)
Oahu
Molokai
East Molokai
West Maui
(Lahaina Volcanics)
Kauai
(Koloa Volcanics)
West Molokai
Maui
Haleakala
(Hana Volcanics)
Lanai
Kahoolawe
Kohala
Mauna Kea
Mauna Loa
Kilauea
200 km
Hawaii
Loihi
Meiji (85 Ma)
Detroit (76-81 Ma)
50°N
EMPEROR
SEAMOUNT
CHAIN
Suiko (61-65 Ma)
Nintoku (55-56 Ma)
40°N
Ojin (55 Ma)
Koko (48-49 Ma)
Kimmei (40 Ma)
Yuryaku (43 Ma)
Daikakuji (42 Ma)
30°N
HAWAIIAN
CHAIN
20°N
HAWAIIAN ISLANDS
160°E
180°E
160°W

Fig 2.

a.

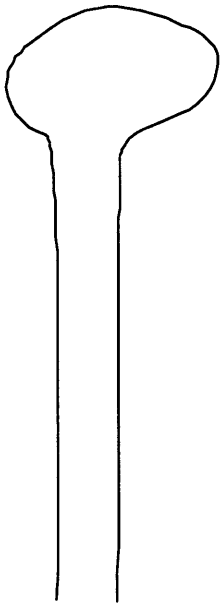

b.

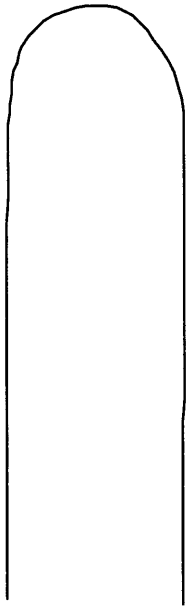

Fig 3.

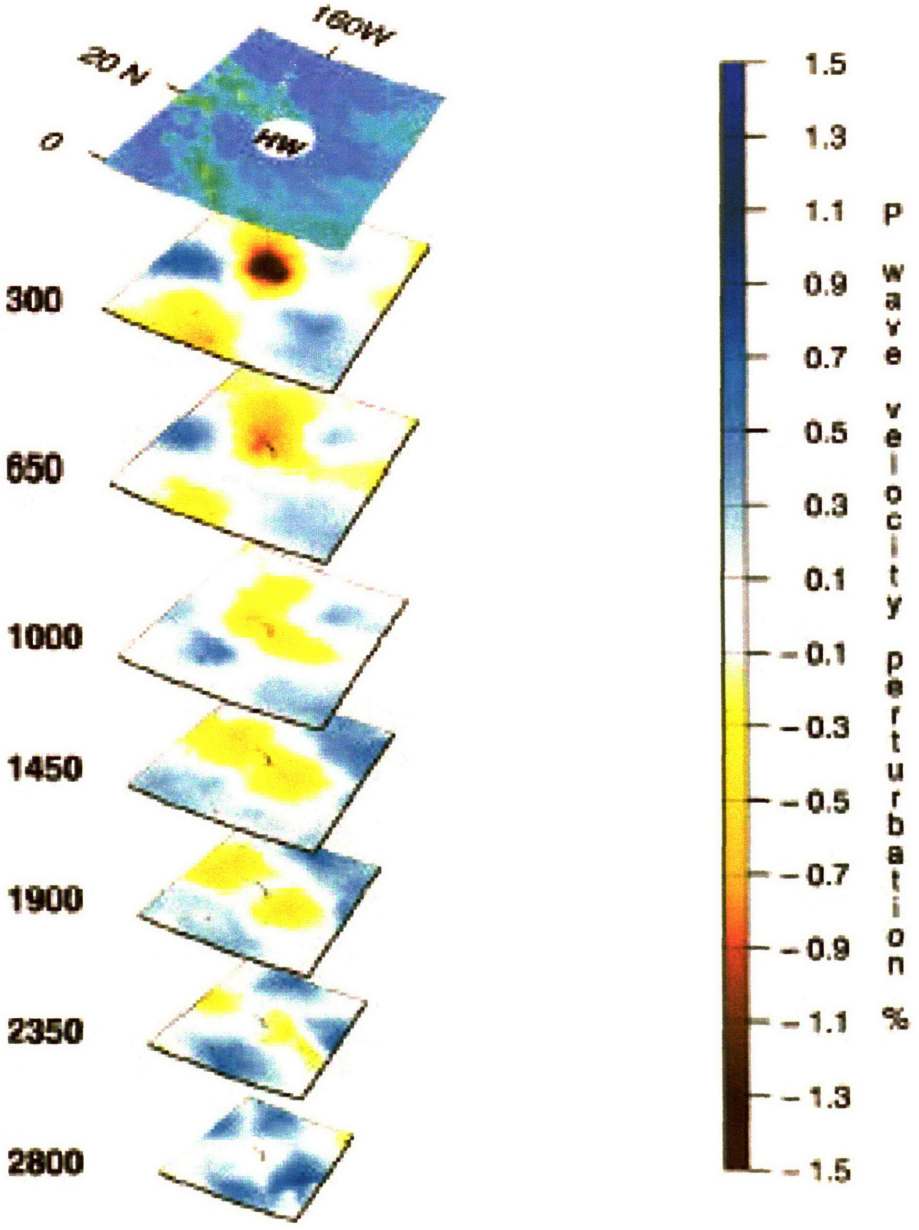
160W
20 N
0
HW
300
650
1000
1450
1900
2350
2800
1.5
1.3
1.1
0.9
0.7
0.5
0.3
0.1
−0.1
−0.3
−0.5
−0.7
−0.9
−1.1
−1.3
−1.5
P wave velocity perturbation %

Fig 4.

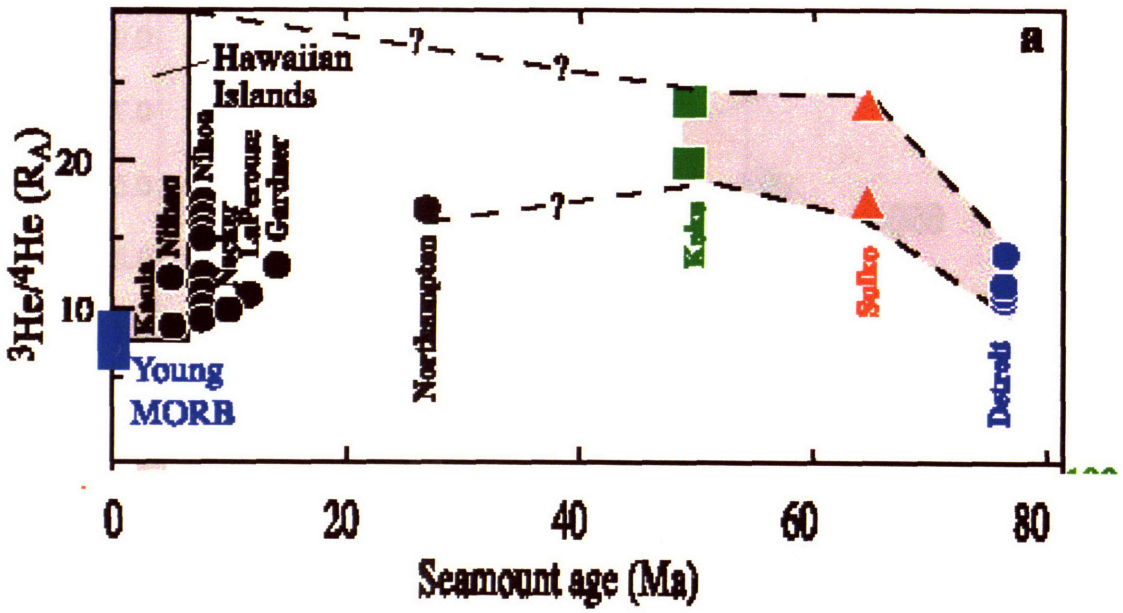
a
Hawaiian Islands
?
?
?
Kauai
Niihau
Nihoa
Necker
La Perouse
Gardner
Northampton
Koko
Suiko
Detroit
Young MORB
$^3He/^4He$ (R_A)
20
10
0
20
40
60
80
Seamount age (Ma)

Fig 5.

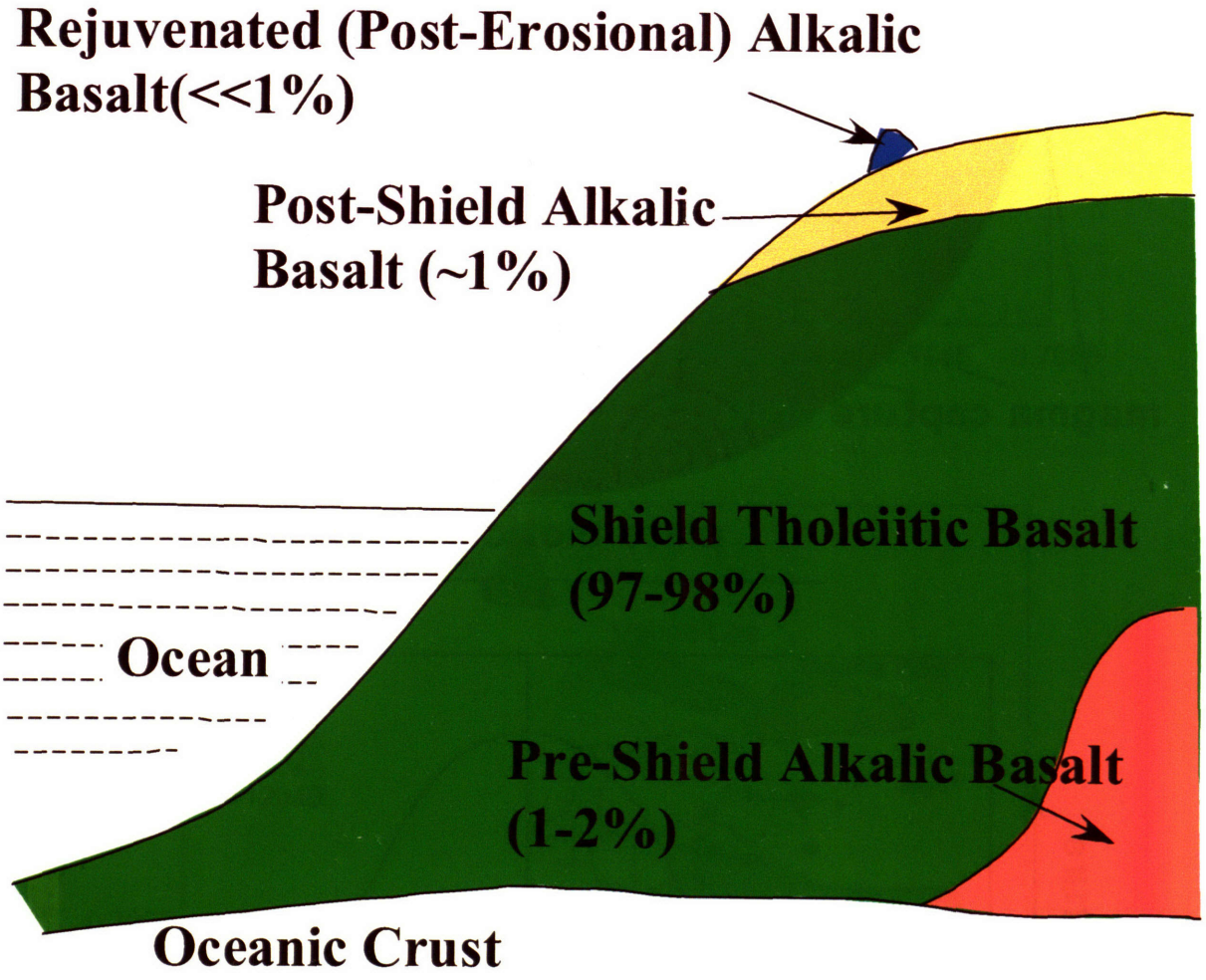
Rejuvenated (Post-Erosional) Alkalic Basalt(<<1%)
Post-Shield Alkalic Basalt (~1%)
Shield Tholeiitic Basalt (97-98%)
Ocean
Pre-Shield Alkalic Basalt (1-2%)
Oceanic Crust

Fig 6.

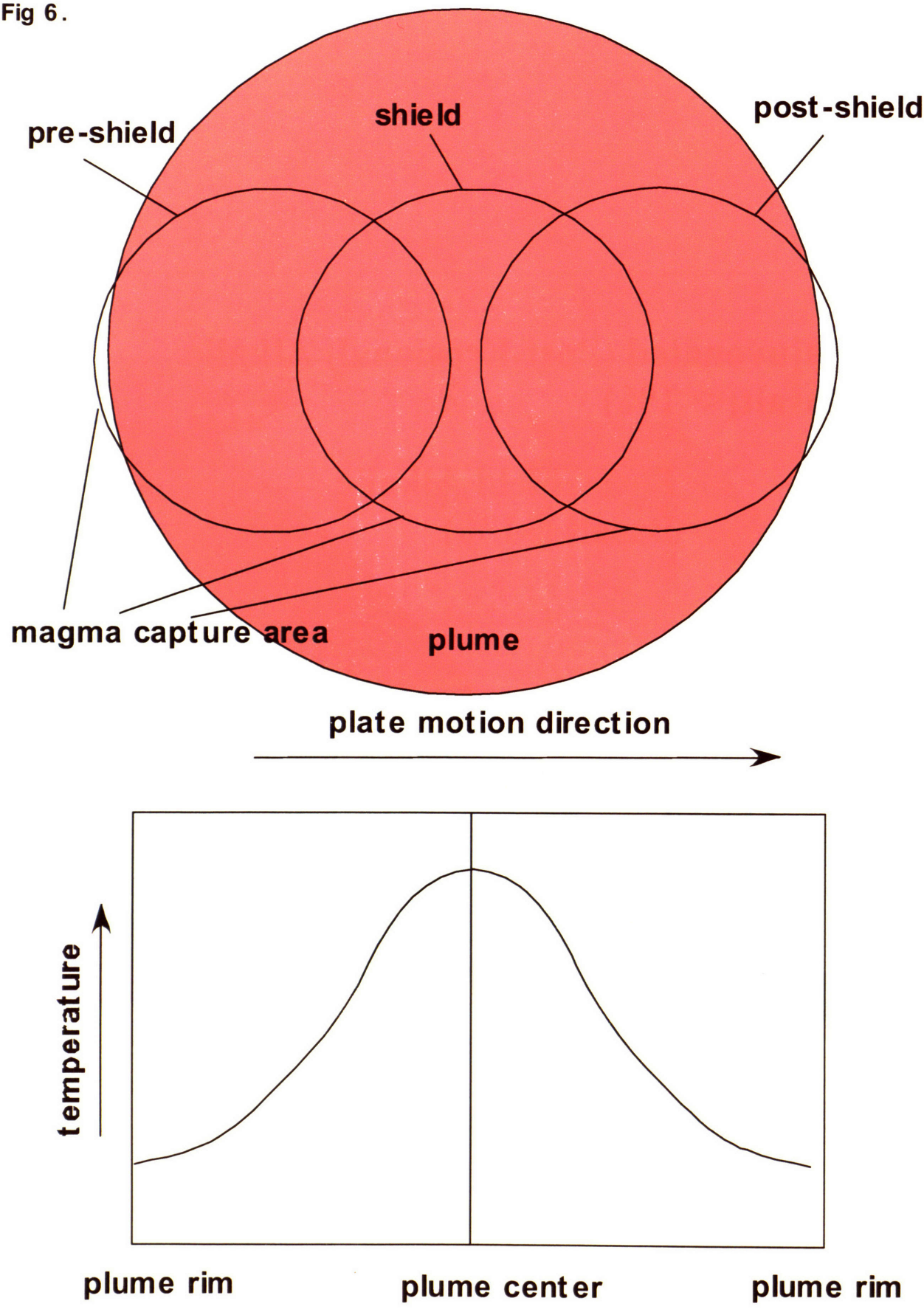
pre-shield
shield
post-shield
magma capture area
plume
plate motion direction
temperature
plume rim
plume center
plume rim

Fig 7.

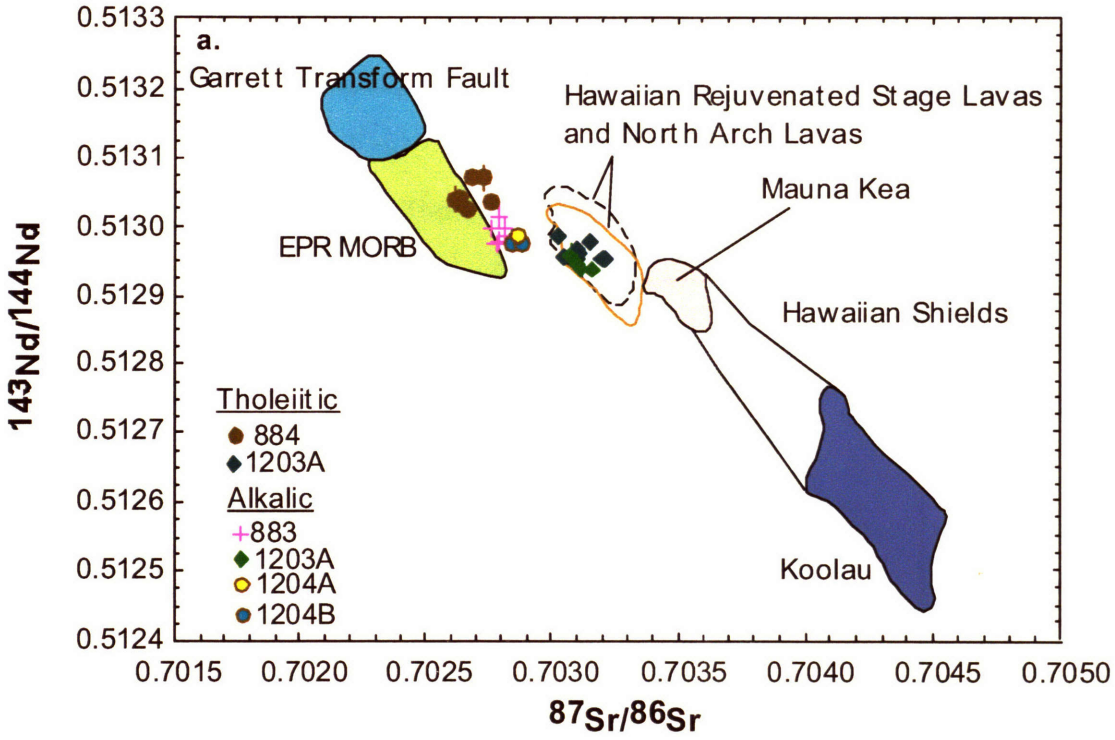
a.
Garrett Transform Fault
Hawaiian Rejuvenated Stage Lavas
and North Arch Lavas
Mauna Kea
EPR MORB
Hawaiian Shields
Koolau
Tholeiitic
884
1203A
Alkalic
883
1203A
1204A
1204B
143Nd/144Nd
87Sr/86Sr
0.5133
0.5132
0.5131
0.5130
0.5129
0.5128
0.5127
0.5126
0.5125
0.5124
0.7015
0.7020
0.7025
0.7030
0.7035
0.7040
0.7045
0.7050

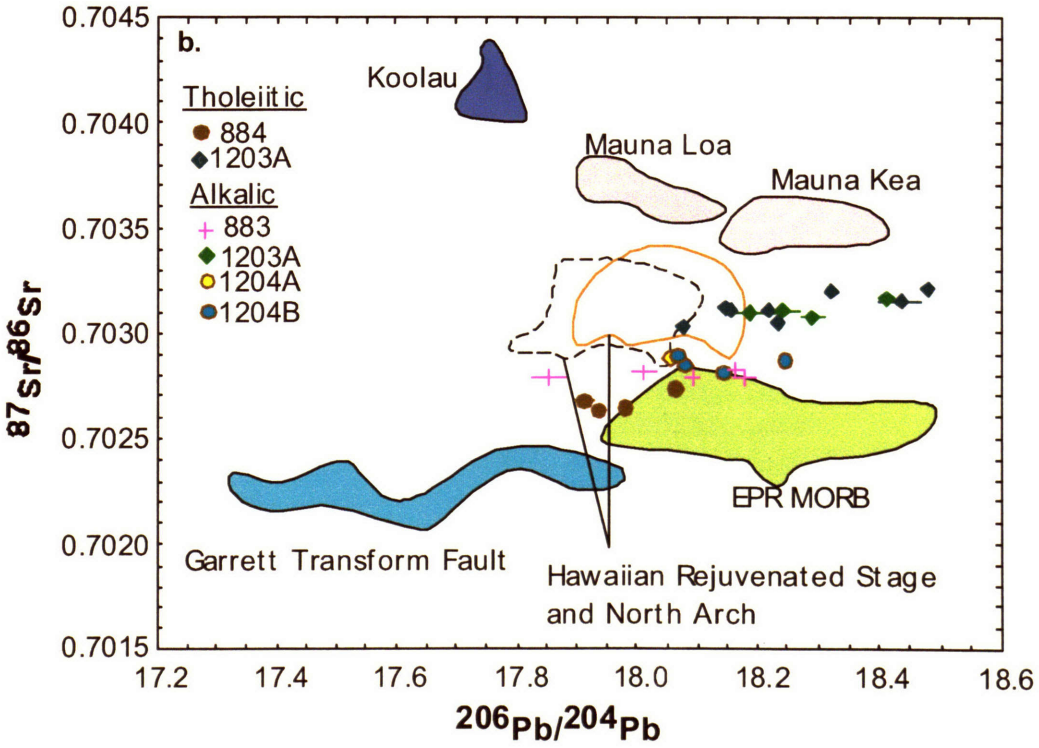
b.
Koolau
Mauna Loa
Mauna Kea
Tholeiitic
884
1203A
Alkalic
883
1203A
1204A
1204B
EPR MORB
Garrett Transform Fault
Hawaiian Rejuvenated Stage
and North Arch
87Sr/86Sr
206Pb/204Pb
0.7045
0.7040
0.7035
0.7030
0.7025
0.7020
0.7015
17.2
17.4
17.6
17.8
18.0
18.2
18.4
18.6

Fig 8.

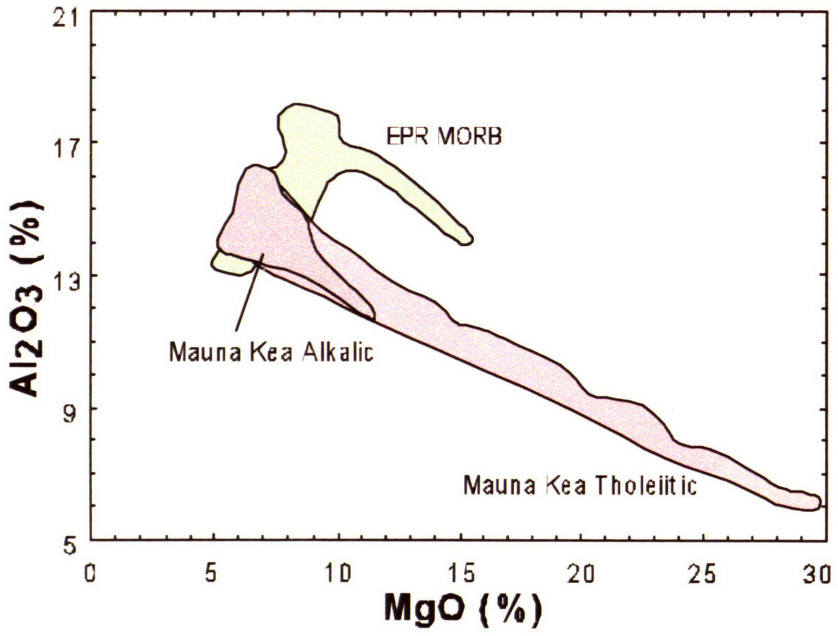
21
17
13
9
5
Al2O3 (%)
0
5
10
15
20
25
30
MgO (%)
EPR MORB
Mauna Kea Alkalic
Mauna Kea Tholeiitic

Fig 9.

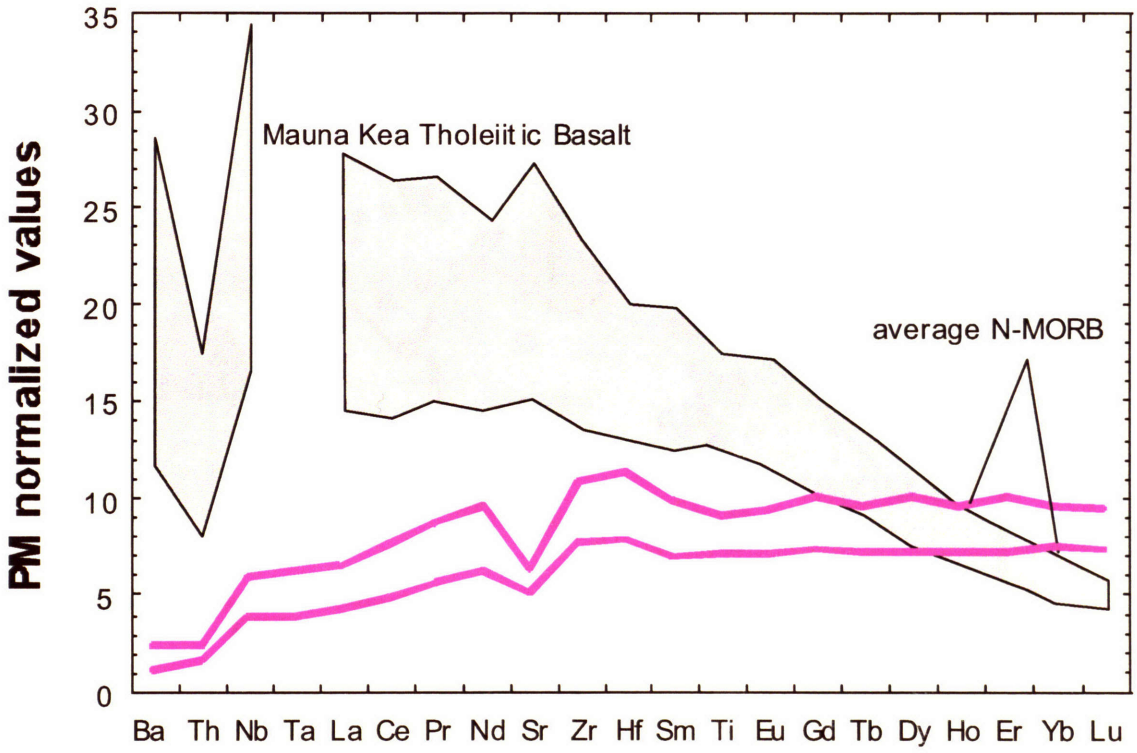
PM normalized values
35
30
25
20
15
10
5
0
Mauna Kea Tholeiitic Basalt
average N-MORB
Ba Th Nb Ta La Ce Pr Nd Sr Zr Hf Sm Ti Eu Gd Tb Dy Ho Er Yb Lu

Fig 10.

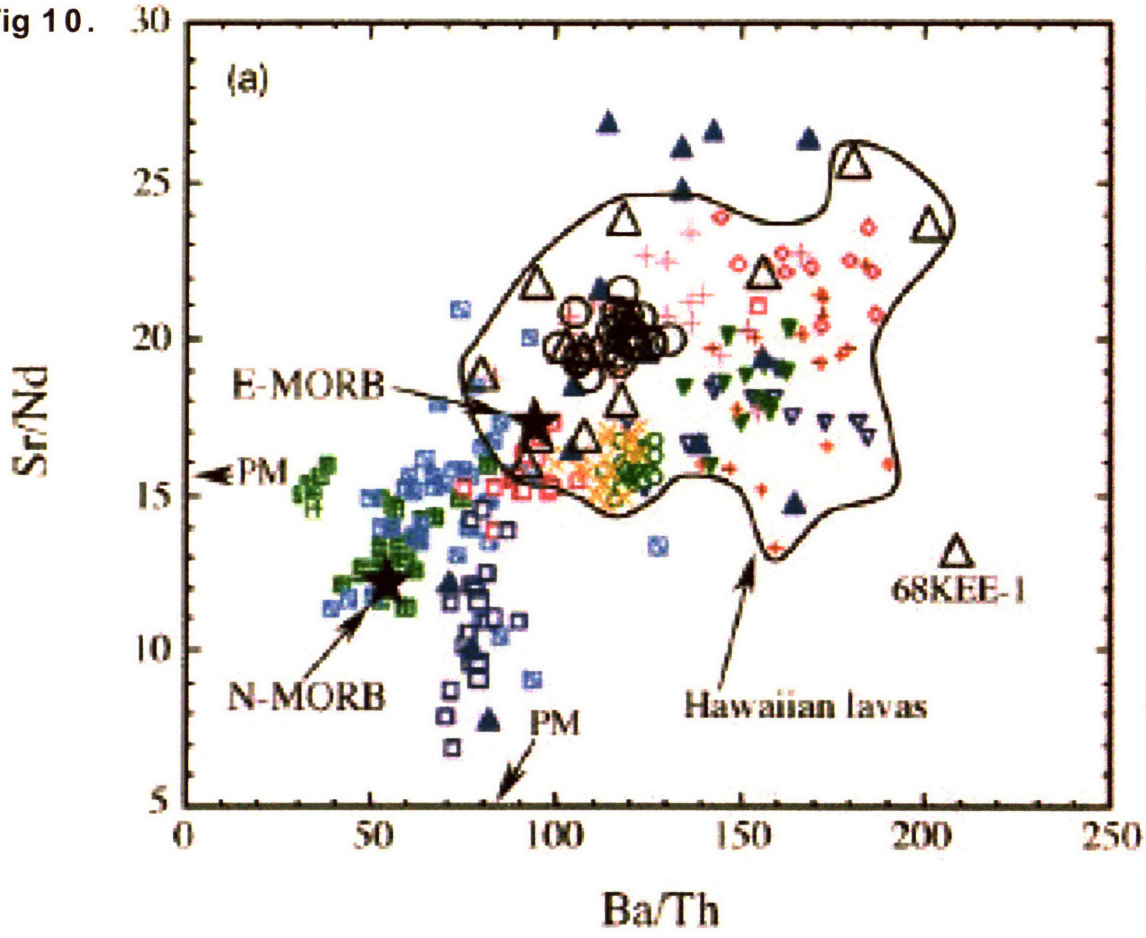

○ North Arch - Yang et al., 2003

Hawaiian rejuvenated lavas

△ Honolulu Volcanics - Yang et al., 2003
◇ Hana Volcanics - Chen *et al.* (1990)

Hawaiian shield and post-shield

+ Koolau - Huang et al. unpublished data
▽ Mauna Kea - Lassiter *et al.* (1996)
- Rhodes (1996)
- Yang *et al.* (1996)
○ Kilauea - Garcia *et al.* (1992, 1996)
× - Pietruszka & Garcia (1999)
◇ Haleakala - Chen *et al.* (1990)
▼ Loihi - Garcia *et al.* (1993; 1995)

Other OIBs

■ Austral Island - Caroff *et al.* (1997)
▣ Society Island - White & Duncan (1996)
□ Grande Comore - Spath *et al.* (1996)
▫ Sierra Negra - Reynolds & Geist (1995)
▲ Iceland - Chauvel & Hemond (2000)

Fig 11.

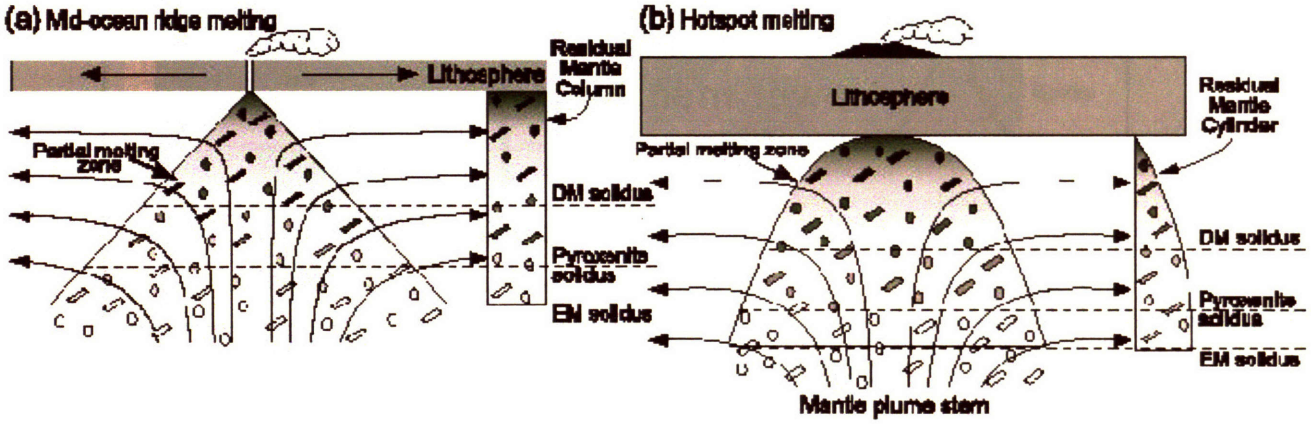
(a) Mid-ocean ridge melting
Lithosphere
Residual Mantle Column
Partial melting zone
DM solidus
Pyroxenite solidus
EM solidus
(b) Hotspot melting
Lithosphere
Residual Mantle Cylinder
Partial melting zone
DM solidus
Pyroxenite solidus
EM solidus
Mantle plume stem

Fig 12.

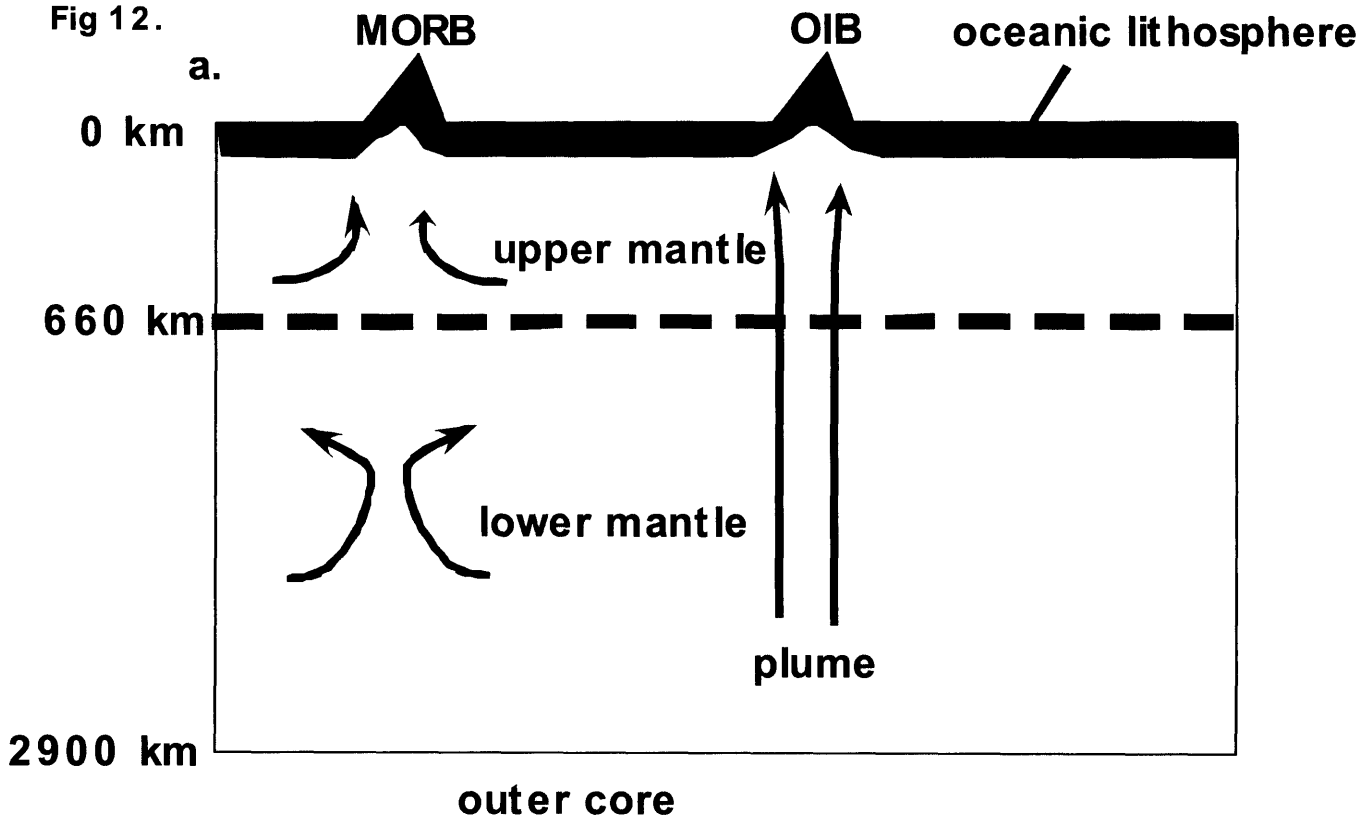
a.
MORB
OIB
oceanic lithosphere
0 km
upper mantle
660 km
lower mantle
plume
2900 km
outer core

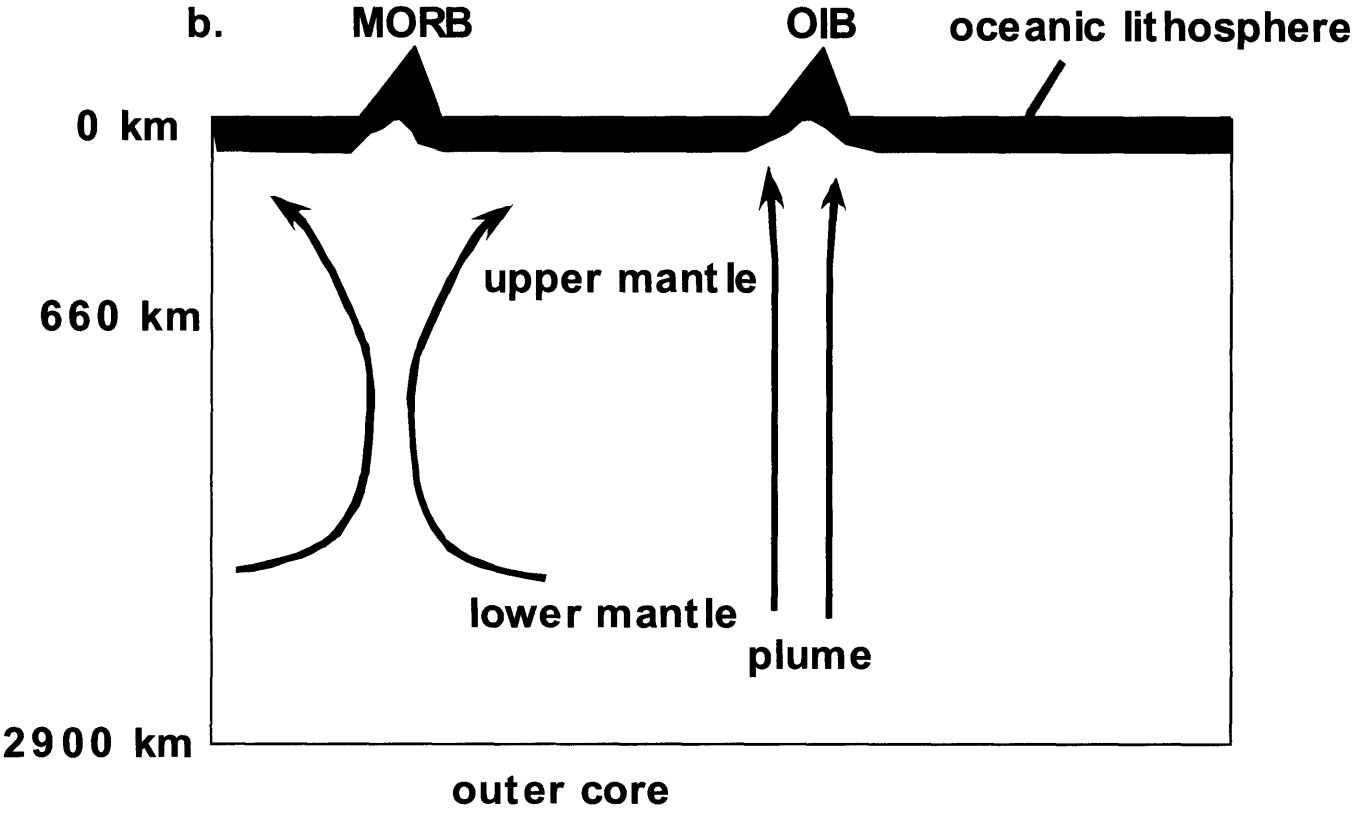
b.
MORB
OIB
oceanic lithosphere
0 km
upper mantle
660 km
lower mantle
plume
2900 km
outer core

Fig 13.

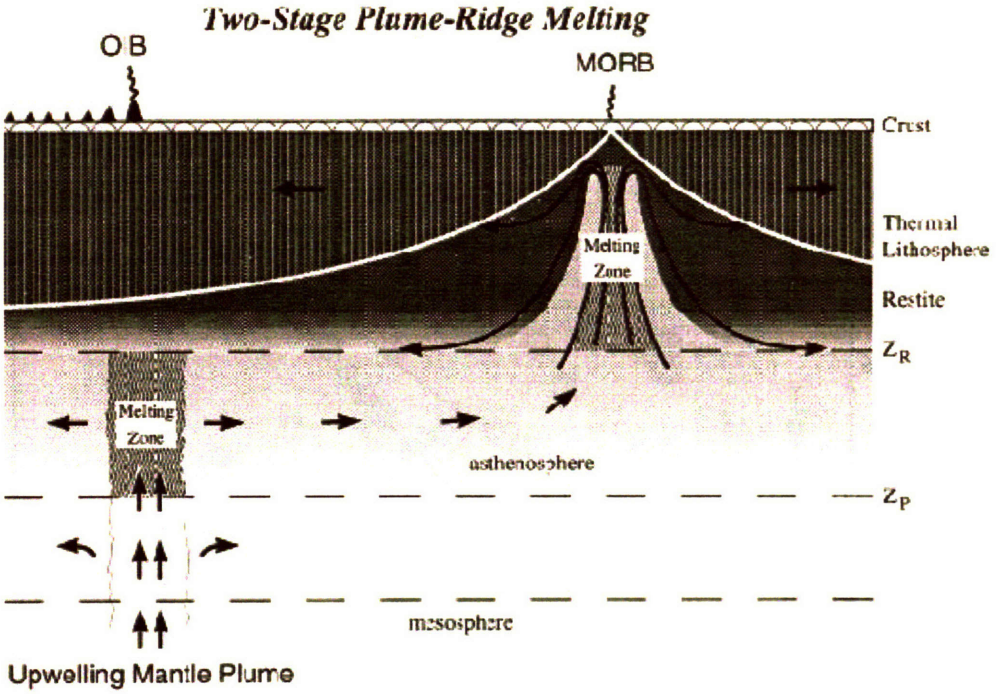
Two-Stage Plume-Ridge Melting
OIB
MORB
Crust
Thermal Lithosphere
Melting Zone
Restite
Z_R
Melting Zone
asthenosphere
Z_P
mesosphere
Upwelling Mantle Plume

Fig 14.

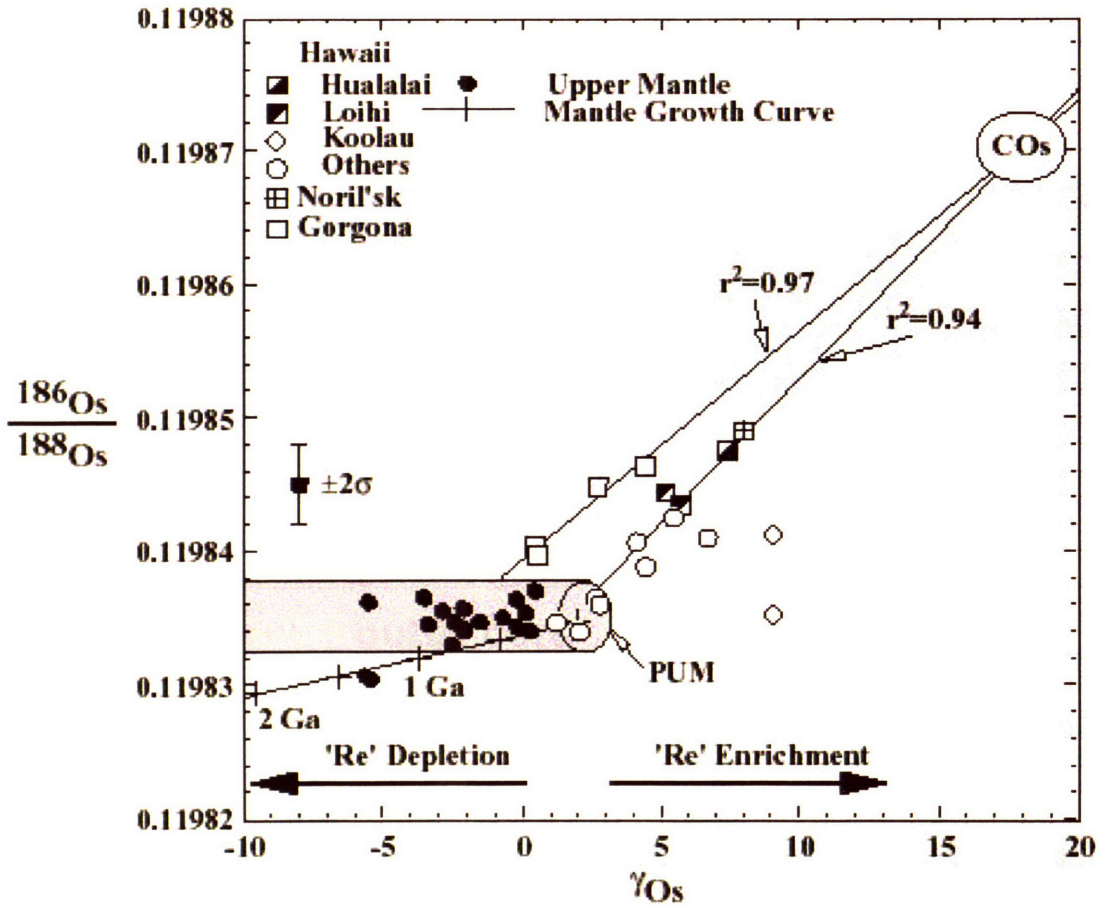
Hawaii
Hualalai
Loihi
Koolau
Others
Noril'sk
Gorgona
Upper Mantle
Mantle Growth Curve
COs
r²=0.97
r²=0.94
±2σ
PUM
1 Ga
2 Ga
'Re' Depletion
'Re' Enrichment
0.11988
0.11987
0.11986
0.11985
0.11984
0.11983
0.11982
-10
-5
0
5
10
15
20
186Os/188Os
γOs

Fig 15.

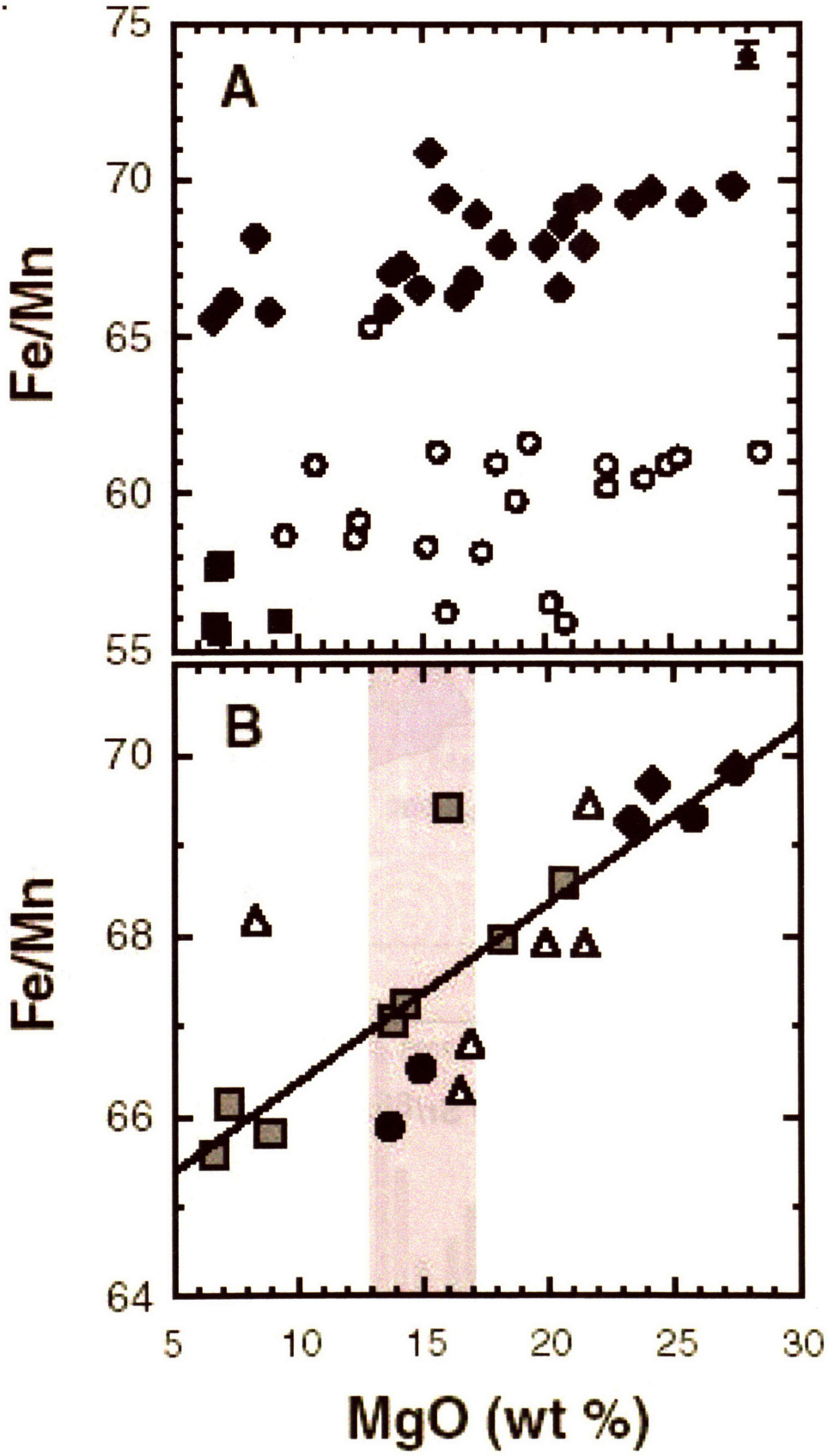

Fig 16.

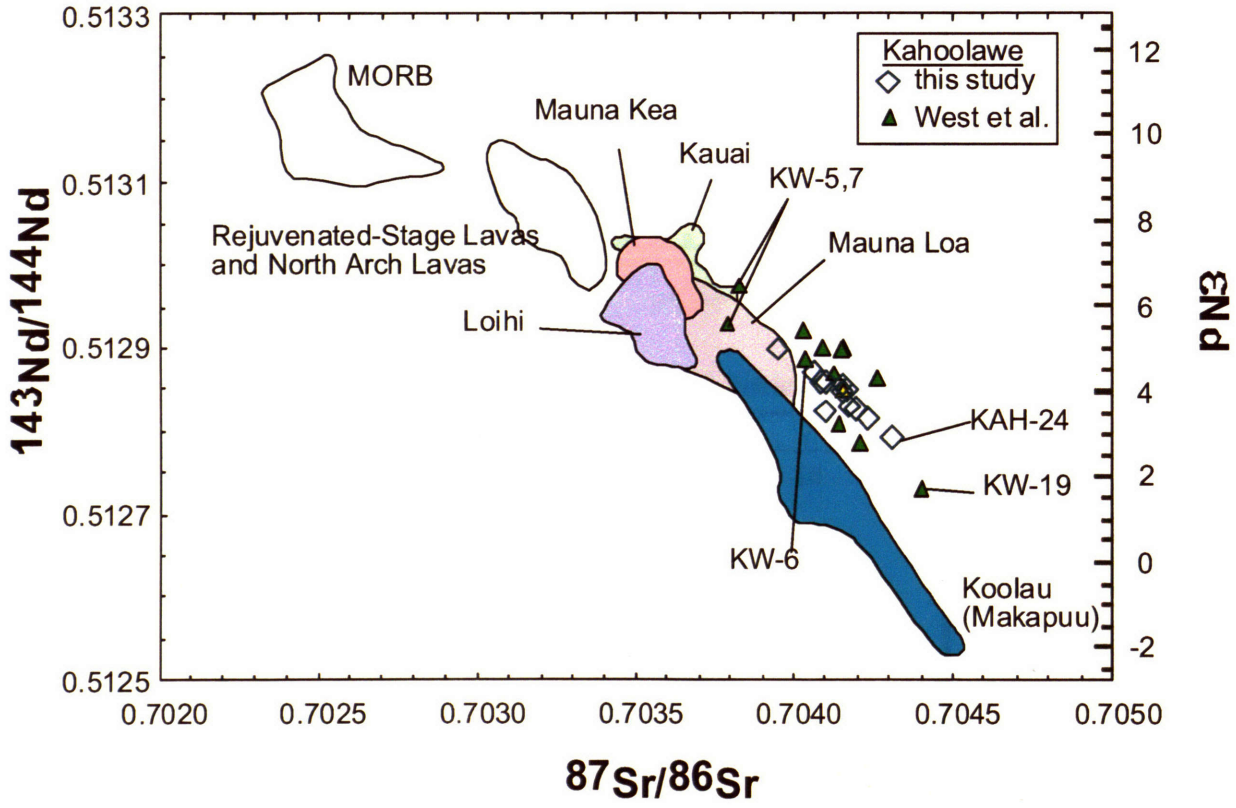
0.5133
0.5131
0.5129
0.5127
0.5125
143Nd/144Nd
0.7020
0.7025
0.7030
0.7035
0.7040
0.7045
0.7050
87Sr/86Sr
12
10
8
6
4
2
0
-2
εNd
Kahoolawe
this study
West et al.
MORB
Mauna Kea
Kauai
KW-5,7
Mauna Loa
Rejuvenated-Stage Lavas
and North Arch Lavas
Loihi
KAH-24
KW-19
KW-6
Koolau
(Makapuu)

Fig 17a.

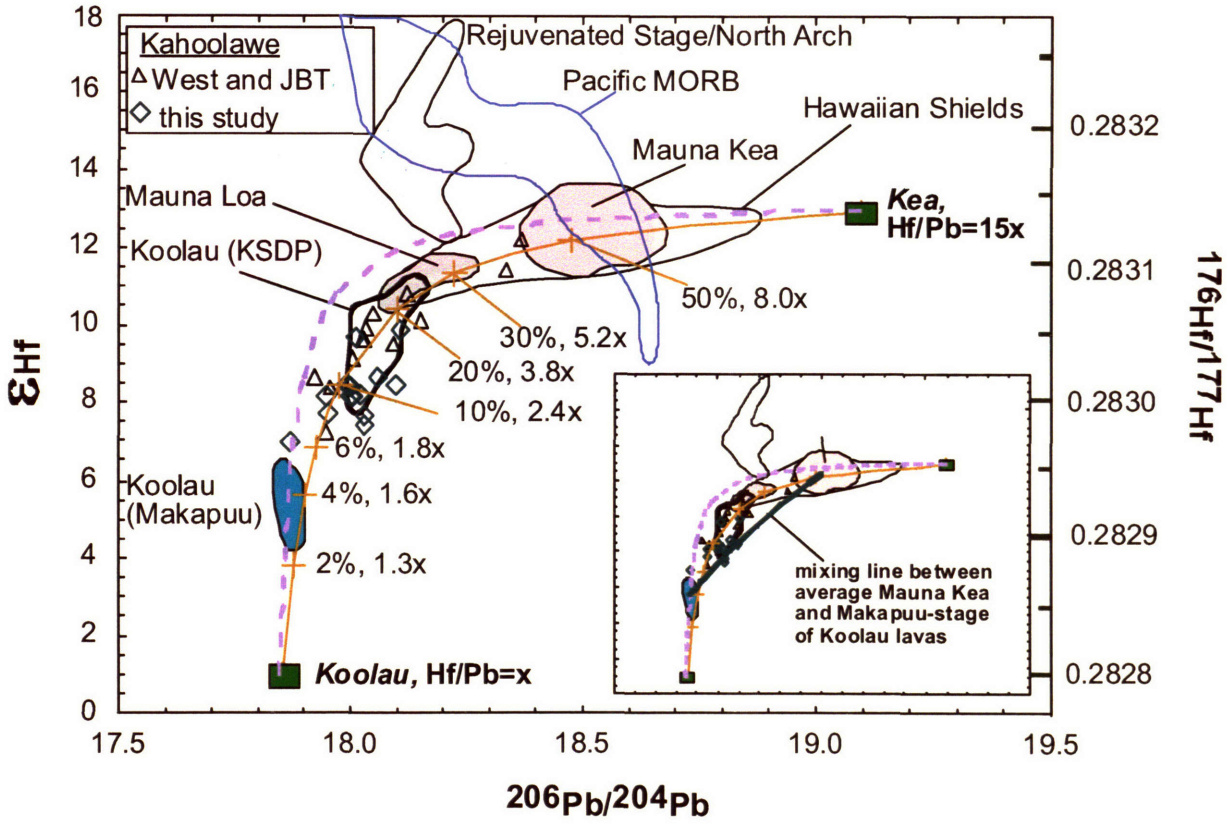

Fig 17b.

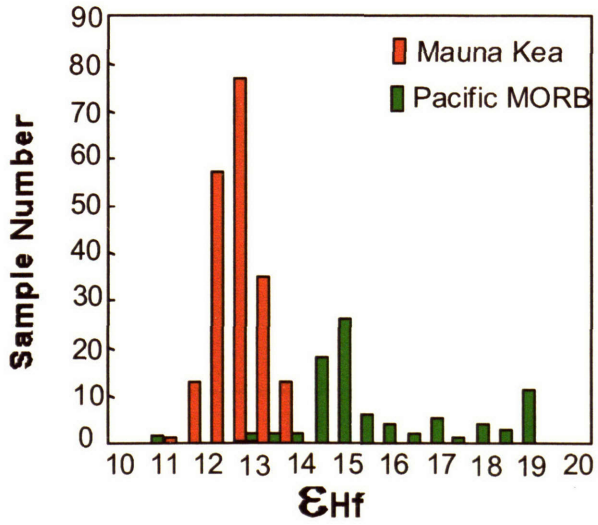

Fig 18.

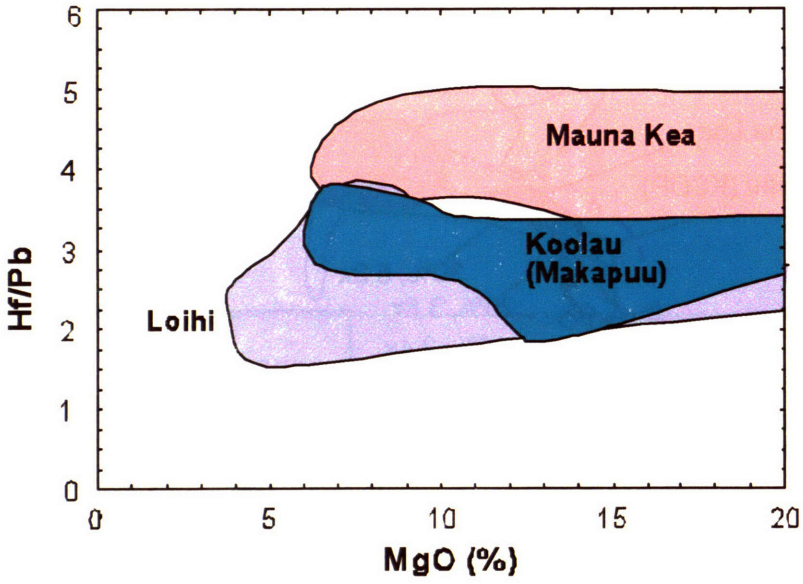

Fig 19.

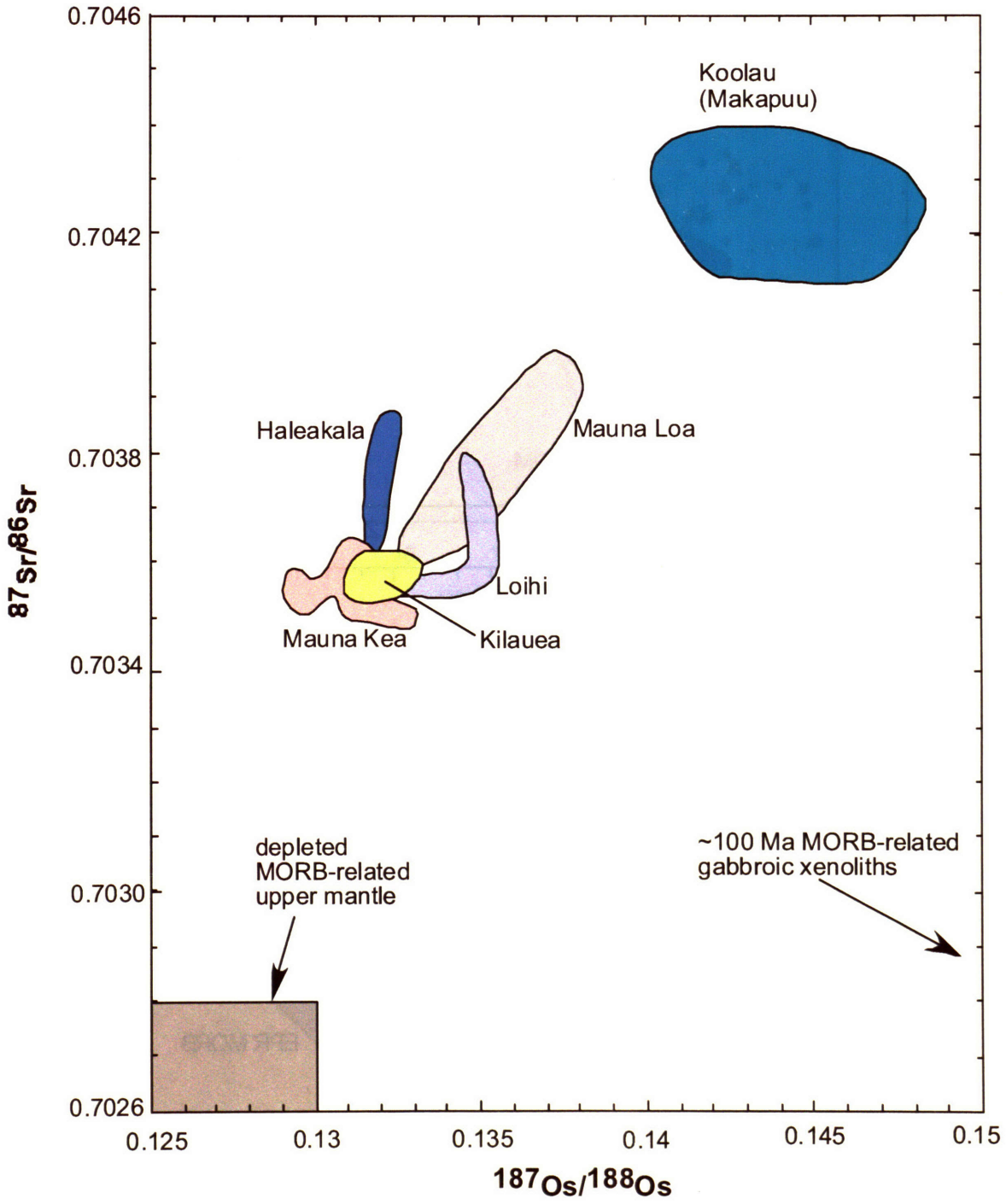
0.7046
0.7042
0.7038
0.7034
0.7030
0.7026
$^{87}Sr/^{86}Sr$
0.125
0.13
0.135
0.14
0.145
0.15
$^{187}Os/^{188}Os$
Koolau
(Makapuu)
Haleakala
Mauna Loa
Loihi
Mauna Kea
Kilauea
depleted
MORB-related
upper mantle
~100 Ma MORB-related
gabbroic xenoliths

Fig 20.

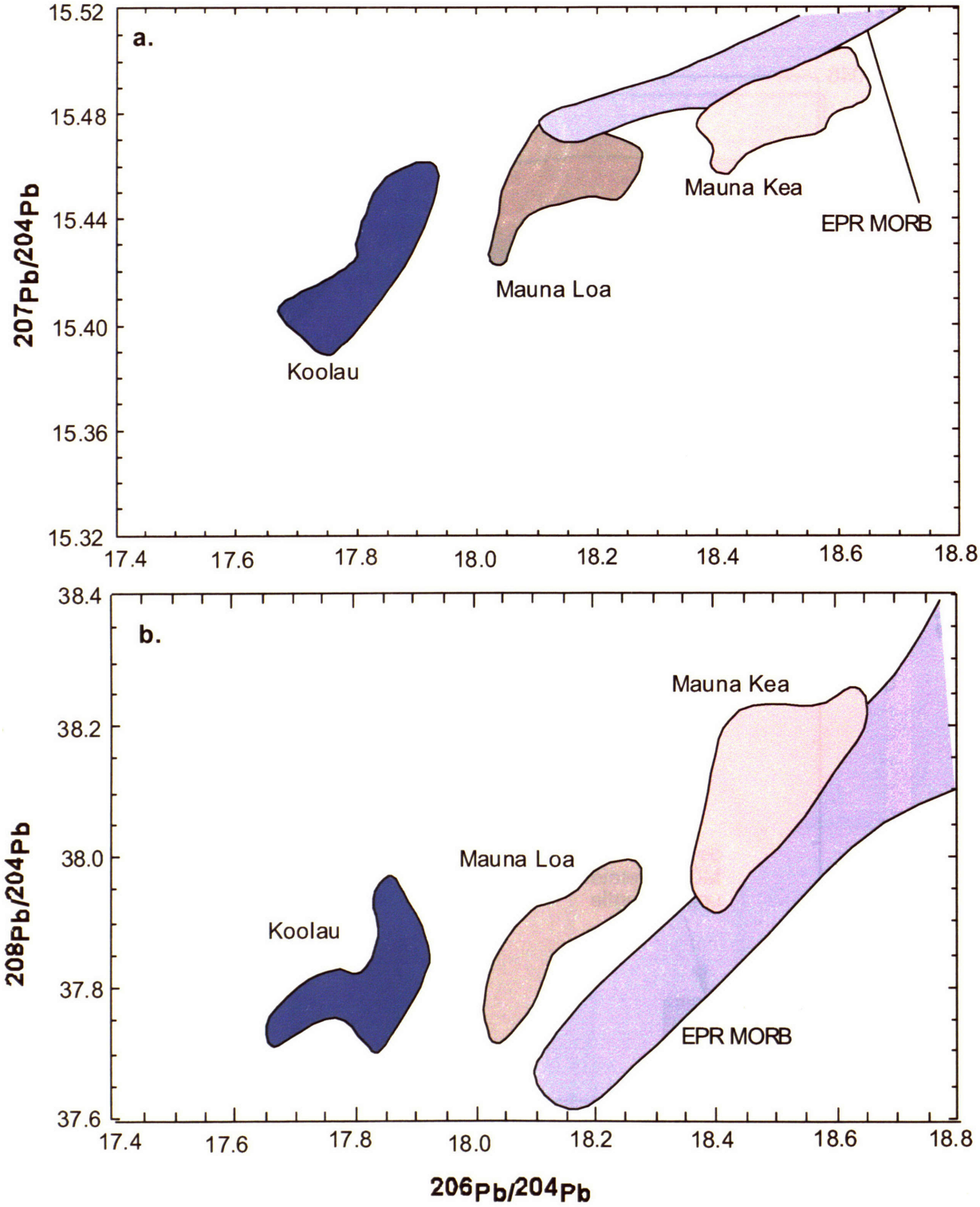
a.
15.52
15.48
15.44
15.40
15.36
15.32
207Pb/204Pb
Mauna Kea
EPR MORB
Mauna Loa
Koolau
17.4
17.6
17.8
18.0
18.2
18.4
18.6
18.8
b.
38.4
38.2
38.0
37.8
37.6
208Pb/204Pb
Mauna Kea
Mauna Loa
Koolau
EPR MORB
206Pb/204Pb

Fig 21.

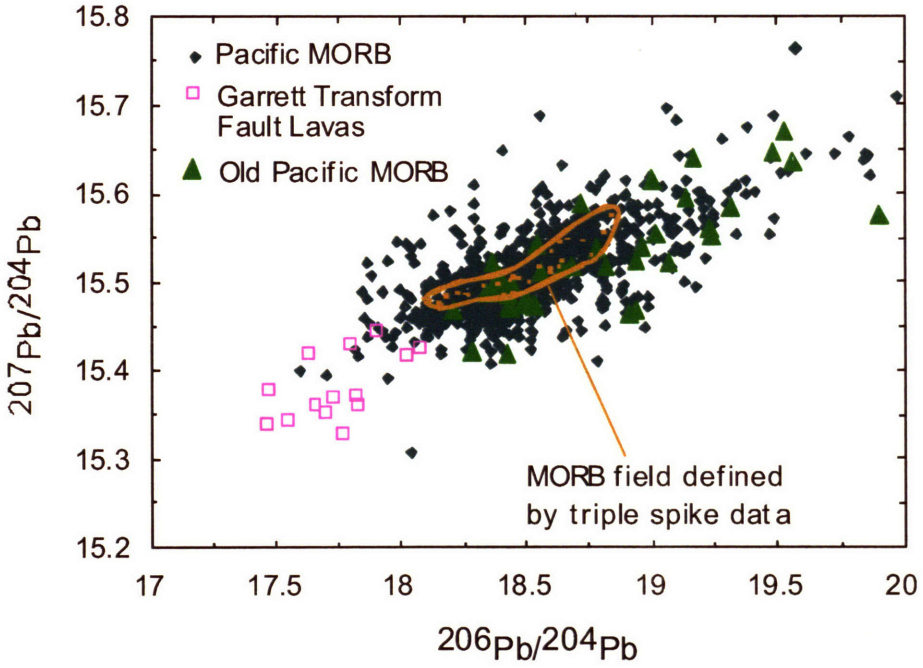
Pacific MORB
Garrett Transform Fault Lavas
Old Pacific MORB
MORB field defined by triple spike data
15.8
15.7
15.6
15.5
15.4
15.3
15.2
17
17.5
18
18.5
19
19.5
20
207Pb/204Pb
206Pb/204Pb

Fig 22.

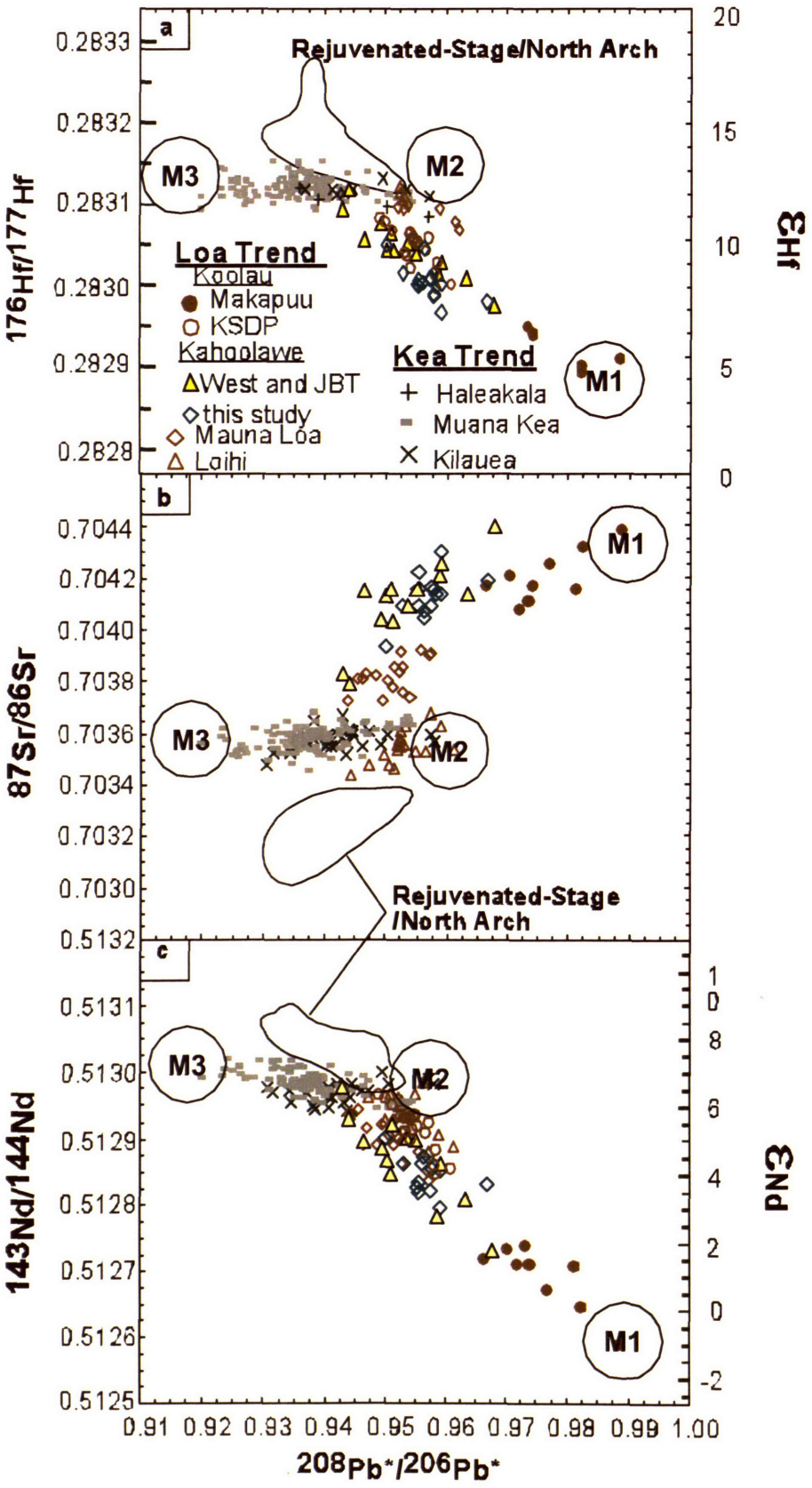
a
b
c
Rejuvenated-Stage/North Arch
M1
M2
M3
Loa Trend
Koolau
Makapuu
KSDP
Kahoolawe
West and JBT
this study
Mauna Loa
Loihi
Kea Trend
Haleakala
Muana Kea
Kilauea
Rejuvenated-Stage
/North Arch
176Hf/177Hf
εHf
87Sr/86Sr
143Nd/144Nd
εNd
208Pb*/206Pb*
0.2833
0.2832
0.2831
0.2830
0.2829
0.2828
20
15
10
5
0
0.7044
0.7042
0.7040
0.7038
0.7036
0.7034
0.7032
0.7030
0.5132
0.5131
0.5130
0.5129
0.5128
0.5127
0.5126
0.5125
10
8
6
4
2
0
-2
0.91 0.92 0.93 0.94 0.95 0.96 0.97 0.98 0.99 1.00

Fig 23.

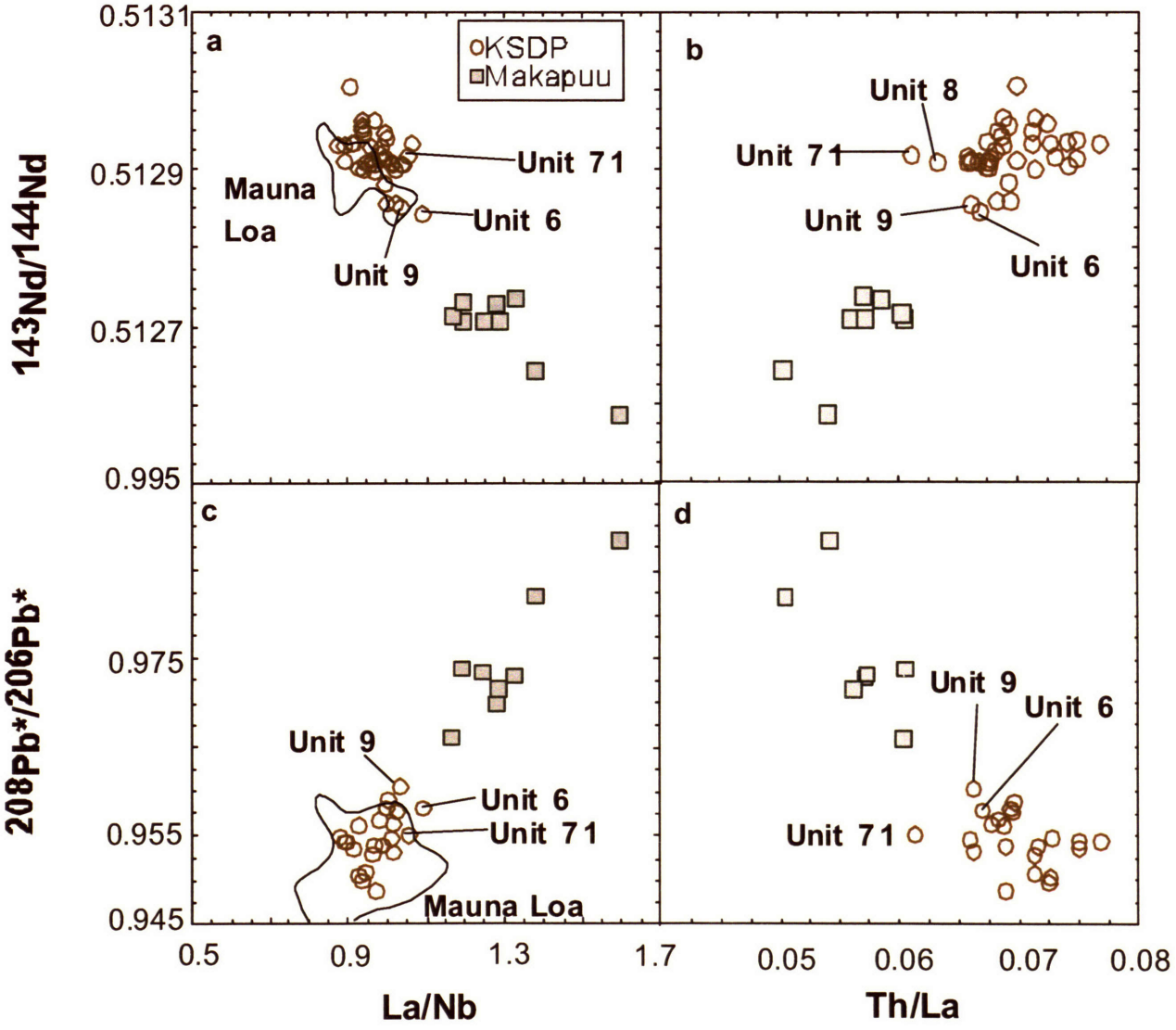
a
KSDP
Makapuu
Unit 71
Mauna
Loa
Unit 6
Unit 9
b
Unit 8
Unit 71
Unit 9
Unit 6
c
Unit 9
Unit 6
Unit 71
Mauna Loa
d
Unit 9
Unit 6
Unit 71
0.5131
0.5129
0.5127
0.995
0.975
0.955
0.945
143Nd/144Nd
208Pb*/206Pb*
0.5
0.9
1.3
1.7
La/Nb
0.05
0.06
0.07
0.08
Th/La

Fig 24.

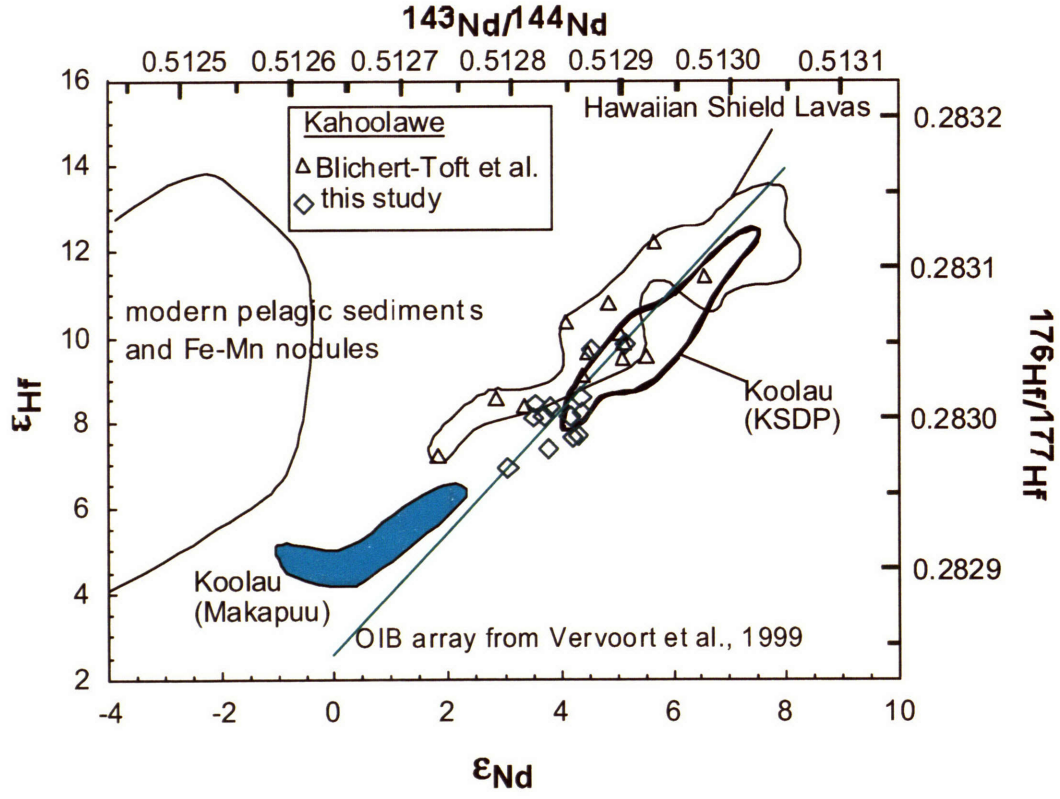
143Nd/144Nd
0.5125 0.5126 0.5127 0.5128 0.5129 0.5130 0.5131
Kahoolawe
Blichert-Toft et al.
this study
Hawaiian Shield Lavas
modern pelagic sediments
and Fe-Mn nodules
Koolau
(KSDP)
Koolau
(Makapuu)
OIB array from Vervoort et al., 1999
εHf
εNd
176Hf/177Hf
16
14
12
10
8
6
4
2
-4 -2 0 2 4 6 8 10
0.2832
0.2831
0.2830
0.2829

Fig 25.

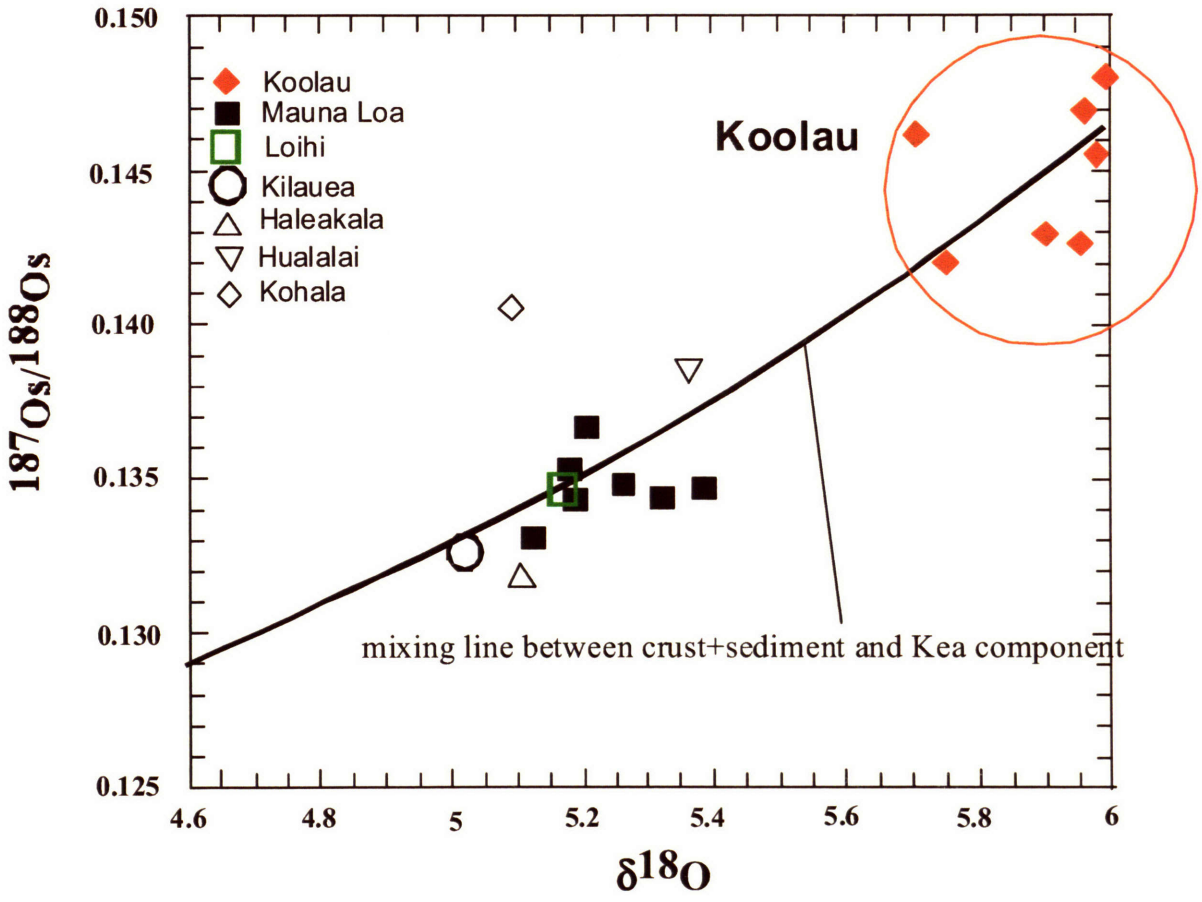
0.150
0.145
0.140
0.135
0.130
0.125
$^{187}Os/^{188}Os$
4.6
4.8
5
5.2
5.4
5.6
5.8
6
$\delta^{18}O$
Koolau
Mauna Loa
Loihi
Kilauea
Haleakala
Hualalai
Kohala
Koolau
mixing line between crust+sediment and Kea component

Fig 26.

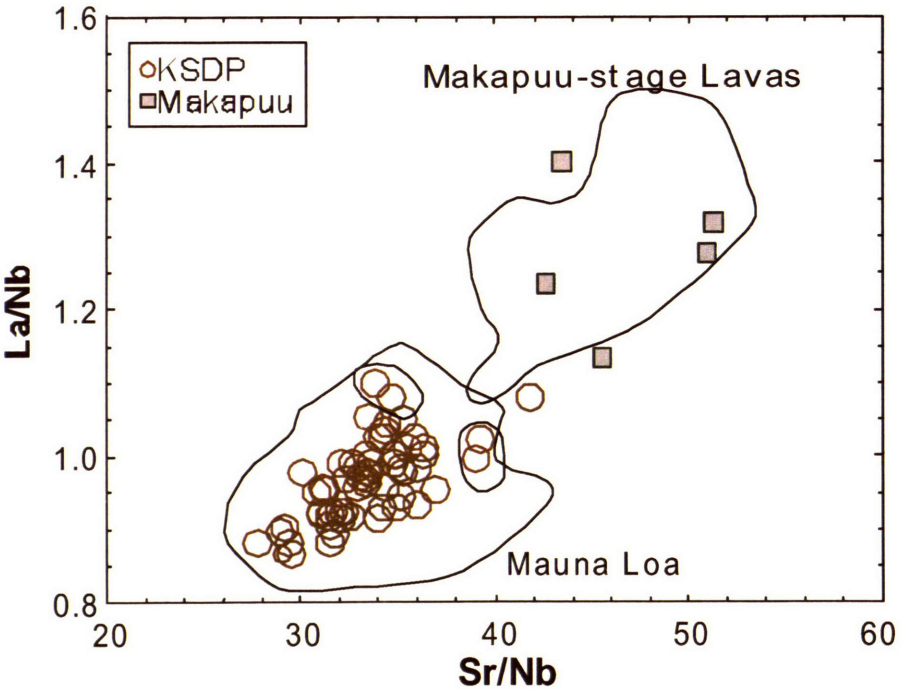
KSDP
Makapuu
Makapuu-stage Lavas
Mauna Loa
La/Nb
Sr/Nb
1.6
1.4
1.2
1.0
0.8
20
30
40
50
60

Fig 27.

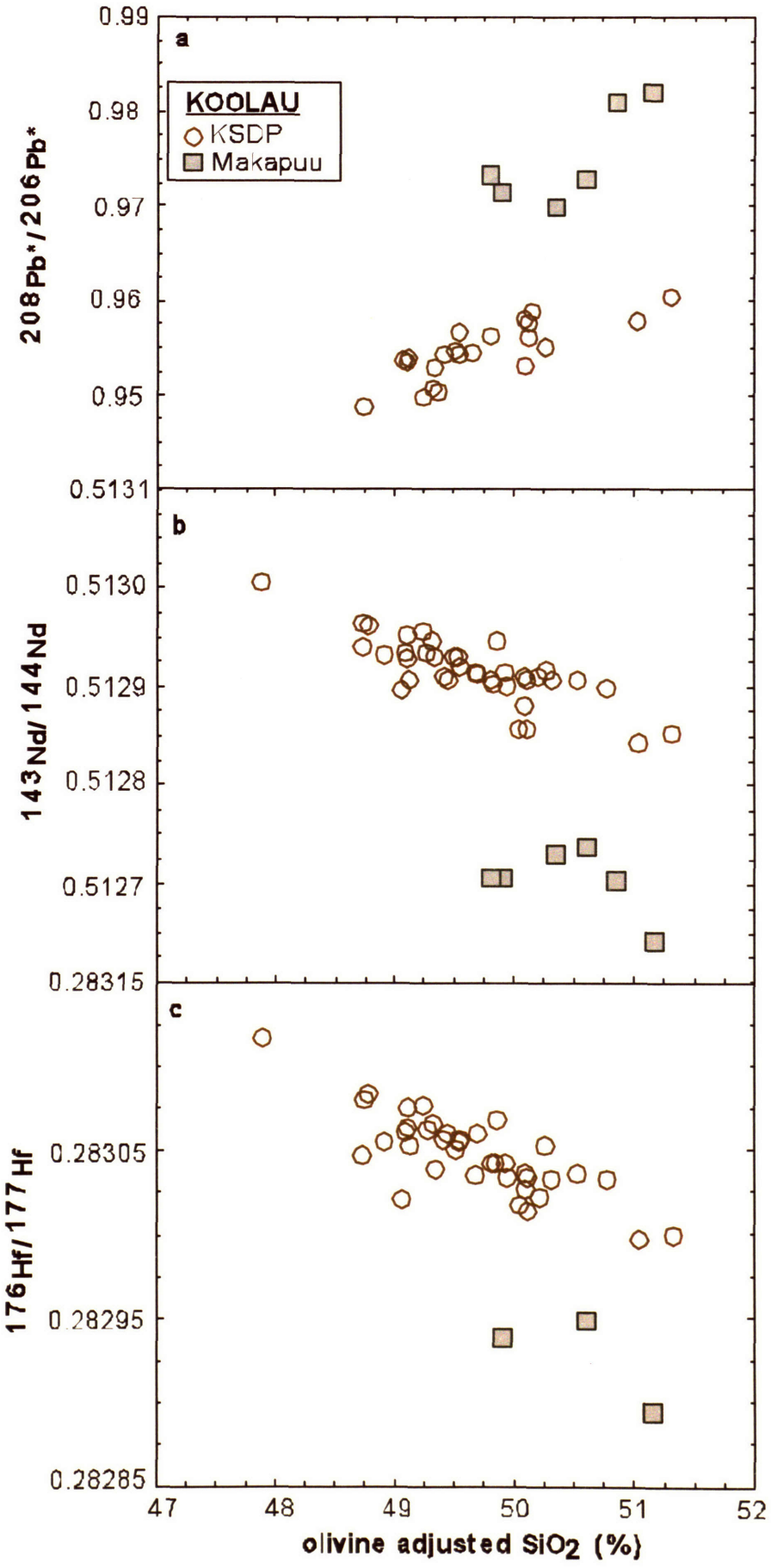
a
KOOLAU
KSDP
Makapuu
208Pb*/206Pb*
0.99
0.98
0.97
0.96
0.95
b
143Nd/144Nd
0.5131
0.5130
0.5129
0.5128
0.5127
c
176Hf/177Hf
0.28315
0.28305
0.28295
0.28285
47
48
49
50
51
52
olivine adjusted SiO2 (%)

Fig 28.

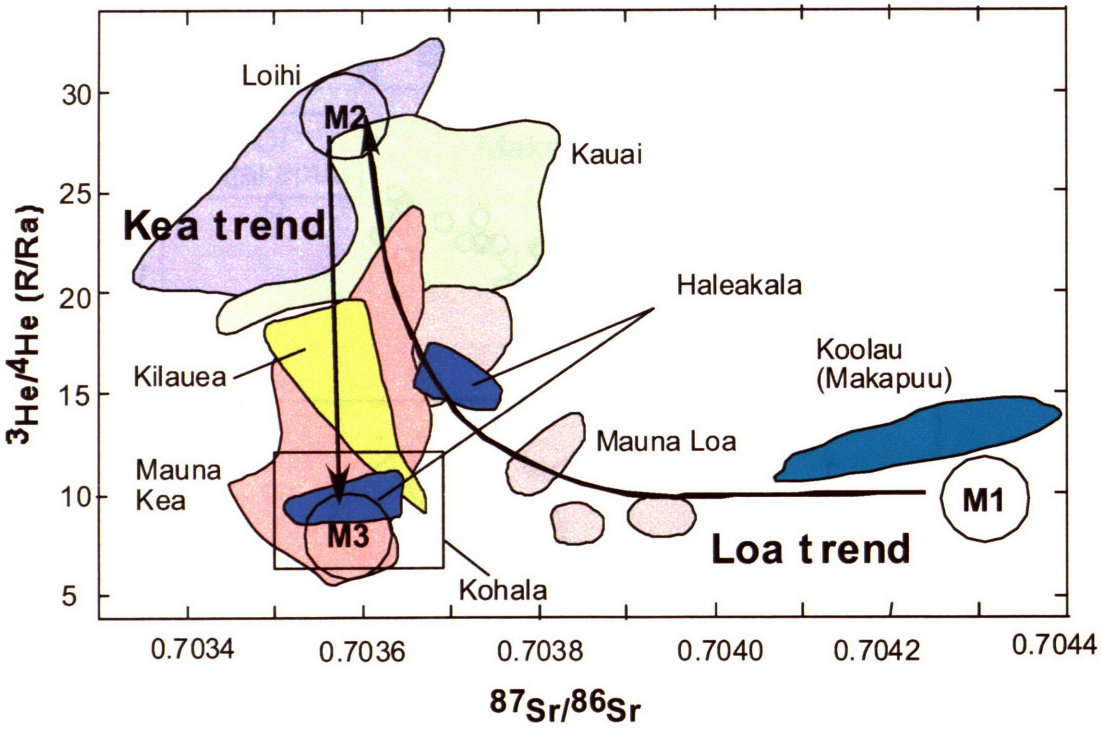
Loihi
M2
Kauai
Kea trend
Haleakala
Kilauea
Koolau
(Makapuu)
Mauna Loa
Mauna
Kea
M1
M3
Loa trend
Kohala
30
25
20
15
10
5
0.7034
0.7036
0.7038
0.7040
0.7042
0.7044
$^{3}He/^{4}He$ (R/Ra)
$^{87}Sr/^{86}Sr$

Fig 29.

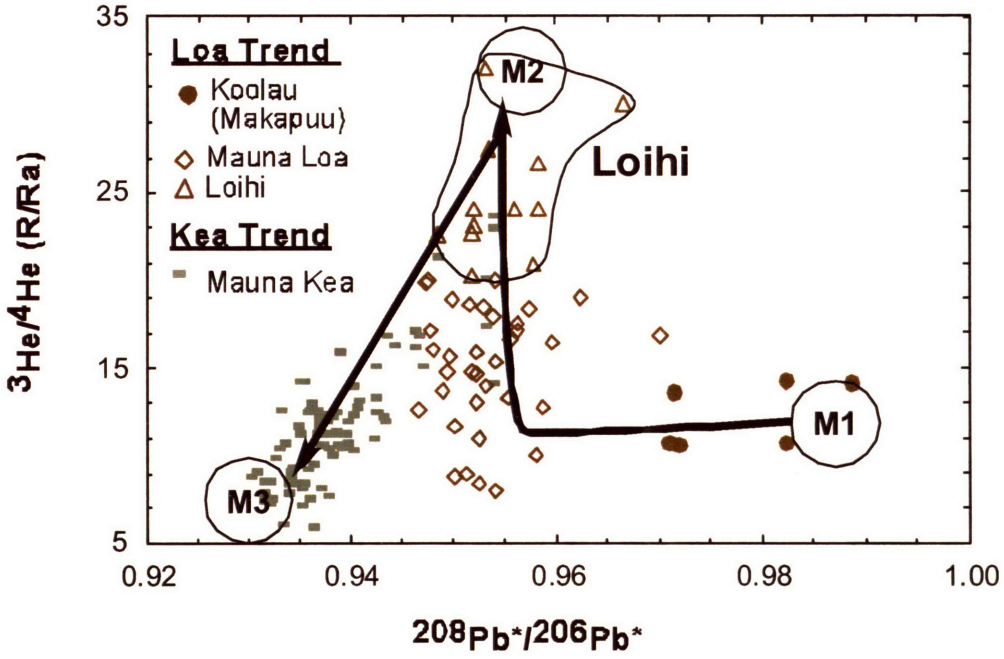
Loa Trend
Koolau (Makapuu)
Mauna Loa
Loihi
Kea Trend
Mauna Kea
M1
M2
M3
Loihi
35
25
15
5
0.92
0.94
0.96
0.98
1.00
3He/4He (R/Ra)
208Pb*/206Pb*

Fig 30a.

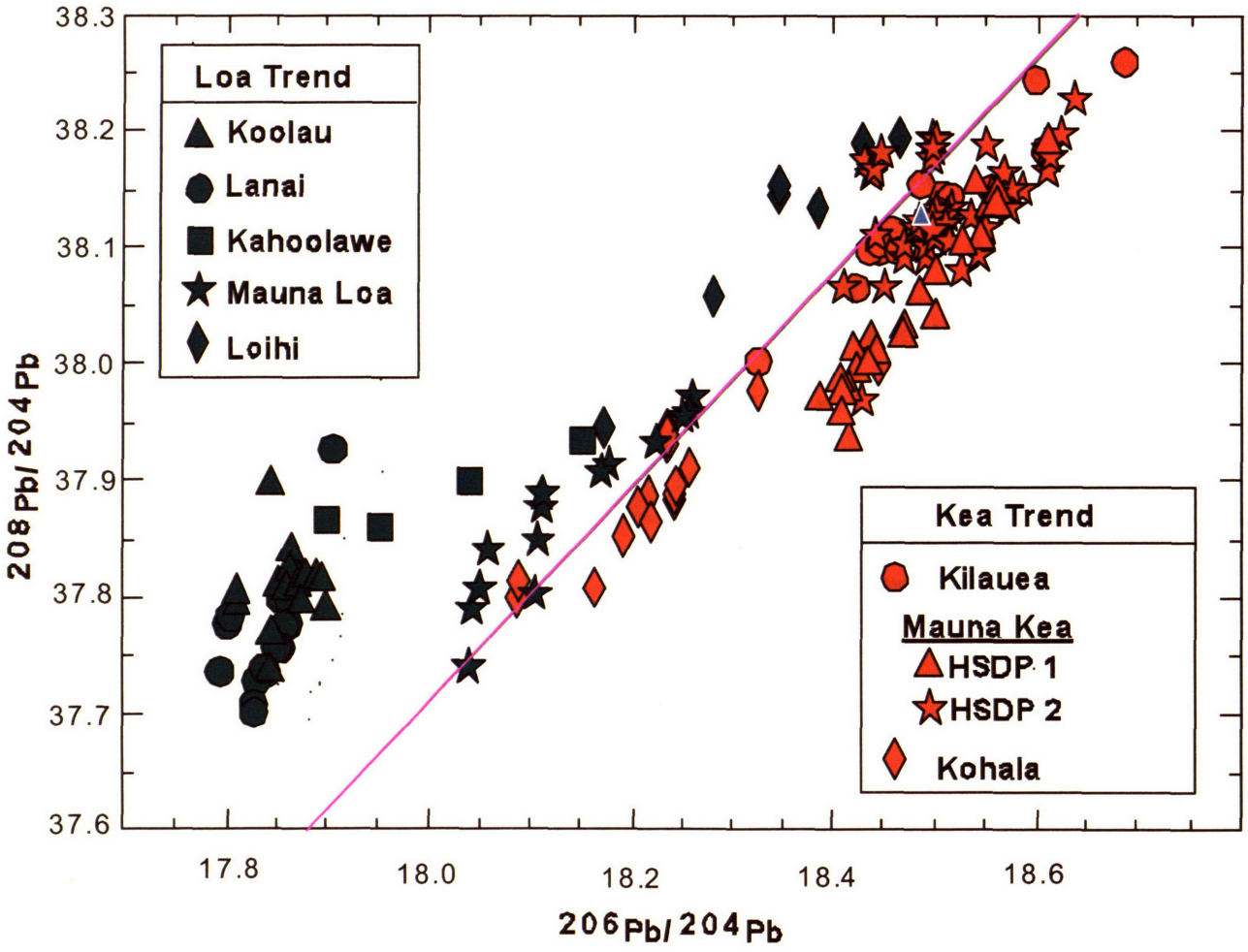
Loa Trend
Koolau
Lanai
Kahoolawe
Mauna Loa
Loihi
Kea Trend
Kilauea
Mauna Kea
HSDP 1
HSDP 2
Kohala
208Pb/204Pb
206Pb/204Pb
38.3
38.2
38.1
38.0
37.9
37.8
37.7
37.6
17.8
18.0
18.2
18.4
18.6

Fig 30b.

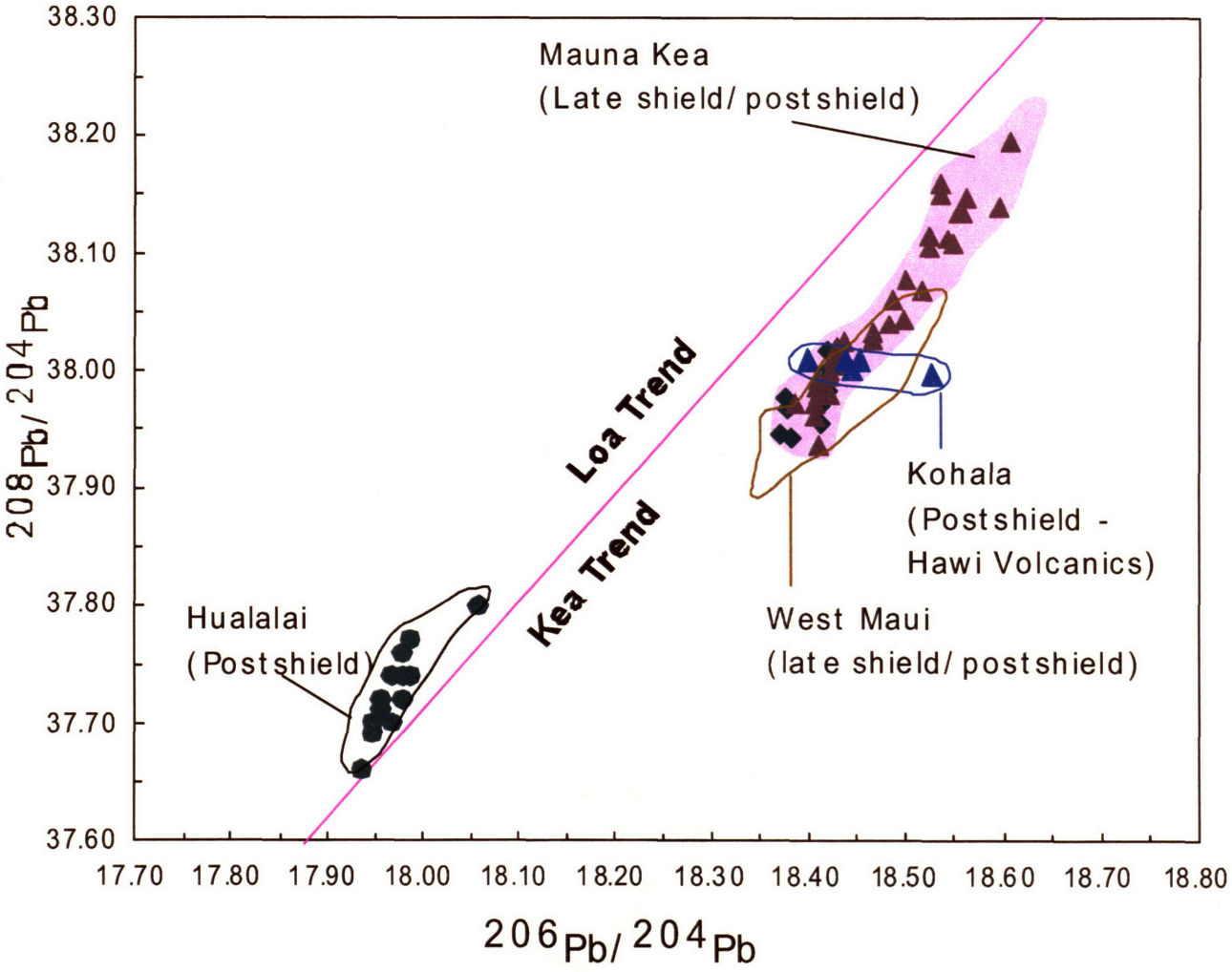
Mauna Kea
(Late shield/ postshield)
Loa Trend
Kea Trend
Kohala
(Postshield -
Hawi Volcanics)
West Maui
(late shield/ postshield)
Hualalai
(Postshield)
38.30
38.20
38.10
38.00
37.90
37.80
37.70
37.60
208Pb/204Pb
17.70
17.80
17.90
18.00
18.10
18.20
18.30
18.40
18.50
18.60
18.70
18.80
206Pb/204Pb

Fig 31.

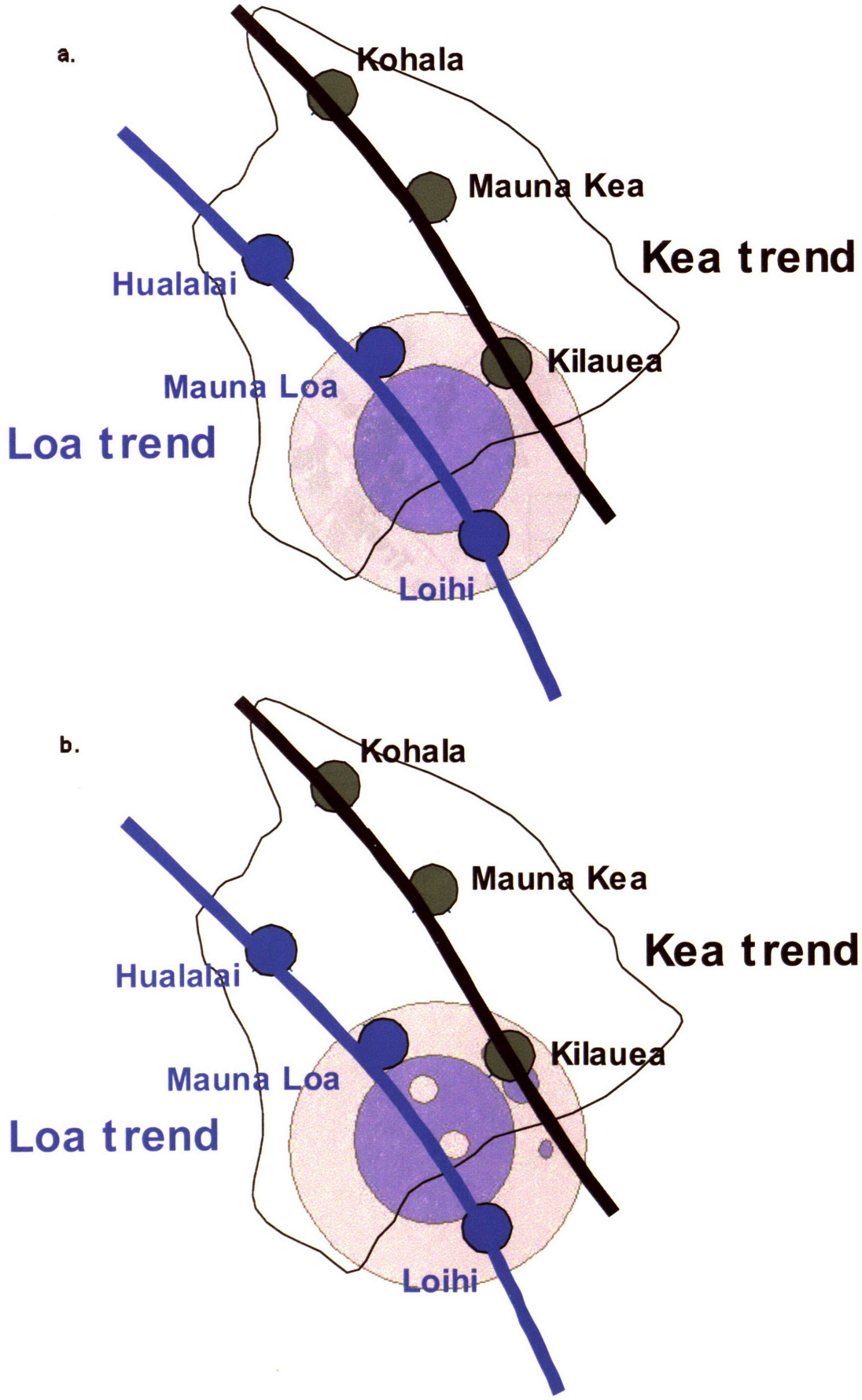
a.
Kohala
Mauna Kea
Kea trend
Hualalai
Kilauea
Mauna Loa
Loa trend
Loihi
b.
Kohala
Mauna Kea
Kea trend
Hualalai
Kilauea
Mauna Loa
Loa trend
Loihi

Fig 31.

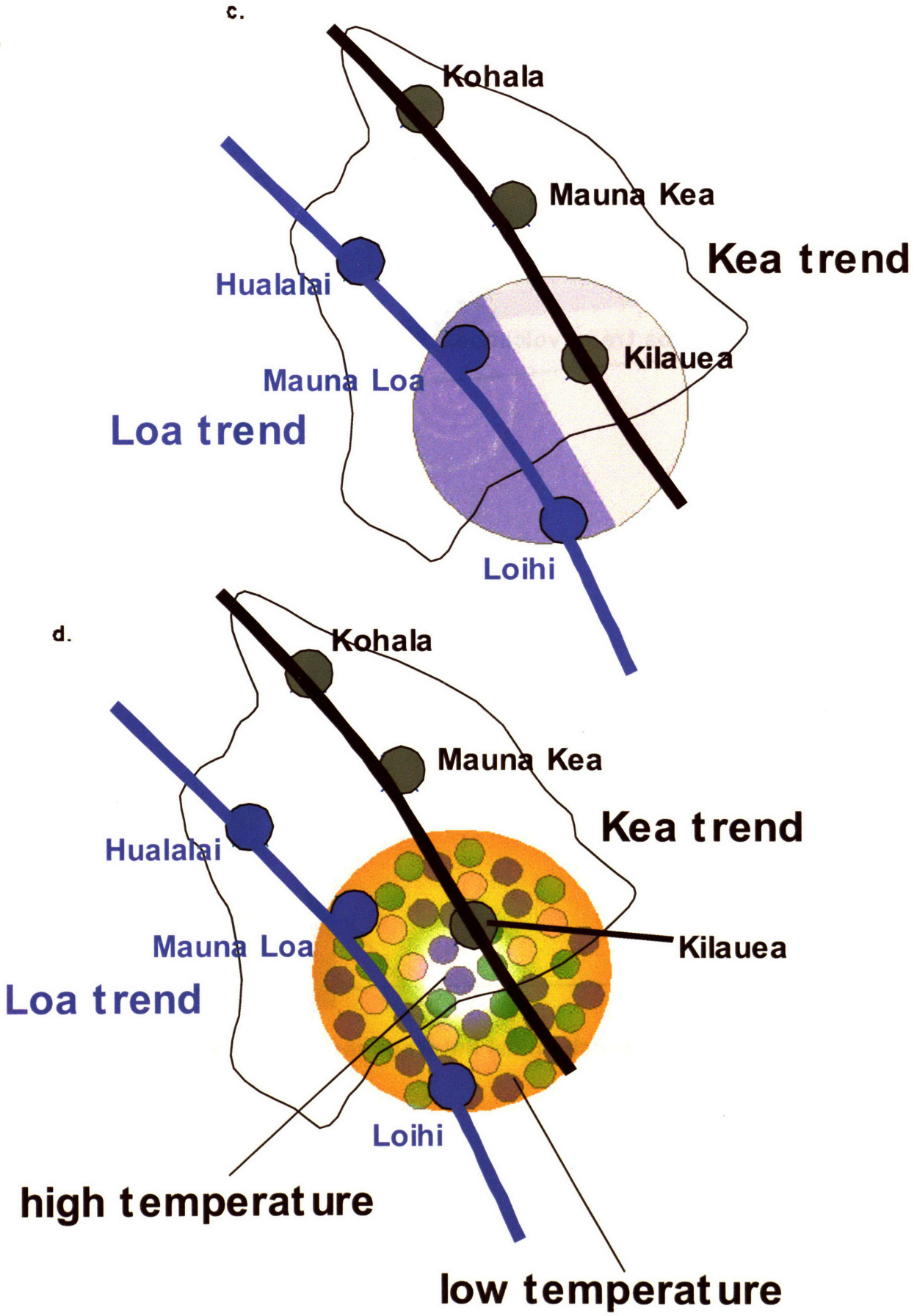
c.
Kohala
Mauna Kea
Kea trend
Hualalai
Kilauea
Mauna Loa
Loa trend
Loihi
d.
Kohala
Mauna Kea
Kea trend
Hualalai
Kilauea
Mauna Loa
Loa trend
Loihi
high temperature
low temperature

Fig 32.

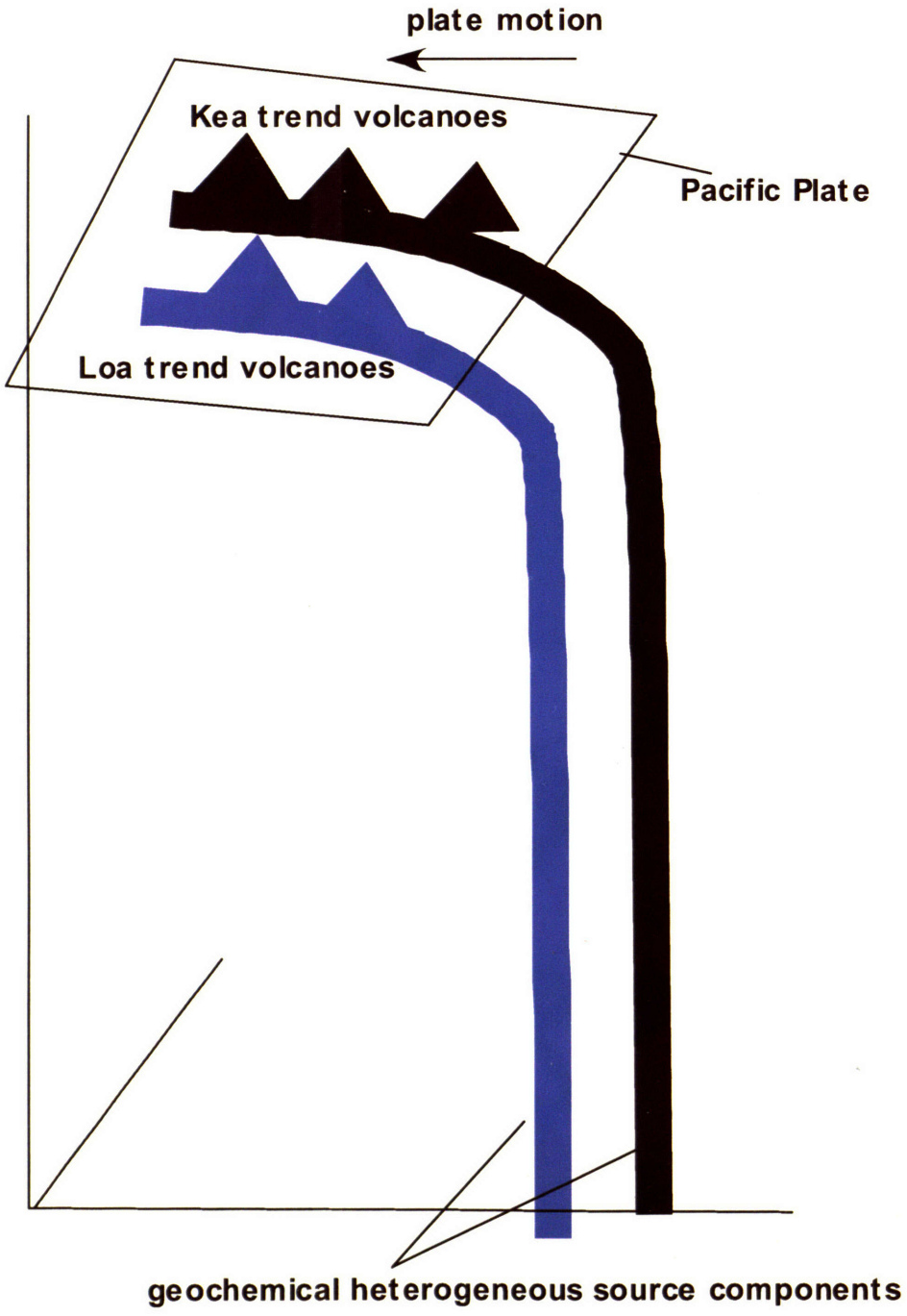

320S-35